Evaluation of *Galleria mellonella* larvae as a model to study microbial pathogenesis and host – pathogen interactions; a cellular and proteomic approach

A thesis submitted to the National University of Ireland, Maynooth for the degree of Doctor of Philosophy

Gerard Sheehan B.Sc.

August 2019

Supervisor
Prof. Kevin Kavanagh
Department of Biology
Maynooth University
Co. Kildare

Head of Department
Prof. Paul Moynagh
Department of Biology
Maynooth University
Co. Kildare

Declaration

This Thesis has not been submitted in whole or in part to this or any other university for any degree, and is the original work of the author except where otherwise stated.

Results presented in Chapter 7 was carried out with Dr. Wendy van de Sande (University Medical Centre Rotterdam, Rotterdam, The Netherlands) as part of a collaborative project. Results generated by Dr. Wendy van de Sande have been clearly delineated throughout this Chapter.

Signed: Gerard Sheehan

Gerard Sheehan, B.Sc.

Date: 28-12-19

Acknowledgements

The success of this PhD was certainly a team effort, every single person I have had the privilege of meeting in my seven years in Maynooth has contributed to shaping me into the person I am today and making Maynooth a home away from home for the best years of my life (so far!). First and foremost, without Prof. Kevin Kavanagh, none of this would have been possible. It was his commitment as an educator, his belief in my abilities, his patience as a supervisor, his expertise as a scientist, and his friendliness as a mentor and friend which has made this PhD a memorable and fruitful experience. I will cherish my memories in the lab, and I hope I am as productive and happy elsewhere as I was in the Medical Mycology lab. To Ciaran and Justin in Qualflow for increasing my knowledge of beer and biofilms, I really enjoyed our visits to HQ in Donabate.

To Amie and Rónán (Real name; Dr. Squire) the living legends (OG), you are lifelong friends and I have fond memories of 'thinking of science' and I will forever watch my back with ye around. A special mention to Anatte for all the help at the start of the project and many hours of ranting/raving about something or other. Ahmad, Dejana, Rachel and Ziga thanks for everything it's been great. To everyone who made the morning 'Anyone for Tea' ritual the highlight of my day (Niall 'the baker/BBQ expert' Conlon, Charley, Derv, Hazel, Rose). Jamie and Eoin, thanks for the invite to bioinfo-magic for new-Tea which was great for sharing knowledge and crac <3.

A massive thank you to all the helpful staff in the Dept. of Biology especially Patricia for popping into the lab for a check in, to Tina for the chats during coffee making and the millions of emails about beer line packages, Francis for teaching me how to clean, Ica for all the help with microscopy and cryoviz, Caroline for assistance with QE, Nick and Noel for their technical support.

To my brother David (Davy) you're a legend and I would be lost without you. My time in Maynooth would have been very different without you here. It was amazing having you in the lab (Summer 2018). To my Mam, you're the greatest woman I know, your support, love and strength (for the past 25 years) are a constant motivator and I would not be here without you (both literally and figuratively). To Niamh, words can't describe the support you've given me through this process, thank you for listening to my rants about failing experiments, writing and when everything seemed too much.

Peer-reviewed publications

Gerard Sheehan & Kevin Kavanagh (2018) Analysis of the early cellular and humoral responses of *Galleria mellonella* larvae to infection by *Candida albicans, Virulence* 9:1, 163-172, DOI: 10.1080/21505594.2017.1370174.

Gerard Sheehan, Gudmundur Bergsson, Noel G McElvaney, Emer P Reeves, Kevin Kavanagh (2018). The human cathelicidin antimicrobial peptide LL-37 promotes the growth of the pulmonary pathogen *Aspergillus fumigatus*. *Infect Immun* 86: e00097-18. DOI: 10.1128/IAI.00097-18.

Gerard Sheehan, Gráinne Clarke, Kevin Kavanagh (2018). Characterisation of the cellular and proteomic response of *Galleria mellonella* larvae to the development of invasive aspergillosis. *BMC Microbiology* 18:1. DOI: 10.1186/s12866-018-1208-6.

Gerard Sheehan, Marcus Nagl, Kevin Kavanagh (2018). Exposure to N-chlorotaurine induces oxidative stress responses in *Aspergillus fumigatus. J. Med. Microbiol 68(2):279-288.* DOI: 10.1099/jmm.0.000900.

Kevin Kavanagh & **Gerard Sheehan** (2018) The Use of *Galleria mellonella* Larvae to Identify Novel Antimicrobial Agents against Fungal Species of Medical Interest. *J. Fungi* 19;4(3). pii: E113. DOI: 10.3390/jof4030113.

Gerard Sheehan, Amy Garvey, Michael Croke & Kevin Kavanagh (2018) Innate humoral immune defences in mammals and insects: The same, with differences? *Virulence* 9:1, 1625-1639. DOI: 10.1080/21505594.2018.1526531.

Gerard Sheehan & Kevin Kavanagh (2019). Proteomic Analysis of the Responses of *Candida albicans* during Infection of *Galleria mellonella* Larvae. *J. Fungi* 5, 7. DOI: 10.3390/jof5010007.

Gerard Sheehan, Amy Dixon, Kevin Kavanagh (2019). Utilisation of *Galleria mellonella* larvae to characterise the development of *Staphylococcus aureus* infection. *Microbiology* 165(8):863-875. DOI: 10.1099/mic.0.000813.

Gerard Sheehan & Kevin Kavanagh (2020). Proteomic profiling of immune priming in *Galleria mellonella* larvae. (in preparation).

Gerard Sheehan, Laura Tully, Kevin Kavanagh (2019). *Candida albicans* increases the pathogenicity of *Staphylococcus aureus* during polymicrobial infection of *Galleria mellonella. Virulence* (in review).

Gerard Sheehan, Gemma Farrell, Kevin Kavanagh (2019). Immune priming, the secret weapon of the insect world? (submitted; *Virulence*).

Gerard Sheehan, Mickey Konings, Wendy W. J. van de Sande, Kevin Kavanagh (2019). Proteomic analysis of the processes leading to *Madurella mycetomatis* grain formation in *Galleria mellonella* larvae. *PLOS Neglected Tropical Diseases* (in preparation).

Publications not covered in this thesis

Farooq Ahmad Wani, Amaduddin, Babita Aneja, **Gerard Sheehan**, Kevin Kavanagh, Rabia Ahmad, Mohammad Abid and Rajan Patel (2019). Synthesis of Novel Benzimidazolium Gemini Surfactants and Evaluation of Their Anti-*Candida* Activity. *ACS Omega* 4 (7), 11871-11879. DOI: 10.1021/acsomega.9b01056.

Luigi Principe, Graziella Vecchio, **Gerard Sheehan**, Kevin Kavanagh, Gianluca Morroni, Valentina Viaggi, Alessandra di Masi, Daniele Roberto Giacobbe, Francesco Luzzaro, Roberto Luzzati, Stefano Di Bella (2019). Evaluation of *in vitro* and *in vivo* potential of Zinc chelators as antibiotic adjuvants against metallo β-lactamase (MBL)-producing bacteria. *J. Infect. Dis* (submitted).

Ahmad Ajdidi, **Gerard Sheehan**, Khaled Abu Elteen and Kevin Kavanagh (2019). Assessment of *in vitro* and *in vivo* antifungal activity of atorvastatin. *J. Med. Microbiol*. (in press).

Dejana Kosanovic, **Gerard Sheehan**, Helen Grogan, Kevin Kavanagh (2019). Characterisation of the interaction of *Pseudomonas putida* and *Psuedomonas tolaasii* with *Trichoderma aggressivum* - competitors of *Agaricus bisporus*. *Eur. J. Plant Pathol* (in review).

Oral Presentations

Gerard Sheehan, Gudmundur Bergsson, Noel G McElvaney, Emer P Reeves, Kevin Kavanagh Title: Why is the CF lung is promoting the growth of a fungal pathogen? Thesis in 3 min competition. 4th February 2017. Maynooth University.

Gerard Sheehan & Kevin Kavanagh. Title: Analysis of the early responses of *Galleria mellonella* larvae to infection by *Candida albicans.* Presentation to visiting academics (April 2017).

Gerard Sheehan & Kevin Kavanagh. Title: The early immune response of *G. mellonella* to infection by *C. albicans'.* Dept. of Biology Summer Research Day. June 2017 (MU).

Gerard Sheehan, Gudmundur Bergsson, Noel G McElvaney, Emer P Reeves, Kevin Kavanagh. Title The human cathelicidin antimicrobial peptide LL-37 augments the growth of *A. fumigatus'*. Irish Fungal Society June 2017 (Limerick IT).

Gerard Sheehan, Gudmundur Bergsson, Noel G McElvaney, Emer P Reeves, Kevin Kavanagh. Title: Exposure of the pulmonary pathogen *Aspergillus fumigatus* to human cathelicidin LL37 leads to increased growth. Lunch time seminar presentation (Dec 2017), (MU).

Gerard Sheehan, Gráinne Clarke, Kevin Kavanagh. Title: Characterisation of the response of *Galleria mellonella* larvae to the development of invasive aspergillosis'. Royal Entomology Society - Infection & Immunity Special Interest Group (Liverpool University, UK) (March 2018).

Gerard Sheehan, Gráinne Clarke, Kevin Kavanagh. Title: Analysis of the response of *Galleria mellonella* larvae to the development of disseminated *Aspergillus* infection. Lunch time seminar presentation (May 2018), (Maynooth University).

Gerard Sheehan & Kevin Kavanagh. Title: The use of *Galleria mellonella* larvae to elude fungal pathogenesis from an interactome approach. Presentation to visiting academics (TruLarv) 25th May 2018 MU.

Gerard Sheehan, Gudmundur Bergsson, Noel G McElvaney, Emer P Reeves, Kevin Kavanagh Title: The human cathelicidin antimicrobial peptide LL-37 promotes the growth and virulence of pulmonary pathogen *Aspergillus fumigatus*. Dept. of Biology Summer Research Day. June 2018 (MU).

Gerard Sheehan, Gráinne Clarke, Kevin Kavanagh. Title: *Galleria mellonella* larvae to study invasive and disseminated aspergillosis *in vivo.* Irish Fungal Society Annual meeting 18th June 2018, MU.

Gerard Sheehan Title: Using insects, Saving mice. Maynooth University 'Thesis-in-3' competition. October 2018, MU.

Gerard Sheehan, Mickey Konings, Wendy W. J. van de Sande, Kevin Kavanagh. Title: Proteomic analysis of the processes leading to *Madurella mycetomatis* grain formation in *Galleria mellonella* larvae. 11th April 2019. Belfast (UK), Microbiology Society Annual conference.

Gerard Sheehan, Stefano Di Bella, Luigi Principe, Alessandra Di Masi, Graziella Vecchio, Kevin Kavanagh. Title: Utilisation of *Galleria mellonella* larvae for identifying novel therapeutic options for the treatment of antibiotic resistant bacterial pathogens. 16th April 2019, Dept of Biology Seminar Series, MU.

Gerard Sheehan, Mickey Konings, Wendy W. J. van de Sande, Kevin Kavanagh. Title: Proteomic analysis of the processes leading to *Madurella mycetomatis* grain formation in *Galleria mellonella* larvae. 5th June 2019. Dept of Biology Research Day, MU.

Poster Presentations

Gerard Sheehan & Kevin Kavanagh. Title: Dissecting *Candida albicans* infection in the invertebrate host (*Galleria mellonella* larvae); a cellular and proteomic approach. 8th April 2018. Birmingham (UK), Microbiology Society Annual conference.

Gerard Sheehan, Gudmundur Bergsson, Noel G. McElvaney, Emer P. Reeves & Kevin Kavanagh. Title: The Human Cathelicidin Antimicrobial Peptide LL-37 stimulates the Growth of the Pulmonary Pathogen *Aspergillus fumigatus.* 14th June 2018. Birmingham University (UK), Early Career Microbiologists Forum Summer Conference.

Gerard Sheehan, Gudmundur Bergsson, Noel G. McElvaney, Emer P. Reeves & Kevin Kavanagh. Title: The Cathelicidin antimicrobial peptide (LL-37) stimulates the growth and pathogenicity of the pulmonary lung pathogen *Aspergillus fumigatus*. 9th April 2019. Belfast (UK), Microbiology Society Annual Conference.

Awards and Achievements

Microbiology Society Annual Conference Travel Grant Award April 2018 (Birmingham, UK), April 2019 (Belfast, UK).

Early Career Microbiologist Summer Conference Travel Grant Award 2018 (University of Birmingham, UK), 2019 (Trinity College Dublin, Ireland).

Runner-Up Best Oral Presentation Dept. of Biology Annual Research Day 2018, Maynooth University, Ireland.

Winner 'Thesis in 3' Competition 2018, Maynooth University, Ireland.

Appointed Microbiology Society Early Career Microbiologists' Forum Eukaryotic Division Representative 2019.

Table of contents

Declaration	i
Acknowledgements	ii
Peer reviewed publications	iii
Publications not covered in this thesis	iv
Oral Presentations	v
Poster Presentations	vi
Awards and Achievements	vi
Table of contents	vii
List of figures	xv
List of tables	xxii
Abbreviations	xxiii
Abstract	xxv

Chapter 1 Introduction

1.1	Insects as an alternative infection model to mammalian systems	2
1.2	Insect model systems	3
1.2.1	*Drosophila melanogaster*	3
1.2.2	*Bombyx mori*	3
1.2.3	*Galleria mellonella*	3
1.3	The innate immune response of insects	8
1.3.1	The insect prophenoloxidase activating (proPO) system	9
1.3.2	Antimicrobial peptides in insects and mammals	11
1.3.3	*Galleria mellonella* antimicrobial peptides and humoral mediators	15
1.3.4	Insect cellular immune response	16
1.3.4.1	Phagocytosis	17
1.3.4.2	Nodulation/ encapsulation	19
1.4	Immune priming or ‘memory’ responses in Insects	20
1.5	Mammalian innate immune response – to fungal pathogens	21
1.5.1	Cathelicidin antimicrobial peptide (LL-37)	22
1.5.2	N-chlorotaurine	25

1.6	Humoral immune signaling pathways in mammals and insects	27
1.6.1	The Toll and Toll-like pathway	27
1.6.2	The IMD and TNF-α signalling pathways	30
1.6.3	The blood/hemolymph clotting system in insects and mammals	32
1.6.3.1	The role of clotting systems	32
1.6.3.2	Similarities between insect and mammalian clotting factors	32
1.6.4	Melanisation in insects and mammals	35
1.7	Utilisation of *G. mellonella* larvae for measuring relative toxicity *in vivo*	37
1.8	Use of *G. mellonella* larvae for assessing antifungal activity *in vivo*	39
1.8.1	Drug assessment against pathogenic yeast	39
1.8.2	Drug assessment against filamentous fungi	42
1.9	Pathogens assessed using *G. mellonella* larvae	45
1.9.1	*Candida albicans*; a model fungal pathogen	45
1.9.2	*Staphylococcus aureus*	46
1.9.3	The pulmonary pathogen *Aspergillus fumigatus*	47
1.9.4	*Madurella mycetomatis*	50
1.10	Label-free mass spectrometry for whole cell proteomic analysis	52
1.11	Objectives of this study	53

Chapter 2 Materials & Methods

2.1	General laboratory practice and sterilisation procedures	55
2.1.1	Chemicals and reagents	55
2.1.2	Sterilisation procedures	55
2.1.3	Phosphate buffered saline (PBS)	55
2.1.4	Statistical analysis	56
2.2	Fungal and Bacterial strains and culture	56
2.2.1	*Aspergillus* strains and culture conditions	56
2.2.2	Harvesting of *Aspergillus* conidia	56
2.2.3	*Candida albicans* strain growth and harvest	57

2.2.4	*S. aureus* strain and culture	57
2.3	Microbial quantification and maintenance	57
2.3.1	Calculation of *S. aureus* culture cell concentration	57
2.3.2	Maintenance of microbial stocks (long term)	57
2.4	*G. mellonella* larval storage and experimental conditions	58
2.4.1	*G. mellonella* storage and food	58
2.4.2	Inoculation of *G. mellonella* larvae	58
2.4.2.1	Inoculation of *G. mellonella* larvae with *M. mycetomatis*	59
2.4.3	Beta glucan solution	60
2.4.5	Determination of hemocyte density	60
2.4.6	Determination of fungal/bacterial load in *G. mellonella* larvae	60
2.4.7	Flow cytometry of hemocyte sub-populations in *G. mellonella* larvae	60
2.4.8	Determination of fungicidal activity of hemocytes	60
2.4.9	Phagocytosis/ extracellular killing assay	62
2.4.10	Extraction of *G. mellonella* hemolymph	63
2.4.11	*Ex vivo* hemolymph fungicidal activity assay	63
2.5	Microscope based techniques	63
2.5.1	Cryo-imaging to assess disseminated infection in *G. mellonella* larvae	63
2.5.2	Fluorescent and Confocal Microscopy	63
2.5.3	Determination of *M. mycetomatis* burden of infection	64
2.6	General Protein Methodology	65
2.6.1	Bradford Protein assay	65
2.6.2	Qubit® protein quantification	65
2.6.3	Acetone precipitation of protein samples	66
2.6.4	Protein sample preparation	66
2.7	Workflow for Proteomics	67
2.7.1	Protein sample clean-up	67
2.7.2	Preparation of peptide sample prior to loading on LC-MS/MS Q-Exactive	67
2.7.3	Parameters for Mass Spectrometry data collection	68
2.7.4	Parameters for analysing quantitative results and statistical analysis.	68
2.7.5	Data availability	70

2.8	Analysis of the responses of *Aspergillus* to chemical agents	72
2.8.1	Assessment of susceptibility of *Aspergillus* conidia to compounds	72
2.8.2	Determination of the viability of *A. fumigatus* conidia	72
2.8.3	Effect of chemical agent on growth of *A. fumigatus* hyphae	72
2.9	Organic extraction from *Aspergillus* culture filtrates	73
2.9.1	Extraction of mycotoxins from *Aspergillus* culture filtrate	73
2.10	Reverse Phase High Performance Liquid Chromatography (RP–HPLC)	73
2.10.1	Quantification of mycotoxins by RP-HPLC	73
2.11	Proteins extraction from fungal cells	75
2.11.1	Whole cell protein extraction from *A. fumigatus*	75
2.11.2	Whole cell protein extraction from *C. albicans*	75
2.12	Ninhydrin colorimetric method for determination of amino acid concentration	76

Chapter 3 Comprehensive analysis of the host – pathogen interactome between *Candida albicans* and *Galleria mellonella*

3.1	Introduction	78
3.2	The effect of *C. albicans* infection on *G. mellonella* larvae viability	80
3.3	Characterisation of proliferation of *C. albicans* inside *G. mellonella* larvae	80
3.4	Alterations in hemocyte density following inoculation with *C. albicans*	81
3.5	Alterations in hemocyte density in larvae administrated β - (1, 3) glucan	85
3.6	Cellular immune response of *G. mellonella* larvae to yeast β - (1, 3) glucan	84
3.7	Effect of β - glucan administered on fungicidal activity of hemocytes	86
3.8	Characterisation of dissemination of *C. albicans* infection in *G. mellonella* larvae	87
3.9	Analysis of Proteomic response of *G. mellonella* larvae to *Candida* infection	87
3.10	Characterisation of *C. albicans* proteins secreted during infection of *G. mellonella* larvae	92

3.11	Assessment of fungicidal activity of larval hemolymph on *C. albicans (ex vivo)*	95
3.12	Proteomic response of *C. albicans* to *G. mellonella* hemolymph (*ex vivo*)	95
3.13	Effect of empirical antifungals on reducing symptoms associated with *C. albicans* systemic infection	101
3.13.1	Effect of amphotericin B and caspofungin on the survival of *C. albicans* infected larvae	101
3.13.2	Cryo-imaging of infected and anti-fungal treated larvae	103
3.14	Discussion	104

Chapter 4 Characterisation of *Galleria mellonella* larvae as a model to study the development of *Staphylococcus aureus* infection

4.1	Introduction	112
4.2	Response of *G. mellonella* larvae to *S. aureus* infection	114
4.3	Dissemination of *S. aureus* infection through larvae	115
4.4	Alteration in hemocyte density and function in response to *S. aureus* infection	119
4.5	Analysis of the humoral immune response of larvae to *S. aureus* infection	122
4.6	Discussion	125

Chapter 5 The evaluation of *Galleria mellonella* larvae as an *in vivo* model to study polymicrobial infection and assess novel combination antimicrobial chemotherapy

5.1	Introduction	130
5.2	Response of *G. mellonella* larvae to co-infection by *C. albicans* and *S. aureus*	132
5.3	Dissemination of co-infection throughout the host	135
5.4	Humoral immune response of *G. mellonella* larvae to co-infection	138
5.5	Evaluation of the efficacy of antimicrobial chemotherapy on the survival of *G. mellonella* larvae co-infected with *C. albicans* and *S. aureus*	141
5.6	Discussion	147

Chapter 6 Characterisation of the cellular and proteomic response of *Galleria mellonella* larvae to the development of invasive aspergillosis

6.1 Introduction 154

6.2 Responses of *G. mellonella* larvae to *A. fumigatus* infection 156

6.3 Alterations in hemocyte density in response to *Aspergillus* infection 157

6.4 Change in hemocyte subpopulations in response to heat killed *A. fumigatus* 158

6.5 Changes in hemocyte function in response to *A. fumigatus* 159

6.6 Modelling invasive and disseminated aspergillosis in *G. mellonella* 159

6.7 Examination of fungal nodule formation in *G. mellonella* larvae following *Aspergillus* infection 163

6.8 Analysis of alterations in *G. mellonella* proteome following *A. fumigatus* infection 166

6.9 Effect of empirical antifungals on reducing symptoms associated with invasive *A. fumigatus* infection 170

6.9.1 Effect of amphotericin B and caspofungin on the survival of *A. fumigatus* infected larvae 170

6.9.2 Cryo-imaging of infected and anti-fungal treated larvae following infection with *A. fumigatus* 172

6.10 Discussion 173

Chapter 7 A proteomic analysis of the processes leading to *Madurella mycetomatis* grain formation in *Galleria mellonella* larvae

7.1 Introduction 178

7.2 Responses of *G. mellonella* larvae to infection by *M. mycetomatis* 180

7.3 Analysis of *M. mycetomatis* grain formation in *G. mellonella* larvae over time 182

7.4 Quantification of the number of peptides and proteins from *G. mellonella* larvae in *M. mycetomatis* infected hemolymph 183

7.5 Temporal proteomic analysis of the host- pathogen interactome between *G. mellonella* larvae and *M. mycetomatis* 183

7.5.1 Proteome of grains at 24 h post inoculation 183

7.5.2 Proteome of hemolymph at 24 h post inoculation 185

7.5.3	Proteome of grains at 3 days post inoculation	187
7.5.4	Proteome of hemolymph at 3 day post inoculation	187
7.5.5	Proteome of grains at 7 days post inoculation	190
7.5.6	Proteome of hemolymph at 7 days post inoculation	191
7.6	Discussion	194
7.6.1	*M. mycetomatis* perspective	194
7.6.1.2	Proteins involved in extracellular vesicle formation	194
7.6.1.3	Proteins able to bind host extracellular matrix	195
7.6.1.4	Proteins able to make extracellular material	196
7.6.1.5	Proteins able to cross-link the extracellular grain matrix	196
7.6.1.6	Response of *M. mycetomatis* to the host	197
7.6.2	*G. mellonella* larvae perspective	198
7.6.2.1	Immune response to *M. mycetomatis* grain	198
7.6.2.2	Detoxification of grain associated cellular damage	199
7.6.2.3	Interaction of host with *M. mycetomatis* grain	199
7.6.3	Comparison of the host to *M. mycetomatis* compared to other fungi	199
7.6.3.1	Fungal invasion through the host	199
7.6.3.2	Grain formation	200
7.6.3.3	Anti-microbial response	200
7.6.3.4	Detoxication of fungal virulence factors	202
7.6.3.5	Fungal recognition	202
7.7	Conclusion	203

Chapter 8 Proteomic profiling of immune priming in *Galleria mellonella* larvae

8.1	Introduction	205
8.2	Immune priming of *G. mellonella* and resistance to infection	207
8.3	Alterations in the density of circulation hemocytes following immune priming of *G. mellonella* larvae	209
8.4	Humoral immune proteome of immune primed *G. mellonella* larvae	211
8.5	Discussion	217

Chapter 9 Analysis of the effect of the human cathelicidin antimicrobial peptide LL-37 on the growth of the pulmonary pathogen *Aspergillus fumigatus*

9.1	Introduction	224
9.2	Effect of LL-37 on the growth of *Candida albicans*	226
9.3	The growth response of *A. fumigatus* to LL-37	226
9.4	The growth response of *A. fumigatus* to cellular stress agents	229
9.5	Responses of *A. fumigatus* mycelium to LL-37	231
9.6	Responses of *A. fumigatus* mycelium to cellular stress agents	232
9.7	Fluorescent microscopic analysis of effect of LL-37 on *Aspergillus*	233
9.8	Effect of LL-37 on gliotoxin secretion by *A. fumigatus*	237
9.9	Analysis of Proteomic response of *Aspergillus fumigatus* to LL-37	239
9.10	Effect of LL-37 on the pathogenicity of *A. fumigatus* in the *Galleria mellonella* model of invasive aspergillosis	242
9.11	Discussion	245

Chapter 10 Analysis of the response of *Aspergillus fumigatus* to N-chlorotaurine

10.1	Introduction	251
10.2	Effects of N-chlorotaurine on the growth of *A. fumigatus*	253
10.3	Effect of NCT on the growth *Aspergillus* mycelium	253
10.4	Effects of N-chlorotaurine on the growth and viability of *A. fumigatus*	257
10.5	N-chlorotaurine induces alterations in extracellular amino acid levels from *A. fumigatus*	258
10.6	N-chlorotaurine induces alterations in gliotoxin levels from *A. fumigatus*	258
10.7	The whole cell proteomic response of *A. fumigatus* to N-chlorotaurine	261
10.8	Effect of combination N-chlorotaurine and Azole treatment on *A. fumigatus*	265
10.9	Toxicity of N-chlorotaurine in *G. mellonella* larvae	267
10.10	Post-antibiotic effect of N-chlorotaurine on *A. fumigatus*	268
10.11	Discussion	270

Chapter 11 General Discussion

11.1 General Discussion 275

11.2 Future research 285

Chapter 12 Bibliography

12 Bibliography 286

Chapter 13 Appendices

13 Appendices: List of Tables 303

List of Figures

Chapter 1

Fig 1.1 The advantages associated with using *G. mellonella* larvae

Fig 1.2 Increased popularity of the use of *G. mellonella* larvae in biomedical research in recent years

Fig 1.3 Schematic diagram of the proPO-system for melanin production in insects

Fig 1.4 Schematic diagram of the mechanism of action and function of antimicrobial peptides in insects and mammals

Fig 1.5 *G. mellonella* larval hemocytes visualised by microscopy

Fig 1.6 Schematic representation of similarities which exist between the insect hemocyte and mammalian granulocyte (e.g. neutrophil)

Fig 1.7 Diagram of the process of nodulation and encapsulation in insects

Fig 1.8 Structure and function of h-CAP18 derived antimicrobial peptide LL-37

Fig 1.9 Biosynthesis of N-chlorotaurine from human monocyte/granulocyte

Fig 1.10 Diagrammatic representation of the similarities between invertebrate Toll signalling and vertebrate toll-like signalling

Fig 1.11 Comparison of insect IMD pathway and mammalian TNF-α pathway

Fig 1.12 Schematic comparison of the hemolymph/blood clotting system in insects versus mammals

Fig 1.13 Examples of uses of *G. mellonella* larvae to assess the *in vivo* toxicity and efficacy of a range of antifungals and chemical agents

Fig 1.14 *C. albicans* infection of *G. mellonella* larvae

Fig 1.15 *G. mellonella* larvae as a model to study the toxicity, efficacy, immune modulatory effects etc.

Fig 1.16 Summary of *C. albicans* diseases, virulence and factors influencing disease development

Fig 1.17 *Aspergillus* colonisation as commonly observed in the cystic fibrosis lung

Fig 1.18 Infection process of invasive Aspergillosis in the immunocompromised lung

Fig 1.19 The biology, epidemiology, pathogenesis and symptoms of *M. mycetomatis* infection

Chapter 2

Fig 2.1 General procedures associated with using *G. mellonella* larvae

Fig 2.2 Schematic demonstration of set up for intracellular and extracellular killing assay.

Fig 2.3 Protein standard curve

Fig 2.4 General workflow for proteomic analysis of complex protein samples

Fig 2.5 Detection of purified Gliotoxin by RP-HPLC

Fig 2.6 Gliotoxin standard curve

Fig 2.7 Amino acid standard curve

Chapter 3

Fig 3.1 Graphical abstract for Chapter 3

Fig 3.2 Effect of *C. albicans* cells on viability of *G. mellonella* larvae over 72 h

Fig 3.3 Fluctuations in fungal cell density in *C. albicans* infected larvae

Fig 3.4 Alteration in circulating hemocyte density following inoculation with inoculation with *C. albicans* and incubated 30 ^{o}C

Fig 3.5 Effect of β - (1, 3) glucan on *G. mellonella* larvae hemocyte density

Fig 3.6 Flow cytometry analysis of hemocyte sub-populations

Fig 3.7 Fungicidal activity of hemocytes from *G. mellonella*

Fig 3.8 Cryoviz visualisation showing the stages of disseminated candidosis in *G. mellonella* after 6 and 24 h infection

Fig 3.9 Confocal microscopy of fungal nodules from *G. mellonella* larvae

Fig 3.10 Shotgun quantitative proteomic analysis of *G. mellonella* infected with *C. albicans*

Fig 3.11 Volcano plots of all identified proteins based on relative abundance differences between *G. mellonella* larvae treated at 0, 6 or 24 h

Fig 3.12 Bar charts showing changes to number of proteins given biological processes (A) and molecular function (B), cellular component (C) at level 3 ontology and enzyme categories (D)

Fig 3.13 Candidacidal activity of *G. mellonella* larval hemolymph *ex vivo*

Fig 3.14 Shotgun proteomics of responses of *C. albicans* (2.5×10^7 ml^{-1}) to *G. mellonella* hemolymph (100%) after 6 h incubated at 30 °C

Fig 3.15 Shotgun quantitative proteomic analysis of *C. albicans* incubated in *G. mellonella* 100% hemolymph for 6 h at 30 ºC

Fig 3.16 Interactome of proteins increased (A) and decreased (B) in abundance in *C. albicans* incubated in *G. mellonella* hemolymph

Fig 3.17 Survival of *G. mellonella* larvae following infection by *C. albicans* and then administrated anti-fungal agents

Fig 3.18 Cryo-imaging of *G. mellonella* larvae infected with *C. albicans* followed by administration of antifungal therapy

Chapter 4

Fig 4.1 Graphical abstract for Chapter 4

Fig 4.2 Effect of *S. aureus* cells on viability of *G. mellonella* larvae over 72 h

Fig 4.3 *S. aureus* c.f.u. per $larva^{-1}$ obtained from *G. mellonella* larvae infected with *S. aureus* cells (2×10^6 $larva^{-1}$) over 72 h

Fig 4.4 Cryo-imaging visualisation of disseminated *S. aureus* infection of *G. mellonella* larvae at 6, 24 and 48 h

Fig 4.5 Visualisation of GFP-labelled *S. aureus* cells within bacterial nodules in *G. mellonella* larvae inoculated with 2×10^6 viable cells

Fig 4.6 Visualisation of WT *S. aureus* cells within bacterial nodules in *G. mellonella* larvae inoculated with 2×10^6 viable cells

Fig 4.7 Alteration in circulating hemocyte density following inoculation with viable *S. aureus* cells

Fig 4.8 Microbicidal activity of hemocytes extracted from *G. mellonella* larvae at 0, 6 and 24 h after inoculation with *S. aureus* heat killed cells (2×10^6 $larva^{-1}$)

Fig 4.9 Response of *ex vivo* hemocytes to *S. aureus*

Fig 4.10 Principal component analysis (PCA) of *G. mellonella* hemolymph proteomic profiles following infection with viable *S. aureus* cells for 0, 6 and 24 h

Fig 4.11 Proteomic responses of *G. mellonella* larval hemolymph following infection by 2×10^6 *S. aureus* cells after 6 (A) and 24 (B) h

Chapter 5

Fig 5.1 Graphical abstract for Chapter 5

Fig 5.2 Survival of *G. mellonella* larvae following mono- and co-infection with *C. albicans* and *S. aureus*

Fig 5.3 Alteration in circulating hemocyte density following inoculation with *S. aureus* cells alone and in combination with *C. albicans*

Fig 5.4 *S. aureus* CFU larva^{-1} obtained from *G. mellonella* larvae infected with *S. aureus* cells (2×10^6 and 2×10^6 larva^{-1}) or co-infected larvae over 48 h

Fig 5.5 Cryo-imaging of *G. mellonella* larvae co-infected with *C. albicans* and *S. aureus*

Fig 5.6 Proteomic response of *G. mellonella* larvae to co-infection by *C. albicans and S. aureus*

Fig 5.7 Proteomic responses of *G. mellonella* larval hemolymph following co-infection by *C. albicans* (1×10^5 larva^{-1}) and *S. aureus* (2×10^4 larva^{-1}) after 6 (A) and 24 (B) h

Fig 5.8 Susceptibility of *C. albicans, S. aureus* and combination to anti-microbial chemotherapy

Fig 5.9 Viability of co-infected *G. mellonella* larvae following administration of antimicrobial chemotherapy

Fig 5.10 Effect of antimicrobial chemotherapy on the symptoms associated with disseminated disease in co-infected larvae

Chapter 6

Fig 6.1 Chapter 6 graphical abstract

Fig 6.2 Effect of viable and heat killed (HK) *A. fumigatus* conidia on viability of *G. mellonella* larvae over 72 h

Fig 6.3 Alteration in circulating hemocyte density following inoculation with viable and heat killed *A. fumigatus* conidia

Fig 6.4 Flow cytometric analysis of hemocyte sub-populations

Fig 6.5 Fungicidal activity *G. mellonella* hemocytes

Fig 6.6 Intracellular (A) and extracellular (B) killing activity of hemocytes from larvae exposed to heat killed *A. fumigatus* (1×10^6 20 μl^{-1})

Fig 6.7 Cryo-imaging visualisation of the stages of invasive and disseminated aspergillosis in *G. mellonella* larvae after 6- and 24-h infection

Fig 6.8 Visualisation of development of *A. fumigatus* conidia and hyphae in fungal nodules/granulomas in *G. mellonella* larvae inoculated with 1×10^6 viable conidia

Fig 6.9 Visualisation of development of *A. fumigatus* conidia and hyphae in fungal nodules/granulomas in *G. mellonella* larvae inoculated with 1×10^6 viable conidia

Fig 6.10 The acute *ex vivo* cellular response of *G. mellonella* hemocytes to *A. fumigatus*

Fig 6.11 Principal component analysis (PCA) and hierarchical clustering of *G. mellonella* hemolymph proteomic profiles following infection with viable *A. fumigatus* conidia for 0, 6 and 24 h

Fig 6.12 Proteomic responses of *G. mellonella* larvae following infection by 1×10^6 viable *A. fumigatus* conidia after 6 (A) and 24 (B) h

Fig 6.13 Survival of *G. mellonella* larvae following infection by *A. fumigatus* and then administrated anti-fungal agents

Fig 6.14 Cryo-imaging of *G. mellonella* larvae infected with *A. fumigatus* followed by administration of antifungal therapy

Chapter 7

Fig 7.1 Graphical abstract for Chapter 7

Fig 7.2 *M. mycetomatis* infection in *Galleria mellonella* larvae

Fig 7.2 Proteomic responses of *G. mellonella* larvae following infection by *M. mycetomatis* mycelium (4 mg 40 μl^{-1}) after 24 h post infection as compared to control larvae

Fig 7.3 Proteomic responses of *G. mellonella* larvae following infection by *M. mycetomatis* mycelium (4 mg 40 μl^{-1}) after 3 days post infection as compared to control larvae

Fig 7.4 Proteomic responses of *G. mellonella* larvae following infection by *M. mycetomatis* mycelium (4 mg 40 μl^{-1}) after 7 days post infection as compared to control larvae

Fig 7.5 Average LFQ intensities for a number of *G. mellonella* immune related proteins and their temporal dynamics in hemolymph during infection with *M. mycetomatis* for 24 h, 3 days and 7 days post infection

Chapter 8

Fig 8.1 Graphical abstract for Chapter 8

Fig 8.2 Survival of *G. mellonella* larvae immune-primed (fungal, bacterial, temperature) and infected with *C. albicans* or *S. aureus*

Fig 8.3 Alterations in circulating hemocyte density from *G. mellonella* larvae immune-primed (fungal, bacterial, temperature) over 24 h

Fig 8.4 Proteomic profiling of immune priming in *G. mellonella* larvae

Fig 8.5 Principal component analysis (PCA) of *G. mellonella* hemolymph proteomic profiles following immune priming with heat killed *C. albicans*, heat killed *S. aureus*, temperature (37 ºC) and control (30 ºC) for 24 h

Fig 8.6 Average LFQ intensities of proteins related to antimicrobial peptides, microbial recognition and immune related proteins from the proteome of control, fungal, bacterial and temperature primed larvae

Chapter 9

Fig 9.1 Chapter 9 graphical abstract

Fig 9.2 The effect of LL-37 on *C. albicans* viability

Fig 9.3 The effect of LL-37, scrambled LL-37 and RK-31 on the growth of *A. fumigatus*

Fig 9.4 The effect of LL-37 on *A. fumigatus* in minimal essential medium

Fig 9.5 The effect of LL-37 on *A. fumigatus* in minimal essential medium supplemented with 5% fetal calf serum

Fig 9.6 The effect of LL-37 on the growth of *A. fumigatus* in YEPD medium

Fig 9.7 The effect of calcofluor white on the growth of *A. fumigatus*

Fig 9.8 The effect of saponin on the growth of *A. fumigatus*

Fig 9.9 The effect of hydrogen peroxide (H_2O_2) on the growth of *A. fumigatus*

Fig 9.10 The effect of LL-37 on biomass accumulation of *A. fumigatus*

Fig 9.11 The effect of a low concentration of cellular stress inducing agents on biomass accumulation of *A. fumigatus*

Fig 9.12 Photomicrographs of *A. fumigatus* hyphae from cultures exposed to LL-37, scrambled and RK-31

Fig 9.13 Effect of LL-37 on the growth of *A. flavus*

Fig 9.14 Photomicrographs of *A. flavus* hyphae from cultures exposed to LL-37, scrambled and RK-31

Fig 9.15 Release of gliotoxin from *A. fumigatus* exposed to LL-37

Fig 9.16 Release of gliotoxin from *A. fumigatus* exposed to stress agents

Fig 9.17 Shotgun quantitative proteomic analysis of LL-37 treated *A. fumigatus*

Fig 9.18 Label free proteomics of *A. fumigatus* exposed to 5 μg ml^{-1} LL-37 for 24 h (A) or 48 h (B)

Fig 9.19 Effect of pre-incubation of *A. fumigatus* in LL-37, scrambled LL-37 and RK-31 on the viability of *Galleria mellonella* larvae

Fig 9.20 Effect of pre-incubation of *A. fumigatus* in LL-37, scrambled LL-37 and RK-31 on the fungal load *G. mellonella* larva^{-1}

Chapter 10

Fig 10.1 Chapter 10 graphical abstract

Fig 10.2 Effect of N-chlorotaurine on the growth of *A. fumigatus* strains

Fig 10.3 Effect of N-chlorotaurine on the growth of *A. flavus*

Fig 10.4 The effect of N-chlorotaurine on growth of *A. fumigatus* strains ATCC 26933 (A), ATCC 46645 (B) and Af 293 (C)

Fig 10.5 The effect of N-chlorotaurine on growth of *A. flavus*

Fig 10.6 The effect of N-chlorotaurine on the viability of *A. fumigatus* conidia

Fig 10.7 Amino acid leakage from *A. fumigatus* mycelium

Fig 10.8 Effect of N-chlorotaurine on gliotoxin (intracellular and extracellular) from *A. fumigatus* mycelium

Fig 10.9 Effect of N-chlorotaurine on extracellular gliotoxin from *A. fumigatus* (ATCC46645) mycelium

Fig 10.10 Effect of N-chlorotaurine on extracellular gliotoxin from *A. fumigatus* (Af293) mycelium

Fig 10.11 Shotgun quantitative proteomic analysis of N-chlorotaurine (6.8 mM) treated *A. fumigatus* (ATCC 26933)

Fig 10.12 Enrichment analysis for proteins detected in *A. fumigatus* treated with N-chlorotaurine

Fig 10.13 Shotgun proteomics of 24-h preformed *A. fumigatus* ATCC 26933 mycelium exposed to N-chlorotaurine (6.8 mM) for 24 h

Fig 10.14 Synergistic activity between N-chlorotaurine and itraconazole in reducing *A. fumigatus* mycelium biomass

Fig 10.15 Viability of *G. mellonella* larvae following injection with varying concentrations of NCT

Fig 10.16 The post-antibiotic effect of N-chlorotaurine on *A. fumigatus*

List of Tables

Chapter 1

Table 1.1 Selected examples of utilisation of *G. mellonella* larvae to assess fungal virulence

Table 1.2 A comparison of the antimicrobial peptides present in insects and humans

Table 1.3 A comparison of humoral receptors, anti-microbial peptides, cascades and enzymes in mammalian and insect humoral immune responses

Table 1.4 Examples of use of *G. mellonella* larvae with antifungal agents

Chapter 2

Table 2.1 Peptides and sequences used in this study

Table 2.2 Buffers and solutions used in protein sample preparation

Table 2.3 Buffers and solutions used in protein sample clean-up

Table 2.4 Proteomic data submission to ProteomeXchange Consortium

Table 2.5 Buffers needed for HPLC operation

Chapter 11

Table 11.1 Summary of the key proteins identified during infection by different pathogens in *G. mellonella* larvae at 24 h post infection relative to the relevant 0 h control

Abbreviations

ACN	Acetonitrile
AMP	Anti-microbial Peptide
ANOVA	Analysis of variance
ApoLp-III	Apolipophorin-III
ApoE	Apolipoprotein E
APS	Ammonium persulphate
ATCC	American Type Culture Collection
ATP	Adenosine triphosphate
β	beta
βGBP	beta-1, 3-glucan recognition protein
BP	Biological process
BSA	Bovine serum albumin
°C	Degrees centigrade
CC	Cellular component
c.f.u.	colony forming units
cm	Centimeter
d	Day
ddH2O	Deionised water
dH2O	Distilled water
DAPI	4',6-diamidino-2-phenylindole
DMSO	Dimethyl sulfoxide
DNA	Deoxyribonucleic acid
DNase	Deoxyribonuclease
dNTP	Deoxynucleotide 5'-triphosphate
DTT	Dithiothreitol
EC	Enzyme category
EDTA	Ethylene diamine tetra acetic acid
EF	Elongation factor
FACS	Fluorescence Activated Cell Sorter
FDR	False discovery rates
g	Grams
g	g-force
GO	Gene ontology
GST	Glutathione S transferase
GTP	Guanidine tri-phosphate
h	Hours
HCl	Hydrochloric acid
Hsp	Heat shock protein
IAA	Iodoacetamide
Ig	Immunoglobulin
IMD	Immune Deficiency pathway
Kg	Kilo
kDa	Kilodaltons
LFQ	Label free quantification
L	Litre
LPS	Lipopolysaccharide
LC-MS	Liquid chromatography mass spectrometry
M	Molar
min	Minute

mL	Millilitre
mM	Millimolar
MP	Molecular function
MOPS	Mopholinepropanesulfonic acid
mRNA	Messenger ribonucleic acid
MRSA	Methicillin resistant *Staphylococcus aureus*
MS/MS	Tandem mass spectrometry
µg	Microgram
µl	Microliter
µM	Micromolar
NADPH	Nicotinamide Adenine Dinucleotide Phosphate
NCT	N- Chlorotaurine
ng	Nanogram
nl	Nanoliter
nm	Nanometer
OD	Optical density
PAGE	Polyacrylamide gel electrophoresis
PRR	Pathogen associated molecular pattern
PBS	Phosphate buffered saline
PCR	Polymerase Chain Reaction
pg	picogram
PG	Peptidoglycan
PGRP	Peptidoglycan recognition protein
pH	Potential hydrogen
PO	Phenoloxidase
ProPO	Prophenoloxidase
ppm	Parts per million
PRR	Pattern recognition receptor
PRIDE	PRIDE PRoteomics IDEntifications
RNA	Ribonucleic acid
RNase	Ribonuclease
ROS	Reactive oxygen species
rpm	Revolutions per minute
SAB	Sabouraud
S.E.	Standard error
SOD	Superoxide dismutase
SSDA	Statistically significantly differentially abundant
STRING	Search Tool for the Retrieval of INteracting Genes/Proteins
TFA	Trifluoroacetic acid
TLR	Toll like receptor
U	Unit
UV	Ultraviolet
V	Volts
v	Volume
v/v	Volume per volume
w/v	Weight per volume
YEPD	Yeast Extract-Peptone-D-Glucose

Abstract

The popularity of *Galleria mellonella* larvae as a model to study microbial virulence is due to the similarities that exist between the mammalian and insect immune responses, adherence to the 3R policy and the financial and legal/ ethical burden associated with using vertebrate animal models. *G. mellonella* larvae have been widely used to assess the virulence of a range of microbial species and the results obtained using larvae closely match those obtained in murine studies. The aim of this project was to utilise *G. mellonella* to assess the pathogenicity of various human pathogens and compare these results to pathologies that occur in mammals.

G. mellonella larvae were infected with *Candida albicans, Aspergillus fumigatus*, *Madurella mycetomatis* or *Staphylococcus aureus,* or co-infected with *C. albicans* and *S. aureus* and the host – pathogen interactome characterised by a variety of cellular and proteomic techniques. Infection of larvae with *C. albicans* and *A. fumigatus* produced disseminated disease and a similar immune response to the human condition. Infection with *S. aureus* produced nodules which are similar to abscesses; a hallmark of soft tissue infection in humans. Proteomic profiling of *M. mycetomatis* grains produced within larvae revealed a range of novel processes (e.g. extracellular vesicle formation, host extracellular matrix binding and response to stress/ host) which are essential in the production of grains *in vivo*. Co-infection of larvae by *C. albicans* and *S. aureus* was characterised, and larvae proved to be an excellent alternative model to study trans-kingdom polymicrobial infection.

Larvae were immunological primed by fungal and bacterial cells, and by temperature (37 ^{o}C) and their 1) resistance to infection, 2) fluctuations in hemocyte density and 3) alterations in humoral immune response were examined. The effect of two antimicrobial effectors (LL-37 and N-chlorotaurine) of the innate immune response on *A. fumigatus* were assessed. Exposure to the AMP LL-37 increased the growth of *A. fumigatus*, the levels of extracellular gliotoxin production, the abundance of proteins associated with growth, virulence and allergenic responses, and increased mortality in *G. mellonella* larvae. The neutrophil derived oxidant N-chlorotaurine reduced the growth and viability of *A. fumigatus*, decreased the production of gliotoxin and induced an oxidative stress response.

This study demonstrated that larvae are an excellent, cost effective and easy to use model to study host – pathogen interactions, microbial pathogenesis, polymicrobial infection and combination antimicrobial drug efficacy.

Chapter 1

Introduction

1.1 Insects as an alternative infection model to mammalian systems

Insects are an extremely successful group of invertebrates with approximately 10^{20} individuals occupying all ecological niches (Ben-Dov, 1993; Leonardi *et al.*, 2012). Their omnipresence is as a result of a highly efficient and versatile immune response (Hoffmann, 1995; Kavanagh and Reeves, 2004). Insects and vertebrates divergence occurred approximately 500 million years ago as evidenced from molecular analysis and fossil records (Sanders and Lee, 2010), but despite this the immune system of insects shares strong functional, structural and biochemical similarities to the innate immune response of vertebrates. Vertebrates have an adaptive immune response which produces long-lived antibodies and memory cells, whereas in recent years the concept of 'immunological memory' in insects has been well documented in the literature but also subjected to much debate and controversy (Cooper & Eleftherianos 2017). Nevertheless, the similarities which exist have allowed insects to be used to assess the virulence of a range of bacterial and fungal pathogens and generate results comparable to those obtained using vertebrates (e. g. mice).

The use of insects as an infection model generated 346 research publications in 2018 which mention; 'insect infection model' as compared to 43 publications in 2000 as found in Pub Med (Accessed 09nd August 2019). The global demand for novel alternative *in vivo* models is a direct result of adherence to the 3R policy (replace, reduce, refine) and due to the strict ethical and legal restrictions and the time and cost considerations associated with using vertebrate systems (Rollin, 2009). It is estimated that approximately 115 million vertebrates are used each year in biomedical testing, this number is also probably underestimated as many countries do not report this data (e.g. China, India, Australia) (Loeb *et al.*, 1989). Both insects and mammals are susceptible to similar pathogens and generate similar pathologies (Mukherjee *et al.*, 2013) and both share similar detoxification systems to xenobiotics (Maguire *et al.,* 2016; Maguire *et al*., 2017a; Maguire *et al*., 2017b).

The insect screening system provides a novel way to examine the mechanism of microbial virulence and interaction with host tissue and to assess the efficacy of antimicrobial agents without the disadvantages associated with vertebrate systems. This has led to a multitude of insect mini models being established and these include

Drosophila melanogaster (Lemaitre and Hoffmann, 2007), *Bombyx mori* (Panthee *et al.*, 2017) and *Galleria mellonella* (Kavanagh and Reeves, 2004).

1.2 Insect model systems

1.2.1 Drosophila melanogaster

Drosophila melanogaster is a well-established model due to the range of molecular tools available such as genome editing and mutant library availability, and the results obtained using flies have been translated into modern medicine e.g. discovery of Toll and its role in antifungal immunity in *Drosophila* resulted in the identification of toll-like receptors (TLR) in mice and in humans (Alarco *et al*., 2004; Chamilos *et al.,* 2011). Their small size limits the collection of large amounts of hemolymph and hemocytes, and for this reason *ex vivo* cell assays are troublesome. Propagation temperature of between 22 and 25 ^{o}C limits temperature dependent studies of human pathogens. However host – pathogen interactions have been analysed in great detail at the genomic and transcriptomic level (Kemp and Massey, 2007; Dionne and Schneider, 2008).

1.2.2 *Bombyx mori*

The silkworm *Bombyx mori* is a large insect (5 cm) thus making it advantageous for handling, injection of a specific inoculum/ volume and amenable to drug pharmacodynamic studies. *B. mori* larvae can be infected with *Staphylococcus aureus*, *Pseudomonas aeruginosa*, and *Vibrio cholera* but are cured by antibiotics and these results were mirrored using mice (Kaito *et al.*, 2002). Larvae were also used to assess the virulence of *Candida albicans* and *Cryptococcus neoformans* (Ishii *et al.,* 2015). Larvae were also used to assess the efficacy of antifungal agents amphotericin B, flucytosine, and fluconazole against *C. neoformans* (Matsumoto *et al.*, 2012) and the effect of trichodermin, epiisororidin E, and verrucarin A against *C. albicans* (Uchida *et al.*, 2016).

1.2.3 *Galleria mellonella*

G. mellonella are a popular choice over other insect models due to their ease of inoculation, low cost and the ability to generate results in 24 – 48 h (Fuchs *et al.*, 2010; Cook and McArthur, 2013) (**Fig. 1.1**) and this has resulted in a significant increase in their use in recent years (**Fig. 1.2**). The low cost of larvae means it is

possible to perform many replicates and produce statistically valid results. *G. mellonella* larvae are easy to house and their use has none of the legal or ethical constraints that restrict the use of mammals. Larvae are amenable to incubation at 37 ºC which means that many temperature dependent virulence factors of human pathogens are active.

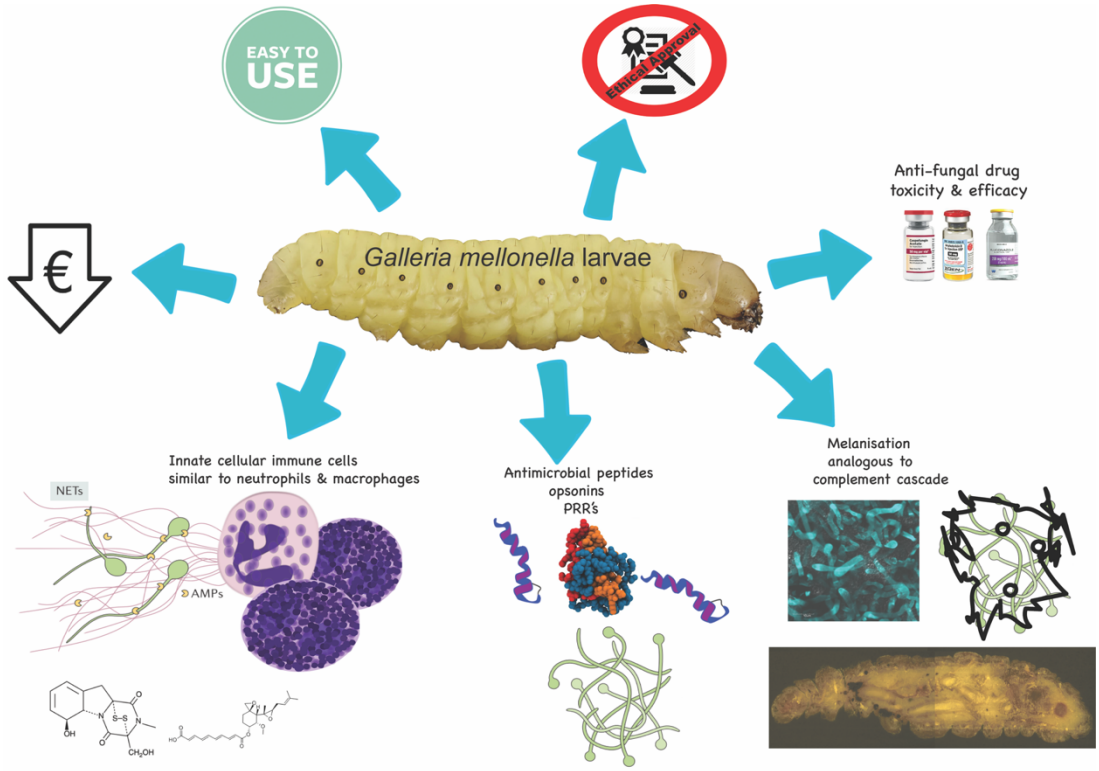

Fig. 1.1. The advantages associated with using *G. mellonella* larvae. Larvae are inexpensive to purchase, easy to use, are not subject to the ethical or lethal restrictions associated with mammalian testing, and can be employed for testing the toxicity and efficacy of a range of novel antifungal drugs. These advantages are possibly due to the similarities between the mammalian innate immune response and the insect immune system.

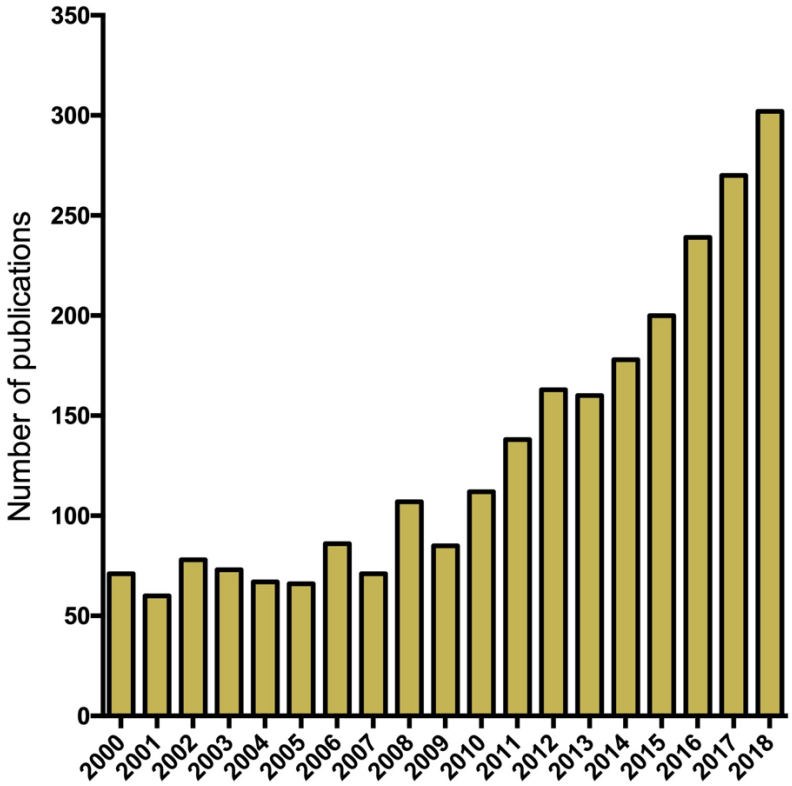

Fig. 1.2. Increased popularity of the use of *G. mellonella* larvae in biomedical research in recent years. The number of research papers published between the years 2000 and 2018 utilising *G. mellonella* larvae to study microbial infection as determined from Web of Science.

In addition, *G. mellonella* larvae may be easily and accurately inoculated via intra-hemocoel injection, by force feeding or by rolling on a layer of spores and a number of parameters may be employed to assess their response to infection. These include mortality, extent of melanisation, alteration in hemocyte density and/or function, changes in microbial load, formation of pupa, movement, alteration in gene expression and variations in the proteome. Another advantage is that due to their size and ease of handling it is possible to administer a defined inoculum by force feeding or intra-hemocoel injection to larvae. Larvae can be used for pharmacokinetic and pharmacodynamics studies and larvae produce a large volume (80 – 100 µl larva^{-1}) of hemolymph (analogous to mammalian blood) which can be analysed by a variety of methods (Astvad *et al.*, 2017; Maguire *et al.*, 2017b; Maurer *et al.*, 2018). Hemocytes (immune cells) can be isolated from larvae and subjected to a range of *ex vivo* cellular assays in response to microbial pathogens and/or to determine the effect of chemical agents (Bergin *et al*., 2005; Renwick *et al*., 2007; Banville *et al*., 2011;

Fallon *et al.,* 2011). There are some disadvantages associated with the use of larvae such as a lack of mutant strains and larvae may not be a suitable model for some microbial species. However many of the disadvantages detailed by Tsai *et al.* (2016) have been addressed in the past three years (Mukherjee & Vilcinskas 2014; Champion *et al.,* 2016; Tsai *et al*., 2016).

The immune responses of larvae have been recently documented at the proteomic, transcriptomic and epigenetic level due to advances in technologies such as label-free proteomics, and the sequencing of the *G. mellonella* genome opens new avenues of research (Mukherjee and Vilcinskas, 2014; Browne *et al.*, 2015; Heitmueller *et al.*, 2017).

Interestingly, infection of *G. mellonella* larvae with *C. albicans* (Cotter *et al.,* 2000; Brennan *et al*., 2002) and *Aspergillus fumigatus* (Reeves *et al.*, 2004a; O'Hanlon *et al.*, 2011; Slater *et al.*, 2011) shows a strong correlation to the results obtained using mice. *G. mellonella* larvae are excellent models to study the virulence of *Candida* species (Jacobsen, 2014) and larvae have been utilised to develop an infection model for *C. neoformans* (Mylonakis *et al.*, 2005) (**Table 1.1**). *C. neoformans* serially passaged in *G. mellonella* larvae showed an enhanced ability to kill mice if administered by intra-tracheal or intravenous route, although their ability to kill *G. mellonella* larvae remained unchanged.

Table 1.1 Selected examples of utilisation of *G. mellonella* larvae to assess fungal virulence.

Reference	Fungal virulence and infection
Leger *et al.,* 2000	*Aspergillus flavus* pathogenicity in *Galleria mellonella*
Brennan *et al*. 2002	The virulence of *Candida albicans* mutants correlates between mice and *Galleria mellonella* larvae
Cotter *et al.* 2002	Using insects for assessing pathogenicity of yeasts
Reeves *et al.* 2004	Gliotoxin Production and Virulence of *Aspergillus fumigatus* in *Galleria mellonella*
Velagapudi *et al*. 2009	*Cryptococcus neoformans* virulence is similar in mice and *Galleria mellonella* larvae
Slater *et al.* 2011	Pathogenicity of *Aspergillus fumigatus* mutants in *Galleria mellonella* matches that in mice
Navarro-Velasco *et al*. 2011	*Galleria mellonella* to study *Fusarium oxysporum* mutants.
Forastiero *et al*. 2013	*Galleria mellonella* to study the virulence of the *Candida tropicalis* and determine antifungal drug efficacy
Thomaz *et al*. 2013	*Galleria mellonella* to study *Paracoccidioides lutzii* and *Histoplasma capsulatum*
Maurer *et al.* 2015	*Galleria mellonella* to assess infection, virulence and amphotericin B resistance of *Aspergillus terreus*
Borman *et al.* 2016	Virulence of *Candida auris* and other *Candida* spp. In *Galleria mellonella*

1.3 The innate immune response of insects

The innate immune system is the first line of defence against invading pathogens in both insects and mammals. Although innate immune responses are non-specific, they are widely distributed throughout the body allowing them to play a crucial role in the maintenance of homeostasis and the prevention of disease and infection (Romo *et al.,* 2016). The insect and mammalian innate immune systems consist of humoral and cellular responses. The cellular response is mediated by hemocytes (e.g. granulocyte, plasmatocyte) in insects and myeloid cells (neutrophil, macrophage) in mammals and involves the targeting of pathogens through processes such as phagocytosis, superoxide production, encapsulation and enzyme release. Insect hemocytes display many structural and functional similarities to neutrophils of the mammalian immune response (Bergin *et al*., 2005; Renwick *et al*., 2007; Browne *et al.,* 2013).

There are many structural, functional and biochemical similarities between immune processes that exist in insects and in mammals. For example, both share homologous coagulation cascades, the insect prophenoloxidase system shares similarities with the mammalian complement cascade, however there are differences such as melanisation which exist in both insects and mammals but have completely different functional properties in both.

1.3.1 The insect prophenoloxidase activating (proPO) system

In insects melanin production depends upon the activation of the prophenoloxidase activating (proPO) system which is rapidly triggered upon pathogen invasion or injury to the cuticle. Upon activation of the proPO system, a pathogen can be killed directly through the production of toxic compounds. Alternatively, phagocytosis and encapsulation of the invading pathogen, or hemolymph coagulation may also be induced by this system (Cerenius *et al.,* 2008). Activation of the proPO cascade leads to the production of melanin which is catalysed by the redox enzyme phenoloxidase.

Melanisation in insects involves a number of cascades that must be carefully regulated due to the production of toxic and reactive intermediates which may be detrimental to the host. ProPO activation can be triggered by pathogen associated molecular patterns (PAMP) such as bacterial lipopolycaccharide and peptidoglycan or fungal β-1,3-glucan binding to their respective pattern recognition receptors. ProPO activation can also occur independently of PAMPs such as in the case of wounding and the presence of cells with altered apoptosis (Cerenius *et al.*, 2008; Chen *et al.*, 2014). Activation of the proPO system results in the induction of a serine protease cascade but PO is also activated by apolipophorin III and inhibited by lysozyme and anionic peptide-2 in *G. mellonella* (Park *et al.*, 2005). Consequently, the phenoloxidase activating system is initiated when prophenoloxidase-activating enzyme is converted from its inactive pro form (pro-ppA), to its active form (ppA). PpA can catalyse the proteolytic cleavage of prophenoloxidase (proP) to phenoloxidase (PO) (**Fig. 1.3**). Active PO is involved in hydroxylation of monophenols. Hydoxylation is followed by the oxidation of phenols to form quinines. Finally, quinine polymerisation is catalysed by phenoloxidase-monophenyl-L-dopa to form melanin (Zhao *et al*., 2007; Lu *et al*., 2014). Excluding the final step in which melanin is produced, the proPO system displays similarities to the complement system of vertebrates. In both the complement system of mammals and the proPO system of insects, there is production of cytotoxic and opsonic components as summarised in **Fig. 1.3** (Cerenius *et al.*, 2010). Furthermore, there is some similarity between the sequences of insect proPO and the mammalian complement proteins C3 and C4 (Shokal and Eleftherianos, 2017).

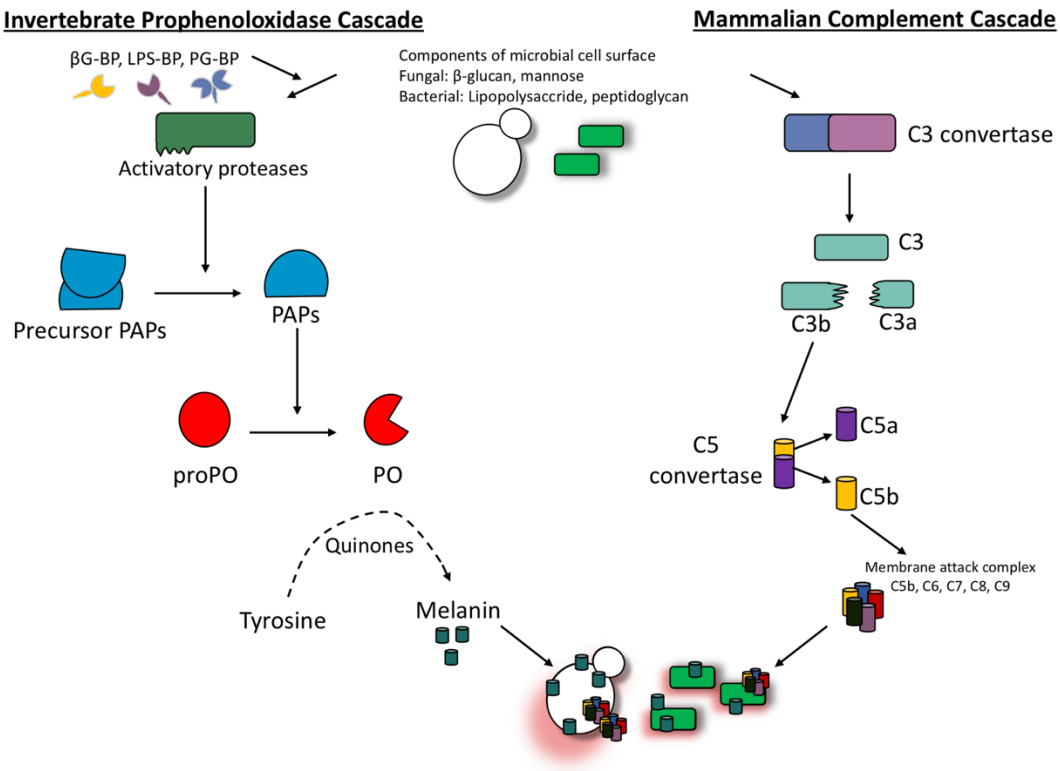

Fig. 1.3. Schematic diagram of the proPO-system for melanin production in insects. PAMPs such as β-1,3 glucan, LPS and peptidoglycan amongst others bind pattern recognition receptors such as β-1,3 glucan-binding protein (βG-bp), lipopolysaccharide-binding protein (LPD-BP) and peptidoglycan-binding protein (PG-BP), respectively. This results in the activation of the serine protease cascade which initates the conversion of prophenoloxidase-activating enzyme from its pro-form (pro-ppA) to its active form (ppA). PpA then catalyzes the conversion of prophenoloxidase (proPO) to phenoloxidase (PO). PO in combination with phenols and O_2 results in the formation of quinones which polymerise to form melanin. Similarily, the alternative complement pathway generates C3b by C3 convertase which with other proteins froms the C5 convertage. This enzyme cleaves C5 to C5a and C5b, the latter of which recuits and assembles C6, C7, C8 and multiple C9 molecules to form a pore forming membrane attack complex which is deposited on the microbial cell surface ultimately resulting in cell lysis.

1.3.2 Antimicrobial peptides in insects and mammals

Antimicrobial peptides (AMPs) are a group of widely expressed molecules that are produced as an early defence mechanism by multicellular organisms such as plants and animals. These peptides are produced in response to a broad spectrum of pathogens including bacteria, viruses, fungi and parasites but have also been found to target cancer cells (Wiesner and Vilcinskas, 2010; Zhang and Gallo, 2016). Most of the identified AMPs share some common characteristics including a size of 12-50 amino acids, a net positive charge and an amphipathic structure. Furthermore, AMPs can be classified based on their secondary structure. These secondary peptide structures include α-helical, β-sheets, a mixture of α-helical and β-sheet structures or extended loop structures (Lai & Gallo 2009; Van Der Weerden *et al.,* 2013). Depending on the particular AMP and its target pathogen, AMPs can target and kill pathogens using two distinct modes of action (**Fig. 1.4**). Upon binding the microbial membrane, AMPs may induce cell lysis through disruption of the membrane. Alternatively, the peptide may induce pore formation through electrostatic interactions, allowing the AMP to target intracellular components of the pathogen such as DNA and RNA. Through binding intracellular proteins, the synthesis of DNA, RNA, proteins and the cell wall integrity may be altered resulting in cell death (Gergely *et al*., 2011). Additionally, AMPs have a chemotactic role in mammals which links the innate and adaptive immune response through recruiting and/or activating immune cells including T- lymphocytes, dendritic cells and monocytes. For example, human LL-37 induces chemotaxis of human neutrophils (De Yang *et al.*, 2000).

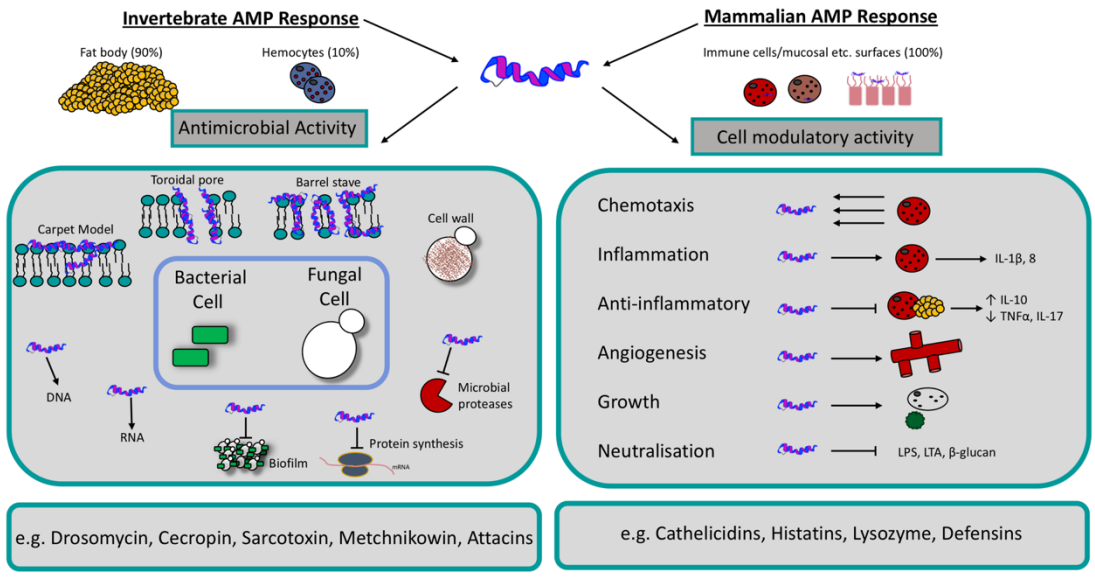

Fig. 1.4. Schematic diagram of the mechanism of action and function of antimicrobial peptides in insects and mammals. Both insect and mammalian AMPs display direct microbicidal activity by initiating cell lysis at the cell surface or interfering with intracellular targets. Some AMPs possess anti-biofilm activity (e.g. LL-37), inhibit protein synthesis (e.g. apidaecin) or inhibit microbial proteases (e.g. histatin-5). Some AMPs also possess pleotropic cell-modulatory activities such as angiogenesis, re-epithelisation, chemotaxis, anti-inflammatory and growth effects depending on cell type.

Lysozymes are cationic proteins that target and kill Gram-positive bacteria through hydrolysing the peptidoglycan β-(1,4) glycosidic bonds in the bacterial cell wall (Ragland and Criss, 2017). Many lysozymes in insects and mammals also display chitinase activity which contributes to their antimicrobial function. Lysozyme is found in the midgut and hemocytes of insects and the neutrophils, macrophages, monocytes, tears and saliva of mammals (Hultmark, 1996). In mammals, lysozyme is expressed constitutively while expression is usually upregulated upon pathogen entry in insects (Gandhe *et al.,* 2007). The *G. mellonella* transcriptome possesses four c-lysozyme and one i-lysozyme homologue, its protein is present in unstimulated larvae, is augmentable during infection, possesses antifungal activity, induces apoptosis in *C. albicans* cells, acts in synergy with apolipophorin III and possesses immunomodulatory activity (Mak *et al.,* 2010; Vogel *et al*., 2011; Zdybicka-Barabas *et al*., 2013; Zdybicka-Barabas *et al*., 2014; Sowa-Jasiłek *et al*., 2016). Upon comparative analysis, the c-lysozyme of *Musca domestica* was found to contain a 122-amino acid long polypeptide with a 38% sequence identity to human lysozyme (Ito *et al.*, 1995). Therefore, there are both structural and functional similarities found between insect and mammalian lysozymes.

Defensins are an abundant group of AMPs found in insects and mammals and are characterised by a group of cysteine-rich cationic peptides that contain several disulfide bridges. Defensins are also small, ranging from 28-44 amino acids in size and display antimicrobial activity against a range of pathogens including bacteria (particularly Gram-positive bacteria), fungi and viruses (Evans and Harmon, 1995; Gallo *et al.*, 2002). Defensins function by targeting microbial cytoplasmic membranes and induce the formation of voltage-dependent ion channels. The formation of these ion channels alters the cell's permeability therefore initiating the loss of cytoplasmic ions such as potassium. Ion loss ultimately results in microbial lysis (Ganz, 2003; Pazgier *et al.*, 2006).

Cecropins are amphipathic α-helical AMPs of 11 amino acids in length that have the ability to target and kill bacteria and filamentous fungi (Andrä *et al.,* 2000; Faruck *et al.,* 2016). In insects, members of this family can be isolated from the hemolymph of moths and flies following bacterial infection (Qu *et al*., 1982; Mak *et*

al., 2001; Kim *et al*., 2004; Mukherjee *et al*., 2011). These cecropins are 35-40 residues long, possess a C-terminal helical stretch and display broad spectrum activity against Gram-positive and Gram-negative bacteria, as well as some fungi (Bulet *et al.*, 1999). In Gram-negative bacteria, the hydrophobic C-terminal domain of cecropin interacts with the phospholipid membrane of the bacteria leading to membrane disruption and bacterial cell death (Lee and Lee, 2014). It displays antibacterial activity against multidrug resistant *Acinetobacter baumannii* and *Pseudomonas aeruginosa*, induces *C. albicans* apoptosis and has been shown to possess immunomodulatory effects on macrophages (Lee *et al.,* 2015; Yun & Lee 2016). There is evidence of cecropins in bovine adrenal glands and pig intestines, but they are more prominent in insects (Vilmos and Kurucz, 1998).

At present over 290 AMPs have been identified in insects therefore it may be more informative to discuss insect AMPs in *G. mellonella* as an example **(Table 1.2)** (Wang *et al.,* 2016).

Table 1.2. A comparison of the antimicrobial peptides present in insects and Humans

Human		*Galleria mellonella*		*Drosophila melanogaster*	
Name	Characteristic	Name	Characteristic	Name	Characteristic
Cathelicidin	α helical	**Cecropins**	α helical	Cecropins	α helical
Defensin	Cysteine rich	**Gallerimycin**	Cysteine rich	Drosomycin	Cysteine rich
Histatin-5	Histidine rich	**Galliomicin**	Cysteine rich	Metchnikowin	Proline rich
Dermcidin	Anionic peptide	**Moricin-like peptides**	α helical	Attacins	Glycine rich
		Gloverin-like peptides	Glycine rich	Drosocin	Proline rich

1.3.3 *Galleria mellonella* antimicrobial peptides and humoral mediators

G. mellonella produces at least 18 putative AMPs and their humoral immune response to a range of bacterial and fungal pathogens has been well documented in recent years with advances in transcriptomic and proteomic technologies (Brown *et al.*, 2009; Browne *et al.*, 2015). Gallerimycin is a cationic 57 amino acid inducible cysteine-rich defensin peptide with anti-filamentous fungi activity against *Metarhizium anisopliae* and is inducible during bacterial infection (Schuhmann *et al.*, 2003; Seitz *et al.*, 2003; Lee *et al.*, 2004b). Gallerimycin alone does not possess anti-bacterial activity but displays synergistic activity with cecropin-A which expands the antimicrobial spectrum of gallerimycin by causing extensive non-lytic depolarisation of *E. coli* membrane resulting in inhibition of growth (Moghaddam *et al*., 2016).

Bioactivated galliomicin is a 43 amino acid AMP which contains 6 cysteine residues and exhibits anti-filamentous activity (Lee *et al.*, 2004b), is induced by *C. albicans* (Bergin *et al.*, 2006), physical stress (Mowlds *et al.,* 2008) and extremes (4 ^{o}C & 37 ^{o}C) in temperature (Mowlds and Kavanagh, 2008), indicating it is induced indiscriminately in times where infection may be likely. Other invertebrate α-helical AMPs include the moricins, isolated exclusively from the *Lepidopteran* insects. Moricins are 42-residues long α-helical peptides with eight turns along the peptide. The N-terminal residues (5-22) are amphipathic and responsible for bacterial membrane permeability, while the C-terminal residues (23-36), are hydrophobic and needed for full antimicrobial activity (Yi *et al.*, 2014). Moricins are secreted as pro-peptides under the control of (NF-kB)/Rel and GATA transcription factors and are activated via proteolysis and increase the permeability of bacterial and fungal membranes. *G. mellonella* has seven moricin-like peptides in its transcritome and these are highly active against yeasts and filamentous fungi (Brown *et al.*, 2008). Gloverins are glycine rich, heat stable antibacterial polypeptides believed to bind LPS and possibly components of the fungal cell wall. It was previously demonstrated that *E. coli* induces gloverin expression in *Bombyx mori* (Yi *et al.*, 2013). With the recent release of the *G. mellonella* genome, there is much opportunity to study the role of individual humoral immune proteins/peptides during the infection process in larvae (Lange *et al.*, 2018).

Apolipophorin III is an 18 kDa protein which is part of the lipophorin complex and is responsible for lipid transport (Niere *et al.*, 1999; Niere *et al.*, 2001). It also augments the activity of lyzosyme (Zdybicka-Barabas and Cytryñska, 2013), potentiates the activity of AMPs (Park *et al.*, 2005), regulates phenoloxidase activity (Zdybicka-Barabas and Cytryńska, 2011; Zdybicka-Barabas *et al.*, 2014) is a PRR and opsonin of lipopolysaccharide, lipoteichoic acids and fungal β-glucan (Wojda, 2017). Insect metalloproteinase inhibitor (IMPI) is a 8.6 kDa glycosylated, heat-stable peptide which is induced following bacterial and fungal infection in *G. mellonella* and functions to inhibit the activity of secreted metalloproteinases which act as virulence factors to degrade host defences (Griesch *et al.,* 2000; Vilcinskas & Wedde 2002; Wedde *et al*., 2007; Vertyporokh & Wojda 2017).

Hemolin Immunoglobulin superfamily member hemolin is induced by *Candida* challenge and has been shown to act as a pattern recognition receptor and opsonin in insects (Shaik and Sehnal, 2009). Peptidoglycan recognition-like proteins bind to peptidoglycan via a conserved domain homologous to T4 bacteriophage lysozyme. Peptidoglycan recognition proteins from *Holotrichia diomphalia* (PGRP-SA) binds β-glucan and induced phenoloxidase activation (Seitz *et al.*, 2003). Immune related hdd1 and hdd11 was found up-regulated in *Hyphantria cunea* 2 h following inoculation of *E. coli* (Gandhe *et al.,* 2007). Its homologues e.g. nodular, plays an essential in nodule formation, aggregation of yeast via binding β-glucan, and RNAi knockdown results in increased fungal burden. To date no study has examined the role of hdd11 or hdd1 during infection of *G. mellonella* larvae.

1.3.4 Insect Cellular Immune Response

Hemocytes (immune cells) from *G. mellonella* can be differentiated into at least five types of cells **(Fig. 1.5)**. Prohemocytes are precursor cells which can differentiate into other cell types. Granulocytes (8 – 12 μm in diameter) are usually spherical with lobulated nuclei and plasmatocytes (8 – 10 μm) are small round/spindle shaped cells and their plasma membrane display philopodia and pseudopodia. These types of cells are the most abundant in hemolymph which have adherent properties and engage in phagocytosis, encapsulation, and nodulation processes. Spherulocytes are large (10 – 15 μm), polymorphic, oval type cells which transport cuticle components and are generally low in abundance in hemolymph and

oenocytoids (12 – 20 µm) contain acidophilic granules and their main function is to carry phenoloxidase precursors (Neuwirth, 1973; Price and Ratcliffe, 1974; Strand, 2008).

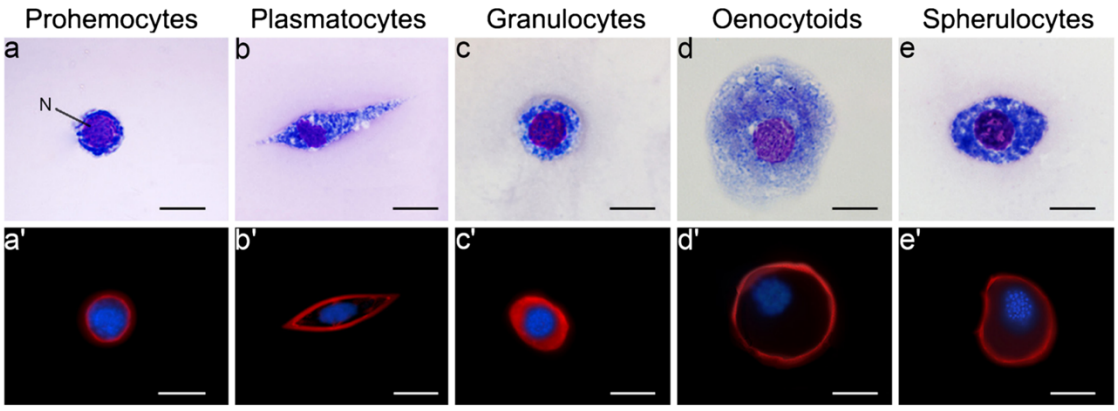

Fig. 1.5. *G. mellonella* larval hemocytes visualised by microscopy. Image adapted from (Arteaga Blanco *et al.*, 2017). Light (top) and fluorescence (bottom) microscope images of *G. mellonella* larvae hemocytes. Cells stained with DAPI (blue) and phalloidin fluorescein-isothiocynate for F-actin (red). Scale bar; 5 µm.

1.3.4.1 Phagocytosis

Insect hemocytes possess a functional NADPH oxidase complex capable of generating superoxide and incorporating proteins with homology to $p40^{phox}$, $p47^{phox}$, $p67^{phox}$ and $gp91^{phox}$ of mammalian neutrophils (Bergin *et al.*, 2005) **(Fig. 1.6)**. Mammalian neutrophils and insect hemocytes display similar responses to the *A. fumigatus* toxin fumagillin, nocodazole (inhibitor of tubulin formation) and cytochalasin B (weakens actin formation) (Fallon *et al.,* 2010; Banville *et al*., 2011; Fallon *et al*., 2011). Neutrophils and hemocytes engage in lectin-mediated phagocytosis and share homologous receptors on their cell surfaces for pathogen recognition, cellular communication and migration. Hemocyte Toll and Immune Deficiency pathways activate NF-κB-like mediated anti-microbial peptide (AMP) production, with adult *Drosophila* Toll/ Dorsal signalling choreographing the insect anti-fungal immune response (Medzhitov *et al.,* 1997).

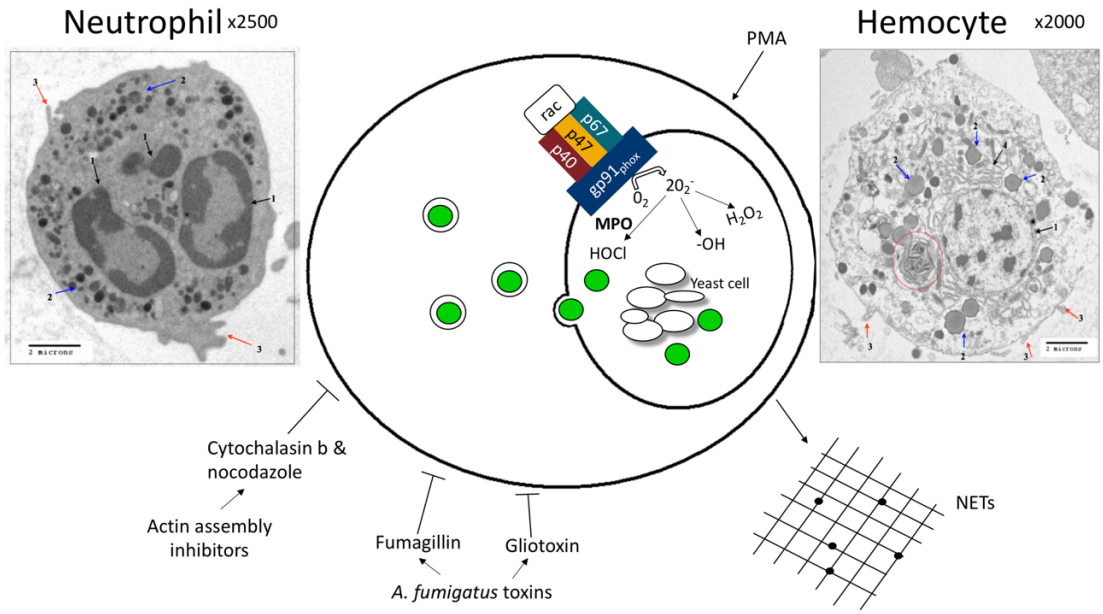

Fig. 1.6. Schematic representation of similarities which exist between the insect hemocyte and mammalian granulocyte (e.g. neutrophil). Both cells engage in phagocytosis of opsonised microbial cells, possess a functional NADPH oxidase complex capable of generating superoxide and incorporating proteins with homology to $p40^{phox}$, $p47^{phox}$, $p67^{phox}$ and $gp91^{phox}$, and display similar responses to the *A. fumigatus* toxin fumagillin, nocodazole (inhibitor of tubulin formation) and cytochalasin B (weakens actin formation).

1.3.4.2 Nodulation/ encapsulation

Nodulation and encapsulation responses are effective against a large number of invading microbial cells or parasites, which lead to formation of macro-cellular aggregates as a result of microbial recognition, hemocyte recruitment, adhesion and degranulation, phenoloxidase activation, melanisation and reactive oxygen species (ROS) generation which begin almost immediately after hemocoel penetration by a foreign object/invader (Chain and Anderson, 1983) **(Fig. 1.7)**. Nodulation is the binding of multiple hemocytes to aggregations of bacteria and fungi, whereas encapsulation refers to multiple hemocytes binding to a larger invader (e.g. protozoans, nematodes and parasitoids) that cannot be phagocytised by a single cell (Ratcliffe & Gagen 1977; Satyavathi *et al.,* 2014). Encapsulation in *G. mellonella* larvae begins with foreign particle recognition by granular type cells which lyse/degranulate which allows for attachment of plasmatocytes in multiple layers to result in the formation of a capsule (Schmit & Ratcliffe 1978; Pech 1996).

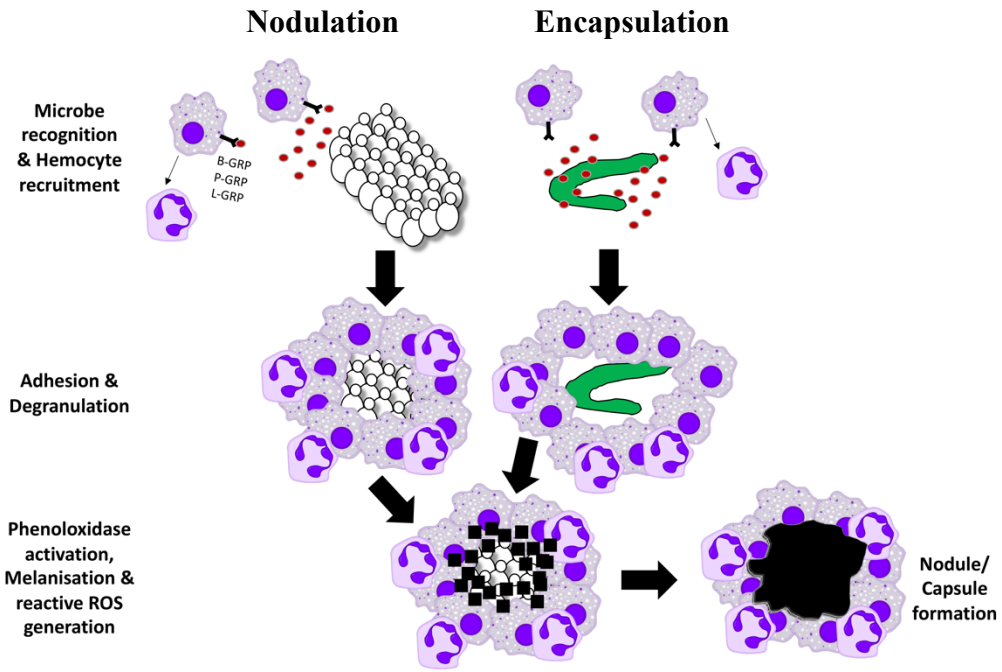

Fig. 1.7. Diagram of the process of nodulation and encapsulation in insects. Both nodulation and encapsulation begin by the recognition of foreign material or PAMPs which leads to hemocyte recruitment, adhesion and hemocyte lysis followed by phenoloxidase activation, melanotic responses and ROS production and ultimately nodule or capsule formation depending on the specific invader/material.

1.4 Immune priming or 'memory' responses in Insects

Adaptive immunity is characterised by memory of a microbe which the organism has previously encountered and overcome and the use of this memory to allow a quick and strong defence against a subsequent insult (Elkon and Rhiannon, 2012). The traditional view of adaptive immunity in vertebrates consists of somatic recombination in B- lymphocytes and T- lymphocytes resulting in long lived memory through the generation of specific subsets of memory B- lymphocytes which following re-infection proliferate thus overcoming the lag associated with the initial adaptive response activation (Chinen *et al.,* 2013).

The adaptive immune system also has the ability to remember previous pathogen attacks, resulting in a more effective immune response to subsequent infection (Cooper and Alder, 2006). The mammalian adaptive immune system first evolved in jawed fish over 500 million years ago after the divergence of vertebrates and invertebrates (Flajnik and Kasahara, 2010). While insects do not have an adaptive immune response mediated by B- lymphocytes and T- lymphocytes, and antibodies they display immunological priming as a result of prior exposure which enhances survival to a subsequent insult as a result of an elevated humoral and cellular response (Mowlds *et al*., 2010; Browne *et al*., 2013; Cooper & Eleftherianos 2017). The deficiency of an adaptive response allows the researcher to study in detail the interactions between a pathogen and the innate immune response without interference from the adaptive response (Cooper & Eleftherianos 2017).

Immune priming displays variation depending upon insect species in terms of duration of priming, specificity and energy costs. Changes in immune mediators as a result of priming have been linked with the first encounter with the microbial invader but is also observed in abiotically stressed insects (e.g. temperature (Wojda and Jakubowicz, 2007), physical (Mowlds *et al.,* 2008)). This has been observed in a number of insect species including *G. mellonella* (Bergin *et al.,* 2006), *D. melanogaster* (Irving *et al.,* 2001), *Anopheles gambiae* (Heard *et al.,* 2005), molluscs and sea urchins (Zhang and Loker, 2004). Interestingly, antimicrobial drugs (e.g. caspofungin (Kelly and Kavanagh, 2011) and silver based drugs (Rowan *et al.,* 2009)) can invoke an immune response and confer increased survival to pathogens in which these drugs have no intrinsic antimicrobial activity on (e.g. *S. aureus*).

1.5 Mammalian innate immune response – to fungal pathogens

Human fungal pathogens, although few in numbers (approx. 100 species) are responsible for more than a million life-threatening infections per year (Bongomin *et al.*, 2017). Fungal infections are difficult to prevent, diagnose and treat due to a lack of effective vaccines, diagnostics and antifungal agents. Advancements in healthcare procedures associated with the treatment of blood cancers, comes with side effects such as myelosuppression resulting in the loss of one's immune system, and this is associated with an increase in the incidence of systemic fungal diseases (Brown *et al.,* 2012). Furthermore, global warming will ultimately result in increased average temperatures and fungal colonisation of novel ecological niches (Garcia-Solache & Casadevall, 2010). The innate immune response is the first line of defence against fungal pathogens and consists of the cellular and humoral arms as well as anatomical barriers (e.g. skin, respiratory tract) (Margalit and Kavanagh, 2015).

Neutrophils are phagocytic granulocytic cells which employ a range of oxidative and non-oxidative mechanisms that effectively eliminate fungal conidia and hyphae. These mechanisms include phagocytosis, NADPH- oxidase-mediated generation of ROS, production of lactoferrin and degranulation of antimicrobial proteases (elastase and cathepsin-G), peptides (LL-37), and proteins (lactoferrin), and the formation of (Feldmesser 2006; Zarember *et al.,* 2007) neutrophil extracellular traps (NETs) (Tkalcevic *et al.,* 2000, Byrd *et al.,* 2013). The importance of neutrophils during fungal infections is exemplified in chronic granulomatous disease characterised by mutations in $p47_{phox}$ which affect the ability of NADPH oxidase to generate ROS, thus leaving patients extremely susceptible to invasive aspergillosis (IA) (Grimm *et al.,* 2011). Furthermore, decreased circulating neutrophil numbers is a risk factor for the development of invasive candidiasis (Byrd *et al.,* 2013).

1.5.1 Cathelicidin antimicrobial peptide (LL-37)

Cathelicidin antimicrobial peptides (CAMP) are expressed in all mammals as α-helical peptides ranging from 23 to 40 residues (Tomasinsig and Zanetti, 2005). The human CAMP gene is located on chromosome 3p21.31 as four exons and is expressed as hCAP-18, a 16 kDa preprotein consisting of a 30 residue signal sequence, a highly conserved cathelin domain and a C-termini antimicrobial domain (Larrick *et al.*, 1996). Cleavage of the C-terminal domain by neutrophil protinease-3, keratinocyte kallikrein, seminal plasma gastricsin and microbial proteases liberates the bioactive LL-37, a cationic (+6 at physiological pH) membrane active amphipathic peptide (Eissa *et al.*, 2011; Rapala-Kozik *et al.*, 2015; Sørensen *et al.*, 2017) **(Fig. 1.8)**.

The peptide is abundant in the specific granules of mature neutrophils contributing to both intracellular and extracellular killing and is present in other leukocytes, lymphocytes, wound fluid, a variety of epithelial and mucosal sites at concentrations of 2-5 μg ml^{-1} at homeostatic conditions to 50 μg ml^{-1} during inflammation/ infection (Robert *et al.*, 1998; Bowdish *et al.*, 2005). LL-37 displays a range of functions in relation to local infection directly by eliciting microbicidal activity targeting the outer layers of microbial cells and indirectly by its alarmin, angiogenic and re-epithelialisation properties (Koczulla *et al.*, 2003; Ramos *et al.*, 2011; Li *et al.*, 2014). Skin derived kallikrein 5/7 cleavage of LL-37 in sweat yields shorter peptide fragments KR-20, RK-31, and KS-30 that display augmented antimicrobial activity and decreased IL-8 expression when compared with LL-37. Initial low concentrations of LL-37 are primarily responsible for cell recruitment and accumulation, followed by peptide saturation in the infection microenvironment (Murakami *et al.*, 2004).

hCAP-18 is constitutively expressed by many cell types and modulated by inflammatory triggers and by-products of microbial growth. Vitamin D3 response elements are present in the hCAP-18 promoter and act synergistically with Dectin-1, NLR and TLR pathways in monocytes and keratinocytes for induction. An absence of saliva and plasma LL-37 is characteristic of morbus Kostmann syndrome, a severe congenital neutropenia associated with recurrent periodontal disease (Putsep *et al.,* 2002). LL-37 is increased in the bronchoalveolar lavage fluid of Cystic Fibrosis (CF)

patients and elevated LL-37 was correlated with local neutrophil density and augmented LL-37 levels in *P. aeruginosa* colonised individuals, indicating LL-37 plays a central role in the pulmonary inflammatory aspect of CF (Bergsson *et al.*, 2009). LL-37 also enhanced lung epithelial cell barrier function which directly prevents *P. aeruginosa* invasion (Byfield *et al.*, 2017). In the chronic inflammatory dermatological condition rosacea increased cutaneous TLR-2, LL-37 and KLK-5/7 levels with neutrophil infiltration and increased serum hydroxyvitamin D status are correlated to the symptoms of aberrant immune responses, vascular dysfunction with local neurogenic involvement (Yamasaki *et al.,* 2011).

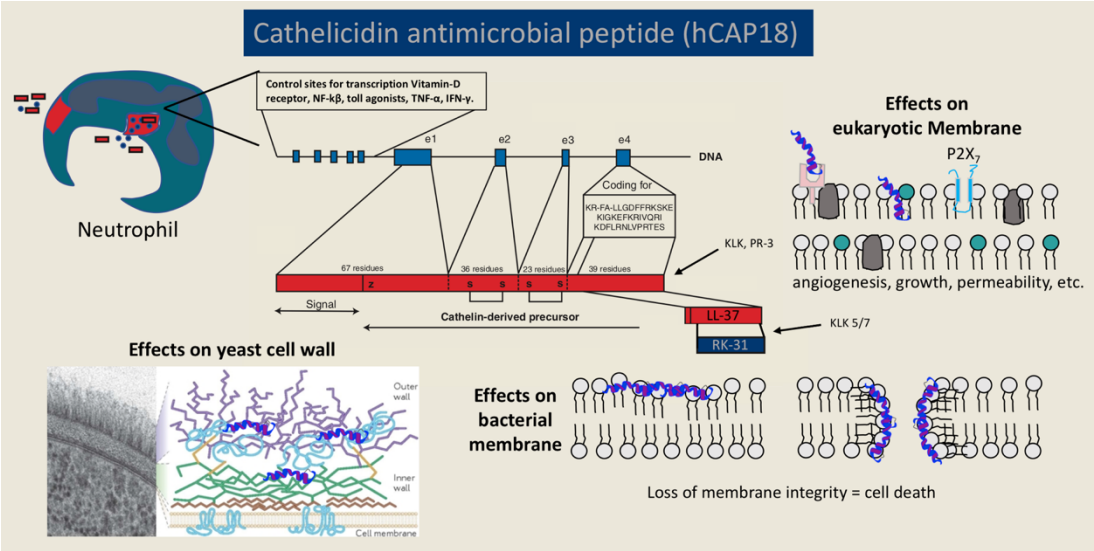

Fig. 1.8. Structure and function of h-CAP18 derived antimicrobial peptide LL-37. Production of LL-37 from the hCAP18 gene is regulated by the vitamin D receptor, Nf-kβ mediated gene transactivation, toll like receptor agonists, TNF-α and IFN-γ signalling. LL-37 has pleotropic effects on eukaryotic cell membranes, results in loss of membrane integrity and cell death in bacterial membranes and can interact with receptors and polymers of the yeast cell wall and membrane.

LL-37 displays pleotropic immunomodulatory properties with many groups reporting classical ligand receptor interactions while others report LL-37 mediated transactivation of transmembrane bound receptors (Xhindoli *et al.*, 2016). Nevertheless, LL-37 induces monocyte, neutrophil and T lymphocyte chemotaxis, modulates inflammatory cytokine production, impacts key non-immune biological processes such as apoptosis, angiogenesis, wound healing and maintenance of epithelial barrier integrity. LL-37 was found to activate eosinophils and bronchial epithelial cells promoting an inflammatory milieu which may have consequences for allergic bronchopulmonary aspergillosis, a disease characterised by eosinophil infiltration (Jiao *et al.*, 2017).

LL-37 is believed to exert its antimicrobial activity via membrane interactions according to the carpet model, where peptides coat the membrane inducing curvature until a critical concentration is reached resulting in breakdown in membrane integrity most likely by the formation of toroidal pores as a result of oligomeric structure formation (Thennarasu *et al.*, 2010). Mammalian membranes are protected from the pore forming effects of LL-37 due to the presence of cholesterol in their plasma membranes which increases bilayer thickness, allows tight packing of acyl chain and compressibility, while decreasing the translational diffusion rates of phospholipids. For example, *Helicobacter pylori* displays resistance to LL-37 dependent on scavenging and utilisation of host cholesterol (McGee *et al*., 2011). Interestingly, LL-37 can induce some degree of leakage in unsaturated and cholesterol containing membranes (Shahmiri *et al.*, 2016). LL-37 displays candidacidal activity by targeting the fungal membrane resulting in complete membrane disintegration and efflux of cellular ATP and protein (Veerman and Amerongen, 2005). LL-37 can bind immunomodulatory β-glucan and also alters cell wall architecture and induces wall reorganisation events via interactions with Xog1p (β-1,3-exoglucanase), resulting in exposure of β-glucan and loss of cellular integrity (Tsai *et al.*, 2014). LL-37 demonstrates microbicidal activity against clinically important microbes *Burkholderia cepacia* (79 μg ml^{-1}), *P. aeruginosa* (16 μg ml^{-1}), *Staphylococcus aureus* (9 μg ml^{-1}), *Haemophilus influenza* (< 10 μg ml^{-1}) and *Stenotrophomonas maltophilia* (1.9 μg ml^{-1}) (Turner *et al.*, 1998; Noore *et al.*, 2013; Tsai *et al.*, 2014).

1.5.2 N-chlorotaurine

Activated neutrophils, through a series of enzymatic reactions, produce superoxide and hydrogen peroxide from NADPH oxidase and superoxide dismutase, respectively, and hypochlorous acid (HOCl) is formed from hydrogen peroxide (H_2O_2) and chloride by myeloperoxidase (Klebanoff, 2005) **(Fig. 1.9)**. HOCl in the presence of taurine results in the formation of N-chlorotaurine (NCT; Cl-HN-CH_2-CH_2-SO_3H) (Zgliczyński *et al.*, 1971; Test *et al.*, 1984). NCT is the most abundant representation of this class of compounds and is a long lived oxidant (Grisham *et al.*, 1984). Chloramine has been detected in supernatants from stimulated granulocytes at concentrations ranging from 30 to 100 µM (Test *et al.*, 1984). NCT is the main constituent of these compounds reaching concentrations of between 10 to 50 µM (Weiss *et al.*, 1982; Grisham *et al.*, 1984).

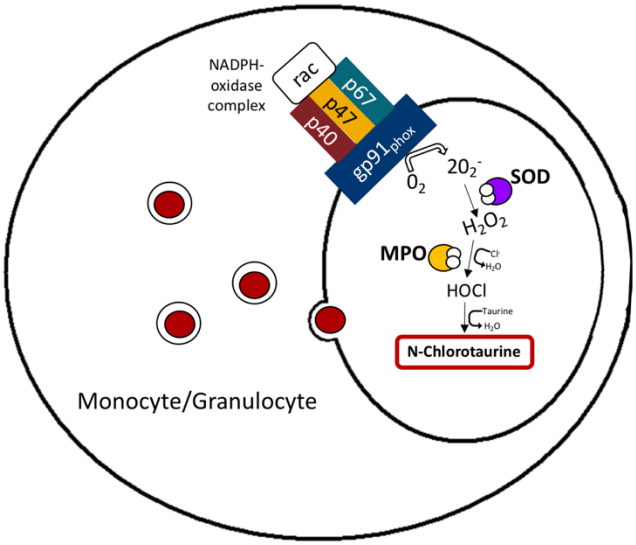

Fig. 1.9. Biosynthesis of N-chlorotaurine from human monocyte/granulocyte. Activation of the NADPH oxidase complex capable of reducing oxygen (O_2) to superoxide (O_2^-) which can be converted to hydrogen peroxide (H_2O_2) by superoxide dismutase. Myeloperoxidase utilises H_2O_2 in the presence of chloride, to generate hypochlorous acid (HOCl) which in the presence of taurine forms N-chlorotaurine.

NCT is bactericidal, fungicidal, virucidal and vermicidical at concentrations ranging from 100 µM to 55 mM and non-cytotoxic up to 0.5 mM (Nagl *et al.*, 2000; Gottardi & Nagl 2010). Bronchial exudates from CF patients display chloramine concentrations of 118 ± 25 µM (Witko-Sarsat *et al.*, 1995), indicating a high level of

NCT present extracellularly *in vivo* which is continually replenished by activated neutrophilic and eosinophilic granulocytes, monocytes and, in small amounts, probably macrophages (Epstein and Weiss, 1989; Marcinkiewicz and Kontny, 2014). Furthermore, the microbicidal activity of NCT is enhanced in CF sputum medium against a range of common CF pathogens (Gruber *et al.*, 2017). NCT is non-toxic and well tolerated. For example, inhalation and topical application to the skin, eye, middle ear, oral cavity and bladder with 1% (10 mg ml; 55 mM) appears to be safe (Gottardi and Nagl, 2010). NCT eradicated bacterial conjunctivitis within 5 days in a Phase IIa open pilot study (Nagl *et al*., 2000). Furthermore, NCT was superior to a combination of neomycin, polymyxin B and hydrocortisone at decreasing inflammation and infection of external otitis (Neher *et al.*, 2004). NCT (1%; 55 mM) results in a > 5 $\log_{10}$ fold reduction in the colony forming units (CFU) of MRSA, *Streptococcus pyogenes, E. coli and P. aeruginosa* after 1 h incubation (Gottardi and Nagl, 2010). NCT significantly deceased the viability of medically important fungi including *C. albicans* (up to 4.7 $\log_{10}$ fold reduction in CFU) and *A. fumigatus* (up to 2.6 $\log_{10}$ fold reduction in CFU) after 4 h exposure (Gottardi and Nagl, 2010). NCT decreased virulence factor production and activity from *C. albicans* (secreted aspartyl proteinases) and *A. fumigatus* (gliotoxin), respectively, before viability of these fungi was impaired probably as a result of oxidative stress interfering with protein synthesis (Nagl *et al.*, 2002; Reeves *et al.*, 2006a). Moreover, *Scedosporium spp*. lost virulence in the *G. mellonella* model after sublethal incubation time in NCT (Lackner *et al.*, 2015). A similar effect has been observed with *Staphylococci* and *Streptococci* (Nagl *et al.*, 1999; Gruber *et al.*, 2017). The activity of NCT is augmented in the presence of hydrogen peroxide (Mustedanagic *et al.,* 2017).

Neutrophils are the first line of defence against *A. fumigatus* and this is demonstrated by the high incidence of invasive aspergillosis in CGD patients who lack functional neutrophils (Williams *et al.*, 2017). *A. fumigatus* is engulfed into the phagosome and encounters NCT during the oxidative killing process. Furthermore, *A. fumigatus* comes into contact with NCT in CF bronchoalveolar lavage fluid. *A. fumigatus* has extensive mechanisms to circumvent and detoxify PMNs killing including oxidative mechanisms (Levitz and Diamond, 1985).

1.6 Humoral immune signalling pathways in mammals and insects

1.6.1 The Toll and Toll-like pathway

Toll-like receptors (TLRs) are a group of type I transmembrane receptors that play a role in innate humoral immunity in both insects and mammals. As Toll and TLRs are conserved throughout evolution, they can be found in mammals, invertebrates and plants. Homologies between these receptors can be observed between the cytoplasmic Toll/IL-1R (TIR) domain of both mammalian Toll-like receptors and the *Drosophilia* Toll receptor. In addition to a TIR cytoplasmic domain, Toll receptors can be characterised by an extracellular domain consisting of several leucine-rich repeats (LRRs) (Zhang and Ghosh, 2001). Despite the conservation of these domains in mammals and insects there are some structural and functional differences observed in the individual Toll receptors and genes. Structurally, mammalian Toll-like receptors contain one cysteine cluster at the C-terminal domain of their LRRs while insects contain multiple cysteine clusters on both the C-terminal and N-terminal domains of their LRRs (Imler, 2003). Functionally, the Toll genes are vital in *Drosophilia* embryogenesis where they are involved in dorsal-ventral development. Insect Toll-signalling is also essential in the production of AMPs in response to pathogen invasion, in particular antifungal peptides such as drosomycin, highlighting its role in innate humoral immunity (Lemaitre and Hoffmann, 2007). Conversely, mammalian Toll-like genes are involved in the production of cytokines and co-stimulatory molecules upon pathogen recognition. The production of these molecules results in the activation of T-lymphocytes, thereby linking the mammalian innate and adaptive immune responses (Akira and Hemmi, 2003).

Upon activation of Toll and Toll-like receptors a series of similar signalling pathways is initiated in insects and mammals which lead to activation of homologous transcription factors; NF-κB in mammals and Dorsal and Dif in insects (**Fig. 1.10**). These transcription factors are responsible for the resulting anti-microbial response in both animal groups (Silverman and Maniatis, 2001). Toll pathway activation in mammals occurs directly through binding of microbial associated material to their specific Toll receptor. In insects, activation occurs indirectly where microbial invasion induces the production of a cysteine-knot protein called Spätzle which can bind to Toll receptors (Govind, 2008). Upon *Drosophilia*

Toll activation by Spätzle the adaptor protein myeloid differentiation primary response protein (MyD88) is recruited to the TIR domain of the Toll receptor. A hetero-trimeric complex is formed with MyD88, the kinase Pelle and the protein Tube. As a result of Pelle activation, the inhibitor protein Cactus is phosphorylated and degraded. In its inactive form Cactus is bound to the transcription factors Dif or Dorsal. Therefore, upon Cactus degradation, Dorsal or Dif are free to translocate to the nucleus resulting in the transcription of anti-fungal AMPs (Valanne *et al.,* 2011). A very similar proccess occurs in mammalian Toll-like signalling (**Fig. 1.10**). In mammals, upon binding of microbial derived material such as peptidoglycan or lipopolysaccharide to Toll-like receptor MyD88, which is homologous to *Drosophila* MyD88, is recruited to the TIR domain. This initiates the recruitment of IRAK kinases which are homologous to *Drosophila* Pelle and Tube. Kinase activation results in the phosphorylation and degradation of I-κβ, which is homologous to *Drosophila* Cactus, thereby initiating the translocation of the now unbound NF-κB (homologous to *Drosophila* Dif and Dorsal) to the nucleus for transcription of co-stimulatory molecules, cytokines and chemokines (Ganesan *et al.*, 2011).

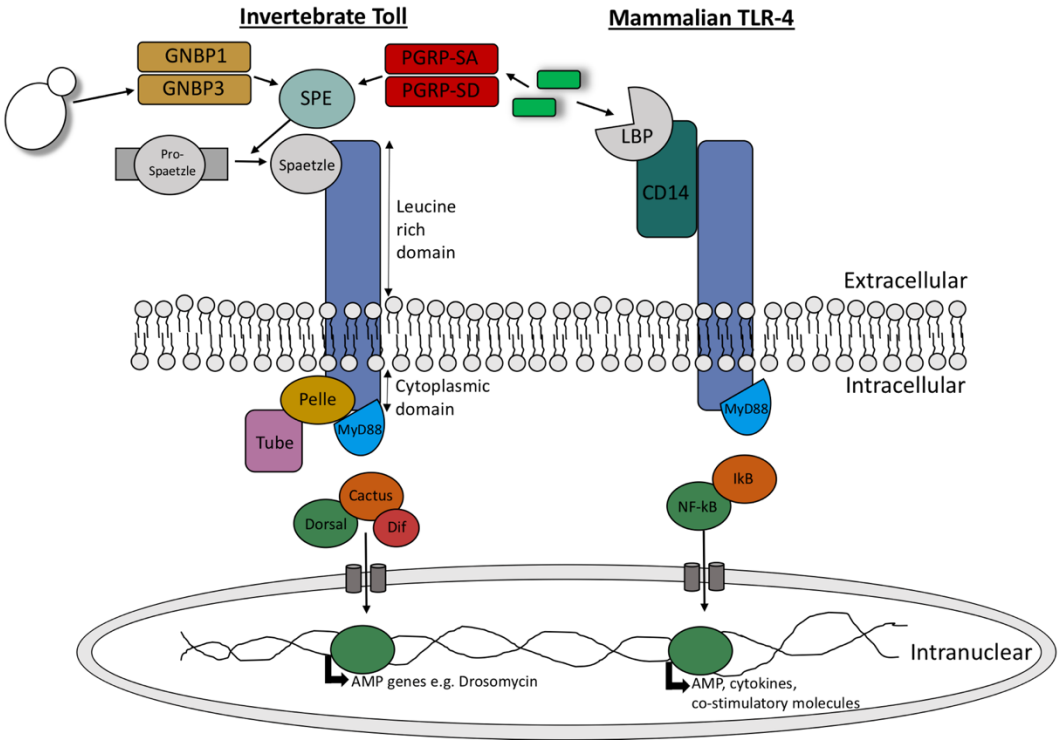

Fig. 1.10. Diagrammatic representation of the similarities between invertebrate Toll signalling and vertebrate toll-like signalling. Upon activation of invertebrate toll receptor and the homologous toll-like receptor in vertebrates, a cascade is induced where the homologous transciption facotors Nf-κB and Dif are activated in vertebrates and invertebrates, respectively. Upon translocation of these transcription factors, AMPs are produced in invertebrates while co-stimulatory molecules and pro-inflammatory cytokines such as IL-1β, IL-6 and IL-8 are produced in vertebrates.

1.6.2 The IMD and TNF-α signalling pathways

In addition to Toll signalling, *Drosophilia* can induce the IMD signalling pathway to produce AMPs. The IMD pathway recognises components of the bacterial cell wall such as peptidoglycan, resulting in the activation of a cascade that ultimately produces AMPs. The IMD pathway displays some similiarities to the mammalian tumour necrosis factor-α (TNF-α) pathway as well as the Toll-like pathway. Both the TNF-α and IMD pathways ultimately result in the production of the homologous transcription factors NF-κB and Relish, respectively (**Fig. 1.11)**. In insects, the IMD pathway is initiated by binding of peptidoglycan to peptidoglycan-recognition proteins (PGRPs) while in mammals, the TNF-α pathway is initiated through the binding of TNF-α to tumor necrosis factor receptor 1 (TNFR1), (Liu, 2005; Kleino and Silverman, 2014). Peptidoglycan recognition in *Drosophila* results in the recruitment of IMD, a death domain protein, the adaptor protein dFADD, and DREDD to form a complex. The activation of this complex promotes the clevage of IMD from the complex and activation of the *Drosophila* TAB2/TAK1 complex. As a result, the *Drosophila* IKK complex is activated and phosphorylates Relish. Rel-68, the N-terminal domain of Relish, can then translocate into the nucleus and initiate the production of anti-bacterial AMPs such as diptericin (Ertürk-Hasdemir *et al.*, 2009). Conversely, TNFR1 activation in mammals initiates the recruitment of RIPP, FADD and caspase 8 which are homologous to *Drosophila* IMD, dFADD and DREDD, respectively. The formation of the RIPP/FADD/caspase 8 complex activates TAK1 (homologous to *Drosophila* TAK1). TAK1 activates the IKK complex (homologous to *Drosophila* IKK complex) which phosphoylates and degrades the inhibitor protein IκB. Upon IκB degradation, NF-κB is released for translocation to the nucleus (Myllymäki and Rämet, 2014). In mammals, TNF pathways are involved in the production of pro-inflammatory cytokines as well as cell survival and apoptosis pathways, therefore also linking the innate and adaptive immune responses (Ting and Bertrand, 2016).

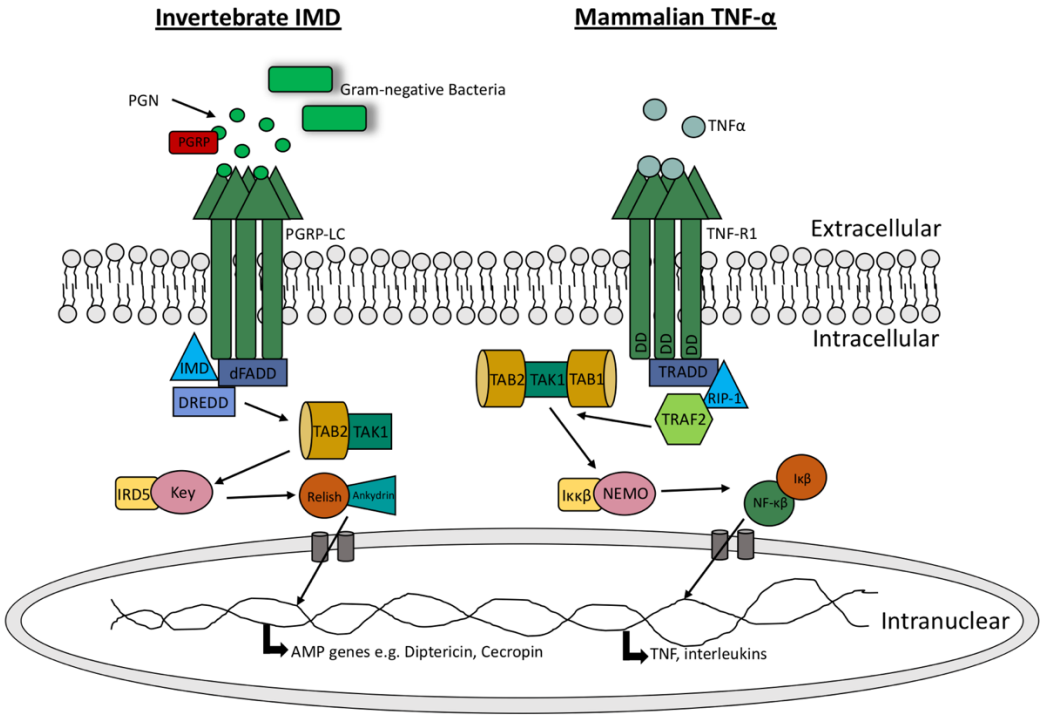

Fig. 1.11. Comparison of insect IMD pathway and mammalian TNF-α pathway. The IMD pathway is activated by binding of peptidoglycan (PGN) to peptidoglycan-recognition proteins (PGRPs) which results in recruitment and formation of a IMD, dFADD and DREDD complex and results in IMD cleavage and subseqeunt activation of TAB2/TAK1. This results in Relish phosphorylation and ultimately the production of AMPs (e.g cecropin). Alternatively in mammals, TNF-α is bound by the tumor necrosis factor receptor 1 (TNF-R1) which results in recuirment of RIPP, FADD and caspase 8. This complex activates TAK1 which activates the IKK complex resulting in phosphoylation and degradation of the inhibitor protein IκB. NF-κB is released for translocation to the nucleus resulting in pro-inflammatory cytokine production.

1.6.3 The blood/hemolymph clotting system in insects and mammals

1.6.3.1 The role of clotting systems

Clotting is an essential component of the innate immune system and promotes hemostasis by inducing the formation of an insoluble matrix/clot by the insect hemolymph or mammalian blood. The formation of a clot also aids in the sealing of wounds and prevention of pathogen entry and infection (Dushay, 2009). Since insects have an open circulatory system, clotting plays a vital role in the insect immune system. The insect clotting system is extremely efficient in order to prevent loss of hemolymph and the spread of infection, and for hemocoel compartmentalisation. Additionally, clotting helps to limit potential tissue damage caused by other immune responses by localising activity to wounding/pathogen entry sites. In contrast, mammals have a closed circulatory system and an adaptive immune response which lessens their reliance on such an efficient clotting system, especially since thrombosis (clot formation) is costly (Haine *et al.,* 2007).

1.6.3.2 Similarities between insect and mammalian clotting factors

Similarities between insect and mammalian clotting cascades can be observed in the family of transglutaminases which are involved in the hardening of a clot. Insect transglutaminases are homologous to human clotting factor XIIIa; one of eight transglutaminases found in humans. Factor XIIIa is involved in the final hardening of the clot in humans while insect transglutaminase is believed to contribute to the clotting cascade at a much earlier stage (Wang *et al.,* 2010; Theopold *et al.,* 2014). Additionally, homologies have been observed between domains of the Drosophila clot fibers constituent hemolectin and domains of human clotting factors V and XIII. Similarities in protein sequence have also been observed between insect hemolectin and human von Willebrand factor (vWF), a glycoprotein involved in hemostasis (Goto *et al.,* 2001; Loof *et al.,* 2011).

Despite the conservation of structure and functions of some clotting factors, greater variation in clotting cascades and clotting factors has been observed between insects and mammals. *Drosophlia* clotting cascades involve a number of clotting factors in three clotting steps to form a hardened clot. Firstly, a primary clot is formed through hemocyte degranulation where an aggregate is formed consisting of hemocytes, cell debris and extracellular matrix (Rowley and Ratcliffe, 1976;

Cerenius and Söderhäll, 2011). Secondly, the prophenoloxidase system (section 1.3.1) and a range of transglutaminases are activated which contribute to the crosslinking and hardening of the clot (Eleftherianos and Revenis, 2011). Finally, plasmatocytes are recruited to seal the clot (Li *et al.*, 2002a). In *Drosophila*, a number of clotting factors have been identified. Hemolectin is the most abundant protein found in the insect clot but many other factors contribute to the formation of a stable clot (Scherfer *et al.*, 2004). Activated transglutaminase (as a result of wounding or infection) interacts with its substrates Fondue and Eig71Ee, causing their subsequent covalent cross linkage and the formation of a hardened clot (**Fig. 1.12**) (Lindgren *et al.*, 2008). Lipophorin, which is analogous to mammalian lipid carrrier, is also involved in the polymerisation of the insect clot. Additionally, the activation of phenoloxidase by the proPO system works alongside transglutaminase through its involvement in the final crosslinking of the clot in addition to having a primary function in the direct killing of pathogens through melanisation (Scherfer *et al.*, 2004).

Mammalian clotting systems are better understood and more clotting factors have been identified. Firstly, primary hemostasis in humans occurs where a platelet plug is formed at the site of bleeding. Secondly, two different pathways can be activated both of which lead to fibrinogen being converted to fibrin; the extrinsic tissue factor (TF) system or the intrinsic contact system. The contact system involves activation of factor XII by collagen exposure in the bleeding vessel. Subsequently, the activation of the factors XI, IX, VIII and X takes place, respectively. Factor X (in the presence of lipids, platelets, calcium and factor V) initates the conversion of prothrombin to thrombin which then converts fibrinogen to fibrin. The production of fibrin finally stabilises the fibrin network/clot (Palta *et al.,* 2014; Smith *et al.,* 2015). TF is constitutively expressed in smooth muscle cells, pericytes and fibroblasts. Upon vessel injury platelets bind to vWF. This event initiates the binding of TF to factor VIIa resulting in platelet activation via PAR1 and PAR4 receptors. Platelet activation ultimately leads to the conversion of prothrombin to thrombin and finally fibrinogen to fibrin, as in the contact system (**Fig. 1.12**) (Mackman *et al.,* 2007; Tanaka *et al.,* 2009).

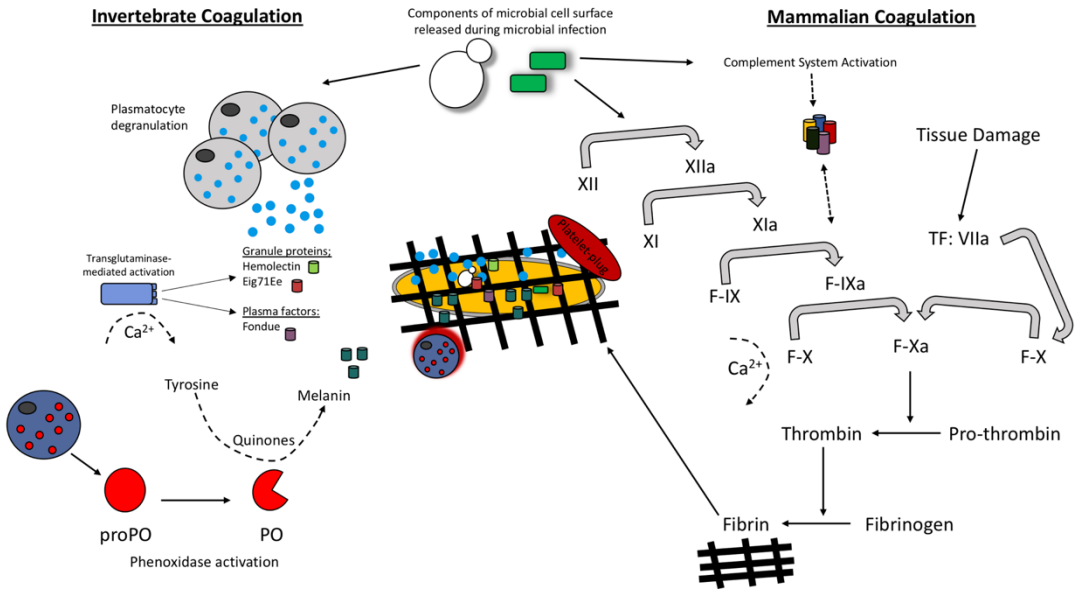

Fig. 1.12. Schematic comparison of the hemolymph/blood clotting system in insects versus mammals. Hemolymph clotting in insects involves co-ordination between plasmatocytes, transgluatimase mediated activation of hemolectin, eig71Ee and fondue as well as phenoxidase activation. During the mammalian blood clotting a series of enzymatic reactions result in the formation of thrombin and subsequently the conversion of fibrinogen to fibrin. Activations of the complement cascade also feeds into mammalian coagulation in the same way as phenoloxidase activation in insects. Similarities can be seen in both systems in that TG is homologous to factor XIIIa. Both factors contribute to the formation of a hemolymph/fibrin network.

1.6.4 Melanisation in insects and mammals

Melanins are a group of pigmented biopolymers dervived from phenolic compounds such as tyrosine. Melanins are believed to have evolved over 500 million years ago and can be found in both insects and mammals despite having a different primary role in both groups. In mammals, the production of melanin pigments is an important component in the colouration of hair, eyes and skin but also contributes to protection from solar radiation (Brenner and Hearing, 2008). In insects, melanin production plays a vital role in the innate immune system, colouration of the exoskeleton, sclerotisation and healing of wounds.

Melanisation in insects involves a number of cascades that must be carefully regulated due to the production of toxic and reactive intermediates which may be detrimental to the host. ProPO activation can be triggered by pathogen associated molecular patterns (PAMP) such as bacterial lipopolycaccharide and peptidoglycan or fungal β-1,3 glucan binding to their respective pathogen recognition receptors. ProPO activation can also occur independently of PAMPs such as in the case of wounding and the presence of cells with altered apoptosis (Cerenius *et al.*, 2008; Chen *et al.*, 2014). Activation of the proPO system results in the induction of a serine protease cascade but PO is activated by apolipophorin III and inhibited by lysozyme and anionic peptide-2 in *G. mellonella* (Park *et al.*, 2005). Consequently, the phenoloxidase activating system is initiated when prophenoloxidase-activating enzyme is converted from its inactive pro form (pro-ppA), to its active form (ppA). PpA can catalyse the proteolytic cleavage of prophenoloxidase (proP) to phenoloxidase (PO). Active PO is involved in hydroxylation of monophenols. Hydoxylation is followed by the oxidation of phenols to form quinines. Finally, quinine polymerisation is catalysed by phenoloxidase-monophenyl-L-dopa to form melanin (Zhao *et al.*, 2007; Lu *et al.*, 2014). Excluding the final step in which melanin is produced, the proPO system displays similarities to the complement system of vertebrates. In both the complement system of mammals and the proPO system of insects, there is production of cytotoxic and opsonic components (Cerenius *et al.*, 2010). Furthermore, there is some similarity between the sequences of insect proPO and the mammalian complement proteins C3 and C4 (Shokal and Eleftherianos, 2017).

Melanisation in mammals plays quite a different role. Melanins (pheomelanin, eumelanin and neuromelanin) are produced by mammalian melanocytes in specific tissues including the brain, skin, hair and eyes. Melaninisation plays a particularly important role in the skin where melanins protect the skin from UV by absorbing UVB rays and facilitates the production of Vitamin D3. In insects injury or PAMP recognition initiates melanisation, while in mammals melanisation is initiated by either the hydroxylation of L-phenylalanine to L-tyrosine or direct hydroxylation of L-tyrosine to L-dihydroxyphenylalanine (L-DOPA), the precursor of both eumelanin and pheomelanin. After a number of oxidoreductions, the reaction intermediates dihydroxyindole and DHI carboxylic acid are produced before being polymerised to form eumelanin (Solano, 2014). Overall, insect melanisation displays more similarities to the mammalian complement system than to mammalian melanisation due to insect melanisation and complement playing an important role in microbial mediated innate immune responses, while mammalian melanisation primarily plays a role in pigmentation and UV protection.

Table 1.3. A comparison of humoral receptors, anti-microbial peptides, cascades and enzymes in mammalian and insect humoral immune responses.

Humoral immune Compoenents	Insect	Mammalian
Receptors	Toll, IMD, β-1,3 glucan, IL-1R, Calreticulin, Hemolin, Lectins, Hemocytin	TLRs, TNFR1, β-1,3 glucan, IL-1R, Calreticulin, C-type lectins, Macrophage mannose receptor
Transcription factors	NF-κβ, I-κβ	NF-κβ, I-κβ
Coagulation cascade	Transglutaminase, Hemolectin	Factor XIIIa, vWF
Immune cascades	Prophenoloxidase cascade	Complement cascade, Melanisation of skin
Metalloproteinase inhibitors	IMPI	Collagenase, Gelatinase
Antimicrobial Peptides	Defensins, cecropins, moricins, gloverins, attacins	Defensins, LL-37, Dermcidin
Antimicrobial Proteins	Lysozyme, Sarcotoxin	Lysozyme, Histatin-5

1.7 Utilisation of *G. mellonella* larvae for measuring relative toxicity *in vivo*

Insects may be used to assess the relative toxicity of a variety of agents, including antifungal agents, and the results show a strong correlation to those obtained using mammals (Maguire *et al.*, 2016). In one case *G. mellonella* larvae were administered, by intra-hemocoel injection or by force feeding, a variety of food additives and the LD_{50} values were determined (Maguire *et al.*, 2016). The values obtained showed a strong correlation to the LD_{50} values determined in rats. Administration of a wide range of compounds to larvae by intra-hemocoel injection allowed differentiation of compounds based on relative toxicity and this correlated well with the toxicity as assessed in cell culture systems and in mammals (Allegra *et al.*, 2018). A strong correlation between the LD_{50} values of a range of chemicals (e.g. 4-methylumbelliferone, umbelliferone, and 7-ethoxycoumarine) in *B. mori* and in mammals was also established and similar metabolic pathways to detoxify the chemicals in both groups of animals were demonstrated (Hamamoto *et al.*, 2009). In an assessment of the relative toxicity of 1, 10 phenanthroline, 1, 10 phenanthroline-5,6-dione and related copper and silver complexes a strong correlation between the response of *G. mellonella* larvae and Swiss mice was established (McCann *et al.*, 2012b) (**Fig. 1.13**).

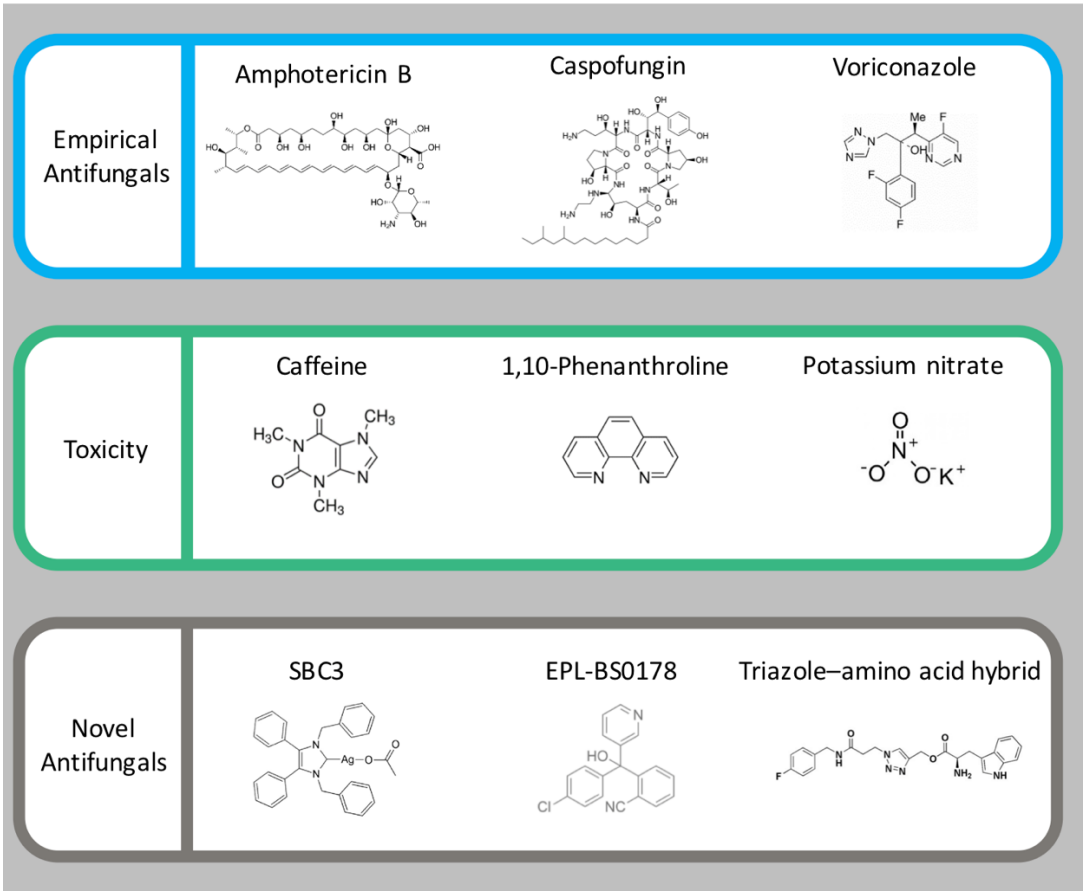

Fig. 1.13. Examples of uses of *G. mellonella* larvae to assess the *in vivo* toxicity and efficacy of a range of antifungals and chemical agents. Structures of empirical antifungals amphotericin B (Kloezen *et al.,* 2018), caspofungin (Kelly & Kavanagh, 2011), voriconazole (Forastiero *et al.,* 2015). Chemicals used for toxicity studies; caffeine (Maguire *et al.,* 2017), 1,10-Phenanthroline (McCann *et al.,* 2012) and potassium nitrate (Maguire *et al.,* 2017). Novel antifungals; SBC3 (1,3-dibenzyl-4,5-diphenyl-imidazol-2-ylidene silver(I) acetate) (Brown *et al.,* 2014) active against *C. albicans*, EPL-BS0178 (Lim *et al*., 2014) active against *M. mycetomatis* and novel triazole–amino acid hybrid (1-(3-(4-fluorobenzylamino)-3-oxopropyl)-1H-1,2,3-triazol-4-yl)methyl 2-amino-3-(1Hindol-3-yl)propanoate) (Aneja *et al.,* 2016).

As well as being suitable to assess the relative *in vivo* toxicity of compounds, larvae may also be used to study the mode of action of selected compounds and show equivalent results to those found in vertebrates. Administration of potassium nitrate **(Fig. 1.13)** to *G. mellonella* larvae produced a response comparable to that observed in mammals and this included an elevated hemocyte density but hemocytes showed reduced fungicidal activity (Maguire *et al.*, 2017a). Larvae administered potassium nitrate also showed alterations in proteins involved in mitochondrial function, metabolism and nitrate metabolism and these effects were also observed in mammals.

A series of novel copper phenanthroline-phenazine cationic complexes which display promising chemotherapeutic potential decrease *G. mellonella* survival dependent upon enhanced nuclease activity, this is evident at the proteomic level with enrichment of metabolic and detoxification pathways. These results indicate that larvae may be used to assess the tumoricidal activity of novel anti-neoplastic agents (Rochford *et al.*, 2018).

1.8 Use of *G. mellonella* larvae for assessing antifungal activity *in vivo*

1.8.1 Drug assessment against pathogenic yeast

One of the advantages of using *G. mellonella* larvae is that the *in vivo* activity of novel and conventional antifungal agents can be quickly established (**Table 1.4)** and this can inform subsequent synthesis of novel derivatives or help establish relative dosage prior to use in mammals. *G. mellonella* larvae can be rescued (i.e. increased survival and decreased symptoms e.g. melanisation) from a lethal inoculum of *C. albicans* (5×10^5 larva^{-1}) by an intra-hemocoel dose of amphotericin B (1 mg kg^{-1}; dose comparable to clinical dosing levels (maximum 1.5 mg/kg/day^{-1}) two h post infection **(Fig. 1.14)**.

Table 1.4. Examples of use of *G. mellonella* larvae with antifungal agents

	Assessment of antifungal activity
Rowan *et al.* 2009	Use of *Galleria mellonella* larvae to evaluate the *in vivo* antifungal activity of [Ag2(mal)(phen)3]
Kelly *et al.* 2011	Caspofungin primes the immune response of the larvae of *Galleria mellonella* and induces a non-specific antimicrobial response
Li *et al.* 2013	Using *Galleria mellonella-Candida albicans* infection model to evaluate antifungal agents
Fuchs *et al*. 2016	Micafungin elicits an immunomodulatory effect in *Galleria mellonella* and mice
Aneja *et al.* 2016	Effect of novel triazole-amino acid hybrids on growth and virulence of *Candida* species: *in vitro* and *in vivo* studies
Ames *et al*. 2017	*Galleria mellonella* as a host model to study *Candida glabrata* virulence and antifungal efficacy

Fig. 1.14. *C. albicans* infection of *G. mellonella* larvae. *G. mellonella* larvae infected with *Candida albicans* (5×10^5 larva^{-1}) 24 h post-infection at 30 ºC. (A) Control larvae administrated PBS (40 µl), (B) larvae administrated *C. albicans* 24 h post-infection, (C) larvae administrated *C. albicans* and amphotericin B (1 mg kg^{-1} 2 h post *C. albicans* infection) 24 h post-infection.

Interestingly a carbene silver(I) acetate complex demonstrated excellent *in vivo* anti-*Candida* activity but was shown not to trigger an immune response in larvae **(Fig. 1.13)**. It was postulated that the relatively small size of the complex was not detected by the larval immune response and thus failed to induce an immune response (Browne *et al.*, 2014). A group of novel triazole-amino acids hybrid compounds were assessed for their anti-*Candida* activity *in vitro,* and *in vivo* using *G. mellonella* larvae. The results showed the compounds did not provoke an immune response in larvae and that administration of compound to larvae resulted in increased survival and reduced yeast cell proliferation (Aneja *et al*., 2016).

Gu *et al*. (2018) demonstrated that the combination of tetracycline and fluconazole at concentrations equivalent to therapeutic doses in humans rescued larvae from a lethal inoculum of azole resistant *C. albicans* CA10 compared to fluconazole alone and this was due to a four-fold decrease in fungal burden and fewer infection sites throughout larvae (Gu *et al.*, 2018). Silva *et al.* (2018) examined the antifungal efficacy of a range of antifungals on *Candida haemulonii* complex (*C. haemulonii, C. duobushaemulonii and C. haemulonii var. vulnera*) and non-*albicans* species, with the former demonstrating resistance to first line antifungals (e.g. fluconazole, amphotericin B) in *G. mellonella* larvae (Silva *et al.*, 2018).

Candida tropicalis dose dependently killed *G. mellonella* larvae at both 30 ^{o}C and 37 ^{o}C but larval hemocytes phagocytosed *C. tropicalis* cells slower than those of *C. neoformans*. Amphotericin B, caspofungin (2, 4 mg kg^{-1}; comparable to clinical dosing levels), fluconazole and voriconazole all produced protective effects *in vivo* at clinically relevant doses but amphotericin B (4 mg kg^{-1}) and fluconazole (3, 6, and 12 mg kg^{-1}; comparable to clinical dosing levels) significantly decreased fungal burden and melanised nodule formation in larval tissue as evident from tissue sections (Mesa-Arango *et al.*, 2013).

The response of *G. mellonella* larvae to infection with *Candida glabrata* was studied and infection was shown to be temperature and dose dependent and the response of the larvae to infection included melanisation and alterations in the hemocyte density. No protection from infection was achieved by administering fluconazole to larvae post infection, although amphotericin B and caspofungin

administration increased larval survival (Ames *et al.*, 2017). *G. mellonella* larvae have also been utilised for assessing the *in vivo* activity of amphotericin B, flucytosine, and fluconazole following challenge with *C. neoformans* (Mylonakis *et al.*, 2005). Combination therapy consisting of pedalitin and amphotericin B act in synergy against *C. neoformans* infection to improve survival, fungal burden and histopathology in both *G. mellonella* larvae and in BALB/c mice (Sangalli-Leite *et al.*, 2016).

Larvae provide a quick and convenient means to assess the potential of novel antifungal therapies prior to murine testing. *G. mellonella* larvae and mice have been employed to assess the efficacy of antimicrobial peptides in combination with caspofungin for treating *C. albicans* infections. There was strong agreement between results since treatment of infected larvae and mice with caspofungin and DsS3 (1-16) resulted in enhanced survival of larvae and mice compared to untreated controls and those that received the agents individually (MacCallum *et al.*, 2013).

1.8.2 Drug assessment against filamentous fungi

G. mellonella larvae have been widely used to study azole resistance in *A. fumigatus* (Gomez-Lopez *et al.*, 2014). Alaczar-Fuoli *et al.* (2015) demonstrated voriconazole selected for *Aspergillus lentulus* in mixed infections with *A. fumigatus*, which together respond differentially to larval hemocytes and induce distinct histological features (e.g. melanisation). Larvae did not respond to a therapeutic dose of voriconazole in mixed *Aspergillus* infection (Alcazar-Fuoli *et al.*, 2015). Haemofungin is a novel synthetic drug-like molecule which causes fungal cell swelling and lysis by inhibiting ferrochelatase, the last enzyme in the haem biosynthetic pathway, and is active at low concentrations against pathogenic moulds and yeast. In larvae, haemofungin is non-toxic up to 22.7 mg kg^{-1}. Most interestingly, a concentration of 5.7 mg kg^{-1} haemofungin improved larval survival to *A. fumigatus* comparable to that of amphotericin (2 mg kg^{-1}) (Ben Yaakov *et al.*, 2016).

G. mellonella larvae have been used to assess the virulence of amphotericin B resistant and susceptible isolates of *Aspergillus terreus* and to assess the potential of amphotericin B for the control of infection. The results demonstrated that amphotericin B was active against the fungus but also stimulated the larval immune response (Maurer *et al.*, 2015). *G. mellonella* larvae have been utilised to assess the virulence potential of a range of mucormycetes (e.g. *Rhizopus* spp., *Rhizomucor* spp., *Mucor* spp.) and demonstrated the virulence potential was strain and infection dose specific. In addition, the ability of the fungus to tolerate oxidative stress was also a critical factor in its ability to cause disease (Maurer *et al.*, 2018). The *in vivo* antifungal potential of liposomal amphotericin B, posaconazole, isavuconazole and nystatin against the fungal pathogens was assessed in larvae. Good control of infection was achieved with nystatin and posaconazole, but not with liposomal amphotericin B and isavuconazole (Maurer *et al.*, 2018). *Madurella mycetomatis* infection results in the formation of large subcutaneous lesions in humans and antifungal therapy is difficult due to the formation of grains within infected tissue. *G. mellonella* larvae are susceptible to infection by *M. mycetomatis* and infected tissue also shows the presence of grains. Larvae have been used to identify potential antifungal therapies for use in humans and highlighted that amphotericin B and terbinafine prolonged larval survival while azoles proved ineffective (Kloezen *et al.*, 2017). A recent study screened 800 compounds and tested the ten most active compounds for anti-fungal efficacy in larvae against *M. mycetomatis*. Several compounds enhanced survival and/or reduced fungal burden. Fenarimol analogues, especially EPL-BS0178 appeared most potent possibly due to their polarity, permeability and tissue distribution allowing penetration of *M. mycetomatis* grains *in vivo* (Lim *et al.*, 2018).

White nose syndrome is a fungal disease of bats caused by *Pseudogymnoascus destructans* and this has been responsible for the deaths of millions of bats in North America in recent years. *G. mellonella* larvae were shown to be susceptible to disease by *P. destructans* and were used to demonstrate that trifluoperazine and amphotericin B could be used to prevent infection and thus highlighted potential treatment options for use in bats (Beekman *et al.*, 2018).

G. mellonella larvae have been adapted to study the virulence of *Fusarium* spp and to investigate anti-fungal therapy and have generated results similar to those obtained from murine studies. Larval killing was dependent upon temperature (more rapid at 30 ºC compared to 37 ºC), strain, inoculum and conidia morphology (Coleman *et al.*, 2011). *Mucor circinelloides* is an opportunistic fungal pathogen that commonly infects patients with an aberrant immune status and presents as nasal, facial or subcutaneous necrosis and disseminated disease (Rogers, 2008). Bastidas *et al.* (2012) found that the immunosuppressive agent rapamycin, possessed antifungal activity mediated by interactions with FKBP12 and a Tor homolog. *G. mellonella* larvae infected with a lethal dose of *M. circinelloides* R7B were treated with rapamycin (33 mg kg^{-1} body weight) and resulted in a 50% survival as compared to the 0% in controls after 5 days (Bastidas *et al.*, 2012).

Trichosporon species are opportunistic anamorphous basidiomycetes, which cause infections ranging from superficial to systemic in the immunocompromised host and are estimated to be in the top three most common non-*Candida* yeast infection that cause invasive disease in hematological cancer patients (Ribeiro *et al*., 2008; Colombo *et al.,* 2011). *Trichosporon asahii, T. asteroides and T. inkin* all infected *G. mellonella* larvae and immunosuppressed mice with species specific differences. However, significant differences were observed between *T. asteroids* species in mice. Both fluconazole and voriconazole improved survival in *G. mellonella* and mice amongst the three species examined. However, amphotericin B improved survival in mice but not in larvae (Mariné *et al.*, 2015).

G. mellonella larvae have also been employed to study infection by *Paracoccidioides brasiliensis* and *Paracoccidioides lutzii* the main causative agents of paracoccidioidomycosis, an endemic mycosis in South and Central America. Typically, murine studies can take up to 60 days for infection/therapy, with patient treatment lasting up to 18 months, however results obtained from larvae infected with *Paracoccidioides* were recorded within 7 days. Larvae were protected from *Paracoccidioides* infection following amphotericin B or itraconazole at therapeutic doses, which decreased fungal burden in larval tissue (de Lacorte Singulani *et al.*, 2016) (**Fig. 1.15)**.

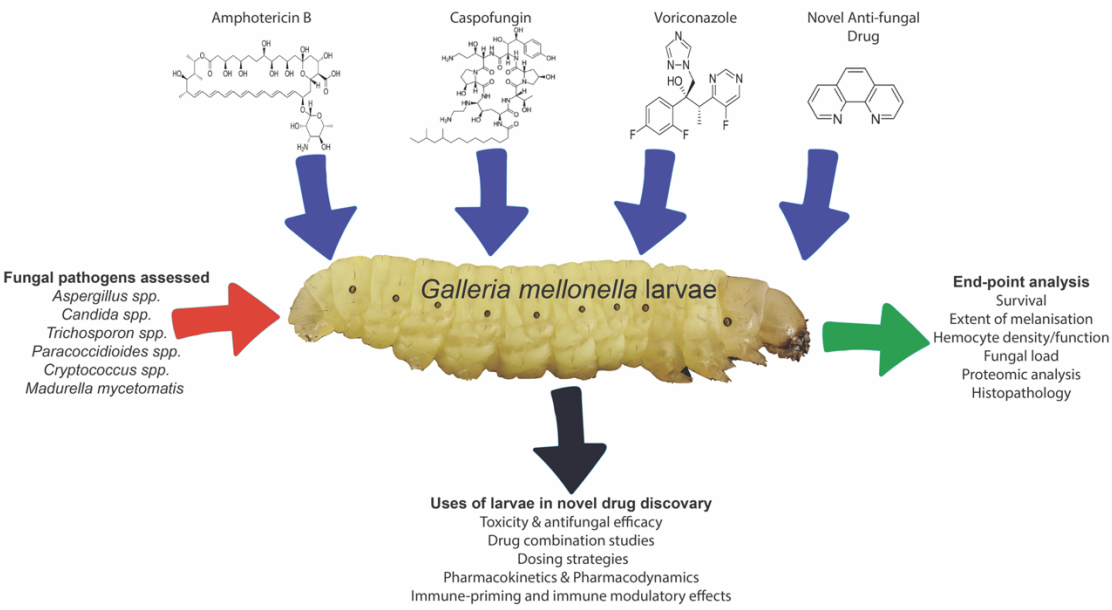

Fig. 1.15. *G. mellonella* larvae as a model to study the toxicity, efficacy, immune modulatory effects etc. of empirical and novel anti-fungal agents. A variety of fungal pathogens can be assessed using a range of end points which have been widely characterised in recent years.

1.9 Pathogens assessed using *G. mellonella* larvae

The advent of immunosuppressive therapy has created a new niche for invasive fungal pathogens. In the immunocompetent host, most fungal pathogens (e.g. *C. albicans*) possess low virulence *in vivo,* and for this reason and others, *G. mellonella* larvae are an excellent host to study the virulence of a range of fungi such as *A. fumigatus*, *Paracoccidioides lutzii*, *Histoplasma capsulatum*, and *C. neoformans* (Reeves *et al.*, 2004a; Thomaz *et al.*, 2013; Trevijano-Contador *et al.*, 2014; Alcazar-Fuoli *et al.*, 2015).

1.9.1 *Candida albicans;* a model fungal pathogen

C. albicans is the most common nosocomial fungal pathogen of humans and causes a broad spectrum of diseases depending on the immune status of the host with a mortality rate of 40% in certain patient groups (**Fig. 1.16**) (Brown *et al.*, 2012). *C. albicans* possesses an arsenal of virulence factors to establish a focal point of infection, adhere to and invade host cells, detoxify the cellular immune response and degrade components of the humoral immune response (Calderone and Fonzi, 2001). The *C. albicans* cell wall is a complex mesh of polysaccharides, proteins and sterols

which help to form a physical barrier against the immune response but also signals are relayed from the wall depending on the stimulus in order for the fungal cell to adequately mount an appropriate stress response (Ruiz-Herrera *et al.*, 2006).

In *G. mellonella* larvae stimuli such as physical stress, temperature extremes or exposure to a sub-lethal dose of *C. albicans* increase hemocyte density and the expression of AMP genes and this has been shown to protect larvae from a later potentially lethal challenge with *C. albicans.* Caspofungin and microfungin protect larvae from *Candida* infection but also possess immunomodulatory effects on larvae and in mice (Kelly and Kavanagh, 2011; Fuchs *et al.*, 2016).

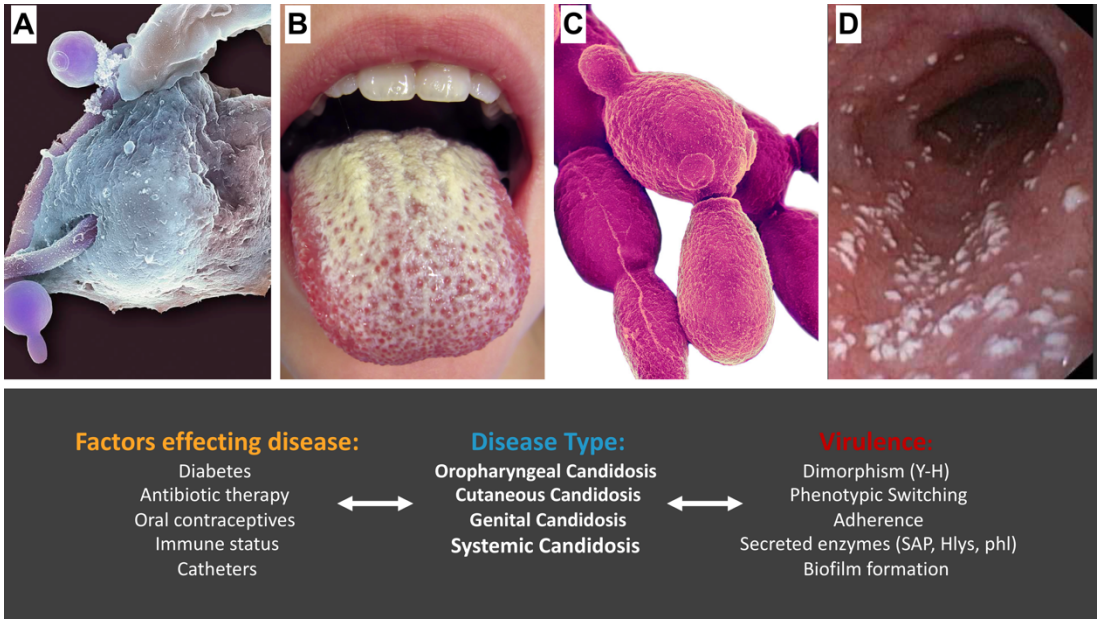

Fig. 1.16. Summary of *C. albicans* diseases, virulence and factors influencing disease development. Interactions between *C. albicans* hyphae and neutrophil (A), oral candidosis (B), yeast forms of *C. albicans* (C), oropharyngeal candidosis (D).

1.9.2 *Staphylococcus aureus*

Staphylococcus aureus is a facultative anaerobic, Gram- positive bacterium which colonises approximately 30% of the world's population on a range of body sites. *Staphylococcus* is the most frequent cause of biofilm – medical device related infections (Otto, 2008) most likely due to its status as a skin commensal. The most frequent sites of *S. aureus* colonisation are the nose, skin and GI tract (Brown *et al.*, 2014). *S. aureus* colonisation is mostly non-symptomatic, however in the correct

situation it is capable of causing a wide variety of diseases from furuncles and boils to serious infections such as pneumonia, toxic shock syndrome and endocarditis (Tong *et al.*, 2015). The virulence of *S. aureus* is multifaceted and due to an arsenal of effectors which enable interactions with the host, immune cell evasion and the induction of tissue damage (Lowy, 1998).

S. aureus 33 kDa protein α-toxin can induce pro-inflammatory conditions and pore formation in mammalian cells resulting in necrosis. It has been suggested that α-toxin creates an enhanced infection microenvironment for disease progression (Bhakdi and Tranum-Jensen, 1991). A range of superantigens are able to induce inflammation which can result in toxic shock syndrome and sepsis by non-specific activation of T-cell proliferation through interactions with MHC class II molecules on antigen presentation cells (Spaulding *et al.*, 2013). *S. aureus* can inhibit the mammalian complement pathway via Chemotaxis Inhibitory Protein of Staphylococci binding of the C5a receptor and Staphylococcal Complement Inhibitor blocking of C3 convertase activity (Jongerius *et al.*, 2007; Burman *et al.*, 2008). Coagulase and von Willebrand factor binding protein activate fibrin clot formation, facilitating the formation of staphylococcal aggregates in the blood and this is mediated by clumping factors A and B (Moreillon *et al.*, 1995; Hartleib *et al.*, 2000). Fibronectin-binding proteins A and B (FnBPA/B) bind to integrin α5β1, enabling the tethering of *S. aureus* to endothelial cells and phagocytic cells during infection (Shinji *et al.*, 2011).

1.9.3 The pulmonary pathogen *Aspergillus fumigatus*

A. fumigatus is a significant pulmonary pathogen in individuals who are immunocompromised (e.g. myelosuppression) and in those who display defects in immune equilibrium, commonly observed in the CF lung (**Fig. 1.17**) and presents itself in the form of allergic bronchopulmonary aspergillosis (ABPA) (Margalit and Kavanagh, 2015). In the latter, *A. fumigatus* airborne conidia penetrate the lower airways, germinate and grow within the thick tenacious CF mucus. CF patients colonised by *A. fumigatus* can become sensitised to *A. fumigatus* secreted allergens and eventually develop a type 2 hypersensitivity reaction to *A. fumigatus* allergens, toxins and proteases that are readily secreted into the mucus which can directly cause cell damage and peeling at the bronco – epithelium interface (Stevens *et al.*, 2003).

In the case of invasive aspergillosis (**Fig. 1.18**) patients primary immunodeficiencies are associated with hematological malignancies (e.g. leukaemia), chronic obstructive pulmonary disease, solid organ and hematopoietic stem cell transplant recipients, extended corticosteroid use and HIV-positive individuals (Dagenais & Keller 2009; Gangneux *et al.,* 2010). Prolonged neutropenia or altered neutrophil function (CGD) can result in angioinvasion (in the former) and ultimately disseminated fungal growth (both) (Segal & Romani 2009; Ben-Ami *et al.,* 2010).

G. mellonella larvae have been used to assess the virulence of *A. fumigatus* mutants and correlated the data with results obtained using mice (Reeves *et al.*, 2004a; Slater *et al.*, 2011). *A. fumigatus* toxins gliotoxin and fumagillin inhibit the function of insect hemocytes and human neutrophils as well as increase the susceptibility of larvae to infection by *A. fumigatus* (Renwick *et al.*, 2007; Fallon *et al.*, 2010; Fallon *et al.*, 2011a).

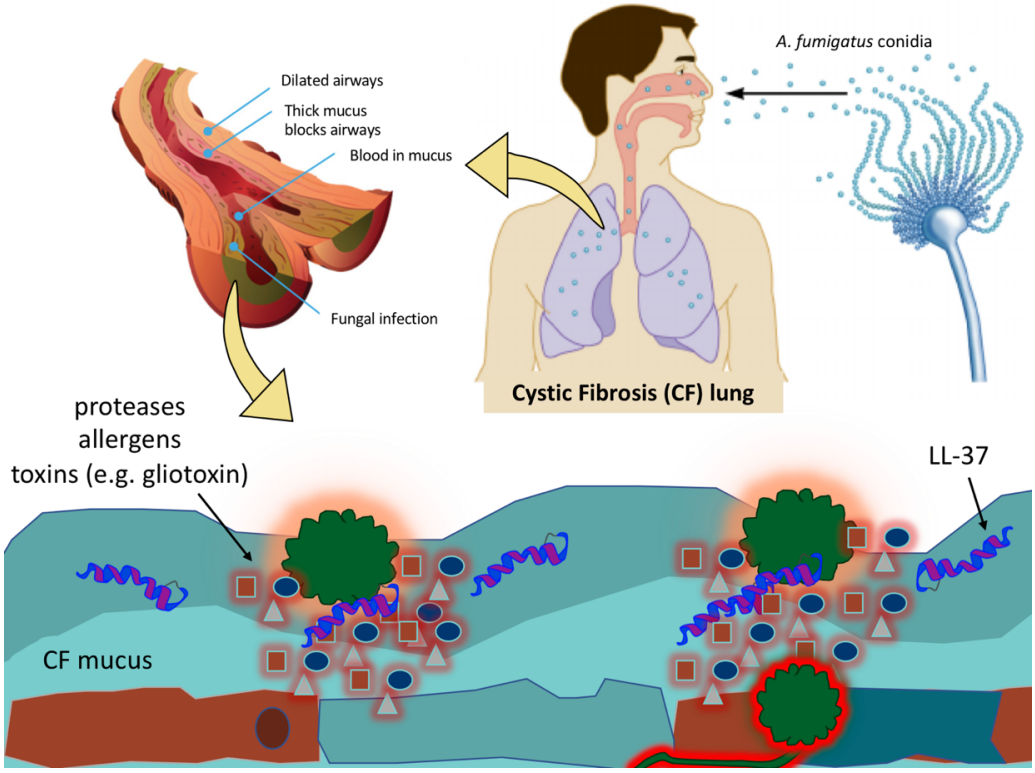

Fig. 1.17. *Aspergillus* colonisation as commonly observed in the cystic fibrosis lung. *Aspergillus* conidia which are inhaled, are not expelled by due to defective mucociliary clearance, and produce a range of allergens, toxins and enzymes which can overtime results in a hypersensitivity reaction and the onset of ABPA.

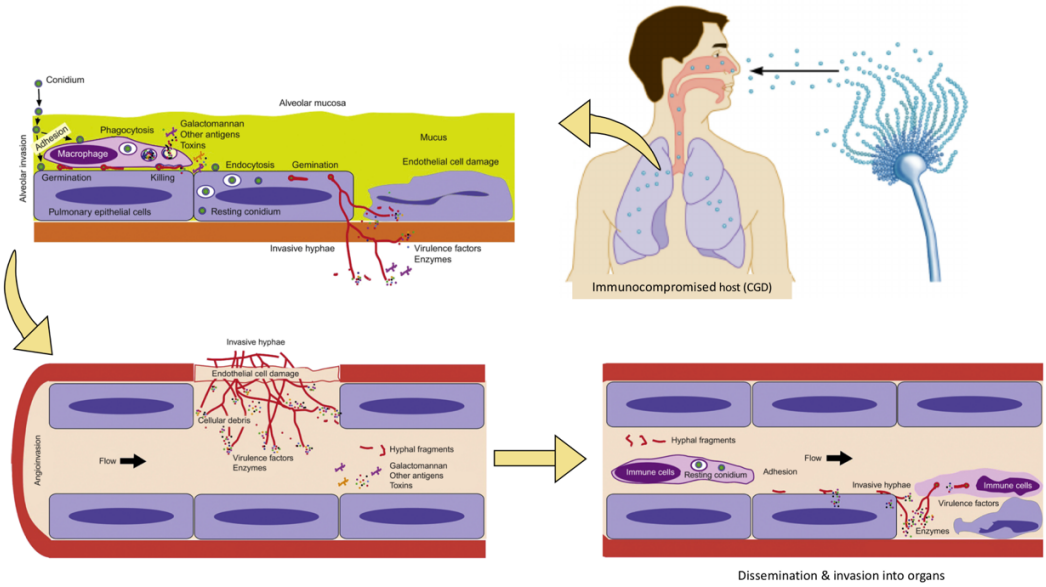

Fig. 1.18. Adapted from (Abad *et al.*, 2010). **Infection process of invasive Aspergillosis in the immunocompromised lung.** Inhaled *A. fumigatus* conidia escape immune cell killing, colonise and invasive through the pulmonary epithelium. This is followed by *A. fumigatus* invasion of blood capillaries, dissemination of the fungus throughout the host and the onset of organ invasion.

1.9.4 *Madurella mycetomatis*

Madurella mycetomatis is the dominate causative agent of eumycetoma, a chronic granulomatous type infection which is severely debilitating to its sufferers due to its occurrence at the extremities of the body (**Fig. 1.19**). Mycetoma is endemic in tropical/subtropical regions but the highest prevalence in associated with the African continent. The disease symptoms may take years to develop and are associated with the development of massive lesions which may ultimately require amputation. Most cases are usually seen in the feet (70%), followed by hands (12%), then legs and knee joints (Ahmed *et al*., 2004). The disease is severely debilitating, especially because of lesions that arise in the extremities and thus the socioeconomic consequences of the disease are severe.

However, lesions are painless and this is suggested to be a result of substances secreted by the pathogen with anaesthetic effect (Fahal, 2004). A key feature of mycetoma is the presence of grains inside the tissue and these grains may be formed as a defence mechanism by the fungus against the host immune system (Ahmed *et al.*, 2004). Grains consist of lipids, protein and melanin and the melanin is located on hyphal walls as thick layers. Furthermore, zinc, copper and calcium concentrations are significantly higher in *M. mycetomatis* infected samples than controls which contribute to the formation of the grain cement matrix (Ibrahim *et al.*, 2013).

M. mycetomatis strains form grains by interactions with *G. mellonella* larvae hemocytes and these grains are identical to those extracted from human and mammalian biopsies (Kloezen *et al.*, 2015). However, grain formation was more efficient in larva as an adjuvant was necessary to induce grain formation in mice. Furthermore, *M. mycetomatis* species and inoculum affect larval mortality and fungal CFUs obtained from larvae (Kloezen *et al.*, 2015). Interestingly, amphotericin B but not itraconazole could prevent grain formation of *M. mycetomatis* in mice, this result was also observed in larvae (Van De Sande *et al.*, 2015; Kloezen *et al.*, 2017).

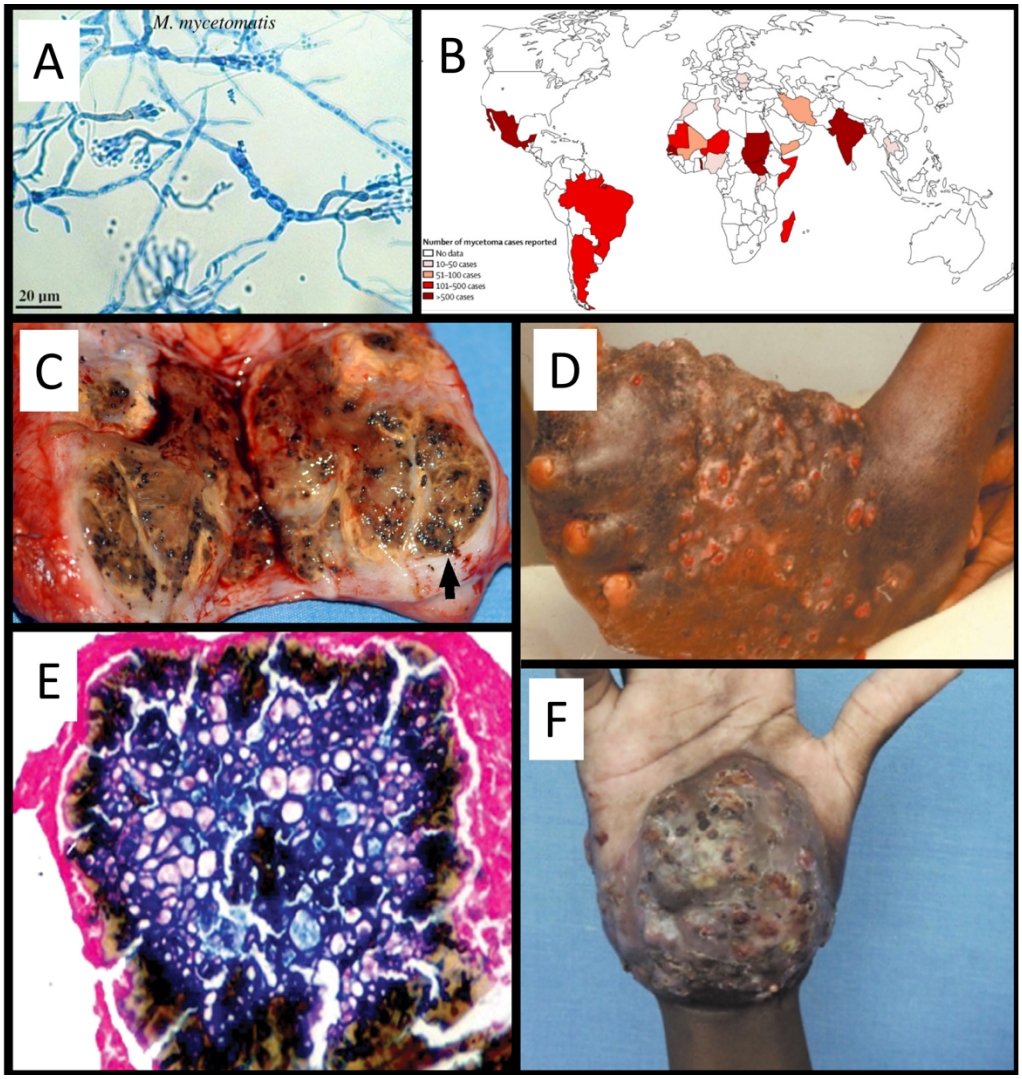

Fig. 1.19. (Adapted from Ahmed *et al.* 2004; Ibrahim *et al.* 2013; Zijlstra *et al.* 2016) **The biology, epidemiology, pathogenesis and symptoms of *M. mycetomatis* infection.** (A) Structure of *M. mycetomatis* phialides with rounded conidia, (B) eumycetoma prevails in the mycetoma belt located 30 ° south and 15 ° north of the equator and encompasses countries such as Argentina, India, Somalia and Sudan, (C) grain (black arrow) development in human biopsy sample, (D) Mycetoma foot, (E) histological section of a *M. mycetomatis* grain illustrating melanin (black) produced by the fungus and (F) eumycetoma of the hand.

1.10 Label free mass spectrometry for whole cell proteomic analysis

In recent years there have been major advances in mass spectrometry (MS) due to technological and bioinformatical advances which have increased the reliability, reproducibility and efficiency of label-free MS proteomic studies (Walther and Mann, 2010; Di Falco, 2018). Liquid chromatography in combination with advanced mass spectrometry has many advantages over gel based methods in terms of range and number of proteins detected, quantitative capacity, identification of proteins with extreme isoelectric points, and/or post translational modifications (Tuli & Ressom 2009; Doyle 2011). Furthermore, comparison between treatments can allow relative quantification. It is for these reasons that label-free MS has replaced gel based approaches in many areas of proteomics and has revolutionised our understanding of how the organism, cell or tissue respond at the proteomic level to a range of biotic and abiotic stimuli (Owens *et al*., 2014; Browne *et al*., 2015; Deslyper *et al*., 2016; Maher *et al.,* 2018; Surlis *et al*., 2018; Green *et al*., 2019).

Label free methods intrinsically reduce sample bias and exogenous contaminants due to the lack of artificially labelling of analytes. Bioinformatic technologies are utilised to interpret MS data for quantification of peptide ion intensities to produce relative quantification. Liquid chromatography alignment software can be used to optimise the chromatographic profiles of peptides and to account for a drift in peptide retention time, further increasing reproducibility (Mallick and Kuster, 2010; Cox *et al.*, 2011). Sequence coverage can be improved when peptide ions (first MS) are subject to tandem MS (MS/MS) to generate sequence specific information for database searching and identification (Cox *et al.*, 2011).

To date the majority of proteomic studies involving insects and fungal pathogens utilise simple 1 dimensional and 2 dimensional gel analysis techniques (Bergin *et al*., 2006; Yanay *et al.,* 2008; Kelly & Kavanagh 2011; Zdybicka-Barabas & Cytryńska, 2011). However in the past five years, label-free MS proteomic studies have been utilised to study the whole proteome of fungal pathogens to a range of stimuli e.g. the responses of *A. fumigatus* under iron-limiting conditions (Moloney *et al.*, 2016) and the oxidative stress responses of *Armillaria mellea* (Collins *et al.*, 2017) and also the insect hemolymph/full body and brain proteome to a range of

stimuli such as food preservatives (Maguire *et al.*, 2016; Maguire *et al.*, 2017b; Maguire *et al.*, 2017a), entomopathogenic culture filtrate (Mc Namara *et al.*, 2017), temperature/physical stress (Browne *et al.*, 2015) and parasitic infection (Surlis *et al.*, 2018).

1.11 Objectives of this study

The primary aim of this study was to assess the humoral immune responses of *Galleria mellonella* larvae to infection by a variety of microbial pathogens and to assess the responses of these pathogens to agents of the innate immune system of vertebrates in order to further validate the use of larvae to study the pathogenesis of fungal pathogens. The specific aims were:

1. To study the interaction between fungal or bacterial pathogen alone or in combination with *G. mellonella* larvae.
2. Analyse the response of fungal pathogens to innate immune effectors.
3. To assess the response of fungal pathogen to larval hemolymph.
4. To characterise disseminated disease in larvae.
5. Characterise the immune-proteomic mediators involved in immunological priming/memory in *G. mellonella* larvae.

Chapter 2

Materials and Methods

2.1 General laboratory practice and sterilisation procedures

2.1.1 Chemicals and reagents

All reagents were of the highest purity and were purchased from Sigma Aldrich Ltd, Somerset, U.K. unless otherwise stated. N-chlorotaurine (NCT) (molecular mass 181.57 g mol^{-1}, lot 2015-02-05) was prepared as a crystalline sodium salt at pharmaceutical grade, as reported previously (Nagl *et al.,* 2002), stored at -20°C, and freshly dissolved in sterile distilled water to a concentration of 0.68, 6.8, 13.77 mM for each experiment. Synthetic LL-37 peptide, scrambled LL-37 and RK-31 were purchased from Innovagen (Sweden), (<95% purity) and dissolved in ddH_2O (Table 2.1).

Table 2.1: Peptides and sequences used in this study

Chemical Name	Amino Acid Sequence/Chemical Name	Molecular weight (g/mol)
LL-37	LLGDFFRKSKEKIGKEFKRIVQRIKDFLRNLVPRTES	4493.33
Scrambled LL-37	GLKLRFEFSKIKGEFLKTPEVRFRDIKLKDNRISVQR	4493.33
RK-31	RKSKEKIGKEFKRIVQRIKDFLRNLVPRTES	3800.51

2.1.2 Sterilisation procedures

All micro-centrifuge tubes and pipette tips were stored in a sealed container and autoclaved at 121 °C for 15 minutes prior to use. All liquid growth media and agar media were autoclaved at 121 °C for 15 minutes before use and agar media allowed to cool until hand hot and poured under sterile conditions using sterile 9 cm petri-dishes.

2.1.3 Phosphate buffered saline (PBS)

One PBS (NaCl 8.0 g l^{-1}; KCl 0.2 g l^{-1}; Na_2HPO_4 1.15 g l^{-1}; KH_2PO_4 0.5 g l^{-1}; pH 7.3) tablet (Oxoid) was dissolved in 100 ml deionised water and autoclaved at 121 °C for 15 minutes. PBS was stored at room temperature.

2.1.4 Statistical analysis

All experiments were performed on three independent occasions and results are expressed as the mean ± standard error (S.E). Analysis of changes in hemocyte density, FACS results, hemocyte killing activity and protein abundance were performed by two-way ANOVA with all statistical analysis listed performed using GraphPad Prism v 6.00 for Mac, GraphPad Software, San Diego California USA, (www.graphpad.com). Survival curves for *G. mellonella* larvae were created using Kaplan–Meier plots and statistical analysis was carried out using the log rank test or survival was plotted as bar graphs in Prism. Differences were considered significant at $p < 0.05$.

2.2 Fungal and Bacterial strains and culture

2.2.1 *Aspergillus* strains and culture conditions

A. fumigatus strains ATCC 26933, ATCC 46645, Af293 were obtained from the American Type Culture Collection and *A. flavus* was a kind gift from Prof. R. Araujo, Faculty of Medicine of Porto, Portugal. *Aspergillus* was grown in sabouraud dextrose broth (SAB), YEPD broth (2% w/v glucose, 1% w/v yeast extract, 2% peptone), minimal essential medium (Sigma) or minimal medium (2% w/v glucose, 0.5% w/v yeast nitrogen base (without amino acids or ammonium sulfate), 0.5% w/v ammonium sulfate) broth at 37 ^{o}C and 200 rpm. Stocks were grown (for 3 days) on Sabouraud agar and used within 5 days.

2.2.2 Harvesting of *Aspergillus* conidia

Aspergillus conidia were harvested in a Class II safety cabinet. Plates were initially washed with 10 ml PBS supplemented with 0.01% (v/v) Tween 80 and centrifuged at 1,500 × g for 5 minutes at room temperature. The supernatant was removed, and the conidia pellet was washed twice in sterile PBS to remove excess Tween 80. The concentration of conidia in the suspension was calculated by hemocytometry.

2.2.3 *Candida albicans* strain growth and harvest

C. albicans MEN (a kind gift from Prof. D. Kerridge, Cambridge, UK) was cultured in YEPD broth (2% (w/v) glucose, 2% (w/v) bactopeptone (Difco Laboratories), 1% (w/v) yeast extract (Oxoid Ltd., Basingstoke, England)) at 30 °C and 200 rpm in an orbital shaker. Stocks were maintained on YEPD agar plates (as above but supplemented with 2% (w/v) agar). To control bacterial contamination for fungal load experiments (section 2.4.6), hand warm agar was supplemented with erythromycin (0.01 mg ml^{-1}). Plates were stored at 4 ºC and used within 3-5 days.

2.2.4 *S. aureus* strain and culture

S. aureus (Clinical isolate) and *S. aureus* strain SH1000 GFP tagged (A kind gift from Dr. J. Geoghegan, TCD, Ireland) was transferred aseptically using a sterile loop from a single colony grown on nutrient agar to nutrient broth (Oxoid) and grown overnight at 37°C and 200 rpm to the early stationary phase. Stocks were maintained on nutrient agar plates. Nutrient broth or nutrient agar (Oxoid) was prepared by adding (13 g l^{-1}) of powder to deionised water and autoclaving. Nutrient agar semi-warm solution was poured aseptically into sterile petri dishes once hand warm and allowed to set before sealing and storing the plates at 4 ^{o}C.

2.3 Microbial quantification and maintenance

2.3.1 Calculation of *S. aureus* culture cell concentration

S. aureus was grown in nutrient broth (Oxoid) at 37°C and 200 rpm to the early stationary phase. The bacterial culture was measured on a spectrophotometer. and the resulting value was adjusted to an OD_{600} of one which was diluted 1/10 and re-adjusted using PBS until the OD_{600} read 0.1, equivalent to 4.01×10^7 cells ml^{-1}. Appropriate dilutions of cells were prepared prior to inoculation into larvae.

2.3.2 Maintenance of microbial stocks (long term)

Storage of bacterial and fungal strains long term was achieved by freezing stocks of liquid culture in 50% (v/v) glycerol and placing at -80 ^{o}C.

2.4 *G. mellonella* larval storage and experimental conditions

2.4.1 *G. mellonella* storage and food

Sixth instar larvae of the greater wax-moth *G. mellonella* (Livefoods Direct Ltd, Sheffield, U.K), were stored in the dark at 15 °C to prevent pupation. Healthy (non-melanised, free of infection) larvae weighing 0.22 ± 0.03 g were selected and used within two weeks of receipt. Ten healthy larvae per treatment and controls (20 µl PBS for appropriate incubation time); (n = 3 i.e. experiments were repeated on 3 separate occasions) were placed in sterile nine cm Petri dishes lined with Whatman filter paper and containing wood shavings. Larvae were acclimatised to 30°C (*C. albicans*) or 37 °C (*S. aureus, A. fumigatus*) for 1 h prior to all experiments and incubated at either 30°C or 37 °C for all studies. All experiments were performed independently on three separate occasions.

2.4.2 Inoculation of *G. mellonella* larvae

Larvae were injected through the last left pro-leg, with a Myjector U-100 insulin syringe (Terumo Europe N.V., 3001 Leuven, Belgium) (**Fig. 2.1 A & B**). Great care was taken with each injection to maintain a high accuracy of drug or pathogen delivery. All *in vivo* experiments were performed on three separate occasions using a group size of 10 larvae per dish and average results were calculated. For viability studies larvae were injected with sterile PBS as a control for the injection of larvae.

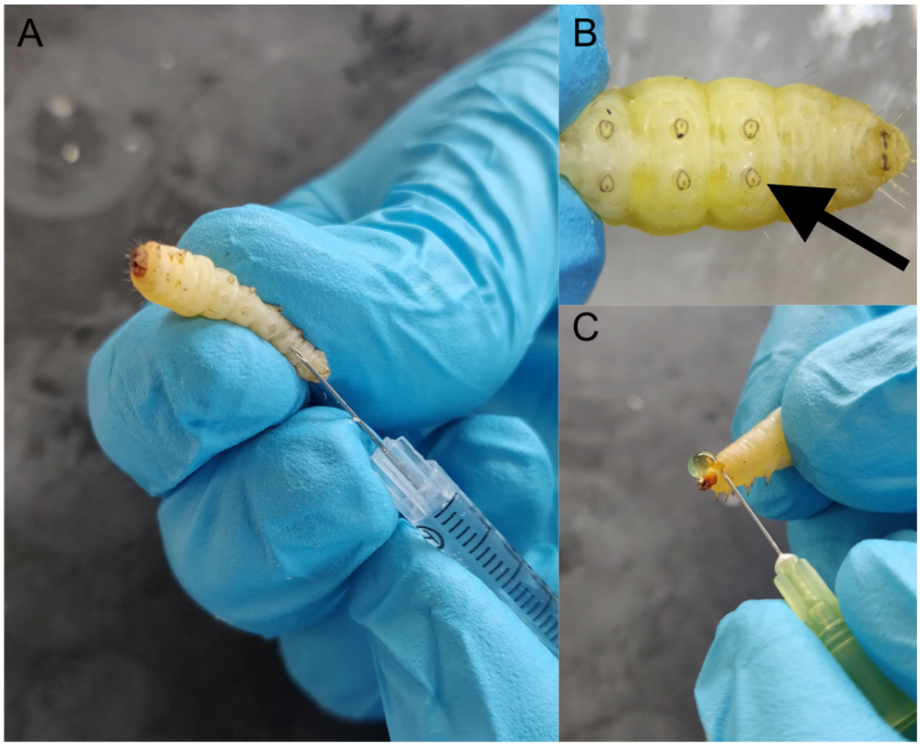

Fig. 2.1. General procedures associated with using *G. mellonella* larvae. Larvae were inoculated with a specific volume (e.g. 20 µl) through the last left proleg using a syringe (A), magnified image of last left proleg (B), demonstration of the method to obtain hemolymph from larvae (C).

2.4.2.1 Inoculation of *G. mellonella* larvae with *M. mycetomatis*

This procedure was carried out by the Dr. Wendy van de Sande group (University Medical Centre Rotterdam, Rotterdam, The Netherlands) as part of a collaborative project. *M. mycetomatis* mycelia obtained from sabouraud dextrose plates were sonicated for 20 s at 28 micron (Soniprep, Beun de Ronde, The Netherlands) and added to 200 ml colorless RPMI 1640 medium supplemented with L-glutamine (0.3 g l^{-1}), 20 mM mopholinepropanesulfonic acid (MOPS) and chloramphenicol (100 mg $liter^{-1}$; Oxoid). After 2 weeks incubation at 37°C, the mycelia were separated and washed by vacuum filtration (Nalgene, Abcoude, The Netherlands). Wet weights of the mycelia were determined and a suspension containing 100 mg wet weight ml^{-1} in PBS was sonicated for 2 min at 28 micron. The resulting homogenous suspension was washed once in PBS and diluted to a final inoculum size of 4 mg wet weight per 40 µl PBS.

2.4.3 β-glucan solution

β-glucan derived from *S. cerevisiae* (Sigma Aldrich Chemical Co., catalogue number G5011-25MG) (molecular weight 5.85 kDa) was resuspended in dH_2O by vigorous vortexing and sonication in PBS at 1 mg ml^{-1}.

2.4.5 Determination of hemocyte density

Hemocyte density was determined by bleeding (**Fig. 2.1C**) five larvae (two drops hemolymph (40 µl) $larva^{-1}$) into a pre-chilled micro-centrifuge tube to prevent melanisation. The collected hemolymph was diluted in PBS supplemented with 0.37% (v/v) mercaptoethanol and cell density was assessed with a hemocytometer and expressed as hemocytes per ml of hemolymph.

2.4.6 Determination of fungal or bacterial load in *G. mellonella* larvae

Three larvae were homogenised using an autoclaved pestle and mortar in 3 ml of sterile PBS. This was serially diluted with PBS, and 100 µl aliquots of the resulting dilutions were plated on YEPD plates containing erythromycin (0.01 mg ml^{-1}) to prevent bacterial overgrowth. These plates were incubated at 30 °C for 48 h. The fungal load was calculated as the microbial cell density per larva and was based on the number of colonies that grew at specific dilutions.

2.4.7 Flow cytometry of hemocytes sub-populations in *G. mellonella* larvae

Hemolymph was extracted from larvae (n = 20) and diluted in ice cold PBS. Hemocytes were enumerated and the density was adjusted to 1×10^6 cells ml^{-1}. Hemocytes were washed in 1% BSA/PBS, 1500 × *g* for 5 min at 4 ºC and re-suspended in BSA/PBS at a density of 1×10^6 cells ml^{-1}. Hemocyte populations were characterised using a FACS BD Accuri™ C6 cytometer and cells were differentiated based on side and forward scatter with a total of 10,000 events measured per sample.

2.4.8 Determination of fungicidal activity of hemocytes

Hemocytes were extracted from larvae (n = 10) and incubated at a density of 1×10^6 ml^{-1} at 30 ºC (Heat killed [HK] *C. albicans* 5 x 10^5) or 37 ºC (HK *A. fumigatus* (1 x 10^6), HK *S. aureus* (OD 0.01)) in PBS in a thermally controlled stirring chamber. Cell free hemolymph opsonised *C. albicans* (2×10^6 cells) was

added and killing was measured as described by Bergin *et al.* (2005). Aliquots were taken at 0, 20, 40, 60 and 80 min, diluted and plated onto YEPD agar plates supplemented with erythromycin (0.01 mg ml^{-1}). Plates were incubated and the resulting number of colonies enumerated counted and expressed in terms of percentage of the original number of cells at time zero.

2.4.9 Phagocytosis/extracellular killing assay

Experimental set up is illustrated in **Fig. 2.2**. Larvae were bled into 10 ml PBS on ice, centrifuged for 10 min at 1500 × *g,* supernatant discarded and cells washed three times using ice cold PBS. Hemocytes were resuspended and counted using a hemocytometer and adjusted to 2×10^6 hemocytes per 500 μl^{-1} PBS. At the same time, a culture of *C. albicans* was harvested by centrifugation and washed using PBS three times and resuspended in PBS and a cell count performed. *C. albicans* cells were opsonised using diluted hemolymph (from the first part of the experiment) for 20 min. *C. albicans* cells were washed and adjusted to 2×10^6 cells per 500 μl^{-1} PBS. Hemocytes and *C. albicans* were mixed in microcentrifuge tubes and incubated at 30 ^oC at 200 rpm. At time = 10, 20, 30 microcentrifuge tubes were taken, placed on ice.

Microcentrifuge tubes were centrifugated at 1500 × *g* for 5 min and supernatant collected into tubes labelled extracellular *C. albicans*, hemocytes were washed a further two times with supernatant being added to the 'extracellular *C. albicans'* tube. Hemocytes were resuspended in 1 ml and 10 µl saponin [10% w/v] added and vortexed to lysis hemocytes. These tubes were considered intracellular *C. albicans*. Both intracellular and extracellular *C. albicans* were diluted and plated on YEPD agar plates. 48 h later resulting colonies were counted.

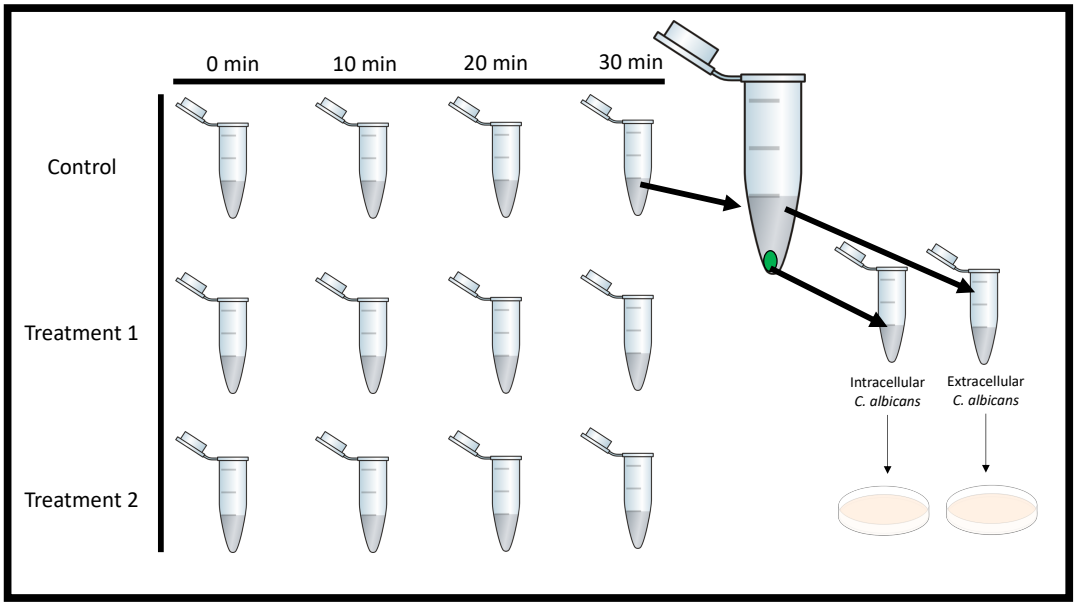

Fig. 2.2. Schematic demonstration of the experimental set-up for intracellular and extracellular killing assay with hemocytes.

2.4.10 Extraction of *G. mellonella* hemolymph

Hemolymph was extracted from larvae by bleeding through the head with a sterile 23G needle and hemolymph was squeezed through the head region into a pre-chilled microcentrifuge tube. Hemocytes were excluded by centrifugation at 1500 × g for five minutes at 4 ºC. Hemolymph supernatant was carefully collected and hemocytes discarded. Hemolymph was diluted in PBS (1/10) to produce the working stock. The working stock was diluted a further 1/10 and protein quantification was performed by Bradford protein assay (section 2.6.1) and protein adjusted to the relevant concentration (75 µg for peptide purification for mass spectrometry) by using the working stock.

2.4.11 *Ex vivo* hemolymph fungicidal activity assay

Hemolymph (1 ml) was extracted from *G. mellonella* larvae, hemocytes were removed by centrifugation (10000 × g for 10 minutes) and diluted with PBS. *C. albicans* cells (1×10^6 ml^{-1}) were suspended in 1 ml of each dilution of hemolymph (100, 50, 25%; maintained at 30 °C) and PBS and aliquots taken at 0, 2, 4, 6 and 24 h and plated on YEPD agar plates supplemented with erythromycin (0.01 mg ml^{-1}). The effect of hemolymph on yeast cell viability was determined by enumerating resulting colonies after 48 h incubation.

2.5 Microscope based techniques

2.5.1 Cryo-imaging to assess disseminated infection in *G. mellonella* larvae

G. mellonella were placed on ice to inhibit any movement. They were embedded in Bioinvision Cryo-Imaging Embedding Compound and flash-frozen in the vapour of liquid nitrogen and stored at – 80 ºC and later mounted on a stage for sectioning. Sectioning and imaging was carried out every 10 µm using a Cryoviz™ (Bioinvision Inc., Cleveland, OH) cryo-imaging system.

2.5.2 Fluorescent and Confocal Microscopy

Cell samples were washed with PBS and stained (e.g. Calcofluor white, FM-4-64) for 30 min at 16 ºC. The cells were washed with PBS and a cover slide was placed on top. The cover slides were fixed *in-situ* by applying a clear sealing solution around the perimeter of the slide which also prevented the sample drying out. Cells were viewed with an Olympus Fluoview 1000 Confocal microscope and an Olympus BX61 fluorescent microscope.

2.5.3 Determination of *M. mycetomatis* burden of infection

This procedure was carried out by the Dr. Wendy van de Sande group (University Medical Centre Rotterdam, Rotterdam, The Netherlands) as part of a collaborative project. At 24 h, day 3 and day 7 after inoculation larvae hemolymph and grains were collected of 5 larvae per time point. At the same time points an additional 5 larvae were fixed in 10% buffered formalin to assess the burden of infection. Since the larval exoskeleton is impenetrable to most fixative reagents, 100 µl of the 10% buffered formalin was injected into the larvae (Kloezen *et al.*, 2015). After 24 h fixation, whole larvae were dissected longitudinally into two halves with a scalpel and fixated in 10% formalin for at least another 48 h. The two halves of larvae were routinely processed for histology. Sections were stained with hematoxylin and eosin (HE) and Grocott methanamine silver staining.

To assess the number of grains per larvae, the grains were manually counted under a light microscope mounted with a Canon EOS70D camera (Canon Inc) by two independent scientists. Grains were magnified 40x and visualised on the computer screen using the supplied EOS Utility software (Canon Inc) and categorised into large, medium or small sizes using the enlargement display frame present in the Live View Shooting mode. Under 40x magnification, the enlargement display frame has a width and height of approximately 250 µm and 160 µm and sums up to a dimension of 0.04 mm^2. Grains that were larger than half of the display frame were categorised as large (>0.02 mm^2). Grains that were larger than a quarter of the frame but smaller than half of the frame are categorised as medium (0.01 ± 0.019 mm^2) and those between one-eighth to a quarter of the display frame (0.005 ± 0.009 mm^2) were categorised as small. The sum of all large, medium and small grains present in larvae was used to represent the total number of grains in the larvae. To determine the total size of grains in the larvae, the sum of all grains in a larva multiplied by the minimum size of their respective category (large: 0.02 mm^2, medium: 0.01 mm^2 and small: 0.005 mm^2) was used.

2.6 General Protein Methodology

2.6.1 Bradford protein assay

Bovine serum albumin standards (100 - 1500 µg ml^{-1}), were made in 800 µl ddH_2O and 200 µl Biorad Bradford protein assay reagent (Bio-Rad Munich Germany), quantified using a spectrophotometer at 595 nm (Eppendorf Biophotometer) and a standard curve (**Fig. 2.3**) prepared. Protein sample (20 µl) was added to 980 µl of Bradford protein assay reagent (diluted 1/5 from stock in PBS). The samples were inverted, allowed to stand for 5 minutes and read spectrophotometrically at 595 nm.

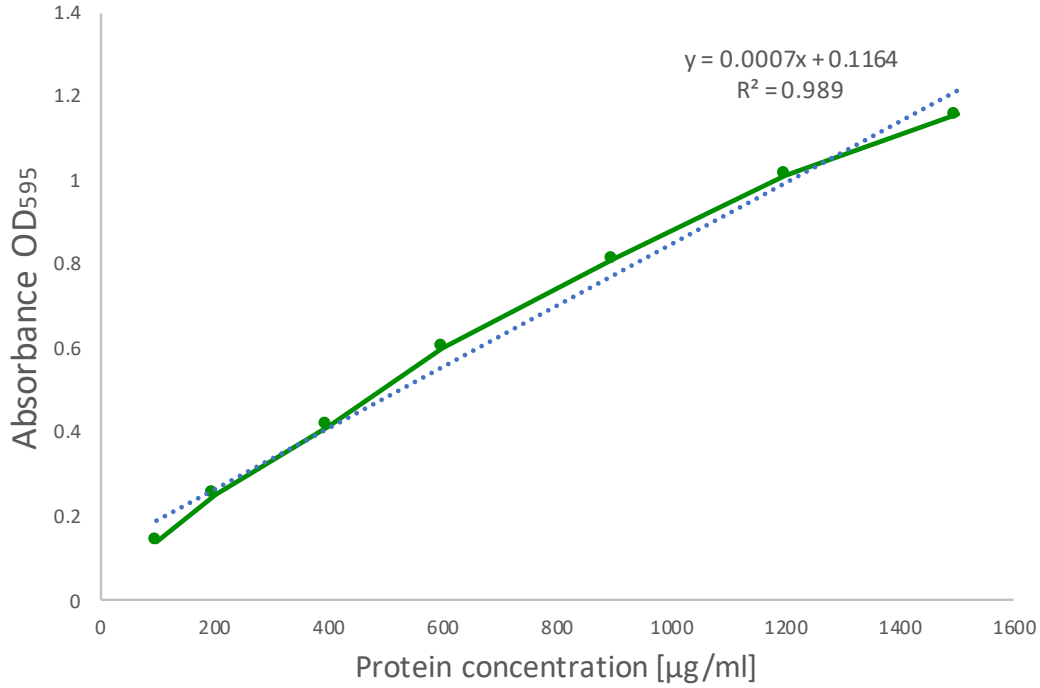

Fig. 2.3. Protein standard curve. Standard curve of protein concentration versus absorbance at OD_{595} generated by bovine serum album standards (1500 – 100 µg ml^{-1}) and quantified using a spectrophotometer.

2.6.2 Qubit® protein quantification

Protein quantification was carried out using the Qubit® Quant-IT™ protein assay kit on a Qubit® fluorometer version 2.0 following the manufacturer's instructions. In total 2 µl of sample was added to 198 µl of working buffer (199 µl of buffer B and 1 µl of dye A reagent), gently mixed and incubated (in the dark at 16 ^{o}C) for 15 min before measuring the protein concentration.

2.6.3 Acetone precipitation of protein samples

Acetone precipitation was used to concentrate protein from a dilute sample volume. The required volume of protein which corresponded to a calculated quantity of protein from Bradford assay quantification was aliquoted to a pre-chilled microcentrifuge tube and 100% ice-cold acetone was added to the tube at a ratio of 1:3 (sample volume: 100% acetone). Protein was left to precipitate overnight at -20 ^{o}C.

2.6.4 Protein sample preparation

Overnight acetone precipitated protein samples were centrifuged at 13000 × *g* for 10 minutes at 4 ^{o}C to pellet protein, acetone removed, and samples allowed to airdry. Pellets were resuspended in 25 µl resuspension buffer (**Table 2.2**). Samples were sonicated (5 minutes) and vortexed (1 minute) to aid sample resuspension. Protein quantification was carried out using a Qubit flurometer and the Qubit protein assay kit (ThermoFisher Scientific, U.S.A). To each sample 105 µl of 50 mM ammonium bicarbonate was added. Samples were subjected to the reducing agent 0.5 M DTT [1 µl] and incubated at 56 ^{o}C for 20 minutes, allowed to cool, then followed by the addition of the alkylating agent 0.55 M IAA [2.7 µl] and incubated in the dark for 15 minutes. Finally, 1 µl of ProteaseMAX solution and typsin solution were added to the samples and incubated for 24 h at 37 ^{o}C.

Table 2.2. Buffers and solutions used in protein sample preparation

Material and Amount	Material and Amount
Sample Resuspension Buffer (pH 8) 7.2 g Urea 2 M Thiourea 0.1 M Tris-HCL 20 ml ddH_2O	**200 mM Ammonium Bicarbonate** 0.394g Ammonium bicarbonate 25 ml water
50 mM Ammonium Bicarbonate 2.5 ml 200 mM Ammonium Bicarbonate 25 ml ddH_2O	**0.55 M Iodoacetamide (IAA)** 0.05 g IAA 500 µl 50 mM Ammonium Bicarbonate
0.5 M Dithiothreitol (DTT) 0.019 g DTT 250 µl 50 mM Ammonium Bicarbonate	**ProteaseMax solution** 1 mg ProteaseMax (Promega) 100 µl 50 mM Ammonium Bicarbonate
Trypsin solution (0.5 µg µl^{-1}) 20 µg Sequence grade modified trypsin (Promega) 40 µl trypsin reconstitution buffer (Promega)	

2.7 Workflow for Proteomics

2.7.1 Protein sample clean-up

All buffers for this procedure are presented in **Table 2.3**. Trypsin digested peptides samples were briefly centrifuged in a microcentrifuge to collect condensate. Samples were supplemented with 1 µl trifluoroacetic acid (TFA) in order to acidify the sample and deactivate trypsin and incubated at 16 ^{o}C (room temperature) for 10 minutes. Samples were centrifuged at 13000 × *g* for 10 minutes to remove debris and supernatant transferred to a fresh tube. In total 110 µl of peptide sample was added to 37 µl of sample buffer.

Pierce C-18 spin columns (Medical Supply Company, Ireland) were placed into 2 ml microcentrifuge tube. C-18 spin columns were activated [addition of 200 µl activation buffer, centrifuge 1500 × g for 1 minute, remove flow through, repeat a total of 3 times] and equilibrated [addition of 200 µl equilibration buffer, centrifuge 1500 × g for 1 minute, remove flow through, repeat a total of three times]. Peptide sample (147 µl) was added to the C-18 spin column which was placed in a new receiver tube and centrifuged at 1500 × g for 1 min. The peptide flow through was reapplied to the column and this step was repeated a total of three times. The C-18 column was placed in a fresh receiver tube, and 200 µl of Wash buffer added in order to remove containments (e.g. urea, ammonium bicarbonate). The C-18 column was placed in a new receiver tube and 25 µl elution buffer applied to the column followed by centrifugation for a total of three times to yield a total volume of 75 µl. Samples were concentrated using a SpeedyVac concentrator (Thermo Scientific, Massachusetts, U.S.A) and stored at – 20 ^{o}C until needed (**Fig. 2.4**).

2.7.2 Preparation of peptide sample prior to loading on LC-MS/MS Q-Exactive

Results from protein quantification from Qubit protein quantification assay (section 2.6.2) were used to determine the volume of sample loading buffer needed to produce a sample concentration of 0.75 µg μl^{-1}. Samples were vortexed for 1 minute, subjected to water bath sonication for 5 min and centrifugated at 13000 × *g* for 5 minutes. A volume of 20 µl of peptide supernatant was removed and transferred to sample vials (VWR).

Table 2.3. Buffers and solutions used in protein sample clean-up

Material and Amount	Material and Amount
Sample buffer (2% TFA, 20% Acetonitrile) 200 µL Acetonitrile 20 µl TFA 780 µl ddH_2O	**Equilibration Buffer/Wash Buffer (0.5% TFA, 5% Acetonitrile)** 150 µl TFA 1.5 ml Acetonitrile 25.8 ml ddH_2O
Activation buffer (50% Acetonitrile, 50% water) 10 ml Acetonitrile 10 ml ddH_2O	**Elution buffer (70% Acetonitrile, 30% water)** 700 µl Acetonitrile 300 µl ddH_2O
Loading buffer (0.05% TFA, 2% Acetonitrile) 500 µl TFA 20 ml Acetonitrile	

2.7.3 Parameters for Mass Spectrometry data collection

One microliter of peptide mix was eluted onto a Q-Exactive (ThermoFisher Scientific, U.S.A) high resolution accurate mass spectrometer connected to a Dionex Ultimate 3000 (RSLCnano) chromatography system. Peptides were separated by an increasing acetonitrile gradient on a Biobasic C18 Picofrit™ column (100 mm length, 75 mm ID), using a 65 min reverse phase gradient at a flow rate of 250 nL/min. All data were acquired with the mass spectrometer operating in automatic data dependent switching mode. A high-resolution MS scan (300-2000 Dalton) was performed using the Orbitrap to select the 15 most intense ions prior to MS/MS.

2.7.4 Parameters for analysing quantitative results and statistical analysis

Protein identification from the MS/MS data was performed using the Andromeda search engine in MaxQuant (version 1.2.2.5; http://maxquant.org/) to correlate the data against a 6-frame translation of the EST contigs for *G. mellonella* with the addition of the proteomes of insect species [*Hyalophora cecropia, Manduca sexta, Bombyx mori*] (Cox *et al.*, 2011; Vogel *et al.*, 2011) the proteome of *C. albicans* (strain SC5314 / ATCC MYA-2876), *S. aureus* (strain NCTC 8325) *Neosartorya fumigata* (strain ATCC MYA-4609 / Af293 / CBS 101355 / FGSC A1100*) (A. fumigatus)* and *M. mycetomatis* (strain mm55). The following search parameters were used: first search peptide tolerance of 20 ppm, second search peptide tolerance 4.5 ppm, carbamidomethylation of cysteines was set as a fixed modification, while oxidation of methionines and acetylation of N-terminals were set

as variable modifications and a maximum of 2 missed cleavage sites allowed. False Discovery Rates (FDR) were set to 1% for both peptides and proteins and the FDR was estimated following searches against a target-decoy database. Peptides with minimum length of seven amino acid length were considered for identification and proteins were only considered identified when more than one unique peptide for each protein was observed.

Results processing, statistical analyses and graphics generation were conducted using Perseus v. 1.5.5.3. LFQ intensities were log_2-transformed and ANOVA of significance and t-tests between control and treated proteome(s) was performed using a p-value of 0.05 and significance was determined using FDR correction (Benjamini-Hochberg). Proteins that had non-existent values (indicative of absence or very low abundance in a sample) were also used in statistical analysis of the total differentially expressed group following imputation of the zero values using a number close to the lowest value of the range of proteins plus or minus the standard deviation. After data imputation these proteins were included in subsequent statistical analysis.

The Blast2GO software tools was utilised to assign gene ontology terms (GO terms) relating to biological processes (BP), molecular function (MF), cellular component (CC) and enzyme categories (EC). Identified proteins were grouped into functional categories based on the FunCat (Functional Catalogue) and GO (Gene Ontology) annotations, using the FungiFun application (Priebe *et al.*, 2011). The Search Tool for the Retrieval of INteracting Genes/Proteins (STRING) (Jensen *et al.*, 2009) v10.5 (http://string-db.org/) was used to map known and predicted protein:protein interactions. UniProt gene lists (extracted from Perseus) were inputted and analysed in STRING using the medium confidence (0.5) setting to produce interactive protein networks for proteins increased and decreased in abundance. Uncharacterised proteins were subjected to functional analysis by online tools (InterPro, Pfam) which provide functional analysis of proteins by classifying proteins into families and predicting domains which can provide insights into their function.

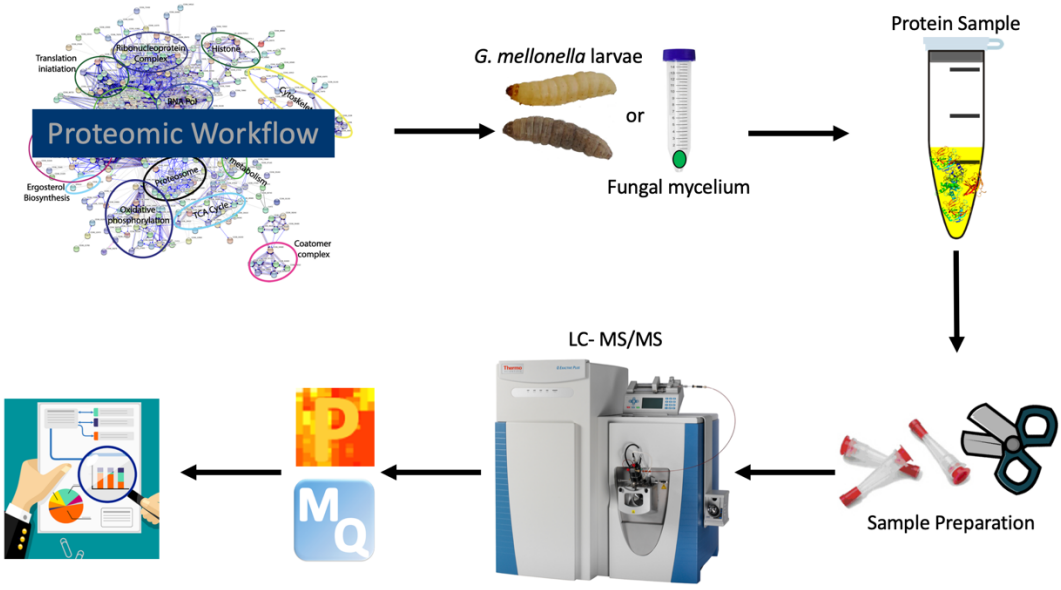

Fig. 2.4. General workflow for proteomic analysis of complex protein samples. Protein is extracted from infected *G. mellonella* larvae (section 2.4.9) or fungal material (section 2.11). Protein is trypsinised and purified (section 2.7.1) and loaded on a Q-Exactive high resolution accurate mass spectrometer (section 2.7.2, 2.7.3) and data collected and analysed by a variety of software packages (section 2.7.4).

2.7.5 Data availability

The mass spectrometry proteomics data and MaxQuant search output files from this thesis have been deposited to the ProteomeXchange Consortium (http://www.proteomexchange.org/) (Côté *et al.*, 2012) via the PRIDE partner repository with the dataset identifier numbers in **Table 2.4**.

Table 2.4. Proteomic data submission to ProteomeXchange Consortium. Chapter number, submitted title, species and identifier number of the proteomic results generated in this thesis which has been deposited to the ProteomeXchange Consortium.

Chapter Number	Title	Species	Identifier number
3	Analysis of the early cellular and humoral responses of *Galleria mellonella* larvae to infection by *Candida albicans*	*Galleria mellonella*	PXD006879
3	Proteomic responses of *Candida albicans* to *Galleria mellonella* larvae hemolymph	*Candida albicans*	PXD011997
4	Utilisation of *Galleria mellonella* larvae to characterise development of *Staphylococcus aureus* infection	*Galleria mellonella*	PXD012766
5	*Candida albicans* increases the pathogenicity of *Staphylococcus aureus* during polymicrobial infection of *Galleria mellonella*	*Galleria mellonella*	PXD014273
6	The acute host – pathogen interactions between *Aspergillus fumigatus* and *Galleria mellonella*	*Galleria mellonella*	PXD008196
7	Proteomic analysis of the processes leading to *Madurella mycetomatis* grain formation in *Galleria mellonella* larvae	*Madurella mycetomatis Galleria mellonella*	PXD013532
8	Proteomic profiling of immune priming in *Galleria mellonella* larvae	*Galleria mellonella*	PXD014651
9	The human cathelicidin antimicrobial peptide LL-37 promotes the growth of the pulmonary pathogen *Aspergillus fumigatus*	*Aspergillus fumigatus var. fumigatus*	PXD008143
10	The responses of the pulmonary pathogen *Aspergillus fumigatus* to the neutrophil derived oxidant N- chlorotaurine	*Aspergillus fumigatus var. fumigatus*	PXD009853

2.8 Analysis of the responses of *Aspergillus* to chemical agents

2.8.1 Assessment of susceptibility of *Aspergillus* conidia to compounds

SAB agar plates containing sporulating *Aspergillus* colonies were washed with 0.1 % (v/v) Tween 80 (Merck) in PBS (pH 7.2) (Sigma Aldrich) to isolate conidia. Conidia were washed twice in sterile PBS, centrifuged (1500 × *g*, 5 min in a Beckman GS-6 centrifuge) and enumerated using a hemocytometer. The chemical was serially diluted in growth medium on the 96 plate (Corning® Costar®) and *Aspergillus* conidia (1×10^4 well^{-1}) were added to each well. Plates were incubated at 37 ºC and growth was quantified by measuring at OD 570 readings (Bio-Tek Synergy HT) at 24 h.

2.8.2 Determination of the viability of *A. fumigatus* conidia (quantitative killing)

A. fumigatus conidia (5×10^7) were incubated in 1 ml PBS supplemented with chemical agents at varying concentrations for 0, 1, 4, 24 h at 37°C. Aliquots (20 µl) were taken and serially diluted at each time point, and 100 µl of diluted sample was spread onto SAB agar plates. Resulting colonies were counted and expressed in terms of % growth relative to the control (n = 3). The detection limit was 10^2 c.f.u. ml^{-1} after 1 h incubation.

2.8.3 Effect of chemical agent on growth of *A. fumigatus* accumulation

Flasks containing SAB (25 or 50 ml) were inoculated with 2.5×10^6 or 5×10^6 *Aspergillus* conidia to give a density of 1×10^5 ml^{-1} and incubated at 37 ºC (*A. flavus*; 30 ºC) and 200 rpm for 24 h. Cultures were supplemented with the chemical agent being investigated and incubated for a further 24 or 48 h when hyphal wet weights were determined (n = 4).

2.9 Organic extraction from *Aspergillus* culture filtrates

2.9.1 Extraction of mycotoxins from *Aspergillus* culture filtrate

Flasks containing SAB (50 ml) were inoculated with 5×10^6 *Aspergillus* conidia to give a density of 1×10^5 ml^{-1} and incubated at 37 ^oC (*A. flavus*; 30 ^oC) and 200 rpm for 24 h. Cultures were supplemented with the chemical agent being investigated or ddH_2O (control) and incubated for a further 24 or 48 h. *Aspergillus* cultures were filtered using mira-cloth and 0.22 µm cellulose filters (Sarstedt) and mixed with an equal volume (20 ml) of chloroform (Hyper Solv; BDH) and mixed for 2 h. The chloroform fraction was collected and evaporated to dryness in a Büchi (Brinkmann Instruments; Westbury, NY) rotor evaporator. Dried extracts were dissolved in 500 µl methanol (Hyper Solv, BDH) and stored at -70 ^oC.

2.10 Reverse Phase High Performance Liquid Chromatography (RP–HPLC)

2.10.1 Quantification of mycotoxins by RP-HPLC

Organic extracts were analysed by Reversed Phase-HPLC (Spectra-Physics). The mobile phase was 34.9% (v/v) acetonitrile (Hyper Solv, BDH), 0.1% (v/v) trifluoroacetic acid (Sigma Aldrich) and 65% (v/v) ddH_2O. The elution profile was 5 minutes of Buffer B (**Table 2.5**) at 5% followed by a linear gradient mobile phase with Buffer B to 100 % acetonitrile for 20 minutes. The column was eluted fully with 100 % Buffer B for 3 minutes and was re-equilibrated with 95 % Buffer A (**Table 2.5**), 5 % Buffer B for 5 minutes prior to further analysis. Organic extracts extract (20 µl) was injected onto a C18 Hewlett Packard column at a flow rate of 1 ml min^{-1}. The retention times of gliotoxin was 18.4 minutes (**Fig. 2.5**). A standard curve of peak area versus gliotoxin concentration **(Fig. 2.6)** was constructed using commercially available gliotoxin standards (5, 10, 15, 20, 25 µg/ 20 $µl^{-1}$) resuspended and diluted in HPLC-grade methanol (Sigma Aldrich).

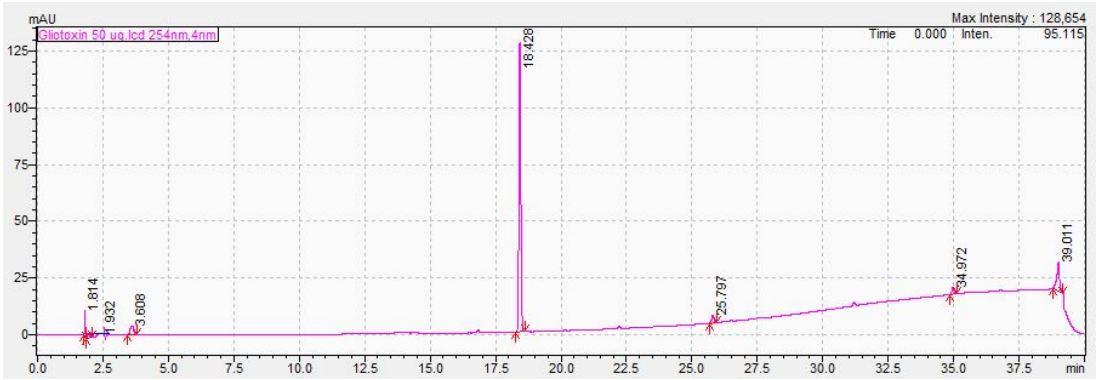

Fig. 2.5. Detection of purified Gliotoxin by RP-HPLC. Gliotoxin detection was performed at 254 nm with a retention time of approximately 18.428 minutes. Image shows detection of gliotoxin (1 µg 20µl^{-1}).

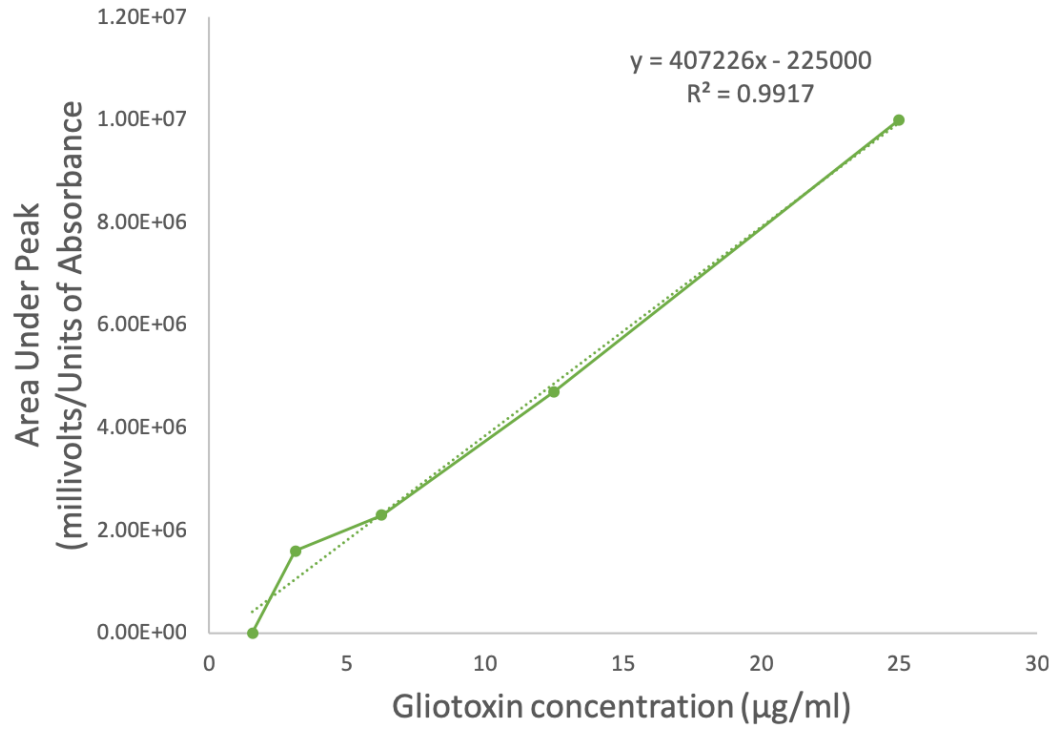

Fig. 2.6. Gliotoxin standard curve**.** Standard curve of area under the peak versus gliotoxin concentration (5, 10, 15, 20, 25 µg/20 µl). All values are the mean of three independent replicates.

Table 2.5. Buffers needed for HPLC operation

Buffer Name and Amount	Buffer Name and Amount
Buffer A HPLC grade water (1 L) 1 ml TFA acid (0.1%)	**Buffer B** HPLC grade Acetonitrile (1 L) 1 ml TFA acid (0.1%)

2.11 Proteins extraction from fungal cells

2.11.1 Whole cell protein extraction from *A. fumigatus*

Mycelium (1 g) was ground to a fine powder in a pestle and mortar with liquid nitrogen followed by the addition of 6 ml of protein extraction buffer (0.4 M NaCl, 10 mM Tris HCl, 2 mM EDTA, 10% (v/v) glycerol) supplemented with apotinin, peptstain A, TLCK, leupeptin (1 μg ml^{-1}). The suspension was disrupted using a sonication probe (Bandelin Sonopuls, Bandelin Electronic, Berlin) at 20% power, cycle 6 for 10 seconds. This was repeated twice with the sample being cooled on ice between each sonication. Protein supernatants were obtained by centrifugation (10,000 × *g*, 4 °C for 20 min).

2.11.2 Whole cell protein extraction from *C. albicans*

C. albicans cell suspension was centrifuged at 8000 × g for 10 min, washed 3 times with PBS and resuspended in lysis buffer (6 M urea, 2 M thiourea, 0.1 M Tris-HCl and supplemented with protease inhibitors [apotinin, peptstain A, TLCK, leupeptin (1 μg ml^{-1})] and pH adjusted to 8). The suspension was disrupted using a sonication probe (Bandelin Sonopuls, Berlin) at 20% power, cycle 6 for 10 seconds. Protein supernatants were obtained by centrifugation (10,000 × *g*, 4 °C for 20 min).

2.12 Ninhydrin colorimetric method for determination of amino acid concentration

Amino acid leakage by *A. fumigatus* was determined using the ninhydrin colorimetric method and expressed in terms of aspartic acid and glutamic acid **(Fig. 2.7)** (Rosen, 1957). Ninhydrin (Sigma-Aldrich) was dissolved in ethanol to give a final concentration of 0.35% (w/v) and 250 µl was added to 1 ml of *A. fumigatus* cell free culture filtrate and heated to 95 ºC for 4 min followed by cooling on ice. The absorbance at 570 nm was recorded on a spectrophotometer (Beckman DU 640).

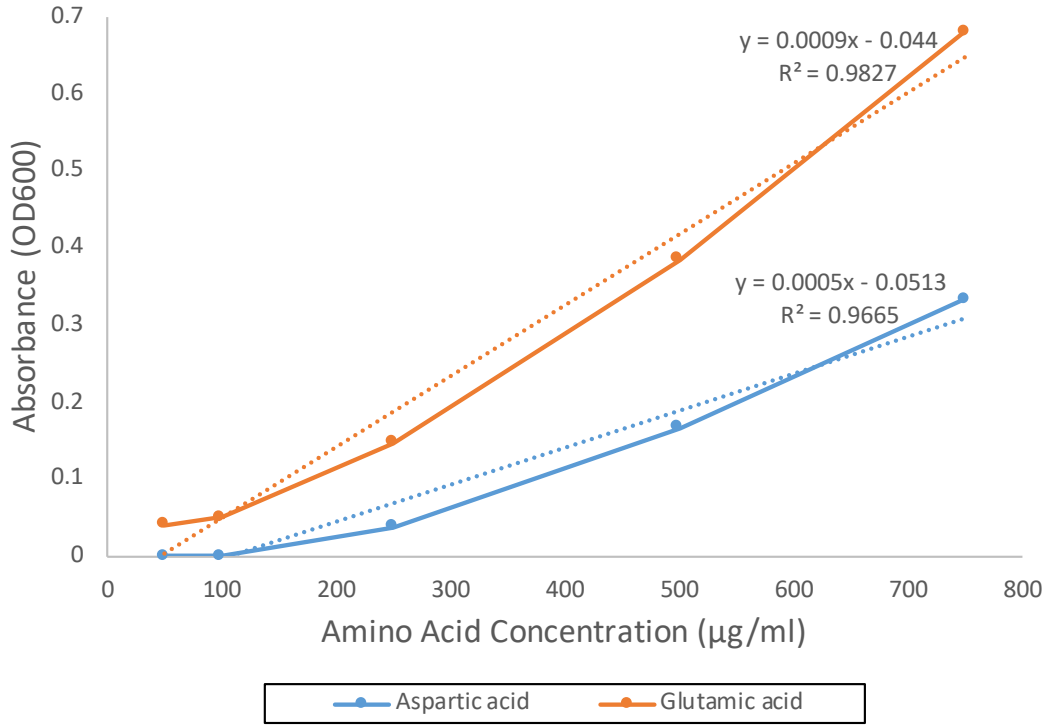

Fig. 2.7. Amino acid standard curve. Standard curve of absorbance (OD_{600} nm) versus amino acid (aspartic acid and glutamic Acid) concentration (750, 500, 250, 100, 50 µg ml^{-1}). All values are the mean of three independent replicates.

Chapter 3

Comprehensive analysis of the host – pathogen interactome between *Candida albicans* and *Galleria mellonella*

3.1 Introduction

While the use of *G. mellonella* larvae has greatly facilitated research, little attention has been directed to the study of the early stages of the pathogen – host interaction. The characterisation of the early stages of infection may facilitate the use of *G. mellonella* larvae to study initial pathogen – mammalian host interactions.

Insects hemocytes display distinct anatomical and biochemical similarities to human phagocytes. Pathways such as IMD and Toll have homologues in mammals and lead to the production of a variety of antimicrobial peptides (AMPs) which play an essential role in curtailing microbial growth. These include a range of anti-fungal peptides such as gallerimycin, a cationic inducible cysteine rich defensin like peptide with antifungal activity and galliomicin a 43 amino acid AMP which is induced by *C. albicans* (Schuhmann *et al.*, 2003; Seitz *et al.*, 2003; Lee *et al.*, 2004b; Bolouri Moghaddam *et al.*, 2016). Lepidopterans also produce moricins which are α-helical peptides which are highly active against yeasts and filamentous fungi (Brown *et al.*, 2008). Insect cecropins are a class of α-helical peptides which target the fungal membrane and induce apoptosis of *C. albicans* and possess immunomodulatory effects on mammalian macrophages (Lee *et al.,* 2015; Yun and Lee, 2016).

Larvae infected with different doses of *A. fumigatus* conidia displayed differential activation of cellular and humoral immune responses (Fallon *et al.,* 2011). *G. mellonella* larvae are capable of discriminating between the extent of infection and mounting dose dependent cellular and humoral responses to β-glucan and this effect was mediated by alterations in the density of circulating hemocytes and in the abundance of a range of immune related proteins (Mowlds *et al.*, 2010).

The aim of the results presented in this Chapter was to characterise the host – pathogen interactome between *C. albicans* and *G. mellonella* by; (1) characterising the early infection processes and dissemination of *C. albicans* in larvae and (2) to assess the responses of *C. albicans* as it interacts with the larval immune response and detail the cellular and humoral immune responses to *C. albicans* (**Fig. 3.1).**

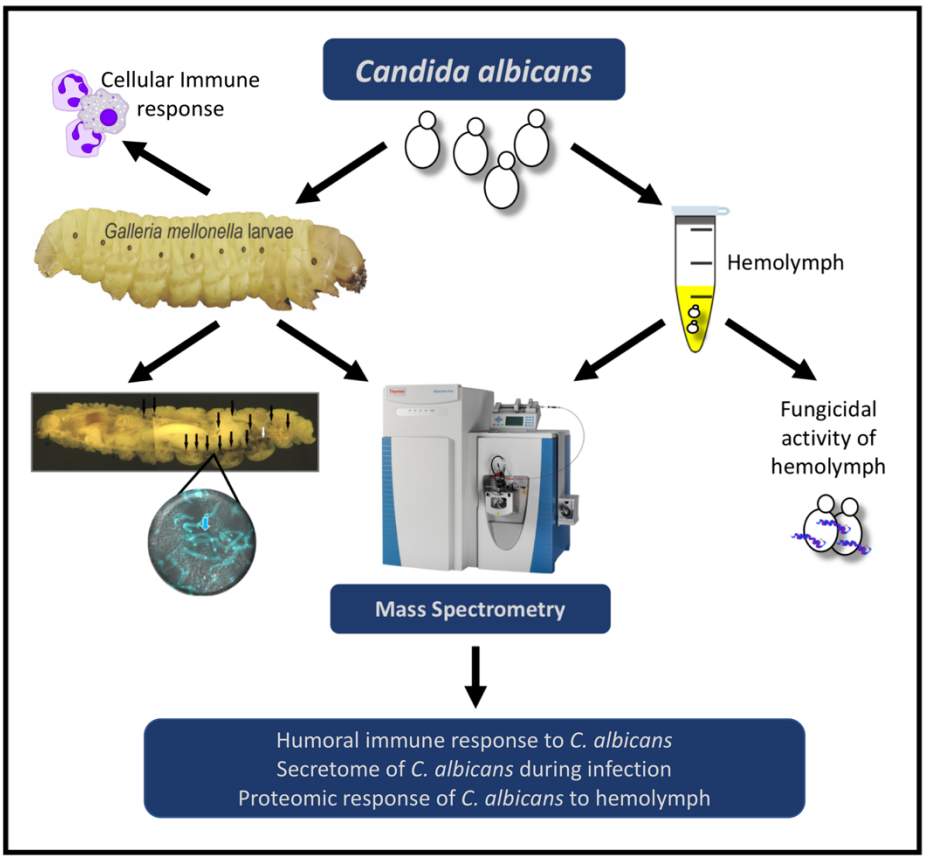

Fig. 3.1. Graphical abstract for Chapter 3.

3.2 The effect of *C. albicans* infection on *G. mellonella* larvae viability

Infection of *G. mellonella* larvae with *C. albicans* at 1×10^4 20 μl^{-1} and 1×10^5 20 μl^{-1} did not alter viability 72 h post infection. However, an inoculum of 5×10^5 20 μl^{-1} decreased larval survival to 70 ± 5.77% at 24 h, 55 ± 2.88% at 48 h and 28.33 ± 4.41% at 72 h. Whereas an inoculum of 1×10^6 20 μl^{-1} reduced larval viability at 24 (53.33 ± 3.33%), 48 (33.33 ± 3.33%) and 72 (6.66 ± 3.33%) h. Infection of larvae with *C. albicans* cells at a density of 1×10^7 20 μl^{-1} resulted in no larval survival 24 h post infection (**Fig. 3.2**).

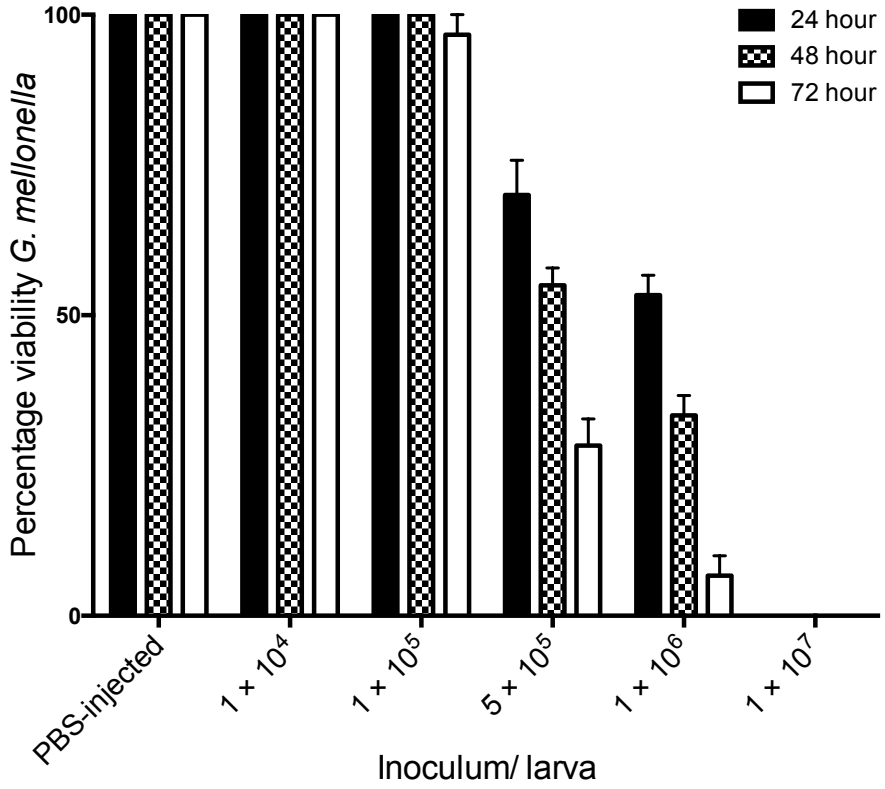

Fig. 3.2: Effect of *C. albicans* cells on viability of *G. mellonella* larvae over 72 h. *G. mellonella* larvae were inoculated with 20 µl of *C. albicans* at doses ranging from 1×10^4 to 1×10^7 incubated at 30 °C and viability was assessed over 72 h. All values are the mean ± S.E of three independent experiments.

3.3 Characterisation of proliferation of *C. albicans* inside *G. mellonella* larvae

Following inoculation of larvae with 5×10^5 20 μl^{-1}, fungal load ml^{-1} was determined by crushing, diluting and plating larval homogenate on YEPD-erythromycin agar plates (section 2.4.6). The yeast cell density in infected larvae decreased from $2.1 \pm 0.35 \times 10^4$ ml^{-1} at time 0 to $0.66 \pm 0.05 \times 10^4$ ml^{-1} ($p < 0.01$) at

two h post infection. *C. albicans* cell density remained stable until six h (0.77 ± 0.15 × 10^4 ml^{-1}) but increased to 4.4 ± 0.06 × 10^4 ml^{-1} at 12 h. By 24 h the yeast cell density had reached 1.68 ± 0.15 × 10^7 ml^{-1} ($p < 0.01$) and at 48 h had reached 9.38 ± 1.7 × 10^7 ml^{-1} ($p < 0.0001$) **(Fig. 3.3).**

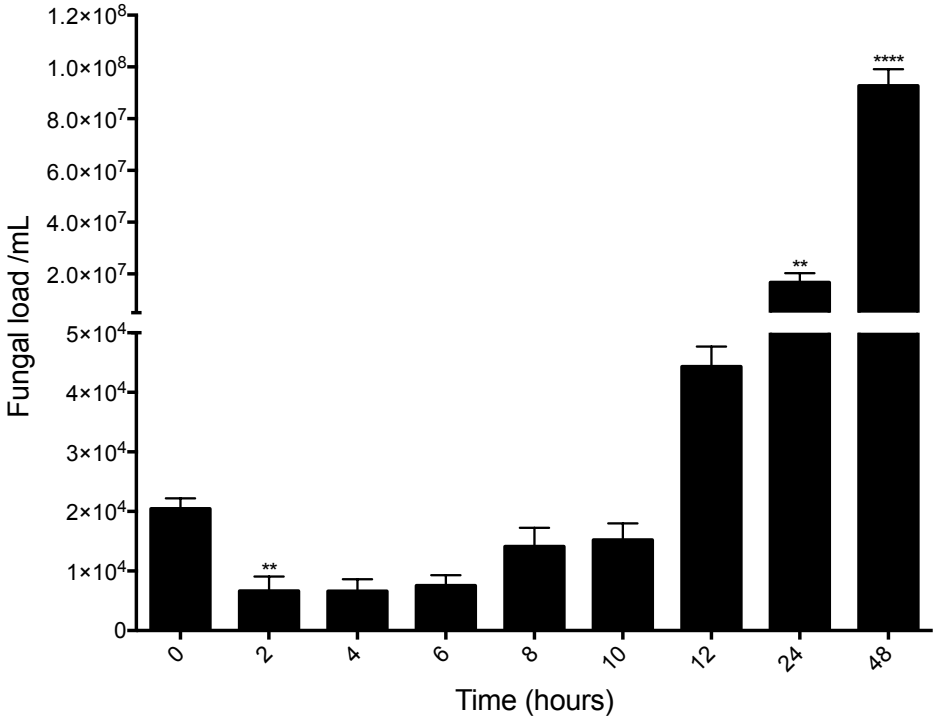

Fig. 3.3. Fluctuations in fungal cell density in *C. albicans* infected larvae. Between zero and two h there was a decrease in *C. albicans* fungal load, however by 24 and 48 h fungal load was significantly increased. Statistical significance was determined by comparing each time point to the previous time point (**: $p < 0.01$, ****: $p < 0.0001$). All values are the mean ± S.E. of three independent replicates.

3.4 Alterations in hemocyte density following inoculation with *C. albicans*

G. mellonella larvae were inoculated with 20 µl *C. albicans* (5 × 10^5 20 $µl^{-1}$) and hemocyte density was assessed over 48 h. The density of circulating hemocytes initially decreased from to 2.55 ± 0.2 × 10^6, ($p < 0.001$) relative to PBS injected larvae (4.95 ± 0.35 × 10^6) at two h post infection, however there was a significant increase in circulating hemocyte density by 6 h post infection (6.18 ± 0.32 × 10^6, $p < 0.01$) relative to PBS injected larvae (5.39 × 0.35 × 10^6. By 12 h the hemocyte density had declined to 1.47 ± 0.1 × 10^6 ($p < 0.001$) as compared to the relevant control (4.58 ± 0.89 × 10^6**) (Fig. 3.4)**.

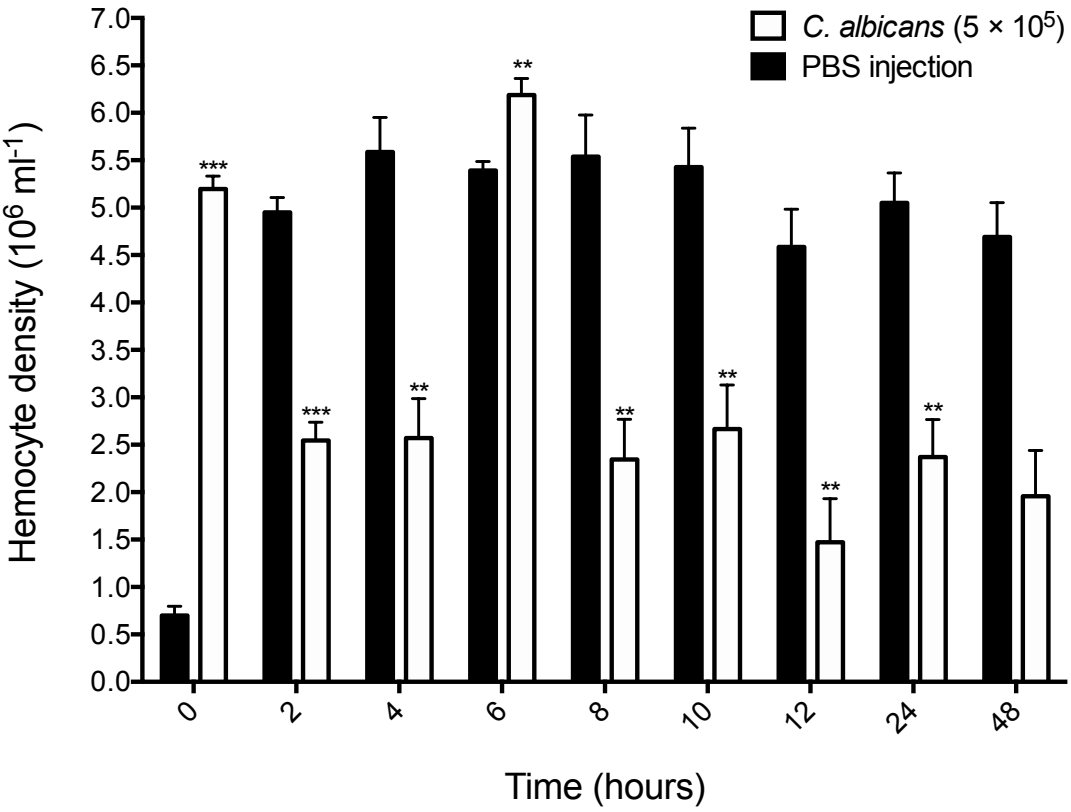

Fig. 3.4. Alteration in circulating hemocyte density following inoculation with *C. albicans* and incubation at 30 ºC. *G. mellonella* larvae were inoculated with 20 µl viable *C. albicans* (5×10^5 20 μl^{-1}) and hemocytes were extracted and enumerated from zero h to 48 h post inoculation. Statistical analysis was performed by comparing each timepoint to its relative PBS control (**: $p < 0.01$, ***: $p < 0.001$). All values are the mean ± S.E. of three independent experiments.

3.5 Alterations in hemocyte density in larvae administrated β-(1, 3) glucan

Following administration of a β-(1, 3) glucan solution (20 µg 20 µl^{-1}) into *G. mellonella* larvae there was a significant spike in hemocyte density at 6 (6.25 ± 0.25 × 10^6 larva^{-1}) h as compared to 0 (5.17 ± 0.22 × 10^6 larva^{-1}, $p < 0.05$) h post injection. By 24 (5.01 ± 4.45 × 10^6 larva^{-1}, $p < 0.01$) h hemocyte density has decreased as compared to 6 h.

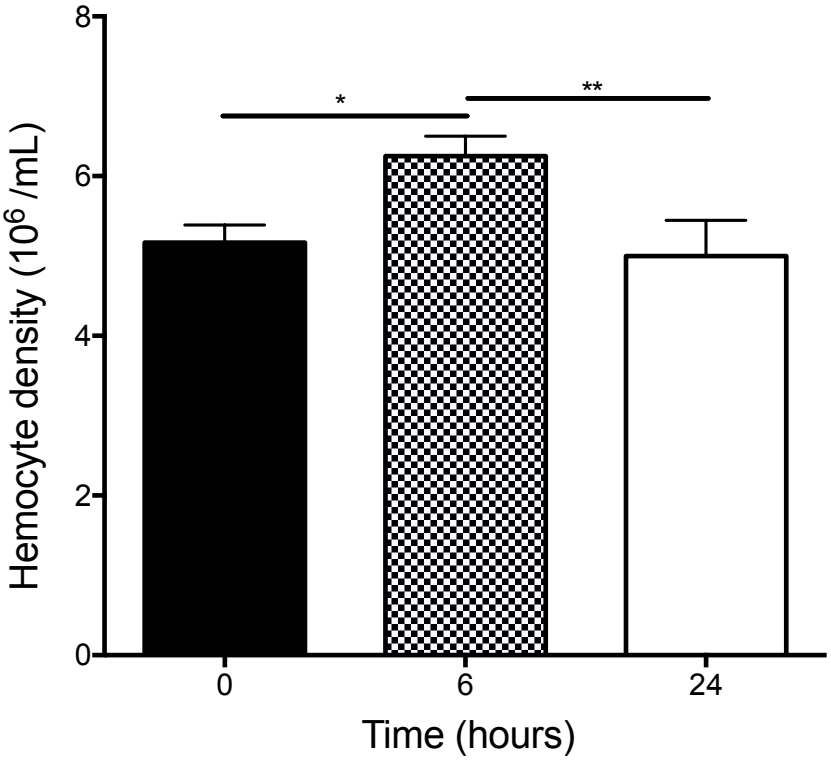

Fig. 3.5. Effect of β-(1, 3) glucan on *G. mellonella* larvae hemocyte density. All values are the mean ± S.E of three independent experiments.

3.6 Cellular immune response of *G. mellonella* larvae to yeast β-(1, 3) glucan

In order to characterise the changes in the hemocyte population by flow cytometry in larvae, *G. mellonella* larvae were administered 20 µl of a β-(1, 3) glucan (20 µg 20 μl^{-1}) solution, a component of the yeast cell wall for 0, 6 and 24 h. β-glucan was employed as it was previously demonstrated to induce an immune response in *G. mellonella* larvae and enabled the use of the flow cytometry facility to differentiate hemocytes without the risk of yeast contamination of the instrument (Mowlds *et al.*, 2010; Browne *et al.*, 2015).

Larvae administered β-glucan for six or 24 h had a hemocyte density of 6.25 ± 1.7 × 10^6 ($p < 0.05$) and 5 ± 2.7 × 10^6, respectively. PBS injected larvae, herein referred to as control larvae, showed a hemocyte density of 5.1 ± 1.6 × 10^6. Flow cytometric analysis was employed to establish if there was a change in the relative proportion of each hemocyte sub-population in naïve larvae and in those larvae administrated β-glucan for 6 and 24 h. Hemocyte populations were differentiated on the basis of size and granularity and at least five distinct sub-populations (Browne *et al.*, 2015) labelled P1 to P5, were identified **(Fig. 3.6)**. Larvae administered β-glucan for 24 h showed a significant increase ($p < 0.05$) in the relative abundance of P1 hemocytes (small, granular cells) as compared to control larvae. The total percentage of the P1 sub-population of hemocytes in 6 h β-glucan challenged larvae was 3.78 ± 0.56% and 13.15 ± 1.7% in larvae administered β-glucan for 24 h. There was a significant increase in P5 hemocytes (very large, non-granular cells) at six h β-glucan exposure. P2 and P3 (medium sized, granular cells) were both significantly decreased at 24 h compared to naïve larvae.

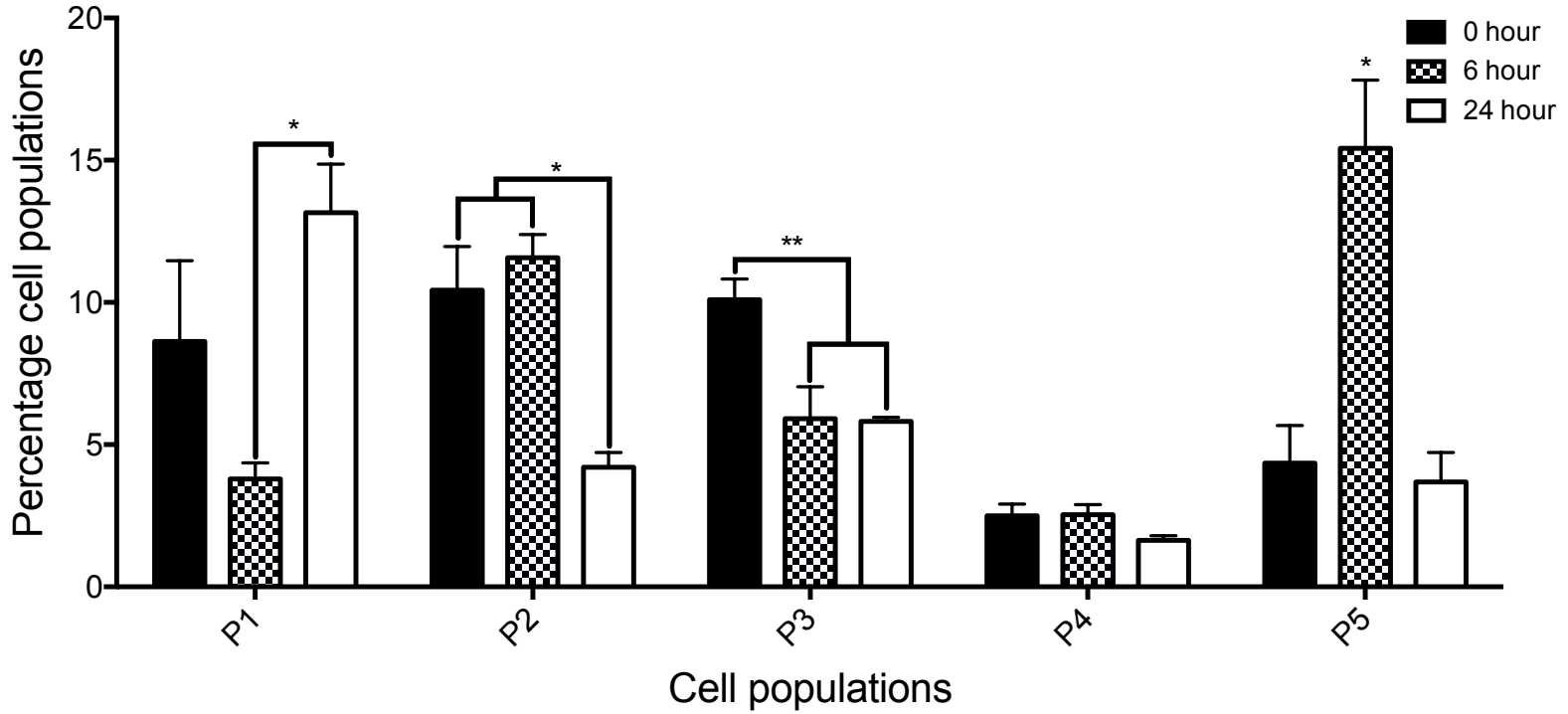

Fig. 3.6. Flow cytometric analysis of hemocyte sub-populations. Fluctuations in hemocyte sub-populations in larvae administered β-glucan at 0, 6 and 24 h. Hemocyte sub-populations were measured based on size and granularity as described (*: $p < 0.05$, **: $p < 0.01$). All values are the mean ± SE of 3 independent determinations.

3.7 Effect of β-glucan administered on fungicidal activity of hemocytes

Hemocytes were extracted from β-glucan administered larvae and their ability to kill *C. albicans* cells was assessed as described (section 2.4.8) (**Fig. 3.5**). Hemocytes from control larvae killed 24 ± 6.67% of the yeast cells after 60 min, while hemocytes from larvae administered β-glucan for 6 and 24 h killed 53 ± 2.37% and 65 ± 2.12%, ($p < 0.01$) after 60 min, respectively. At 80 min hemocytes from control larvae killed 72 ± 2.89% yeast cells while those from larvae administered β-glucan for 6 or 24 h killed 81 ± 3.33% or 86 ± 1.22% ($p < 0.05$), respectively.

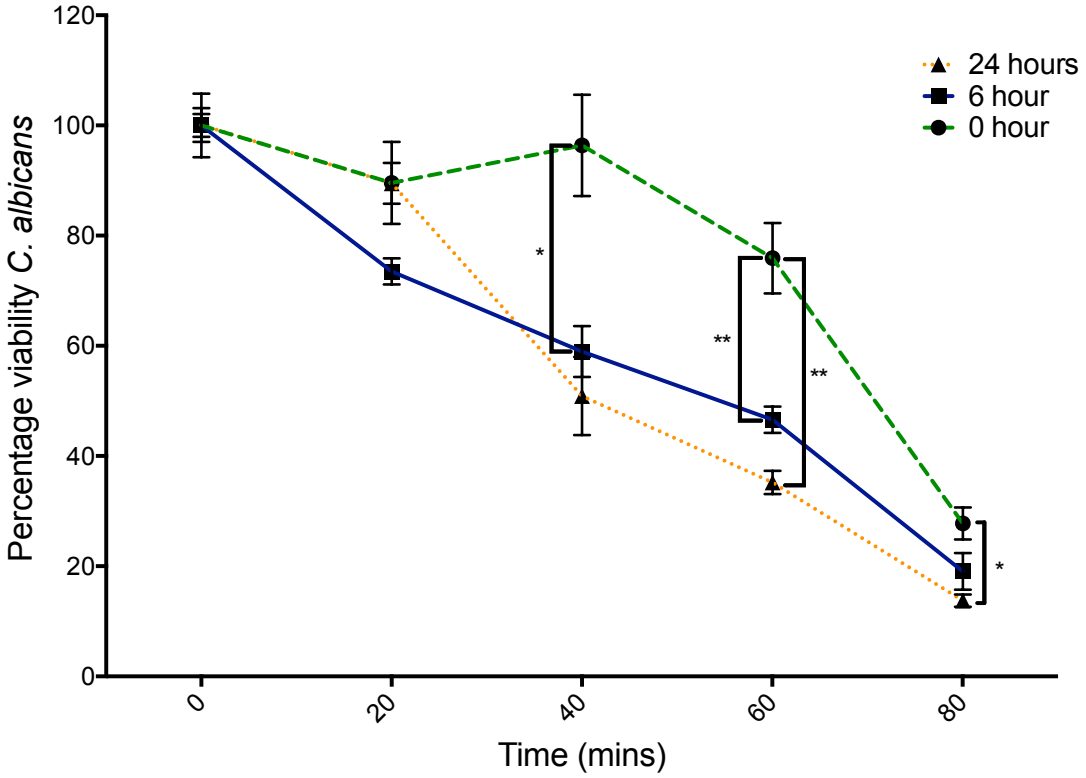

Fig. 3.7. Fungicidal activity of hemocytes from *G. mellonella*. *Ex vivo* fungicidal activity of hemocytes from *G. mellonella* larvae administrated 20 µg β-1,3-glucan larva^{-1} (*: $p < 0.05$, **: $p < 0.01$). All values are the mean ± SE of 3 independent replicates.

3.8 Characterisation of dissemination of *C. albicans* infection in *G. mellonella* larvae

Cryo-imaging was used to visualise the dissemination of *C. albicans* (5×10^5 $larva^{-1}$) infection from the point of inoculation throughout the larva (**Fig. 3.8**). Nodules appeared around the perimeter of the hemocoel 6 h post infection (see black arrows) indicating dissemination of the *C. albicans* blastospores from the site of infection. By 24 h there was extensive melanisation of larval tissue and cuticle (white arrows) indicating invasion from the insect hemocoel into surrounding tissue, and the formation of large fungal nodules (black arrows) at the site of inoculation and throughout the larva (**Fig. 3.8**). Visualisation of melanised lesions dissected from infected larvae by confocal microscopy at 6 and 24 h revealed the presence of hyphae (blue arrow) dispersed throughout nodules (**Fig. 3.9**). At 24 h hyphae (blue arrow) and yeast cells (orange arrow) are visible.

3.9 Analysis of Proteomic response of *G. mellonella* larvae to *Candida* infection

Label free quantitative proteomic analysis was conducted on the *G. mellonella* cell free hemolymph proteome after exposure to *C. albicans* for 0, 6 and 24 h. In total, 3167 peptides were identified representing 586 proteins with two or more peptides and 21, 125 and 113 (6 h v 0 h, 24 h v 0 h, 24 h v 6 h, respectively) proteins were determined to be differentially abundant (ANOVA, $p < 0.05$) with a fold change of > 2. A total of 55 proteins were deemed exclusive (i.e. with LFQ intensities present in all three replicates of one treatment and absent in all three replicates of the other two treatments). These proteins were also used in statistical analysis of the total differentially expressed group following imputation of the zero values as described. After data imputation these proteins were included in subsequent statistical analysis. A principal component analysis (PCA) performed on all filtered proteins distinguished the 0, 6 and 24 h *C. albicans* treated samples indicating a clear difference between each proteome (**Fig. 3.6).** Hierarchical clustering of z-score normalised intensity values for all significantly differentially abundant proteins (n = 259) produced the three replicates of each sample group (**Fig. 3.6).** Furthermore, 2 major protein clusters were identified: 0 h and 6 h abundant proteins (Cluster A) and 24 h abundant proteins (Cluster B).

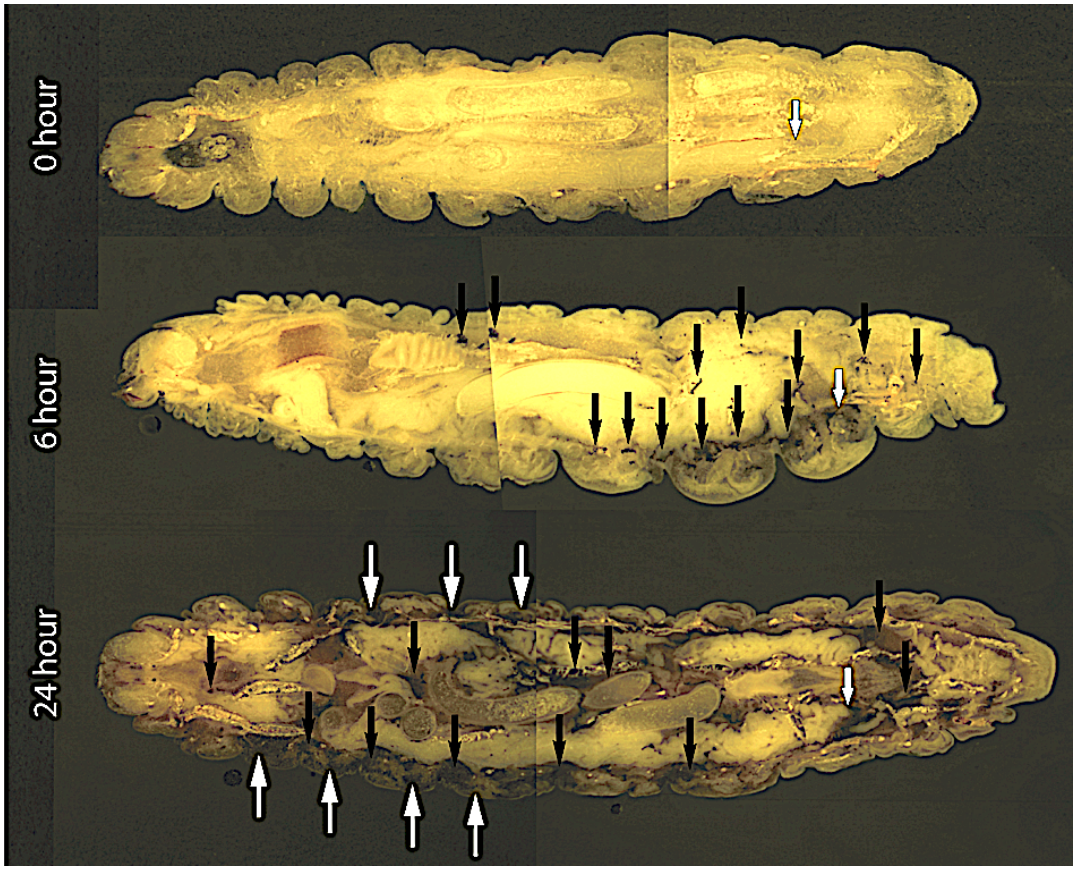

Fig. 3.8. Cryoviz visualisation showing the stages of disseminated candidosis in *G. mellonella* after 6 and 24 h infection. Larvae were inoculated with 5 × 10^5 *C. albicans* cells and incubated for 6 and 24 h. Larvae were embedded in Cryo-imaging embedding compound and sectioned (10 µm) using a Cryoviz cryo-imaging system. (Point of inoculation (white-edged arrow), fungal nodules/granulomas (black arrow), cuticle melanisation (white arrows). This experiment was repeated on 3 separate occasions with representative images provided.

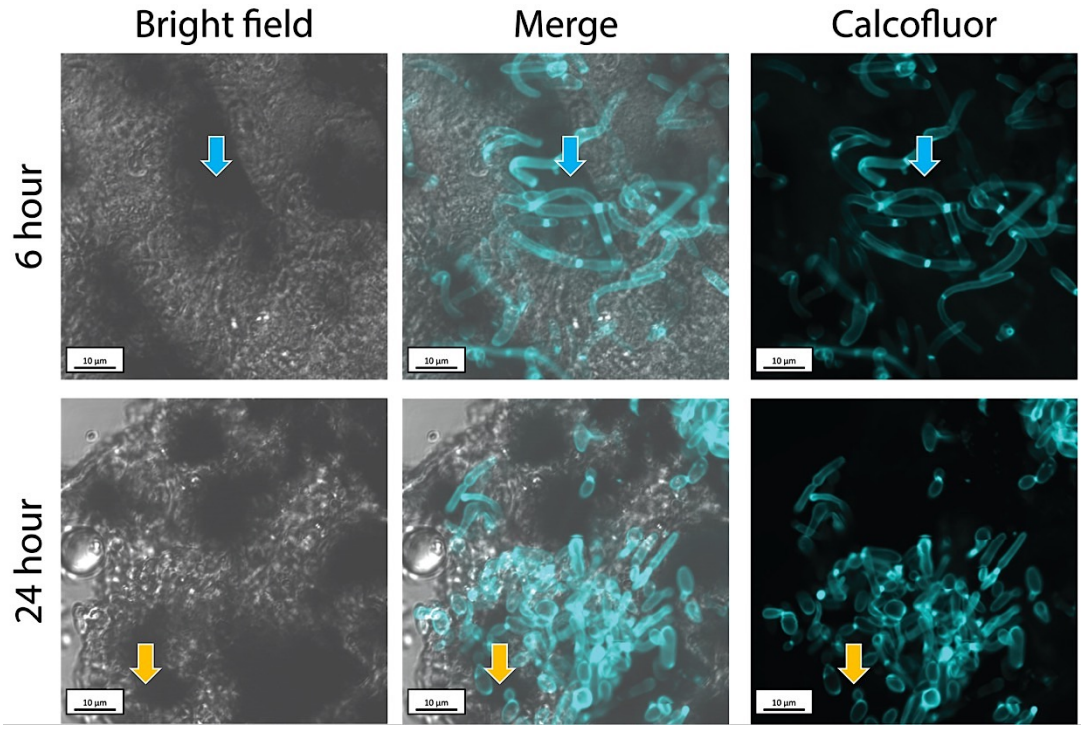

Fig. 3.9. Confocal microscopy of fungal nodules from *G. mellonella* larvae. Visualisation by confocal microscopy of development of *C. albicans* yeast and hyphal cells in fungal nodules dissected from infected *G. mellonella* larvae inoculated with 5×10^5 yeast cells 20 μl^{-1} inoculum. Fungal nodules were dissected from larvae and stained with Calcofluor white. Confocal microscopy revealed the formation of melanised plaques (black clumps within nodules). Fluorescent microscopy of fungal nodules using Calcofluor white fluorescence revealed *C. albicans* hyphae (blue arrow) at 6 h post infection. By 24 h there is the appearance of both hyphal forms and yeast cells (orange arrow) (scale bar corresponds to 10 µm). This experiment was repeated on 3 separate occasions with representative images provided.

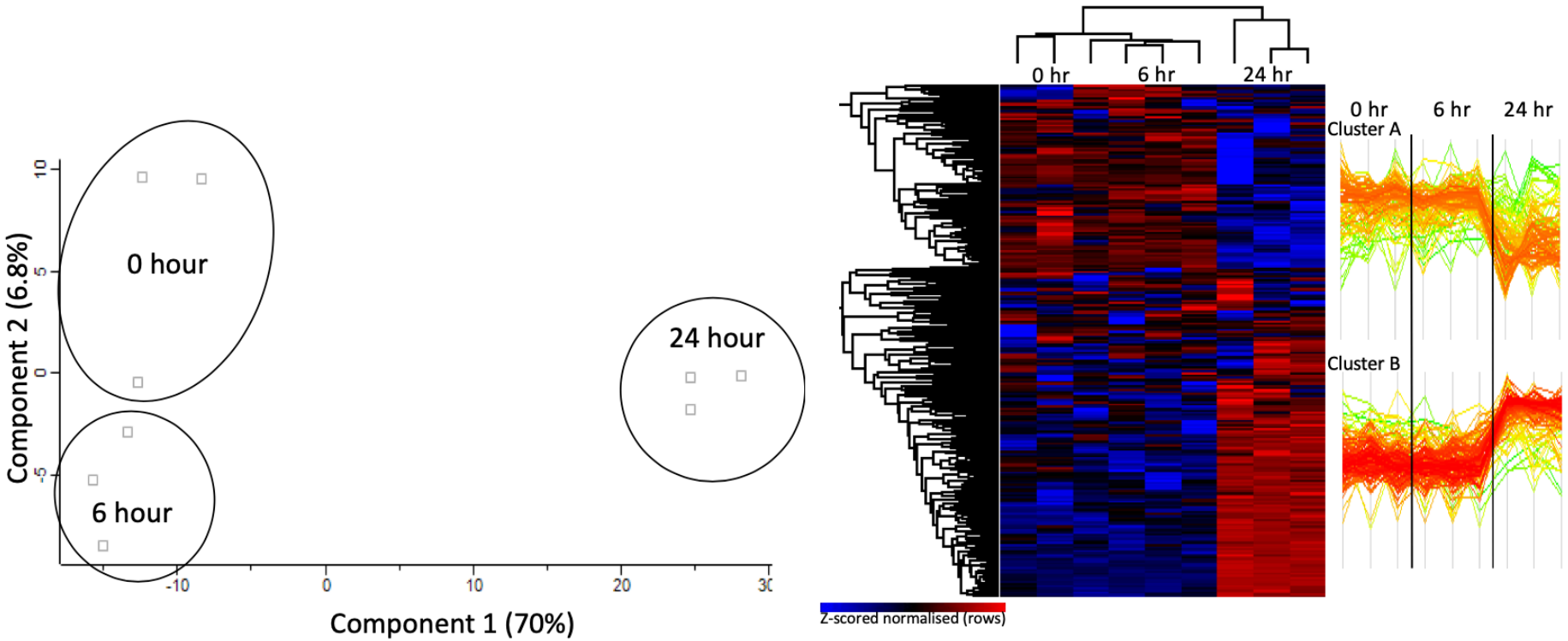

Fig. 3.10. Shotgun quantitative proteomic analysis of *G. mellonella* infected with *C. albicans*. A; Principal component analysis (PCA) of *G. mellonella* infected with *C. albicans* at 0, 6 and 24 h with a clear distinction between each time point. B; Two-way unsupervised hierarchical clustering of the median protein expression values of all statistically significant differentially abundant proteins. Hierarchical clustering (columns) identified 3 distinct clusters comprising the three replicates from their original sample groups.

Proteins increased in relative abundance in the larvae challenged with *C. albicans* for 6 h compared to the control were mitochondrial aldehyde dehydrogenase (+10 fold), prophenoloxidase-activating proteinase-1 (+5 fold), cecropin-A (+4.5 fold), hdd11 (+4 fold) and peptidoglycan recognition - like protein B (+2.3 fold) (**Table A3.1A**). Proteins decreased in relative abundance in the larvae challenged with *C. albicans* for 6 h compared to the control were uncharacterised protein (-5.6 fold), integument esterase 2 precursor (-4.8 fold), chemosensory protein 7 precursor (-4.6 fold) and translationally-controlled tumor protein homolog (-2.9 fold) (**Fig. 3.11A, Table A3.1B**).

Proteins increased in relative abundance in larvae inoculated with *C. albicans* for 24 h compared to the control larvae were muscle protein 20-like protein (+174 fold increased), tropomyosin 2 (+141 fold), glutathione-S-transferase-like protein (+114 fold), peptidoglycan recognition protein - LB (+72 fold), mitochondrial aldehyde dehydrogenase (+54 fold) gloverin (+52 fold), hdd11 (+49 fold), serpin-4B (+35 fold), Mn superoxide dismutase (+30 fold), cecropin-D (+23 fold) and moricin-like peptide B (+21 fold) (**Table A3.2A**). Proteins decreased in relative abundance in larvae inoculated with *C. albicans* for the 24 h were β-1,3-glucan recognition protein precursor (-28.6 fold), prophenoloxidase subunit 2 (-25 fold), catalase (-5 fold), kunitz-like protease inhibitor precursor (-5 fold), lysozyme-like protein 1 (-5 fold) and putative Gram negative bacteria - binding protein precursor (-4.5 fold) (**Fig. 3.11B, Table A3.2B**).

Blast2GO annotation software was used to group proteins based on conserved GO terms in order to identify processes and pathways potentially associated with infection by *C. albicans*. GO terms were categorised by biological processes (BP), molecular function (MF) and cellular components (CC). Enzyme categories (EC) were also included in the analysis (**Fig. 3.12**).

Biological processes such as single-organism metabolic process, organic substance metabolic process and immune response were significantly enriched within the 6 and 24 h infected larvae. A range of molecular functions such as ion binding and oxidoreductase activity were increased at 24 h relative to 0 h *C. albicans* infected larvae. GO terms such as intracellular, intracellular part and supramolecular polymer were enriched within the 24 h infected hemolymph for cellular component.

Enzyme categories such as oxidoreductases and hydrolases were also increased amongst the infected larval hemolymph proteome.

3.10 Characterisation of *C. albicans* proteins secreted during infection of *G. mellonella* larvae

Hemolymph from *C. albicans* infected larvae was isolated (t = 24 h) and MS analysis performed. A total of 101 *C. albicans* proteins released during infection were detected in *G. mellonella* hemolymph. Seventeen uncharacterised proteins were detected during infection. Enrichment analysis using FunCat GO terms, identified biological processes such as interaction with host (p = 1.4029e-8), cellular response to heat (p = 0.040686) and pathogenesis (p = 0.032202). Molecular functions such as protein binding (p = 6.8596e-7) and cellular components such as cytoplasm (p = 7.7444e-7) and hyphal cell wall (p = 7.6282e-9) were all significantly enriched within this subset of proteins. Proteins associated with the extracellular region (p = 6.8596e-7) and cell surface (p = 1.7438e-12) were also enriched indicating these proteins are released or secreted during infection in larval hemolymph (**Table A3.3)**.

Proteins that were implicated in pathogenesis were 14-3-3 protein homolog, cell wall protein 1, potential fungal zinc cluster transcription factor, cell wall protein IFF5, cell surface mannoprotein MP65, heat shock protein homolog SSE1, secreted protein RBT4, secreted β-glucosidase SUN41, heat shock protein 90 homolog and enolase 1 (**Table A3.4)**

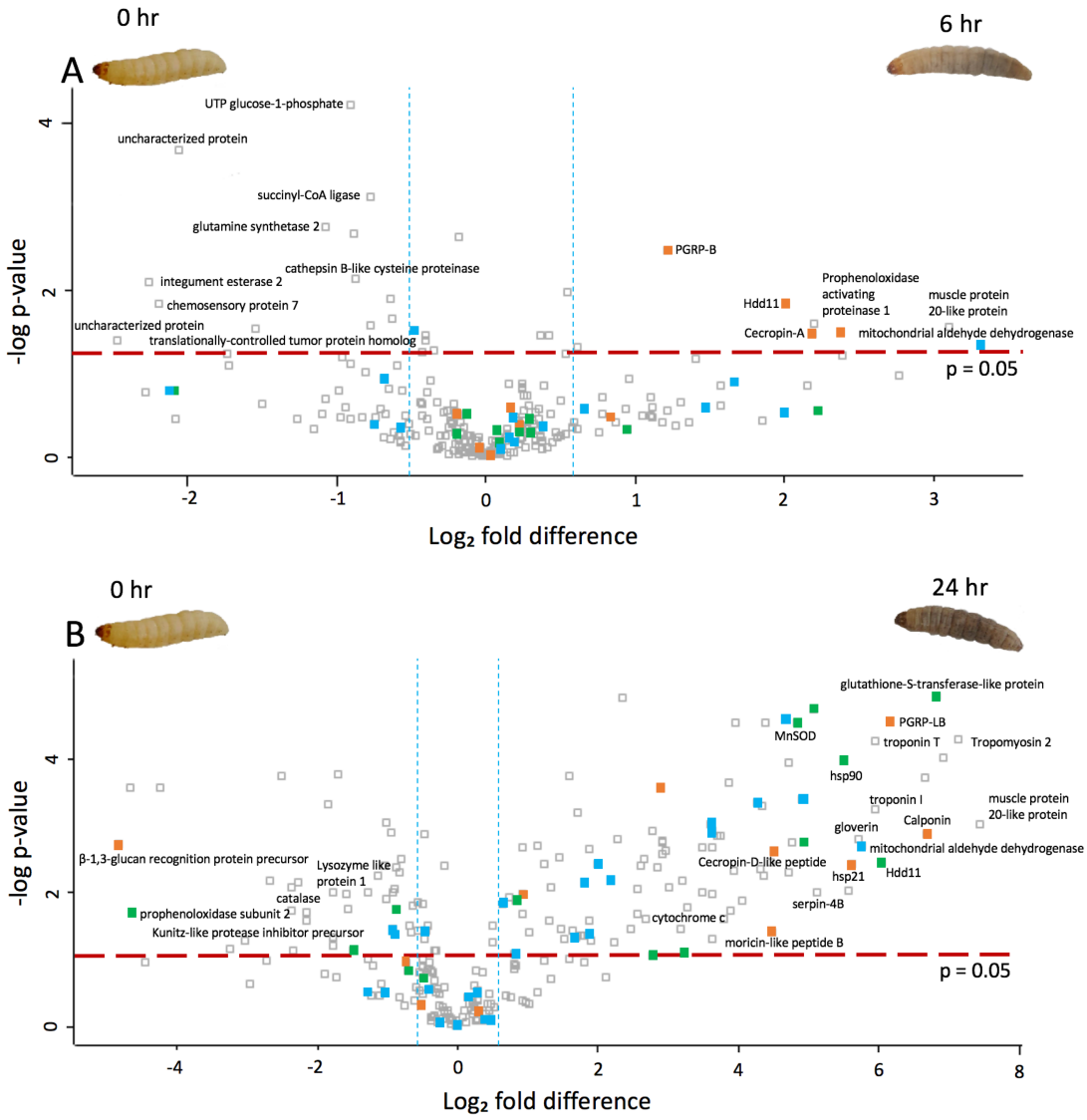

Fig. 3.11. Volcano plots of all identified proteins based on relative abundance differences between *G. mellonella* larvae treated at 0, 6 or 24 h. Volcano plots showing the distribution of quantified proteins according to p value (−log10 p-value) and fold change (log2 mean LFQ intensity difference). Proteins above the line are considered statistically significant (p value < 0.05) and those to the right and left of the vertical lines indicate relative fold changes ± 1.5. The top 20 differentially abundant proteins are labelled and all proteins associated with the stress response (green), immune response (orange) and oxidoreductase activity (blue) were highlighted for 6 h versus 0 h **(A)** and 24 h and 0 h and **(B)** *C. albicans* treated.

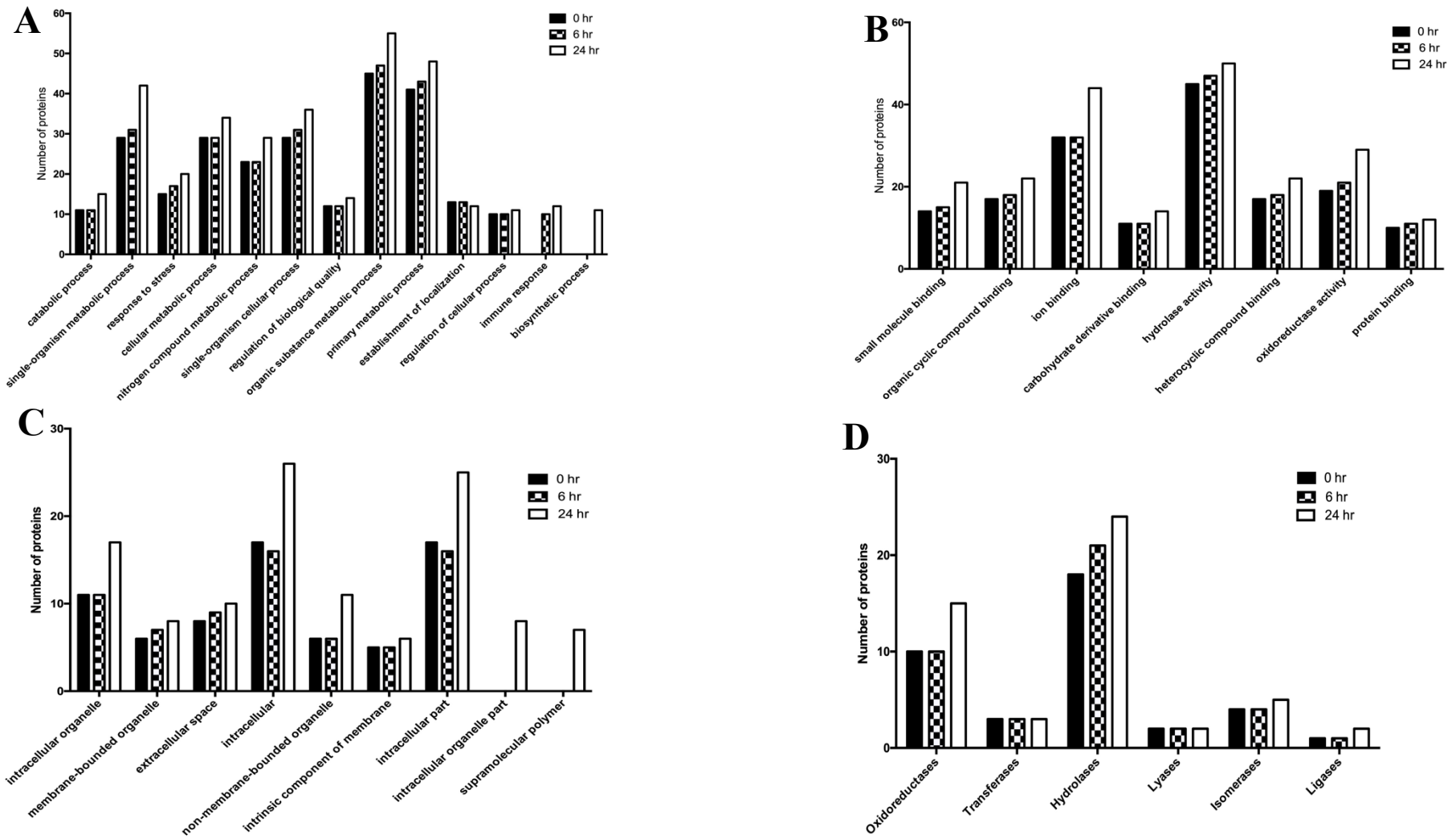

Fig. 3.12. Bar charts showing changes to number of proteins given biological processes (A) and molecular function (B), cellular component (C) at level 3 ontology and enzyme categories (D). Proteins were assigned groups based on involvement in biological processes, molecular function and cellular component for 0, 6 and 24 h *C. albicans* inoculated larvae.

3.11 Assessment of fungicidal activity of larval hemolymph on *C. albicans (ex vivo)*

In order to uncover the fate of *C. albicans* cells when first introduced into the larval hemolymph the fungicidal activity of hemolymph was determined by incubation of yeast cells (10^6 cells ml^{-1}) in different concentrations of hemolymph *ex vivo* over 24 h. There was a 76% decrease in the viability of *C. albicans* after incubation in 100% hemolymph ($0.23 \pm 0.03 \times 10^6$, $p < 0.05$) as compared to PBS ($0.99 \pm 0.01 \times 10^6$) after 0 h incubation. This effect was also observed after 4 h ($0.38 \pm 0.03 \times 10^6$, $p < 0.05$) and 6 h ($0.25 \pm 0.04 \times 10^6$ $p < 0.05$) incubation as compared to the control. However, incubation of yeast cells in 50% and 25% hemolymph after 0 h resulted in no significant decrease in *C. albicans* viability. Incubation of *C. albicans* in hemolymph (50% and 25%) for 2, 4 and 6 h resulted in a decrease in yeast viability. After 24 h, the growth of *C. albicans* in whole hemolymph remained below the control, however diluted hemolymph (50% ($1.35 \pm 0.23 \times 10^6$) and 25% ($1.91 \pm 0.08 \times 10^6$)) stimulated the growth of *C. albicans* (**Fig. 3.13**).

3.12 Proteomic response of *C. albicans* to *G. mellonella* hemolymph (*ex vivo*)

In order to understand how *C. albicans* responds to and survives the fungicidal activity of hemolymph and ultimately disseminates throughout the host, label-free quantitative proteomic analysis was conducted on the proteome of *C. albicans* exposed to *G. mellonella* hemolymph (100%) and PBS (control) for 6 h at 30 ^oC (**Fig. 3.14**). In total, 19696 peptides were identified representing 1231 proteins with two or more peptides and 786 (hemolymph treated versus PBS treated *C. albicans*) proteins were determined to be statistically significant differentially abundant (SSDA; ANOVA, $p < 0.05$) with a fold change of > 1.5 (260 increased and 526 decreased). A total of 361 proteins were deemed exclusive (i.e. with LFQ intensities present in all three replicates of one treatment and absent in all three replicates of the other treatment). These proteins were also used in statistical analysis of the total differentially expressed group following imputation of the zero values as described. After data imputation these proteins were included in subsequent statistical analysis. A principal component analysis (PCA) performed on all filtered proteins distinguished the hemolymph and PBS treated *C. albicans* samples indicating a clear difference between each proteome **(Fig. 3.15**).

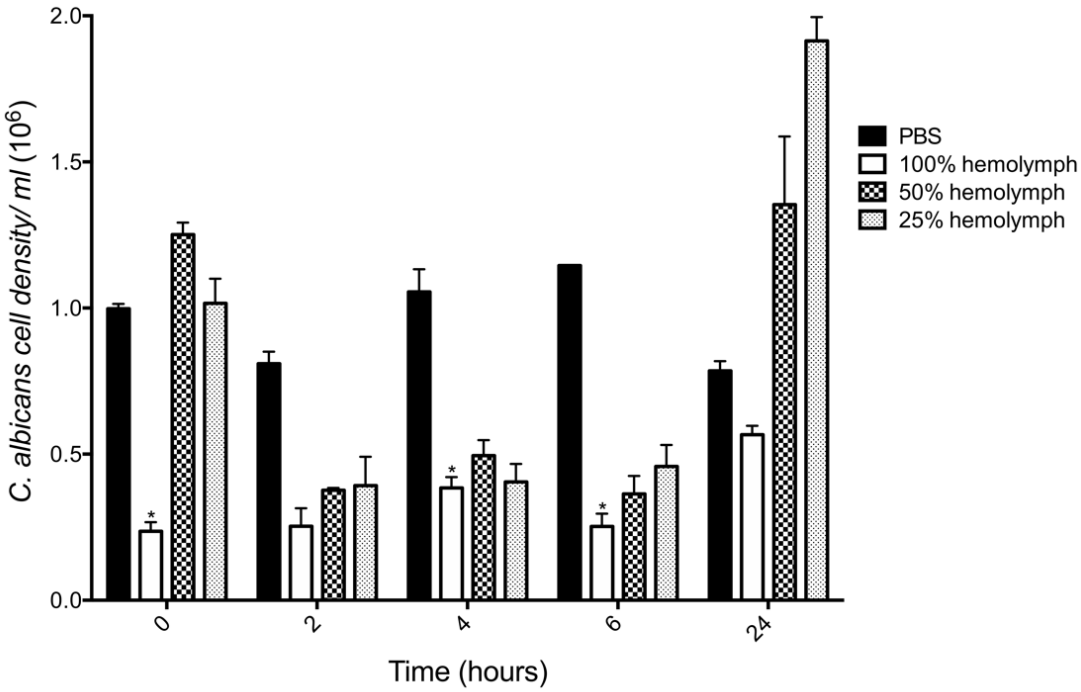

Fig. 3.13. Candidacidal activity of *G. mellonella* larval hemolymph *ex vivo*. *C. albicans* was incubated (30 °C) in varying concentrations (100, 50, 25%) of *ex vivo* hemocyte-free hemolymph or PBS and dilutions were plated on YEPD agar plates to assess viability. Incubation of *C. albicans* in 100% hemolymph decreased yeast cell viability by 76% after t = 0 incubation, this was also observed after 4 and 6 h. All values are the mean ± S.E of three independent experiments.

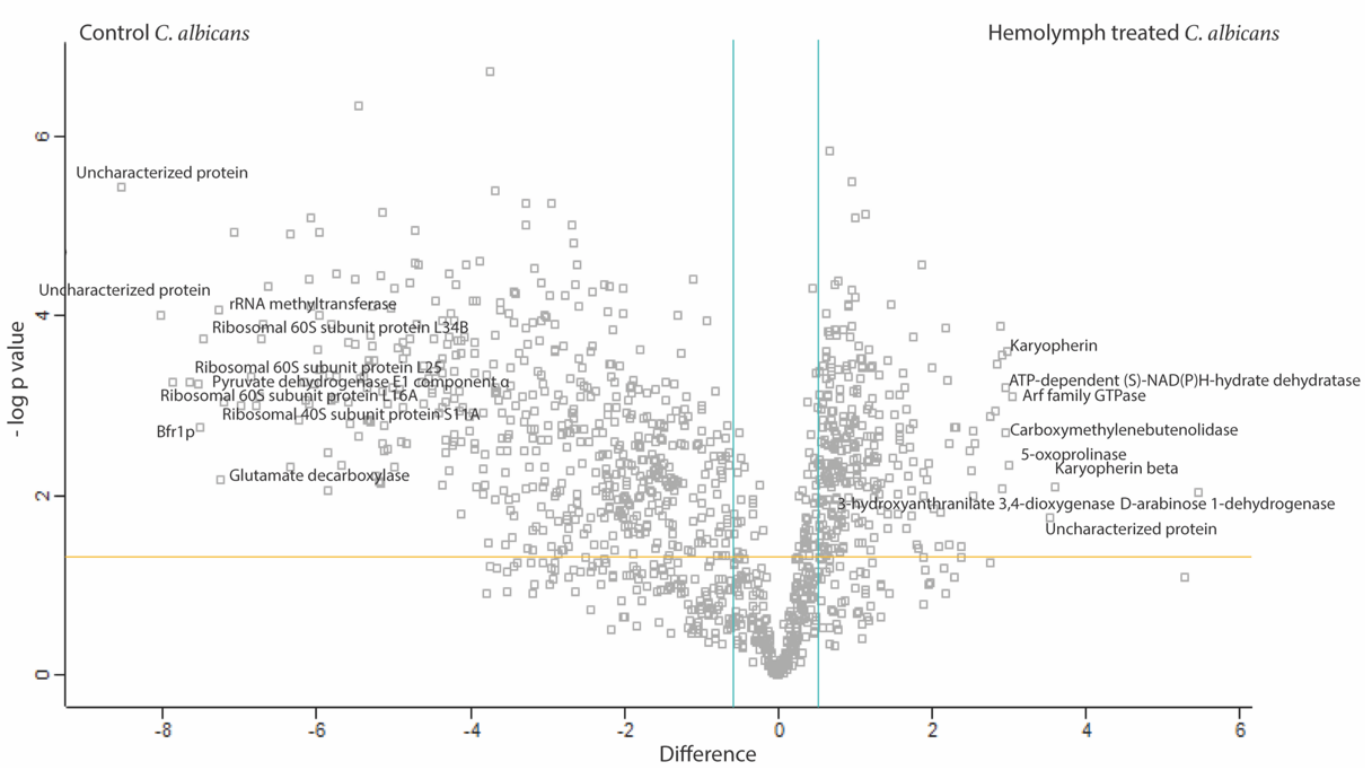

Fig. 3.14. Shotgun proteomics of responses of *C. albicans* (2.5×10^7 ml^{-1}) to *G. mellonella* hemolymph (100%) after 6 h and incubation at 30 °C. Volcano plots showing the distribution of quantified proteins according to p value (−log10 p-value) and fold change (log2 mean LFQ intensity difference). Proteins above the horizontal line are considered statistically significant (p value < 0.05) and those to the right and left of the vertical lines indicate relative fold changes ± 1.5. *C. albicans* responds to hemolymph by altering the abundance of a range of proteins associated with a variety of biological process (enrichment for; translation, glycolytic process, protein folding, oxidation-reduction process and interaction with host), molecular functions (structural constituent of ribosome, RNA binding, and metallopeptidase activity) and cellular components (cytoplasm, ribosome and cell surface).

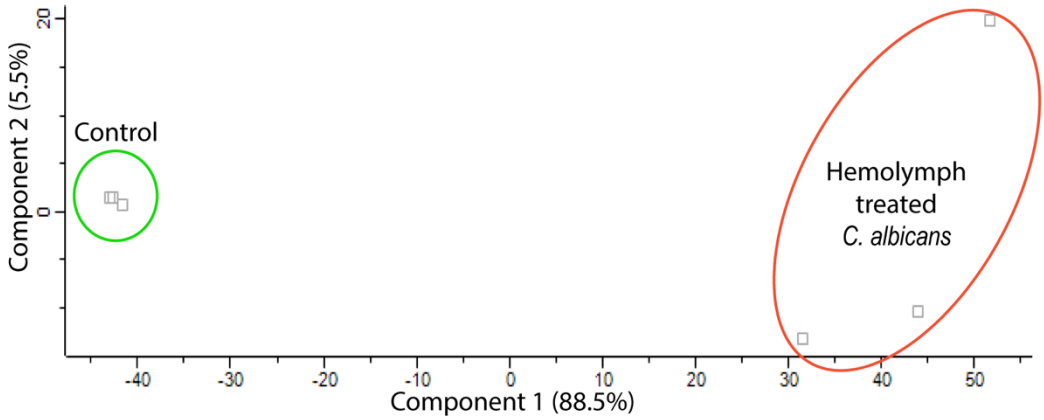

Fig. 3.15. Shotgun quantitative proteomic analysis of *C. albicans* incubated in *G. mellonella* 100% hemolymph for 6 h at 30 ºC. Principal component analysis (PCA) of *C. albicans* incubated in 100% hemolymph and PBS for 6 h with a clear distinction between control and treatment.

FungiFun analysis revealed enrichment for biological processes such as translation (p = 6.6882e-35), glycolytic process (1.8762e-7), protein folding (1.1493E-06), oxidation-reduction process (9.7092E-06) and interaction with host (0.00022661) in the *C. albicans* incubated in hemolymph. Molecular functions such as structural constituent of ribosome (p = 3.2372e-19), RNA binding (p = 0.000003489) and metallopeptidase activity (0.013756). Cellular components of the cytoplasm (p = 2.7786e-36), ribosome (p = 1.7021e-19) and cell surface (p = 1.5316e-9) were also enriched within the SSDA proteins from *C. albicans* incubated in hemolymph *ex vivo* (**Table A3.5).** These results were confirmed by STRING analysis (**Fig. 3.16**).

The top 10 proteins increased in abundance in *C. albicans* incubated in hemolymph were D-arabinose 1-dehydrogenase (+44 fold), karyopherin β (+12 fold), uncharacterised protein (+11.5 fold), Arf family GTPase (+8 fold), 5-oxoprolinase (+8 fold), karyopherin (+8 fold), carboxymethylenebutenolidase (+8 fold), ATP-dependent (S)-NAD(P)H-hydrate dehydratase (+8 fold), 3-hydroxyanthranilate 3,4-dioxygenase (+8 fold) and Leu42p (+7.5 fold) **(Table A3.6A)**. The top 10 proteins decreased in abundance in *C. albicans* incubated in hemolymph were uncharacterised protein (-374 fold), uncharacterised protein (-

259.5 fold), ribosomal 60S subunit protein L16A (-235 fold), ribosomal 60S subunit protein L25 (-201.5 fold), pyruvate dehydrogenase E1 component subunit α (-187 fold), Bfr1p (-184 fold), ribosomal 60S subunit protein L34B (-176 fold), rRNA methyltransferase (-155.5 fold), glutamate decarboxylase (-152 fold) and ribosomal 40S subunit protein S11A (-149 fold**) (Table A3.6B).**

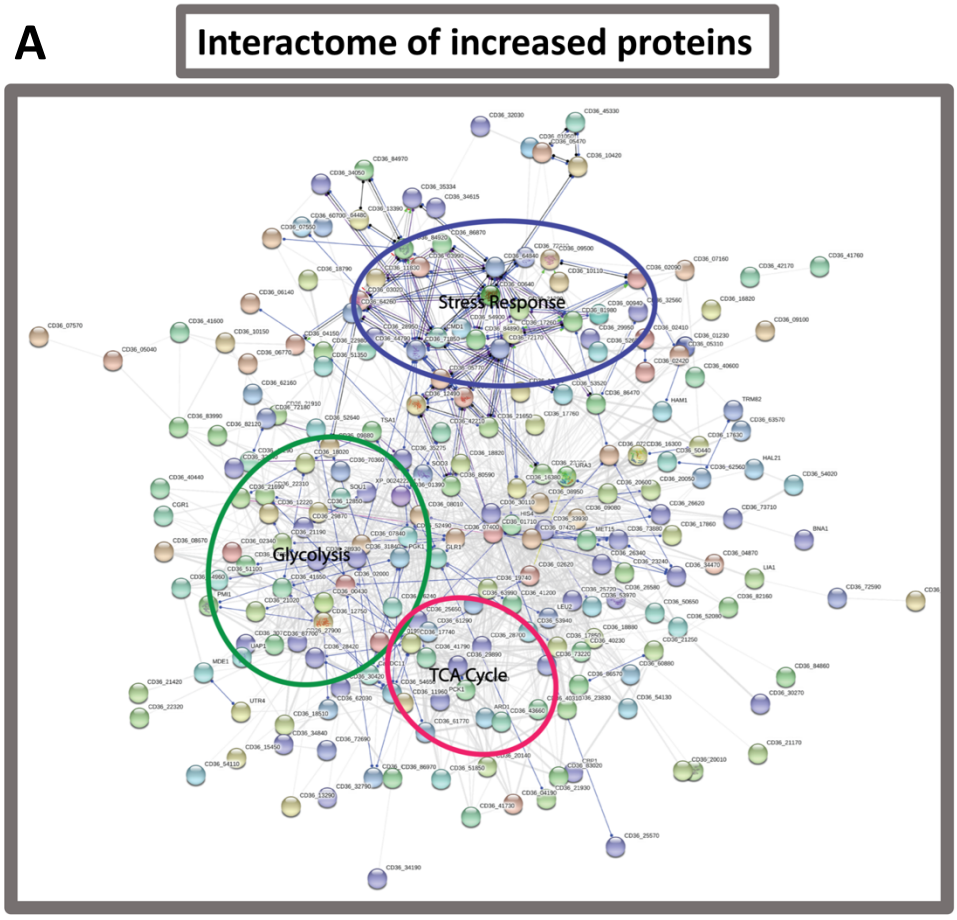

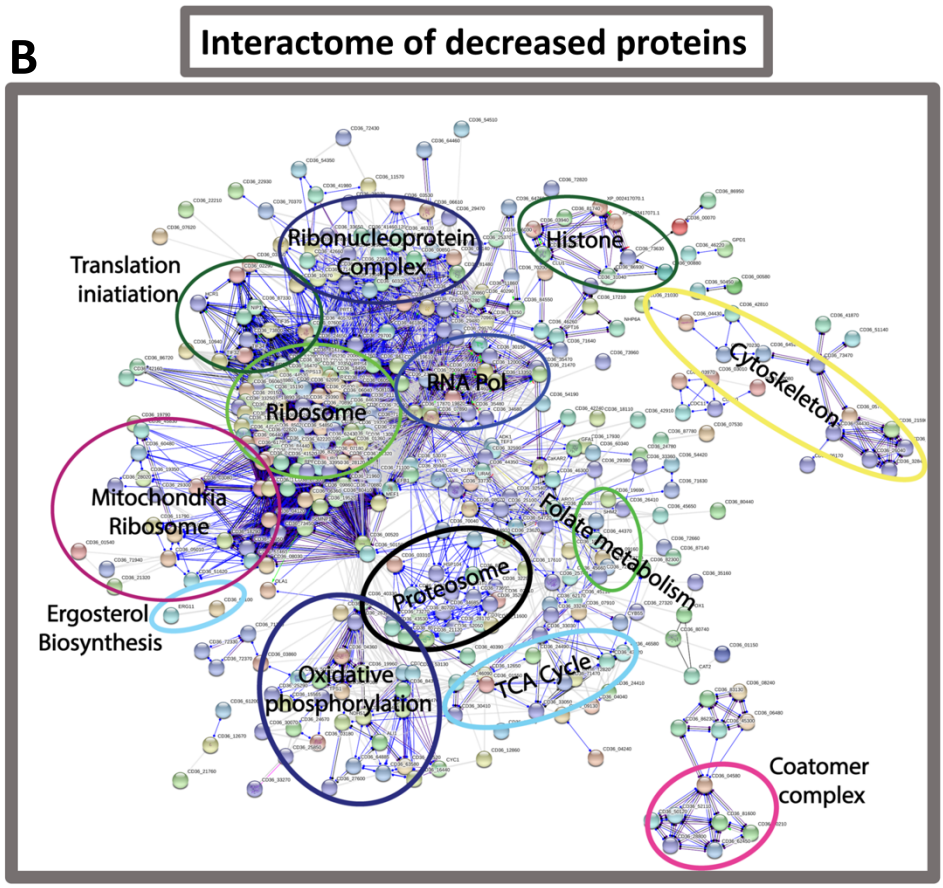

Fig. 3.16. Interactome of proteins increased (**A**) and decreased (**B**) in abundance in *C. albicans* incubated in *G. mellonella* hemolymph. Protein interaction information was obtained from the STRING database using gene lists extracted for statistically significant differentially abundant (SSDA) proteins from pair wise t-tests ($p < 0.05$). Each node represents a protein and each connecting line represents an interaction, the extent of evidence for which is represented by the width of the line. Statistically enriched biological process Gene Ontology descriptors were examined to identify clusters of proteins enriched within SSDA protein lists.

3.13 Effect of empirical antifungals on reducing symptoms associated with *C. albicans* systemic infection

3.13.1 Effect of amphotericin B and caspofungin on the survival of *C. albicans* infected larvae

Larvae injected with 20 µl of PBS, amphotericin B (30 mg kg^{-1}) or caspofungin (8.75 mg kg^{-1}) showed no decrease in viability after 96 h. Larvae that were infected with *C. albicans* and followed up with PBS one h later resulted in decreased survival at 24 (70 ± 5.77%), 48 (55 ± 2.88), 72 (28.33 ± 4.41%) and 96 (5 ± 1.05%) h. Larvae followed up one h later with amphotericin B at a dose of 30 mg kg^{-1} (100 ± 6.34%, $p < 0.0001$) and 3 mg kg^{-1} (100 ± 2.93%, $p < 0.0001$) displayed enhanced survival relative to those followed up with PBS at 24 h post infection. This effect was also observed for amphotericin B at a dose of 30 mg kg^{-1} (100 ± 2.44%, $p < 0.0001$) and 3 mg kg^{-1} (100 ± 5.34%, $p < 0.0001$) at 48 h post infection. Interesting, larvae that received a dose of 30 mg kg^{-1} amphotericin showed viability of 80 ± 4.51% ($p < 0.0001$) 96 h post infection as compared to 5 ± 1.05% in the PBS treated.

Larvae that were followed up with caspofungin at a dose of 8.75 mg kg^{-1} (24 h; 100% ± 4.54% [$p < 0.0001$] 48 h; 80% ± 4.87% [$p < 0.0001$]) and 0.875 mg kg^{-1} (24 h; 100% ± 3.59% [$p < 0.0001$], 48 h; 60% ± 4.65%) also showed increased survival relative to the PBS injected control following *C. albicans* infection at 24 and 48 h, respectively.

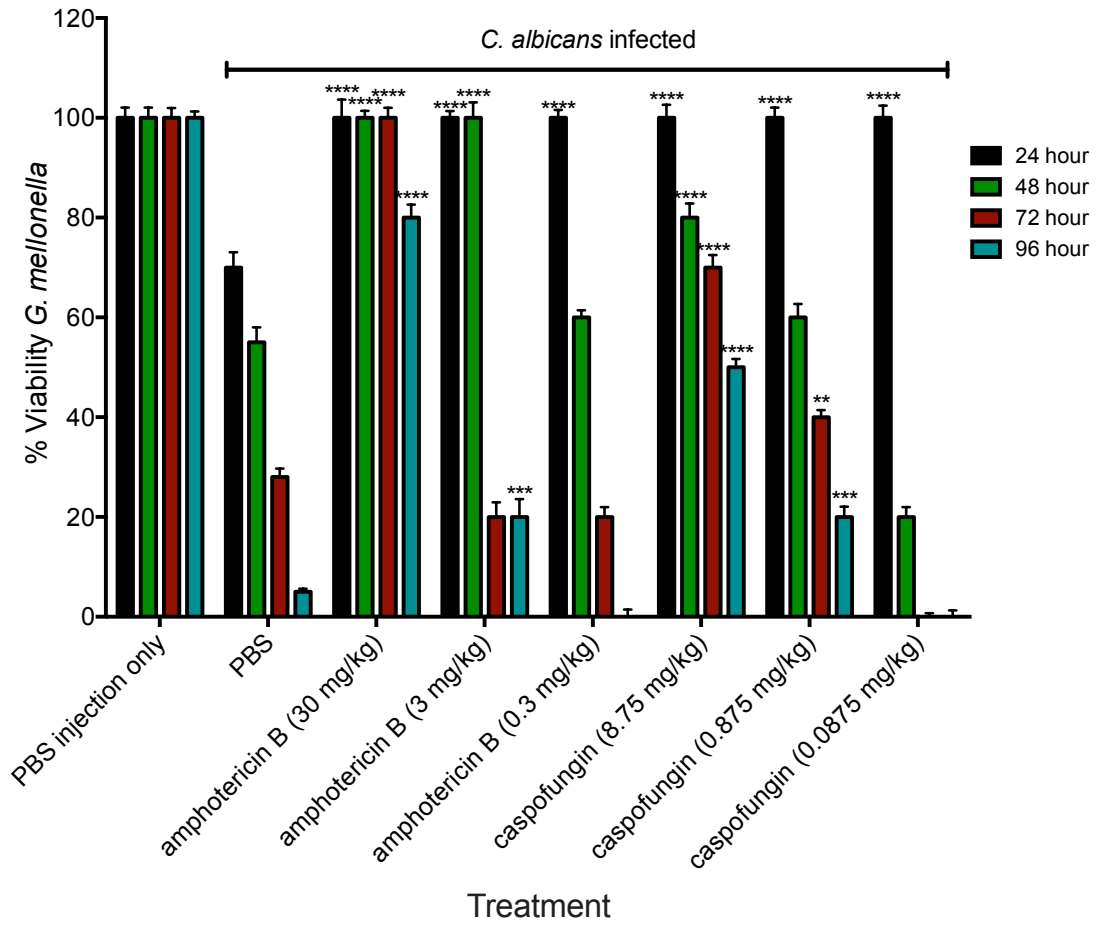

Fig. 3.17. Survival of *G. mellonella* larvae following infection by *C. albicans* and then administrated anti-fungal agents. Larvae were inoculated with *C. albicans* (5×10^5 20 μl^{-1}) and followed with PBS or varying doses of amphotericin B (3 – 30 mg kg^{-1}) or caspofungin (0.087 – 8.75 mg kg^{-1}). Larvae were incubated at 30 ^oC and viability assessed over 96 h. All values are the mean ± S.E. of three independent experiments.

3.13.2 Cryo-imaging of infected and anti-fungal treated larvae

The efficacy of antifungal agents (amphotericin B and caspofungin) in reducing the symptoms associated *C. albicans* infection was assessed by cryo-imaging. *C. albicans* causes significant melanisation of *G. mellonella* larvae 24 h post infection. However, the addition of amphotericin B (3 mg kg^{-1}) one h post infection reduced melanisation of the cuticle and the appearance of nodules throughout the larvae. This effect was also observed at a lower concentration with caspofungin (0.875 mg kg^{-1}) (**Fig. 3.18**).

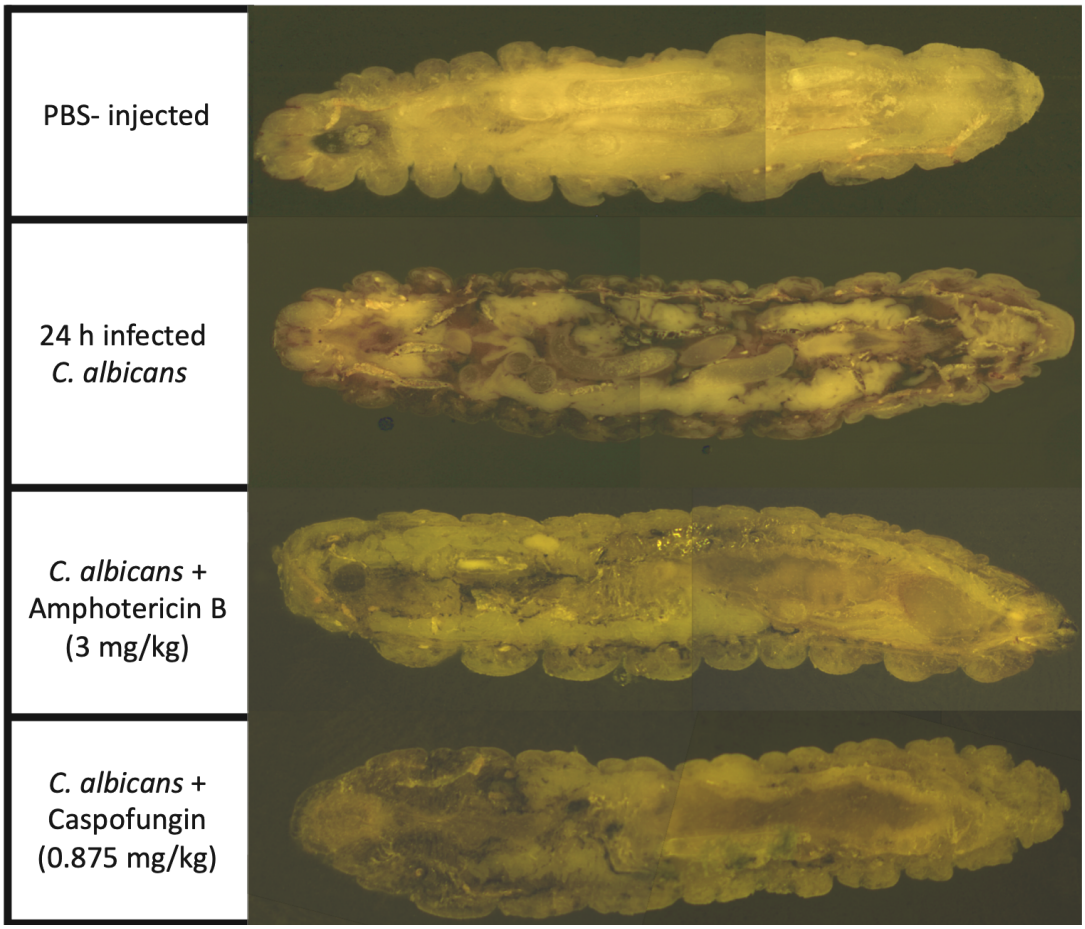

Fig. 3.18. Cryo-imaging of *G. mellonella* larvae infected with *C. albicans* followed by administration of antifungal therapy. Larvae were inoculated with PBS or *C. albicans* (5×10^5 20 μl^{-1}) and followed up one-h later with 20 µl of amphotericin B (3 mg kg^{-1}) or caspofungin (0.875 mg kg^{-1}). Larvae were incubated at 30 ^oC for 24 h and prepared for cryoviz imaging.

3.14 Discussion

The similarities between the immune responses of insects and the innate immune response of mammals can be further exploited through using insects as models to study disease development and progression (Kavanagh and Reeves, 2004; Browne *et al.,* 2013) *G. mellonella* larvae infected with *Listeria* show neural pathologies similar to those in mammals thus opening the possibility of examining neural disease and repair mechanisms in insects (Mukherjee *et al.*, 2013). This finding could enable the use of *G. mellonella* larvae for studying pathogenesis of other pathogens such as *S. aureus* or *C. albicans*.

C. albicans possesses an arsenal of virulence factors to establish a focal point of infection, adhere to and invade host cells, detoxify the cellular immune response and degrade components of the humoral immune response (Hebecker *et al.*, 2014). The *C. albicans* cell wall is also a complex mesh of polysaccharides, proteins and sterols which help to form a physical barrier against the immune response but also signals are relayed from the wall depending on the stimulus in order for the fungal cell to adequately mount an appropriate stress response (Ruiz-Herrera *et al.*, 2006).

The results presented here describe the development of *C. albicans* in *G. mellonella* larvae over 24 h and detail the initial cellular and humoral immune responses that the insect employs to limit fungal development. Infection with *C. albicans* resulted in a dose dependent decrease in larval viability over 72 h. An inoculum of 1×10^5 resulted in no change in viability, while an inoculum of 5×10^5 20 μl^{-1} decreased larval viability at 24 (70 ± 5.77%), 48 (55 ± 2.88) and 72 (28.33 ± 4.41%) h (**Fig. 3.2**). Following inoculation with *C. albicans* (5×10^5 20 μl^{-1}), yeast cell density decreased (**Fig. 3.3**) between 0 and 2 h which may be associated with nodulation by hemocytes at the focal point of infection (Browne *et al.,* 2013; Mesa-Arango *et al.*, 2013; Gago *et al.*, 2014). The hemocyte density increased at 6 h possibly due to the release of sessile hemocytes normally attached to the fat body and inner surface of the hemocoel of larvae (**Fig. 3.4**) (Ratcliffe, 1985; Bergin *et al.,* 2003). It has been demonstrated that thermal or physical stress can lead to an elevated hemocyte density and this can be associated with decreased susceptibility to infection (Mowlds *et al.,* 2008; Browne *et al.*, 2015). Yeast cell proliferation in

larvae did not commence until 8 h post infection and then rose to $1.68 \pm 0.15 \times 10^7$ ml^{-1} at 24 h and $9.38 \pm 1.7 \times 10^7$ ml^{-1} at 48 h.

In order to characterise the changes in the hemocyte population in larvae, larvae were administered β-glucan which also produced a rise in circulating hemocyte density after 6 h (**Fig. 3.5)**. Flow cytometric analysis demonstrated an increase in the relative abundance of large, non-granular cells (P5) at 6 h (**Fig. 3.6**). At 24 h post β-glucan administration there was an increase in the relative abundance of small, granular cells (P1). Hemocytes from larvae administered β-glucan for 6 or 24 h demonstrated a superior ability to kill *C. albicans* cells thus indicating a higher proportion of microbicidal active cells in the respective populations (**Fig. 3.7**).

The use of cryo-imaging revealed infection by *C. albicans* commenced immediately with extensive melanisation around the area of inoculation at 6 h (**Fig. 3.8**). There were discrete nodules at the middle of the larvae and these consisted of viable fungal hyphae. By 24 h larvae were heavily infected with disseminated *C. albicans* as observed by extensive cuticular melanisation and the appearance of large nodules throughout the host. A similar process has been documented in patients with chronic candidiasis where immune cells surround the pathogen and initiate an inflammatory response to prevent dissemination (Misme-Aucouturier *et al.*, 2017). Dissection of nodules at 6 and 24 h revealed the presence of hyphae at 6 h with the appearance of yeast cells at 24 h (**Fig. 3.9**).

Quantitative shotgun proteomics was employed to analyse the response of *G. mellonella* larvae to *C. albicans* infection at 6 and 24 h (**Fig. 3.11**). Six h following *C. albicans* infection there was an increase in the abundance of immune proteins. These are constitutively expressed and augmentable upon microbial detection for example prophenoloxidase-activating proteinase-1 (+5 fold) contributes to insect immunity by converting prophenoloxidase to phenoloxidase which participates in melanotic encapsulation, wound healing, and cuticle sclerotisation (Zou *et al.,* 2005). Cecropin-A (+4.5 fold) is a 37 amino acid antimicrobial peptide first isolated from *H. cecropia*. It demonstrates antibacterial activity against multidrug resistant *A. baumannii* and *P. aeruginosa*, induces *C. albicans* apoptosis and recently has been shown to have immunomodulatory effects on macrophages (Lee *et al.,* 2015; Yun

and Lee, 2016). Immune related hdd1 (+4 fold) was found up-regulated in *Hyphantria cunea* 2 h following inoculation of *E. coli* (Shin *et al.*, 1998).

Muscle proteins (muscle protein 20-like protein, tropomyosin 2, calponin, troponin I, troponin T, troponin C, β actin) were increased from 30-fold to 175-fold in hemolymph after 24 h and may be associated with tissue disruption due to fungal proliferation and hyphal formation. Antimicrobial peptides and immune proteins (peptidoglycan recognition protein - LB, gloverin, hdd11, cecropin-D-like peptide, moricin-like peptide B, hemolin) were increased in abundance in response to *Candida* infection at 24 h. Gloverins are glycine rich, heat stable antibacterial polypeptides believed to bind LPS and possibly components of the fungal cell wall. It was previously demonstrated that *E. coli* but not yeast or saline injection induced gloverin expression in *B. mori* (Yi *et al.*, 2013). Moricins are secreted pro-peptides under the control of (NF-κB)/Rel and GATA transcription factors and are activated via proteolysis and increase the permeability of bacterial and fungal membranes. *G. mellonella* moricins are highly active against yeasts and filamentous fungi (Brown *et al.*, 2008). Immunoglobulin superfamily member hemolin was induced by *Candida* challenge and has been shown to act as a pattern recognition receptor in insects (Yu and Kanost, 2002; Browne *et al.*, 2015).

Cellular stress proteins (glutathione-S-transferase-like protein, mitochondrial aldehyde dehydrogenase, heat shock protein hsp21.4, heat shock protein 90, putative mitochondrial Mn superoxide dismutase) were increased from 4-fold to 114-fold in hemolymph at 24 h and function to protect cells from geno- and proteotoxicity. Mitochondrial aldehyde dehydrogenase is important in the protection against nitrate induced oxidative stress in *G. mellonella* (Maguire *et al.*, 2017a). Immune related proteins (e.g. β-1,3 - glucan recognition protein precursor (29 fold) and lysozyme-like protein 1 (5 fold)) were decreased in abundance at 24 h, possible due to binding of yeast cells and resulting in decreased abundance in hemolymph. Proteomic profiling of RAW 264.7 macrophages exposed to *C. albicans* demonstrated increased abundance of tropomyosin, β-actin, elongation factor 2, triosephosphate isomerase, heat shock protein 71 kDa, annexin A1 and glyceraldehyde-3-phosphate dehydrogenase which are indicative of oxidative stress, immune response, unfolded

protein response and apoptosis (Martínez-Solano *et al.*, 2009; Reales-Calderón *et al.*, 2012).

Proteins released by *C. albicans* during infection of larvae were also analysed. In total 101 *C. albicans* proteins were found in hemolymph during infection and biological processes such as interaction with host (p = 1.4029e-8), cellular response to heat (p = 0.040686) and pathogenesis (p = 0.032202) were enriched. Interestingly, cell wall protein 1 is a heme-binding protein involved in heme-iron utilisation and required for biofilm formation and is preferentially expressed during the mycelium growth phase, induced by iron starvation and ciclopirox (Weissman and Kornitzer, 2004; Sigel *et al.*, 2005; Pérez *et al.*, 2006). Peroxiredoxin is a thiol specific peroxidase that catalyses the reduction of hydrogen peroxide and also plays a role in cell wall protection against oxidative stress (Urban *et al.*, 2005). Enolase 1 binds to plasminogen and results in enhanced invasion of human brain microvascular endothelial cells (Jong *et al.*, 2003). Heat shock protein SSA1 binds to histatin 5, an important antimicrobial peptide against *C. albicans* oral infection (Li *et al.*, 2003). Cell surface mannoprotein MP65 which is a major antigen and induces T- cell proliferation, is required for hyphal morphogenesis and surface adherence during infection (Pietrella *et al.*, 2006; Sandini *et al.*, 2011). Antigenic secreted protein RBT4 acts as a virulence factor during infections and plays a role in protection against phagocyte attack (Braun *et al.*, 2000). Moreover, a range of cell wall derived proteins were detected in hemolymph such as chitin synthase, cell wall protein PGA59, cell wall protein IFF5 and secreted β-glucosidase SUN41. Proteins associated with translation (translation initiation factor eIF2B subunit Δ, translation factor GUF1, translation elongation factor 1 subunit β) and the ribosome (60S ribosomal protein L27) were detected in hemolymph and may have been released from *C. albicans* during cell death.

Exposure of yeast cells to larval hemolymph resulted in significant reduction in viability. At t = 0, 100% hemolymph significantly reduced the viability of *C. albicans* by 76% ($0.23 \pm 0.03 \times 10^6$, $p < 0.05$) as compared to the PBS treatment ($0.99 \pm 0.01 \times 10^6$) (**Fig. 3.13**). This indicates that the candicidal activity of hemolymph is highly active even in naïve larvae. *C. albicans* viability remained significantly lower than that of the control at 4 and 6 h. *G. mellonella* hemolymph is

rich in antimicrobial peptides and proteins such as cecropins, moricins, gloverins, 6-tox, lysozyme, gallerimycin and galliomicin. Furthermore, cecropin-A induced apoptosis of *C. albicans* by disrupting intracellular ion balance and the glutathione antioxidant system (Yun and Lee, 2016). A range of these AMPs are inducible thus indicating that naïve hemolymph has significant constitutively expressed antifungal molecules.

In order to characterise the molecular responses of *C. albicans* to hemolymph, protein was extracted from the yeast cells after 6 h exposure to hemolymph *ex vivo* and subjected to mass spectrometry (**Fig. 3.14, 3.15**). STRING analysis of proteins decreased in abundance from *C. albicans* cells incubated in hemolymph revealed enrichment for biological processes associated with the ribosome, translation and ribonucleoprotein complex (**Fig. 3.16**). A decrease in these proteins indicates a decrease in global protein synthesis. Gene expression associated with protein synthesis was decreased late during experimental *C. albicans* bloodstream infection in mice and this decrease in protein synthesis was associated with an increase in gene expression associated with glycolysis, oxidative stress, fermentation and genes associated with interaction with the host which it may use to escape from the bloodstream (Fradin *et al.*, 2003). Larval hemolymph induced increases in the abundance of *C. albicans* proteins associated with the same processes. Incubation of *C. albicans* in human serum and *G. mellonella* hemolymph activate similar processes in order for the fungal cell to survive the host. Furthermore, proteins associated with oxidative phosphorylation, the TCA cycle and the mitochondria were all decreased in abundance probably resulting in an overall decrease in cellular respiration (Gyurko *et al.*, 2000). *C. albicans* deficient in respiration were resistant to histatin 5 and disruption of mitochondria also allows increased growth in the presence of amphotericin B (Gyurko *et al.*, 2000; Geraghty and Kavanagh, 2003). Therefore, a decrease in mitochondrial respiration may allow the cell to withstand the hostile environment within hemolymph during infection.

Proteins associated with an oxidative stress response such as thioredoxin, thioredoxin reductase, superoxide dismutase, glutathione-disulfide reductase, thioredoxin peroxidase were increased in abundance in hemolymph-incubated *C. albicans*. There is also an increase in a range of heat shock proteins (hsp) such as hsp

homolog SSE1, hsp SSA1, hsp SSA2 and hsp SSC1. Hsp SSA1 and SSA2 induce host cell endocytosis which lead to increased virulence (Sun *et al.*, 2010). They also play a role in resistance to antimicrobial peptides and antifungal agents (Cho *et al.*, 2003; Li *et al.*, 2003; Nagao *et al.*, 2012). Interestingly, hsp SSA1 and peroxiredoxin TSA1 were also found secreted into *G. mellonella* hemolymph during infection in this study. Candidapepsin-9 is a glycosylphosphatidylinositol-anchored protease and important virulence factor found to activate human neutrophils more effectively than any other secreted aspartyl proteinase (Hornbach *et al.*, 2009) and was increased 1.8 fold in *C. albicans* incubated in hemolymph in this study.

Lastly, the efficacy of empirical antifungal agents (amphotericin B and caspofungin) was assessed on the survival and reduction of symptoms associated with disseminated *C. albicans* infection. Caspofungin and other echinocandins inhibit the synthesis of 1,3- β-glucan, an important polymer in the biosynthesis of the fungal cell wall, thus toxicity is low in humans and it displays excellent *in vivo* activity (Petraitiene *et al*., 2002). Amphotericin B is well known for its *in vivo* efficacy and binds of ergosterol in the fungal cell membrane, resulting in pore formation and eventually fungal cell death. Amphotericin is equally known for its toxic side effects such as nephrotoxicity which it exerts through the binding of cholesterol which is present at high levels in kidney cell membranes (Fanos and Cataldi, 2014).

Both amphotericin B (30 and 3 mg kg^{-1}) and caspofungin (8.75 and 0.875 mg kg^{-1} which correspond to 70 and 7 mg m^2, respectively) enhanced survival of larvae at clinically relevant doses (**Fig. 3.17)**. Currently, the guidelines for treatment of candidaemia in non-neutropenic patients is amphotericin B (3 mg/kg/day^{-1}) or caspofungin (70 mg loading dose /50 mg once daily) (Allen, 2010; Cornely *et al.*, 2012; Pea and Lewis, 2018). Cryo-imaging revealed significantly less melanisation and nodule formation in larvae administered amphotericin B (3 mg kg^{-1}) or caspofungin (0.875 mg kg^{-1}) as compared *C. albicans* infected control larvae (**Fig. 3.18)**.

The response of *G. mellonella* larvae to infection by *C. albicans* can be divided into two phases. In phase 1, extending from 0 – 6 h, there was a decrease in

fungal load per larva correlating with an increase in hemocyte density and increased abundance of antimicrobial peptides and immune proteins. In phase 2 (6 – 24 h) yeast cell proliferation occurs, the hemocyte population declines, larval death occurs and proteomic analysis reveals increased abundance of proteins associated with tissue degradation. In murine invasive candidiasis the kidney is the principle site of dissemination which launches an acute phase response consisting of complement activation, cellular recruitment, protease inhibition and opsonisation which is analogous to the initial cellular and humoral response of *G. mellonella* to infection and essential for resistance to *C. albicans* infection (Tsoni *et al.*, 2009; MacCallum, 2009). In a fatal mouse model of systemic invasive candidiasis, yeast cells quickly disseminate from blood to distal locations including the kidney. Inoculation results in an early robust peripheral blood neutrophilia which subsequently decreased between day 4 and 7, followed by murine death (Lionakis *et al.*, 2011). The murine response in the first 24 h is crucial as the kidney is relatively neutropenic. The results presented here found a reduction in hemocyte density possibly as a result of local accumulation (nodulation) of hemocytes, followed by an increase in the population of granular cells (P1) at 24 h. The early stage of detection and action during systemic infection may be non-specific (e.g. AMPs, melanisation, nodulation) in order to gauge the extent of fungal burden and allocate immune recourses accordingly. In the second stage from 6 to 24 h, a large scale, specific response (e.g. granular cells, increased AMP) is launched to an already uncontrollable and disseminated fungal infection (e.g. larval death, increased abundance of muscle proteins).

From the pathogen perspective *C. albicans* disseminates through *G. mellonella* larvae in a similar way to mammals. The effect of hemolymph on *C. albicans* activates processes associated with a decrease in protein synthesis and increased proteins associated with pathogenesis, glycolysis and responses to oxidative stress. Some of these proteins are secreted and detectable in hemolymph during infection and play a role in pathogenesis. These results demonstrate that *G. mellonella* larvae are a useful model to study the pathogenesis of *C. albicans* infection while overcoming some of the disadvantages (e.g. no legal/ethical considerations, easy to use and cost effective) associated with using mammalian systems.

Chapter 4

Characterisation of *Galleria mellonella* larvae as a model to study the development of *Staphylococcus aureus* infection

4.1 Introduction

Staphylococcus aureus is a facultative anaerobic, Gram- positive bacterium which colonise approximately 30% of the world's population on a range of body sites. *Staphylococcus* species are the most frequent cause of biofilm – medical device related infections most likely due to them being a body commensal (Otto, 2008). *S. aureus* colonisation is mostly non-symptomatic, however in the correct situation it is capable of causing a wide variety of diseases from furuncles and boils to serious infections such as pneumonia, toxic shock syndrome and endocarditis (Tong *et al.*, 2015).

The virulence of *S. aureus* is multifaceted and due to an arsenal of effectors which enable interactions with the host, immune cell evasion and the induction of tissue damage (Lowy, 1998). *S. aureus* 33 kDa protein α-toxin can induce pro-inflammatory conditions and pore formation in mammalian cells resulting in necrosis. It has been suggested that α-toxin creates an enhanced infection microenvironment for disease progression (Bhakdi and Tranum-Jensen, 1991). A range of superantigens are able to induce inflammation which can result in toxic shock syndrome and sepsis by non-specific activation of T-cell proliferation through interactions with MHC class II molecules on antigen presentation cells (Spaulding *et al.*, 2013). *S. aureus* can inhibit the mammalian complement pathway via Chemotaxis Inhibitory Protein of Staphylococci binding of the C5a receptor and Staphylococcal Complement Inhibitor blocking of C3 convertase activity (Jongerius *et al.*, 2007; Burman *et al.*, 2008). Coagulase and von Willebrand factor binding protein activate fibrin clot formation, facilitating the formation of staphylococcal aggregates in the blood and this is mediated by clumping factors A and B (Moreillon *et al.*, 1995; Hartleib *et al.*, 2000).

Many experimental *in vivo* systems to characterise *S. aureus* infection dynamics have been developed and include cutaneous (Bunce *et al.*, 1992), renal (Weiss *et al.*, 2004), sepsis in mice (Tarkowski *et al.*, 2001) and endocarditis in rats (Santoro and Levison, 1978). Alternative systems are also used to study the development of *S. aureus* infection. These include models to study bloodstream infection and pathogenesis using zebrafish larvae (Prajsnar *et al.*, 2008) and digestive tract infection in *Caenorhabditis elegans* (Sifri *et al.*, 2003). The aim of

this Chapter was to examine the interaction of *S. aureus* with the larval immune response and to characterise similarities with the mammalian response in order to better establish this system as a model for studying *S. aureus* infection processes (**Fig. 4.1**).

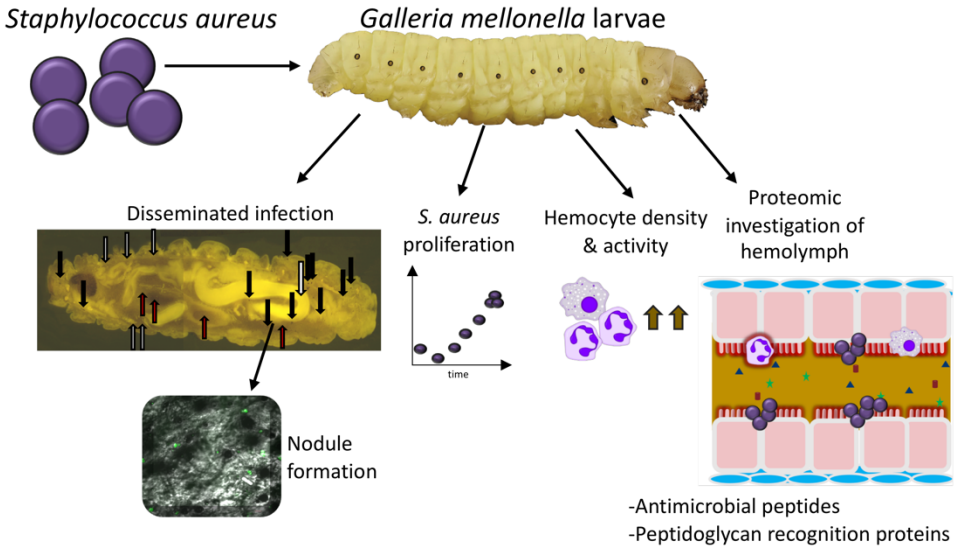

Fig. 4.1. Graphical abstract for Chapter 4.

4.2 Response of *G. mellonella* larvae to *S. aureus* infection

Larvae were infected with an inoculum of *S. aureus* ($2 \times 10^4 - 2 \times 10^6$ cells larva^{-1}), incubated at 37 ºC and viability was assessed over 72 h. An inoculum of 2×10^4 cells larva^{-1} resulted in no change in larval viability over 72 h. An inoculum of 2×10^5 cells larva^{-1} resulted in no change in larval viability over 24 h, however at 48- and 72-h viability was reduced to 96.66 ± 3.33% and 84.43 ± 2.94%, respectively. An inoculum of 2×10^6 cells larva^{-1} resulted in the largest decrease in larval viability at 80 ± 5.77% at 24 h, 55.93 ± 5.55% at 48 h and 10.23 ± 2.97% at 72 h as compared to the PBS injected control (**Fig. 4.2**).

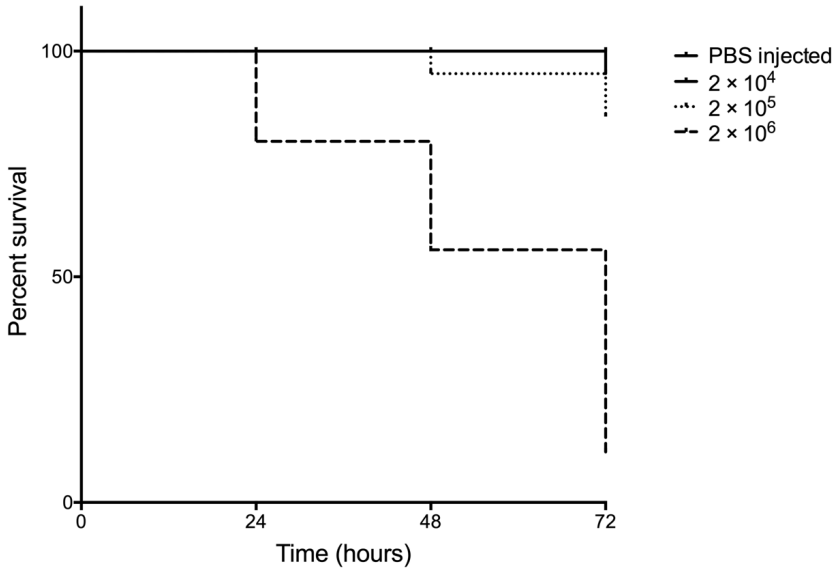

Fig. 4.2. Effect of *S. aureus* cells on viability of *G. mellonella* larvae over 72 h. *G. mellonella* larvae were inoculated with 20 µl *S. aureus* at doses ranging from 2×10^4 to 2×10^6 incubated at 37^{o}C and viability assessed over 72 h.

Between 4 and 6 h post infection *S. aureus* colony forming units (c.f.u.) larva^{-1} increased from $3.14 \pm 0.19 \times 10^5$ to $5.08 \pm 0.28 \times 10^5$ ($p < 0.01$). There was also an increase in *S. aureus* c.f.u. larva^{-1} at 24 ($1.31 \pm 0.11 \times 10^8$, $p < 0.01$), 48 ($2.76 \pm 0.18 \times 10^8$, $p < 0.01$) and 72 ($5.83 \pm 0.44 \times 10^8$, $p < 0.01$) h (**Fig. 4.3**).

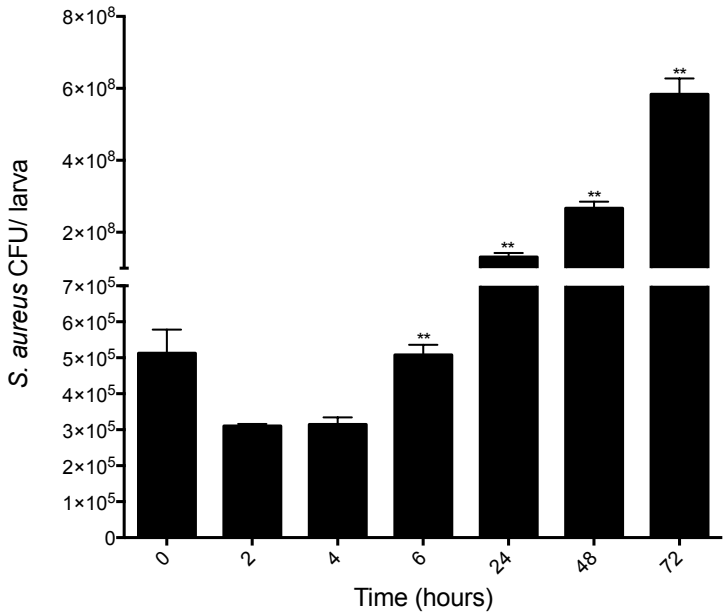

Fig. 4.3. *S. aureus* c.f.u. larva^{-1} obtained from *G. mellonella* larvae infected with *S. aureus* cells (2×10^6 larva^{-1}) over 72 h. Infection with *S. aureus* resulted in an increase in bacterial load in larvae from 6 until 72 h as determined by plating on nutrient agar plates. Statistical analysis was carried by comparing each time point to the previous time point (*: $p < 0.05$, ** $p < 0.01$). All values are the mean ± S.E. of three independent experiments.

4.3 Dissemination of *S. aureus* infection through larvae

Cryo-imaging was employed to visualise the stages of invasion and dissemination of *S. aureus* through *G. mellonella* larvae. Larvae were inoculated (white arrow) with viable *S. aureus* (2×10^6 per 20 µl) as described (section 2.5.1). Small discrete nodules appeared around the perimeter of the hemocoel 6 h post infection (black arrows) indicating dissemination of *S. aureus* from the site of infection. By 24 and 48 h there was extensive melanisation (red arrows) of larval tissue. The formation of large nodules at the site of inoculation was also apparent at 24 and 48 h post infections (**Fig. 4.4**).

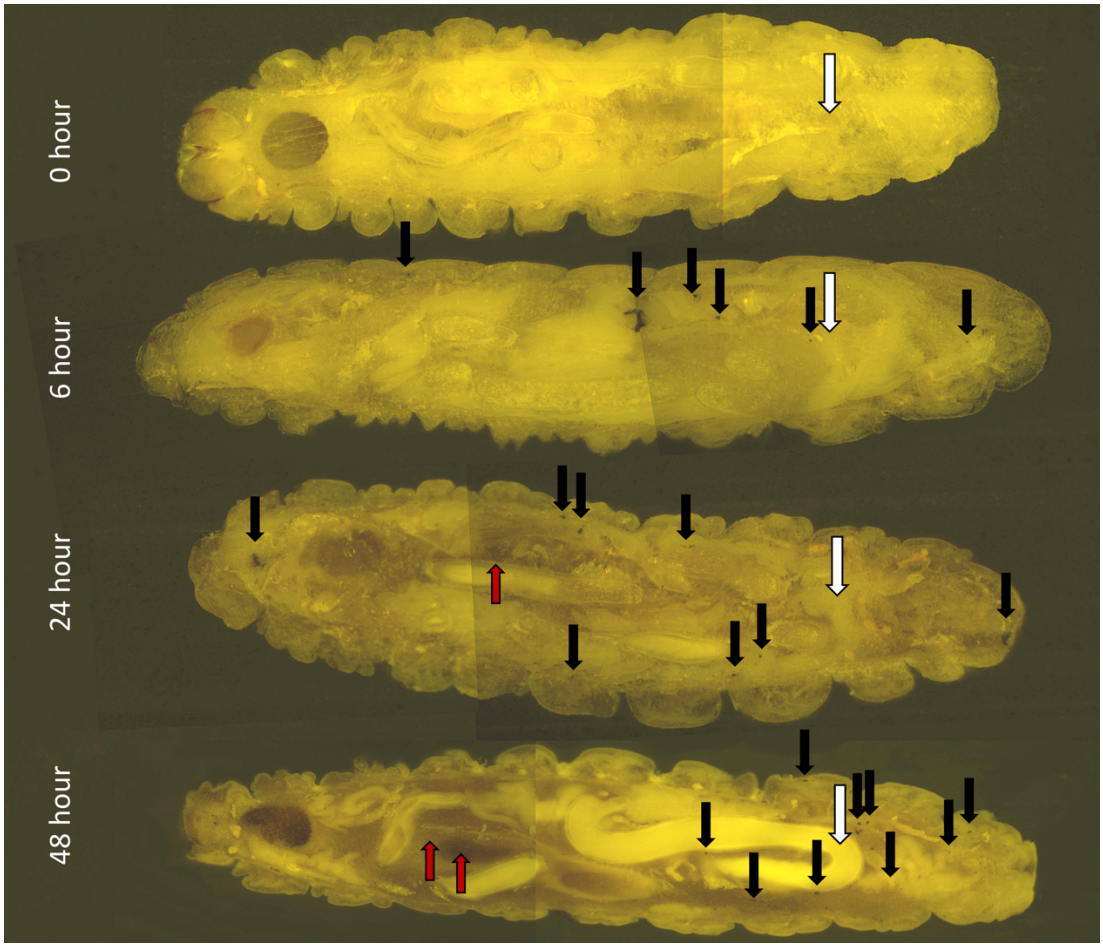

Fig. 4.4. Visualisation of disseminated *S. aureus* infection of *G. mellonella* larvae at 6, 24 and 48 h. Larvae were inoculated with 2×10^6 viable *S. aureus* cells for 6, 24 and 48 h were embedded, sectioned (10 µm) and visualised using a cryo-imaging system. Point of inoculation (white arrow), bacterial nodules (black arrow), extensive melanisation (red arrows). This experiment was repeated on 3 separate occasions with representative images provided.

The use of confocal microscopy was employed at 6, 24 and 48 h post-infection and revealed the presence of GFP labelled viable *S. aureus* (blue arrow) within nodules formed during infection. Interestingly at 6 h, cells were clumped together during the nodulation process (**Fig. 4.5**). Wild type *S. aureus* without GFP produced no fluorescence and was included as a control for auto-fluorescence (**Fig. 4.6**).

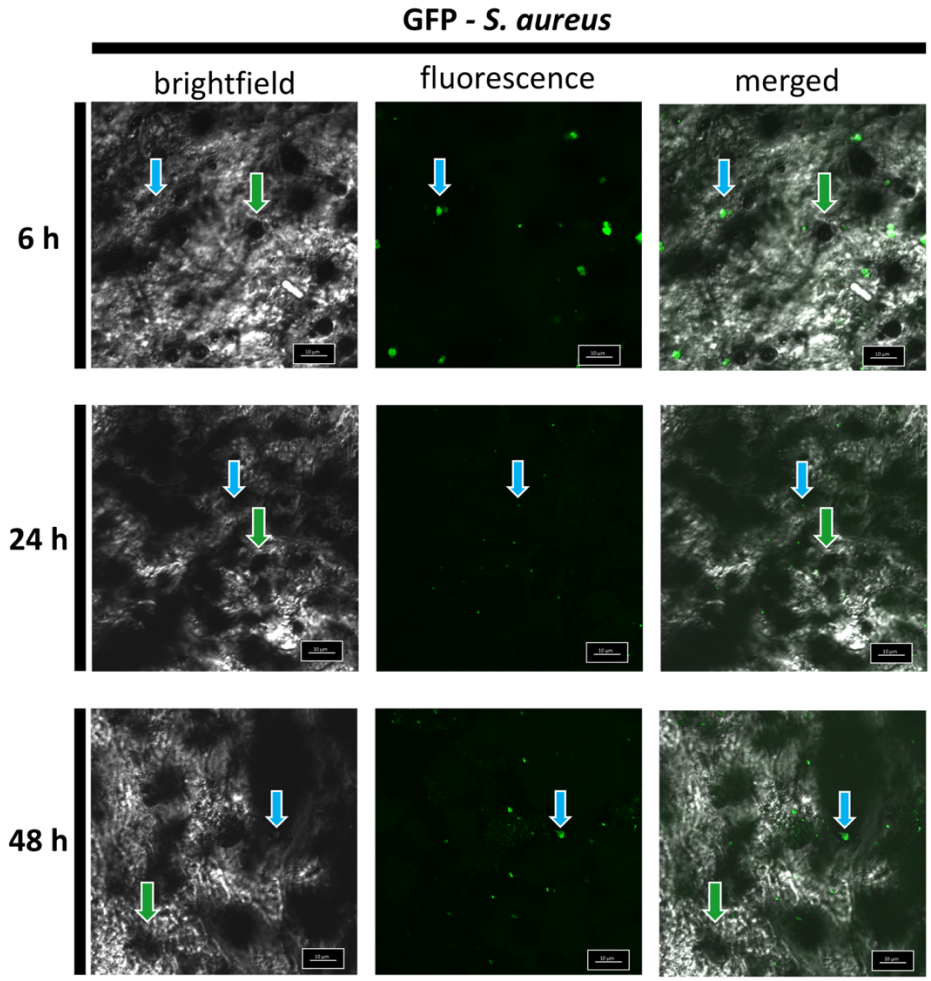

Fig. 4.5. Visualisation of GFP-labelled *S. aureus* cells within bacterial nodules in *G. mellonella* larvae inoculated with 2×10^6 viable cells. Bacterial nodules were dissected from larvae infected with *S. aureus* for 6, 24 and 48 h and visualised using confocal microscopy. Bright field images reveal the formation of melanised plaques (green arrow). Fluorescent microscopy revealed an abundance of *S. aureus* cells (blue arrow) within nodules at 6, 24 and 48 h post infection (scale bar corresponds to 10 μm). This experiment was repeated on 3 separate occasions with representative images provided.

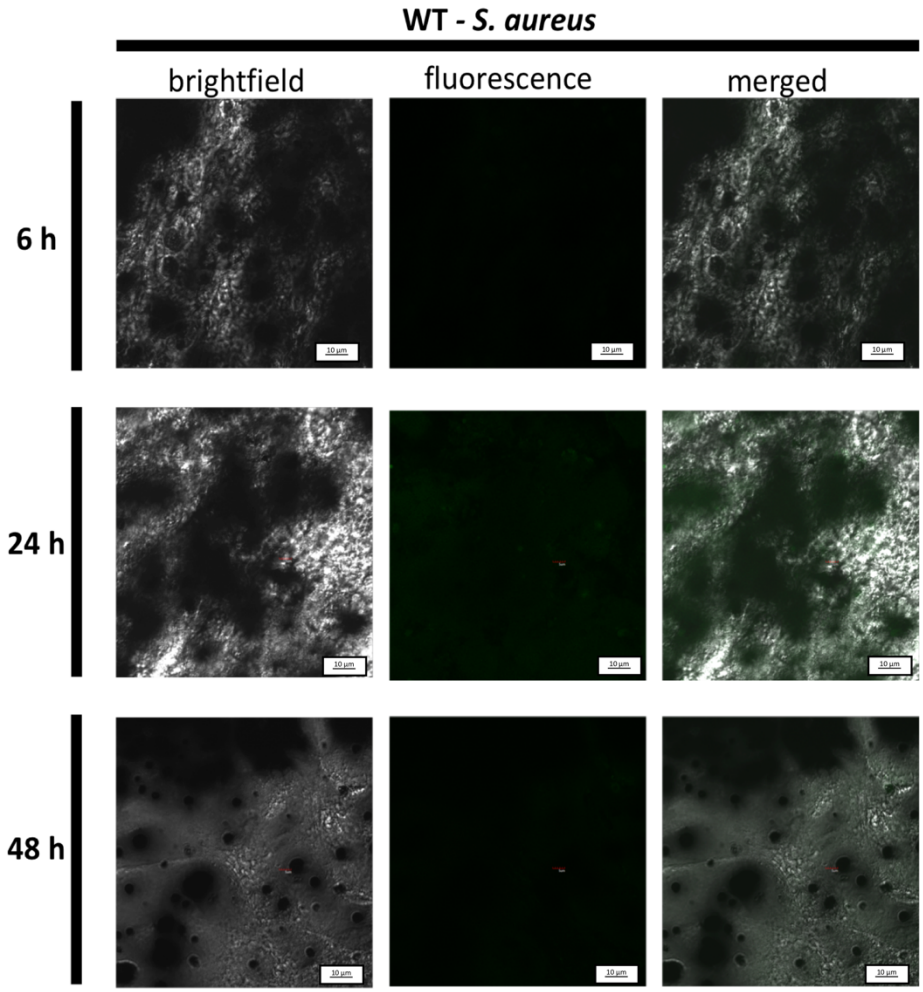

Fig. 4.6. Visualisation of WT *S. aureus* cells within bacterial nodules in *G. mellonella* larvae inoculated with 2×10^6 viable cells. Bacterial nodules were dissected from larvae infected with *S. aureus* for 6, 24 and 48 h and visualised using confocal microscopy. Bright field images reveal the formation of melanised plaques and cellular infiltrates. Fluorescent microscopy of WT non-GFP - *S. aureus* (WT) produced no fluorescent signal (scale bar corresponds to 10 µm).

4.4 Alteration in hemocyte density and function in response to *S. aureus* infection

Inoculation of larvae with *S. aureus* (2×10^6 cells $larva^{-1}$) resulted in a significantly increase in hemocyte density at 4 h ($1.47 \pm 0.25 \times 10^6$ $larva^{-1}$ (60 µl hemolymph), $p < 0.05$) as compared to the PBS control ($4.71 \pm 0.66 \times 10^5$). There was also an increase in hemocyte density at 6 h ($6.23 \pm 8.61 \times 10^5$, $p < 0.05$) compared to the PBS control ($2.81 \pm 0.15 \times 10^5$). Larvae infected with *S. aureus* for 24 ($6.65 \pm 1.66 \times 10^5$, $p < 0.05$) and 72 ($1.29 \pm 0.16 \times 10^6$, $p < 0.05$) h showed a significant increase in hemocyte density compared to the controls (**Fig. 4.7**).

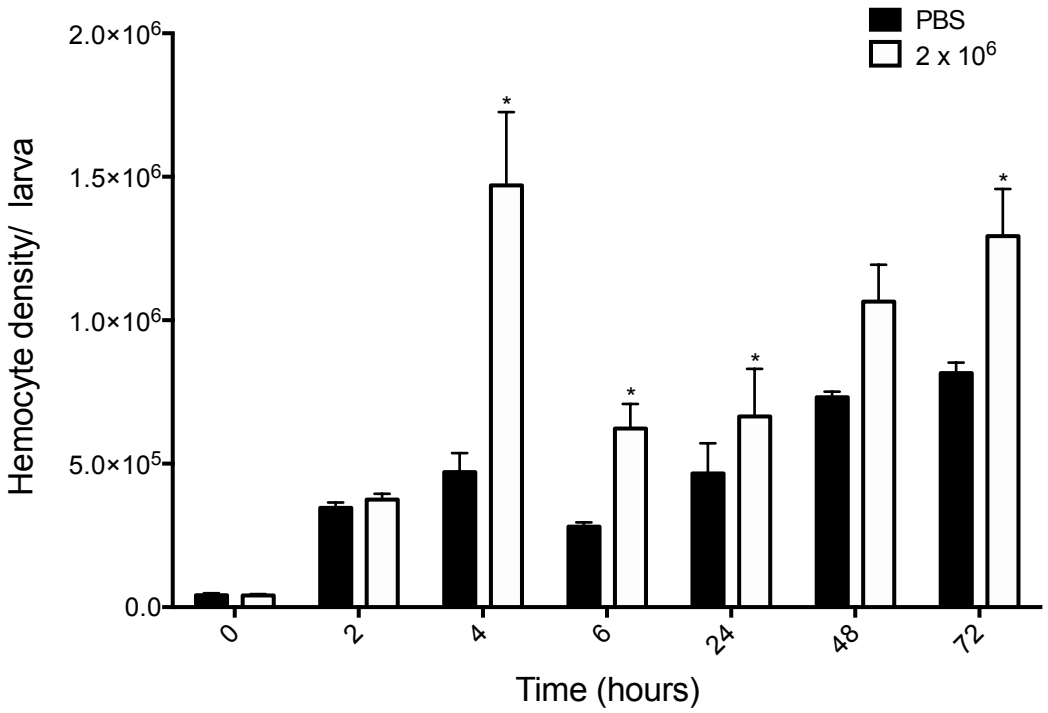

Fig. 4.7. Alteration in circulating hemocyte density following inoculation with viable *S. aureus* cells. *G. mellonella* larvae were inoculated with 20 µl *S. aureus* cells (2×10^6) or PBS and hemocytes were extracted and enumerated from 0 h to 72 h post inoculation. Statistical analysis was performed by comparing treatments to PBS injected controls at respective time points (*: $p < 0.05$). All values are the mean ± S.E. of three independent experiments.

Hemocytes from larvae that were administrated heat killed *S. aureus* (2×10^6 20 μl^{-1}) for 24 h displayed an increased ability to kill yeast cells as compared to hemocytes from control larvae, and larvae administrated heat killed *S. aureus* for 6 h. Hemocytes from larvae administrated *S. aureus* for 24 h reduced the viability of *C. albicans* to 4.47 ± 0.69% ($p < 0.01$) at 60 mins and 2.39 ± 1.39% ($p < 0.05$) at 80 mins compared to the controls at the same time points (60 min; 53.98 ± 10.62%, 80 min 25.63 ± 6.14%) **(Fig. 4.8)**.

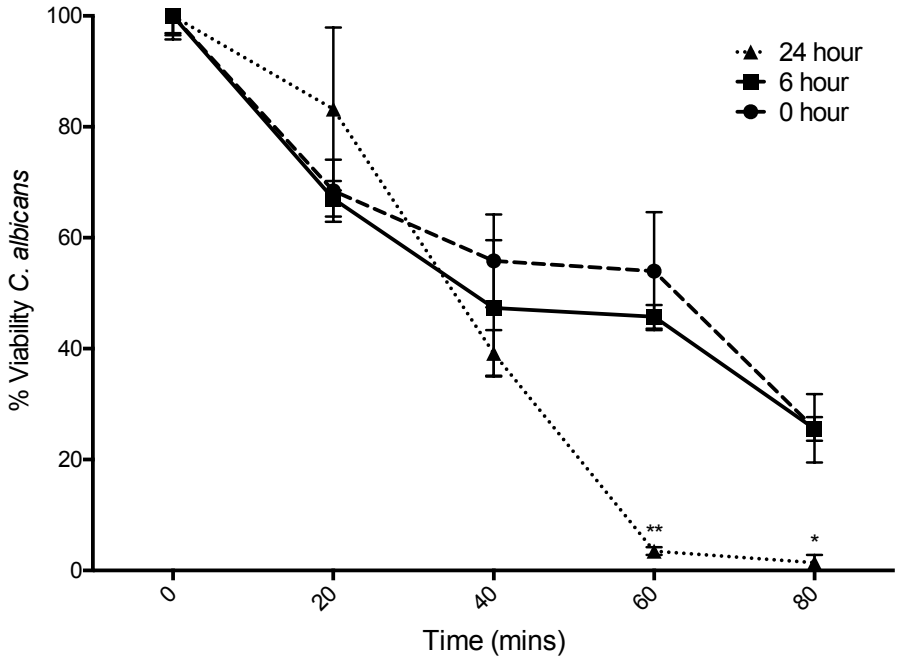

Fig. 4.8. Microbicidal activity of hemocytes extracted from *G. mellonella* larvae at 0, 6 and 24 h after inoculation with heat killed *S. aureus* cells (2×10^6 $larva^{-1}$). Pre-opsonised *C. albicans* cells were incubated with hemocytes (2:1 ratio) for 80 minutes and aliquots taken every 20 minutes diluted and plated on YEPD agar plates (*: $p < 0.05$, **: $p < 0.01$). All values are the mean ± S.E. of three independent experiments.

Incubation of hemocytes with *S. aureus* (2:1 ratio) for 5 and 20 minutes indicated hemocyte lysis around *S. aureus* cells (white arrow) **(Fig. 4.9)**.

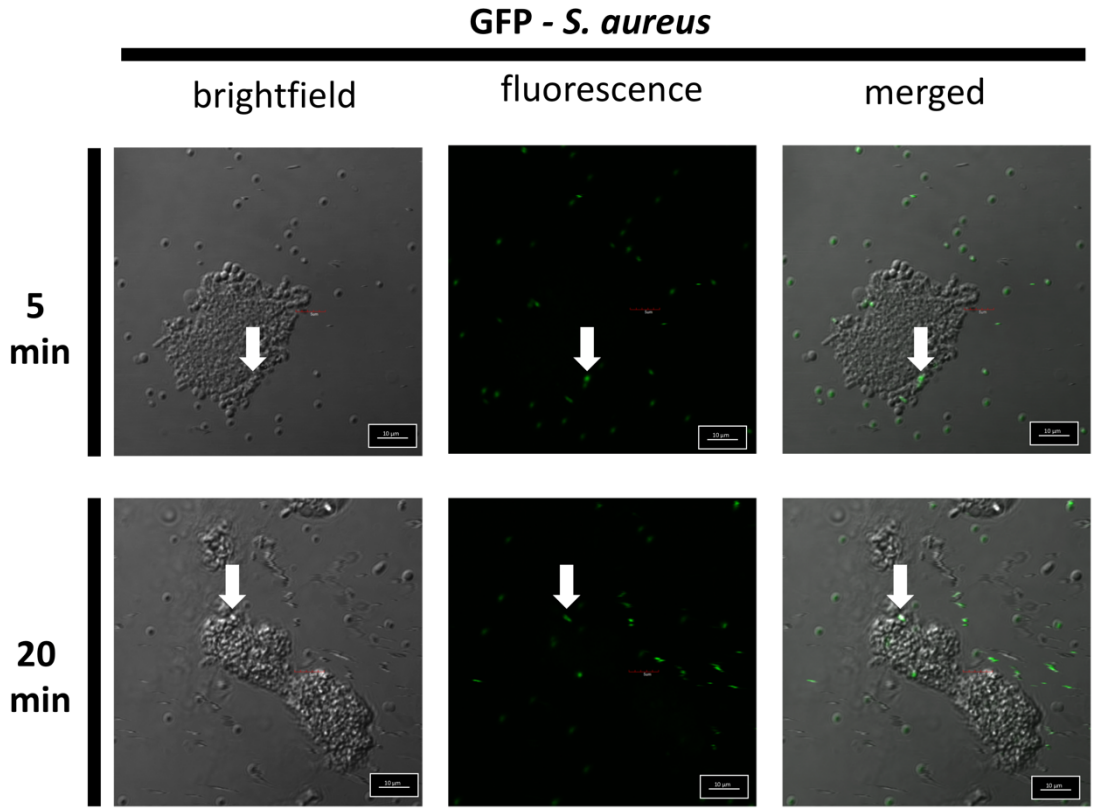

Fig. 4.9. Response of *ex vivo* hemocytes to *S. aureus*. Hemocytes were extracted from *G. mellonella* larvae washed 3 times with PBS and mixed for 5 and 20 min at a 1: 1 ratio *S. aureus* GFP bright field images suggest the lysis of hemocytes around *S. aureus* cells (white arrow) (Scale bar corresponds to 10 µm).

4.5 Analysis of the humoral immune response of larvae to *S. aureus* infection

Quantitative proteomics was performed on hemocyte-free hemolymph (hemocytes were removed by centrifugation 10000 × *g* for 10 minutes) from larvae infected with *S. aureus* (2×10^6 larva) for 0, 6 and 24 h. In total 331 proteins were identified consisting of 2121 peptides. Of these, 18 proteins at 6 h as compared to 0 h and 33 proteins at 24 h as compared to 0 h were found to be differentially abundant with a fold change > 1.5. In total, 12 proteins were found to be exclusive to 6 h and 24 h treatments. A principal component analysis (PCA) of the proteins present at all three time points indicates that there was a distinct difference between the proteomes at 0 h, 6 h and 24 h **(Fig. 4.10)**.

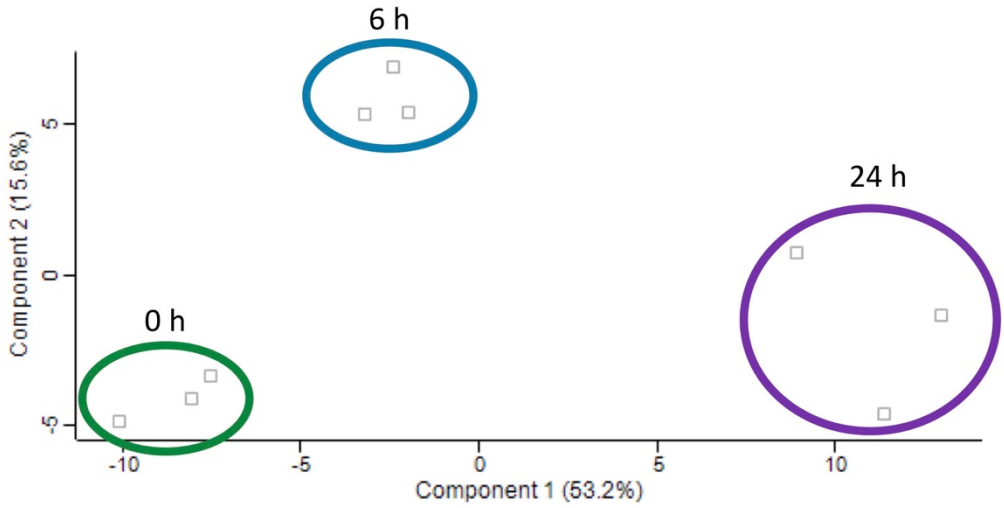

Fig. 4.10. Principal component analysis (PCA) of *G. mellonella* hemolymph proteomic profiles following infection with viable *S. aureus* cells for 0, 6 and 24 h. PCA of three replicates of each treatment included in LFQ analysis with a clear distinction between each time point.

Proteins that were increased in abundance in the 6 h infected larvae when compared to the uninfected control larvae included a hypothetical protein (+43 fold), gloverin (+14 fold), gustatory receptor candidate 25 (+10 fold), peptidoglycan-recognition protein-LB (+9 fold), peptidoglycan recognition like protein B (+5 fold) and β actin (+4 fold). Proteins that were decreased in abundance at 6 h compared to 0 h were α-esterase 45 (-1.6 fold) and hypothetical protein (-2 fold) (**Fig. 4.11A, Table A4.1**).

Proteins increased in abundance in the 24 h *S. aureus* infected larvae compared to 0 h included gloverin (+86 fold), cecropin-D like peptide (+79 fold), hypothetical protein (+46 fold), cecropin-A (+30 fold), gloverin-like protein (+23 fold), lysozyme (+18 fold), peptidoglycan recognition-like protein B (+17 fold), peptidoglycan-recognition protein-LB (+15 fold), inducible metalloproteinase inhibitor protein (+10 fold) and hemolin (+9 fold). Proteins decreased in abundance at 24 h compared to 0 h were cathepsin B-like cysteine proteinase (-4 fold), heat shock protein 25.4 precursor (-3 fold), hypothetical protein (-2.7 fold), serine proteinase (-2.7 fold), hypothetical protein (-2.3 fold) (**Fig. 4.11B, Table A4.2**).

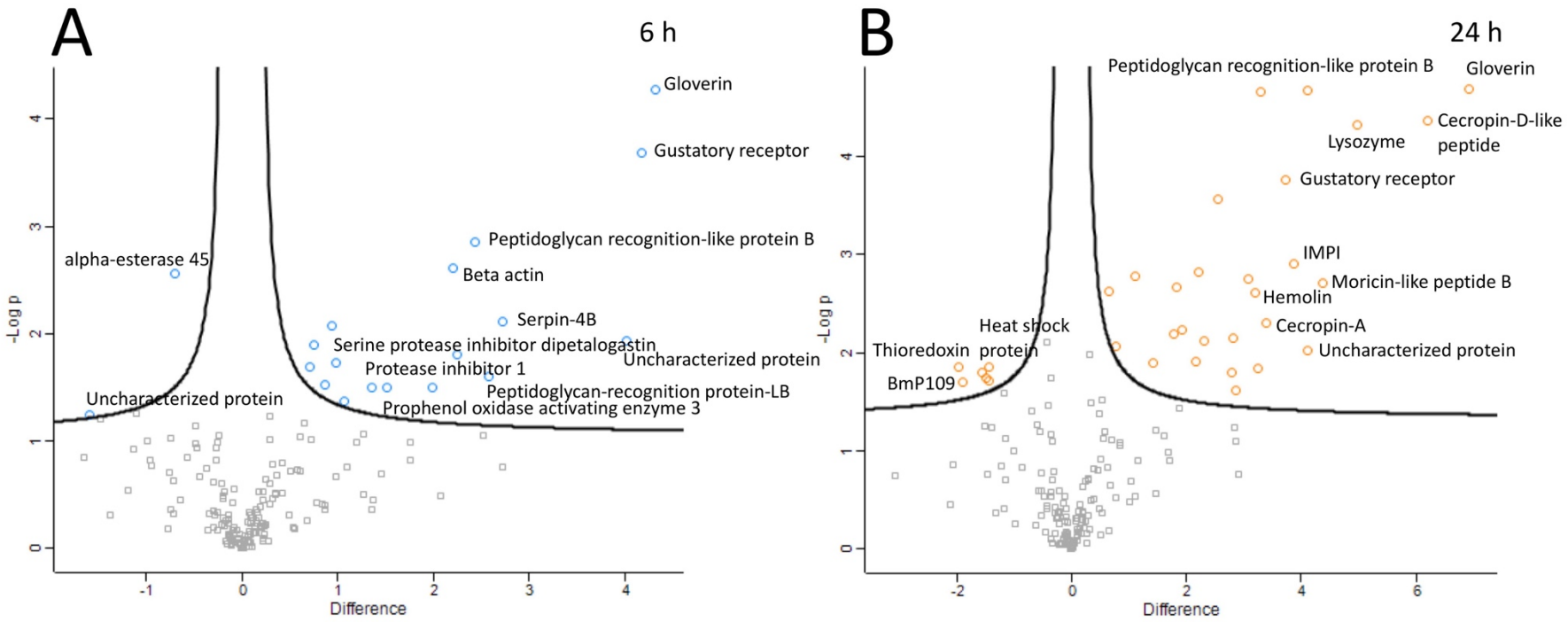

Fig. 4.11. Proteomic responses of *G. mellonella* larval hemolymph following infection by 2×10^6 *S. aureus* cells after 6 (A) and 24 (B) h. Volcano plots represent protein intensity difference (- $\log_2$ mean intensity difference) and significance in differences (- log P-value) based on a two-sided *t*-test. Proteins above the line are considered statistically significant (p value < 0.05) and those to the right and left of the vertical lines indicate relative fold changes > 1.5. Annotations are given for the most differentially abundant proteins identified in hemolymph from larvae infected with *S. aureus* for 6 and 24 h. These plots are based upon post imputed data.

4.6 Discussion

While *G. mellonella* larvae offer a number of advantages which overcome the drawbacks associated with mammalian testing and other model systems, there is now the opportunity to model bacterial infection processes in larvae and to compare these to the processes which occur during mammalian infection. Infection with *S. aureus* dose dependently decreased larval viability at 37 ^{o}C (**Fig. 4.2)**. In mice, an inoculum of 10^8 c.f.u per mouse resulted in 50% survival after 2 days and 0% survival after 4 days (Capparelli *et al.*, 2007). Bacterial load peaked at 72 h and this was associated with a significant decrease in larval viability (**Fig. 4.3)**. In neutrophil depleted mice, *S. aureus* can significantly proliferate within blood and skin samples (Molne *et al.,* 2000).

At 6 h post infection there were small nodules around the site of inoculation but no melanisation of the cuticle (**Fig. 4.4)**. At 6 h *S. aureus* appeared in clumps, but by 24 h single cells were present within nodules and this occurred with extensive melanised nodule formation around the hemocoel of the larvae. By 48 h widespread melanisation of insect hemolymph had occurred possibly due to uncontrolled phenoloxidase activation due to an uncontrollable bacterial burden.

Nodules produced in *G. mellonella* larvae during infection are similar in structure and function to abscesses commonly found during *S. aureus* skin and soft tissue infection in humans (**Fig. 4.5, 4.6)** (Kobayashi *et al.,* 2015). *S. aureus* produces several molecules that contribute to abscess formation which recruit neutrophils, induce host cell lysis and the formation of the fibrin capsule surrounding the abscess (Kobayashi *et al.,* 2015). Abscess formation is associated with a characteristic decrease in *S. aureus* c.f.u. load, but this may be associated with an increase within tissue (Cheng *et al.*, 2009). This was also observed in this Chapter as total *S. aureus* c.f.u. decreased in larvae between 2 and 4 h. *S. aureus* invasion triggers predominantly neutrophils and macrophages infiltration with residence of *S. aureus* within neutrophils. Within 72 h staphylococci are localised within abscess at the centre of the lesions, enclosed by fibrin deposits, and surrounded by layers of immune cells (Cheng *et al.*, 2009; Thomer *et al.,* 2016).

Inoculation of larvae with 2×10^6 *S. aureus* cells resulted in a significant increase in the numbers of circulating hemocytes at 4 h, possibly due to the release of hemocytes usually attached to the linings of internal organs such as fat body (**Fig. 4.7)** (Ratcliffe, 1985b). There was also an increase in hemocyte density at 6 and 24 h post-infection and this is correlated with the replication of *S. aureus* cells within larvae. Interestingly, human neutrophils (which are analogous to insect hemocytes) are first recruited to the site of *S. aureus* infection and the accumulation of neutrophils is effective in *S. aureus* killing (Li *et al.*, 2002b; Robertson *et al.*, 2008; Guerra *et al.*, 2017). In mice infected with 10^7 or 10^8 *S. aureus* cells, circulating granulocyte density peaked at 6 h and was higher in mice infected with the higher dose (Capparelli *et al.*, 2007). BALB/c mice infected with *S. aureus* (10^8) displayed a significant increase in neutrophil density before a spike in *S. aureus* proliferation was observed (Marques, 2015) and in this study hemocyte density peaked prior to accelerated *S. aureus* proliferation.

Hemocytes from larvae exposed to heat killed *S. aureus* for 24 h were more microbicidal as compared to control hemocytes and hemocytes from larvae exposed for 6 h, indicating the possible appearance of a specific cell type (e.g. granulocyte) with superior killing ability (**Fig. 4.8)**. Interactions between *S. aureus* and larval hemocytes resulted in hemocyte degranulation and lysis and this is the early stage of nodule formation around the microbial invader (**Fig. 4.9)**.

Proteomic analysis of larval hemolymph at 6 and 24 h post infection with *S. aureus* revealed a range of proteins which are involved in regulation of the immune response, defence against bacterial infection and nodule formation (**Fig. 4.11)**. There was also an increased abundance of a range of opsonins such as peptidoglycan-recognition protein-LB and peptidoglycan recognition like protein B at 6 h post infection which play an important role in bacterial cell identification and recognition by circulating immune cells (Dziarski, 2004). Components of the prophenoloxidase cascade (prophenoloxidase activating enzyme 3) were also increased in abundance in the proteome of 6 h *S. aureus* infected hemolymph. The phenoloxidase cascade is analogous to the mammalian complement cascade in terms of protein structure, function and mode of action (Söderhäll and Cerenius, 1998; Clow *et al.*, 2004). *S. aureus* interacts with and evades the complement cascade at many levels (Lee *et al.*,

2004a). At 6 h post infection the antimicrobial protein showing the greatest increase in abundance was gloverin. Gloverin is a glycine rich, heat stable antibacterial protein believed to bind LPS and it was previously demonstrated that *E. coli* induced its expression in *Bombyx mori* (Yi *et al.*, 2013).

By 24 h post infection a range of AMPs such as gloverin, cecropin-D-like peptide, lysozyme and moricin-like peptide B were increased in abundance. The AMP family cecropin were first isolated from *H. cecropia* and demonstrate antibacterial activity against multidrug resistant *Acinetobacter baumannii* and *P. aeruginosa* and displays immunomodulatory effects on macrophages (Yun and Lee, 2016). Cecropin-A displays antimicrobial activity against *S. aureus* (Lee *et al.*, 2013). Lysozyme was also increased in abundance in response to *S. aureus* infection and cleaves the β-1,4 glycosidic bonds between N-acetylmuramic acid and N-acetylglucosamine of bacterial peptidoglycan and induce bacterial lysis. However, many *S. aureus* strains display intrinsic resistance to lysozyme and its activity acts in synergy with other AMPs and the cellular immune response (Bera *et al.*, 2005; Chen *et al.*, 2005). Moricins are secreted pro-peptides and are activated via proteolysis and increase the permeability of bacterial membranes (Hara and Yamakawa, 1995). *B. mori* moricin is active against *S. aureus*, targets the membrane and is induced by bacterial infection (Hara and Yamakawa, 1995). A range of human AMPs are essential in the defence against *S. aureus* infection. Pathogenic *S. aureus* primarily induce human β-defensin (hBD) 1 and hBD3. LL-37, which is expressed on the skin and an important defence against *S. aureus* invasion and displays important bactericidal activity against *S. aureus* (Ommori *et al.*, 2013). *S. aureus* induces the expression of hBD3 and hCAP-18, MRSA was more resistant to AMPs than its methicillin-susceptible counterpart (Midorikawa *et al.*, 2003).

A number of proteins involved in nodule formation in *G. mellonella* larvae were also increased in abundance such as putative defence protein hdd11 and hemolin. Hdd11 was increased in hemolymph at 24 h post infection with *S. aureus* and has been found increased in *Hyphantria cunea* during bacterial infection and shares homology with noduler from *Antheraea mylitta* (Woon Shin *et al.*, 1998; Sarauer *et al.*, 2003). Noduler shares a reeler domain with hdd11 and binds both insect hemocytes and bacterial LPS, is enriched within nodules and is important

during the nodulation response (Gandhe *et al.,* 2007). Immunoglobulin superfamily member hemolin was induced by *Candida* challenge and has been shown to act as a pattern recognition receptor in insects (Yu and Kanost, 2002; Browne *et al.*, 2015). Hdd11 and hemolin were also increased abundance in larvae infected with *A. fumigatus* and *C. albicans.*

The results presented here detail the cellular and humoral responses of larvae to *S. aureus* during the development of disseminated disease. These results show similarities to interaction that occurs between *S. aureus* and the immune response of mammals (i.e. rapid bacterial proliferation, nodule formation, alteration in immune cell number, increased antimicrobial peptide abundance). Studying the development of *S. aureus* infection in larvae may give novel insights into the pathogen – host interactions that could improve our understanding of this disease process in mammals. These similarities may also be used to study the efficacy and interaction of novel antibiotics with *S. aureus* in combination with the host immune response, while overcoming the disadvantages associated with using mice in early stage drug development.

Chapter 5

The evaluation of *Galleria mellonella* larvae as an *in vivo* model to study polymicrobial infection and assess novel combination antimicrobial chemotherapy

5.1 Introduction

The human microbiome consists of communities of bacteria and fungi which through their interactions have both positive and negative effects on each other and with their host (Shirtliff *et al.*, 2009). In times of dysbiosis, polymicrobial infection can lead to aggressive forms of diseases which are usually difficult to treat. For example, co-colonisation by *A. fumigatus* and *P. aeruginosa* in the cystic fibrosis lung had poorer clinical outcomes compared to those colonised by *P. aeruginosa* alone (Reece *et al.*, 2017). Up to 38% of candidaemia infections are polymicrobial, and *S. aureus* is one of the most common microbes isolated during these infections (Klotz *et al.*, 2007; Reno *et al.*, 2015). These types of diseases include catheter infections, burn wound infections, septicaemia, ventilator-associated pneumonia, keratitis, denture stomatitis, peritonitis, cystic fibrosis and urinary tract infections (Shirtliff *et al.,* 2009; Schlecht *et al.*, 2015). The interactions between *S. aureus* and *C. albicans* are synergistic and result in increased mortality in animal models which is associated with enhanced invasion, biofilm formation, exacerbated inflammatory responses and intrinsic resistance to antimicrobial chemotherapy (Harriott and Noverr, 2009; Schlecht *et al.*, 2015; Kong *et al.*, 2016; De Carvalho Dias *et al.*, 2017; Kean *et al.*, 2017; Kong *et al.*, 2017; Krüger *et al.*, 2019).

There is a lack of simple *in vivo* systems to assess the development of co-microbial infection in order to study the complex interactions at the cellular and molecular level. The aim of the work presented in this Chapter was to characterise the development of and the larval immune response to mixed microbial co-infection (*C. albicans* and *S. aureus*) in *G. mellonella* larvae and to assess the efficacy of empirical antimicrobial agents in enhancing the survival and reduction of symptoms of co-infected larvae.

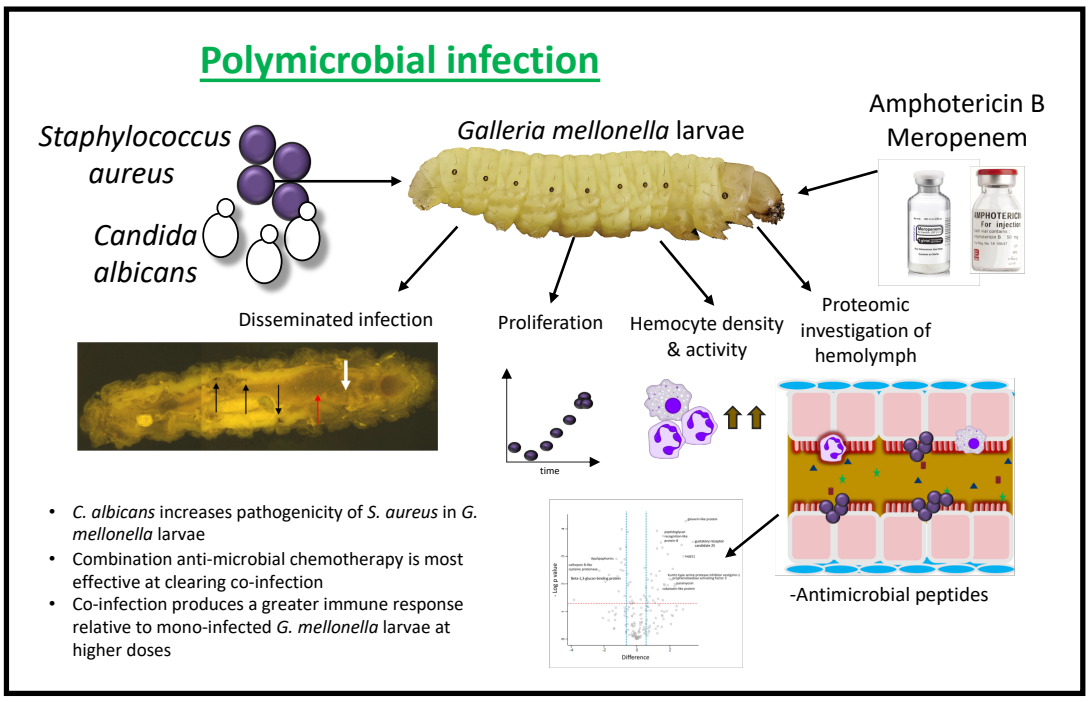

Fig. 5.1. Graphical abstract for Chapter 5.

5.2 Response of *G. mellonella* larvae to co-infection by *C. albicans* and *S. aureus*

Infection of larvae with an inoculum of 1×10^5 *C. albicans* larva^{-1} resulted in no significant decrease in survival over 72 h. Infection of larvae with *S. aureus* (2×10^4 larva^{-1}) resulted in a decrease in larval survival at 72 h to 96.66 ± 5.77%, while an inoculum of 2×10^6 *S. aureus* larva^{-1} resulted in larval survival of 80 ± 10% at 24 h, 55.93 ± 9.62% at 48 h and 10 ± 5.15% at 72 h post infection. Co-infection of larvae with *C. albicans* (1×10^5 larva^{-1}) and *S. aureus* (2×10^4 larva^{-1}) resulted in a significant decrease in survival (24 h; 70 ± 3.33% [$p < 0.01$], 48 h; 10 ± 3.33% [$p < 0.0001$], 72 h; 5 ± 6.66% [$p < 0.0001$]) compared to larvae that received *S. aureus* (2×10^4 larva^{-1}) alone at 24, 48 h (100 ± 0%) and 72 h (96.66 ± 5.77%). Co-infection of *G. mellonella* larvae with *C. albicans* (1×10^5 larva^{-1}) and *S. aureus* (2×10^6 larva^{-1}) reduced larval survival to 30 ± 6.66% ($p< 0.0001$) at 24 h and 0 ± 0% ($p < 0.0001$) at 48 and 72 h post infection, relative to mono-infection with *S. aureus* (2×10^6 larva^{-1}) (**Fig. 5.2**).

Alterations in circulating hemocyte density in co-infected larvae was determined in order to assess the cellular response to co-infection. Firstly, mono-infection with *C. albicans* (1×10^5 larva^{-1}) significantly decreased hemocyte density at 24 ($2.18 \pm 0.22 \times 10^5$ hemocytes larva^{-1} [60 µl hemolymph], $p < 0.001$) and 48 ($2.09 \pm 0.13 \times 10^5$, $p < 0.05$) h relative to the PBS injected control (24 h; $4.58 \pm 0.31 \times 10^5$, 48 h; $7.10 \pm 0.32 \times 10^5$). Inoculation of larvae with *S. aureus* at a dose of 2×10^4 resulted in a significant decrease in hemocyte density at 6 ($1.26 \pm 0.36 \times 10^5$, $p < 0.01$), 24 ($1.30 \pm 0.73 \times 10^5$, $p < 0.0001$) and 48 ($1.42 \pm 0.13 \times 10^5$ $p < 0.01$) h post infection. Interestingly, mono-infection with *S. aureus* 2×10^6 larva^{-1} caused an increase in circulating hemocyte density at 6 ($5.70 \pm 0.25 \times 10^5$, $p<0.0001$) and 24 ($6.55 \pm 0.27 \times 10^5$, $p < 0.01$) h post infection compared to their relative PBS injected controls (**Fig. 5.3)**.

Co-infection with *C. albicans* (1×10^5 larva^{-1}) and *S. aureus* 2×10^4 larva^{-1} resulted in an increase in circulating hemocyte density at 6 ($1.69 \pm 0.13 \times 10^5$, $p < 0.05$), 24 ($3.63 \pm 0.14 \times 10^5$, $p < 0.0001$) and 48 ($5.11 \pm 0.20 \times 10^5$, $p < 0.05$) h post infection compared to larvae only infected with *S. aureus* (2×10^4 larva^{-1}) at the relative timepoints. Co-infection of *C. albicans* (1×10^5 larva^{-1}) with *S. aureus* at an inoculum of 2×10^6 larva^{-1} ($3.19 \pm 0.31 \times 10^5$, $p < 0001$) resulted in a significant decrease in circulating hemocyte density relative to larvae only infected with *S. aureus* 6 h post infection (2×10^5; $3.15 \pm 0.17 \times 10^5$, 2×10^6; $5.70 \pm 0.25 \times 10^5$).

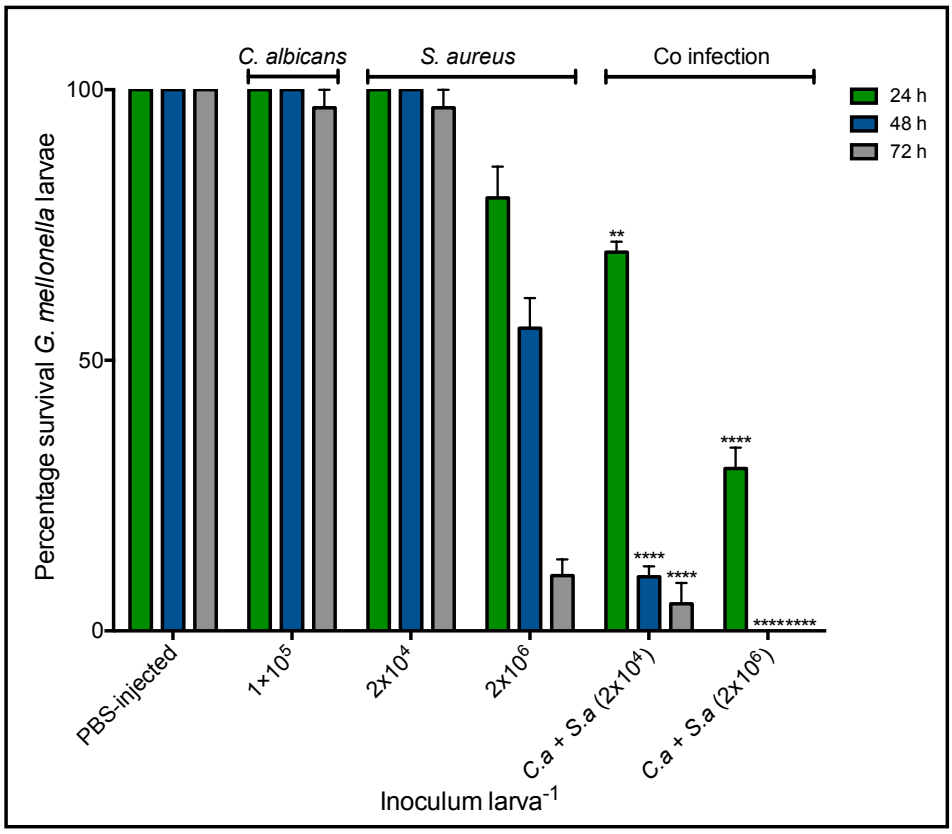

Fig. 5.2. Survival of *G. mellonella* larvae following mono- and co- infection with *C. albicans* and *S. aureus.* Larvae were infected with 20 µl of *C. albicans*, *S. aureus* or co-infected (1×10^5 *C. albicans* with varying concentrations of *S. aureus*) and survival assessed over 72 h. Statistical significance was determined by comparing co-infected larvae to the relevant *S. aureus* mono-infected larvae (**: $p < 0.01$, ****: $p < 0.0001$). All values are the mean ± S.E of three independent experiments.

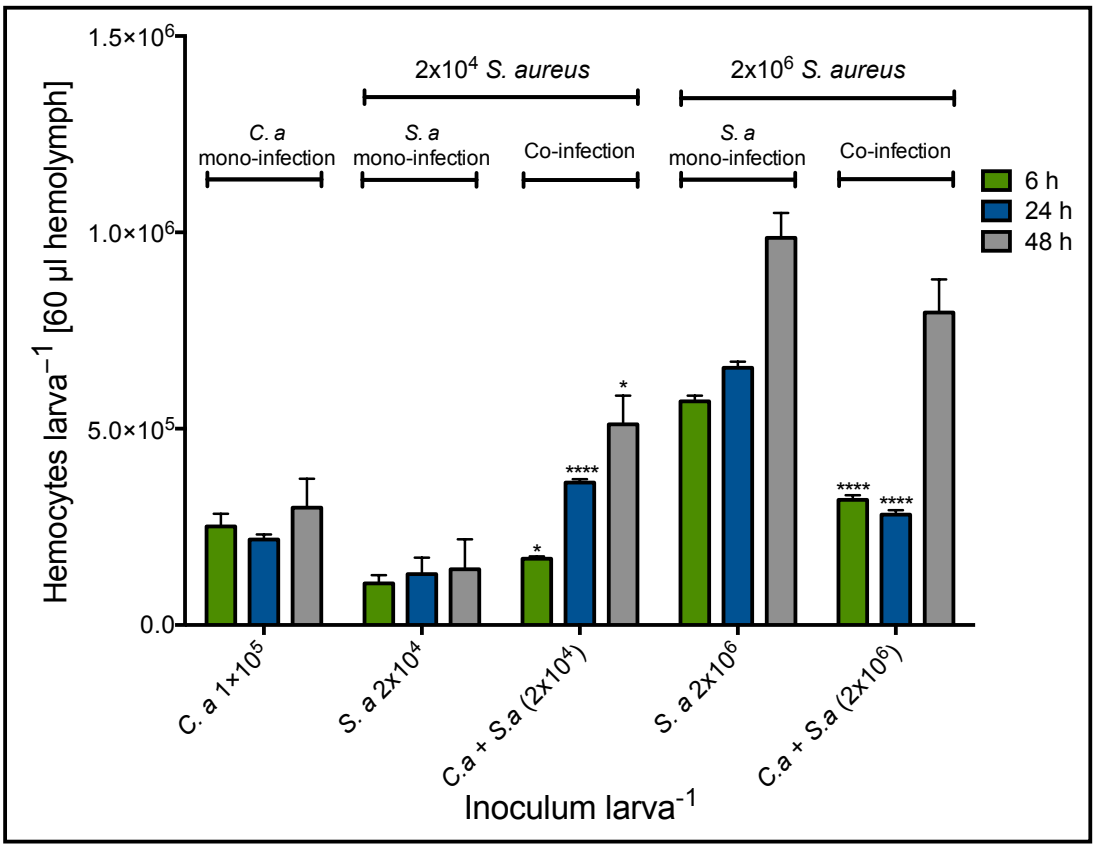

Fig. 5.3. Alteration in circulating hemocyte density following inoculation with *S. aureus* cells alone and in combination with *C. albicans*. *G. mellonella* larvae were inoculated with 20 µl *S. aureus* cells *(*2 × 10^4 and 2 × 10^6 $larva^{-1}$) alone or in combination with *C. albicans* (1 × 10^5 $larva^{-1}$) or PBS injection and hemocytes were extracted and enumerated from 6, 24 and 48 h post inoculation. Statistical analysis was performed by comparing *C. albicans* (*C. a*) or *S. aureus* (*S. a*) only treatments to PBS injected larvae and by comparing co-infected larvae (*C. a* + *S. a*) to *S. aureus* only treated larvae at their at respective doses and time points (*: $p < 0.05$, **: $p < 0.01$, ***: $p < 0.001$, ****: $p < 0.0001$). All values are the mean ± S.E of three independent experiments.

5.3 Dissemination of co-infection throughout the host

The microbial burden of co-infected larvae was assessed by measuring *S. aureus* c.f.u larva^{-1} in co-infected (*C. albicans* [1 × 10^5 larva^{-1} with varying concentrations of *S. aureus* [2 × 10^4 and 2 × 10^6 larva^{-1}]) larvae and comparing these to larvae only infected with *S. aureus* (2 × 10^4 and 2 × 10^6 larva^{-1}). Co-infected larvae (*C. albicans* [1 × 10^5 larva^{-1}] *S. aureus* [2 × 10^4 larva^{-1}]) displayed a significantly higher c.f.u larva^{-1} at 6 (1.51 ± 0.17 × 10^5 c.f.u larva^{-1}, $p < 0.05$), 24 (1.01 ± 0.38 × 10^7 c.f.u larva^{-1} , $p < 0.05$) and 48 (2.01 ± 0.23 × 10^8 c.f.u larva^{-1} , $p < 0.001$) h compared to larvae infected with just *S. aureus* [2 × 10^4 larva^{-1}] at 6 (4.49 ± 0.5 × 10^4 c.f.u larva^{-1}), 24 (4.51 ± 0.37 × 10^5 c.f.u larva^{-1}) and 48 (1.05 ± 0.33 × 10^7 c.f.u larva^{-1}) h. There was a significant increase in *S. aureus* c.f.u at 6 (1.55 ± 0.59 × 10^6 c.f.u larva^{-1} , $p < 0.001$), 24 (2.58 ± 0.52 × 10^8 c.f.u larva^{-1}, $p < 0.05$) and 48 (6.12 ± 0.73 × 10^8, $p < 0.01$) h post infection in co-infected larvae (*C. albicans* [1 × 10^5 larva^{-1}] and *S. aureus* [2 × 10^6 larva^{-1}]) compared to those only infected with *S. aureus* [2 × 10^6 larva^{-1}] at 6 (9.96 ± 0.68 × 10^5 c.f.u larva^{-1}), 24 (9.41 ± 0.34 × 10^7 c.f.u larva^{-1}) and 48 (3.21 ± 0.51 × 10^8 c.f.u larva^{-1}) h (**Fig. 5.4**).

Cryo-imaging was employed to assess the development of dual infection within *G. mellonella* larvae. Larvae were co-infected with *C. albicans* (1 × 10^5 larva^{-1}) and *S. aureus* (2 × 10^4 larva^{-1}) and cryo-imaging performed at 0, 6, 24 and 48 h post infection. Six h post infection there was the appearance of melanised nodules (black arrow) around the site of inoculation (white arrow) and throughout the host. By 24 h post infection there was extensive melanisation (red arrow) of larval tissue especially around the site of inoculation and nodules are found throughout the larva. By 48 h post infection *G. mellonella* larvae survival was 10 ± 3.33% and there was extensive melanisation throughout the larvae as well as a large number of distinct nodules (**Fig. 5.5).**

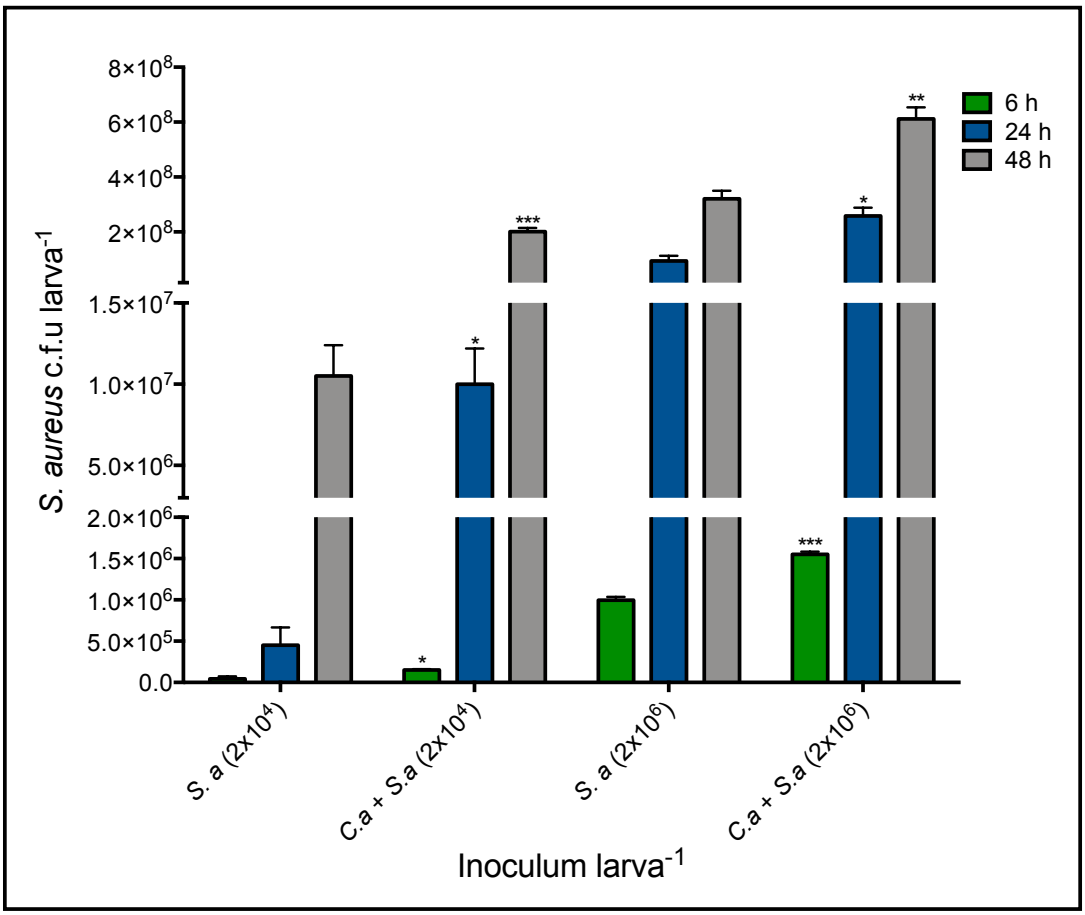

Fig. 5.4. *S. aureus* c.f.u. larva^{-1} obtained from *G. mellonella* larvae infected with *S. aureus* cells (2×10^6 and 2×10^6 larva^{-1}) or co-infected larvae over 48 h. Co-infection with *C. albicans* and *S. aureus* (*C. a* + *S. a*) results in an increase in bacterial load in larvae from 6 to 48 h as determined by plating on nutrient agar plates, statistical analysis was performed by comparing co-infected larvae (*C. a* + *S. a*) to larvae only infected with *S. aureus* (*S. a*) at their respective timepoints (*: $p < 0.05$, ** $p < 0.01$). All values are the mean ± S.E of three independent experiments.

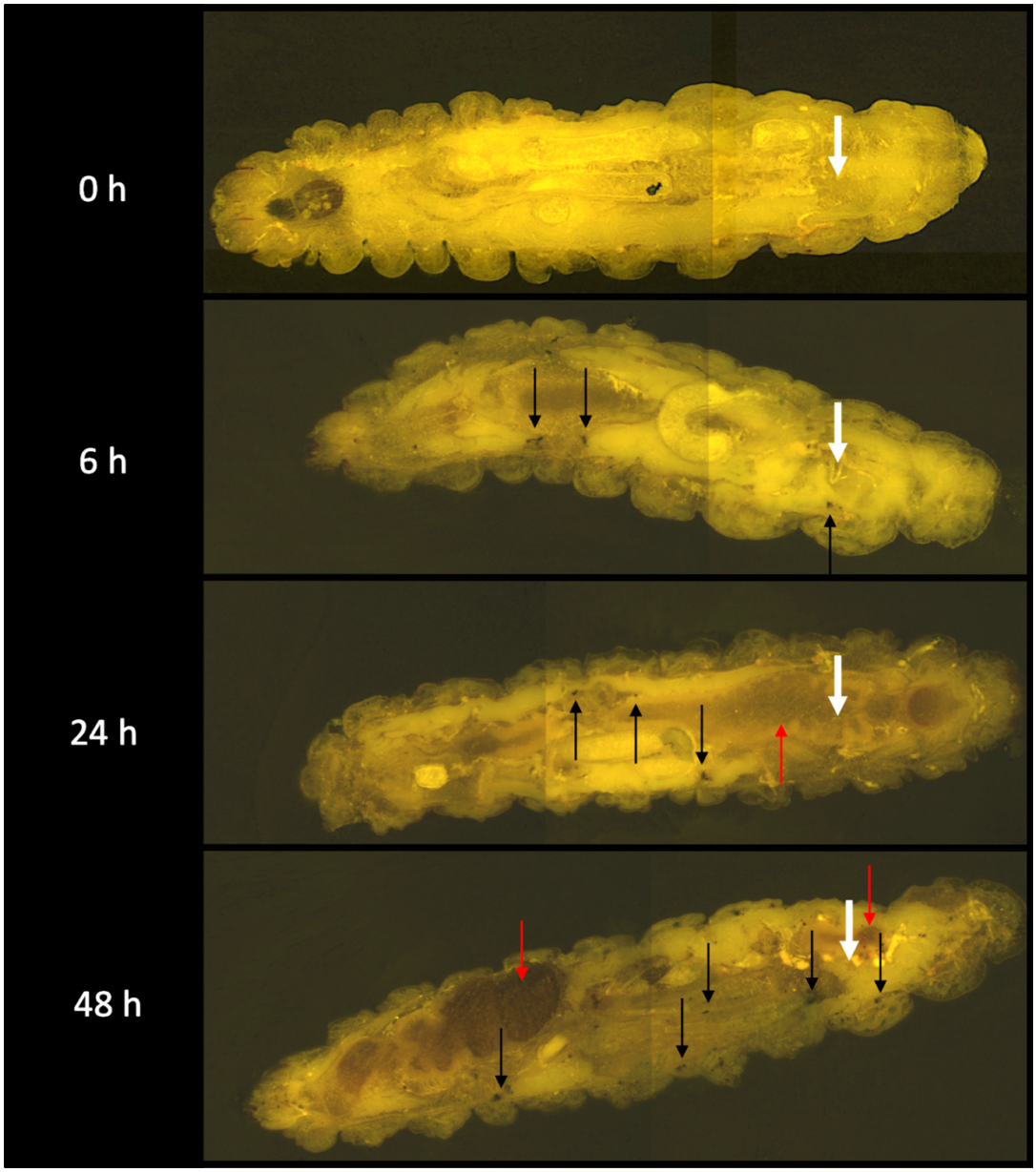

Fig. 5.5. Cryo-imaging of *G. mellonella* larvae co-infected with *C. albicans* and *S. aureus*. Larvae (n = 3) were co-infected with *C. albicans* (1×10^5 larva^{-1}) and *S. aureus* (2×10^4 larva^{-1}) for 0, 6, 24 and 48 h. Larvae (average size = 2 cm) were embedded, sectioned (10 µm) and visualised using a Cryoviz cryo-imaging system. (Point of inoculation (white arrow), nodules (black arrow), extensive melanisation (red arrows). This experiment was repeated on 3 separate occasions with representative images provided.

5.4 Humoral immune response of *G. mellonella* larvae to co-infection

Quantitative proteomic analysis was performed on the cell free hemolymph of infected *G. mellonella* larvae following co-infection with *C. albicans* [1×10^5 $larva^{-1}$] and *S. aureus* [2×10^4 $larva^{-1}$] for 0, 6 and 24 h. In total 2293 peptides were identified, representing 351 proteins with two or more peptides and 48 and 83 (6 hr v 0 hr and 24 hr v 0 hr, respectively) proteins were determined to be differentially abundant (ANOVA, $p < 0.05$) with a fold change of > 1.5. A total of 34, 46 and 84 proteins for 0, 6 and 24 h, respectively, were deemed exclusive (**Fig. 5.6A**). These proteins were subsequently used to statistically analyse the total differentially expressed group after imputation of the zero values as described and were then included in statistical analysis after data imputation. A principal component analysis (PCA) was performed on all filtered proteins and distinguished the 0, 6 and 24 h *C. albicans* and *S. aureus* treated samples. A clear difference between the 0, 6 and 24 h proteome was observed **(Fig. 5.6B**).

Proteins increased in relative abundance in the larvae co-infected for 6 h compared to the control were gustatory receptor candidate 25 (+10.5 fold), gloverin-like protein (+7.9 fold), putative defence protein hdd11 (+7.1 fold), actin 3 (+6.6 fold) and paramyosin (+5 fold). Proteins decreased in relative abundance in the larvae co-infected for 6 h compared to the control were cathepsin B-like cysteine proteinase (-4.9 fold), apolipophorin (-2.4 fold), β-1, 3-glucan-binding protein (-2.3 fold) and methionine-rich storage protein (-2.2 fold) (**Fig. 5.7A, Table A5.1**).

Proteins increased in relative abundance in co-infected larvae at 24 h compared to the control larvae were cecropin-A (+45.4 fold), gustatory receptor candidate 25 (+41.7 fold), cecropin-D-like peptide (+37.8 fold), putative defence protein hdd11 (+33.3 fold), gloverin (+19.3 fold) peptidoglycan-recognition protein-LB (+14.0 fold), serpin-4B (+12.9 fold) and salivary cysteine-rich peptide precursor (+12.6 fold). Proteins decreased in relative abundance in larvae co-infected for 24 h compared to the control larvae were apolipophorin (-62.4 fold), α-esterase 45 (-7.7 fold), serine proteinase (-6.2 fold), saposin-related precursor (-5.8 fold), carboxylesterase CarE-11 precursor (-5.6 fold) and cathepsin B-like cysteine proteinase (-4 fold) (**Fig. 5.7B, Table A5.2)).**

A range of *C. albicans* and *S. aureus* proteins were also detected in infected *G. mellonella* larval hemolymph 24 h post infection. A total of 23 *C. albicans* proteins were identified in co-infected *G. mellonella* larval hemolymph including hsp70 family ATPase, hsp SSA2 and peroxiredoxin TSA1-A (**Table A5.3**). In addition 20 *S. aureus* proteins such as staphopain B and HTH-type transcriptional regulator SarR were detected in hemolymph 24 h post infection (**Table A5.4**).

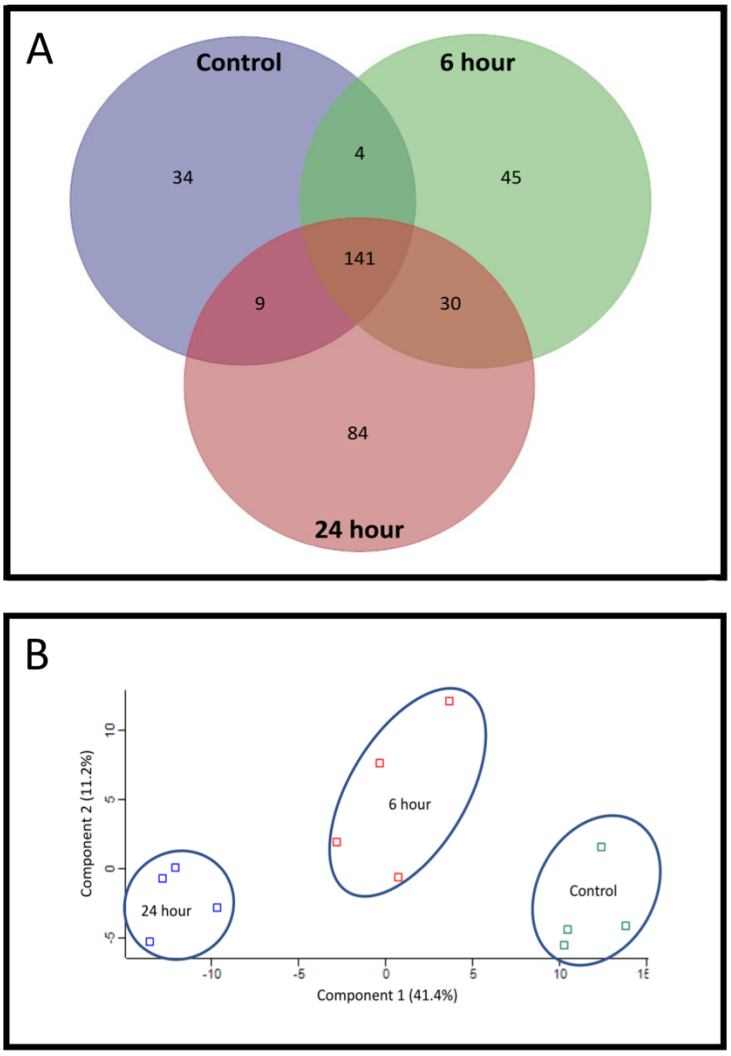

Fig 5.6. Proteomic response of *G. mellonella* larvae to co-infection by *C. albicans and S. aureus*. (A) Venn diagram of number of proteins detected in control, 6 h and 24 h co infected larvae. In total 34, 45 and 84 proteins were deemed exclusive to the control, 6 h and 24 h hemolymph proteome from co-infected larvae. (B) Principal component analysis of larva hemolymph proteomic profiles following co-infection with *C. albicans* and *S. aureus* for 0, 6 and 24 h. PCA of three replicates of each treatment included in LFQ analysis with a clear distinction between each time point.

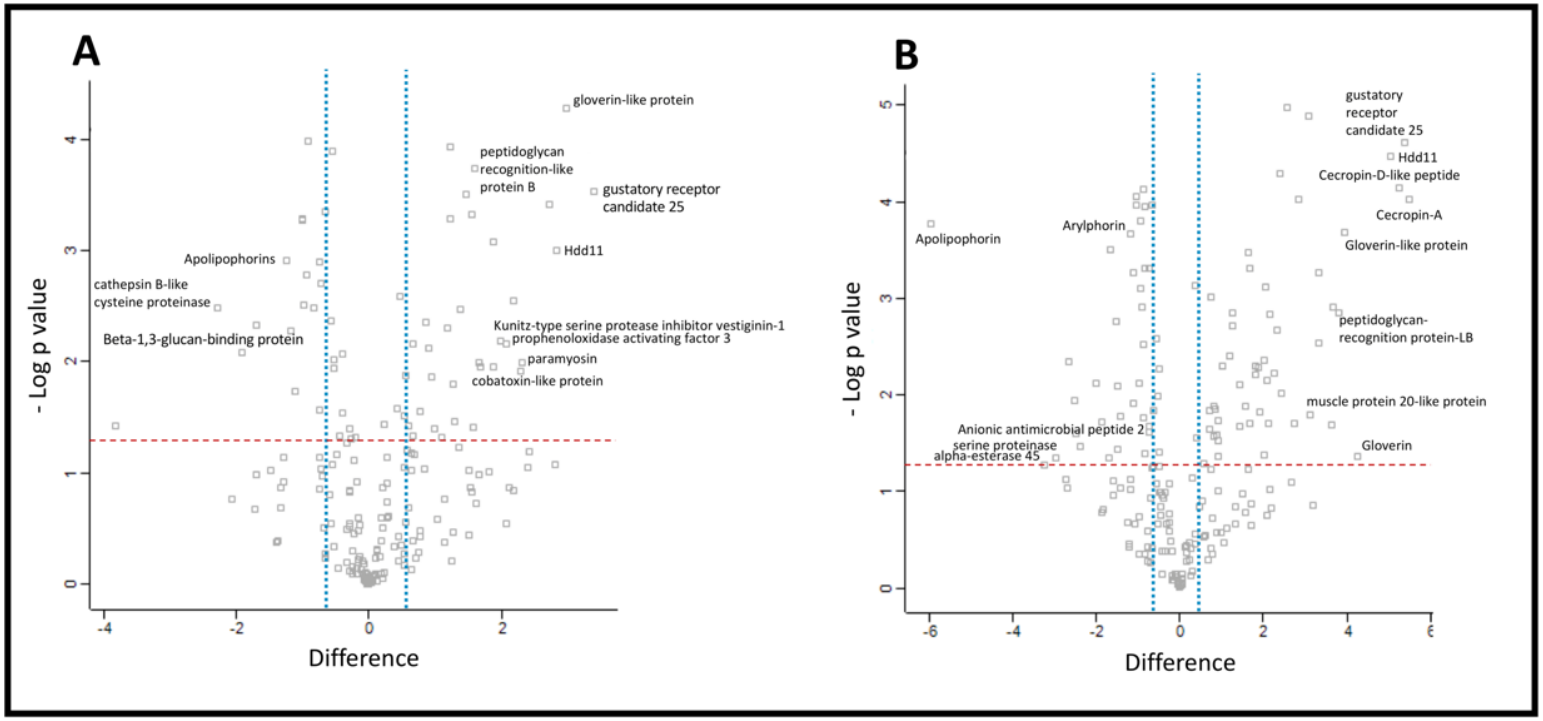

Fig. 5.7. Proteomic responses of *G. mellonella* larval hemolymph following co-infection by *C. albicans* (1×10^5 larva^{-1}) and *S. aureus* (2×10^4 larva^{-1}) after 6 (**A**) and 24 (**B**) h. Volcano plots represent protein intensity difference (- $\log_2$ mean intensity difference) and significance in differences (- log P-value) based on a two-sided *t*-test. Proteins above the line are considered statistically significant (p value < 0.05) and those to the right and left of the vertical lines indicate relative fold changes > 1.5. Annotations are given for the most differentially abundant proteins identified in hemolymph.

5.5 Evaluation of the efficacy of antimicrobial chemotherapy on the survival of *G. mellonella* larvae co-infected with *C. albicans* and *S. aureus*

The *in vitro* susceptibility of *C. albicans*, *S. aureus* to antimicrobial therapy [amphotericin B and meropenem] was first examined. Meropenem had no effect on the growth of *C. albicans*, however amphotericin B reduced the growth of *C. albicans* to 20 ± 7.3% ($p < 0.001$) at a concentration 3.90 μg ml^{-1}, and to 6.80 ± 0.39% ($p < 0.001$) at a concentration of 250 μg ml^{-1} relative to untreated cells (**Fig. 5.8A**). Interestingly, amphotericin B did reduce the growth of *S. aureus* to 60.12 ± 10.79% at 15.62 μg ml^{-1} ($p < 0.05$) and 14.91±0.86% ($p < 0.0001$) at a concentration of 250 μg ml^{-1} relative to untreated *S. aureus*. Meropenem was very active against *S. aureus* and reduced growth to 14.01 ± 2.23% ($p< 0.0001$) at the lowest concentration tested; 0.97 μg ml^{-1} (**Fig. 5.8B**).

The effect of both single therapy (amphotericin B or meropenem alone) or dual therapy (amphotericin B and meropenem in combination) on the combined growth of *C. albicans* and *S. aureus* was determined. Amphotericin B was more effective at reducing the growth of co-incubated microbes by reducing their growth to 65.63 ± 12.91% ($p < 0.01$) at a concentrations of 15.62 μg ml^{-1} whereas a concentration of 125 μg ml^{-1} reduced growth to 32.34 ± 4.86% ($p < 0.0001$) relative to untreated cells. Meropenem treatment alone had no effect on the combined growth of *C. albicans and S. aureus.* Furthermore, combination therapy was more active at lower concentrations at reducing the growth of *S. aureus* and *C. albicans* relative to monotherapy of amphotericin B. A concentration of amphotericin B and meropenem at 7.81 μg ml^{-1} reduced growth to 24.78 ± 14.50% ($p < 0.0001$). A concentration of 15.62 μg ml^{-1} reduced growth of co-incubated microbes to 14.07±2.70% ($p < 0.0001$) as compared to amphotericin (65.62 ± 12.91%, $p < 0.01$) or meropenem (114.78 ± 2.3%) alone (**Fig. 5.8C**). Based on these results concentrations of meropenem, amphotericin or combination (1.95, 7.81, 31.25 and 125 μg ml^{-1}) were selected to assess their *in vivo* efficacy against polymicrobial co-infection.

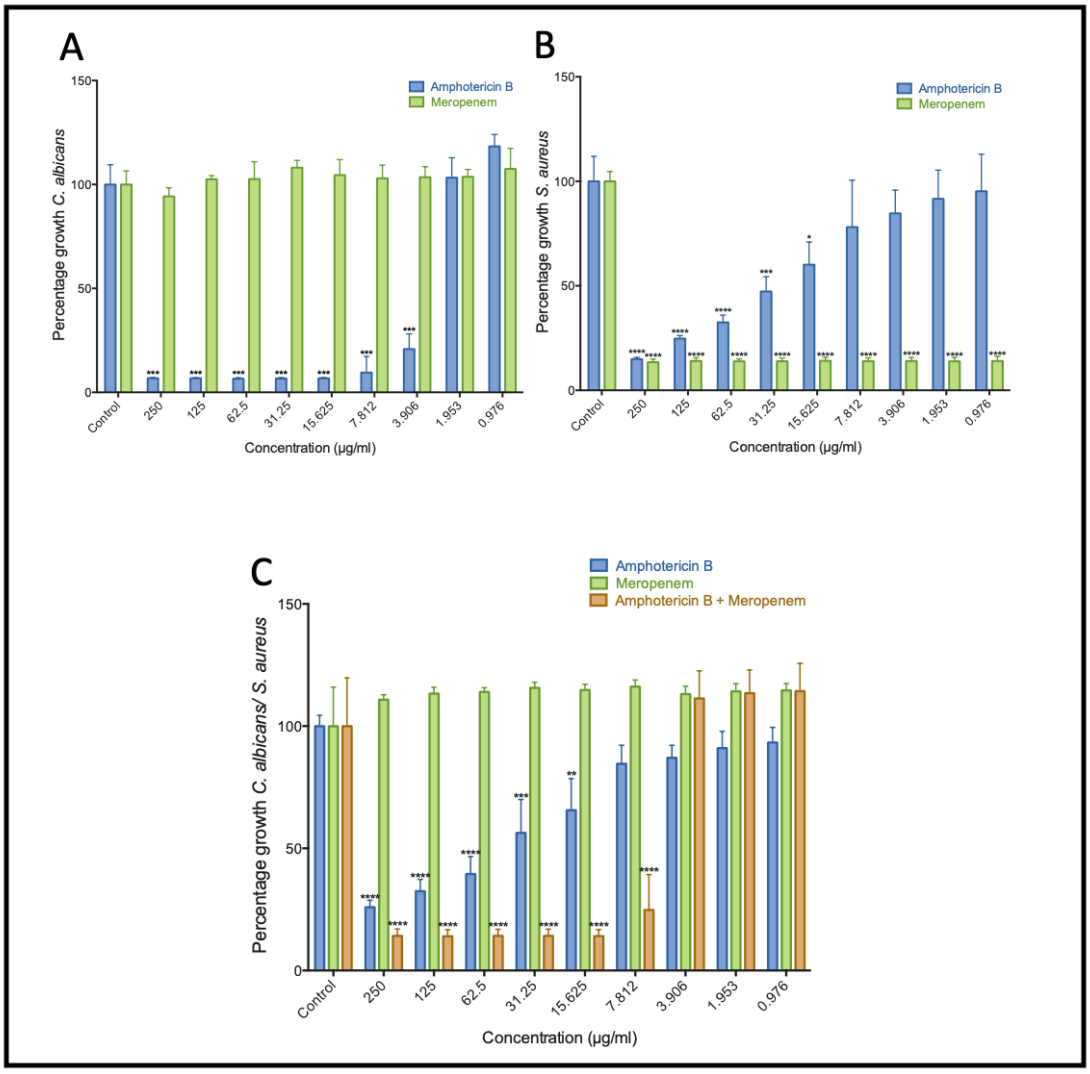

Fig. 5.8. Susceptibility of *C. albicans, S. aureus* and combination to anti-microbial chemotherapy. The effect of a range of concentrations (0.97 – 250 µg ml^{-1}) of amphotericin B, meropenem and dual therapy [amphotericin B and meropenem] on the growth of *C. albicans* (A; 1 × 10^4 $well^{-1}$), *S. aureus* (B; OD 0.1/$well^{-1}$) and combination (C; *C. albicans* [1 × 10^4 $well^{-1}$] *S. aureus* [OD 0.1/$well^{-1}$]) were determined in YEPD medium after 24 h incubation at 37 °C and growth was quantified by measuring at OD 570 readings. Statistically significance was determined by One-way ANOVA by comparing concentrations of antimicrobial drug to control (untreated cells) (*: $p < 0.05$, **: $p < 0.01$, ***: $p < 0.001$, ****: $p < 0.0001$).

Antimicrobial efficacy was tested *in vivo* by assessing the survival of co-infected larvae treated with amphotericin B, meropenem or combination therapy. Larvae treated with 40 µl of PBS displayed no significant decrease in survival over 96 h. Larvae were injected with 20 µl of amphotericin B, meropenem or combination therapy (1.95 – 31.25 µg ml^{-1}) with the addition of 20 µl PBS and viability and alterations in hemocyte density assessed over 96 h. Amphotericin B, meropenem or combination therapy did not alter larval viability or result in a significant change in hemocyte density over 96 h (data not presented).

Larvae (n=10) co-infected with *C. albicans* (1×10^5 $larva^{-1}$) and *S. aureus* (2×10^4 $larva^{-1}$) showed decreased survival at 24 (70 ± 3.33%), 48 (10 ± 3.33%), 72 (5 ± 6.66%) and 96 (0 ± 3.33%) h. However, larvae treated with amphotericin B at a concentration of 1.95 showed increased survival at 48 (30 ± 6.66%, $p < 0.01$) and 72 (20 ± 5%, $p < 0.05$) h post infection. A concentration of 31.25 µg ml^{-1} was most successful at increasing larval survival to 90 ± 5% ($p < 0.01$) at 24, 70 ± 0 ($p < 0.0001$) at 48, 50 ± 3.33% ($p < 0.0001$) at 72 and 40 ± 3.33 ($p < 0.0001$) at 96 h post infection (**Fig. 5.9A)**. Treatment of mixed microbial infection with meropenem produced significantly increased survival (1.95 µg ml^{-1}; $p < 0.05$, 7 µg ml^{-1}; $p < 0.0001$, 31.25 µg ml^{-1}; $p < 0.001$) of larvae relative to amphotericin treatment. Meropenem concentrations of 7.81 µg ml^{-1} and 31 µg ml^{-1} resulted in larval survival of 65 ± 3.33 ($p < 0.0001$) and 80 ± 5% ($p < 0.0001$) at 48 h post infection relative to PBS treated coinfected larvae (**Fig. 5.9B**). Combination therapy of co-infected larvae produced significantly higher survival relative to monotherapy. A concentration of 31.25 and 125 µg ml^{-1} resulted in no decrease in larval survival over 96 h. A concentration 7.81 µg ml^{-1} [amphotericin B and meropenem] resulted in increased survival of larvae at 24 (90 ± 5%, $p < 0.05$), 48 (80 ± 3.33%, $p < 0.0001$), 72 (70 ± 5%, $p < 0.0001$) and 96 (60 ± 3.33%, $p < 0.0001$) h post infection relative to PBS treated larvae (**Fig. 5.9C**).

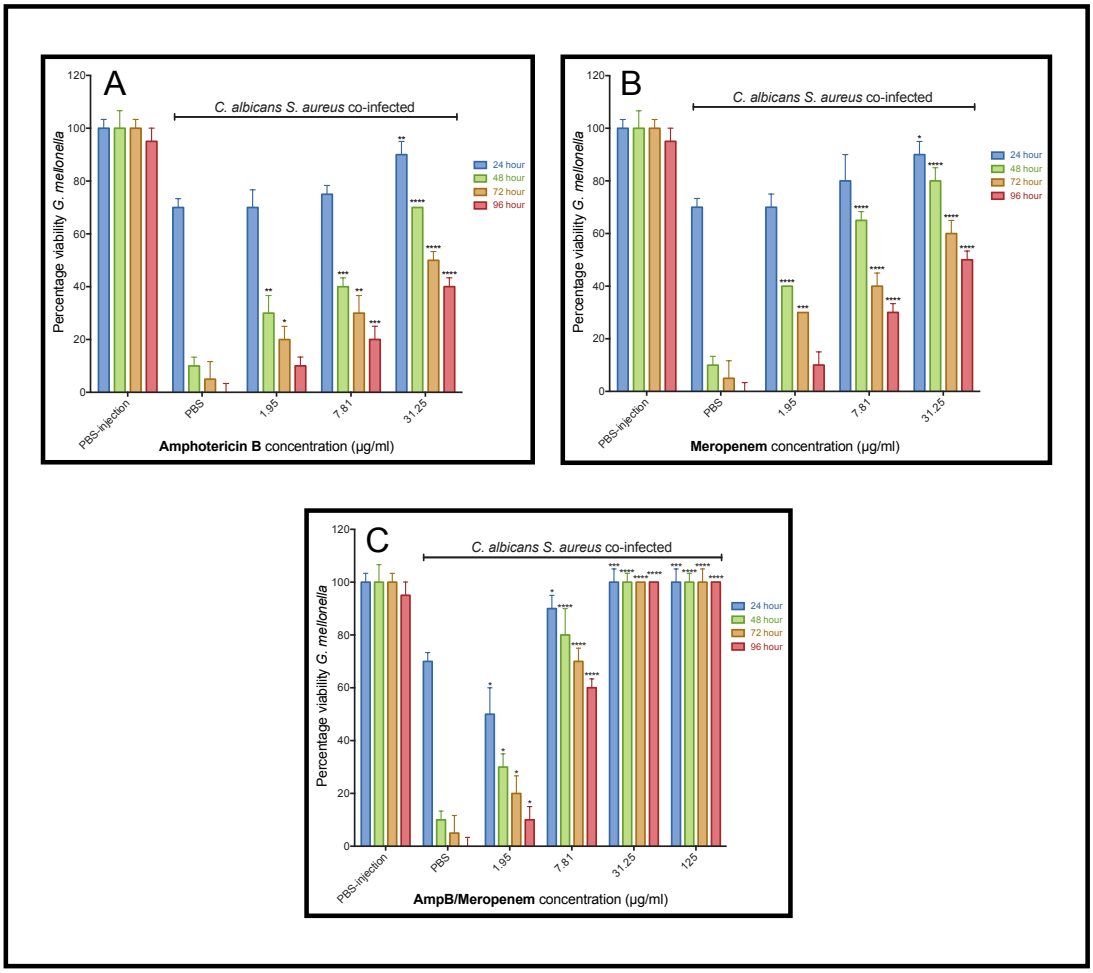

Fig. 5.9. Viability of co-infected *G. mellonella* larvae following administration of antimicrobial chemotherapy. Larvae (n = 10) were co-infected with 20 µl of a suspension of *C. albicans* (1×10^5 larva^{-1}) and *S. aureus* (2×10^4 larva^{-1}), incubated at 37 °C for 2 h, administrated 20 µl antimicrobial chemotherapy (amphotericin B [**A**], meropenem [**B**] or dual therapy [**C**; amphotericin B and meropenem] at a range of concentrations (1.95 µg ml^{-1} to 125 µg ml^{-1}) and viability assessed over 96 h. Larvae were also injected with 40 µl PBS (PBS injection) only. Statistical significance was determined by One-way ANOVA by comparing concentrations of antimicrobial drug to 'PBS' (co-infected control) treated larvae (*: $p < 0.05$, **: $p < 0.01$, ***: $p < 0.001$, ****: $p < 0.0001$). All values are the mean ± S.E of three independent experiments.

Cryo-imaging was performed on co-infected larvae treated with amphotericin B, meropenem or dual therapy at a range of concentrations to assess the efficacy of antimicrobial therapy in reducing the symptoms associated with co-infection. Larvae that received a dose of 1.95 µg ml^{-1} amphotericin B displayed less hemolymph melanisation compared to the control whereas larvae that received meropenem had more nodule formation and melanisation of internal tissues. Larvae treated with dual therapy produced larger nodules but less melanisation of tissue (**Fig. 5.10A**). Larvae treated with a dose of amphotericin B (31.25 µg ml^{-1}) had less nodules than control larvae but those treated with meropenem had more nodules, and combination treated larvae had less nodules and less systemic melanisation than control larvae (**Fig. 5.10B**).

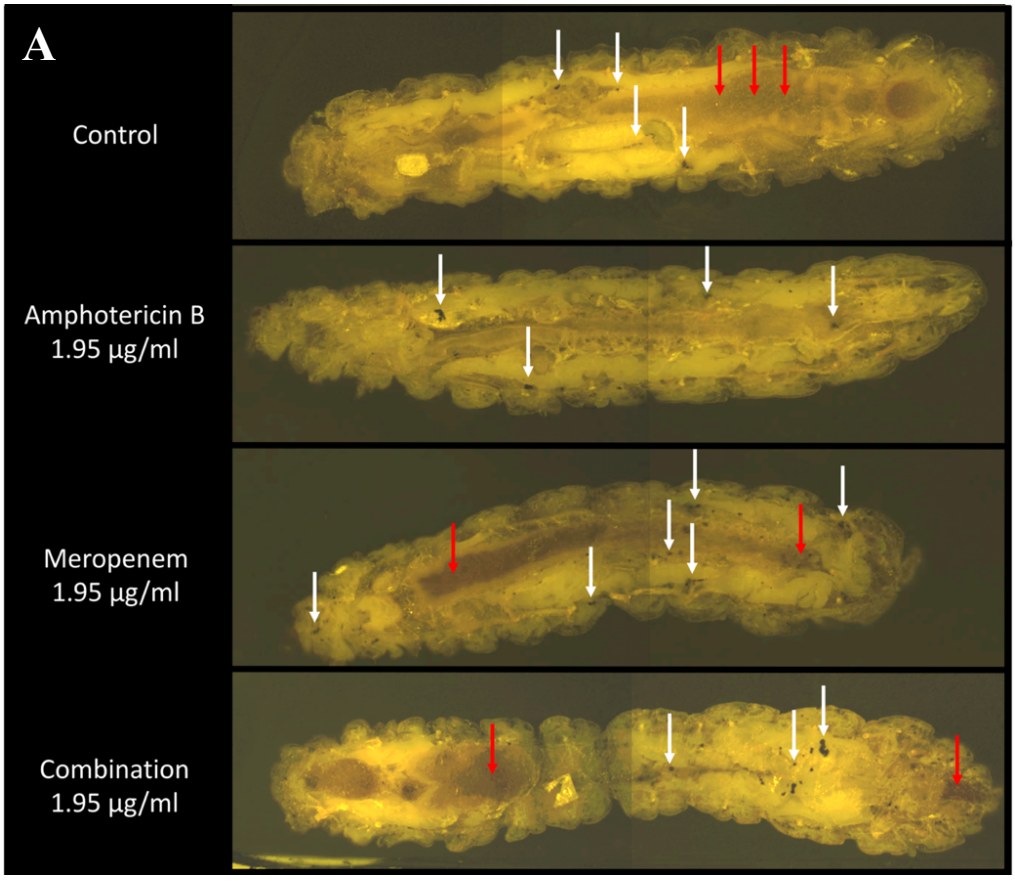

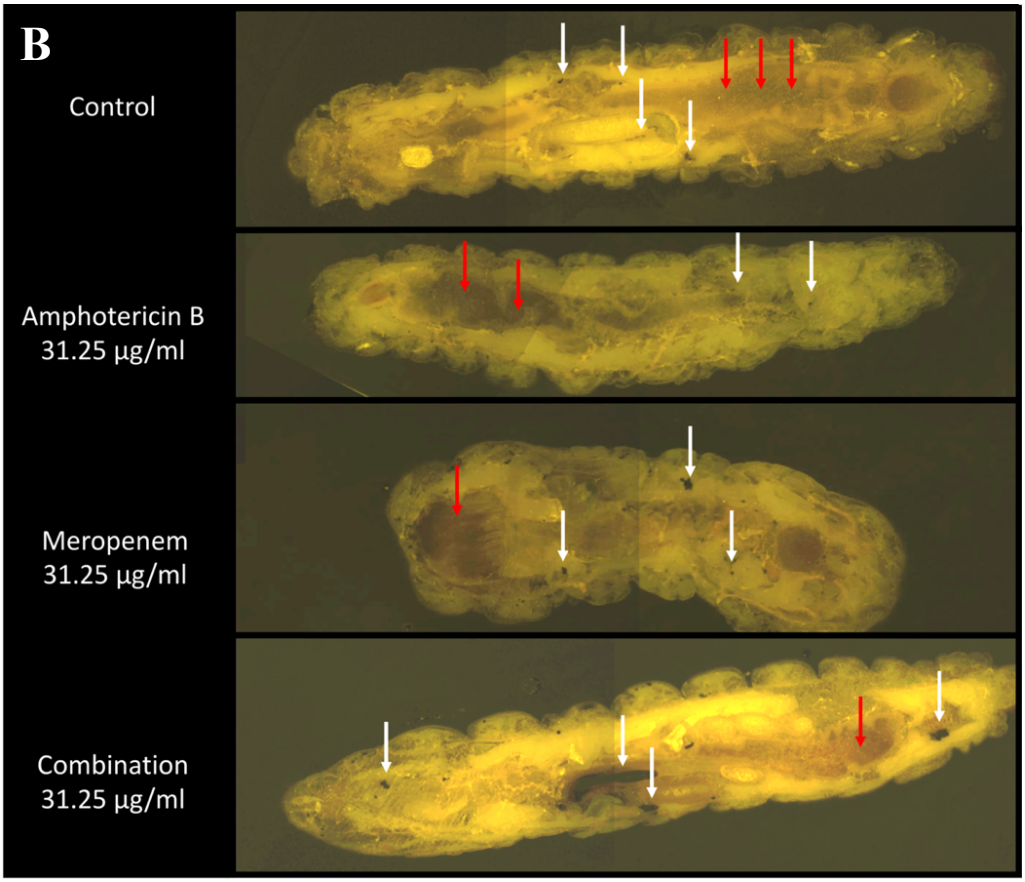

Fig. 5.10. Effect of antimicrobial chemotherapy on the symptoms associated with disseminated disease in co-infected larvae. Co-infected larvae were administrated amphotericin B, meropenem or combination therapy at a concentration of (**A**) 1.95 µg ml^{-1} and (**B**) 31.25 µg ml^{-1} 2 h post infection and subjected to cryo-imaging 24 h post infection. Larvae were embedded, sectioned (10 µm) and visualised using a cryo-imaging system (nodules (white arrow), extensive melanisation (red arrows)).

5.6 Discussion

The incidence of polymicrobial infections is likely underestimated as routine clinical microbiological investigation could never encompass the vast number and diversity of microbes present within the human micro- and mycobiome. Advances in technologies associated with the detection of these microbes will eventually enter the clinic and this will ultimately result in the classification of many mono-infections as polymicrobial infections. With this in mind, this Chapter aimed to develop a cost effective and easily accessible *in vivo* system to study the pathogenesis of polymicrobial infection and the efficacy of antimicrobial chemotherapy on enhancing the survival of co-infected larvae.

Inoculation of larvae with *C. albicans* (1×10^5 larva^{-1}) and *S. aureus* (2×10^4 larva^{-1}) in mono-infection resulted in no decrease in survival, however co-inoculation of larvae with these doses resulted in a significant decrease in survival relative to larvae mono-infected with *S. aureus* (2×10^4 and 2×10^6 larva^{-1}). This suggests that the interactions between *C. albicans* and *S. aureus* may be synergistic which has been previously documented in mice (Harriott and Noverr, 2009; Shirtliff *et al.*, 2009; Peters and Noverra, 2013; Schlecht *et al.*, 2015; Kean *et al.*, 2017; Kong *et al.*, 2017; Krüger *et al.*, 2019). Infection of *G. mellonella* larvae with *S. aureus* (2×10^6 larva^{-1}) or *C. albicans* (5×10^5 larva^{-1}) in mono- infection resulted in 70% and 44% larval mortality after 48 h, respectively. In mice, doses of *C. albicans* and *S. aureus* which are non-lethal 5 days post infection, when combined resulted in 30% survival 2 days post infection (Peters and Noverra, 2013).

Inoculation with a low inoculum of *S. aureus* (2×10^4 larva^{-1}) with *C. albicans* (1×10^5 larva^{-1}) resulted in a significant increase in hemocyte density, however a high inoculum of *S. aureus* (2×10^6 larva^{-1}) with *C. albicans* (1×10^5 larva^{-1}) produced a decrease in hemocyte density relative to *S. aureus* mono-infection as compared to the relevant *S. aureus* inoculum. The increase in hemocyte number is probably as a result of the release of hemocytes usually attached to the linings of internal organs such as the fat body (Ratcliffe, 1985b) while the decrease in hemocyte density associated with the higher inoculum may be due to the aggregation of hemocytes at the site of inoculation in order to halt the spread of the infection. Interestingly, mice co-infected with *C. albicans* and *S. aureus* had a

significantly higher number of neutrophils in the peritoneal cavity as compared to mono-infection (Peters and Noverra, 2013). Co-inoculation of larvae results in a significant increase in c.f.u. larva^{-1} relative to mono-infection. In co-infected mice, microbial burden was significantly higher in the kidney and spleen compared to mono infection (Peters and Noverra, 2013). Interestingly, the total *S. aureus* c.f.u in co-infected larvae, regardless of dose was 10.65 ± 4.40 fold higher than *S. aureus* only -infected larvae.

Cryoviz imaging was utilised to assess the dissemination of co-infection throughout the host over 48 h. By 24 h post infection there was significant nodule formation and by 48 h there was extensive melanisation and widespread nodule formation throughout the host. Interestingly, infection of larvae with a higher inoculum of *C. albicans* (5×10^5 larva^{-1}) and *S. aureus* (2×10^6 larva^{-1}) in mono-infection results in more cuticular melanisation and larger granuloma (nodule) type structure formation (section 3.8, section 4.3). This may indicate that co-infection, at a lower cell density which ultimately produced a larger decrease in survival relative to mono-infection, may have activated a less robust immune response to co-infection. Interestingly, Peters & Noverra (2013) found co-infection by *C. albicans* and *S. aureus* was associated with an augmented inflammatory response characterised by up to a +100-fold increase in inflammatory cytokines (e.g. IL-6) and neutrophil influx in mice.

The humoral immune response of larvae to co-infection was determined by tandem mass spectrometry. At 6 h post co-infection antimicrobial peptide gloverin-like protein was increased +7.9 fold. Gloverins are heat stable antibacterial polypeptides which bind to bacterial lipopolysaccharide and components of the fungal cell wall. It was previously demonstrated that *E. coli* and *S. aureus* induce gloverin expression in *Bombyx mori and Manduca sexta* (Xu *et al.*, 2012; Yi *et al.*, 2013). Gloverins display activity against yeast but do not possess anti-*staphylococcal* activity (Xu *et al.*, 2012). In *C. albicans* infected *G. mellonella* larvae, gloverin was not detected 6 h post infection but was increased +52 fold at 24 h post infection, however in *S. aureus* infected larvae gloverin was +20 fold increased at 6 h and +121 fold at 24 h post infection. Similarly, PGRP-B was increased +3 fold in co-infected larvae but +2.3 fold in *C. albicans*, and +6 fold in *S.*

aureus mono-infected larvae (section 3.9, section 4.5). Furthermore, these experiments were performed with five times more *C. albicans* (5×10^5 larva^{-1}) and 100 times more *S. aureus* (2×10^6 larva^{-1}) relative to co-infected larvae (*C. albicans* (1×10^5 larva^{-1}), *S. aureus* (2×10^4 larva^{-1}). Members of the phenoloxidase cascade (e.g. prophenoloxidase activating factor 3) were increased up to +4.2 fold in co-infected larvae 6 h post co-infection but were only increased +2.4 fold in *C. albicans* and +2.85 fold in *S. aureus* at 6 h post mono-infection. The phenoloxidase cascade is a series of enzymatic reactions which result in the formation phenoloxidase which participates in melanotic encapsulation, wound healing, and cuticle sclerotisation and this reaction is analogous to the mammalian complement cascade in terms of protein structure and function (Wojda, 2017).

By 24 h post co-infection cecropin-A was increased +45 fold as compared to control larvae. Cecropin-A is a 37 amino acid antimicrobial peptide first isolated from *H. cecropia*. It has antibacterial activity against multidrug resistant bacteria (e.g. *S. aureus*), induces *C. albicans* apoptosis and displays immune-modulatory effects on human macrophages (Lee *et al.*, 2013; Lee *et al.,* 2015; Yun and Lee, 2016). Cecropin-A was increased in *C. albicans* mono-infected larvae (+4.5 fold) at 6 h post infection larvae but was increased +10.5 fold 24 h post *S. aureus* infection. Moricin-like peptide was increased +21 fold and +20.8 fold during *C. albicans* and *S. aureus* mono-infection, respectively but was not detected in co-infected larvae. Moricins are secreted pro-peptides and are activated via proteolysis and increase the permeability of bacterial and fungal membranes. *G. mellonella* moricins are highly active against yeasts and *S. aureus* (Hara and Yamakawa, 1995; Brown *et al.*, 2008). Hdd11 was increased +7.1 and +33.33 fold at 6- and 24 h post co-infection. However, hdd11 was +49 fold and +7.24 fold increased at 24 h post *C. albicans* and *S. aureus* infection, respectively. Hdd11 shares homology with noduler from the tasar silkworm (*Antheraea mylitta*) (Woon Shin *et al.*, 1998; Sarauer *et al.*, 2003). Noduler shares a reeler domain with hdd11 and binds both insect hemocytes, bacterial LPS and fungal β-glucan, is enriched within nodules (section 7.5) and is important during the nodulation response (Gandhe *et al.,* 2007). Apolipophorin was -1.9 fold decreased in abundance in mono *C. albicans* infected larvae and not detected during *S. aureus* infection but was found to be significantly decreased (-64.2 fold) during co-infection by *S. aureus* and *C. albicans.* Apolipophorin plays a

role in lipid transport (Niere *et al.*, 1999; Niere *et al.*, 2001) but has immune-modulatory activity and augments the activity of lyzosyme (Zdybicka-Barabas and Cytryñska, 2013), potentiates the activity of antimicrobial peptides (Park *et al.*, 2005), regulates phenoloxidase activity (Zdybicka-Barabas and Cytryńska, 2011; Zdybicka-Barabas *et al.*, 2014) and is a pathogen recognition receptor and opsonin for bacterial lipopolysaccharide and lipoteichoic acids, and fungal β-glucan (Wojda, 2017). Furthermore, lysozyme was decreased (-4.9 fold) during *C. albicans* mono-infection of larvae and increased (+31.38 fold) during *S. aureus* mono infection but was not detected in co-infected larvae.

In total 23 *C. albicans* and 20 *S. aureus* proteins were found in hemolymph during co-infection of *G. mellonella* larvae. *C. albicans* heat shock protein SSA2 and peroxiredoxin TSA1-A and *S. aureus* staphopain B were found in hemolymph 24 h post-infection. SSA1 can induce host cell endocytosis of *C. albicans* which leads to increased virulence (Sun *et al.*, 2010) and plays a role in resistance to antimicrobial peptides and antifungal agents (Cho *et al.*, 2003; Li *et al.*, 2003; Nagao *et al.*, 2012). Peroxiredoxin TSA1-A was also detected in larvae mono-infected with *C. albicans* (section 3.10) and plays a role in cell protection against oxidative stress (Urban *et al.*, 2005). *S. aureus* staphopain B decreased the phagocytic activity of neutrophils and cleaved CD31 resulting in increased clearance by macrophages (Smagur *et al.*, 2009). It is possible these proteins display activity against insect hemocytes and antimicrobial peptides or play a role in the detoxification of the host immune response.

The incidence of co-infection is likely underestimated and *in vivo* data suggest that co-infection caused by *C. albicans* and *S. aureus* results in higher mortality and increased fungal burden (Peters and Noverra, 2013). *In vitro* data also demonstrated that the presence of *C. albicans* or *S. aureus* decreases each other's sensitivity to antifungal or antibacterial agents, respectively (Harriott and Noverr, 2009; Kean *et al.*, 2017). The efficacy of a novel combination of amphotericin B and meropenem was assessed in *G. mellonella* larvae co-infected with *C. albicans* and *S. aureus*. Amphotericin B binds ergosterol in the fungal cell membrane, resulting in pore formation, cell leakage and eventually fungal cell death (Fanos and Cataldi, 2014). Meropenem binds to penicillin binding proteins involved in bacterial cell wall

synthesis (Hawkey and Livermore, 2012), demonstrates activity against *S. aureus* and is active in combination with other antibiotics (e.g. piperacillin/tazobactam) against MRSA. Furthermore, the use of meropenem is not associated with an increased risk of the development of an invasive *Candida* infection, unlike ciprofloxacin (Gonzales *et al.*, 2015; Jensen *et al.*, 2015). Currently, the recommended treatment of candidaemia in non-neutropenic patients is amphotericin B at a dose of 3 mg/kg/day^{-1} (Allen, 2010; Cornely *et al.*, 2012; Pea and Lewis, 2018). The adult dose for meropenem is from 500 mg to 1000 mg per 8 h (7 – 14 mg kg^{-1} for a 70 kg adult) and meropenem is commonly used to treat acute bacterial meningitis, pneumonia, complicated skin and soft tissue infections and is the first port of call for the treatment of suspected bacterial infection in neutropenic patients (Hawkey and Livermore, 2012). The doses selected in this study for amphotericin B and meropenem (1.95, 7.81, 31.25 and 125 μg ml^{-1}) correspond to 0.18, 0.71, 2.84 and 11.36 mg kg^{-1} respectively.

Amphotericin displayed excellent *in vitro* activity against *C. albicans* (MIC_{50}; 3.90 μg ml^{-1}) but also had activity against *S. aureus* (MIC_{50}: 15.62 μg ml^{-1}), while meropenem only displayed activity against *S. aureus* (MIC_{50}: 0.97 μg ml^{-1}). Interestingly, meropenem alone had no effect on the growth of *C. albicans* and *S. aureus* in combination, whereas amphotericin B displayed good activity against the combination (MIC_{50}: 15.62 μg ml^{-1}) and the addition of meropenem with amphotericin reduced growth (MIC_{50}: 7.81 μg ml^{-1}). Meropenem displayed better *in vivo* activity over amphotericin B in co-infected larvae and this may indicate that *S. aureus* is the primary cause of decreased survival but *C. albicans* enhances this effect (c.f.u. results; increased *S. aureus* growth in co-infection compared to mono-infection). This may have negative implications for patients which are presumably infected with only *S. aureus* but may be also infected with *C. albicans*. Treatment of co-infected larvae with a combination of amphotericin B and meropenem at 31.25- and 125- μg ml^{-1} was most effective and resulted in no larval mortality over 96 h.

Co-infected larvae were treated with amphotericin B, meropenem or combination (1.95 and 31.25 μg ml^{-1}) and subjected to cryo-imaging. Interestingly, larvae which received a dose of 31.25 μg ml^{-1} of amphotericin B, meropenem or combination displayed less melanisation compared to larvae which received PBS.

This highlights a novel use of cryo-imaging to determine the efficacy of antimicrobial chemotherapy at the whole organism/symptoms level.

In conclusion, the results presented in this Chapter demonstrate that the *G. mellonella* larvae model is an excellent *in vivo* system to study co-infection by dual species, inter-kingdom microbial pathogens and is also an effective system for screening novel combinations of antimicrobial agents against co-infection. This model could be adapted for other common interactions (antagonistic or synergistic) which exist during infection of the human host (e.g. *A. fumigatus* with *P. aeruginosa*, *S. aureus* etc., *C. albicans* with *E. coli, Lactobacilli, P. aeruginosa* or dual species, intra-kingdom infection). This is particularly important as advances in healthcare which ultimately result in inhibition of the host immune response (e.g. spleen tyrosine kinase (SYK) inhibitors) will facilitate the emergence of new pathogens which are better adapted to survival in diverse ecological niches which will thrive in the immunocompromised host.

Chapter 6

Characterisation of the cellular and proteomic response of *Galleria mellonella* larvae to the development of invasive aspergillosis

6.1 Introduction

A. fumigatus can induce allergic, saprophytic and invasive disease depending upon the host immune status. In the case of invasive disease, inhaled conidia germinate, form hyphae within alveoli and migrate beyond the pulmonary epithelium and into the bloodstream (angioinvasive), ultimately disseminating throughout the host if anti-fungal therapy is not commenced (Dagenais and Keller, 2009; Margalit and Kavanagh, 2015). In the murine model of chronic granulomatous disease (CGD), invading hyphae are found within granulomatous lesions predominated by neutrophils that probably function to prevent the spread of conidia (Dennis *et al.*, 2006).

Larvae of *G. mellonella* have been utilised to study the virulence of *A. fumigatus* and provided results comparable to those from murine studies. *A. fumigatus Δpes*3 mutants displayed significantly higher mortality in *G. mellonella* larvae than WT *A. fumigatus* which was mirrored in two murine models of pulmonary aspergillosis (corticosteroid-treated and neutropenic) (O'Hanlon *et al.*, 2011). Mutant strains of *A. fumigatus* (Δ*sid*A, Δ*sid*C, Δ*sid*D, Δ*sid*F, Δ*paba* and Δ*cpc*A) demonstrated almost complete correlation of virulence when assessed in *G. mellonella* and mice (Slater *et al.*, 2011). Hemocytes can discriminate between non-germinated, germinating and hyphal forms of *A. fumigatus* which is also the case with human neutrophils (Renwick *et al.*, 2006; van de Veerdonk *et al.*, 2017). *Aspergillus terreus* infection in *G. mellonella* demonstrated unique histological findings (i.e. invasion of tissue) consistent with those observed in disseminated aspergillosis in mammals (Maurer *et al.*, 2015).

The aim of the work presented in this Chapter was to analyse the response of *G. mellonella* larvae to *A. fumigatus* infection and to examine similarities with invasive aspergillosis in mammals. While *G. mellonella* larvae are now widely used as *in vivo* models a greater understanding of the pathogen – host interaction may allow the identification of a range of end points and further validate use of larvae for studying disease processes *in vivo*.

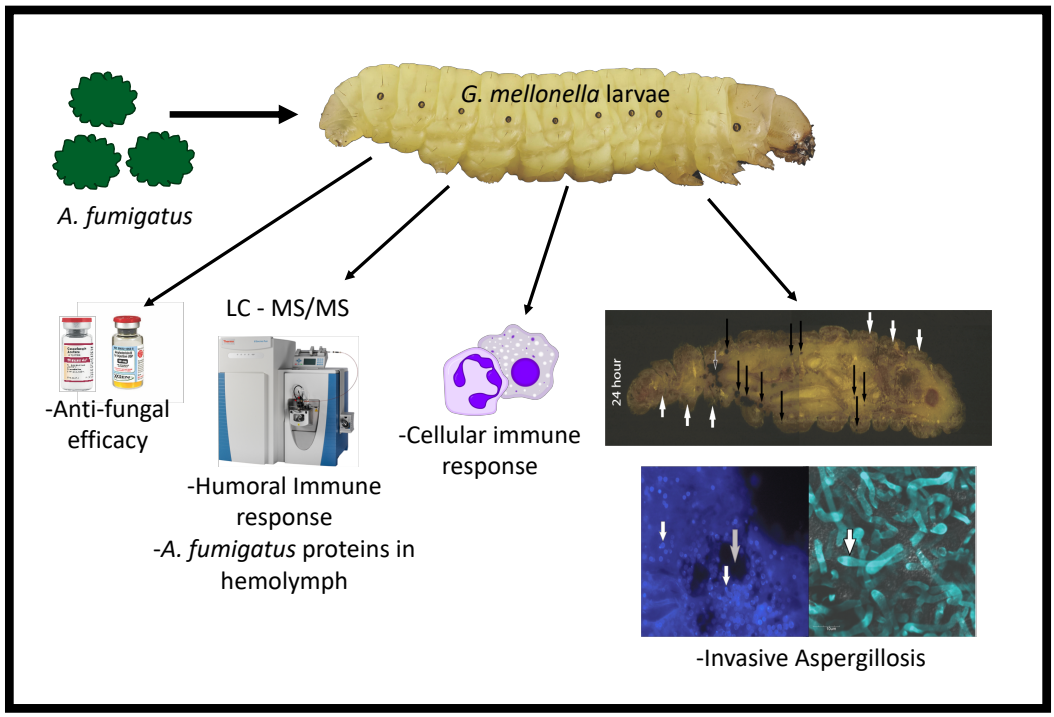

Fig. 6.1. Chapter 6 graphical abstract.

6.2. Responses of *G. mellonella* larvae to *A. fumigatus* infection

Larvae were inoculated with heat killed (HK) and viable conidia of *A. fumigatus*, incubated at 37 ºC and viability was assessed over 72 h. An inoculum of heat killed conidia ranging from 1×10^4 to 1×10^7 larva^{-1} yielded no change in larval viability over 72 h. An inoculum of 1×10^4 viable conidia larva^{-1} resulted in no change in larval viability over 72 h whereas 1×10^5 viable conidia larva^{-1} caused 16.7 ± 5.7% mortality after 72 h. A dose of 1×10^6 viable conidia resulted in 30 ± 5.7% and 90 ± 3.3% mortality after 48 h and 72 h respectively. Inoculation of larvae with conidia at a dose of 1×10^7 larva^{-1} reduced viability to 77 ± 3.3% and 0 ± 0% at 24 and 48 h respectively (**Fig. 6.2**).

6.3 Alterations in hemocyte density in response to *Aspergillus* infection

Inoculation of larvae with viable conidia (1×10^6 larva^{-1}) induced an initial spike in circulating hemocyte density at 2 h ($7.43 \pm 0.50 \times 10^6$, $p < 0.01$) which stabilised at 4 h ($4.88 \pm 0.15 \times 10^6$) (**Fig. 6.3)**. Hemocyte density increased at 6 ($6.42 \pm 0.20 \times 10^6$, $p < 0.05$) and 8 h ($6.95 \pm 0.48 \times 10^6$, $p < 0.05$). At 12 ($3.03 \pm 0.20 \times 10^6$) and 24 h ($6.74 \pm 0.43 \times 10^6$) post infection there were fluctuations in hemocyte density. Inoculation of larvae with heat killed conidia (1×10^6 larva^{-1}) also produced similar cellular responses. Notably, hemocyte density peaked at 2 h ($12.33 \pm 0.95 \times 10^6$, $p < 0.001$) but fell at 4 h ($3.5 \pm 0.85 \times 10^6$) and did not decrease at 12 h ($7.52 \pm 0.66 \times 10^6$) as observed with viable conidia.

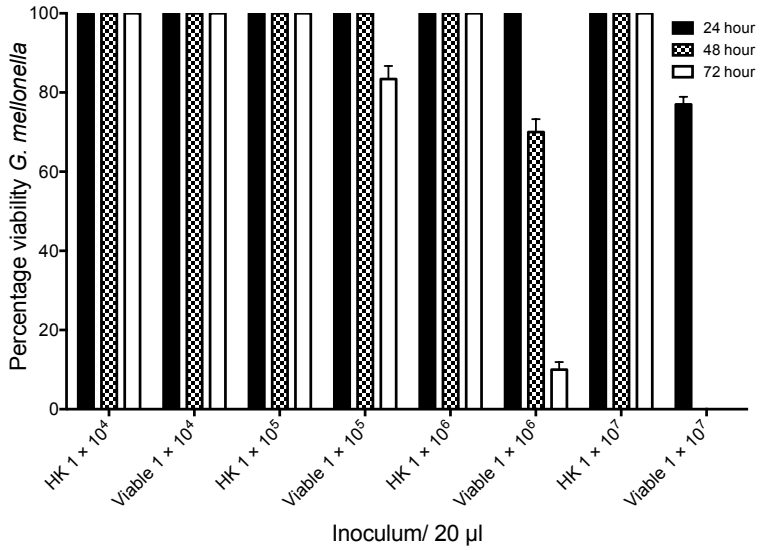

Fig. 6.2. Effect of viable and heat killed (HK) *A. fumigatus* conidia on viability of *G. mellonella* larvae over 72 h. *G. mellonella* larvae were inoculated with 20 µl *A. fumigatus* at doses ranging from 1×10^4 to 1×10^7 incubated at 37 °C and viability assessed over 72 h. All values are the mean ± S.E of three independent experiments.

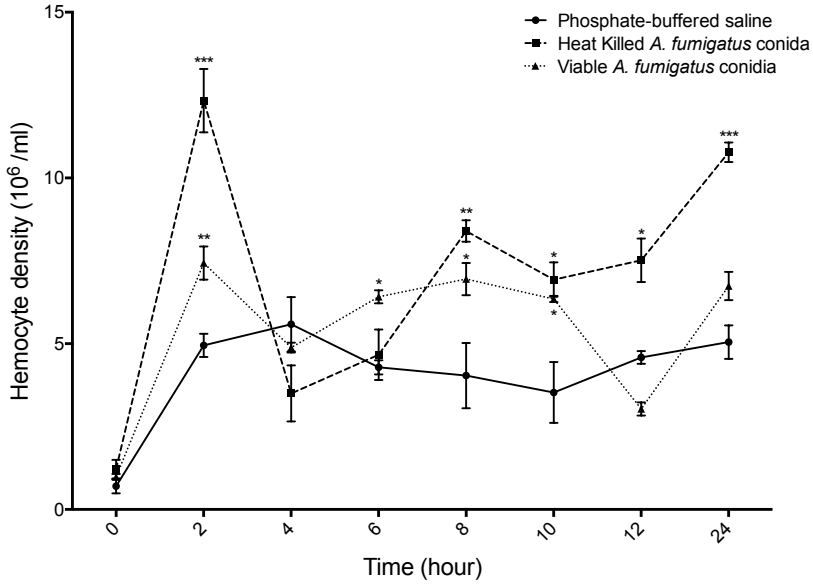

Fig. 6.3. Alteration in circulating hemocyte density following inoculation with viable and heat killed *A. fumigatus* conidia. *G. mellonella* larvae were inoculated with 20 µl heat killed conidia (1×10^6), viable *A. fumigatus* conidia (1×10^6) or PBS and hemocytes were extracted and enumerated from 0 h to 24 h post inoculation. Statistical analysis was performed by comparing treatments to PBS injected controls at respective time points (*: $p < 0.05$, **: $p < 0.01$, ***: $p < 0.001$). All values are the mean ± S.E of three independent experiments.

6.4 Change in hemocyte subpopulations in response to heat killed *A. fumigatus*

Changes in the types of hemocytes were assessed by flow cytometric analysis. An inoculum of 1×10^6 heat killed conidia $larva^{-1}$ increased the abundance of P1 cells (large, non-granular) at 6 h (26.75 ± 1.92 %, $p < 0.05$) as compared to the zero-h injected control (13.90 ± 3.12), P1 cells decreased by 24 h (9.71 ± 2.93 $p < 0.05$) which was associated with a statistically significant increase in P2 cells (small, very granular) (38.37 ± 1.77%, $p < 0.01$) at this time point (**Fig. 6.4**).

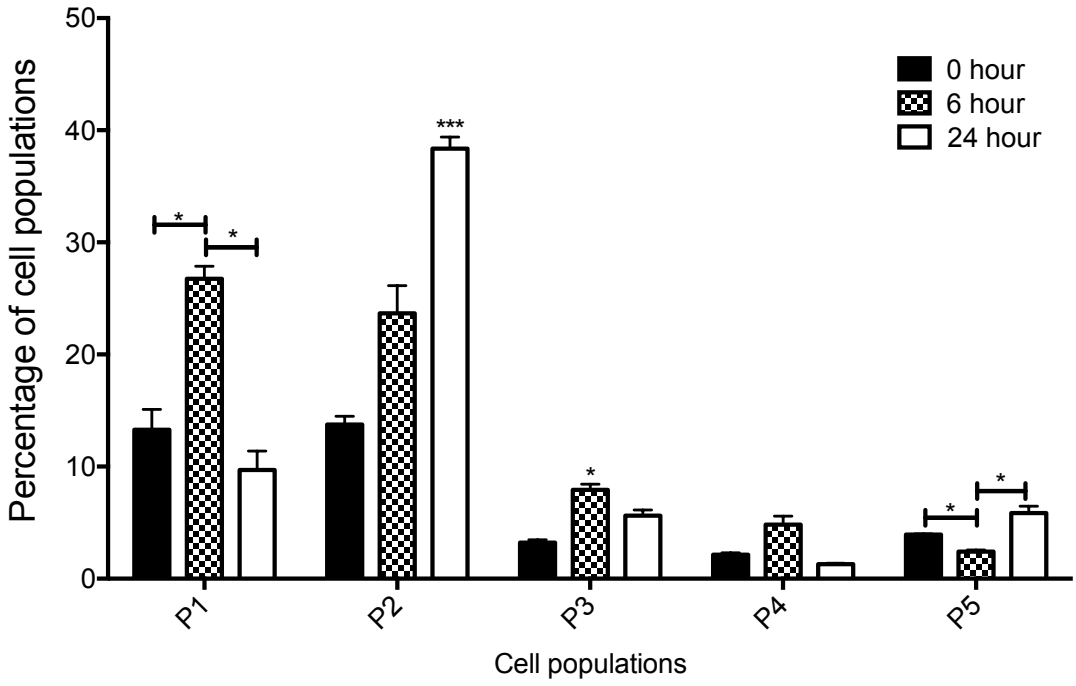

Fig. 6.4. Flow cytometric analysis of hemocyte sub-populations. Fluctuations in hemocyte sub-populations in larvae administered heat killed *A. fumigatus* at 0 h, 6 h and 24 h. Hemocyte sub-populations were measured based on size and granularity as described (*: $p < 0.05$, ***: $p < 0.001$). All values are the mean ± S.E of 3 independent determinations.

6.5 Changes in hemocyte function in response to *A. fumigatus*

Changes in hemocyte function following inoculation of larvae with heat killed *A. fumigatus* conidia were characterised by an *ex vivo* hemocyte microbicidal activity assay. Hemocytes from larvae inoculated with heat killed conidia for 6 h significantly decreased the viability of *C. albicans* to 11.94 ± 5.17% ($p < 0.05$) as compared to hemocytes from controls (37.07 ± 5.38%) and larvae inoculated for 24 h (40.67 ± 4.04%), at 80 mins. Interesting, hemocytes from 6 (101.49 ± 3.96%, $p < 0.05$) and 24 (95.17 ± 3.06%, $p < 0.05$) h inoculated larvae were slower at killing yeast cells at t = 20 min, compared to hemocytes from control larvae (62.93 ± 2.98%) (**Fig. 6.5)**.

The intracellular and extracellular killing activity of hemocytes (at t = 0, 6 and 24 h) was also assessed (section 2.4.9). These results demonstrate that hemocytes from larvae exposed to HK *A. fumigatus* conidia for 6 h had more viable intracellular ($6.65 \pm 0.17 \times 10^4$, $p < 0.01$) (**Fig. 6.6A**) and extracellular ($2.32 \pm 0.04 \times 10^4$, $p < 0.01$) *C. albicans* (**Fig. 6.6B**) as compared to 0 h (intracellular [$5.02 \pm 0.03 \times 10^4$], extracellular [$1.54 \pm 0.02 \times 10^4$]) extracted hemocytes at 10 mins post incubation.

6.6 Modelling invasive and disseminated aspergillosis in *G. mellonella*

Cryo-imaging was employed to visualise the stages of invasive aspergillosis disease in *G. mellonella* larvae. Larvae were inoculated with viable *A. fumigatus* conidia through the last left proleg in the posterior region (see white-edged arrow). Small discrete nodules appeared in the anterior region and around the perimeter of the hemocoel 6 h post infection (see black arrows) indicating dissemination of the *A. fumigatus* conidia from the site of infection. By 24 h there is extensive melanisation of larval tissue and cuticle (see white arrows) indicating invasion from the insect hemocoel into surrounding tissue, and formation of both large diffuse fungal nodules at the site of inoculation and smaller distinct fungal nodules throughout the larva (**Fig. 6.7**).

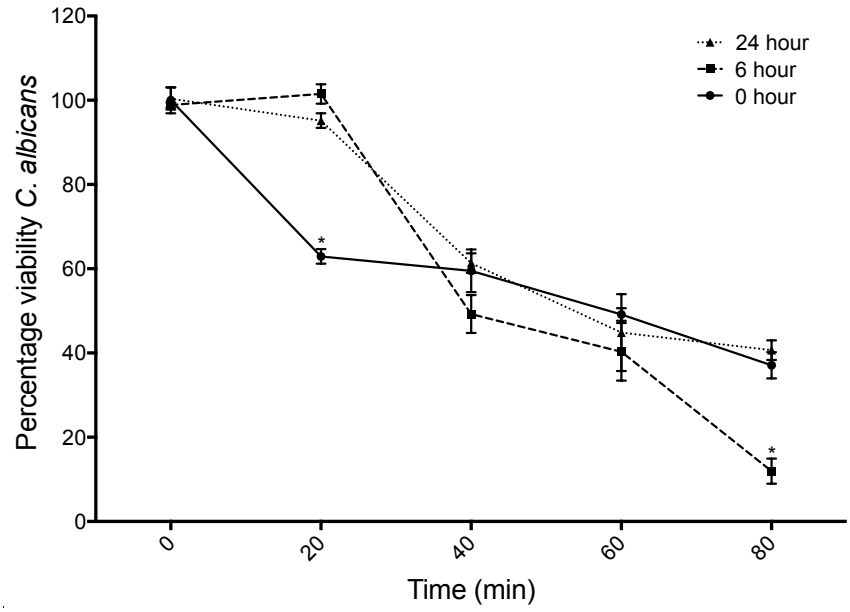

Fig. 6.5. Fungicidal activity *G. mellonella* hemocytes. Fungicidal activity of hemocytes extracted from *G. mellonella* larvae at 0, 6 and 24 h post inoculation with *A. fumigatus* heat killed conidia (1×10^6 larva^{-1}). Opsonised *C. albicans* cells were incubated with hemocytes (2:1 ratio) for 80 min and aliquots taken every 20 min diluted and plated on YEPD agar plates. (*: $p < 0.05$). All values are the mean ± S.E of three independent experiments.

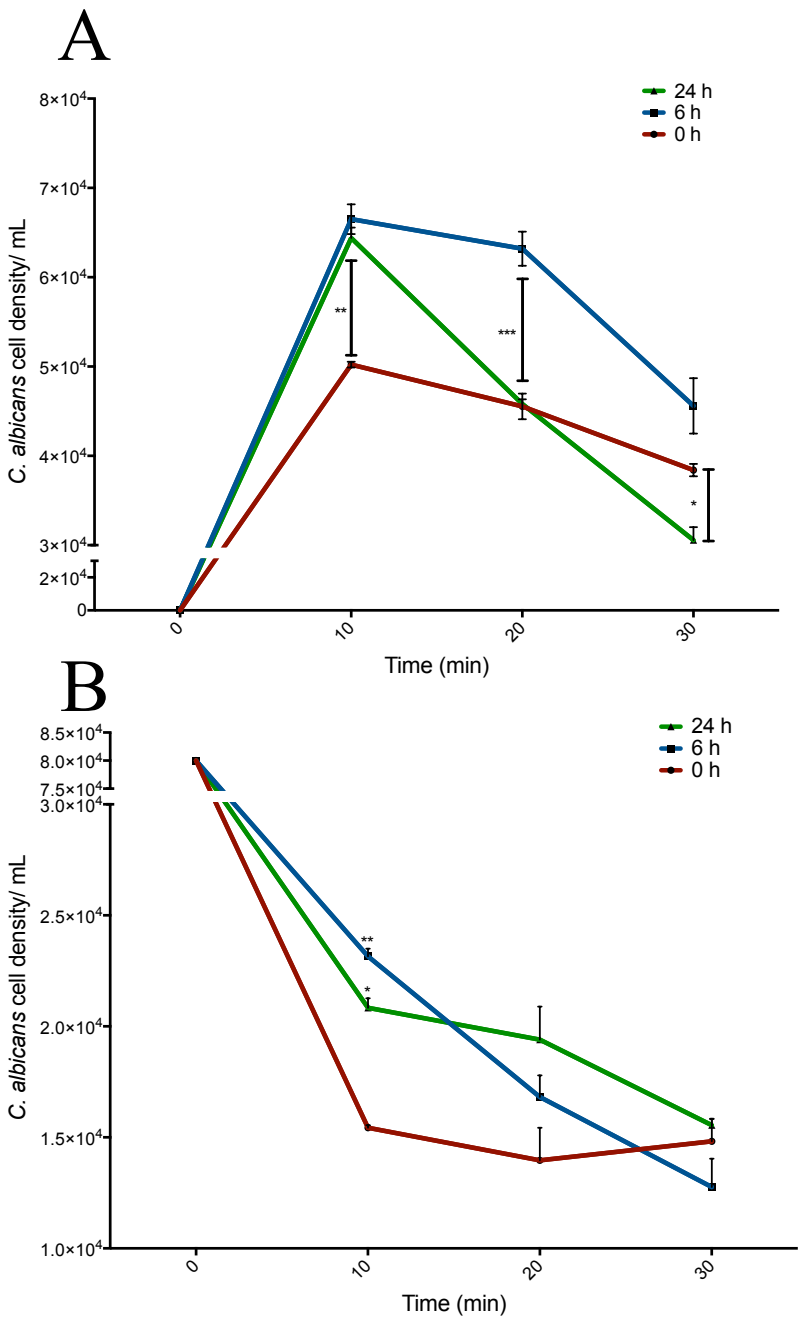

Fig. 6.6. Intracellular (A) and extracellular (B) killing activity of hemocytes from larvae exposed to heat killed *A. fumigatus* (1× 10^6 20 μl^{-1}). Hemocytes from larvae were mixed with *C. albicans*, incubated over 30 min and extracellular *C. albicans* cells were plated, while hemocytes were lysed and plated on YEPD-erythromycin agar plates. Resulting colonies were counted and expressed in terms of *C. albicans* cells ml^{-1} of solution. Statistical analysis was performed by comparing 6 and 24 h to 0 h extracted hemocytes at their respective incubation times (*: $p < 0.05$, **: $p < 0.01$, ***: $p < 0.001$). All values are the mean ± S.E. of three independent experiments.

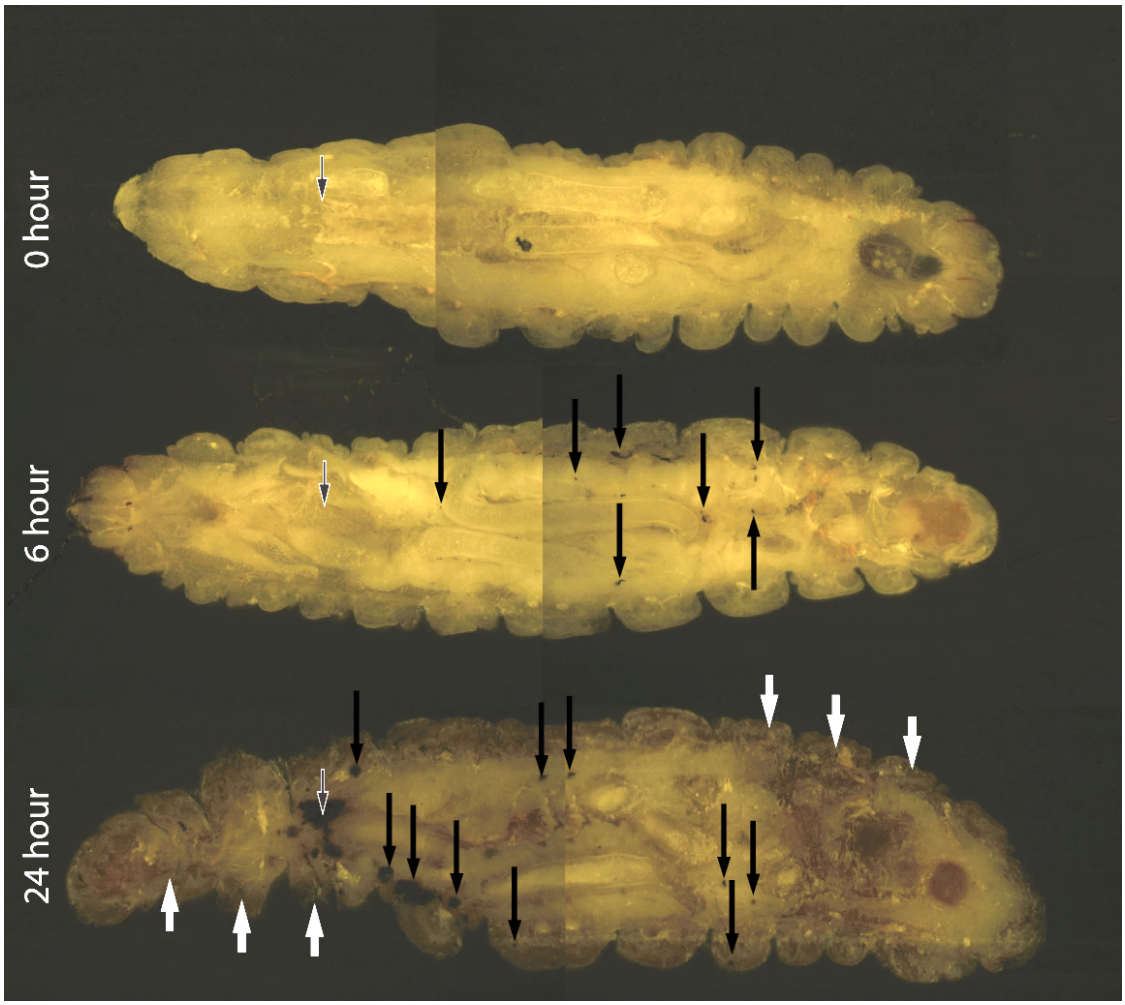

Fig. 6.7. Cryo-imaging visualisation of the stages of invasive and disseminated aspergillosis in *G. mellonella* larvae after 6 and 24 h infection. Larvae were inoculated with 1×10^6 viable *A. fumigatus* conidia for 6 and 24 h were embedded in cryo-imaging embedding compound and sectioned (10 μm) using a cryo-imaging system (Point of inoculation (white-edged arrow), fungal nodules/granulomas (black arrow), cuticle melanisation (white arrows). This experiment was repeated on 3 separate occasions with representative images provided.

6.7 Examination of fungal nodule formation in *G. mellonella* larvae following *Aspergillus* infection

Melanised lesions from larvae infected with *A. fumigatus* for 6 or 24 h were extracted and dissected. Dense hemocyte infiltration (green arrow) and melanised plaques (grey arrow) were visible by light microscope (**Fig. 6.8**). Confocal laser scanning microscopy of nodules isolated at 6 and 24 h and analysis of fluorescence due to calcofluor white binding confirmed the presence of germinated conidia (germ tube; black arrow) at 6 h and dense hyphal infiltration (white arrow) at 24 h post infection (**Fig. 6.8**). Interestingly, the use of fluorescence microscopy at 6 and 24 h revealed the presence of germinated conidia (white arrow) and hyphae (red arrow), respectively and fungal nodules stained with FM 4-64 illustrated the presence of hemocyte membrane (**Fig. 6.9**). Incubation of hemocytes with *A. fumigatus* (2:1 ratio) for 20 min suggests hemocyte phagocytosis (white arrow) and lysis around conidia (blue arrow) as well as attachment of viable hemocytes to the outer perimeter (red arrow) as evident from bright-field and FM 4-64 stained images (**Fig. 6.10**) and reported elsewhere (Schmit and Ratcliffe, 1977). Conidia and hyphae remained viable inside granulomatous tissue after grinding, diluting and plating on MEA agar plates (data not presented).

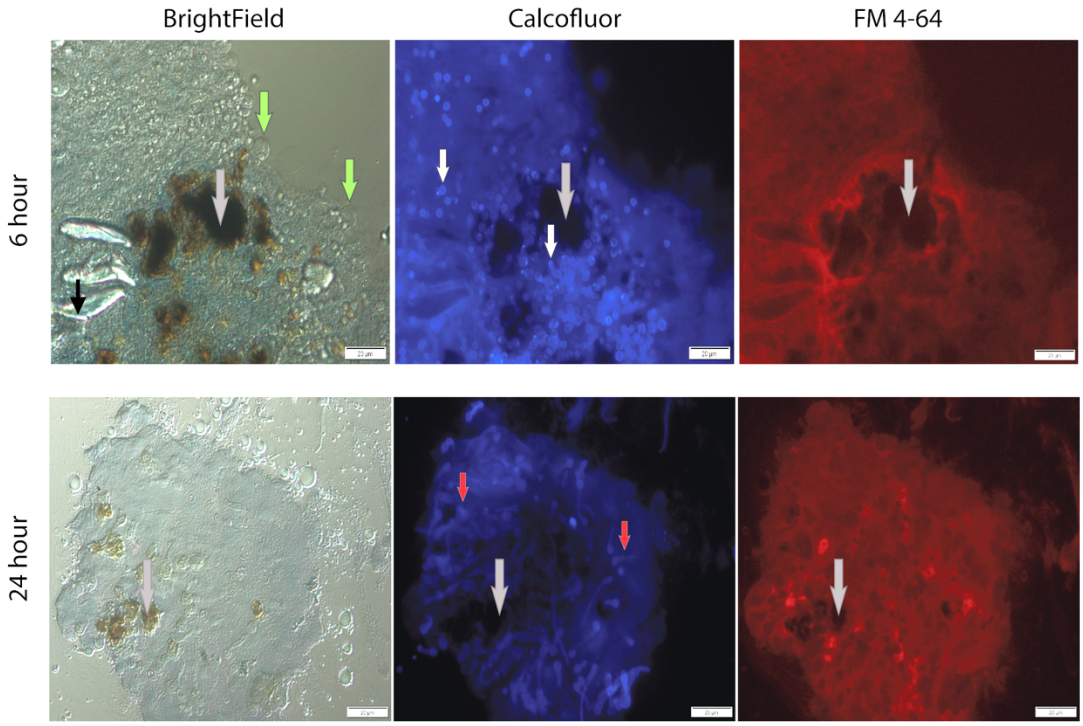

Fig. 6.8. Visualisation of the development of *A. fumigatus* conidia and hyphae in fungal nodules in *G. mellonella* larvae inoculated with 1×10^6 viable conidia. Fungal nodules were dissected from larvae and stained with Calcofluor white and FM 4-64. Bright field images reveal the formation of melanised plaques (grey arrow) and cellular infiltrates (green arrow). Fluorescent microscopy using Calcofluor white revealed germinating conidia (oval shaped; white arrow) at 6 h and dense hyphal infiltration (red arrow) at 24 h post infection. Corresponding images obtained from fungal nodules stained with FM 4-64 demonstrates the accumulation of hemocyte membrane at 6 and 24 h (scale bar corresponds to 20 μm). This experiment was repeated on 3 separate occasions with representative images provided.

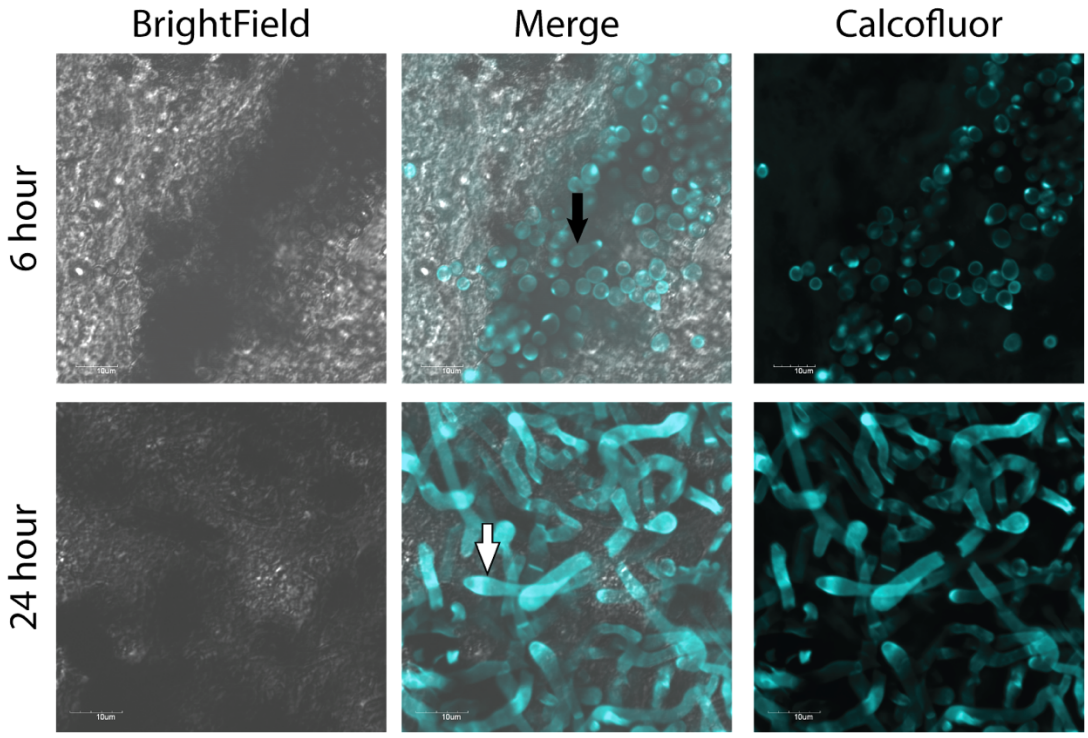

Fig. 6.9. Visualisation of the development of *A. fumigatus* conidia and hyphae in fungal nodules in *G. mellonella* larvae inoculated with 1×10^6 viable conidia. Fungal nodules were dissected from larvae and stained with Calcofluor white. Confocal laser scanning microscopy using Calcofluor white revealed germinated conidia (germ tube) and germinating conidia (oval shaped) at 6 h and dense hyphal infiltration at 24 h post infection within fungal nodules (Black arrow; germinated conidia, white arrows; hyphae) (Scale bar corresponds to 10 µm).

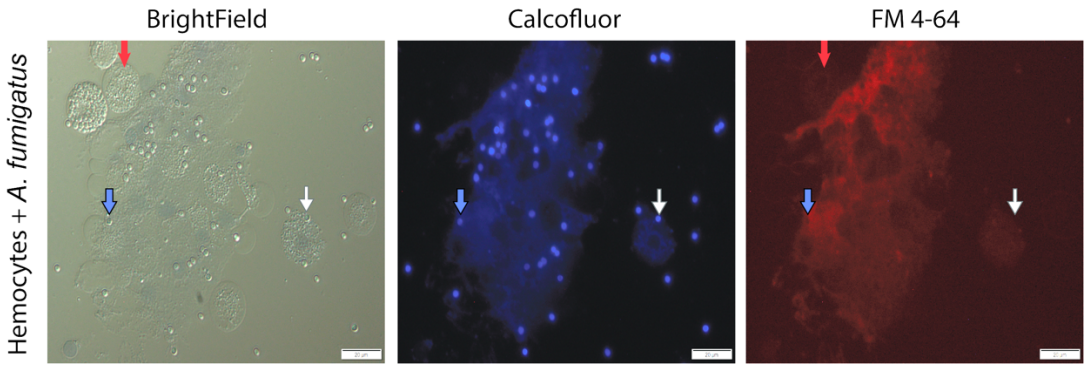

Fig. 6.10. The acute *ex vivo* cellular response of *G. mellonella* hemocytes to *A. fumigatus*. Hemocytes were extracted from *G. mellonella* washed three times with PBS and mixed for 20 min at a 2 : 1 ratio with viable *A. fumigatus* conidia. Bright field images suggest the phagocytosis (white arrow), accumulation and lysis (Blue arrow) of hemocytes around conidia as well as viable hemocytes attached to the outer perimeter (red arrow) (Scale bar corresponds to 20 µm).

6.8 Analysis of alterations in *G. mellonella* proteome following *A. fumigatus* infection

Label free quantitative proteomic analysis was performed on the *G. mellonella* cell free hemolymph after exposure of larvae to viable *A. fumigatus* conidia (1×10^6 $larva^{-1}$) for 0, 6 and 24 h. In total, 2517 peptides were identified representing 252 proteins with two or more peptides and 26 and 103 (6 h v 0 h and 24 h v 0 h, respectively) proteins determined to be differentially abundant (ANOVA, $p < 0.05$) with a fold change of > 1.5. A total of 17 proteins were deemed exclusive (i.e. with LFQ intensities present in all four replicates of one treatment and absent in all four replicates of the other two treatments). These proteins were also used in statistical analysis of the total differentially expressed group following imputation of the zero values as described. After data imputation these proteins were included in subsequent statistical analysis.

A principal component analysis (PCA) performed on all filtered proteins distinguished the 0, 6 and 24 h *A. fumigatus* treated samples indicating a clear difference between each proteome (**Fig. 6.11A**). Hierarchical clustering of z-score normalised intensity values for all significantly differentially abundant proteins (n = 252) produced the three replicates of each sample group (**Fig. 6.11B**). Furthermore, 2 major protein clusters were identified: 0 h and 6 h abundant proteins and 24 h abundant proteins.

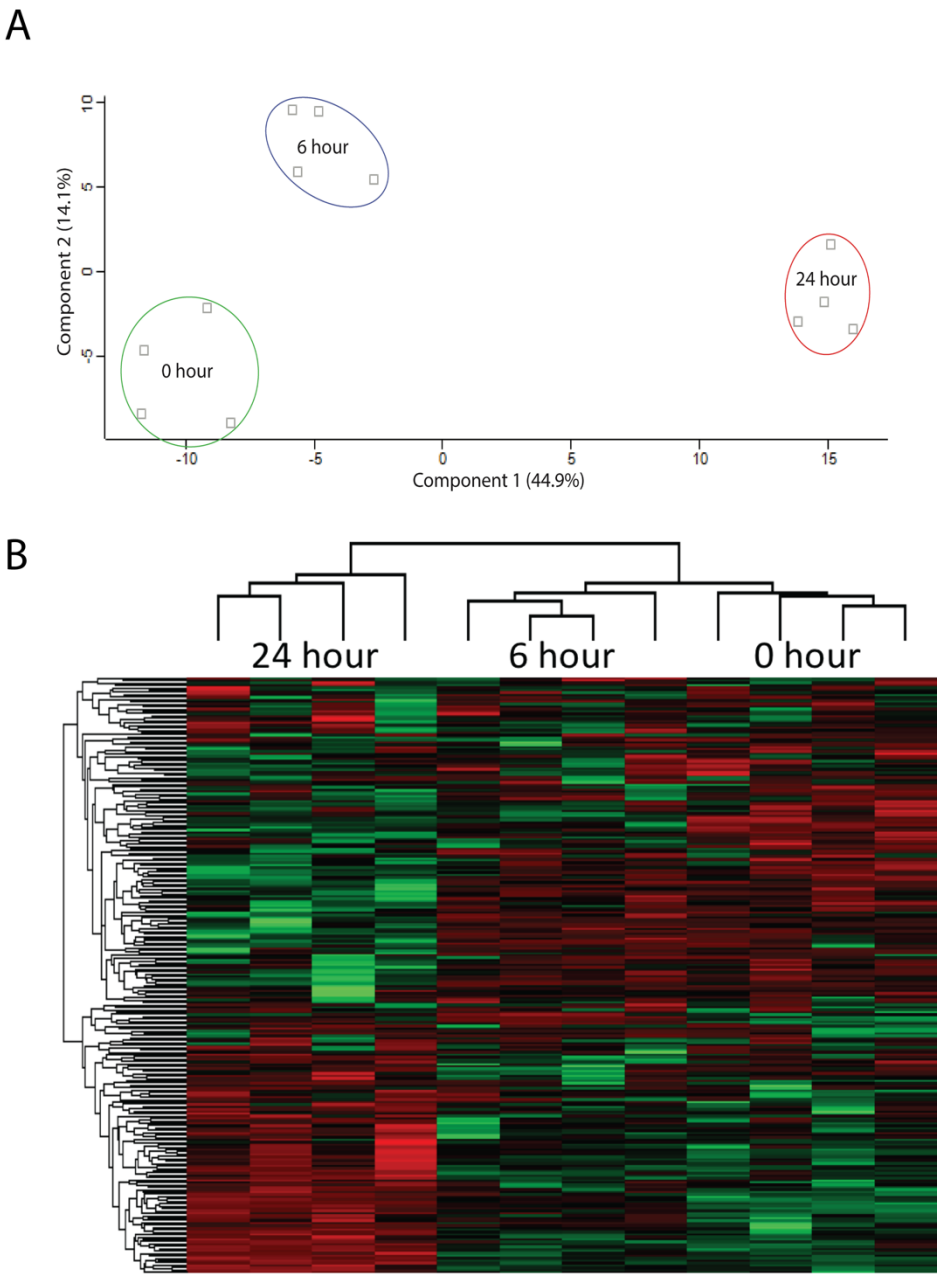

Fig. 6.11. Principal component analysis (PCA) and hierarchical clustering of *G. mellonella* hemolymph proteomic profiles following infection with viable *A. fumigatus* conidia for 0, 6 and 24 h. (A) PCA of four replicates of each treatment included in LFQ analysis with a clear distinction between each time point. (B) Two-way unsupervised hierarchical clustering of the median protein expression values of all statistically significant differentially abundant proteins. Hierarchical clustering (columns) identified 2 distinct clusters comprising the four replicates from their original sample groups.

Proteins increased in relative abundance in larvae 6 h post infection with 1 × 10^6 conidia versus non-infected larvae were gustatory receptor candidate 25 (+37 fold), gloverin-like protein (+14 fold), cecropin-A (+11 fold), lysozyme (+5 fold), moricin-like peptide B (+4 fold), muscle protein 20-like protein (+3 fold), peptidoglycan recognition-like protein B (+3 fold) and prophenoloxidase activating enzyme 3 (+2 fold). Proteins decreased in relative abundance in 6 h infected larvae compared to control larvae were juvenile hormone binding protein (-18 fold), succinyl-CoA ligase (-4 fold), serpin 3a (-2 fold), α-esterase 45 (-2 fold) and apolipophorin III (-2 fold) (**Fig. 6.12A, Table A6.1**).

Proteins increased in relative abundance in larvae exposed to *A. fumigatus* for 24 h versus control larvae were gustatory receptor candidate 25 (+126 fold), moricin-like peptide D (+33 fold), DNA-directed RNA polymerase II subunit RPB (+22 fold), growth-blocking peptide (+16 fold), moricin-like peptide C1 (+16 fold), muscle protein 20-like protein (+12 fold), protease inhibitor 1 precursor (+12 fold), chemosensory protein (+11 fold), immunoglobulin I-set domain containing protein (+10 fold), chitinase A1 (+10 fold), inducible metalloproteinase inhibitor protein (+8 fold), cecropin-A (+8 fold), cecropin-D-like peptide (+7 fold), peptidoglycan-recognition protein-LB (+6 fold), gloverin-like protein (+5 fold), hemolin (+5 fold), hemicentin (+4 fold), spatzle-1 precursor (+4 fold) and immune-related hdd1 (+4 fold). Proteins decreased in relative abundance in larvae 24 h post infection versus control larvae were fibrohexamerin (-13 fold), dimeric dihydrodiol dehydrogenase (-8 fold), glyceraldehyde-3-phosphate dehydrogenase (-6 fold), β-1,3-glucan-binding protein (-4 fold), C-type lectin 10 precursor (-2 fold) and ecdysteroid-regulated 16 kDa protein (-2 fold) (**Fig. 6.12B, Table A6.2**).

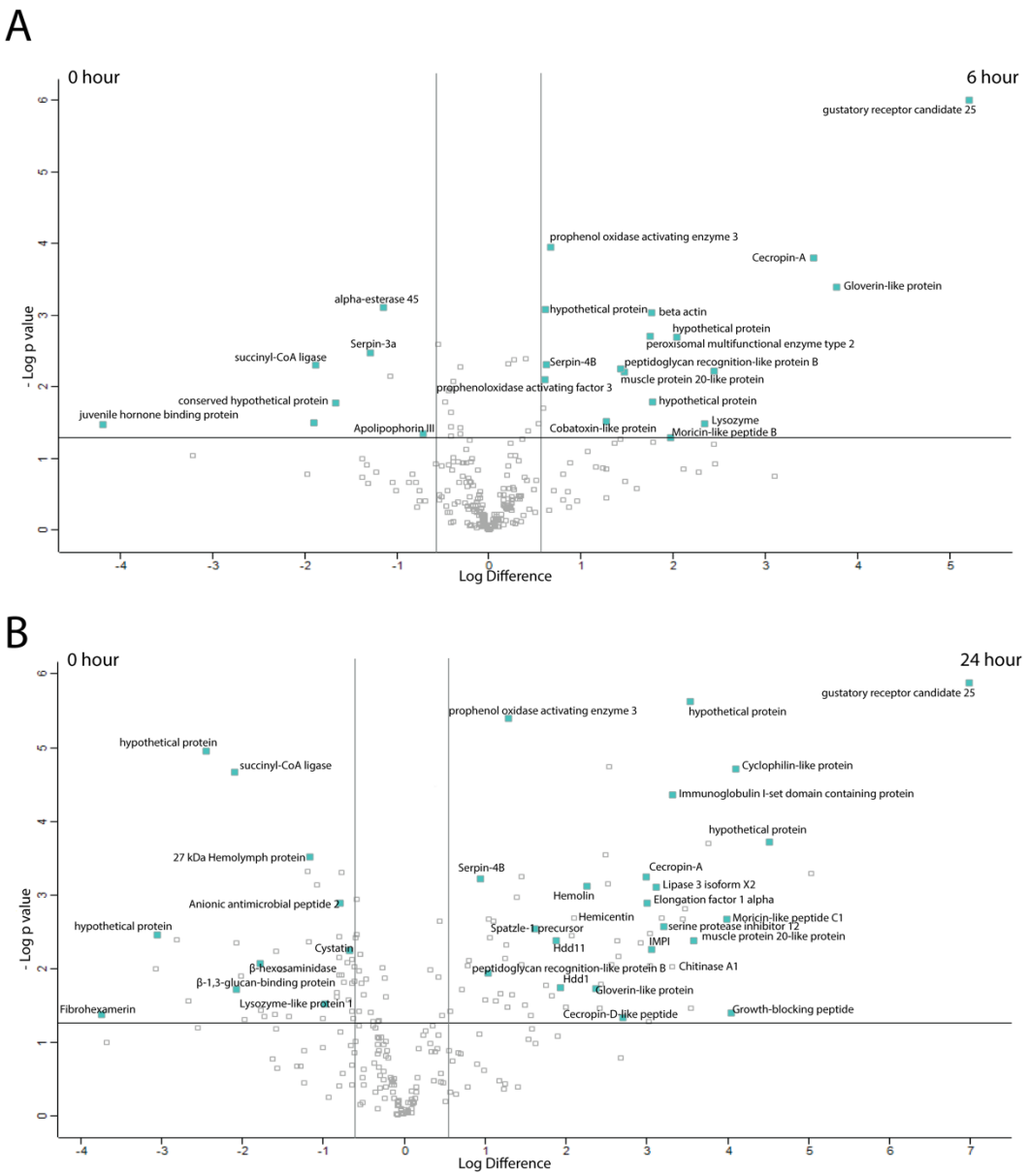

Fig. 6.12. Proteomic responses of *G. mellonella* larvae following infection by 1 × 10^6 viable *A. fumigatus* conidia after 6 (A) and 24 (B) h. Volcano plots represent protein intensity difference (- $\log_2$ mean intensity difference) and significance in differences (- log P-value) based on a two-sided *t*-test. Proteins above the line are considered statistically significant (p value < 0.05) and those to the right and left of the vertical lines indicate relative fold changes > 2 as compared to the 0 h control. Annotations are given for the most differentially abundant proteins identified in hemolymph from larvae infected with *A. fumigatus* for 6 and 24 h. These plots are based upon post imputed data.

6.9 Effect of empirical antifungals on reducing symptoms associated with invasive *A. fumigatus* infection

6.9.1 Effect of amphotericin B and caspofungin on the survival of *A. fumigatus* infected larvae

Larvae injected with 20 µl of PBS, amphotericin B (30 mg kg^{-1}) or caspofungin (8.75 mg kg^{-1}) showed no decrease in viability following incubation at 37 °C for 96 h. Larvae that were infected with *A. fumigatus* (1×10^6 20 μl^{-1}) and followed up with PBS one h later resulted in decreased survival at 24 (100 ± 0%), 48 (70 ± 3.29), 72 (10 ± 1.90%) and 96 (0 ± 0.60%) h. Larvae infected with *A. fumigatus* (1×10^6 20 μl^{-1}) followed up one h later with amphotericin B at a dose of 30 mg kg^{-1} (100 ± 3.14%, $p < 0.0001$) and 3 mg kg^{-1} (100 ± 3.08%, $p < 0.0001$) displayed enhanced survival relative to those followed up with PBS at 48 h post infection. This effect was also observed for amphotericin B at a dose of 30 mg kg^{-1} (100 ± 3.14%, $p < 0.0001$) and 3 mg kg^{-1} (100 ± 3.08%, $p < 0.0001$) at 72 h post infection. Interesting, larvae that received 30 mg kg^{-1} amphotericin showed viability of 80 ± 2.09% ($p < 0.0001$) 96 h post infection as compared to 0 ± 0.06% in the PBS treated control.

Infected larvae that were treated with caspofungin at a dose of 8.75 mg kg^{-1} (48 h; 90% ± 2.81% ($p < 0.01$), 72 h; 75 ± 2.45%, $p < 0.0001$) and 0.875 mg kg^{-1} (48 h; 70% ± 2.68%, 72 h; 50 ± 3.33%, $p < 0.001$) also showed increased survival relative to the PBS injected following *A. fumigatus* infection at 24 and 48 h, respectively (**Fig. 6.13**).

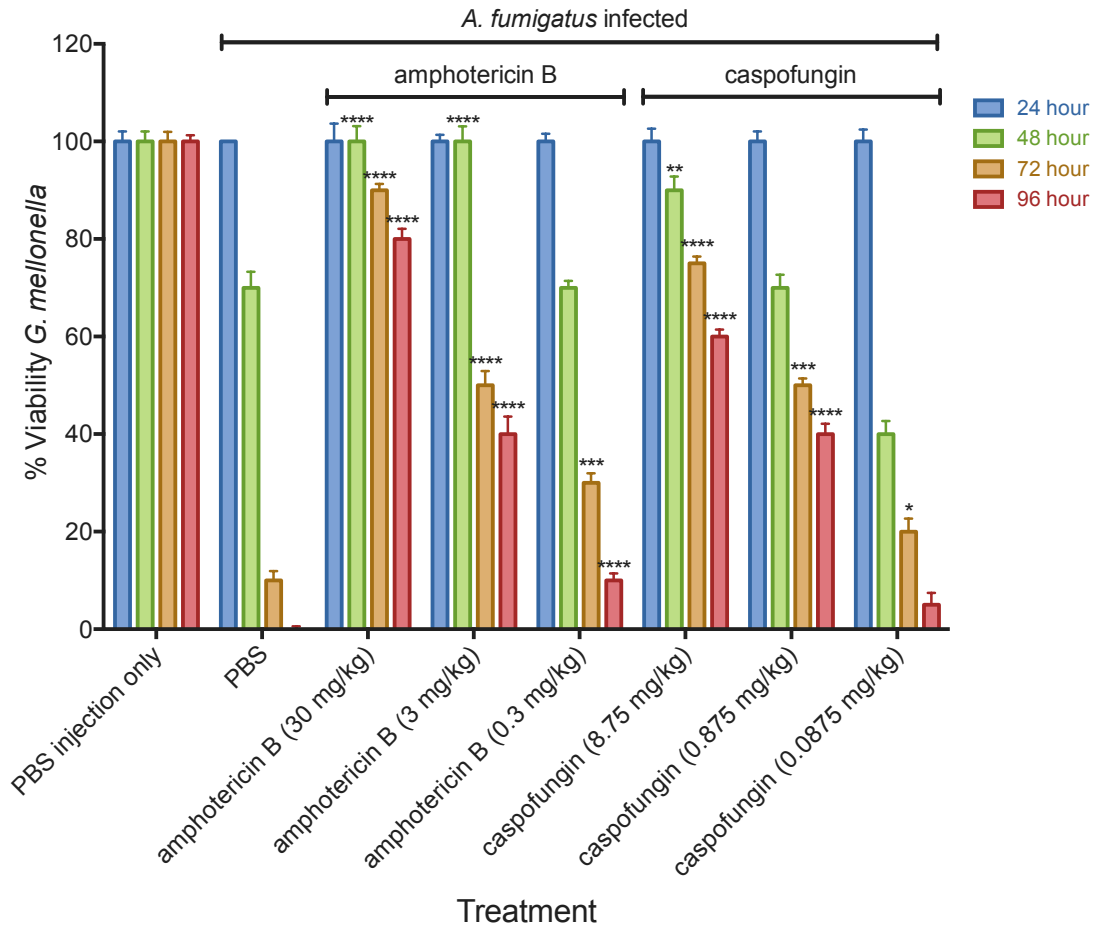

Fig. 6.13. Survival of *G. mellonella* larvae following infection by *A. fumigatus* and treatment with anti-fungal agents. Larvae were inoculated with *A. fumigatus* (1×10^6 20 μl^{-1}) and followed with PBS or varying doses of amphotericin B (3 – 30 mg kg^{-1}) or caspofungin (0.087 – 8.75 mg kg^{-1}). Larvae were incubated at 37 ^oC and viability assessed over 96 h. All values are the mean ± S.E. of three independent experiments. Statistical significance was determined by comparing anti-fungal treated larvae to PBS treated larvae (PBS) (*: $p < 0.05$, **: $p < 0.01$, ***: $p < 0.001$, ****: $p < 0.0001$).

6.9.2 Cryo-imaging of infected and anti-fungal treated larvae following infection with *A. fumigatus*

The efficacy of antifungal agents (amphotericin B and caspofungin) in reducing the symptoms associated *A. fumigatus* infection was assessed by cryo-imaging. *A. fumigatus* caused significant melanisation of *G. mellonella* larvae 24 h post infection. However, the addition of amphotericin B (3 mg kg^{-1}) one h post infection reduced melanisation of the cuticle and the appearance of nodules throughout the larvae. This effect was also observed at a lower concentration with caspofungin (0.875 mg kg^{-1}). Interestingly, administration of amphotericin B or caspofungin prevents the formation of macro-cellular nodules in larvae (**Fig. 6.14**).

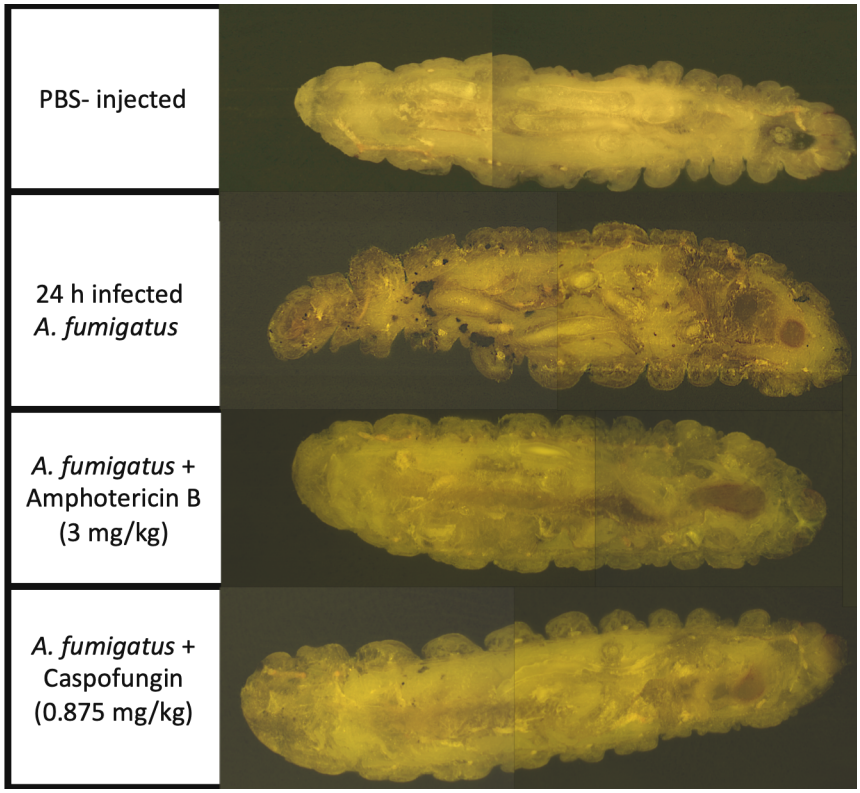

Fig. 6.14. Cryo-imaging of *G. mellonella* larvae infected with *A. fumigatus* followed by administration of antifungal therapy. Larvae were inoculated with PBS or *A. fumigatus* (1×10^6 20 μl^{-1}) and followed up one-h later with 20 µl of amphotericin B (3 mg kg^{-1}) or caspofungin (0.875 mg kg^{-1}). Larvae were incubated at 37 ^oC for 24 h and prepared for cryoviz imaging.

6.10 Discussion

G. mellonella larvae are widely utilised in determining *in vivo* antimicrobial drug activity, in assessing relative toxicity of compounds and in quantifying the virulence of bacterial and fungal pathogens (Hornsey and Wareham, 2011; Desbois and Coote, 2012; Mukherjee *et al.*, 2013; Jia *et al.*, 2016). While *G. mellonella* larvae offer many advantages as *in vivo* models, there is the possibility of extending their use for modelling diseases processes (Mukherjee *et al.*, 2013). This creates an opportunity to model infection processes in larvae that show similarities to those in mammals and to design therapies in the insect system that may be translated into mammals. The results presented here characterised the immune response of *G. mellonella* to *A. fumigatus* and describe the dissemination of the fungus through the host in the first 24 h of infection.

Inoculation of larvae with viable conidia (1×10^6 larva^{-1}) resulted in a significant increase in the density of circulating hemocytes at 2 h as compared to the control possibly due to the release of sessile hemocytes normally attached to the inner surface of the hemocoel or fat body of larvae (Ratcliffe, 1985b). Heat killed conidia produced a greater increase in hemocyte density and it is possible that loss of the rodlet/hydrophobin layer on their surface may trigger a larger immune response (Aimanianda *et al.*, 2009). Heat killed conidia and germinating conidia display β-glucan on their cell surface and recruit neutrophils into the airways of C57BL/6 mice (Hohl *et al.*, 2005). Hemocyte density was significantly elevated for 6, 8 and 10 h post infection with viable conidia and this may be associated with the formation of hyphae and secretion of metabolites from *A. fumigatus*.

Interestingly, flow cytometric analysis revealed an increased abundance of P1 cells (large, non-granular) at 6 h as compared to the zero-h injected control. By 24 h the population of small, very granular type cell (P2) increased relative to the zero-h injected control. Hemocyte populations from larvae inoculated with heat killed *A. fumigatus* for 6 h displayed increased fungicidal activity as compared to hemocyte populations from control and 24 h treated larvae. However, intracellular and extracellular killing of *C. albicans* was significantly less from hemocytes extracted from larvae exposed to heat killed *A. fumigatus* for 6 h relative to 0 h exposed larvae.

In this case the type of cell present at 6 h (large, non-granular) may have increased phagocytic activity due to the greater number of *C. albicans* cells inside hemocytes.

In mice, *A. fumigatus* increased the activity of both macrophages and neutrophils, which are essential in conidia and hyphal destruction by phagolysosome mediated killing, degranulation and NET formation (Philippe *et al.*, 2003; Bellocchio *et al.*, 2004). Interestingly, mice exposed to conidia show a significant increase in total immune cell density (in bronchoalveolar lavage fluid) but specifically an increase in macrophages after 4 h and neutrophils 48 h post exposure (Buskirk *et al.*, 2014). Histology of the CGD invasive aspergillosis mouse lung showed germinated conidia early and the formation of hyphae after 24 h with neutrophil infiltration and pyogranulomatous lesions surrounded by granulocytes (Dennis *et al.*, 2006).

Cryoviz imaging and fluorescent microscopy characterised the dissemination and development of *Aspergillus* within larvae. By 6 h, fungal infection had spread to distal sites of the larvae and is marked by the formation of well-defined melanised nodules consisting of granulocyte infiltration and encapsulation of *A. fumigatus* germinating conidia. Here, hemocytes accumulate around antigenic *A. fumigatus* conidia preventing its spread. Hemocyte membrane was found surrounding *A. fumigatus* conidia and hyphae which is consistent with encapsulation responses of *G. mellonella* larvae to foreign material (Dubovskiy *et al.*, 2016). Larvae at twenty four h post infection were characterised by melanisation of the cuticle, the appearance of *de novo* nodules and expansion of fungal nodules from the site of inoculation throughout the host. These nodules show similarities to granulomatous structures which are characteristic of invasive aspergillosis in the CGD murine model. Histology from the CGD murine lung illustrates granulomatous lesions with significant hyphal invasion (Dennis *et al.*, 2006). However, insect granulomatous structures lack lymphocytes, key components of mammalian granulomas. *A. fumigatus* remained viable and grew through melanised nodules 6 and 24 h post infection thus highlighting the importance of nodulation as an early response to an invading fungal inoculum.

Quantitative proteomics was employed to characterise the larval humoral immune response to *A. fumigatus*. At 6 h there was an increase in the abundance of antimicrobial peptides and proteins (gloverin, moricin, lysozyme, cecropin) and

proteins associated with the prophenoloxidase cascade (serpin-4B, prophenoloxidase activating enzyme 3 and prophenoloxidase activating factor 3) in hemolymph. During the mammalian innate immune response to *A. fumigatus,* a range of antimicrobial peptides (defensins, cathelicidins) and proteins (lactoferrin, lysozyme) are produced and these are essential in curtailing early fungal establishment and growth (Alekseeva *et al.*, 2009; Zhang *et al.*, 2014). Furthermore, the prophenoloxidase cascade is analogous to the mammalian complement protein cascade in terms of protein structure, function and mode of action (Söderhäll and Cerenius, 1998; Clow *et al.*, 2004).

At 24 h post infection antimicrobial peptides and prophenoloxidase family members are increased in abundance but also proteins associated with tissue invasion (muscle protein 20 like protein), recognition and opsonisation of fungal cells (hemolin, peptidoglycan recognition like protein B) and inhibition of fungal proteinases (insect metalloproteinase inhibitor (IMPI)) (Gillespie *et al.,* 1997; Gillespie *et al.*, 2000). IMPI is induced following fungal infection in *G. mellonella* and functions to inhibit the activity of secreted metalloproteinases which act as virulence factors to degrade host defences (Vertyporokh and Wojda, 2017). *A. fumigatus* produces a variety of metalloproteinases most notably is Asp f5/mep, a 42 kDa Zn/Mep which possesses collagenlytic and elastinolytic activity and is important for immune cell recruitment in the murine lung (Vasco *et al.*, 2005; Namvar *et al.*, 2015). Gustatory protein was increased in abundance at 6 and 24 h post *A. fumigatus* infection and was also increased in *G. mellonella* larvae in response to entomopathogenic fungal culture filtrate and is hypothesised to be associated with altered feeding responses and possibly toxin avoidance in insects (Chapman, 2003; Mc Namara *et al.*, 2017). Hdd1 and hdd11 were found increased in 24 h *A. fumigatus* infected larval hemolymph. Both are induced following bacterial infection in *Hyphantria cunea* with the former sharing homology with mucin-5AC-like protein from *Plutella xylostella* and the later homologous with Noduler from *Antheraea mylitta* (Woon Shin *et al.*, 1998; Sarauer *et al.*, 2003). Noduler shares a reeler domain with hdd11 and binds both insect hemocytes and fungal β-1, 3 glucan, is enriched in nodules and may act as a facilitator of nodulation (Gandhe *et al.,* 2007). Interestingly, 27 kDa hemolymph protein, Lysozyme–like protein 1, C-type lectin 10 precursor and β-glucan binding protein were significantly decreased at 24 h

possibly as a result of binding to hyphal structures and facilitating hemocyte recognition of fungal structures. Anionic antimicrobial peptide 2 was decreased in abundance 24 h after *A. fumigatus* infection (**Fig. 6B**) and was also decreased in *G. mellonella* infected with *C. albicans* (Mak *et al.,* 2010). At 6 h post infection there is a decrease in Apolipophorin III in hemolymph. Apolipophorin III mediates recognition of fungal conidia, activates the phenoloxidase cascade and dose dependently enhances melanised nodule formation (Halwani *et al.,* 2000; Whitten *et al.*, 2004). Its decreased abundance in hemolymph may be as a result of increased binding to *A. fumigatus* at the site of nodule formation (Fallon *et al.,* 2011).

Infection with *A. fumigatus* generates pathologies in larvae which are similar to those which occur during mammalian infection. The effects of antifungal therapy in enhancing the survival and reducing the symptoms associated with *A. fumigatus* infection of larvae were assessed. Injection of larvae with amphotericin B and caspofungin was non-toxic in larvae and resulted in no decreased survival over time. Amphotericin B and caspofungin increased survival of larvae at a range of clinically relevant doses compared to infected larvae which received PBS treatment only. Interestingly, larvae which received antifungal therapy displayed no cuticular melanisation and no fungal nodule formation.

Due to the lack of a comparable respiratory system to mammals, the use of *G. mellonella* to study *A. fumigatus* interactions at the bronco – alveolar surface is not possible. Furthermore, larvae are not suitable for modelling chronic infection but are an excellent model to study the acute stages of infection. The results presented here, reveal similarities between the development of invasive aspergillosis in mammals and in *G. mellonella* larvae. This work has characterised the cellular and humoral immune responses of *G. mellonella* larvae to *A. fumigatus* as well as the morphological changes of conidia and dissemination of hyphae throughout larvae. These results document significant parallels between the mammalian and insect immune responses to *A. fumigatus* infection, and illustrate how the development of invasive aspergillosis in larvae shows similarities to that which occurs in mammals. Studying the development of invasive aspergillosis in larvae may give novel insights into the pathogen – host interactions that could improve our understanding of this disease process in humans.

Chapter 7

A proteomic investigation of the processes leading to *Madurella mycetomatis* grain formation in *Galleria mellonella* larvae

7.1 Introduction

Madurella mycetomatis is the dominant causative agent of eumycetoma, a chronic granulomatous type infection which is severely debilitating to sufferers due to its occurrence at the extremities of the body (Ahmed *et al.*, 2004). Mycetoma is endemic in tropical and subtropical regions but the highest prevalence is associated with the African continent (Fahal *et al.*, 2018). The disease symptoms may take years to develop and are associated with large swellings on the extremities which hinder the patients in their daily activities. Although, the lesions can be extensive, they are not associated with pain. This may be a result of substances secreted by the pathogen with anaesthetic capabilities (Ahmed *et al.*, 2004). A key feature of mycetoma is the presence of grains inside the tissue and these grains may be formed as a defence mechanism by the fungus against the host immune system (Ahmed *et al.*, 2004). Grains consist of lipids, protein and melanin and the melanin is located on hyphal walls as thick layers. Furthermore, zinc, copper and calcium concentrations were found to be significantly higher in *M. mycetomatis* infected samples than controls which contribute to the formation of the grain cement matrix (Ibrahim *et al.*, 2013). Grains are only found *in vivo,* and animal models are needed to produce these grains (Ahmed *et al.*, 2004; Kloezen *et al.*, 2015).

The use of *G. mellonella* larvae as a model of grain development by *M. mycetomatis* has been documented previously (Kloezen *et al.*, 2015). *M. mycetomatis* strains form grains by interactions with larval hemocytes which are similar to human neutrophils and these grains are identical to those extracted from human and mammalian biopsies (Kloezen *et al.*, 2015). Using *G. mellonella* larvae, grain formation can be followed over time, and different grain developmental stages were noted (Kloezen *et al.*, 2015). These developmental stages also resembled the developmental stages in murine grains. In mice, grain formation could be prevented by administering amphotericin B but not by itraconazole (Van De Sande *et al.*, 2015; Kloezen *et al.*, 2017). In larvae, prolonged survival was noted with amphotericin B, but not with itraconazole (Van De Sande *et al.*, 2015; Kloezen *et al.*, 2017). Larvae have also been used to screen for novel anti-*M. mycetomatis* agents. A total of 800 compounds were screened and the ten most active compounds were assessed for anti-fungal efficacy in larvae against *M. mycetomatis*. Several compounds enhanced survival and/or reduced fungal burden. Fenarimol analogues, especially EPL-

BS0178 appeared most potent possibly due to their polarity, permeability and tissue distribution allowing penetration of *M. mycetomatis* grains *in vivo* (Lim *et al.*, 2018). These screening approaches have been useful in identifying potential novel compounds to treat mycetoma caused by *M. mycetomatis,* however a more directed approach could also be taken. By identifying which processes in pathogen and host are involved in grain formation, novel grain inhibiting targets might be identified.

This Chapter aimed to use the *G. mellonella* grain model to profile the proteomic changes of larvae following infection by *M. mycetomatis* and to identify proteins secreted by *M. mycetomatis* during grain formation and into hemolymph during infection in order to understand the biological processes involved in grain formation *in vivo.*

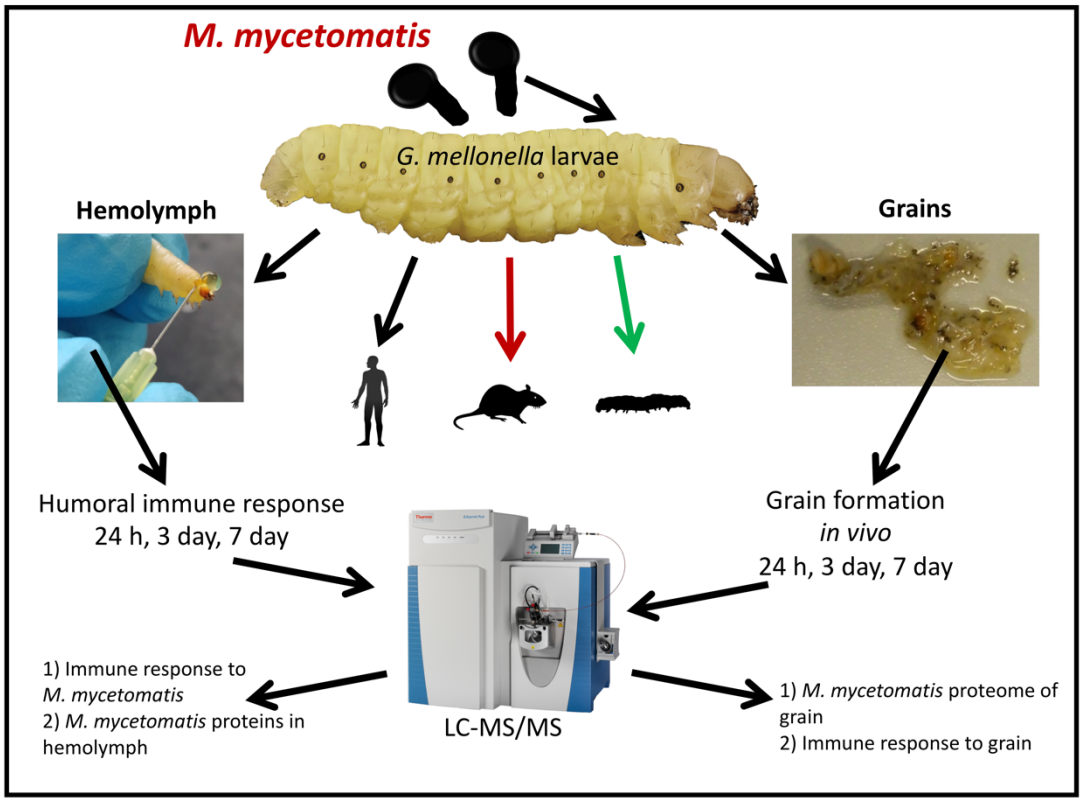

Fig. 7.1. Graphical abstract for Chapter 7.

7.2 Responses of *G. mellonella* larvae to infection by *M. mycetomatis*

(NOTE: The work in section 7.2 was performed in the Van de Sande group as part of a collaborative project). When *G. mellonella* larvae were infected with *M. mycetomatis* a rapid decrease in larval survival was noted **(Fig. 7.2A**, (Kloezen *et al.,* 2015)**)**. All larvae infected with 4 mg *M. mycetomatis* hyphal suspension per larva died within 8 days of infection **(Fig. 7.2A)**. During the course of infection, the number of grains per larva and the size of the grains within the larvae remained constant **(Fig. 7.2B and 7.2C)**. No statistical significant differences were noted in grain size from 24 h grains compared to 3 days or 7 days grains (Mann-Whitney, $p>0.05$). However, the morphology of the grains did differ per time point. At 24 h, cement material was present within the grain and individual hemocytes were trapped within this cement material **(Fig. 7.2D)**. Hyphal cells were also clearly seen, however at this time point encapsulation was not noted. At 3 days post infection, the cement material was fully formed and no individual hemocytes were found inside the grains **(Fig. 7.2E)**. Some hemocytes were seen surrounding the grain. Furthermore, the grain became encapsulated. At 7 days after inoculation most larvae had died **(Fig. 7.2A)**. The surviving larvae showed grains with many hemocytes surrounding them **(Fig. 7.2F)**. The capsule surrounding the grain was also less prominent and it often started to degrade.

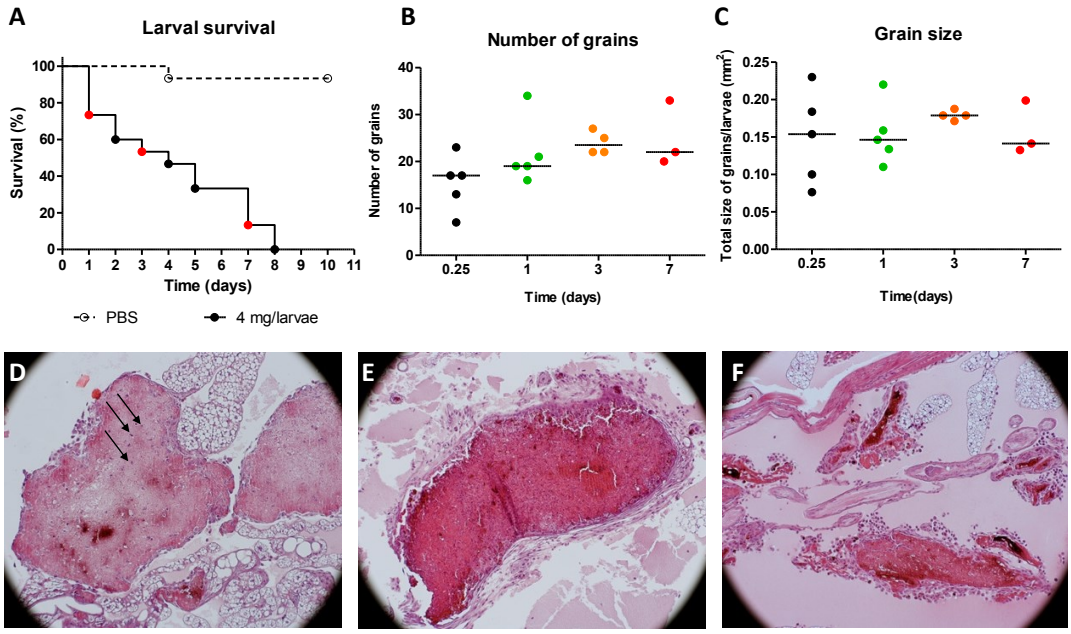

Fig. 7.2. This figure and the results from it were produced from the Dr. Wendy van de Sande group (University Medical Centre Rotterdam, Rotterdam, The Netherlands). *M. mycetomatis* infection in *Galleria mellonella* larvae. **A**: survival curves of larvae inoculated with PBS (dashed black line) or 4 mg wet weight *M. mycetomatis* per larvae (black line). Red dots in this graph represent the time points in which samples were taken for proteomic profiling and histology. **B**: Number of grains found per larvae at 0.25 (6 h), 1, 3- and 7-days post inoculation. **C**: Average size of the grains per larva at 0.25 (6 h), 1, 3- and 7-days post inoculation. **D**: Hematoxylin and eosin (HE) staining of *M. mycetomatis* grains within *G. mellonella* larvae at 24 h. Within the cement material of the grain individual hemocytes (arrows) are seen, magnification 200x. **E**: HE staining of 3 day old *M. mycetomatis* grains. No individual hemocytes within the cement material are seen. Hemocytes are seen outside the grain as well as a capsule, magnification 200x. **F**: HE staining of 7 day old *M. mycetomatis* grains. Cement material is present, the capsule is disappearing and many hemocytes are outside the grain (magnification 200x).

7.3 Analysis of *M. mycetomatis* grain formation in *G. mellonella* larvae over time

To determine which processes were involved in grain formation the proteome of *M. mycetomatis* infected larvae at 1 day, 3 days and 7 days after inoculation was determined. In total 4746 peptides were detected representing 499 *G. mellonella* proteins (472 statistically significant and differentially abundant [SSDA] proteins were present in the 24 h grain proteome relative to the 0 h hemolymph proteome, 488 SSDA present were identified in the 3 day grain proteome relative to the 24 h grain proteome and 96 SSDA proteins were identified in the 7 day grain proteome relative to the 3 day grain proteome).

Over time different *M. mycetomatis* proteins were found to be expressed in the grain. The number of *M. mycetomatis* proteins inside the grain remained relatively stable over time, with 87 *M. mycetomatis* proteins identified at 1 day after inoculation, 51 proteins at 3 days after inoculation and 48 proteins found 7 days after inoculation. However, the nature of these proteins differed. From the proteins identified, only 22 *M. mycetomatis* proteins were identified on all three time points tested **(Table A7.1)**. These included house keeping proteins such as actin, α-tubulin, histones, ribosomal proteins and the woronin body **(Table A7.1)**. Within these first 7 days, the grain appeared to remain metabolic active as on all time points enolase, ATP synthase and malate dehydrogenase were identified indicating that both glycolysis and the Kreb's cycle were functioning. Stress response related proteins such as Hsp60 and Hsp70 were also identified. Some of the *M. mycetomatis* proteins were not contained in the grain but were found to be secreted in larval hemolymph. Of these proteins three were found to be secreted at all time points, two at 3 days and 7 days and the other 75 on only a single time point. The three *M. mycetomatis* proteins found in hemolymph at all three times were actin, α-tubulin and Hsp70. The two proteins found to be excreted only at 3 days and 7 days were histone H4 and GTP-binding protein ypt1.

7.4 Quantification of the number of peptides and proteins from *G. mellonella* larvae in *M. mycetomatis* infected hemolymph

In order to understand how the *G. mellonella* humoral immune system responds to *M. mycetomatis,* label-free quantitative proteomic analysis was conducted on the proteome of larvae infected with *M. mycetomatis* for 0 h, 24 h, 3 days and 7 days at 37 ^{o}C. In total, 3217 peptides were identified representing 330 proteins with two or more peptides and 110 (24 h v 0 h), 114 (3 day v 0 h) and 154 (7 day v 0 h) proteins were determined to be statistically significant differentially abundant (SSDA; ANOVA, $p < 0.05$) with a fold change of > 1.5. A total of 361 proteins were deemed exclusive (i.e. with LFQ intensities present in all three replicates of one treatment and absent in all three replicates of the other treatment). These proteins were also used in statistical analysis of the total differentially expressed group following imputation of the zero values as described. After data imputation these proteins were included in subsequent statistical analysis.

7.5 Temporal proteomic analysis of the host – pathogen interactome between *G. mellonella* larvae and *M. mycetomatis*

7.5.1 Proteome of grains at 24 h post inoculation

At 24 h after inoculation a total of 87 *M. mycetomatis* proteins were found within the *M. mycetomatis* grain. Proteins identified included actin, heat shock protein 70 (hsp 70), malate dehydrogenase, heat shock protein 90 (hsp90), mitochondrial outer membrane protein porin, enolase, protein Ecm33, elongation factor 2, histone H2A, ATP-dependent RNA helicase, histone H2B, nucleoside diphosphate kinase, superoxide dismutase, glyceraldehyde-3-phosphate dehydrogenase, phosphoglycerate kinase, citrate synthase, transaldolase, 6-phosphogluconate dehydrogenase, fructose-bisphosphate aldolase (Fba), elongation factor 1, transketolase and peptidyl-prolyl cis-trans isomerase (PPIase) corresponded to proteins also encountered in cell extracts of *A. fumigatus, A. flavus, A. terreus, A. niger, A. nidulans, Coccidioides posadasii, M. circinelloides, S. cerevisiae, C. albicans, C. tropicalis, C. parapsilosis, C. glabrata* and *C. neoformans* (Champer *et al.*, 2016) and represent common fungal proteins **(Table A7.1)**. A range of proteins associated with virulence (putative fungistatic metabolite, cyanovirin-N, phospholipase, enolase), nutrient acquisition from hemolymph (trehalose-

phosphatase, trehalase), detoxification of the immune response (catalase-peroxidase, flavohemoprotein, superoxide dismutase), allergenic reactions (major allergen Asp f 2) and cell wall organisation/repair (putative β-glucosidase A, woronin body major protein) made up the vast majority of proteins within *M. mycetomatis* grains. Proteins identified in the grain which were associated with the stress response were the 78 kDa glucose-regulated protein, ATP synthase subunit α, histone H2A, catalase-peroxidase, uncharacterised protein (Accession: A0A175VYV0), actin, flavohemoprotein, superoxide dismutase (Accession: A0A175W4W0, Accession: A0A175W7X9) and mitochondrial peroxiredoxin PRX1.

Out of the 499 *G. mellonella* proteins identified, 472 SSDA proteins were present in the 24 h grain proteome relative to the 0 h hemolymph proteome **(Tables A7.2A and A7.2B)**. *G. mellonella* proteins increased in grains at 24 h as compared to hemolymph control proteome were associated with the immune response (cecropin-D-like peptide (+176 fold), gloverin (+115 fold), 6tox (+47 fold), lysozyme (+18 fold), prophenoloxidase subunit 2 (+12 fold), gloverin-like protein (+11 fold) and macrophage migration inhibitory factor (+7 fold)), protection against cellular stress (heat shock protein (hsp) (+810 fold), hsp 90 (+144 fold), thioredoxin (+128 fold), prophenol oxidase activating enzyme 3 (+47 fold), superoxide dismutase (116 fold) and glutathione-S-transferase-like protein (+24 fold)), nodulation (hdd11 (+147 fold), hdd1 (+26 fold), hdd23 (+21 fold), hemolin (+19 fold), hdd1-like protein (+19 fold), apolipoprotein D-like protein (+2 fold)) and a range of proteins that are primarily associated with intracellular processes (mitochondria, ribosome, proteasome) **(Table A7.2A).** *G. mellonella* proteins decreased in abundance at 24 h as compared to hemolymph control proteome were hexamerin (-310 fold), arylphorin (-13 fold), cationic peptide CP8 (-5 fold), transferrin (-5 fold) and also apolipophorin (-4 fold) and lysozyme-like protein 1 (-3 fold) **(Table A7.2B).**

7.5.2 Proteome of hemolymph at 24 h post inoculation

In the hemolymph, in total 18 *M. mycetomatis* proteins were identified. The most prominent *M. mycetomatis* proteins were heat shock 70 kDa protein, heat shock protein 90, putative DNA helicase ino80, tubulin α chain, putative flavin-containing monooxygenase 1, putative sterigmatocystin biosynthesis P450 monooxygenase stcF, putative N-acetylglucosamine-6-phosphate deacetylase and TEL2-interacting protein 1 **(Table A7.3)**.

When the 330 *G. mellonella* proteins were compared to the proteome of uninfected *G. mellonella* proteins, 110 of the *G. mellonella* proteins were determined to be statistically significant differentially abundant (SSDA; ANOVA, $p < 0.05$) with a fold change of > 1.5. *G. mellonella* proteins that were increased in abundance in larval hemolymph at 24 h were transgelin (+191 fold), hdd11 (+47 fold), cecropin-D-like peptide (+33.5 fold), hdd1 (+28 fold), tropomyosin 2 (+25 fold), thioredoxin (+15.5 fold), hemicentin-like protein 1 (+15 fold), prophenol oxidase activating enzyme 3 (+11 fold), glutathione-s-transferase-like protein (+10 fold), inhibitor of metalloproteinases [IMPI]; (+9 fold) and gloverin (+6 fold) **(Table A7.4A)**. A number of proteins were decreased in abundance at 24 h as compared to 0 h hemolymph such as hexamerin (-15 fold), β-1,3-glucan recognition protein (-10 fold), apolipophorin (-6 fold), C-type lectin 21 precursor (-4 fold) and anionic antimicrobial peptide 2 (-2 fold) (**Table A7.4B)**. These proteins were subjected to GO analysis by the Blast2GO software tool. A number of GO terms belonging to biological process (small molecule metabolic process, response to stress, cellular component organisation and biosynthetic process), molecular function (ion binding, oxidoreductase activity, structural constituent of ribosome and organic cyclic compound binding) and cellular component (intracellular organelle, membrane-bounded organelle, intracellular and endomembrane system) were significantly enriched within the dataset **(Table A7.5)**.

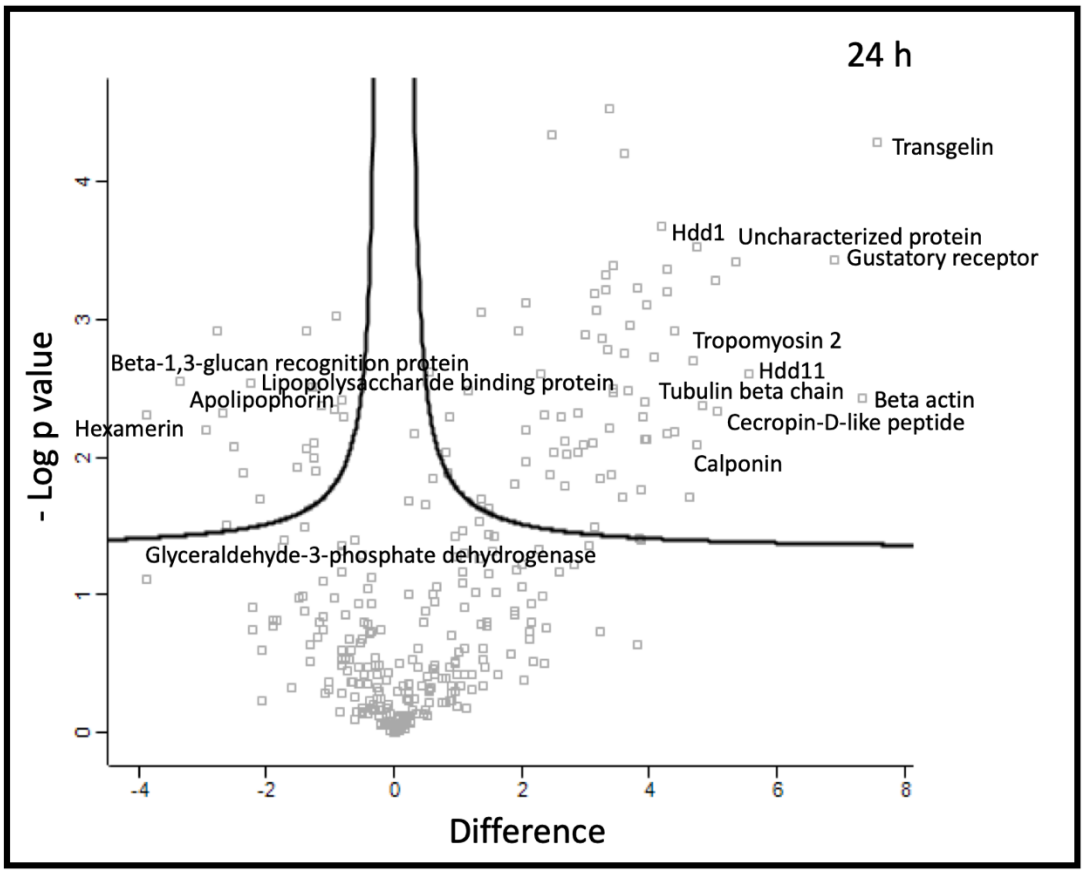

Fig. 7.2. Proteomic responses of *G. mellonella* larvae following infection by *M. mycetomatis* mycelium (4 mg 40 μl^{-1}) after 24 h post infection as compared to control (PBS- injected) larvae. Volcano plots represent protein intensity difference (− log2 mean intensity difference) and significance in differences (− log P-value) based on a two-sided t-test. Proteins above the line are considered statistically significant (p value < 0.05) and those to the right and left of the vertical lines indicate relative fold changes > ±1.5. These plots are based upon post imputed data.

7.5.3 Proteome of grains at 3 days post inoculation

In the grain 51 *M. mycetomatis* proteins were identified. These proteins included cyanovirin-N, enolase, iron-sulfur cluster assembly protein, protein Ecm33, two component system protein A, mitochondrial peroxiredoxin PRX1, heat shock protein 60, heat shock protein 90, heat shock 70 kDa protein and malate dehydrogenase. Interrogation of the 3 day *M. mycetomatis* grain proteome via Blast2GO revealed enrichment of GO terms associated with biological process (catabolic process, macromolecule localisation, oxidation-reduction process and response to stress), molecular function (hydrolase activity, protein binding and drug binding), cellular component (non-membrane-bounded organelle, ribonucleoprotein complex and cell periphery) and enzyme categories (hydrolases, transferases and oxidoreductases.

Out of the 499 *G. mellonella* proteins, 488 SSDA were identified in the 3 day grain proteome relative to the 24 h grain proteome **(Table A7.6)**. Grains from *M. mycetomatis* infected larvae infected for 3 days [which were compared to grains isolated from 24 h infected larvae] showed an increase in *G. mellonella* proteins such as AGAP010145-PA (+39 fold), ATP synthase subunit α (+13 fold), transferrin (+12 fold), hdd11 (+4 fold), hemicentin-like protein 2 (+3 fold), as well as a range of proteins associated with the ribosomal (ribosomal protein L7, 40S ribosomal protein S16, 60S ribosomal protein L13a, ribosomal protein S27A, L35, S12, L37 **(Table A7.6A)**. A reduction in the abundance of antimicrobial peptides cobatoxin-like protein (-14 fold), cecropin-D-like peptide (-5 fold), gloverin (-4 fold) and anionic antimicrobial peptide 2 (-3 fold) **(Table A7.6B)** was observed in the 3 day grain compared to the 24 h grain.

7.5.4 Proteome of hemolymph at 3 days post inoculation

In total, 26 *M. mycetomatis* proteins were detected in *G. mellonella* larval hemolymph at 3 days after inoculation **(Table A7.3)**. The most abundant were heat shock 70 kDa protein, α-1,4 glucan phosphorylase, 3-dehydroshikimate dehydratase, trans-aconitate 2-methyltransferase, small COPII coat GTPase SAR1, tricalbin-3, 60S ribosomal protein L27, clathrin heavy chain, succinyl-CoA:3-ketoacid-coenzyme A transferase and malate dehydrogenase **(Table A7.3)**.

In terms of *G. mellonella* hemolymph proteins 114 of the *G. mellonella* proteins were SSDA as compared to non-infected larvae **(Table A7.7)**. A range of *G. mellonella* proteins were increased in abundance at 3 days as compared to 0 h hemolymph including hdd11 (+337 fold), transgelin (+223 fold), heat shock-like protein (+115 fold), hdd1 (+30 fold), glutathione-s-transferase-like protein (+25 fold), hemicentin (+24 fold), prophenoloxidase activating factor 3 (+14 fold) and superoxide dismutase (+9 fold), **Table A7.7A.** Proteins decreased in abundance at 3 days as compared to 0 h hemolymph were apolipophorin (-33 fold), hexamerin (-10 fold), cationic peptide CP8 (-4 fold) and 27 kDa hemolymph protein (-3.5 fold) **(Table A7.7B, Table A7.7B)**. These proteins were subjected to GO enrichment analysis by the Blast2GO software tool. A number of GO terms belonging to biological process (organic substance metabolic process, response to stress, defence response and innate immune response), molecular function (ion binding, catalytic activity, purine ribonucleoside binding and metal ion binding) and cellular component (extracellular region, cytoplasm and intracellular) were significantly enriched within the dataset **(Table A7.5)**.

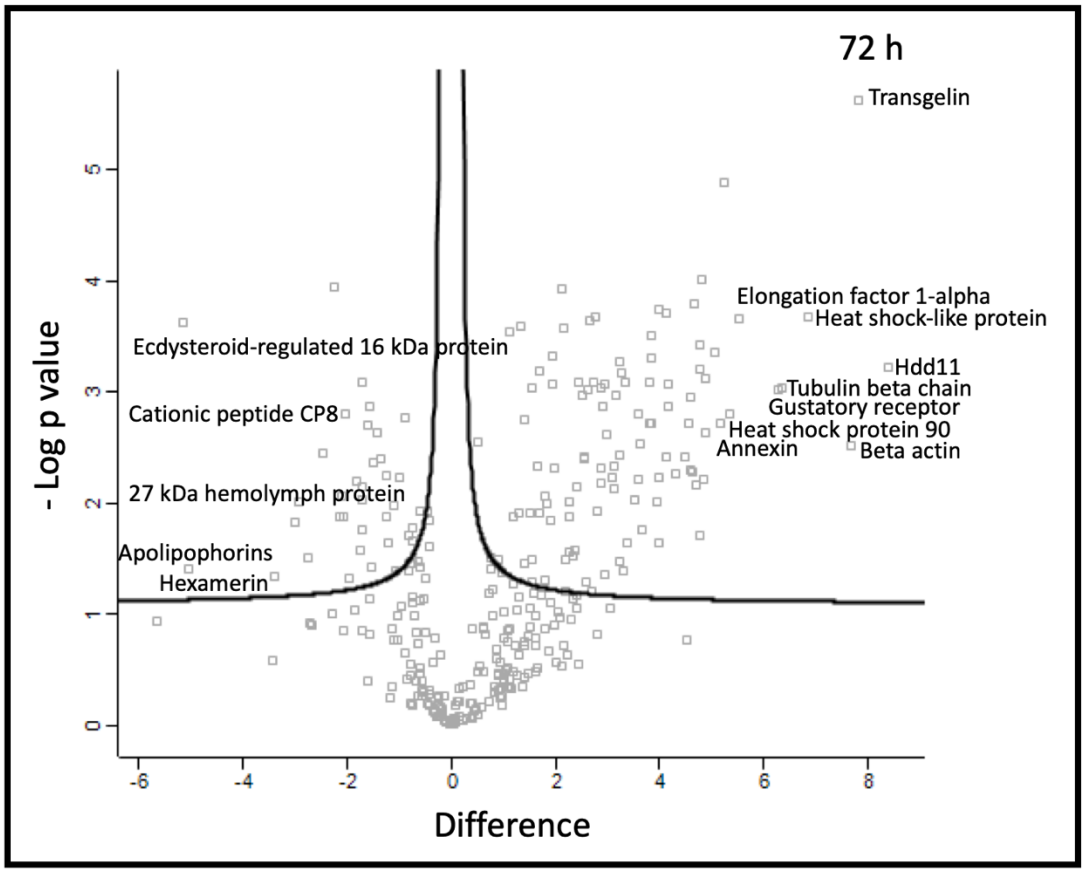

Fig. 7.3. Proteomic responses of *G. mellonella* larvae following infection by *M. mycetomatis* mycelium (4 mg 40 μl^{-1}) after 3 days post infection as compared to control (PBS- injected) larvae. Volcano plots represent protein intensity difference (− log2 mean intensity difference) and significance in differences (− log P-value) based on a two-sided t-test. Proteins above the line are considered statistically significant (p value < 0.05) and those to the right and left of the vertical lines indicate relative fold changes > ±1.5. These plots are based upon post imputed data.

7.5.5 Proteome of grains at 7 days post inoculation

At 7 days post inoculation, 18 *M. mycetomatis* proteins were identified in grains **(Table A7.1)**. These proteins included T-complex protein 1 subunit γ, putative voltage-gated potassium channel subunit β, peroxisomal hydratase-dehydrogenase-epimerase, ketol-acid reductoisomerase, mitochondrial and phosphoenolpyruvate carboxykinase. Interrogation of the 3 day *M. mycetomatis* grain proteome via Blast2GO revealed enrichment of GO terms associated with biological process (cellular component organisation, establishment of localisation, cellular component biogenesis, regulation of cellular process), molecular function (heterocyclic compound binding, organic cyclic compound binding, ion binding, protein binding), cellular component (endomembrane system, proteasome regulatory particle, supramolecular polymer) and enzyme categories (hydrolases).

In total, 96 *G. mellonella* hemolymph proteins were determined to be SSDA in the 7 days grain proteome relative to the 3 day grain proteome **(Table A7.9)**. For example, lysozyme-like protein 1 (+9 fold), hemolymph proteinase 16 (+9 fold) and hemicentin-like protein 2 (+9 fold) were increased in abundance **(Table A7.9A)** while heat shock protein 25.4 (-358 fold), 27 kDa hemolymph protein (-76 fold), apolipophorin (-75 fold), hemolin (-29 fold) and hdd11 (-9 fold) were decreased in abundance within 7 day grain samples **(Table A7.9B)**.

7.5.6 Proteome of hemolymph at 7 days post inoculation

In total, 36 *M. mycetomatis* proteins were detected in *G. mellonella* larval hemolymph at 7 days post infection. The most abundant were vegetative incompatibility protein HET-E-1, actin, long-chain-fatty-acid-CoA ligase 1, heat shock 70 kDa protein, chromodomain helicase hrp3, tubulin α chain, dehydrodolichyl diphosphate synthase complex subunit NUS1, peroxisomal long-chain fatty acid import protein 2, catechol 1,2-dioxygenase, GTP-binding protein ypt1, ribosomal protein, conidiation-specific protein 6, ras-related protein YPTC6, heat shock 70 kDa protein and superoxide dismutase 1 copper chaperone.

A range of *G. mellonella* proteins were deemed altered (n=154) in abundance in hemolymph 7 day post infection relative to the proteome of control larval hemolymph. At this time point proteins such as hdd11 (+533 fold), heat shock-like protein (+250 fold), hemicentin (+54 fold), hemolin (+44 fold), thioredoxin (+41 fold), hemicentin-like protein 1 (+37 fold), glutathione-S-transferase-like protein (+21 fold), cecropin-A (+12 fold), 6tox (+3 fold), ferritin (+3 fold) and apolipoprotein D-like Protein (+3 fold) were increased in abundance as compared to the 0 h hemolymph proteome **(Table A7.10A)**. At the same timepoint hexamerin (-64 fold), putative hydroxypyruvate isomerase (-50 fold), 27 kDa hemolymph protein (-9 fold), cationic peptide CP8 (-6 fold) and β glucan binding protein (-3 fold) were all decreased in abundance relative to the 0 h proteome **(Table A7.10B)**. These proteins were subjected to GO analysis by the Blast2GO software tool. A number of GO terms belonging to biological process (organic substance metabolic process, response to stress, carbohydrate derivative metabolic process and defence response), molecular function (catalytic activity, ion binding, nutrient reservoir activity and metal ion binding) and cellular component (extracellular region, cytoplasm and intracellular) were significantly enriched within the dataset **(Table A7.11)**. A range of these proteins play an important role in the antimicrobial response and immune-regulation **(Fig. 7.5).**

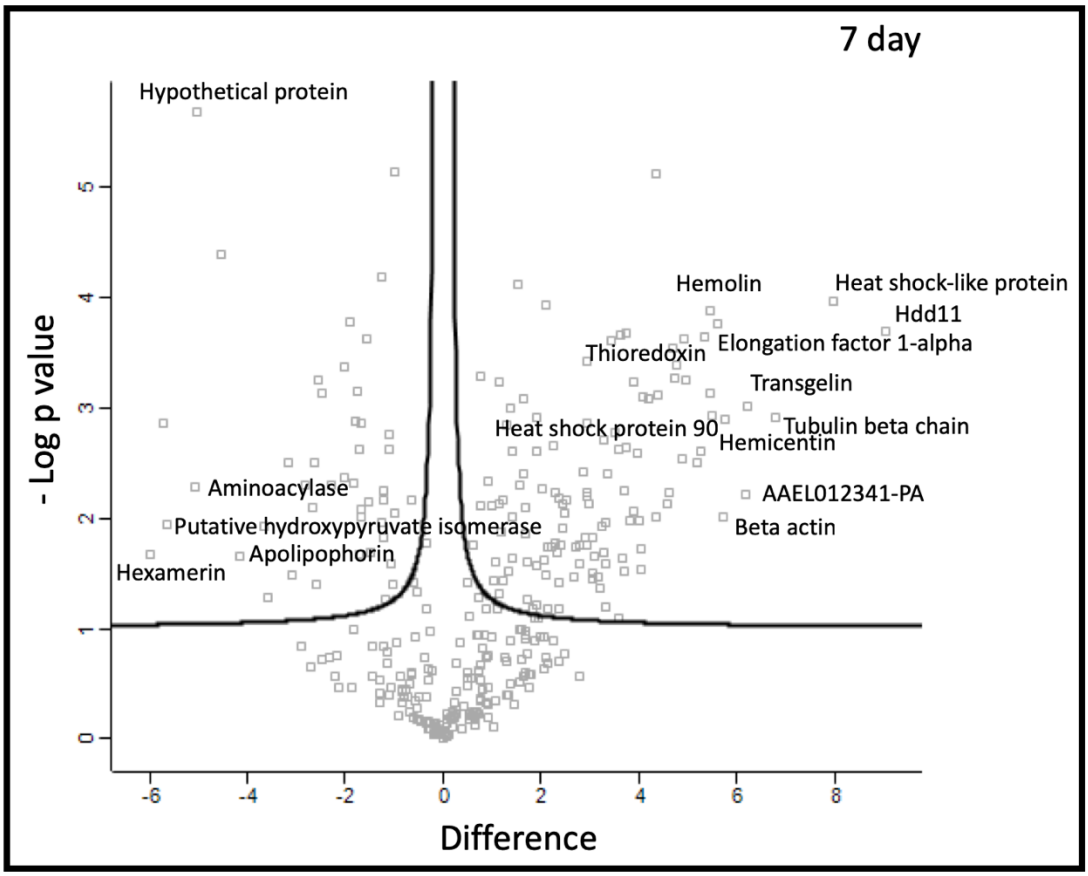

Fig. 7.4. Proteomic responses of *G. mellonella* larvae following infection by *M. mycetomatis* mycelium (4 mg 40 μl^{-1}) after 7 days post infection as compared to control (PBS- injected) larvae. Volcano plots represent protein intensity difference (− log2 mean intensity difference) and significance in differences (− log P-value) based on a two-sided t-test. Proteins above the line are considered statistically significant (p value < 0.05) and those to the right and left of the vertical lines indicate relative fold changes > ±1.5. These plots are based upon post imputed data.

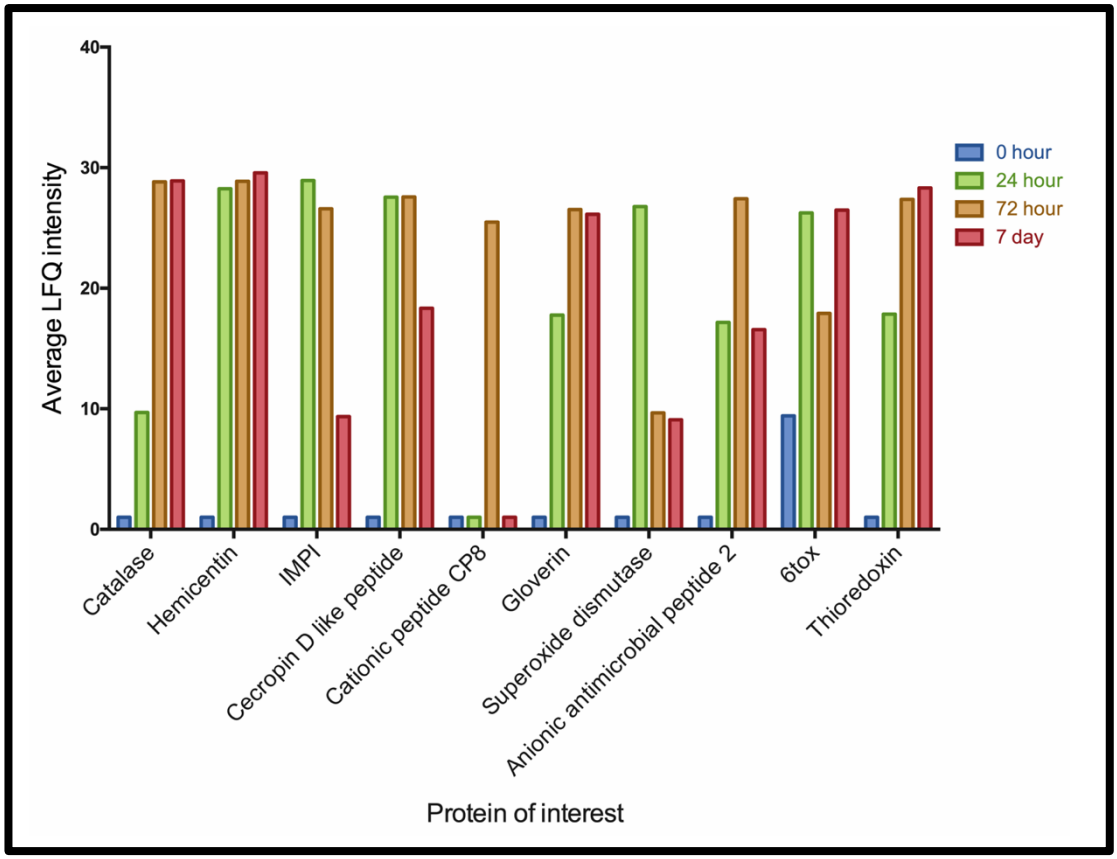

Fig. 7.5. Average LFQ intensities for a number of *G. mellonella* immune related proteins and their temporal dynamics in hemolymph during infection with *M. mycetomatis* for 24 h, 3 days and 7 days post infection.

7.6 Discussion

Eumycetoma grain formation in *G. mellonella* larvae over time was characterised by utilising a proteomic approach. Three time points were studied: 24 h, 3 days and 7 days after fungal inoculation. During all time points both *M. mycetomatis* as well as *G. mellonella* proteins were identified. Interestingly, proteins previously demonstrated to be part of the grain cement material, such as the translationally controlled tumour protein were not identified (van de Sande *et al.*, 2006). In contrast, fructose biphosphate aldolase (Fba1) was identified (De Klerk *et al.*, 2012). The amorphous cement-material present in the grain may hamper the recovery of all protein sequences.

7.6.1 *M. mycetomatis* perspective

Among the *M. mycetomatis* proteins identified a large proportion have been known to be involved in biofilm production in other fungi, which is not surprising since the extracellular matrix produced in the eumycetoma grain does resemble the extracellular matrix in biofilms. Throughout the *M. mycetomatis* infection process in *G. mellonella* larvae, different stages of cement formation were observed. At 24 h after inoculation, the cement material was forming which makes it plausible that many proteins associated with biofilm formation were found. Three days after inoculation cement material was formed and 7 days after inoculation, the capsule surrounding the cement material was broken down. Similar to the formation of biofilms, the proteins identified in the grain biosynthesis process were related to extracellular vesicle formation, proteins which can bind host extracellular matrix, proteins able to make extracellular material, proteins able to cross-link the extracellular grain matrix, proteins able to respond to stress, proteins able to repair the cement material, and especially in mature grains, proteins involved in metabolic conversion.

7.6.1.2 Proteins involved in extracellular vesicle formation

In order to form the extracellular matrix, building blocks need to be transported through the cell wall into the extracellular space. In fungal cells, secretion of these building blocks follows an endoplasmic reticulum-*trans*-Golgi-plasma membrane route, where a coordinated network of vesicle transport promotes vesicular fusion with the plasma membrane and the release of the cargo to the

extracellular space (Rodrigues *et al.*, 2011). In both the grain and the hemolymph, many proteins in vesicle transport were found. Of these, Sly1p, tricalbin-3 and small COPII coat GTPase SAR1 are found in the secretory vesicles in the endoplasmic reticulum (Li, 2005; D'Arcangelo *et al*., 2013), while sortilin and clathrin are mainly found in the Golgi apparatus (Nielsen *et al.*, 2001; Schultzhaus *et al.*, 2017).

The high yield of proteins involved in vesicle production is not surprising. These vesicles have been known to transport a high variety of molecules to the surface of the fungus. In *A. fumigatus,* the enzymes responsible for DHN-melanin production are localised in endosomes (Eisenman and Casadevall, 2012) and the last steps of melanisation occur at the cell wall. In the *M. mycetomatis* grain, DHN-melanin is present and the cement material itself is melanised (Ibrahim *et al.*, 2013). Therefore, if in *M. mycetomatis* these enzymes were secreted via the extracellular vesicles, melanisation of the cement material could occur.

In *C. albicans* and *Pichia fermentans* it was demonstrated that extracellular vesicles are found on the surface of the biofilm as well as embedded in the extracellular matrix and that proteins, RNA and polysaccharides are present within these extracellular vesicles (Zarnowski *et al.*, 2018; Bielska and May, 2019). In *C. albicans* biofilms, the vesicle composition showed a high degree of similarity with the matrix protein and polysaccharide contents, suggesting that extracellular vesicles may be a major source of matrix material (Zarnowski *et al.*, 2018). Also enolase and other moonlighting proteins (i.e. a protein which can perform more than one function e.g. GAPDH) were present in extracellular vesicles from all fungal species examined so far (Rodrigues *et al.*, 2011).

7.6.1.3 Proteins able to bind host extracellular matrix

Moonlighting proteins such as GAPDH, enolase and fructose biosphosphate aldolase are known to bind constituents of the extracellular matrix. The extracellular matrix is the acellular proteinaceous part of vertebrate and invertebrate tissues and it is therefore not surprising that many micro-organisms target the extracellular matrix components for adhesion and induction of host inflammatory response thus leading to colonisation and invasion of host tissue (Barbosa *et al.*, 2006; Singh *et al.*, 2012). In the 24 h grain proteome, many of the *M. mycetomatis* proteins identified, had homologues in *Candida* spp*, Paracoccidiodes* spp and *Aspergillus* spp, and are

known to bind extracellular components such as laminin (GAPDH, EF-2, Eno1, Fba1, transaldolase) (Gil-Navarro *et al.*, 1997; Upadhyay *et al.*, 2009), collagen (GAPDH) (Singh *et al.*, 2012), plasminogen (GAPDH, Eno1, Fba1, Asp f2) (Funk *et al.*, 2016), fibrinogen (β-glucosidase) (Upadhyay *et al.*, 2012) and fibronectin (GAPDH, Ef2, transketolase and 6-phosphogluconate dehydrogenase) (Gil-Navarro *et al.*, 1997; Upadhyay *et al.*, 2009). Laminin and collagen are relatively ancient proteins and known constituents of basal membranes. They are found in the extracellular matrix of invertebrates but fibronectin, fibrinogen and vitronectin are restricted to vertebrates (Hynes and Zhao, 2000) due to their extracellular location on fungal cells and close contact to the host, these moonlighting proteins are often antigenic in other fungal species. In serum of eumycetoma patients, antibodies against *M. mycetomatis* fructose-bisphosphate aldolase and pyruvate kinase have been detected (De Klerk *et al.*, 2012). Immunohistochemistry furthermore demonstrated that Fba1 was indeed expressed in the fungal grain which confirmed our proteomic findings (De Klerk *et al.*, 2012).

7.6.1.4 Proteins able to make extracellular material

In the 7-day hemolymph proteome the dehydrodolichyl diphosphate synthase was identified, which successively adds isopentenyl diphosphate to farnesyl diphosphate resulting in dolichols with different chain lengths (Grabińska and Palamarczyk, 2002). The dolichol biosynthetic pathway is a central part of the mevalonate pathway and is essential for the production of lipid particles, membranes and glycosylation of proteins and as a result in anchoring of proteins towards the cell wall, cell wall integrity and biofilm formation (Yasmin *et al.*, 2012).

7.6.1.5 Proteins able to cross-link the extracellular grain matrix

When the fungus adheres to the host material, building blocks are transported to the extracellular space via extracellular vesicles and extracellular material is produced. The next step in the process of cement forming is to cross-link the extracellular matrix to make a protective biofilm surrounding the hyphal cells. One of the proteins responsible for this is Asp2f homologue found in the 24 h grain proteome. Asp2f can bind plasminogen and its *C. albicans* homologue Pra1 is known to be antigenic in *A. fumigatus* and *C. albicans* (Banerjee *et al.*, 1998; Sentandreu *et al.*, 1998) and functions to acquire zinc from the environment

(Sentandreu *et al.*, 1998; Citiulo *et al.*, 2012). This protein is secreted from the fungal cell, forms a complex with extracellular zinc and is recruited back to the fungal cell. Once near the *C. albicans* cell, the zinc bound by Pra1 is cross-linked to the amyloid regions of the aspartic proteinase Sap6, resulting in large fungal aggregates with elevated zinc concentrations similar to biofilms (Kumar *et al.*, 2017). Although a homologue of Sap6 was not identified in these experiments, another amylolytic protein was found at 3 days post infection, namely α/β-glucosidase agdC. In *A. nidulans* agdC was identified as an amylolytic gene under the control of two $Zn(II)_2Cys_6$-type transcriptional activator genes (Nakamura *et al.*, 2006). If in *M. mycetomatis,* Asp2f also functioned as a zincophore and the amylolytic agdC is able to function as the amylolytic donor, an elevated level of zinc is expected in mycetoma grains. Within mycetoma grains from human biopsies elevated levels of zinc were noted (Findlay and Vismer, 1974; Ibrahim *et al.*, 2013). Findlay *et al*. (1974) found the zinc concentration within the *M. mycetomatis* grain was +1.5 times higher than the normal epidermis, while in the study of Ibrahim *et al*. (2013), a six times higher zinc concentration within the *M. mycetomatis* grains was found as compared to normal tissue (0.34 ± 0.1 ppm) (Findlay and Vismer, 1974; Ibrahim *et al.*, 2013) which could indicate that a similar cross-linking activity of Asp2f also takes place in the production of the cement material noted in the *M. mycetomatis* grains.

7.6.1.6 Response of *M. mycetomatis* to the host

M. mycetomatis steF, a homologue of sterigmatocystin biosynthesis P450 monooxygenase was detected in larval hemolymph during infection. Interestingly, larval glutathione-s-transferase (GST) was also increased in hemolymph in response to *M. mycetomatis*. GST plays an important role in xenobiotic (e.g. sterigmatocystin) metabolism by the addition of glutathione to the xenobiotic and thus protecting the cell from oxidative damage (Allameh *et al.*, 2000; Schaaf *et al.*, 2002).

The larval immune response (AMPs and ROS) will evoke a stress response in *M. mycetomatis.* A range of *M. mycetomatis* proteins were detected in 24 h grains such as SOD, trehalose-phosphatase and treahalse which play an important role in the protection against stress in fungal cells (Perfect *et al.*, 2017). The primary role of trehalose in certain fungi is as a component of the energy reserves i.e. as a

carbohydrate source (Lillie and Pringle, 1980). During stress, trehalose can interact with proteins and phospholipids to protect membrane structures and prevent protein denaturation (Wiemken, 1990; Petitjean *et al.*, 2015). Furthermore, trehalose can scavenge free radicals under oxidative stress conditions and can protect against host defences (Wiemken, 1990; Lewis *et al.*, 1995). Trehalose also has effects on the fungal cell wall and plays a role in capsule formation and virulence in *Cryptococcus gattii* (Ngamskulrungroj *et al.*, 2009). In *C. albicans*, trehalose levels were also found in the earliest phases of biofilm formation, while they were decreased in mature biofilms (Tournu *et al.,* 2013). In the early phases of grain formation, the response to ROS is important, which could explain why trehalose synthesising and modifying enzymes were present. In the more mature grain, nutrients might be more deplete, and trehalose might be degraded into glucose to provide energy (which occurs in mature *C. albicans* biofilms) (Tournu *et al.,* 2013).

7.6.2 *G. mellonella* larvae perspective

7.6.2.1 Immune response to *M. mycetomatis* grain

AMPs such as cecropin-D (+175.74 fold), gloverin (+114.8 fold), 6tox (+47.46 fold), lysozyme (+17.99 fold), gloverin-like protein (+10.84 fold) and anionic antimicrobial peptide 2 (+1.89 fold) were increased in abundance in 24 h grains relative to control hemolymph, while cationic peptide CP8 (-5.44 fold) was decreased in abundance at this timepoint. Interestingly, the grain proteome at 3 days displayed a decreased abundance of AMPs such as cecropin-D (-4.55 fold), gloverin (-3.97 fold), cationic peptide CP8 (-3.39 fold), anionic antimicrobial peptide 2 (-2.92 fold), cobatoxin-like protein (-14.39 fold) relative to 24 h grains. This was also observed at 7 day relative to 3 day grains with anionic antimicrobial peptide 2 (-53.47 fold), cecropin-D-like peptide (-11.52 fold) all decreased in abundance, with the exception of lysozyme-like protein 1 (+9.35 fold) which was increased in abundance.

Components of the phenoloxidase cascade [prophenoloxidase activating enzyme 3 (+47.28 fold), prophenoloxidase subunit 2 (+11.51 fold)] were also increased at this time point. Furthermore, opsonins such as PG-RP - LB (+43.49 fold) and B (+28.51 fold) were enriched within *M. mycetomatis* grains. Interestingly, transferrin (24 h v control; -5.40 fold, 3 day v 24 h; +39.01 fold, 7 day v 3 day; -

44.35 fold) contributes to anti-fungal immunity by scavenging free iron rendering it inaccessible to invading fungal pathogens (Shoham and Levitz, 2005) and transferrin was altered during the different stages of grain formation in *G. mellonella* larvae.

7.6.2.2 Detoxification of grain associated cellular damage

M. mycetomatis grains were highly enriched for a range of detoxification enzymes produced in response to grains. In total, 11 *G. mellonella* larval heat shock proteins were increased in *M. mycetomatis* grains from +5.76 fold to +673.62 fold. However, heat shock protein 25.4 (-358.31 fold) was significantly decreased in 7 day grains relative to 3 day grains. The role of heat shock proteins in vertebrate and invertebrate immunity has been widely documented (Srivastava, 2002). Furthermore, enzymes such as superoxide dismutase (+115.62 fold), three glutathione-S-transferase isoforms, four peroxiredoxin enzymes and two thioredoxin type enzymes were produced and were detected in *M. mycetomatis* grains. Glutathione-S-transferase-like protein (+2.95 fold) and thioredoxin peroxidase (+2.12 fold) were also increased within 3 day grains relative to 24 h grains.

7.6.2.3 Interaction of host with *M. mycetomatis* grain

A range of proteins were also increased such as hdd11 (+147.04 fold), hdd1 (+26.04 fold), hdd23 (+21.03 fold), hdd1-like protein (+18.62 fold) which have been identified as playing an important role in the nodulation response along with hemolin (+19.04 fold). By 3 days post infection, hdd11 (+4.07 fold) was also increased as compared to 24 h grains. But in 7 day old grains hdd11 (-8.68 fold) and hemolin (-28.51 fold) were both decreased relative to the 3 day grain proteome. Immunoglobulin superfamily member hemolin was induced by *Candida* challenge of *G. mellonella* larvae and has been shown to act as a pattern recognition receptor and opsonin in insects (Shaik and Sehnal, 2009).

7.6.3 Comparison of the host to *M. mycetomatis* compared to other fungi

7.6.3.1 Fungal invasion through the host

Muscle protein 20 like protein was increased +190.84 fold in *M. mycetomatis* infected *G. mellonella* larvae 24 h post infection. Interestingly, this protein was increased +173.3 fold in hemolymph during *C. albicans* infection and +11.84 fold during *A. fumigatus* infection of *G. mellonella* larvae 24 h post infection (section 3.9,

section 6.8). Furthermore, tropomyosin 2 was increased +25.48 fold during *M. mycetomatis* at 24 h post infection and +141.3 fold during *C. albicans* infection of larvae. Proteins such as paramyosin, tubulin α chain, troponin T, calreticulin, troponin T, CALNUC, actin 3 and calponin were increased between +2.57 to +190.84 fold and may be associated with tissue disruption due to fungal proliferation and hyphal formation which was also observed in response to *C. albicans* but not *A. fumigatus* infection of larvae (section 3.9, section 6.8).

7.6.3.2 Grain formation

Hdd11 which may play a role in grain formation was increased +47.19 fold in *M. mycetomatis* infected larval hemolymph but was +49.4 and +3.66 fold increased in *C. albicans* and *A. fumigatus* infected *G. mellonella* larvae, respectively (section 3.9, section 6.8). Hdd11 homologue nodular plays an essential role in nodule formation, aggregation of yeast via binding β-glucan, and RNAi knockdown results in increased fungal burden (Gandhe *et al.*, 2007b). Interestingly, immune related hdd1 was also increased +26.71 fold during *M. mycetomatis* infection, but was only increased +13.5 fold and +3.79 fold during *C. albicans* and *A. fumigatus* infection of *G. mellonella* larvae 24 h post infection, respectively (section 3.9, section 6.8). Apolipophorin is an 18 kDa protein which is part of the lipophorin complex and is responsible for lipid transport (Niere *et al.*, 1999; Niere *et al.*, 2001) and also acts as a PRR and opsonin of fungal β-glucan (Wojda, 2017). Apolipophorin was decreased by -6.36 fold in *M. mycetomatis* infected larvae but decreased by -1.99 fold in *C. albicans* infected larvae and not detected during infection by *A. fumigatus* (section 3.9, section 6.8).

7.6.3.3 Anti-microbial response

A range of AMPs were induced in response to *M. mycetomatis* infection. For example, cecropin D was increased +33.46 fold during *M. mycetomatis* infection while it was increased +22.8 fold and +6.54 fold in response to *C. albicans* and *A. fumigatus*, while cecropin-A was increased +2.47 fold during *M. mycetomatis* infection and +7.98 fold to *A. fumigatus* but not detected in response to *C. albicans* infection (section 3.9, section 6.8). Insect cecropins are a class of α-helical peptides which target the fungal membrane and induce apoptosis of *C. albicans* and possess immunomodulatory effects on mammalian macrophages (Lee *et al.*, 2015; Yun and

Lee, 2016). Gloverins are antibacterial polypeptides believed to bind LPS and possibly components of the fungal cell wall. It was previously demonstrated that *E. coli* induces gloverin expression in *Bombyx mori* (Yi *et al.*, 2013). Gloverin was increased +6.38 fold in *M. mycetomatis* infected larvae but was increased +52.5 fold during *C. albicans* infection and +5.16 fold during *A. fumigatus* infection indicating this AMP may be more important against yeast infections (section 3.9, section 6.8).

Interestingly, the AMP moricin was not detected at 24 h post infection with *M. mycetomatis* but was found +20.6 fold increased during *C. albicans* infection and moricin C1 was increased +15.84 fold in *A. fumigatus* infected larvae relative to control larvae (section 3.9, section 6.8). Moricins are secreted as pro-peptides are activated via proteolysis and increase the permeability of bacterial and fungal membranes. *G. mellonella* which has seven moricin-like peptides in its transcriptomics and these are highly active against yeasts and filamentous fungi (Brown *et al.*, 2008). This may indicate that *M. mycetomatis* can manipulate the host response to suppress the expression of moricin AMPs as they were also not detected in *M. mycetomatis* grains, but were detected in response to *A. fumigatus* and exhibit widely documented anti-filamentous fungus activity (Brown *et al.*, 2008).

Members of the prophenoloxidase activating system such as prophenoloxidase activating enzyme 3 were increased in response to *M. mycetomatis* (+10.72 fold), *C. albicans* (+1.8 fold) and *A. fumigatus* (+2.44 fold) infection (section 3.9, section 6.8). Prophenoloxidase activating protease was also increased by +15.65 fold during *M. mycetomatis* infection. This system which is very similar to the mammlaian complement cascade is initiated when prophenoloxidase-activating enzyme is bioactivated and therefore can catalyse the proteolytic cleavage of prophenoloxidase to phenoloxidase which in turn leads to the formation of melanin which is deposited on the microbial cells surface and displays antimicrobial activity and scavenges oxygen (Zhao *et al.*, 2007; Lu *et al.*, 2014). Phenoloxidase is also activated by apolipophorin III and inhibited by lysozyme and anionic peptide-2 in *G. mellonella* (Park *et al.*, 2005).

Furthermore, lysozyme was decreased by -4.9 and -1.78 fold during *C. albicans* and *A. fumigatus* infection of *G. mellonella* larvae, respectively but was not detected during *M. mycetomatis* infection of *G. mellonella* larvae (section 3.9,

section 6.8). Lysozyme was found highly enriched within *M. mycetomatis* grains but absent in hemolymph which suggests, along with other proteins such as apolipophorin and β-glucan recognition protein, that proteins may be shuttled from the hemolymph to the site of infection. Lysozyme exhibits its antifungal mechanism of action at the cell surface (i.e. membrane or cell wall) which ultimately leads to osmotic imbalance and cell death in *C. albicans* (Wu *et al.*, 1999; Woods *et al.*, 2011).

7.6.3.4 Detoxication of fungal virulence factors

Detoxication enzymes play an important role in protecting from geno- and proteo- toxicity induced by secreted microbial virulence factors. Glutathione-S-transferase was +9.93 fold increased in *G. mellonella* larvae in response to *M. mycetomatis* but was +114.1 fold increased during *C. albicans* infection but not detected during *A. fumigatus* infection (section 3.9, section 6.8). Glutathione-s-transferase was increased in the midgut of *G. mellonella* larvae following infection by *Bacillus thuringiensis* and acts with superoxide dismutase to protect against oxidative stress (Dubovskiy *et al.*, 2008). Thioredoxin was increased +15.53 fold in response to *M. mycetomatis* but was only increased +3.2 fold in response to *C. albicans* and +2.20 fold in response to *A. fumigatus* (section 3.9, section 6.8). Insect metalloproteinase inhibitor (IMPI) was +9.30 fold increased in *M. mycetomatis* infected *G. mellonella* larval hemolymph. IMPI was not induced by *C. albicans* but was +8.2 fold increased in abundance in response to *A. fumigatus* 24 h post infection of *G. mellonella* larvae (section 3.9, section 6.8). IMPI is a 8.6 kDa glycosylated, heat-stable peptide which is induced following fungal infection in *G. mellonella* and functions to inhibit the activity of secreted metalloproteinases which act as virulence factors to degrade host defences (Griesch *et al.*, 2000; Vilcinskas and Wedde, 2002; Wedde *et al.*, 2007; Vertyporokh and Wojda, 2017).

7.6.3.5 Fungal recognition

Peptidoglycan recognition (PG-RP)-like proteins bind to peptidoglycan via a conserved domain homologous to T4 bacteriophage lysozyme. Peptidoglycan recognition proteins from *H. diomphalia* bind β-glucan and induced phenoloxidase activation (Seitz *et al.*, 2003). In response to *M. mycetomatis*, a range of peptidoglycan recognition proteins such as PG-RP LB (*M. mycetomatis*; +16.91, *A.*

fumigatus; +5.90) and PG-RP B (*M. mycetomatis*; +12.21, *C. albicans*; +7.5 fold, *A. fumigatus*; +5.61) were increased 24 h post infection (section 3.9, section 6.8). β-glucan recognition protein was decreased -7.7 fold and -1.82 fold following *M. mycetomatis* infection. Interestingly, this protein was also decreased in abundance during *C. albicans* (-28.6 fold) and *A. fumigatus* (-4.06, -2.00, -1.56 fold) infection of *G. mellonella* larvae (section 3.9, section 6.8). The opsonin lipopolysaccharide binding protein was decreased -4.74 fold during *M. mycetomatis* infection but this protein was exclusive to *M. mycetomatis* infected larvae. C type lectin 21 was decreased -4.28 fold in *M. mycetomatis* infected but decreased -2.25 fold in *A. fumigatus* infected larvae (section 3.9, section 6.8).

7.7 Conclusion

M. mycetomatis can produce grains in *G. mellonella* larvae that are similar to grains produced during mammalian infection. These grains contain proteins linked to extracellular vesicle formation, binding to the host extracellular matrix, production and cross-linking of extracellular grain matrix. The host responds to grain formation by the deposition of a range of proteins (AMPs, detoxification associated proteins) in *M. mycetomatis* grains. The humoral immune response to *M. mycetomatis* infection is indicative of fungal infection of larvae (*C. albicans* [Chapter 3] and *A. fumigatus* [Chapter 6]). The host produced a range of anti-fungal AMPs, proteins associated with fungal cell recognition and binding, and proteins which may play a role in detoxification of fungal virulence factors.

Chapter 8

Proteomic profiling of immune priming in *Galleria mellonella* larvae

8.1 Introduction

While insects do not have an adaptive immune response mediated by B-lymphocytes and T- lymphocytes, and antibodies, they display immunological priming as a result of prior exposure to pathogens which enhances survival to a subsequent insult as a result of increased humoral and cellular response (Mowlds *et al*., 2010; Browne *et al*., 2013; Cooper & Eleftherianos 2017). Immune priming displays variation depending upon insect species in terms of duration of priming, specificity and energy costs. Changes in immune mediators as a result of priming have been linked with the first encounter with the microbial invader but is also observed by abiotically stressed insects (e.g. temperature [Wojda and Jakubowicz, 2007], shaking [Mowlds *et al.,* 2008]). This has been observed in a number of insect species including *G. mellonella* (Bergin *et al.,* 2006), *D. melanogaster* (Irving *et al.,* 2001) and *Anopheles gambiae* (Heard *et al.,* 2005) and molluscs and sea urchins (Zhang and Loker, 2004). Interestingly, antimicrobial drugs (e.g. caspofungin [Kelly and Kavanagh, 2011] and silver based drugs [Rowan *et al.,* 2009]) can induce an immune response and confer increased survival to pathogens which these drugs have no intrinsic antimicrobial activity (Kelly and Kavanagh, 2011). This alteration in immune function can be mediated through the cellular immune response i.e. changes in hemocyte density and alterations in immune cell type/function or changes in humoral mediators.

In *G. mellonella* larvae resistance to *A. fumigatus* can be induced by mild physical and/or thermal stress and also by exposure to conidia at a low inoculum via an increase in hemocyte density and in the expression of a number of antimicrobial proteins (Fallon *et al.,* 2011). Pre- exposure of *G. mellonella* larvae to a non-lethal *C. albicans* infection protects larvae from a subsequent infection at an inoculum which would usually prove fatal and this was also observed in larvae infected with *S. cerevisiae* (Bergin *et al.*, 2006). Fluctuations in temperature can also induce immune priming (Mowlds and Kavanagh, 2008). Larvae incubated at 37 ^{o}C for 1 h displayed enhanced survival to a lethal *C. albicans* infection and this was observed with an increase in hemocyte density and the expression of gallerimycin, transferrin, IMPI and galiomicin with the peak expression observed 24 h post incubation (Mowlds and Kavanagh, 2008).

The aim of the work presented in this Chapter was to characterise the humoral immune response of *G. mellonella* larvae primed by fungal and bacterial targets and in response to increased temperature (37 ºC) and dissect how the humoral immune response may influence resistance to bacterial and fungal infection in larvae.

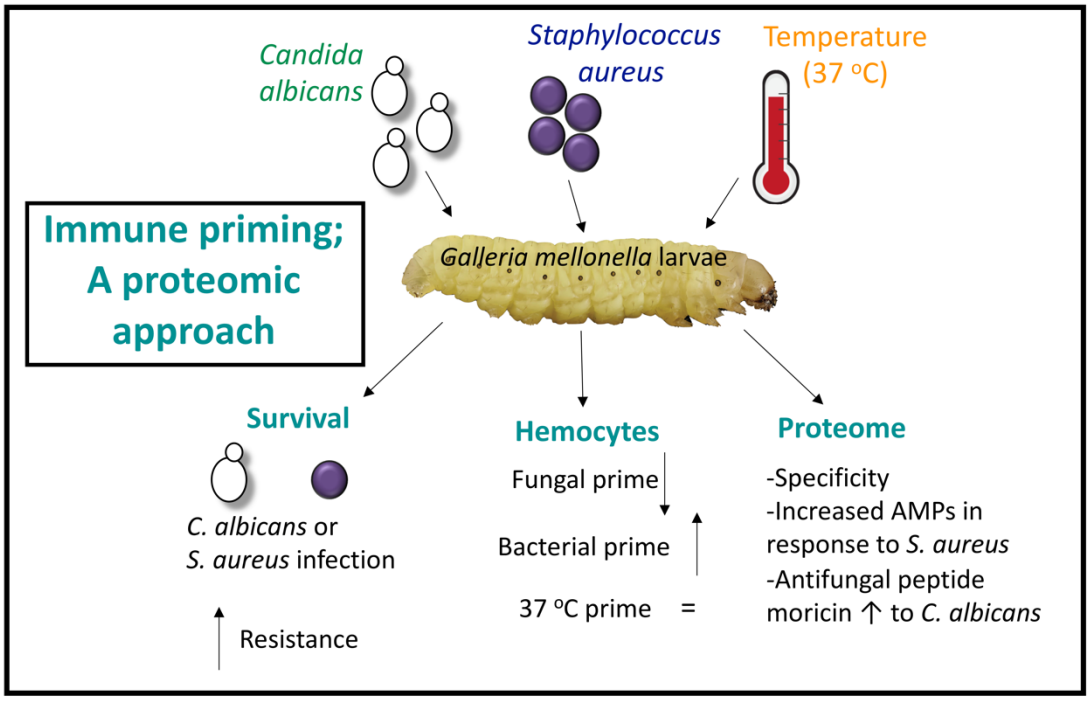

Fig. 8.1. Graphical abstract for Chapter 8.

8.2 Immune priming of *G. mellonella* and resistance to infection.

Larvae immune primed with heat killed fungal cells (*C. albicans* 1×10^6 20 μl^{-1}), heat killed bacteria cells (Bacterial; 20 µl of a 0.1 OD heat killed *S. aureus* PBS solution) or by temperature (37 ºC) for 24 h were infected with *C. albicans* (**Fig. 8.2A**) or *S. aureus* (**Fig. 8.2B**) and survival assessed over 96 h.

Larvae that were immune primed with fungal or bacterial cells displayed significantly higher survival relative to control larvae when infected with *C. albicans*. Fungal cell primed larvae displayed survival of 100 ± 3.33% at 24 h, 80 ± 3.33% $p < 0.01$ at 48 h, 70 ± 3.33%, $p < 0.001$ at 72 h and 50 ± 3.33, $p < 0.001$ at 96 h post infection relative to control larvae (24 h; 100 ± 3.33% , 48 h; 60 ± 6.66% 72 h; 20 ± 3.33%, 96 h; 10 ± 8.35%). Larvae primed with bacteria displayed a significantly enhanced survival (100 ± 6.66%, $p < 0.0001$ at 48 h, 100 ± 6.66%, $p < 0.0001$ at 72 h and 90 ± 4.28%, $p < 0.0001$ at 96 h post infection) relative to control larvae. Interestingly, larvae incubated at 37 ºC displayed significantly less survival at 48 h (30 ± 3.33, $p < 0.001$) relative to 30 ºC control larvae at that time point (**Fig. 8.2A**).

Larvae which were immune primed with heat killed *S. aureus* showed enhanced survival to 100 ± 5.29, $p < 0.01$ at 24 h, 80 ± 2.94, $p < 0.01$ at 48 h, 60 ± 7.82, $p < 0.01$ at 72 h and 50 ± 5.34%, $p < 0.001$ at 96 h as compared to larvae injected with 20 µl PBS and incubated at 30 ºC (survival of 80 ± 5.63% at 24 h, 60 ± 3.33% at 48 h, 40 ± 3.33% at 72 h, 20 ± 3.33% at 96 h).

Larvae immune primed by prior exposure to heat killed *C. albicans* or temperature (37 ºC) were less resistant to *S. aureus* infection as compared to larvae incubated at 30 ºC. Larvae which had prior exposure to *C. albicans* and were infected with *S. aureus* displayed survival of 30 ± 6.24%, $p < 0.01$ at 48 h, 10 ± 2.45%, $p < 0.01$ at 72 h and 0 ± 3.33%, $p < 0.01$ at 96 h post infection. The same occurred with larvae primed at 37 ºC and infected with *S. aureus* which decreased survival of larvae to 30 ± 3.55%, $p < 0.001$ at 48 h and 10 ± 3.33%, $p < 0.01$ at 72 h post infection (**Fig. 8.2B**).

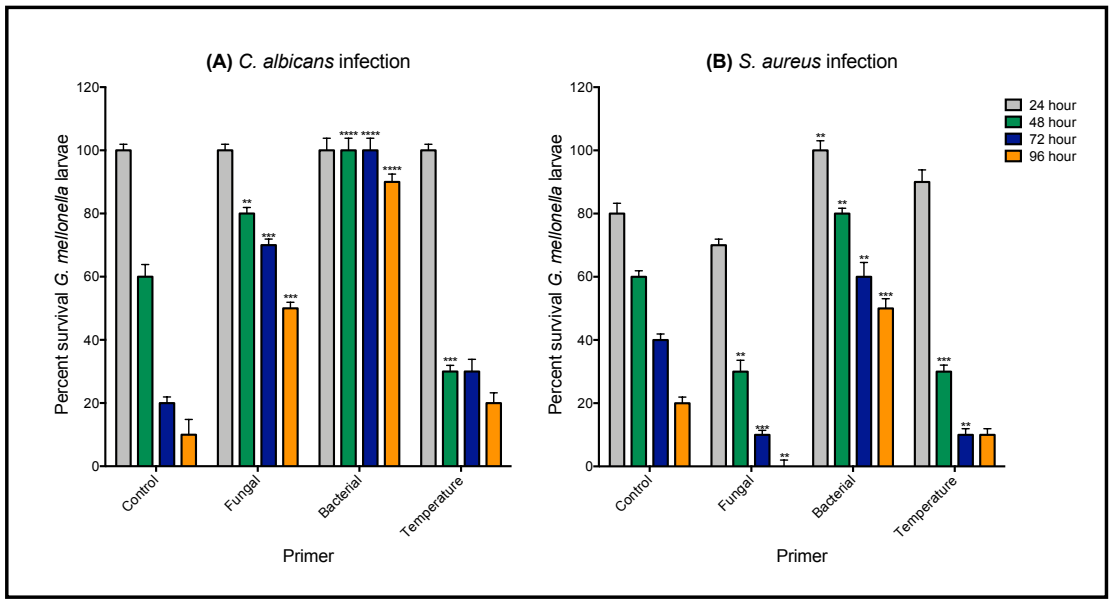

Fig. 8.2. Survival of *G. mellonella* larvae immune-primed (fungal, bacterial, temperature) and infected with *C. albicans* or *S. aureus*. Larvae (n=10) were injected with 20 µl of heat killed *C. albicans* (fungal; 1×10^6 20 μl^{-1}), *S. aureus* (bacterial; 20 µl of a 0.1 OD heat killed *S. aureus* PBS solution) or PBS and incubated at 37 ºC (Temperature) or 30 ºC (fungal, bacterial and control) for 24 h. Twenty four h incubated larvae were then infected with 20 µl of live *C. albicans* (**A**; 5×10^5 20 μl^{-1}) or live *S. aureus* cells (**B**; 20 µl of a 0.1 OD *S. aureus* PBS solution). Survival of larvae was monitored over 96 h and statistical analysis was performed by comparing primed larval survival to control larvae (20 µl PBS and incubated at 30 ºC) at the relative time point (**: $p < 0.01$, ***: $p < 0.001$, ****: $p < 0.0001$). All values are the mean ±S.E. of three independent experiments.

8.3 Alterations in the density of circulation hemocytes following immune priming of *G. mellonella* larvae

The changes in circulating hemocyte density following immune priming 24 h post injection were determined as described. Administration of heat killed *C. albicans* (1×10^6 20 μl^{-1}) resulted in a significant decrease in the number of circulating hemocytes to $6.01 \pm 1.63 \times 10^6$ $larva^{-1}$ ($p < 0.01$) as compared to larvae injected with PBS and incubated at 30 ^oC ($10.41 \pm 1.67 \times 10^6$ $larva^{-1}$). Injection of larvae with heat killed *S. aureus* (20 µl of a 0.1 OD *S. aureus* PBS) solution resulted in a significant increase in the number of circulating hemocytes to $14.08 \pm 2.14 \times 10^6$ $larva^{-1}$ ($p < 0.05$) as compared to control incubated larvae. There was no significant change in hemocyte density following incubation of larvae at 37 ^oC ($8.38 \pm 3.61 \times 10^6$ $larva^{-1}$) relative to 30 ^oC (**Fig. 8.2**).

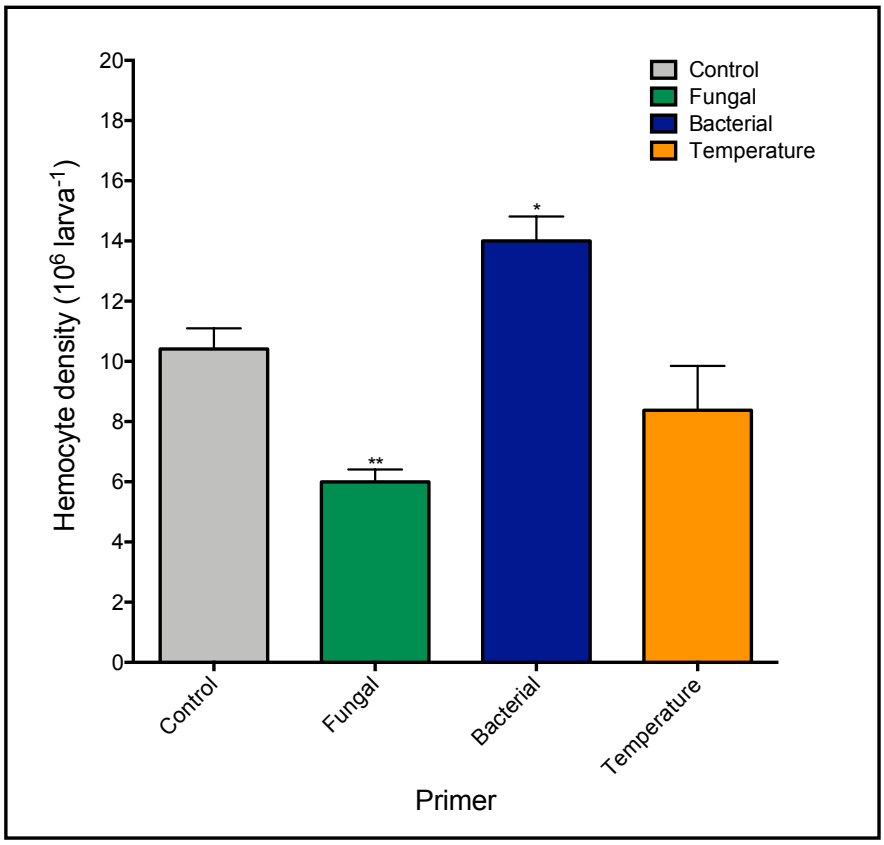

Fig. 8.3. Alterations in circulating hemocyte density from *G. mellonella* larvae immune-primed (fungal, bacterial, temperature) at 24 h post injection. Larvae (n=6) were injected with 20 µl of heat killed *C. albicans* (fungal; 1×10^6 20 μl^{-1}), *S. aureus* (bacterial; 20 µl of a 0.1 OD heat killed *S. aureus* PBS solution) or PBS and incubated at 37 ºC (Temperature) or 30 ºC (Fungal, Bacterial and Control) for 24 h. Hemocytes were extracted and enumerated from primed and control larvae and statistical analysis was performed by comparing primed larvae to control larvae (*: $p < 0.05$, **: $p < 0.01$). All values are the mean ±S.E. of three independent experiments.

8.4 Humoral immune proteome of immune primed *G. mellonella* larvae

Shotgun proteomic analysis was performed on the proteome of cell free hemolymph of *G. mellonella* larvae immune primed by fungal cells **(Fig. 8.4A**), bacterial cells (**Fig. 8.4B**) or by temperature (37 ºC) **(Fig. 8.4C**) 24 h post injection. In total, 1840 peptides were identified, representing 171 proteins with two or more peptides and 39 (fungal primed v control), 24 (bacterial primed v control) and 13 (temperature primed v control) proteins were determined to be SSDA (ANOVA, $p < 0.05$) with a fold change of > 1.5.

A total of 14, 73, 12, and 33 proteins for control, fungal primed, bacterial primed and temperature primed larvae respectively, were deemed exclusive (**Fig. 8.4D**). These proteins were subsequently used to statistically analyse the total differentially expressed group after imputation of the zero values as described and were then included in statistical analysis after data imputation. A principal component analysis (PCA) was carried out on all filtered proteins and distinguished the proteome of control, fungal primed, bacterial primed and temperature primed samples. A clear difference between the control, fungal primed, bacterial primed and temperature primed proteomes was observed (**Fig. 8.5)**.

A range of proteins were increased in abundance in the fungal primed *G. mellonella* larval hemolymph proteome relative to control larval proteome and these consisted of gustatory receptor (+32.73 fold), hdd11 (+27.48 fold), moricin-like peptide C1 (+16.76 fold), peptidoglycan-recognition protein-LB (+15.85 fold) and prophenoloxidase activating enzyme 3 (+11.91 fold). There was also a range of proteins which were decreased in fungal primed larvae relative to control larvae such as prophenoloxidase subunit 2 (-89.07 fold), apolipophorin 2 (-3.08 fold), 3-dehydroecdysone 3, β-reductase (-1.75 fold) and methionine-rich storage protein 2 (-1.67 fold) (**Fig. 8.4A, Fig. 8.6, Table A8.1**).

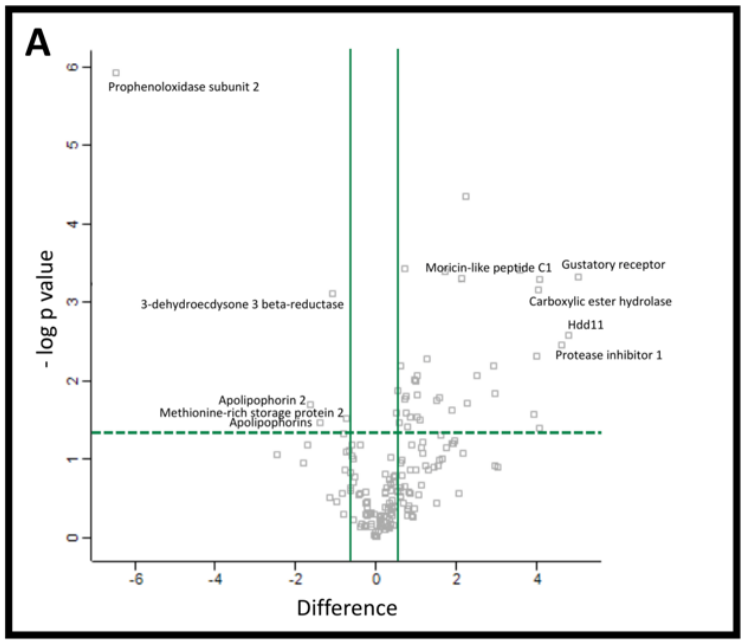
A
Prophenoloxidase subunit 2
Moricin-like peptide C1
Gustatory receptor
3-dehydroecdysone 3 beta-reductase
Carboxylic ester hydrolase
Hdd11
Protease inhibitor 1
Apolipophorin 2
Methionine-rich storage protein 2
Apolipophorins
- log p value
Difference

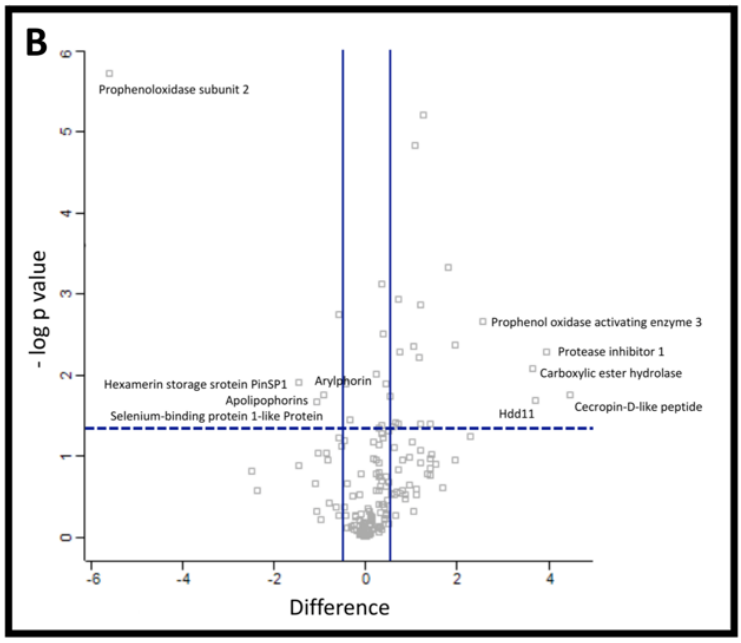
B
Prophenoloxidase subunit 2
Prophenol oxidase activating enzyme 3
Protease inhibitor 1
Carboxylic ester hydrolase
Hexamerin storage srotein PinSP1
Arylphorin
Apolipophorins
Cecropin-D-like peptide
Selenium-binding protein 1-like Protein
Hdd11
- log p value
Difference

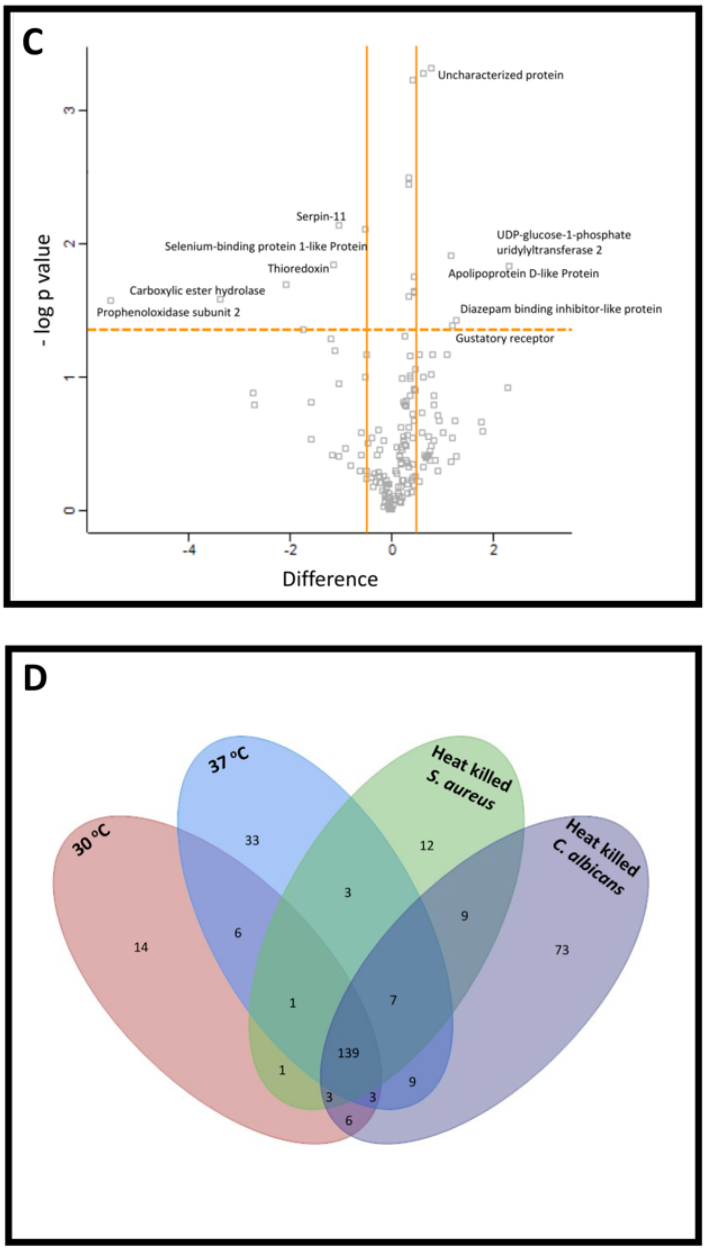

Fig. 8.4. Proteomic profiling of immune priming in *G. mellonella* larvae. Volcano plots (**A**; fungal [heat killed *C. albicans*], **B**; bacterial [heat killed *S. aureus*] and **C**; temperature [37 °C] primed hemolymph proteomes as compared to the proteome of control [30 °C] larvae) represent protein intensity difference (- $\log_2$ mean intensity difference) and significance in differences (- log P-value) based on a two-sided *t*-test. Proteins above the line are considered statistically significant (p value < 0.05) and those to the right and left of the vertical lines indicate relative fold changes > ±1.5. Annotations are given for the most differentially abundant proteins identified in hemolymph. Venn diagram (**Fig. 8.4D**) of the number of shared and exclusive proteins from the proteome of primed and control larvae.

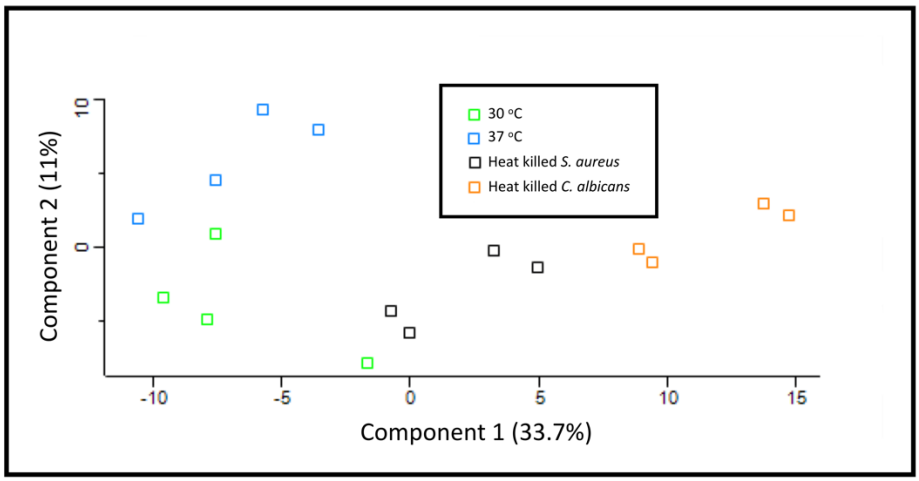

Fig. 8.5. Principal component analysis (PCA) of *G. mellonella* hemolymph proteomic profiles following immune priming with heat killed *C. albicans*, heat killed *S. aureus*, temperature (37 °C) and control (30 °C) for 24 h. PCA of four replicates of each treatment included in LFQ analysis with a distinction between each time point.

Proteins such as cecropin-D-like peptide (+22.23), hdd11 (+12.61), prophenoloxidase activating enzyme 3 (+5.96 fold), lysozyme-like protein 1 (+2.65 fold), hemolin (+2.32 fold) and peptidoglycan recognition protein (+2.13 fold) were increased in abundance in the bacterial primed *G. mellonella* larval hemolymph proteome relative to control larval proteome. A range of proteins such as prophenoloxidase subunit 2 (-48.90), hexamerin storage protein PinSP1 (-2.73 fold), selenium-binding protein 1-like protein (-2.08 fold), apolipophorin (-1.88 fold) were decreased in abundance in the bacterial primed *G. mellonella* larval hemolymph proteome relative to control (30 °C) larval proteome (**Fig. 8.4B**, **Fig. 8.6, Table A8.2**).

The proteome of temperature primed of *G. mellonella* larvae showed a significant increase in the abundance of proteins such as UDP-glucose-1-phosphate uridylyltransferase 2 (+8.74 fold), diazepam binding inhibitor-like protein (+4.95 fold), gustatory receptor (+2.43 fold), apolipoprotein D-like protein (+2.28 fold) and uncharacterised protein (GI number 145504735 [+2.26 fold]). Incubation of larvae at 37 °C decreased the abundance of a range of proteins in the hemolymph of these larvae such as prophenoloxidase subunit 2 (-46.57 fold), carboxylic ester hydrolase

(-10.43 fold), thioredoxin (-3.35 fold), serpin-11 (-2.22 fold) relative to control larvae (**Fig. 8.4C**, **Fig. 8.6, Table A8.3**).

Proteins that were exclusive to the microbial primed (fungal and bacterial n = 9 i.e. not present in any replicate of control or temperature primed larvae) *G. mellonella* larval hemolymph were serine protease inhibitor 12, N-acetylglucosamine-6-sulfatase isoform X1, cecropin-A1, conserved hypothetical protein, integument esterase 2 precursor, moricin-like peptide C3, moricin-like peptide C5, peptidoglycan-recognition protein-LB. Proteins exclusive (n=33) to the 37 ºC primed larval proteome were β-1,3-glucan binding protein, hemicentin, β-hexosaminidase, prophenoloxidase activating factor 3, fructrose-1,6-bisphosphatase, serpin-13. Proteins exclusive (n=12) to bacterial primed *G. mellonella* larval hemolymph were carboxylic ester hydrolase, growth-blocking peptide, chorion b-ZIP transcription factor, protease inhibitor-like protein, salivary cysteine-rich peptide, peptidoglycan-recognition protein-LB, antichymotrypsin-2, coatomer subunit γ, pheromone binding protein, uncharacterised protein LOC113519625 [*G. mellonella*], lebocin-like anionic peptide 1, lebocin-5-like protein (**Fig. 8.4D**). Interestingly, there was 30 proteins SSDA (5 increased and 25 decreased) in *S. aureus* primed hemolymph as compared to *C. albicans* primed hemolymph.

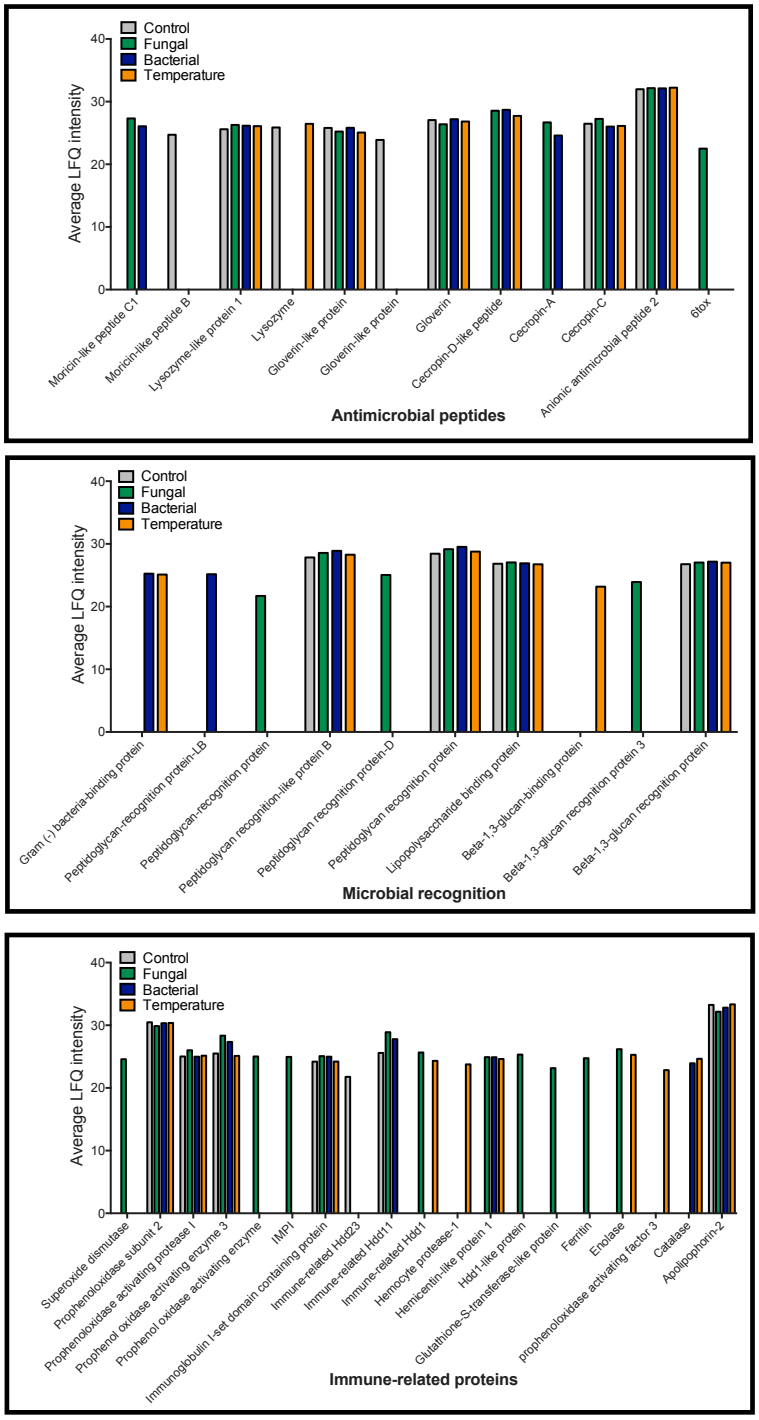

Fig. 8.6. Average LFQ intensities of antimicrobial peptides, microbial recognition and immune related proteins from the proteome of control, fungal, bacterial and temperature primed larvae.

8.5 Discussion

The focus on *G. mellonella* larvae related research has been mostly on their use as an ethical and easy to use alternative to mammals to assess the virulence of pathogenic microorganisms and toxicological investigations on novel chemical agents (Cotter *et al.*, 2000; Maguire *et al.*, 2016). However, larvae are also used to study the immune system of insects belonging to the *Lepidopteran* order.

Immune priming in *G. mellonella* has been well documented in recent years. Infection with sub-lethal doses of *C. albicans* or *A. fumigatus* confers resistance to a subsequent lethal dose (Bergin *et al.*, 2006; Fallon *et al.*, 2011b). Components of microbial cell wall (laminarin (Bergin *et al.*, 2006), β-glucan (Mowlds *et al.*, 2010) and lipopolysaccharide (Wu *et al.*, 2015)) administration can induce protection against subsequent infection by fungal or bacterial cells respectively, and increasing β-glucan doses were correlated with increases in hemocyte density and antimicrobial peptide abundance in larvae (Mowlds *et al.*, 2010).

The effect of temperature on *G. mellonella* larvae has been widely documented and pre-incubation at 37 ºC for 1 h makes *G. mellonella* more resistant to fungal (Mowlds and Kavanagh, 2008; Wojda *et al.*, 2009; Vertyporokh *et al.*, 2015) and bacterial infection (Wojda and Taszłow, 2013) and induced the expression of humoral immune genes (Wojda and Jakubowicz, 2007; Taszlow and Wojda, 2015). The results obtained from these studies have utilised gel-based proteomic techniques, but advances in quantitative shotgun proteomic technology allows for a greater level of sensitivity, the identification of a large number of proteins, accurate quantification and comparison of these proteins with a relevant control (Tuli and Ressom, 2009). The results presented in this Chapter focused on the identification of humoral immune mediators by quantitative mass spectrometry which may confer resistance to bacterial or fungal infection following immunological priming by fungal or bacterial cells, or elevated temperature (37 ºC).

Immune priming of larvae with heat killed *C. albicans* enhanced survival to a subsequent potentially lethal *C. albicans* infection. Priming of larvae with heat killed bacterial cells (*S. aureus*) enhanced larval survival to a subsequent *S. aureus* infection but also to a *C. albicans* infection. This may indicate that a bacterial infection activates a robust immune response which displays broad spectrum anti-

bacterial and anti-fungal activity i.e. humoral or altered cellular immune response, however a fungal infection only induces anti-fungal immunity. Immune priming by incubation at 37 ºC for 24 h resulted in a decreased survival of larvae infected with *C. albicans* or *S. aureus*. Interestingly, incubation of *G. mellonella* at 37 ºC has been widely documented to enhance survival to both bacterial and fungal infection, however these studies examined the effect of 37 ºC following a 1 h (temperature spike) as compared to 24 h in this study (Mowlds and Kavanagh, 2008; Wojda *et al.*, 2009; Wojda and Taszłow, 2013; Vertyporokh *et al.*, 2015).

Hemocyte density was determined 24 h post priming with heat killed *C. albicans, S. aureus* or 37 ºC incubation to assess if the enhanced survival following infection may have been due to alterations in circulating hemocyte density. Interestingly, injection of heat killed fungal cells resulted in a significant decrease in hemocyte density, while injection with heat killed bacterial cells resulted in a significant increase, whereas temperature had no effect on circulating hemocyte density. The decrease in hemocyte density following fungal cell administration could be due to binding of hemocytes to yeasts cells at the site of injection, and the increase in hemocyte density in response to bacterial cells may be due to the release of hemocytes from the lining of internal organs (Ratcliffe, 1985a) in response to the large inoculum size. Mowlds *et al.* (2010) administration of larvae with β-glucan resulted in an increase in survive which was correlated with a dose dependent increase in circulating hemocyte density but also alterations in the humoral immune response. Priming of larvae with LPS also resulted in increases in circulating hemocyte density, increased hemocyte phagocytic activity, increased encapsulation rate and increased bactericidal activity of cell free- hemolymph (Wu *et al.*, 2015).

The humoral immune response of larvae to heat killed fungal and bacterial cells, and to incubation at 37 ºC for 24 h was assessed by tandem mass spectrometry. The humoral response to fungal priming consisted of anti-fungal AMPs (moricin-like peptide C1, cobatoxin-like protein), proteins which may have a role in binding of microbial components (peptidoglycan-recognition protein-LB, peptidoglycan recognition protein, peptidoglycan recognition-like protein B), proteins involved in phenoloxidase regulation (prophenoloxidase activating enzyme 3, serpin-4B, serpin-

like protein, serpin-11, prophenoloxidase subunit 2) and proteins which play a role in the nodulation response (hdd11, hemolin, apolipoprotein D-like protein).

Moricins are a family of AMPs and are secreted as pro-peptides and are activated via proteolysis and increase the permeability of bacterial and fungal membranes (Brown *et al.*, 2008). The N-terminal residues (5-22) are amphipathic and responsible for bacterial membrane permeability, while the C-terminal residues (23-36), are hydrophobic and needed for full antimicrobial activity (Yi *et al.*, 2014). *B. mori* moricin is active against *S. aureus*, targets the membrane and is induced by bacterial infection (Hara and Yamakawa, 1995). Cobatoxin was induced in *Helicoverpa armigera* in response to Gram-positive (*Bacillus thuringiensis*), Gram-negative (*Klebsiella pneumoniae)* and in response to yeast (*C. albicans*) (Wang *et al.*, 2010). Cobatoxin from the *Centruroides noxius* scorpion is a toxin present in venom that blocks voltage-gated and Ca2+-activated channels (Selisko *et al.*, 1998).

Peptidoglycan recognition-like proteins bind to peptidoglycan via a conserved domain homologous to T4 bacteriophage lysozyme. Peptidoglycan recognition proteins from *H. diomphalia* (PGRP-SA) bind β-glucan and induced phenoloxidase activation (Seitz *et al.*, 2003) and play an important role in bacterial cell identification and recognition by circulating immune cells (Dziarski, 2004). A range of components from the prophenoloxidase cascade were increased in response to *C. albicans* priming including a range of serpins. Serpins can limit the activity of phenoloxidase activating proteinases, thereby limiting the reaction speed and avoiding excessive melanisation *in vivo* (Kanost, 1999; Kanost *et al.*, 2004).

Proteins involved in nodulation such as hdd11 were increased in abundance hemolymph during *C. albicans* infection (section 3.9)*, S. aureus* infection (section 4.5), co-infection (*C. albicans*/ *S. aureus* (section 5.4)), *A. fumigatus* infection (section 6.8) and *M. mycetomatis* infection and *M. mycetomatis* grains (section 7.5). Previously, hdd11 was found to be up-regulated in *H. cunea* 2 h following inoculation of *E. coli* (Gandhe *et al.,* 2007). Hdd11 shares homology with noduler from *Antheraea mylitta* (Woon Shin *et al.*, 1998; Sarauer *et al.*, 2003) which plays an essential in nodule formation, aggregation of yeast cells via binding β-glucan, bacterial cells via LPS, and RNAi knockdown of noduler results in increased fungal and bacterial burden during infection (Gandhe *et al.*, 2007b). Immunoglobulin

superfamily member hemolin was induced by *Candida* challenge in *G. mellonella* larvae and has been shown to act as a pattern recognition receptor and opsonin in other insects (Shaik and Sehnal, 2009). Apolipoprotein D like protein was also found increased in response to heat killed *C. albicans*. Apolipoprotein functions as part of the lipophorin complex and is responsible for lipid transport (Niere *et al.*, 1999; Niere *et al.*, 2001) but it also augments the activity of lysozyme (Zdybicka-Barabas and Cytryñska, 2013), potentiates the activity of AMPs (Park *et al.*, 2005), regulates phenoloxidase activity (Zdybicka-Barabas and Cytryńska, 2011; Zdybicka-Barabas *et al.*, 2014) is a PRR and opsonin of lipopolysaccharide, lipoteichoic acids and fungal β-glucan (Wojda, 2017).

A range of AMPs (lebocin-like anionic peptide 1, lebocin-5-like protein, cecropin-D-like peptide, lysozyme-like protein 1) were altered in abundance in response to bacterial cells. Proteins associated with microbial recognition (peptidoglycan recognition protein, peptidoglycan recognition-like protein B) and nodulation (hdd11, arylphorin, apolipophorin) were also enriched within the dataset.

Lebocin is a proline-rich and O-glycosylated protein which is bioactivated by proteolytic cleavage of the precursor protein (Yi *et al.*, 2014). Lebocin and Lebocin-like peptides display anti-*S. aureus* activity but lack anti-*Candida* activity (Cytryńska *et al.*, 2007; Zhang *et al.*, 2019). Interestingly, lebocin was not detected in response to *S. aureus* infection or co-infection of *G. mellonella* larvae (section 4.5, 5.4). Cecropins are amphipathic α-helical AMPs of 11 amino acids in length that have the ability to target and kill bacteria (including *S. aureus*) and some fungi (Bulet *et al.*, 1999; Andrä *et al.*, 2000; Lee *et al.*, 2013; Faruck *et al.*, 2016). In insects, members of this family can be isolated from the hemolymph of moths and flies following bacterial infection (Qu *et al*., 1982; Mak *et al.,* 2001; Kim *et al*., 2004; Mukherjee *et al*., 2011). In Gram-negative bacteria, the hydrophobic C-terminal of cecropin interacts with the phospholipid membrane of the bacteria leading to membrane disruption and bacterial cell death (Lee and Lee, 2014). Cecropin has antibacterial activity against multidrug resistant *A. baumanii* and *P. aeruginosa*, induces *C. albicans* apoptosis and has been shown to display immunomodulatory effects on human macrophages (Lee *et al.,* 2015; Yun & Lee 2016).

Lysozyme was also induced in response to heat killed *S. aureus*. Lysozyme cleaves the β-1,4 glycosidic bonds between N-acetylmuramic acid and N-acetylglucosamine of bacterial peptidoglycan and induces bacterial lysis. However, many *S. aureus* strains display intrinsic resistance to lysozyme but its activity acts in synergy with other AMPs and the cellular immune response (Bera *et al.*, 2005; Chen *et al.*, 2005). Lysozyme displays anti-fungal activity primarily at the cell surface (i.e. membrane or cell wall) which ultimately leads to osmotic imbalance and cell death in *C. albicans* (Wu *et al.*, 1999; Woods *et al.*, 2011). Lysozyme and cecropin fusion peptides display synergistic activity against *E. coli* (Lu *et al.*, 2010). A range of proteins associated with microbial recognition and nodulation were also increased in abundance such as peptidoglycan recognition-like proteins and hdd11. Interestingly, there were no serpins increased in abundance in hemolymph in response to *S. aureus*, unlike the response to *C. albicans*.

In response to temperature, only 13 proteins were altered in abundance (39 in *C. albicans* and 24 in *S. aureus*), including gustatory receptor which was increased +2.43 fold and was also increased in response to heat killed *C. albicans* (+32.73 fold) but not in response to heat killed *S. aureus*. Interestingly, gustatory receptor was increased in abundance in hemolymph of larvae infected with *A. fumigatus* (section 6.8) and in another study it was increased in response to entomopathogenic fungal culture filtrate and is hypothesised to be associated with altered feeding responses and possibly toxin avoidance in insects (Chapman, 2003; Mc Namara *et al.*, 2017). Carboxylic ester hydrolase was decreased -10.43 fold during temperature stress but was increased in response to both *C. albicans* (+16.47 fold) and *S. aureus* (+13 fold). Carboxylic ester hydrolases play an important role in the insects xenobiotic defence system (Qiao *et al.*, 2009).

As the larvae of *G. mellonella* are an apiculture pest they are well adapted to life in the beehive brood, temperatures of which range between 32 and 36 ^{o}C (Kronenberg and Heller, 1982; Becher and Moritz, 2009) and larvae can generate temperatures of 32 and 40 ^{o}C while being maintained in lab culture boxes at an ambient temperature of 28 ^{o}C (Schmolz and Schulz, 1995). Therefore, larvae may be considered in homeostasis at 37 ^{o}C or have become acclimatised to this temperature after 24 h incubation and this was evidenced by the lack of changes in the density of

circulating hemocytes and proteome relative to control larvae incubated at 30 ºC. The decreased survival of larvae incubated at 37 ºC may be associated with optimum growth temperature for the human pathogens *C. albicans* and *S. aureus*.

Immune priming by heat killed *S. aureus* produced inter-kingdom resistance to bacterial and fungal infection and this may be attributed to increases in circulating hemocyte density, and the importance of this has been detailed in other studies (Mowlds *et al.*, 2010; Wu *et al.*, 2015). Alterations in the *S. aureus* primed- larval hemolymph proteome also provided evidence (i.e. cecropin, lysozyme, lebocin AMPs, microbial recognition proteins, decreased serpin abundance relative to *C. albicans* priming) as to why bacterial infection produced resistance to both bacterial and fungal infection. The humoral immune response to heat killed *C. albicans* is specific and results in the increased abundance of primarily antifungal AMPs (moricin-like peptide C1), whereas the *S. aureus* immune response is broad spectrum and results in the increased abundance of cecropin-D-like peptide which displays potent antibacterial and antifungal activity. Similar responses have been observed elsewhere, where challenge of *Tenebrio molitor* by Gram-positive or Gram-negative, but not fungi induced trans-generational immune priming via increased antimicrobial peptide in eggs (Dubuffet *et al.*, 2015). This indicates that the larval immune effector arsenal to bacterial infection may initiate a strong antimicrobial response which, while increasing specific resistance to bacterial infection, also confers resistance to fungal infection mediated by *C. albicans*.

Chapter 9

Analysis of the effect of the human cathelicidin antimicrobial peptide LL-37 on the growth of the pulmonary pathogen *Aspergillus fumigatus*

9.1 Introduction

Cathelicidin antimicrobial peptides (CAMP) are expressed in all mammals as α-helical peptides ranging from 23 to 40 residues (Tomasinsig and Zanetti, 2005). Liberation of the bioactive C-termini antimicrobial domain by neutrophil protinease-3, keratinocyte kallikrein, seminal plasma gastricsin and microbial proteases yields the cationic (+6 at physiological pH) membrane active amphipathic 37 amino acid peptide LL-37 (Eissa *et al.*, 2011; Rapala-Kozik *et al.*, 2015; Sørensen *et al.*, 2017).

LL-37 displays a range of functions in relation to local infection directly by eliciting microbicidal activity targeting the outer layers of microbial cells and indirectly by its alarmin, angiogenic and re-epithelialisation properties (Koczulla *et al.*, 2003; Ramos *et al.*, 2011; Li *et al.*, 2014). Skin derived kallikrein 5/7 cleavage of LL-37 in sweat yields shorter peptide fragments KR-20, RK-31, and KS-30 that display augmented antimicrobial activity and decreased IL-8 expression when compared with LL-37, initial low concentrations of LL-37 are primarily responsible for cell recruitment and accumulation, followed by peptide saturation in the infection microenvironment (Murakami *et al.*, 2004).

LL-37 is believed to exert its antimicrobial activity via membrane interactions according to the carpet model, where peptides coat the membrane inducing curvature until a critical concentration is reached resulting in breakdown in membrane integrity most likely by the formation of toroidal pores as a result of oligomeric structure formation. LL-37 demonstrates microbicidal activity against clinically important microbes *Burkholderia cepacia* (MIC_{50}: 79 μg ml^{-1}), *P. aeruginosa* (MIC_{50}: 16 μg ml^{-1}), *S. aureus* (MIC_{50}: 9 μg ml^{-1}), *Haemophilus influenza* (MIC_{50}: < 10 μg ml^{-1}) and *Stenotrophomonas maltophilia* (MIC_{50}: 1.9 μg ml^{-1}) (Turner *et al.*, 1998; Noore *et al.*, 2013; Tsai *et al.*, 2014). The aim of the results presented in this Chapter was to establish the response of the pulmonary pathogen *Aspergillus fumigatus,* a common pathogen in the CF lung, to LL-37.

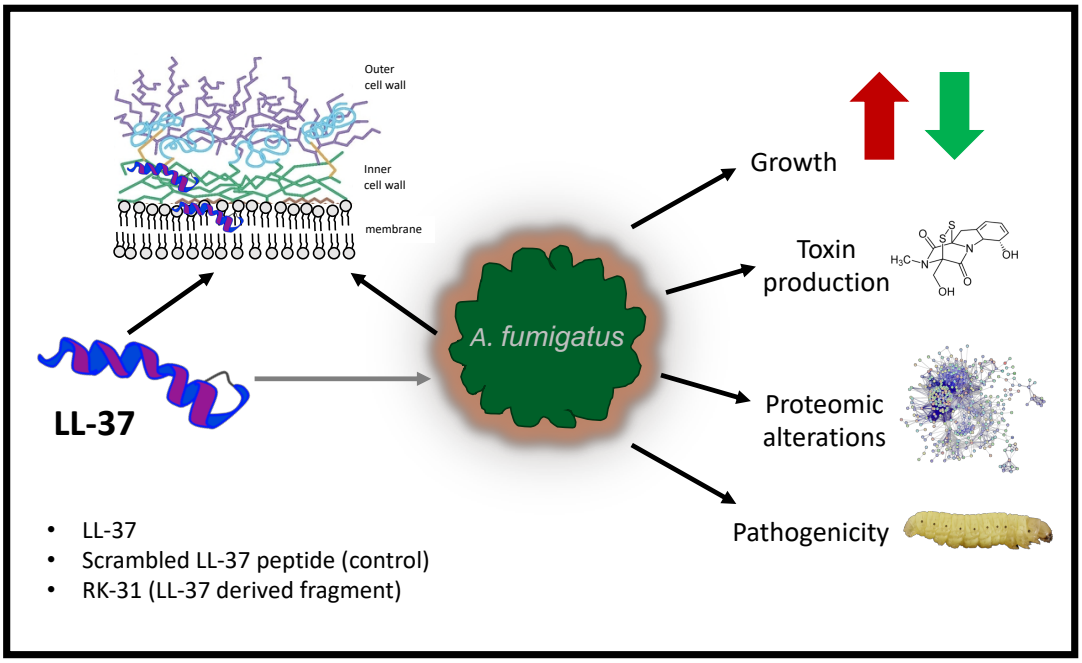

Fig. 9.1. Chapter 9 graphical abstract.

9.2 Effect of LL-37 on the growth of *Candida albicans*

A *C. albicans* culture was achieved by inoculation of YEPD liquid broth with 10^6 ml^{-1} yeast cells and these were incubated for 24 h at 30 ^oC. Stationary phase yeast cells were harvested, adjusted to 10^6 ml^{-1}, resuspended in YEPD and one ml of LL-37 (final concentration of culture; 5 μg ml^{-1}), scrambled LL-37 peptide (5 μg ml^{-1}) and ddH_2O were added and incubated for 5 h. An aliquot was taken, diluted, plated onto YEPD agar plates and *C. albicans* viability was calculated relative to the control cells (ddH_2O treated). LL-37 (5 μg ml^{-1}) significantly reduced the viability of *C. albicans* to 76.67 ± 4.67%, ($p < 0.01$) relative to the scrambled LL-37 peptide (107.22 ± 3.18%) and control (101.67 ± 2.91%) treated cells (**Fig. 9.2**).

9.3 The growth response of *A. fumigatus* to LL-37

An *in vitro* susceptibility assay was employed to establish the effects of intact LL-37, scrambled LL-37 and LL-37 derived fragment (RK-31) on the growth of *A. fumigatus* at concentrations ranging from 31.25 μg ml^{-1} to 0.97 μg ml^{-1} in glucose minimal medium after 24 h ($n = 3$). A concentration of 31.25 μg ml^{-1} increased the growth of *A. fumigatus* to 110.57 ± 2.24% (LL-37) and 147.35 ± 5.54%, $p < 0.05$ (RK-31) while scrambled LL-37 did not (91.91 ± 2.04%). A concentration of 7.81 μg ml^{-1} LL-37 also increased the growth of *A. fumigatus* (185.09 ± 6.02%, $p < 0.05$). Interestingly, a low concentration of LL-37 and RK-31 (1.95 μg ml^{-1}) induced maximum growth of *A. fumigatus* to 199.94 ± 6.17%, $p < 0.05$ and 218.20 ± 4.63%, $p < 0.05$ while the scrambled LL-37 peptide did not (85.12 ± 2.92%) (**Fig. 9.3**). High concentrations of LL-37 (100 μg ml^{-1} – 3.12 μg ml^{-1}) also significantly increased the growth of *A. fumigatus* in minimal essential medium (**Fig. 9.4**), minimal essential medium with 5% FCS (**Fig. 9.5**) and YEPD (**Fig. 9.6**).

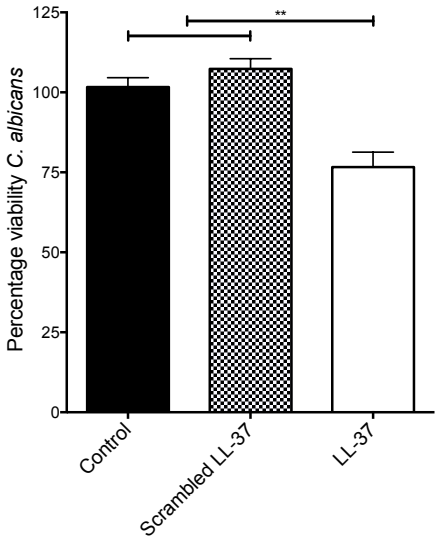

Fig. 9.2. The effect of LL-37 on *C. albicans* viability. Effect of 5 μg ml^{-1} LL-37 and scrambled LL-37 on the viability of *C. albicans* (10^6 ml^{-1} YEPD) following 5 h exposure, LL-37 significantly reduced the viability of *C. albicans* as compared to the scrambled LL-37 peptide and ddH_20 control (**: $p < 0.01$).

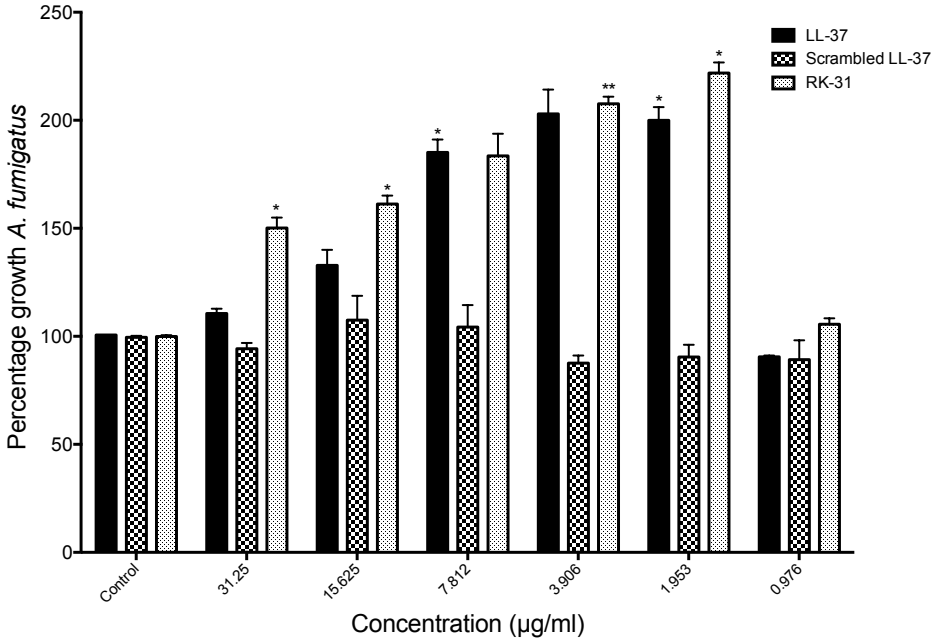

Fig. 9.3. The effect of LL-37, scrambled LL-37 and RK-31 on the growth of *A. fumigatus*. Susceptibility of *A. fumigatus* conidia (initial concentration 10^4 $well^{-1}$) to LL-37, scrambled LL-37 and RK-31 peptides at concentrations ranging from 31.25 μg ml^{-1} to 0.97 μg ml^{-1} after 24 h growth in minimal medium as determined by absorbance at OD_{570}. LL-37 and RK-31 increased the growth of *A. fumigatus* at low concentrations of peptide whilst scrambled LL-37 peptide has no significant effect on *A. fumigatus* growth (*: $p < 0.05$).

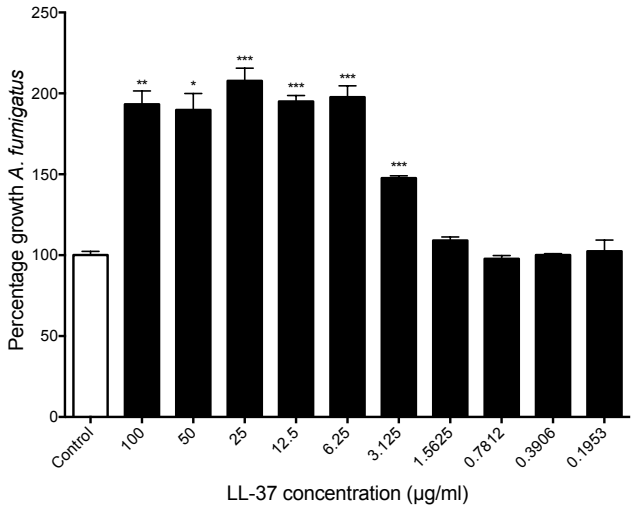

Fig. 9.4. The effect of LL-37 on *A. fumigatus* in minimal essential medium. Conidia were seeded in a 96 plate and the effect of varying concentrations of LL-37 (100 µg ml^{-1} – 0.19 µg ml^{-1}) determined by absorbance at OD_{570} after 24 h growth in minimal essential medium. LL-37 significantly increased the growth of *A. fumigatus* at concentrations ranging from 100 µg ml^{-1} to 3.12 µg ml^{-1} (*: $p < 0.05$, **: $p < 0.01$, ***: $p < 0.001$).

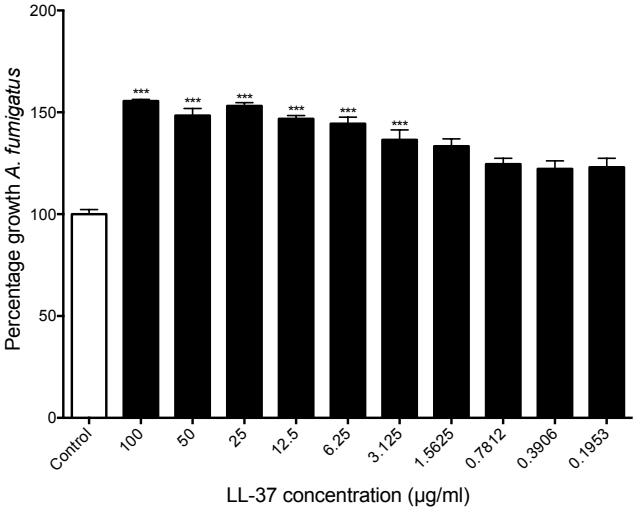

Fig. 9.5. The effect of LL-37 on *A. fumigatus* in minimal essential medium supplemented with 5% fetal calf serum. Conidia were seeded in a 96 plate and the effect of varying concentrations of LL-37 (100 µg ml^{-1} – 0.19 µg ml^{-1}) determined by absorbance at OD_{570} after 24 h growth in minimal essential medium supplemented with 5% fetal calf serum. LL-37 significantly increased the growth of *A. fumigatus* at concentrations ranging from 100 µg ml^{-1} to 3.12 µg ml^{-1} (***: $p < 0.001$).

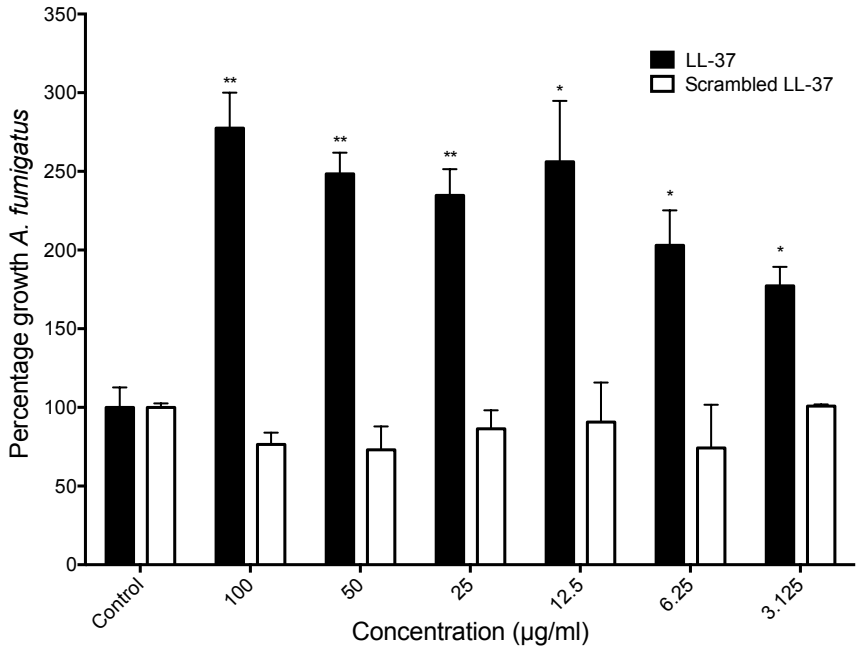

Fig. 9.6. The effect of LL-37 on the growth of *A. fumigatus* in YEPD medium. The effect of intact and scrambled LL-37 on the growth of *A. fumigatus* conidia (10^4 $well^{-1}$) following 24 h growth in YEPD medium as determined by absorbance at OD_{570}. LL-37 stimulates the growth of *A. fumigatus* at high concentrations ranging from 100 µg ml^{-1} – 3.12 µg ml^{-1} whilst addition of scrambled LL-37 peptide has no significant effect on growth (*: $p < 0.05$, **: $p < 0.01$, ***: $p < 0.001$).

9.4 The growth response of *A. fumigatus* to cellular stress agents

Cellular stress agents targeting the cell wall (calcofluor white; (**Fig. 9.7**)) cell membrane (saponin; (**Fig. 9.8**)) and cellular oxidative capacity (hydrogen peroxide (H_2O_2); (**Fig. 9.9**)) were employed to determine if sub-lethal cellular stress agents could stimulate the growth of *A. fumigatus*. Exposure of *A. fumigatus* to calcofluor white (31.25 µg ml^{-1}; 195.37 ± 35.54%, $p < 0.001$) and saponin (100 µg ml^{-1}; 111.90 ± 3.29%, $p < 0.05$) resulted in increased cell growth, however H_2O_2 decreased growth at higher concentrations and did not increase growth at low concentrations compared to the relevant control.

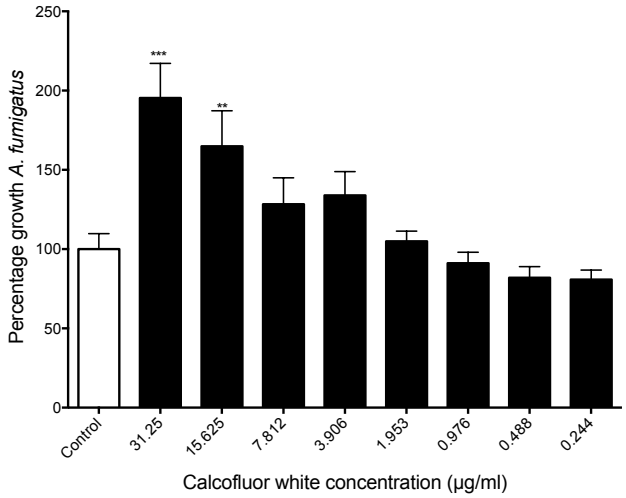

Fig. 9.7. The effect of calcofluor white on the growth of *A. fumigatus.* Conidia were seeded in a 96 plate and the effect of varying concentrations of Calcofluor white (31.25 µg ml^{-1} – 0.24 µg ml^{-1}) determined by OD_{570} after 24 h growth in minimal medium. Calcofluor white significantly increased the growth of *A. fumigatus* at concentrations ranging from 31.25 µg ml^{-1} to 15.62 µg ml^{-1} (**: $p < 0.01$, ***: $p < 0.001$).

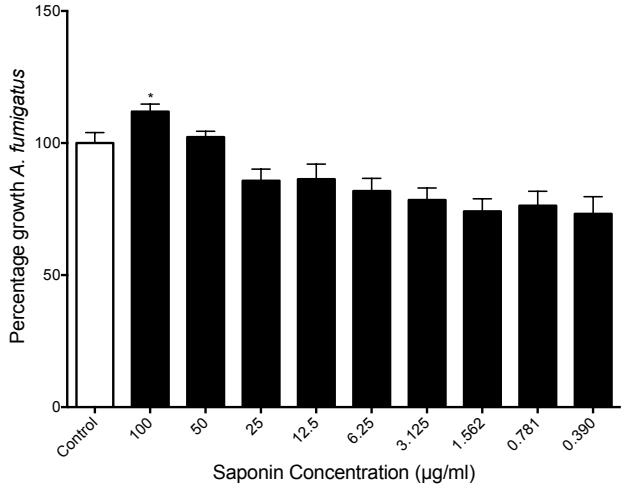

Fig. 9.8. The effect of saponin on the growth of *A. fumigatus.* Conidia were seeded in a 96 plate and the effect of varying concentrations of Saponin (100 µg ml^{-1} – 0.39 µg ml^{-1}) determined by absorbance at OD_{570} after 24 h growth in minimal medium. Saponin significantly increased the growth of *A. fumigatus* at a concentration of 100 µg ml^{-1} (*: $p < 0.05$).

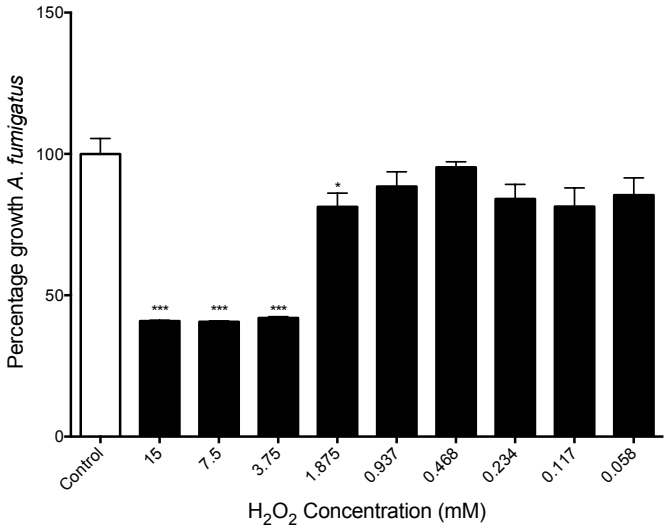

Fig. 9.9. The effect of hydrogen peroxide (H_2O_2) on the growth of *A. fumigatus.* Conidia were seeded in a 96 plate and the effect of varying concentrations of H_2O_2 (15 mM – 0.058 mM) determined by OD_{570} after 24 h growth in minimal medium. H_2O_2 significantly decreased the growth of *A. fumigatus* at concentrations ranging from 15 mM to 3.75 mM (***: $p < 0.001$).

9.5 Responses of *A. fumigatus* mycelium to LL-37

Cultures of *A. fumigatus* (24 h) were supplemented with intact or scrambled LL-37 to give a final concentration of (5 μg ml^{-1}) and incubated for a further 24 or 48 h (n = 3). Addition of LL-37 to cultures for 24 h induced a small increase in growth (2.4 ± 0.23 g versus 2.18 ± 0.10 g (50 ml culture)$^{-1}$), however by 48 h there was a significant increase in growth ($p < 0.001$) (4.37 ± 0.23 g versus 2.67 ± 0.05 g (50 ml culture)$^{-1}$) (**Fig. 9.10**). This increase in growth was not observed following the addition of scrambled LL-37 (5 μg ml^{-1}) after 24 (1.85 ± 0.15 g (50 ml culture)$^{-1}$) or 48 (2.23 ± 0.09 g) h. As a positive control cultures were supplemented with DMSO (final concentration 0.5% v/v) which is known to alter the permeability of fungal cells (Reeves *et al.*, 2004). The results demonstrated an increase in hyphal mass at 24 (2.7 ± 0.077 g) and 48 (3.35 ± 0.06 g, $p < 0.05$) h (**Fig. 9.10**).

9.6 Responses of *A. fumigatus* mycelium to cellular stress agents

Low concentrations of cellular stress inducing agents were used to determine if cell wall, membrane or oxidative stress may cause an increase in wet weight as observed with LL-37 which acts at the membrane – wall interface. Interestingly, a low concentration of H_2O_2 (0.468 mM) resulted in a significant decrease in mycelium wet weight at 24 and 48 h ($p < 0.05$) (**Fig. 9.11**). However, exposure of *A. fumigatus* to 50 µg ml^{-1} of the cell wall stressor calcofluor white resulted in increased mycelium wet weight at 48 h (3.11 ± 0.15 g, $p < 0.05$) as compared to the control.

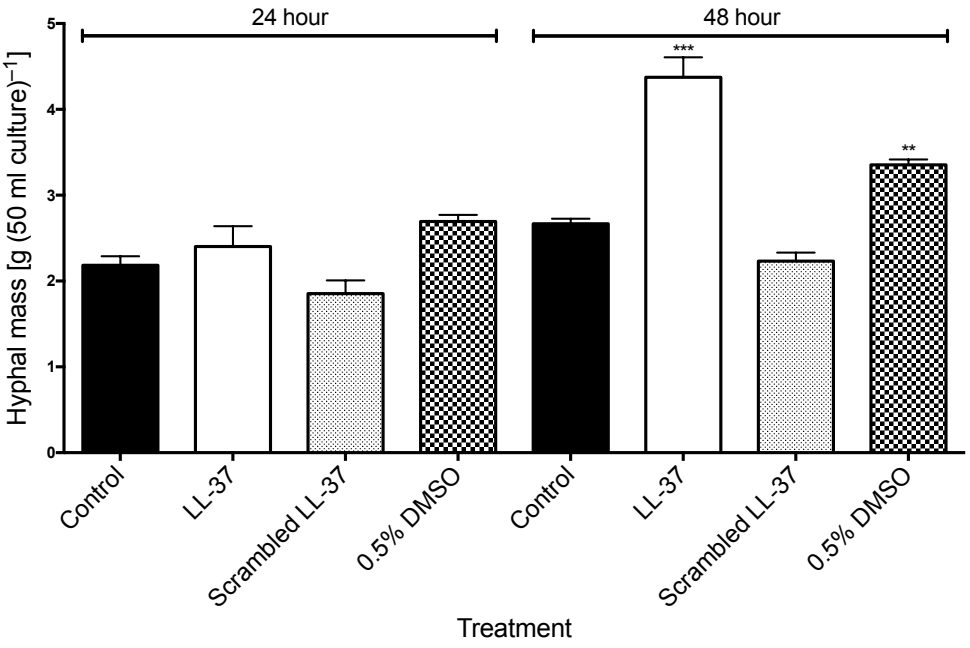

Fig. 9.10. The effect of LL-37 on biomass accumulation of *A. fumigatus*. A 24 h culture of *A. fumigatus (*10^5 ml^{-1}) in sabouraud dextrose broth was supplemented with LL-37, scrambled LL-37, DMSO (0.5% v/v) or ddH20 (control) to give final peptide concentration of 5 µg ml^{-1}. After 24 and 48 h mycelium were weighed. LL-37 increased hyphal mass significantly after 48 h exposure (*: $p < 0.05$, ***: $p < 0.001$).

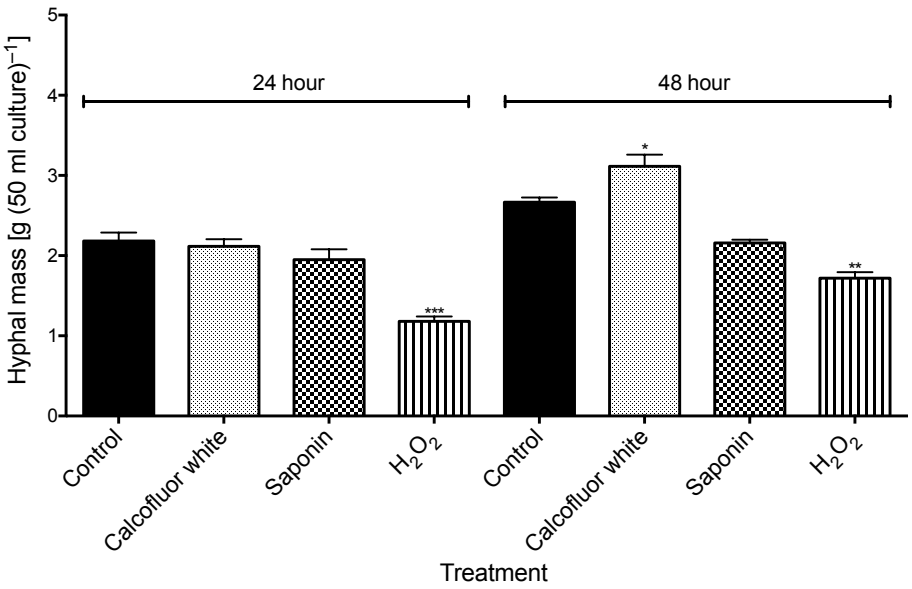

Fig. 9.11. The effect of a low concentration of cellular stress inducing agents on biomass accumulation of *A. fumigatus*. A 24 h culture of *A. fumigatus (*10^5 ml^{-1}) in sabouraud dextrose broth was supplemented with calcofluor white (50 µg ml^{-1}), saponin (100 µg ml^{-1}), H_2O_2 (0.46875 mM) or ddH20 (control). After 24 and 48 h hyphae were weighed. Calcofluor white increased hyphal mass significantly after 48 h exposure (*: $p < 0.05$, **: $p < 0.01$, ***: $p < 0.001$).

9.7 Fluorescent microscopic analysis of effect of LL-37 on *Aspergillus*

Microscopic examination of LL-37, scrambled LL-37 and RK-31 peptide treated and control *A. fumigatus* hyphae revealed no changes in hyphal morphology (**Fig. 9.12**). The effect of LL-37, scrambled LL-37 and RK-31 on the growth of pulmonary pathogen *Aspergillus flavus* was also determined. LL-37 increased the growth of *A. flavus* at 1.93 µg ml^{-1} (137.64 ± 5.90%, $p < 0.05$), however RK-31 and scrambled LL-37 had no significant effect on growth (**Fig. 9.13**). Moreover, these peptides had no effect on *A. flavus* hyphal morphology (**Fig. 9.14**).

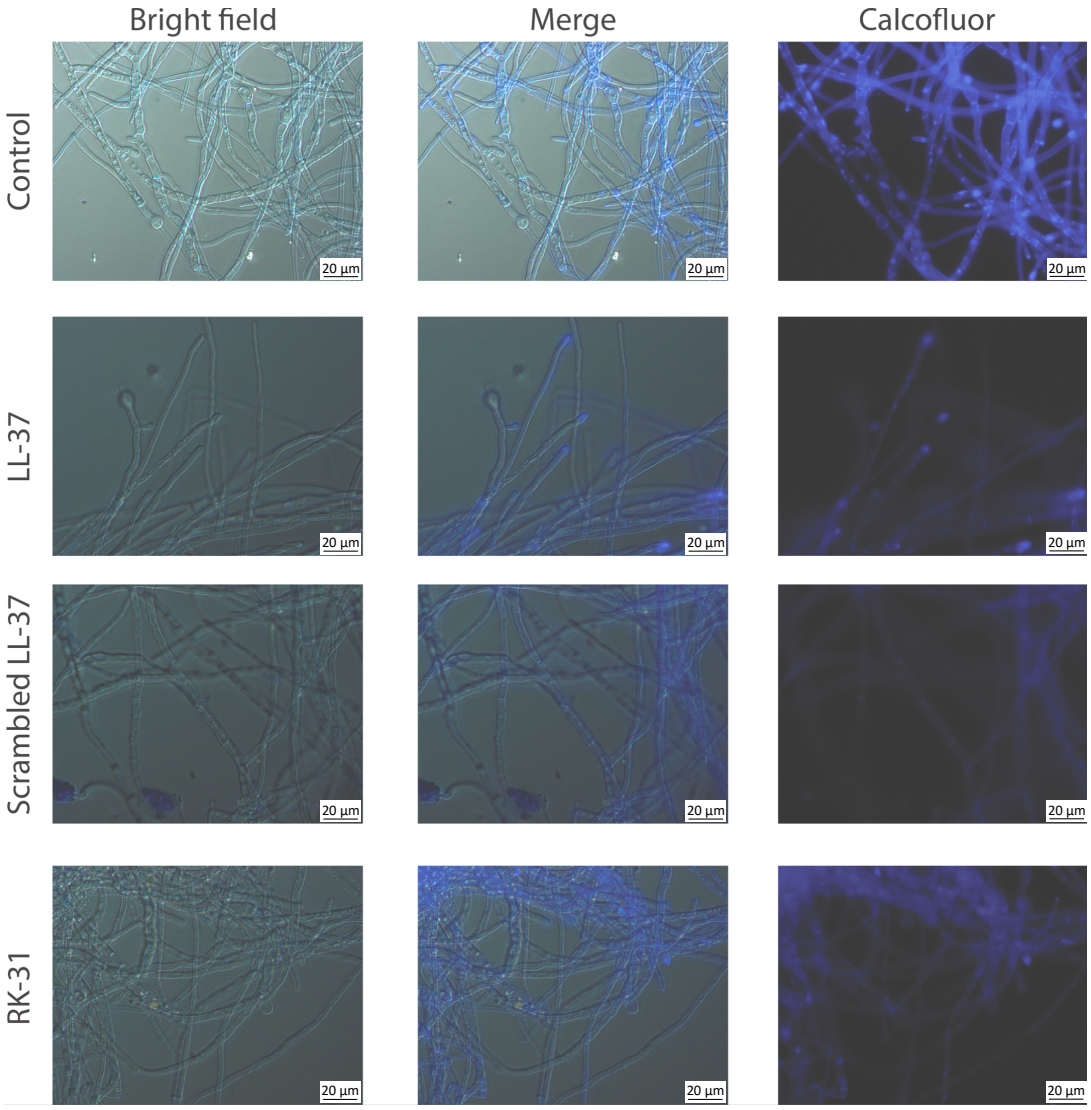

Fig. 9.12. Photomicrographs of *A. fumigatus* hyphae from cultures exposed to LL-37, scrambled and RK-31. *A. fumigatus* mycelium exposed to 31.25 µg ml^{-1} LL-37, scrambled LL-37 and RK-31 for 24 h were stained with Calcofluor white and visualised with an Olympus BX51 fluorescence microscope. LL-37, RK-31 and scrambled LL-37 had no effect on hyphal morphology. The scale bar corresponds to 20 µm.

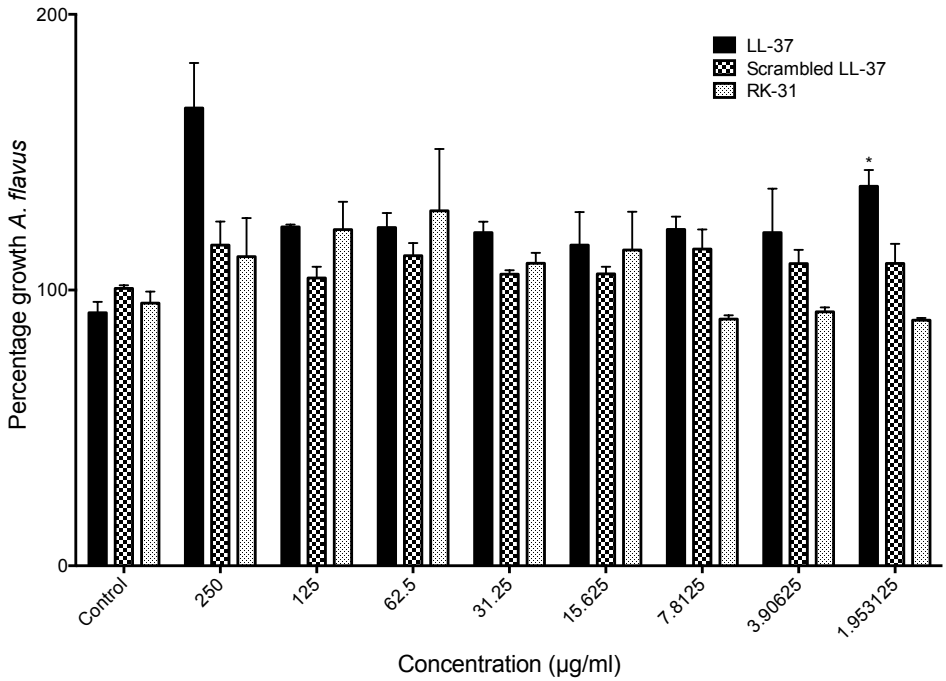

Fig. 9.13. Effect of LL-37 on the growth of *A. flavus*. Susceptibility of *A. flavus* conidia (10^4 well^{-1}) to LL-37, scrambled LL-37 and RK-31 peptides at concentrations ranging from 250 µg ml^{-1} to 1.95 µg ml^{-1} after 24 h growth in minimal medium. LL-37 increased the growth of *A. flavus* at 1.95 µg ml^{-1} of peptide whilst scrambled LL-37 and RK-31 peptide has no significant effect on *A. flavus* growth (*: $p < 0.05$).

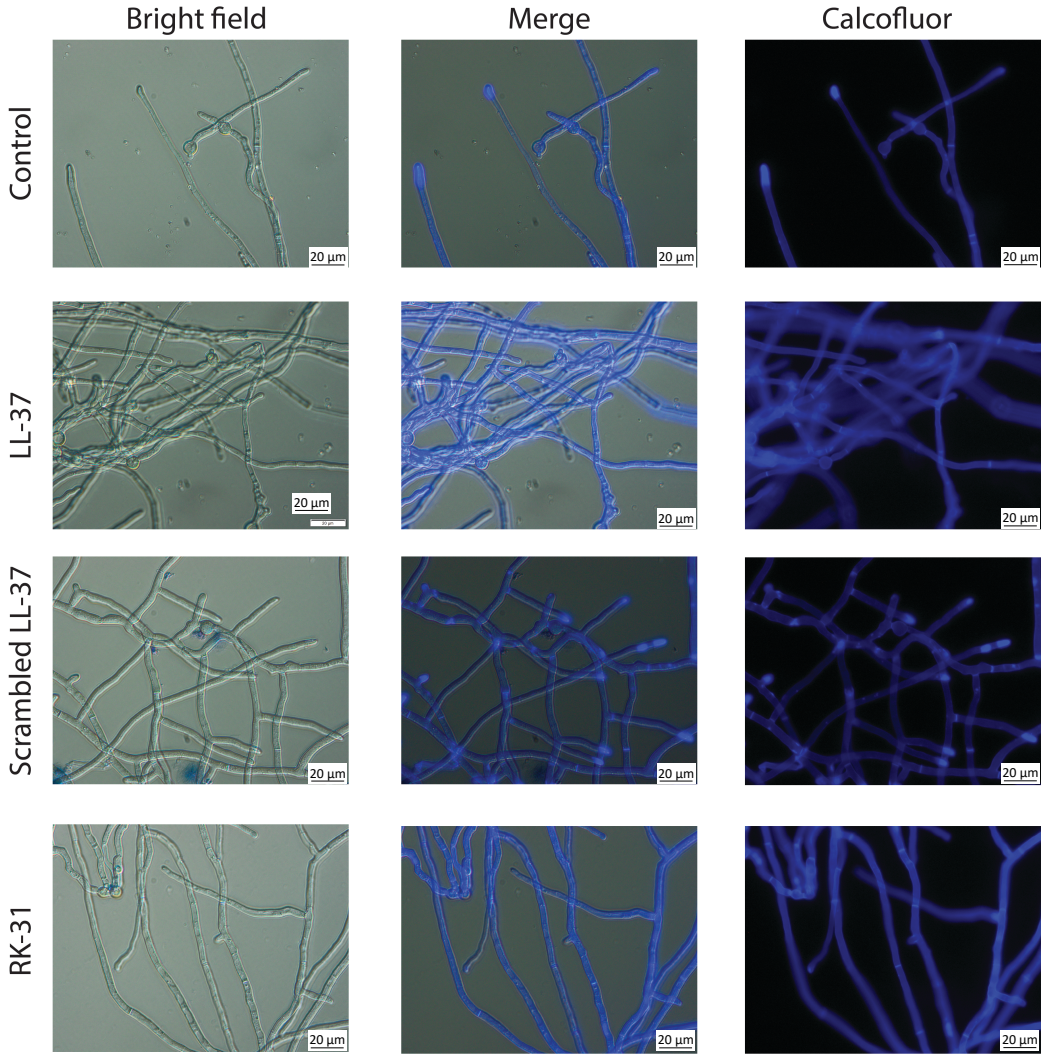

Fig. 9.14. Photomicrographs of *A. flavus* hyphae from cultures exposed to LL-37, scrambled and RK-31. *A. flavus* exposed to 31.25 µg ml^{-1} LL-37, scrambled LL-37 and RK-31 for 24 h were stained with Calcofluor white and visualised with an Olympus BX51 fluorescence microscope. LL-37, RK-31 and scrambled LL-37 had no effect on hyphal morphology. The scale bar corresponds to 20 µm.

9.8 Effect of LL-37 on gliotoxin secretion by *A. fumigatus*

Culture filtrates of 24 and 48 h intact LL-37, scrambled LL-37 or DMSO treated *A. fumigatus* mycelium were collected and assessed for gliotoxin leakage by RP-HPLC in order to determine the effects of LL-37 (intact and scrambled) and DMSO on membrane integrity (n = 3). The biological solvent DMSO was used as a positive control as it known to increase cell membrane permeability and at low concentrations induced gliotoxin leakage from *A. fumigatus* (Reeves *et al.*, 2004).

Mycelium which was cultured in the presence of intact LL-37 (5 μg ml^{-1}) for 24 h released significantly more extracellular gliotoxin (169.15 ± 6.36 ng mg^{-1} hyphae, $p < 0.05$) than control mycelium (102.72 ± 18.81 ng/ mg $hyphae^{-1}$). The addition of scrambled LL-37 (5 μg ml^{-1}) had no significant effect on extracellular gliotoxin concentration after 24 (96.09 ± 15.15 ng/ mg $hyphae^{-1}$) or 48 (99.88 ± 4.08 ng/mg $hyphae^{-1}$) h as compared to their respective controls. An increase in extracellular gliotoxin was also noted for DMSO treated *A. fumigatus* cultures (211.30 ± 15.42 ng/ mg $hyphae^{-1}$, $p < 0.01$). By 48 h, cultures supplemented with LL-37 had gliotoxin levels of 137.82 ± 8.72 ng/ mg $hyphae^{-1}$ compared to 96.32 ± 8.43 ng/mg $hyphae^{-1}$ in the control. Mycelium treated with DMSO for 48 h displayed significantly increased gliotoxin (168.15 ± 15.64 ng/ mg $hyphae^{-1}$, $p < 0.01$) compared to the control (**Fig. 9.15**). Furthermore, the addition of cellular stress inducing agents also resulted in an increase in extracellular gliotoxin (calcofluor white (186.15 ± 12.05 ng/mg $hyphae^{-1}$), saponin (171.52 ± 19.28 ng/mg $hyphae^{-1}$) at 48 h post exposure as compared to the relevant controls (**Fig. 9.16**).

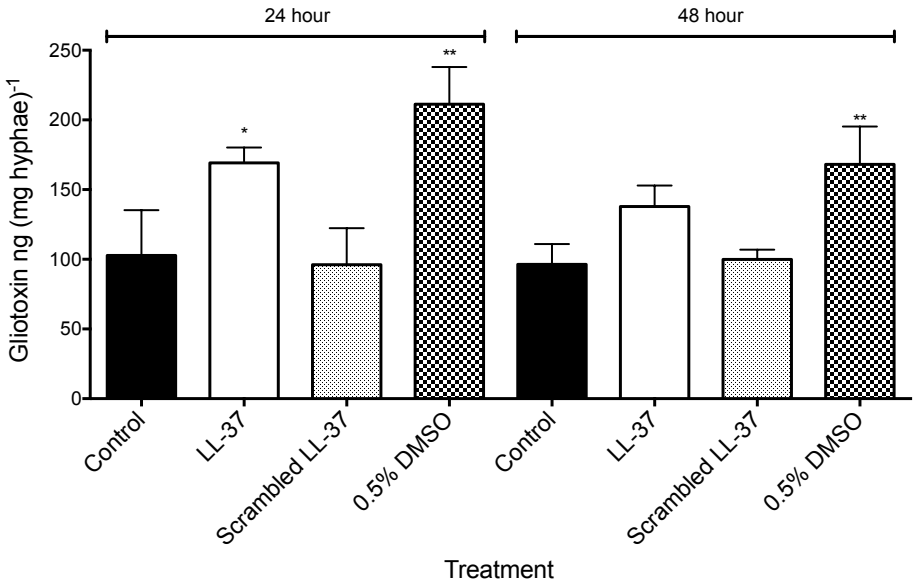

Fig. 9.15. Release of gliotoxin from *A. fumigatus* exposed to LL-37. Gliotoxin quantification in *A. fumigatus* supernatants exposed to LL-37 (5 µg ml^{-1}), scrambled LL-37 (5 µg ml^{-1}) or DMSO (0.5% v/v) for 24 or 48 h was determined by RP-HPLC. LL-37 increased gliotoxin levels at 24 and 48 h (*: $p < 0.05$, **: $p < 0.01$).

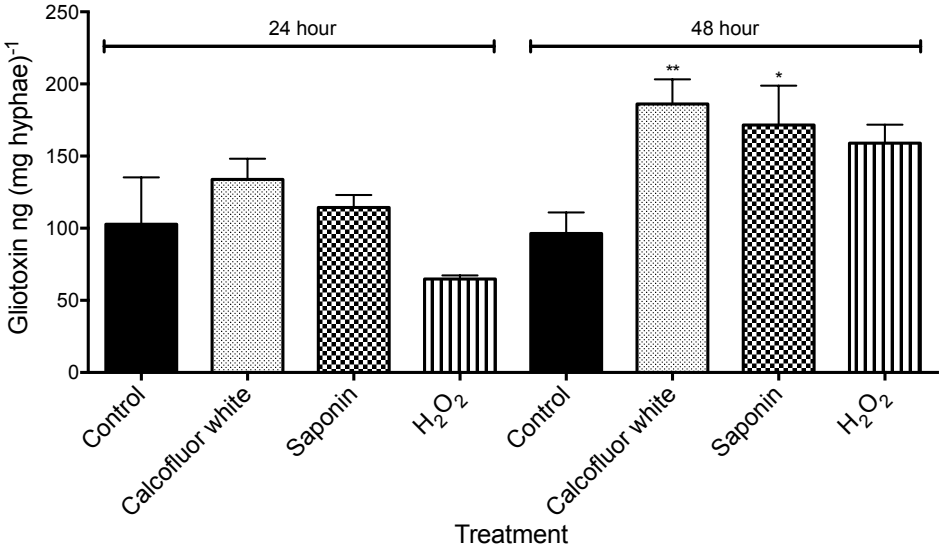

Fig. 9.16. Release of gliotoxin from *A. fumigatus* exposed to cellular stress agents. Gliotoxin quantification in *A. fumigatus* supernatants exposed to a low concentration of cellular stress inducing agents (calcofluor white (50 µg ml^{-1}), saponin (100 µg ml^{-1}), H_2O_2 (0.46875 mM) or ddH_20 (control)) for 24 or 48 h was determined by RP-HPLC. Calcofluor white and saponin increased gliotoxin levels after 48 h (*: $p < 0.05$, **: $p < 0.01$).

9.9 Analysis of proteomic response of *A. fumigatus* to LL-37

Label free quantitative proteomic analysis was conducted on *A. fumigatus* mycelium exposed to LL-37 (5 μg ml^{-1}) for 24 and 48 h. In total, 1524 and 6004 peptides were identified representing 232 and 626 proteins with two or more peptides, respectively. A total of 32 proteins at 24 h and 87 proteins at 48 h were determined to be differentially abundant (ANOVA, $p < 0.05$) with a fold change of > 1.5. A total of 3 (24 h) and 43 (48 h) proteins were deemed exclusive (i.e. with LFQ intensities present in all three replicates of one treatment and absent in all three replicates of the other two treatments). These proteins were also used in statistical analysis of the total differentially expressed group following imputation of the zero values as described. After data imputation these proteins were included in subsequent statistical analysis. A principal component analysis (PCA) performed on all filtered proteins distinguished the control and LL-37 (24 and 48 h) treated samples indicating a clear difference between each proteome (**Fig. 9.17**).

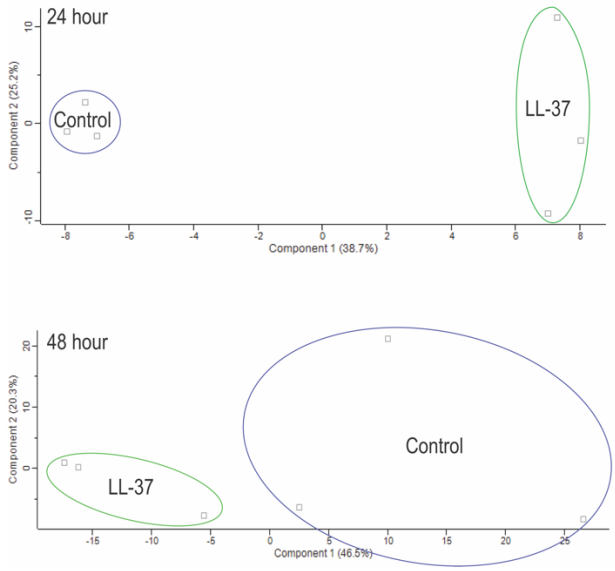

Fig. 9.17. Shotgun quantitative proteomic analysis of LL-37 treated *A. fumigatus*. A; Principal component analysis (PCA) of control and LL-37 treated *A. fumigatus* for 24 and 48 h with a clear distinction between each time point.

Proteins increased in relative abundance in LL-37 (24 h exposure) treated *A. fumigatus* as compared to the control were eukaryotic translation initiation factor eIF-5A (+16 fold), Asp F13 (+10 fold), translation initiation factor 4B (+9.5 fold), translation elongation factor EF-Tu (+7 fold), aspartic endopeptidase Pep1 (+5 fold), 40S ribosomal protein S10a (+4.5 fold), 1,3-β-glucanosyltransferase Gel1 (+2 fold) and aegerolysin family protein (+2 fold). Proteins decreased in relative abundance in LL-37 (24 h exposure) treated *A. fumigatus* were triosephosphate isomerase (-9 fold), secreted dipeptidyl peptidase (-7 fold), inorganic diphosphatase (-5 fold), saccharopine dehydrogenase (-4 fold) and fructose-bisphosphate aldolase (-4 fold) (**Fig. 9.18A, Table A9.1**).

Proteins increased in relative abundance in LL-37 (48 h exposure) treated *A. fumigatus* were malate dehydrogenase (+27 fold), glutathione peroxidase (+9 fold), ribosomal protein L15 (+8.9 fold), translationally-controlled tumor protein homolog (+8.4 fold), hsp70 chaperone (+7.9 fold), eukaryotic translation initiation factor eIF-5A (+6 fold), 60S acidic ribosomal protein P0 (+6 fold), Alcohol dehydrogenase (+5.2 fold), dual-functional monooxygenase/methyltransferase psoF (+4.1 fold) ribonuclease mitogillin (+3.7 fold), FK506-binding protein 2 (+3.5 fold), eIF4A (+2.7 fold), allergen Asp f 15 (+2.5 fold) and glutathione oxidoreductase (+1.7 fold). Proteins decreased in relative abundance in LL-37 treated *A. fumigatus* at this time were associated with the proteasome (proteasome subunit β type (-7 fold), proteasome endopeptidase complex (-2.5 fold), pup1 (-2.1 fold) and proteasome subunit α type (-2 fold)) cell wall (1,3-β-glucanosyltransferase Gel1 (-3 fold)), and carboxypeptidase activity (carboxypeptidase (-2.4 fold) (**Fig. 9.18B, Table A9.2**).

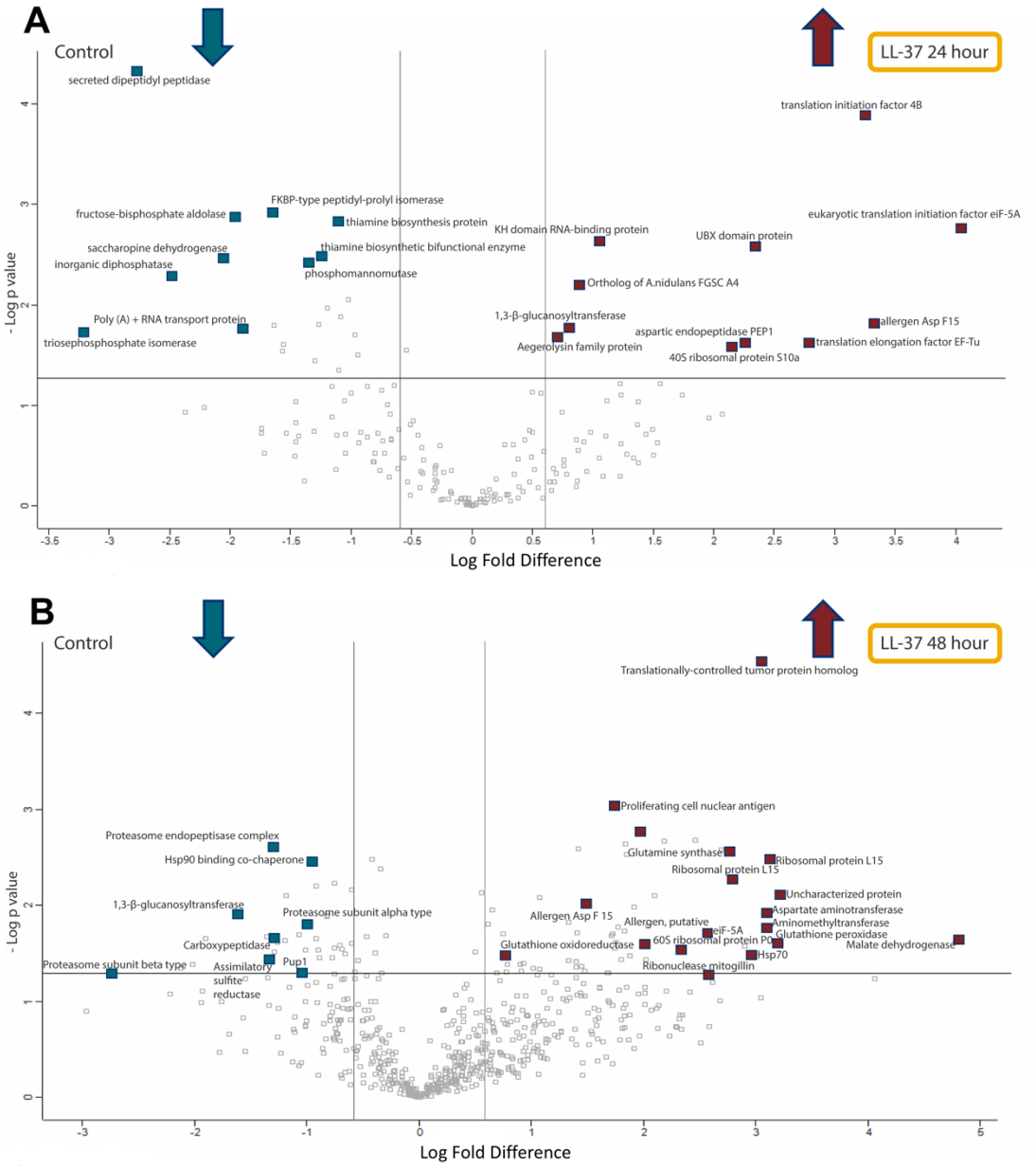

Fig. 9.18. Label free proteomics of *A. fumigatus* exposed to 5 µg ml^{-1} LL-37 for 24 h (A) or 48 h (B). Volcano plots showing the distribution of quantified proteins according to p value (−log10 p-value) and fold change (log2 mean LFQ intensity difference). Proteins above the line are considered statistically significant (p value < 0.05) and those to the right and left of the vertical lines indicate relative fold changes > ±1.5. LL-37 induced increased abundance of proteins associated with growth, virulence and allergic reactions.

9.10 Effect of LL-37 on the pathogenicity of *A. fumigatus* in the *G. mellonella* model of invasive aspergillosis

A. fumigatus conidia were germinated in minimal essential media (with the addition of 5% v/v FCS) for 2 h, incubated in LL-37, scrambled LL-37 or RK-31 at varying concentrations for 2 h, washed and injected into *G. mellonella* larvae and viability and fungal load assessed after 24 and 48 h post infection.

Incubation of *A. fumigatus* in LL-37 significantly decreased the survival of *G. mellonella* larvae after 24 and 48 h. At 24 h a concentration of 5 μg ml^{-1} (83.33 ± 3.33%, $p < 0.01$), 15 μg ml^{-1} (86.67 ± 3.33, $p < 0.05$) and 40 μg ml^{-1} (80.00% ± 0%, $p < 0.001$) LL-37 significantly decreased the viability of *G. mellonella* larvae as compared to *A. fumigatus* incubated in scrambled LL-37 peptide (100 ± 0%). At 48 h this was also observed e.g. a lower concentration of 5 μg ml^{-1} LL-37 decreased larval viability to 16.67 ± 3.33% ($p < 0.001$) as compared to the scrambled LL-37 peptide incubated *A. fumigatus* (36.67 ± 3.33%). Moreover, this effect was observed with LL-37 derived fragment RK-31 which resulted in increased mortality of larvae relative to scrambled LL-37 peptide over 24 and 48 h (**Fig. 9.19**).

The fungal burden of infected larvae was determined at 24 and 48 h post infection (**Fig. 9.20**). Larvae infected with *A. fumigatus* pre-incubated in LL-37 and RK-31 at varying concentrations displayed an increased fungal burden *in vivo.* At 48 h post infection a concentration of 5 μg ml^{-1} LL-37 and RK-31 resulted in a fungal load of 2.74 ± 0.09 × 10^5 c.f.u. $larva^{-1}$ and 3.38 ± 0.18 × 10^5 c.f.u. $larva^{-1}$, respectively as compared to those infected with *A. fumigatus* pre-incubated in scrambled peptide (1.30 ± 0.03 × 10^5 c.f.u. $larva^{-1}$).

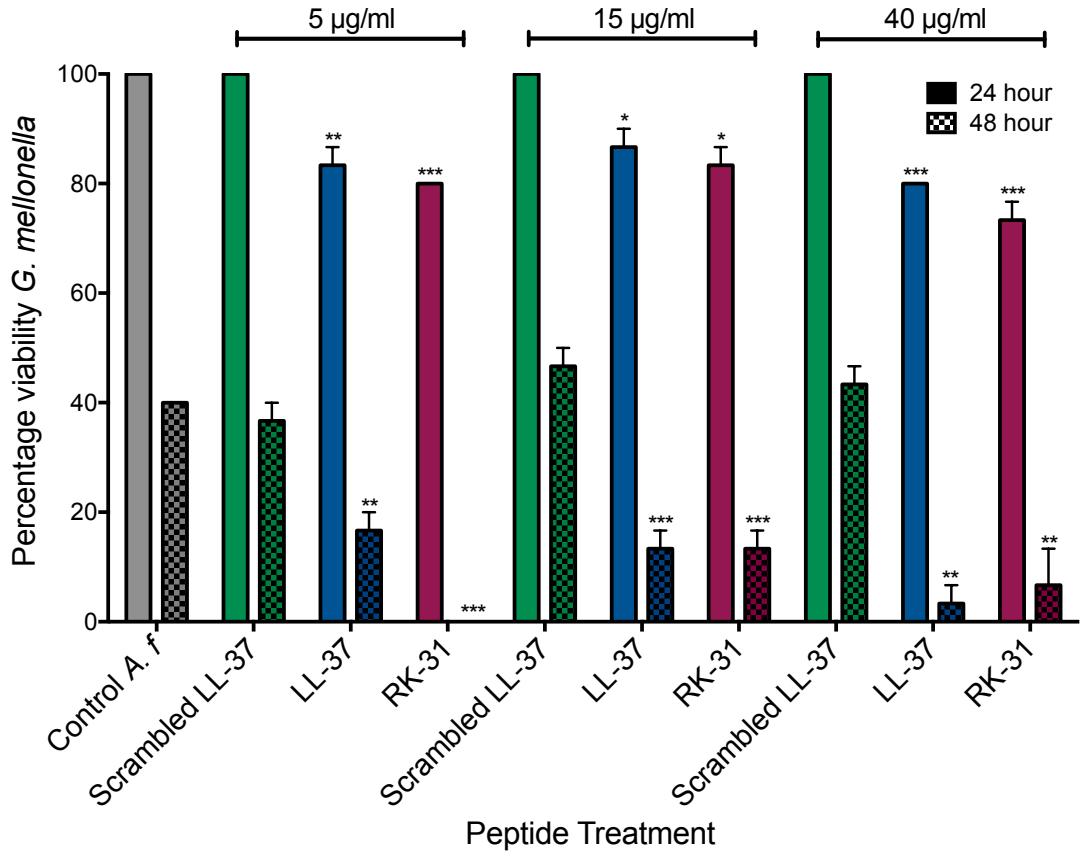

Fig. 9.19. Effect of pre-incubation of *A. fumigatus* in LL-37, scrambled LL-37 and RK-31 on the viability of *G. mellonella* larvae. *A. fumigatus* conidia were incubated in minimal essential medium supplemented with 5% v/v fetal calf serum for 2 h to produce germlings, supplemented with peptides at varying concentrations (5, 15 or 40 µg ml^{-1}) for 2 h, centrifuged and washed with PBS and injected into larvae (initial density; 2.5×10^7 ml^{-1}). Viability was assessed at 24 and 48 h. Statistical analysis was performed by comparing each treatment to the scrambled LL-37 peptide incubated *A. fumigatus* at its respective timepoint (*: $p < 0.05$, **: $p < 0.01$, ***: $p < 0.001$).

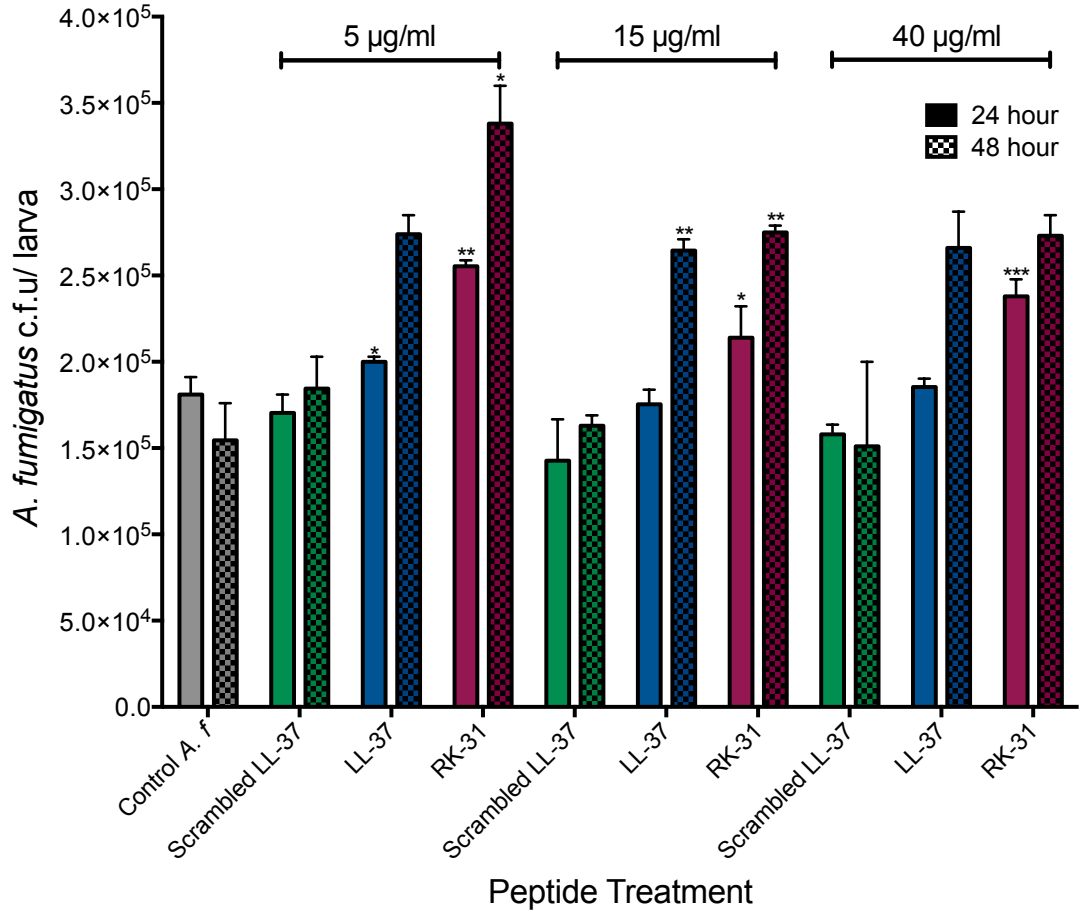

Fig. 9.20. Effect of pre-incubation of *A. fumigatus* in LL-37, scrambled LL-37 and RK-31 on the fungal load *Galleria mellonella* larva^{-1}. Larvae (n = 3) were homogenised in a pestle and mortar, diluted and plated on malt extract agar plates supplemented with 0.1 mg ml^{-1} erythromycin which were incubated over night at 37 ^{o}C. Resulting colonies were counted and expressed in terms of *A. fumigatus* fungal load larva^{-1}. Statistical analysis was performed by comparing each treatment to the scrambled LL-37 peptide incubated *A. fumigatus* at its respective timepoint (c.f.u.: colony forming units) (*: $p < 0.05$, **: $p < 0.01$, ***: $p < 0.001$).

9.11 Discussion

A. fumigatus is a significant pulmonary pathogen in individuals who are immunocompromised (e.g. myelosuppression) and in those who display defects in immune equilibrium, commonly observed in the CF lung and presents itself in the form of allergic bronchopulmonary aspergillosis (ABPA) (Margalit and Kavanagh, 2015). In the latter, *A. fumigatus* airborne conidia penetrate the lower airways, germinate and grow within the thick tenacious CF mucus. CF patients colonised by *A. fumigatus* can become sensitised to *A. fumigatus* secreted allergens and eventually develop a type 2 hypersensitivity reaction to *A. fumigatus* allergens, toxins and proteases that are readily replenished into the mucus which can directly cause cell damage and peeling at the bronco – epithelium interface (Stevens *et al.*, 2003). Therefore, the hypothesis behind this Chapter was that components of the CF mucus could positively or negatively affect the growth of *A. fumigatus*.

LL-37 is an important antimicrobial peptide produced by a variety of pulmonary cells (type II pneumocytes, neutrophils) and augmentable to high concentrations transiently during inflammation and infection. LL-37 has direct and indirect antimicrobial activity against important pathogens of the CF lung and has pleotropic growth effects on eukaryotic membranes, this together with its augmented abundance in the CF lung which is frequently dominated by *A. fumigatus*, makes it an interesting target to study host – pathogen interactions.

As previously reported by Tsai *et al.* (2011, 2014) LL-37 decreased the viability of *C. albicans,* whereas the scrambled version of the peptide did not alter viability. The effect of LL-37 on the pulmonary pathogen *A. fumigatus* was then examined. Interestingly, LL-37 increased the growth of *A. fumigatus*. Doses ranging from 31.25 μg ml^{-1}, which would be indicative of local inflammation, to 5 μg ml^{-1}, which is characteristic of CF BALF, supported the growth of *A. fumigatus in vitro* (Robert *et al.*, 1998; Bowdish *et al.*, 2005). The addition of scrambled LL-37 peptide had no effect on *A. fumigatus* growth while the addition of LL-37 derived fragment RK-31 also produced an increase in growth in high and low nutrient media. This indicates the primary structure of LL-37 is essential to its bioactivity and RK-31, a shorter and purportedly more microbicidal peptide of LL-37 also enhanced *A. fumigatus* growth. LL-37 at a low concentration also increased the growth of *A.*

flavus, a less common CF lung pathogen (Hedayati *et al.*, 2007; Mahgoub and el-Hassan, 1972). Furthermore, microscopic analyses of *A. fumigatus* and *A. flavus* revealed no changes in hyphal morphology and no hyperbranching or aggregation in response to LL-37 or RK-31. LL-37 increased mycelium wet weight after 24 (2.4 ± 0.23 g versus 2.18 ± 0.10 g (50 ml culture)$^{-1}$) and 48 (4.37 ± 0.23 g versus 2.67 ± 0.05), ($p < 0.001$)) h. Addition of scrambled LL-37 to *A. fumigatus* cultures for 24 (1.85 ± 0.15 g (50 ml culture)$^{-1}$) and 48 (2.23 ± 0.09 g) h had no significant effect on mycelium mass. This indicates that peptide size, sequence, charge, helicity, hydrophobicity and amphipathicity are essential for the growth promoting effects induced by LL-37. The use of a low concentration of the biological solvent DMSO, which is known to alter cell permeability, also increased mycelial wet weight at 24 and 48 h. These findings suggest that LL-37 may increase the growth of *A. fumigatus* by acting on the fungal membrane in a similar mechanism to that observed in mammals (Coffelt *et al.*, 2008; Von Haussen *et al.*, 2008).

Employing low concentrations of cellular stress agents resulted in enhanced growth comparable to that observed with LL-37, most notably was calcofluor white and saponin which interact with the fungal cell wall and membrane, respectively (Roncero and Duran, 1985; Yang *et al.*, 2006). Calcofluor white increased the growth of *A. fumigatus* to 195.37 ± 35.54%, ($p < 0.001$) and also increased mycelium biomass (3.11 ± 0.15 g, $p < 0.05$). It was hypothesised that a low level of stress may activate compensatory growth pathways in *A. fumigatus*. At the concentrations examined H_2O_2 appears growth inhibitory rather than stimulatory.

Previous work has demonstrated that LL-37 induced leakage of biological and fungal membranes and the antifungal drug amphotericin B also alters *A. fumigatus* membrane permeability and induces the release of gliotoxin (Reeves *et al.*, 2004; Den Hertog *et al.*, 2006; Thennarasu *et al.*, 2010; Lee *et al.*, 2011; Ordonez *et al.*, 2014). The secretion of gliotoxin was increased in response to LL-37 at 24 (169.15 ± 6.36 ng/ mg hyphae^{-1}, $p < 0.05$) and 48 (137.82 ± 8.72 ng/ mg hyphae^{-1}) h. Gliotoxin has pleotropic effects on its host such as polymorphonuclear leukocyte apoptosis, inhibition of neutrophil phagocytosis and NADPH dependent oxidative burst, inhibition of T lymphocytes epithelia damage, slowed ciliary beating (Amitani *et al.*, 1995; Reeves *et al.*, 2004; Coméra *et al.*, 2007; Martins *et al.,* 2017). Gliotoxin

induces vitamin D receptor down-regulation in pulmonary macrophages and epithelial cells resulting in increased IL-5 and IL-13 production which skew T cell plasticity towards an allergic T_H2 dominated response (Coughlan *et al.*, 2012). Small molecule leakage may facilitate rapid nutrient uptake into the cell possibly accounting for the observed growth increase. The use of calcofluor, and saponin resulted in a significant increase in extracellular gliotoxin 48 h post exposure. Gliotoxin may play an important role in maintenance of cell redox balance and is significantly increased in response to oxidative stress (Gallagher *et al.*, 2012). This suggests cell stress resulting in an alteration in cell redox status may result in increased gliotoxin production to restore cell redox homeostasis, which may have consequences in the CF lung.

Shotgun proteomics was employed to determine the effect of LL-37 on *A. fumigatus* after 24 and 48 h exposure. *A. fumigatus* responds to LL-37 by increasing the abundance of growth associated proteins such as eukaryotic translation initiation factor eIF-5A (+16 fold), translation initiation factor 4B (+9.5 fold), translation elongation factor EF-Tu (+7 fold) and 40S ribosomal protein S10a (+4.5 fold). eIF-5A in eukaryotic cells was strongly associated with hyperproliferative growth, maintenance of cell wall integrity in fungal cells and was found to be important in *A. fumigatus* in response to H_2O_2 (Lessing *et al.*, 2007; Rossi *et al.*, 2013; Acta, 2016).

After 24 h LL-37 exposure *A. fumigatus* also increased the abundance of proteins which may have a role in virulence such as Asp F13 (+10 fold), aspartic endopeptidase Pep1 (+5 fold) and aegerolysin family protein (+2 fold). Asp F13 is a secreted alkaline protease and allergen associated with *A. fumigatus* immune subversion and virulence via cleavage of complement cascade proteins and immunoglobulin class G isotypes and binding of IgE (Rambach *et al.*, 2010; Wartenberg *et al.*, 2011). Pep1 is a hyphal tip secreted aspartic proteinase known to hydrolyse proteins of the basement membrane (elastin, collagen, and laminin) and found during *A. fumigatus* invasion of the neutropenic mouse lung (Lee and Kolattukudy, 1995). *A. fumigatus* also produces a 14 kDa aegerolysin family protein (Asp-hemolysin) found to possess putative hemolytic activity on erythrocytes as well as cytotoxic effects on murine macrophages and endothelial cells (Kumagai *et al.,* 1999). Asp-hemolysin can be detected *in vivo* during infection, however

experimental evidence is lacking for its role in virulence (Vasco *et al.*, 2005). Proteins associated with thiamine metabolism were decreased in abundance 24 h post LL-37 exposure.

Forty - eight h post LL-37 exposure, mycelium proteome displayed enrichment for proteins associated with growth (malate dehydrogenase (+27 fold), ribosomal protein L15 (+8.9 fold), 60S acidic ribosomal protein P0 (+6 fold), eIF-5A (+6 fold), FK506-binding protein 2 (+3.5 fold) and eIF4A (+2.7 fold)) as well as a variety of detoxification and stress response proteins (glutathione peroxidase, hsp70 chaperone, alcohol dehydrogenase, and glutathione oxidoreductase). As with 24 h LL-37 treated mycelium, 48 h exposed mycelium showed increased abundance of proteins associated with virulence. Ribonuclease mitogillin (+3.7 fold) is an 18 kDa purine-specific ribonuclease which cleaves the 28S RNA of eukaryotic ribosomes resulting in protein synthesis inhibition (Vasco *et al.*, 2005). Mitogillin is considered a major allergen of *A. fumigatus* which interacts with IgE from ABPA patients (Weig *et al.*, 2001). Allergen (+ 3.6 fold) is a putative secreted allergen of *A. fumigatus* which possesses domains associated with oxidoreductase activity (redoxin, thioredoxin-like fold, thioredoxin-domain containing protein) and may play a role in cell redox homeostasis. Dual-functional monooxygenase/ methyltransferase psoF and methyltransferase psoC are both essential in pseurotin and fumagillin (psoF) biosynthesis. Pseurotin has been noted to inhibit chitin synthesis and inhibit IgE production from mouse B cells. The toxin fumagillin can retard the ciliary beat frequency of pulmonary epithelial cells, inhibit neutrophil function and decreases host survival to invasive aspergillosis *in vivo* (Fallon *et al.,* 2010, 2011). Exposure of *A. fumigatus* to LL-37 for 48 h results in decreased abundance of proteins associated with protein degradation. The reduction in these proteins may explain the increased abundance of proteins associated with regulatory processes (mRNA and protein synthesis etc.) to an external stimuli (LL-37). Interestingly, Gel1 is increased at 24 h but is decreased at 48 h. Gel1 plays a role in elongation of 1,3-β-glucan chains and is induced under hypoxic conditions and its change in abundance may alter β-glucan concentration in the cell wall (Mouyna *et al.*, 2000; Vödisch *et al.*, 2011).

The effect of LL-37 on the pathogenicity of *A. fumigatus* was assessed *in vivo* using the *G. mellonella* model of invasive aspergillosis (Jackson *et al.,* 2009; Slater *et al.*, 2011). Larvae have been used to assess the efficacy of novel antimicrobial peptides as well as LL-37 *in vivo* (Dean *et al.,* 2011; McCloskey *et al.*, 2019). Pre-incubation of *A. fumigatus* in LL-37 or RK-31 but not scrambled LL-37 resulted in decreased survival of *G. mellonella* larvae at a range of concentrations and this is associated with increased fungal load in larvae. It is most probable that LL-37 and RK-31 activate growth promotion in *A. fumigatus* germlings, which, upon injection into larvae are primed (at the proteomic level: increased growth and virulence associated proteins and increased gliotoxin production) for infection.

Interestingly, a recent study from Luo *et al.* (2019) found that LL-37 is protective for immunocompromised mice infected with *A. fumigatus*. Although these findings are contradictive to the datum presented in this Chapter, there are key differences between the two studies. This work examined concentrations relevant to the CF lung, while Luo *et al.* focused on concentrations up to 100 μg ml^{-1}, different strains were used (Af293 vs. ATCC strain) and they focused on the role of LL-37 in invasive aspergillosis in corticosteroid-treated mice (Luo *et al.*, 2019). Invasive aspergillosis in immunocompromised patients and colonisation/ABPA in CF or asthmatic patients are completely different diseases although caused by the same pathogen. It is likely that LL-37 may have a positive effect on the outcome of IA but may cause a negative effect on the outcome of ABPA in CF patients because of the inflammatory milieu present in the lung which drives dysregulated production of LL-37 (Chen *et al.*, 2004; Xiao *et al.*, 2005).

The results presented in this Chapter demonstrate that LL-37 stimulates the growth of *A. fumigatus* at physiologically relevant concentrations as found in the CF lung. This stimulation of growth may be due to the altered membrane permeability or interactions with the fungal cell wall resulting in the activation of growth associated processes. The enhanced growth of the fungus, the elevated secretion of gliotoxin and the increased abundance of allergic and tissue degrading enzymes may have adverse effects on the pulmonary tissue of CF patients and contribute to the development of disease.

Chapter 10

Analysis of the response of *Aspergillus fumigatus* to N-chlorotaurine

10.1 Introduction

When the immune system becomes severely compromised (e.g. myelosuppression) *A. fumigatus* conidia germinate, produce hyphae and grow between and through alveolar epithelial cells by the production of a range of tissue degrading enzymes and immunosuppressive toxins. *A. fumigatus* virulence is multifaceted and includes the production of low molecular weight toxins, proteolytic enzymes, thermotolerance, immune detoxification mechanisms and metabolic adaptations (Dagenais and Keller, 2009; Chotirmall *et al.*, 2013). *A. fumigatus* produces several non-ribosomal peptides (NRP) such as *pes*1 and *pes*3 (Reeves, *et al.*, 2006; O'Hanlon *et al.*, 2011). The former (*pes*1) plays a role in fungal tolerance to oxidative stress, mediated by the conidial phenotype (Reeves *et al.*, 2006).

Activated neutrophils through a series of enzymatic reactions produce superoxide and hydrogen peroxide with NADPH oxidase and superoxide dismutase, respectively, and hypochlorous acid (HOCl) is formed from hydrogen peroxide (H_2O_2) and chloride by myeloperoxidase (Klebanoff, 2005). HOCl in the presence of taurine results in the formation of N-chlorotaurine (NCT; Cl-HN-CH_2-CH_2-SO_3H) (Zgliczyński *et al.*, 1971; Test *et al.*, 1984). NCT is the most abundant representative of this class of compounds and is a long lived oxidant (Grisham *et al.*, 1984). Chloramine has been detected in supernatants from stimulated granulocytes at concentrations ranging from 30 to 100 μM (Test *et al.*, 1984). NCT is the main constituent of these compounds reaching concentrations of between 10 to 50 μM (Weiss *et al.*, 1982; Grisham *et al.*, 1984). NCT is bactericidal, fungicidal, virucidal and vermicidical at concentrations ranging from 100 μM to 55 mM and non-cytotoxic up to 0.5 mM (Nagl *et al.*, 2000a; Gottardi and Nagl, 2010). Bronchial exudates from CF patients display chloramine concentrations of 118 ± 25 μM (Witko-Sarsat *et al.*, 1995), indicating a high level of NCT present extracellularly *in vivo* which is continually replenished by activated neutrophilic and eosinophilic granulocytes, monocytes and, in small amounts, probably macrophages (Epstein and Weiss, 1989; Marcinkiewicz and Kontny, 2014).

Neutrophils are the first line of defence against *A. fumigatus* and this is demonstrated by the high incidence of invasive aspergillosis in chronic granulomatous disease (CGD) patients who lack functional neutrophils (Williams *et*

al., 2017). *A. fumigatus* is engulfed into the phagosome and encounters NCT during the oxidative killing process. *A. fumigatus* comes into contact with NCT in CF bronchoalveolar lavage fluid. *A. fumigatus* has extensive mechanisms to circumvent and detoxify PMNs killing including oxidative mechanisms (Levitz and Diamond, 1985). In order to elucidate the role of NCT in the human defence system and its potential for topical application as an anti-infective, it was the aim of this Chapter to determine its mode of action on *A. fumigatus* and the response of this pulmonary pathogen (**Fig. 10.1)**.

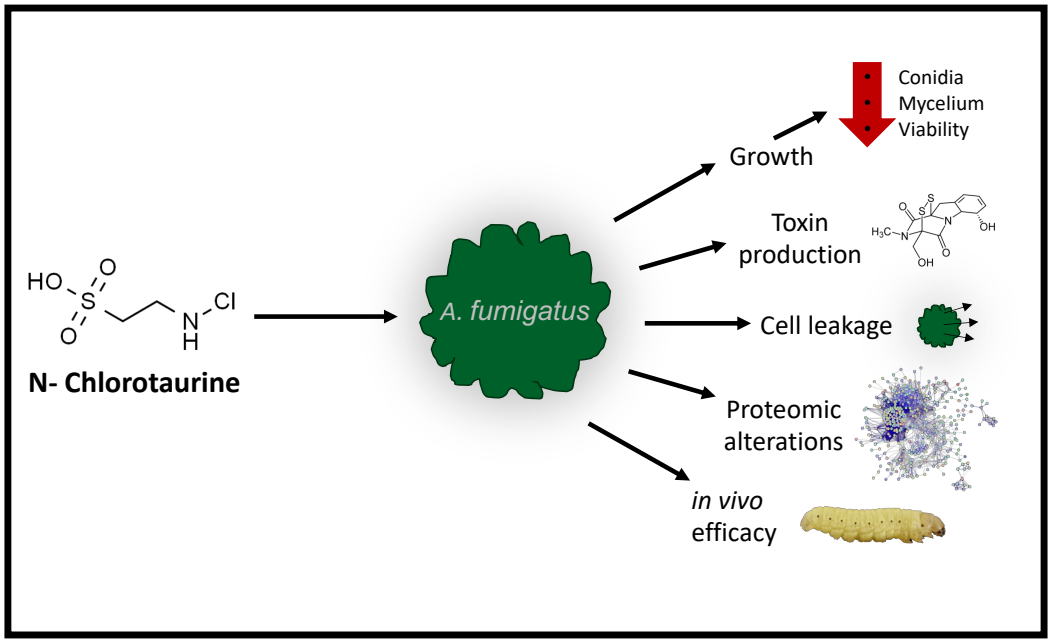

Fig. 10.1. Chapter 10 graphical abstract.

10.2 Effects of N-chlorotaurine on the growth of *A. fumigatus*

The growth response of *A. fumigatus (*ATCC 26933) to NCT was assessed *in vitro* using a susceptibility assay. Exposure of *A. fumigatus* to 6.8 and 55 mM NCT reduced growth to 6.42 ± 0.43% and 5.22 ± 0.43%, respectively, relative to the control in SAB after 48 h ($p < 0.001$). A concentration of 3.44 mM reduced growth by 9.83 ± 3.64%, ($p < 0.05$) **(Fig. 10.2A).** NCT at 55 mM reduced growth of *A. fumigatus* in minimal essential media (MEM) + 5% fetal calf serum (FCS) to 70.67 ± 1.29% ($p < 0.0001$), and 3.4 mM NCT reduced growth to 78.17 ± 11.01%, but this was less in MEM + 5% FCS as compared to SAB **(Fig. 10.2B).** NCT also reduced the growth of other *A. fumigatus* strains (ATCC46645 [**Fig. 10.2C**] & Af293 [**Fig. 10.2D**]) at concentrations ranging from 3.44 to 55 mM. The effect of NCT on the growth *A. flavus* was also determined and 55 mM NCT reduced growth to 6.84 ± 0.04% ($p < 0.0001$) and 3.44 mM NCT reduced growth to 28.37 ± 1.81% ($p < 0.0001$) compared to the control (98.74 ± 4.49%) (**Fig. 10.3**).

10.3 Effect of N-chlorotaurine on the growth *Aspergillus* mycelium

To assess the effect of NCT on mycelium biomass accumulation, 24 h preformed mycelium was supplemented with NCT (0.68 mM to 13.77 mM) for a further 24 h. A NCT concentration of 0.68 mM reduced mycelium biomass (0.75 ± 0.06 g/ (25 ml culture)$^{-1}$, $p < 0.01$) as compared to the control (1.03 ± 0.055 g/ (25 ml culture)$^{-1}$). A concentration of 6.8 (0.64 ± 0.04 g/ (25 ml culture)$^{-1}$, $p < 0.001$) and 13.77 mM (0.18 ± 0.009 g, $p < 0.0001$) resulted in a statistically significant decrease in mycelium wet weight compared to the control **(Fig. 10.4A)**. This decrease in mycelium biomass was also noted with *A. fumigatus* strains ATCC 46645 and Af293 and *A. flavus.* A concentration of 13.77 and 0.68 mM reduced mycelium biomass of *A. fumigatus* ATCC 46645 to 0.138 ± 0.004 g/ (25 ml culture)$^{-1}$, ($p < 0.05$) and 0.637 ± 0.03 g/ (25 ml culture)$^{-1}$, ($p < 0.0001$) respectively as compared to the control (0.741 ± 0.008 g/ (25 ml culture)$^{-1}$) (**Fig. 10.4B**). NCT (13.77 mM) significantly reduced the biomass accumulation of *A. fumigatus* Af293 to 0.319 ± 0.05 g/ (25 ml culture)$^{-1}$, ($p < 0.01$) as compared to the relevant control (0.682 ± 0.03 g g/ (25 ml culture)$^{-1}$) **(Fig. 10.4C**). Furthermore, NCT also reduced the mycelium wet weight of *A. flavus* at 13 mM (0.531 ± 0.03 g/ (25 ml culture)$^{-1}$, $p < 0.01$) and 6.8 mM (0.656 ± 0.01 g/ (25 ml culture)$^{-1}$, $p < 0.01$) as compared to control mycelium (0.857 ± 0.003 g/ (25 ml culture)$^{-1}$) (**Fig. 10.5)**.

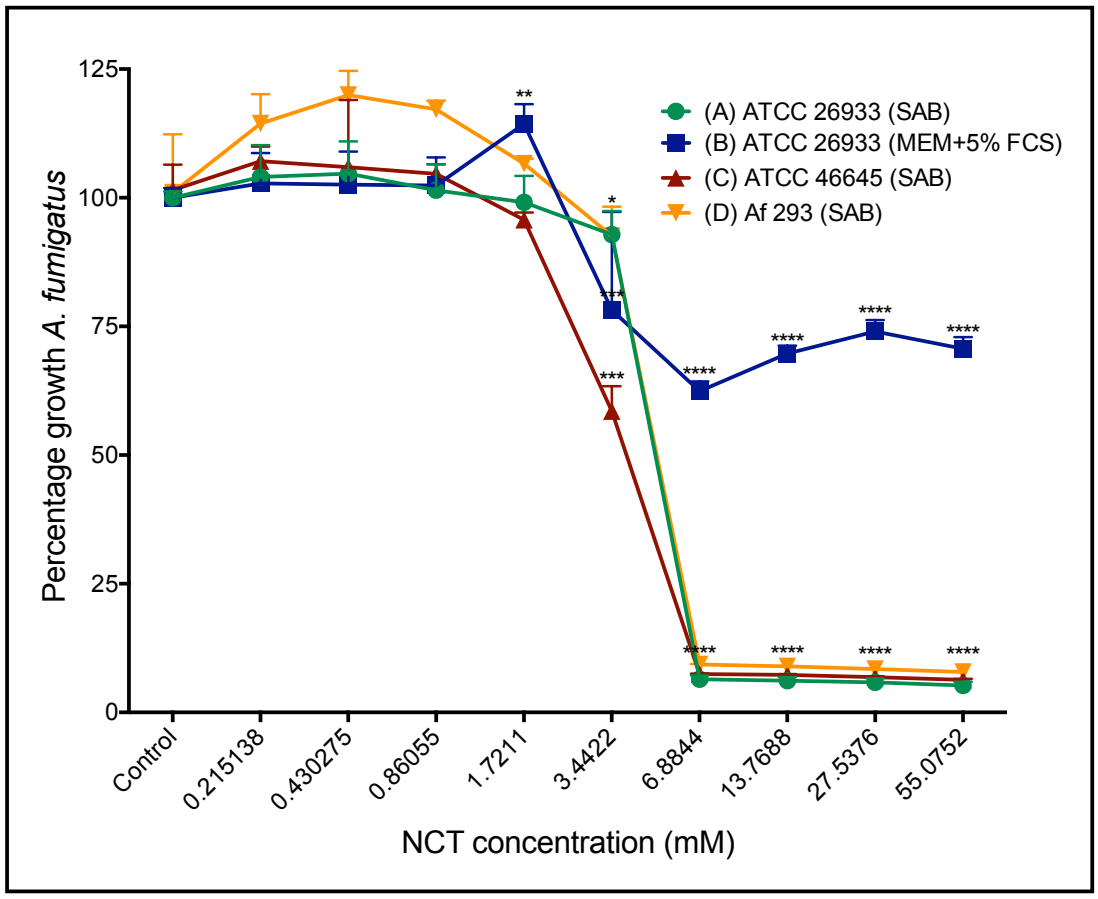

Fig. 10.2. Effect of N-chlorotaurine on the growth of *A. fumigatus* strains. Susceptibility of *A. fumigatus* (ATCC 26933 in sabouraud medium (SAB) [**A**; green], ATCC 26933 in minimal essential medium (MEM) supplemented with 5% v/v fetal calf serum (FCS) [**B**; blue], ATCC 46645 in SAB [**C**; red], Af 293 [**D**; yellow]) conidia (initial concentration 10^4/well^{-1}) to N-chlorotaurine at concentrations ranging from 0.21 mM to 55 mM after 48 h growth in SAB or MEM supplemented with 5% v/v FCS as determined by photometric analysis (absorption at OD_{575}). N-chlorotaurine significantly reduced the growth of *A. fumigatus* at concentrations between 6.8 and 55 mM as compared to the control (**: $p < 0.01$, **: $p < 0.001$, ****: $p < 0.0001$).

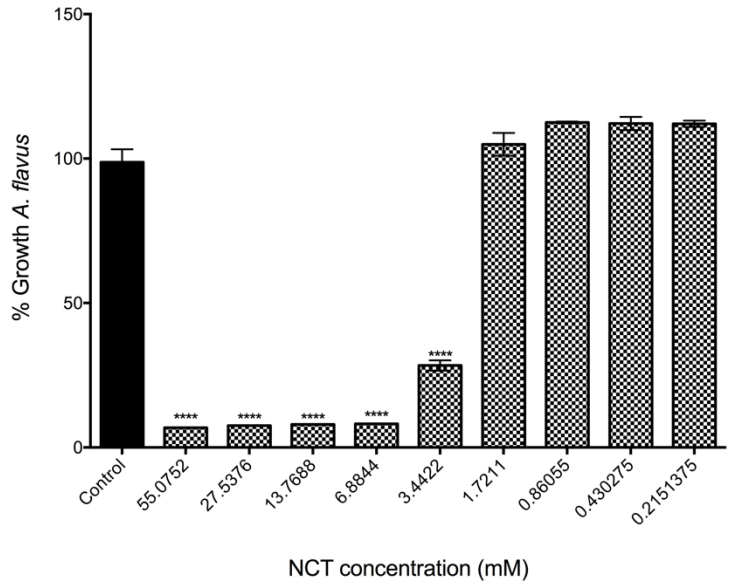

Fig. 10.3. Effect of N-chlorotaurine on the growth of *A. flavus*. Susceptibility of *A. flavus* conidia (initial concentration 10^4/well^{-1}) to N-chlorotaurine at concentrations ranging from 55 mM to 0.21 mM after 48 h growth in SAB medium as determined by photometric analysis. N-chlorotaurine reduced the growth of *A. flavus* at ranging between 55 and 3.44 mM as compared to the control (****, $p < 0.0001$).

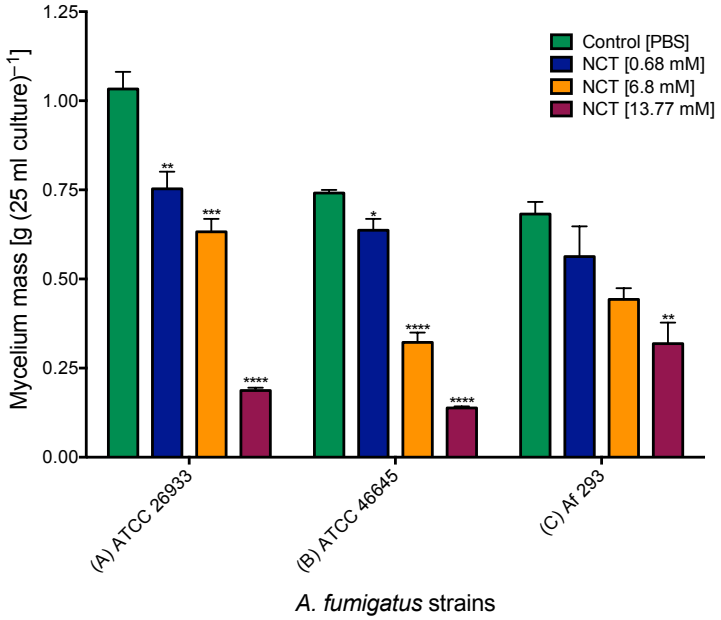

Fig. 10.4. The effect of N-chlorotaurine on growth of *A. fumigatus* strains ATCC 26933 (A), ATCC 46645 (B) and *Af* 293 (C). A 24 h culture of *A. fumigatus (*10^5 ml^{-1}) in sabouraud dextrose broth was supplemented with N-chlorotaurine (0.68, 6.8 and 13.77 mM) or PBS (control). After 24h, mycelia were weighed. N-chlorotaurine dose dependently decreased hyphal mass significantly after 24 h exposure (**: $p < 0.01$, ***: $p < 0.001$, ****: $p < 0.0001$).

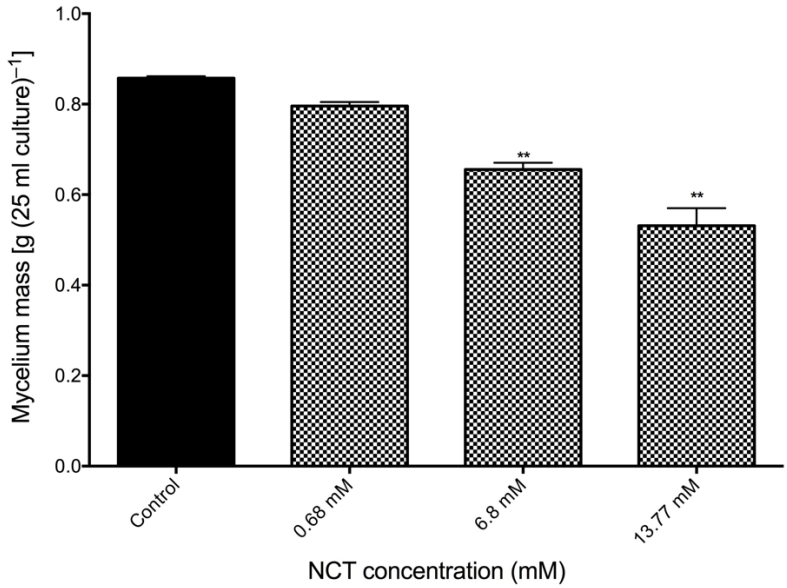

Fig. 10.5. The effect of N-chlorotaurine on growth of *A. flavus*. A 72 h culture of *A. flavus (*10^5 ml^{-1}) in sabouraud dextrose broth was supplemented with N-chlorotaurine (0.68, 6.8 and 13.77 mM) or PBS (control). After 24h, mycelia were weighed. N-chlorotaurine dose dependently decreased hyphal mass significantly after 24 h exposure (**: $p < 0.01$).

10.4 Effects of N-chlorotaurine on the growth and viability of *A. fumigatus*

Incubation of *A. fumigatus* (ATCC 26933) conidia in NCT for 1, 4 and 24 h at concentrations ranging from 6.8 to 68 mM decreased the viability of conidia in a dose and time dependent manner. Incubation of conidia in PBS supplemented with 68 mM NCT reduced viability at 1 (28.73 ± 7.78%, $p < 0.05$), 4 (0 ± 0.0007%, $p < 0.05$) and 24 (0% ± 0.0034%, $p < 0.05$) h and incubation in 6.8 mM NCT reduced viability at 1 (78.4 ± 2.89%), 4 (54.67 ± 3.46%, $p < 0.05$) and 24 (15.78 ± 2.32%, $p < 0.05$) h **(Fig. 10.6)**. Because of rapid inactivation of NCT after the dilution on the plates within 3 min (Lackner *et al.*, 2015), no inactivation substance was necessary after the long incubation times used in this experiment.

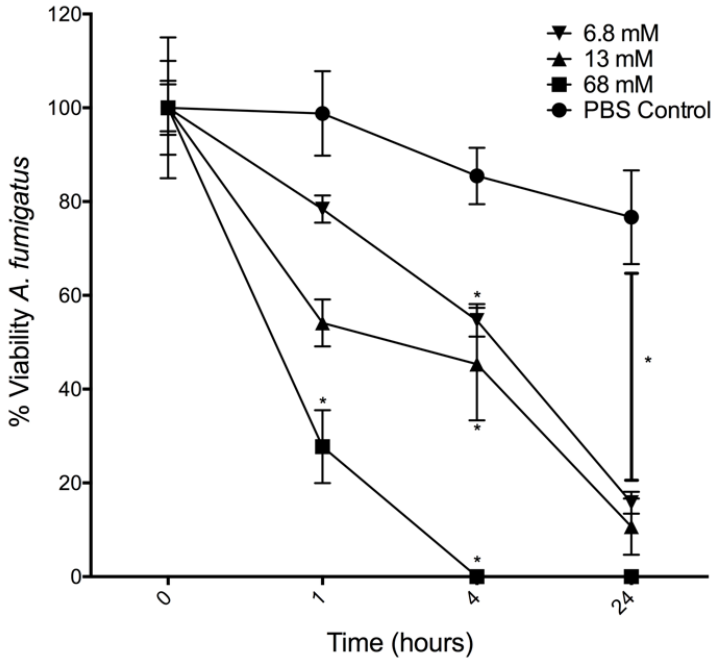

Fig. 10.6. The effect of N-chlorotaurine on the viability of *A. fumigatus* conidia. The viability of *A. fumigatus* ATCC 26933 conidia (initial concentration; 5×10^7 ml^{-1}) after incubation in varying concentrations of N-chlorotaurine (6.8, 13, 68 mM [PBS]) and PBS (control) for 0, 1, 4, 24 h. Cells were removed, diluted, plated at each time point and % viability calculated relative to the PBS 0 h control. N-chlorotaurine statically significantly and dose dependently reduced the viability of *A. fumigatus* conidia at a variety of concentrations over time as compared to the control (*: $p < 0.05$).

10.5 N-chlorotaurine induces alterations in extracellular amino acid levels from *A. fumigatus*

To assess the effect of NCT on membrane permeability, the leakage of extracellular amino acids following treatment with varying concentrations of NCT (0.68 – 13.77 mM) were determined via the ninhydrin colorimetric assay. NCT (13.7 mM) significantly increased amino acid leakage (8.82 ± 1.72 µg mg mycelium^{-1}, $p < 0.0001$) as compared to the control (0.24 ± 0.01 µg mg mycelium^{-1}) **(Fig. 10.7)**.

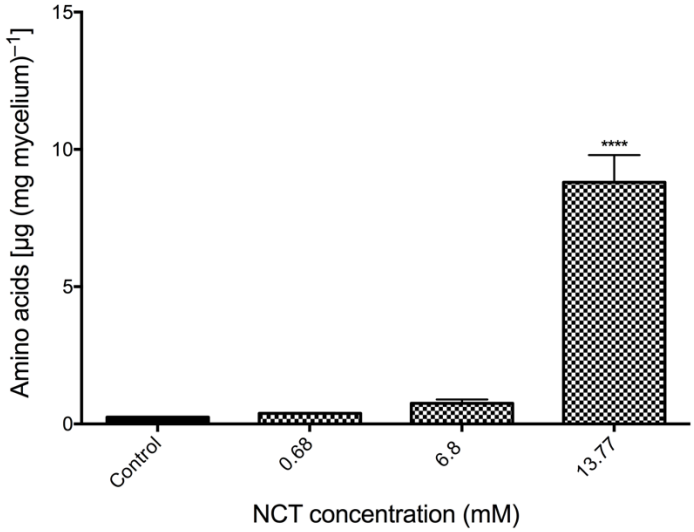

Fig. 10.7. Amino acid leakage from *A. fumigatus* mycelium. Amino acid quantification in *A. fumigatus* ATCC 26933 supernatants exposed to N-chlorotaurine (0.68, 6.8 and 13.77 mM) or PBS (control) for 24 h was determined by ninhydrin colorimetric assay. N-chlorotaurine (13.77 mM) significantly increased extracellular amino acid leakage as compared to the control (****: $p < 0.0001$).

10.6 N-chlorotaurine induces alterations in gliotoxin levels from *A. fumigatus*

A. fumigatus (ATCC 26933) mycelium treated with 6.8 mM NCT (25.67 ± 0.43 ng (mg mycelium)$^{-1}$, $p < 0.0001$) and 0.68 mM (38.38 ± 1.55 ng (mg mycelium)$^{-1}$ $p < 0.001$) NCT for 24 h displayed significantly less extracellular gliotoxin as compared to control mycelium (64.15 ± 3.34 ng (mg mycelium)$^{-1}$). However, exposure to 13.77 mM NCT resulted in a statistically significant increase in extracellular gliotoxin (88.19 ± 1.98 ng (mg mycelium)$^{-1}$, $p < 0.001$) **(Fig. 10.8)**.

Furthermore, NCT (0.68 and 6.8 mM) also reduced extracellular gliotoxin levels in *A. fumigatus* (ATCC 46645) supernatants to 9.70 ± 8.19 ng (mg mycelium)$^{-1}$, ($p < 0.01$) and 18.56 ± 11.78 ng (mg mycelium)$^{-1}$, ($p < 0.05$) respectively, as compared to the control mycelium (77.78 ± 12.35 ng (mg mycelium)$^{-1}$) (**Fig. 10.9**). This effect was observed with *A. fumigatus* (Af293) with the same concentrations of NCT reducing extracellular gliotoxin levels to 2.64 ± 1.49 ng (mg mycelium)$^{-1}$ and 13.81 ± 4.13 ng (mg mycelium)$^{-1}$, respectively as compared to the control (65.87 ± 13.79 ng (mg mycelium)$^{-1}$, $p < 0.05$) (**Fig. 10.10**). For intracellular gliotoxin quantification a similar effect was observed. Treatment of *A. fumigatus* mycelium with 13.77 mM NCT resulted in a significant increase in intracellular gliotoxin (9.42 ± 1.50 ng (mg mycelium)$^{-1}$, $p < 0.01$) relative to control mycelium (2.39 ± 1.18 ng (mg mycelium)$^{-1}$). Interesting, no gliotoxin was detected within mycelium treated with 6.8 mM (**Fig. 10.8)**.

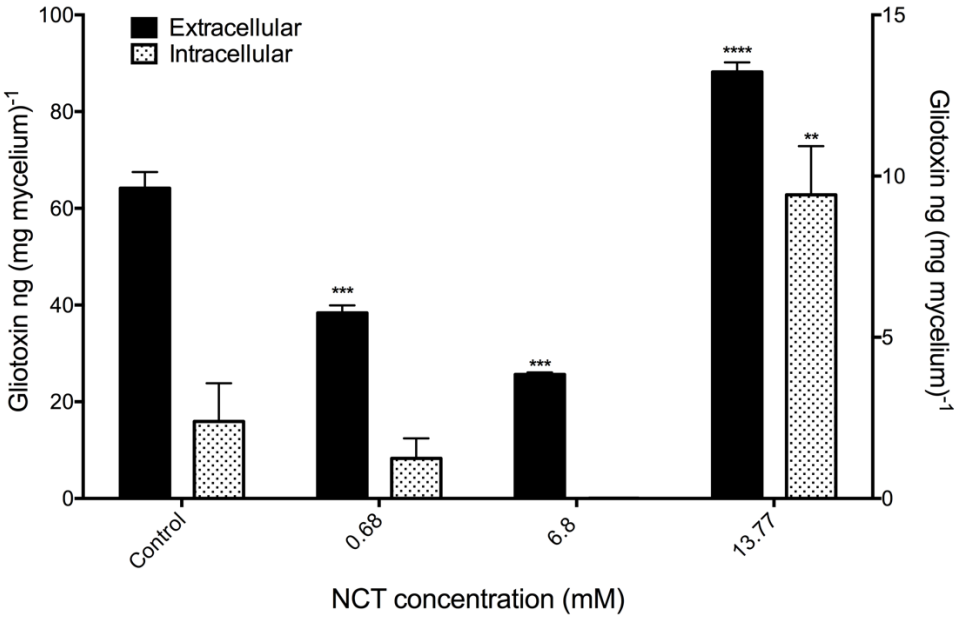

Fig. 10.8. Effect of N-chlorotaurine on gliotoxin (intracellular and extracellular) from *A. fumigatus* mycelium. Gliotoxin quantification (extracellular; closed bars and left Y-axis, intracellular; open bars and right Y-axis) in *A. fumigatus* ATCC 26933 exposed to N-chlorotaurine (0.68, 6.8 and 13.77 mM) or PBS (control) for 24 h was determined by RP-HPLC. N-chlorotaurine decreased gliotoxin levels at a concentration of 0.68 and 6.8 mM. However, N-chlorotaurine (13.77 mM) significantly increased both extracellular and intracellular gliotoxin levels as compared to the respective controls (**: $p < 0.01$, ***: $p < 0.001$, ****: $p < 0.0001$).

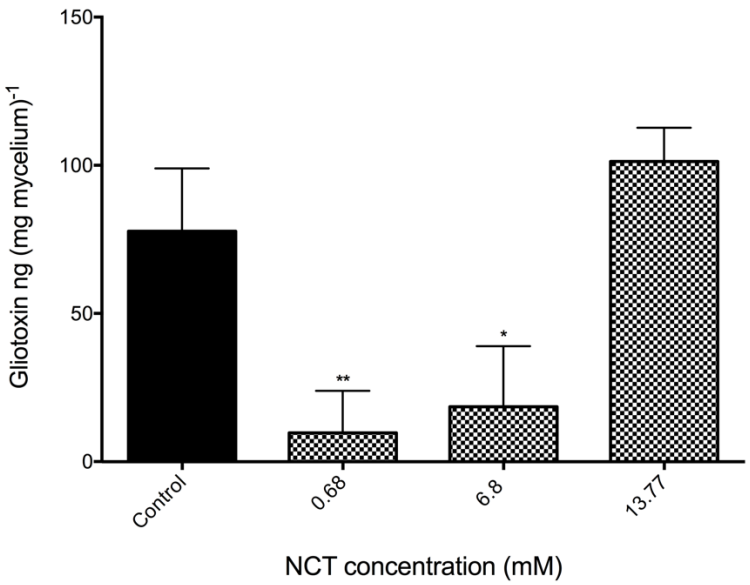

Fig. 10.9. Effect of N-chlorotaurine on extracellular gliotoxin from *A. fumigatus* (ATCC46645) mycelium. Gliotoxin quantification in *A. fumigatus (*ATCC46645) supernatants exposed to N-chlorotaurine (0.68, 6.8 and 13.77 mM) or PBS (control) for 24 h was determined by RP-HPLC. N-chlorotaurine decreased gliotoxin levels at a concentration of 0.68 and 6.8 mM. However, N-chlorotaurine (13.77 mM) significantly increased extracellular gliotoxin levels (*: $p < 0.05$, **: $p < 0.01$).

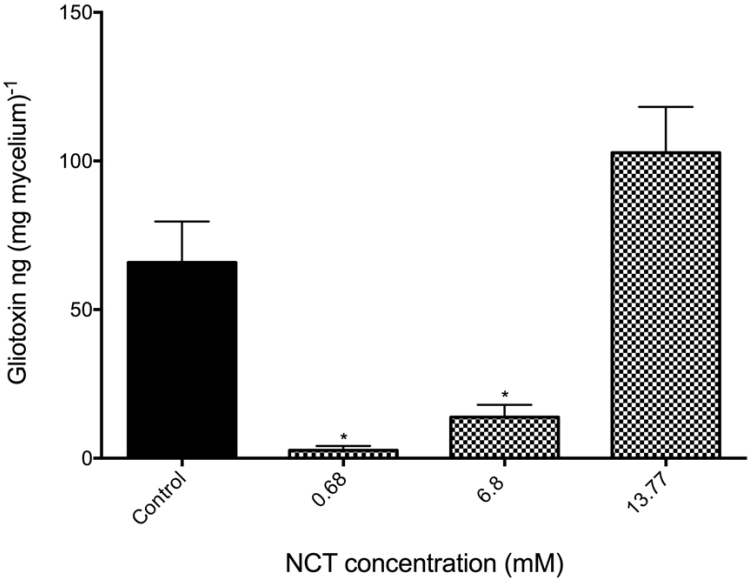

Fig. 10.10. Effect of N-chlorotaurine on extracellular gliotoxin from *A. fumigatus* mycelium. Gliotoxin quantification in *A. fumigatus (*Af293) supernatants exposed to N-chlorotaurine (0.68, 6.8 and 13.77 mM) or PBS (control) for 24 h was determined by RP-HPLC. N-chlorotaurine decreased gliotoxin levels at a concentration of 0.68 and 6.8 mM (*: $p < 0.05$).

10.7 The whole cell proteomic response of *A. fumigatus* to N-chlorotaurine

Shotgun quantitative proteomic analysis was performed on *A. fumigatus* (ATCC 26933) treated with 6.8 mM NCT for 24 h as described. In total, 30538 peptides were identified representing 1932 proteins with two or more peptides and 210 (*A. fumigatus* NCT- treated versus control *A. fumigatus*) proteins were determined to be differentially abundant (ANOVA, $p < 0.05$) with a fold change of > 1.5. A total of 44 proteins were deemed exclusive (i.e. with LFQ intensities present in all 3 replicates of one treatment and absent in all 3 replicates of the other treatment). These proteins were also used in statistical analysis of the total differentially expressed group following imputation of the zero values as described. After data imputation, these proteins were included in subsequent statistical analysis**.** A principal component analysis (PCA) performed on all filtered proteins distinguished the NCT-treated *A. fumigatus* and control *A. fumigatus* samples indicating a clear difference between each proteome (**Fig. 10.11)**.

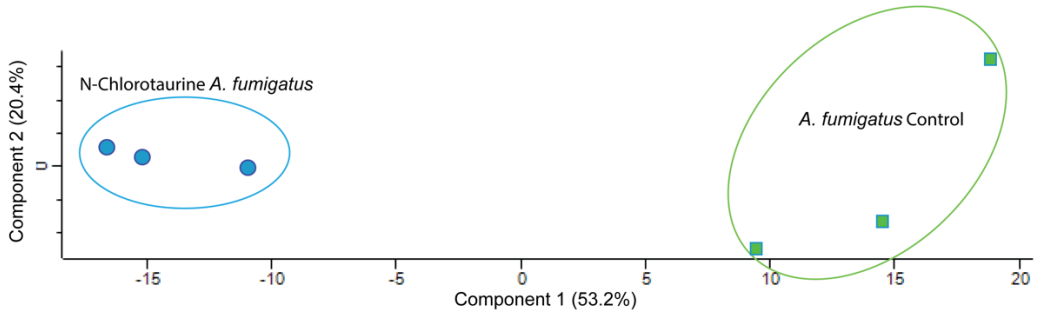

Fig. 10.11. Shotgun quantitative proteomic analysis of N-chlorotaurine (6.8 mM) treated *A. fumigatus* (ATCC 26933). Principal component analysis (PCA) of control and N-chlorotaurine treated *A. fumigatus* for 24 h with a clear distinction between control and treatment

Functional (GO term and FunCat) analysis revealed enrichment for biological processes such as oxidation-reduction process, proteolysis and translation, while molecular functions such as nucleotide binding and oxidoreductase activity were significantly enriched within the SSDA dataset (**Fig. 10.12 A**). FunCat categories associated with electron transport, nitrogen, sulfur and selenium metabolism, catabolism of nitrogenous compounds and sulfate assimilation confirm *A. fumigatus* mycelium responds to NCT by activation of a variety of processes (**Fig. 10.12 B**).

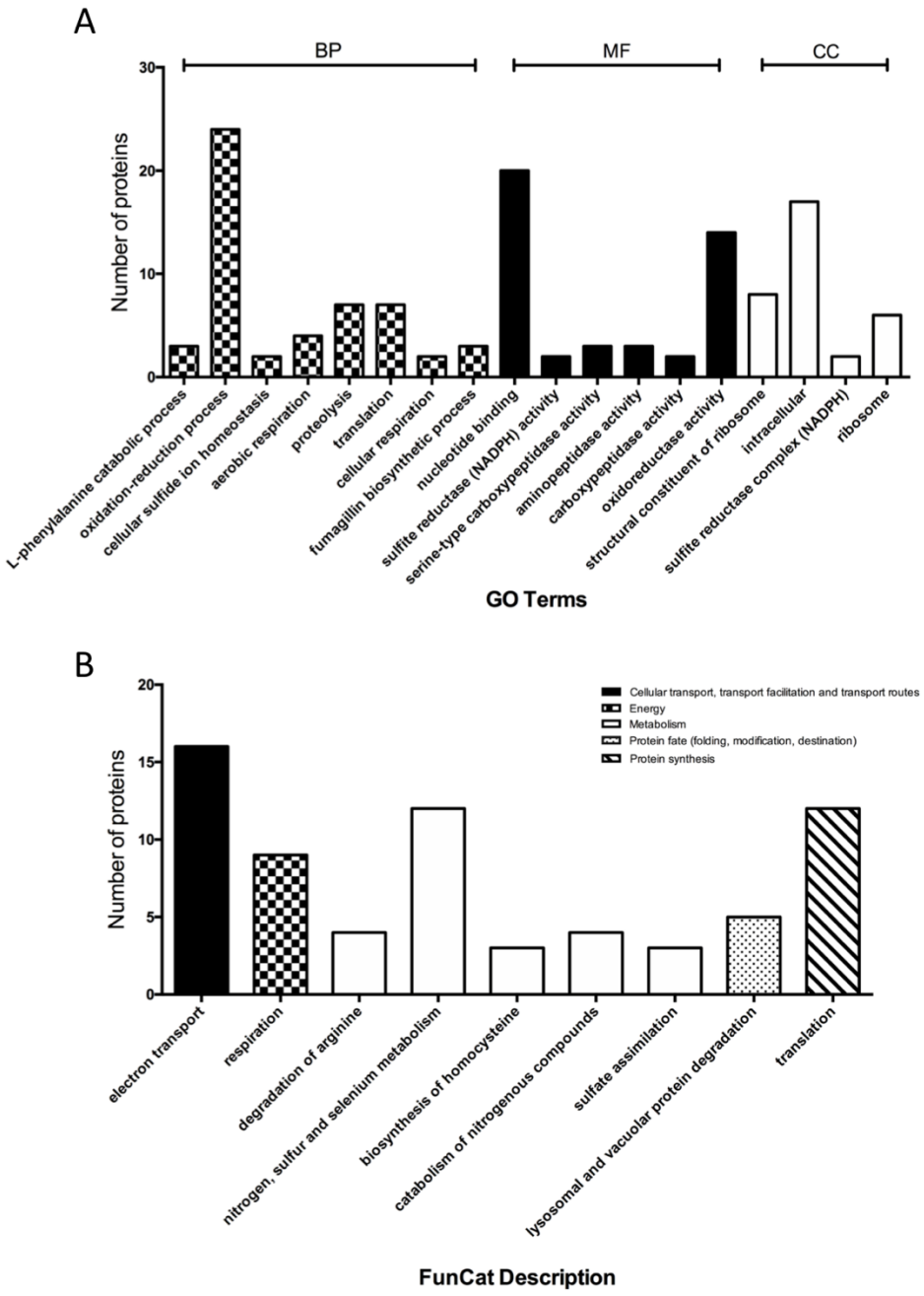

Fig. 10.12. Enrichment analysis for proteins detected in *A. fumigatus* treated with N-chlorotaurine. Proteins which were classified as statistically significant and differentially abundance were assigned functional annotation (Gene Ontology (GO), (**A**); (Biological process [BP], molecular function [MF] & cellular component [CP]), and FunCat categories [**B**]) utilising the FungiFun application.

Proteins that were increased in abundance in NCT treated mycelium were ribosomal proteins (ribosomal protein S28e [+23.1 fold], ribosomal biogenesis protein gar2 [+5.5 fold], ribosome assembly factor mrt4 [+5.1 fold], 40S ribosomal protein S26 [+2.2 fold], 60S ribosomal protein L35Ae [+1.7 fold], 60S ribosomal protein L12 [+1.6 fold], ribosomal protein L16a [+1.6 fold], 60S ribosomal protein L5 [1.5 fold], 60S ribosomal protein L27 [+1.5 fold]) and transcription and translation associated proteins (small nucleolar ribonucleoprotein complex subunit [+4.6 fold], rRNA processing protein pwp1 [+3 fold], mRNA splicing factor (prp17) [+2.9 fold], RNA cytidine acetyltransferase [+2.3 fold], ATP-dependent RNA helicase has1 [+2.2 fold], eEF-3 [+1.9 fold], eEF-1B [+1.8 fold], pre-mRNA-splicing factor [+1.7 fold], rRNA biogenesis protein RRP5 [+1.6 fold]) (**Fig. 10.13)**.

There was also increased abundance of proteins associated with cell response to stress/drug (oxidoreductase, zinc-binding dehydrogenase family protein [+11 fold], superoxide dismutase [Cu-Zn];[+7.7 fold], hsp30-like [+5.6 fold], hsp30/hsp42 [+2.4 fold], nitroreductase family protein [+2.2 fold], glutathione S-transferase GstA [+1.7 fold], ecm33 protein [+1.6 fold], MFS multidrug transporter [+1.5 fold]), mitochondrion associated proteins (cytochrome c oxidase subunit VIa [+12.4 fold], cytochrome c oxidase subunit 2 [+1.7 fold], cytochrome P450 phenylacetate 2-hydroxylase, putative [+1.5 fold]) and secondary metabolite biosynthetic proteins (non-ribosomal peptide synthetase 8, non-ribosomal peptide synthetase 1, NRPS-like enzyme, fumipyrrole biosynthesis protein C) (**Table A10.1)**.

Proteins that were decreased in abundance in response to NCT were associated with sterol biosynthesis (14-α sterol demethylase Cyp51A [-1.5 fold]) and secondary metabolism (NRPS-like enzyme, putative [-7.3 fold], fumagillin dodecapentaenoate synthase [-6.5 fold], fumagillin biosynthesis methyltransferase [5.2 fold], fumagillin biosynthesis acyltransferase [-5 fold], pseurotin biosynthesis protein C [4.3 fold], NRP synthetase 14 [3.9 fold], fumagillin biosynthesis cluster P450 monooxygenase [-3.6 fold], pseurotin biosynthesis protein F [-3.0 fold]) (**Table A10.1).**

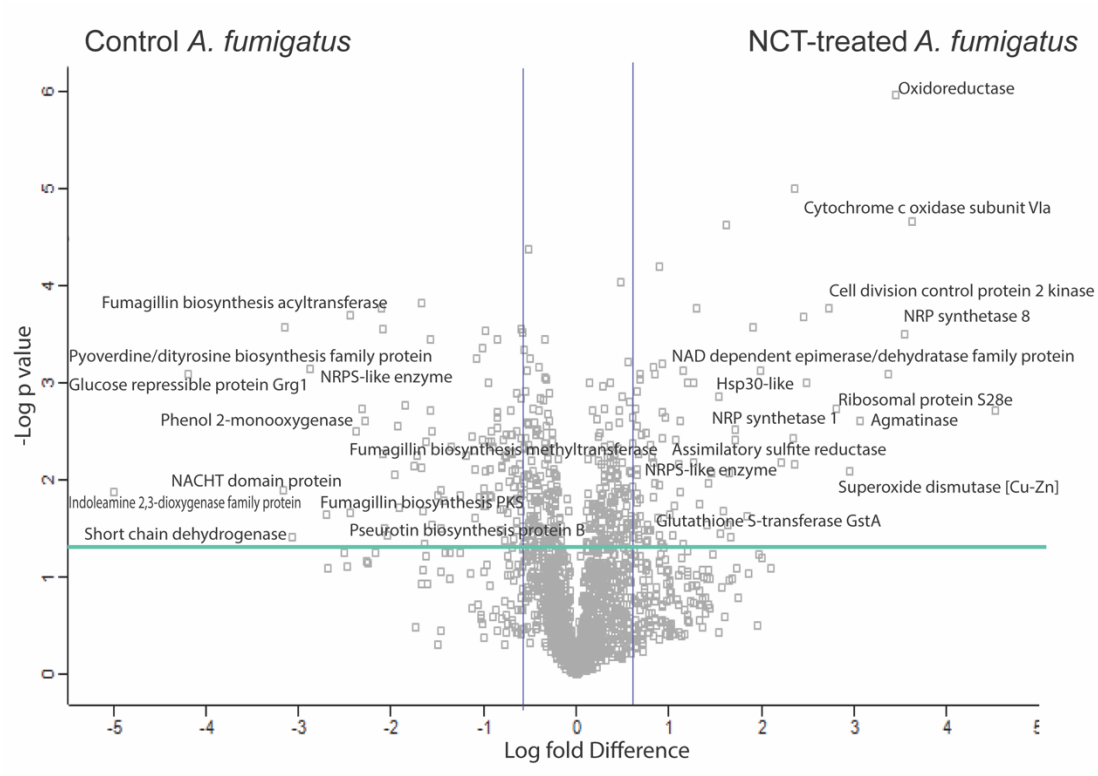

Fig. 10.13. Shotgun proteomics of 24 h preformed *A. fumigatus* ATCC 26933 mycelium exposed to N-chlorotaurine (6.8 mM) for 24 h. Volcano plots showing the distribution of quantified proteins according to p value (−log10 p-value) and fold change (log2 mean LFQ intensity difference). Proteins above the horizontal line are considered statistically significant (p value < 0.05) and those to the right and left of the vertical lines indicate relative fold changes > ±1.5 fold. N-chlorotaurine increased the abundance of proteins associated with cellular response to drug, ribosomal biogenesis and secondary metabolism.

10.8 Effect of combination N-chlorotaurine and Azole treatment on *A. fumigatus*

From the proteomic data NCT induced a decrease in the abundance of the 14-α sterol demethylase Cyp51A (Erg11) by -1.5 fold relative to control treated *A. fumigatus*. Erg11 catalyses the demethylation of lanosterol which is critical for ergosterol biosynthesis in fungi. This protein is the target for the azole family (e.g. fluconazole, itraconazole, voriconazole) of antifungal drugs. As NCT induced decreased expression of erg11 it was hypothesised that NCT and itraconazole may work in synergy in blocking the growth of *A. fumigatus.*

A non-inhibitory dose of NCT (0.68 mM) (1.04 ± 0.08 g [50 ml culture]$^{-1}$) did not significantly reduce the biomass of *A. fumigatus* mycelium relative to control treated cells (1.13 ± 0.02 g [50 ml culture]$^{-1}$). However, a concentration of 5 μg ml^{-1} itraconazole (0.63 ± 0.08 g [50 ml culture]$^{-1}$, $p < 0.001$) significantly reduced the growth of *A. fumigatus* mycelium relative to control treated cells. Most interestingly, when itraconazole was supplemented with the non-inhibitory dose of NCT this resulted in a significantly decrease in mycelium wet weight (0.41 ± 0.01 g [50 ml culture]$^{-1}$, $p < 0.05$) relative to the itraconazole treated cells alone and compared to control treated cells ($p < 0.0001$) (**Fig. 10.14**).

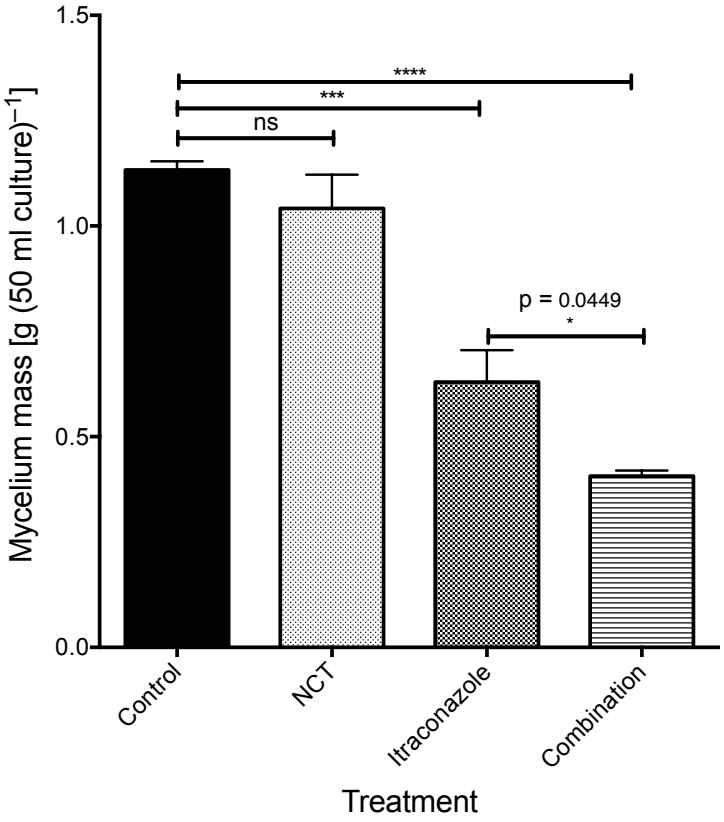

Fig. 10.14. Synergistic activity between N-chlorotaurine and itraconazole in reducing *A. fumigatus* mycelium biomass. Twenty four h pre-formed *A. fumigatus* mycelium ((culture medium; SAB (50 ml), initial inoculum 1×10^5 ml^{-1}) was incubated in PBS alone (control & itraconazole) or PBS supplemented with NCT (0.68 mM) for 4 h, washed in PBS (three times) and returned to their original culture medium (SAB) either supplemented with 2 ml DMSO ((final concentration; 4% v/v), (control & NCT treatment)) or DMSO with the addition of itraconazole (final concentration; 5 μg ml^{-1} in SAB [4% v/v DMSO]) and incubated for 20 h. Mycelium biomass was recorded after a total of 48 h growth (ns: no significance, *: $p < 0.05$, ***: $p < 0.001$, ****: $p < 0.0001$).

10.9 Toxicity of N-chlorotaurine in *G. mellonella* larvae

Intra-hemocoel inoculation of *G. mellonella* larvae with concentrations of NCT ranging from 0.68 to 13.77 mM were non-toxic and resulted in no decrease in viability relative to the PBS injected control. However, NCT at 68.84 mM decreased larval viability to 90 ± 2.88% at 24 h and 70 ± 5.77% at 48 and 72 h (**Fig. 9.15**).

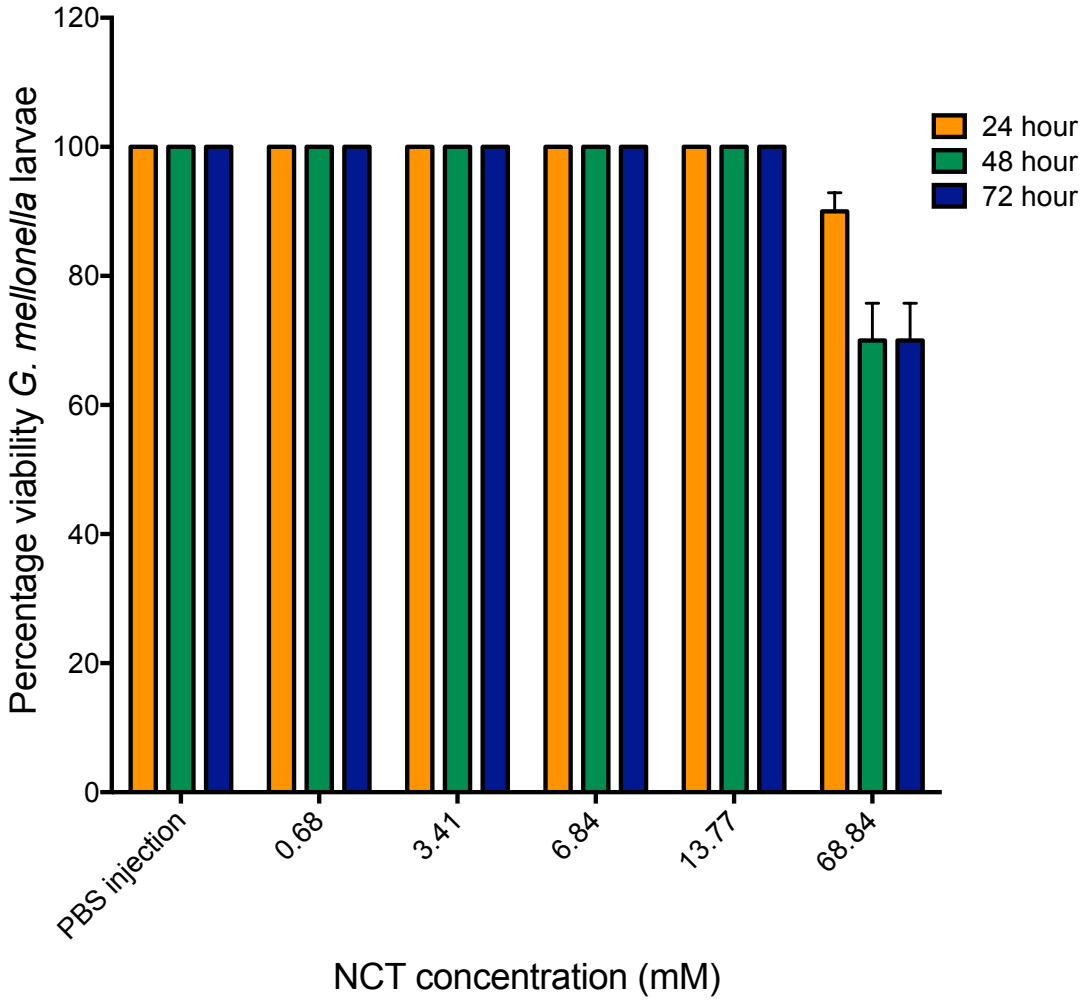

Fig. 10.15. Viability of *G. mellonella* larvae following injection with varying concentrations of N-chlorotaurine. *G. mellonella* larvae were injected with 20 µl of PBS or NCT at varying concentrations and viability assessed over 72 h.

10.10 Post-antibiotic effect of N-chlorotaurine on *A. fumigatus*

Post-antibiotic effect is the lag regrowth of a microbe following exposure to an antimicrobial agent for a short amount of time. This effect has been well documented with NCT in *S. aureus* and *C. albicans* (Nagl *et al*., 1999, 2002). The *in vivo* post antibiotic effect of NCT on *A. fumigatus* was determined using *G. mellonella* larvae.

Inoculation of larvae with PBS resulted in no decrease in larval survival over 108 h. Infection with *A. fumigatus* (un-incubated) reduced viability of larvae over 24 (96.67 ± 3.33%), 48 (86.66 ± 3.33%) and 72 (13.33 ± 3.33%) h. Incubation of *A. fumigatus* in NCT for 1 h over a range of concentrations (6.8, 13 and 68 mM) had no positive or negative effect on the survival of *G. mellonella* larvae relative to the PBS control. Incubation of *A. fumigatus* in NCT for 4 h did result in enhanced survival of larvae for 6.8 (73.33 ± 3.33, $p < 0.05$), 13 (83.33 ± 3.33, $p < 0.05$), 68 (98.33 ± 1.67, $p < 0.0001$) mM at 72 h post infection but not at any other time point. Incubation of conidia in NCT for 24 h was most effective where NCT at 68 mM resulted in increased survival of larvae at 72 (100 ± 0%, $p < 0.01$), 96 (98.33 ± 2.88%, $p < 0.01$) and 108 (96.66 ± 5.77%, $p < 0.01$) h post infection relative to the PBS incubated conidia, respectively (**Fig. 10.16**).

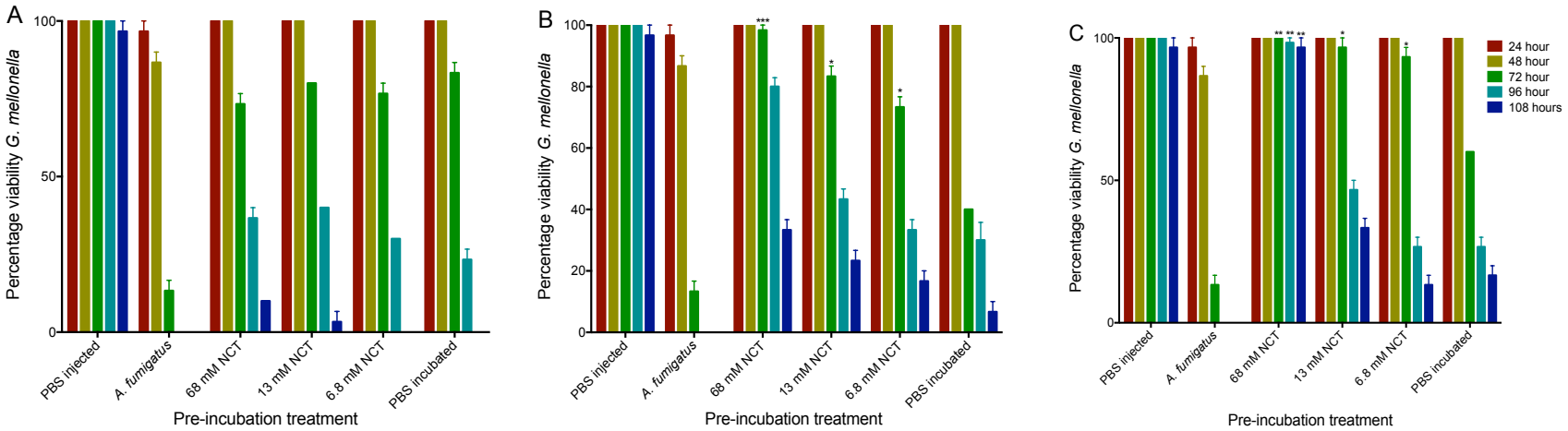

Fig. 10.16. The post-antibiotic effect of N-chlorotaurine on *A. fumigatus*. *A. fumigatus* conidia (5×10^7 ml^{-1}) were incubated in varying concentrations (6.8, 13, 68 mM) of N-chlorotaurine for 1 (**A**), 4 (**B**) and 24 (**C**) h. Cells were washed (twice) and re-suspended in PBS and injected into *G. mellonella* larvae (inoculum; 1×10^6 20 μl^{-1}) and viability assessed over 108 h. Statistical significance was determined by comparing NCT incubated *A. fumigatus* to the PBS incubated control (*: $p < 0.05$, **: $p < 0.01$, ***: $p < 0.001$).

10.11 Discussion

In recent years it has become evident that environmental use of triazoles has selected for multi-azole and pan-azole resistant *A. fumigatus* isolates (Snelders *et al.*, 2009). Mutations in the Cyp51A gene or its transcriptional enhancer in the promoter region is a common mechanism (50 to 80%) related to altered or enhanced production of erg11 (Fraczek *et al.,* 2011; Lazzarini *et al.*, 2016). *In vitro* data, animal models, and some clinical data demonstrate that there may be a benefit of combination anti-fungal therapy in treating *Aspergillus* infections (Johnson and Perfect, 2010). N-chlorotaurine (NCT) shows broad spectrum antimicrobial activity, excellent tolerability *in vivo* and may be a potential anti-fungal therapy for superficial infections (Gottardi and Nagl, 2010; Gottardi *et al.,* 2013; Nagl *et al.*, 2018).

NCT significantly decreased the growth of *A. fumigatus* (ATCC 26933, ATCC 46645, Af293) conidia in an *in vitro* susceptibility assay at concentrations ranging from 6.8 to 55 mM in sabouraud medium and MEM supplemented with 5% v/v FCS as compared to the relevant controls. The lower effect of NCT on growth in MEM can be explained by reaction of NCT with reducing components of the FCS, which is connected with a loss of oxidative activity (chlorine consumption, (Gottardi and Nagl, 2013; Gottardi *et al.,* 2013)). NCT reduced the biomass formation of *A. fumigatus* (ATCC 26933, ATCC 46645, Af293) mycelium after 24 h at concentrations between 0.68 mM and 13.77 mM. Incubation of *A. fumigatus* conidia in NCT decreased their viability at 1, 4 and 24 h. The results are in agreement with the fungicidal activity of NCT against yeasts and moulds found in previous studies (Nagl *et al.*, 2001, 2002; Reeves *et al.*, 2006; Lackner *et al.*, 2015; Nagl *et al.,* 2018).

Within 1 min, NCT forms covalent chlorine covers (chlorination of the external protein matrix of the microbe) around *S. aureus, E. coli*, *P. aeruginosa* and *C. albicans* (Marcinkiewicz *et al.*, 1994; Gottardi and Nagl, 2005), which is associated with a loss of virulence (Nagl *et al.,* 1999, 2002; Lackner *et al.,* 2015). Longer incubation leads to cellular leakage and inactivation of pathogens (Gottardi and Nagl, 2005).

In this work, incubation of 24 h pre-formed mycelium in NCT (13.77 mM) significantly increased extracellular amino acid release indicating small molecule leakage from mycelium, which would damage the cell's ability to respire, grow and activate an oxidative stress response. Amino acid leakage is also observed with a variety of antimicrobials (Johnston *et al.*, 2003; Reeves *et al.*, 2004b; Thati *et al.*, 2007; Kelly and Kavanagh, 2010). Interestingly, incubation of mycelium in 0.68 and 6.8 mM NCT decreased extracellular gliotoxin levels amongst *A. fumigatus* strains. This was observed previously where NCT diminished the activity of gliotoxin by reduction of the disulphide bridge which is essential to its activity (Reeves *et al.*, 2006). However, our results indicate that these NCT treatments also reduced intracellular gliotoxin. Furthermore, NCT leads to decreased production of secreted aspartyl proteinases from *Candida* spp. (Nagl *et al.*, 2002). Conversely, incubation of mycelium in the higher concentration of 13.77 mM NCT resulted in a significant increase in intracellular and extracellular gliotoxin concentration. At this concentration, reduced growth and increased gliotoxin production and secretion from *A. fumigatus* was observed. Therefore, it was hypothesised that gliotoxin was liberated by active and/or passive mechanisms, through the damaged cell and that this effect overlays the reduced production of the toxin at low concentrations. Treatment of *A. fumigatus* with caspofungin and amphotericin resulted in a significant increase in intracellular and extracellular gliotoxin as a result of halted growth, which was observed in mycelium treated with 13.77 mM NCT (Reeves *et al.*, 2004b; Eshwika *et al.*, 2013).

Shotgun proteomics was employed to determine the effect of NCT (6.8 mM) on *A. fumigatus* (ATCC 26933) after 24 h exposure. *A. fumigatus* responds to NCT by increasing the abundance of ribosomal proteins and proteins associated with transcription and translation. Shenton *et al.* (2006) found that a hydrogen peroxide treatment increased the number of ribosomal proteins which may be utilised once the response to oxidative stress has subsided for transcriptional and translational remodelling (Shenton *et al.*, 2006).

There was also an increase in the abundance of proteins associated with cellular response to stress (e.g. oxidoreductase, superoxide dismutase [Cu-Zn], hsp30-like, hsp30/hsp42, nitroreductase family protein, glutathione s-transferase

GstA**,** MFS multidrug transporter). *A. fumigatus* responds to NCT by an increase in superoxide dismutase which detoxifies superoxide anions, glutathione s-transferase which quenches reactive hydroxyl free radicals, a range of heat shock proteins and nitroreductase family protein. This may be an attempt by the fungus to neutralise active chlorine compounds it would encounter within the phagosome.

NCT exposure lead to an increase in the abundance of some secondary metabolism proteins which play a role in the response to oxidative stress (e.g. non-ribosomal peptide synthetase 1 [Pes1], non-ribosomal peptide synthetase 8 [Pes3]). Pes1 confers protection against oxidative stress as the Δ*pes*1 mutant showed attenuated virulence in *G. mellonella*, increased sensitivity to neutrophil phagocytosis, which was mediated by altered conidial surface morphology and increased hydrophilicity (Reeves *et al.*, 2006). Paradoxically, *pes*3 disruption augments *A. fumigatus* virulence (in *G. mellonella*) and increased fungal burden (murine pulmonary aspergillosis model), possibly due to defective innate immune recognition of *A. fumigatus in vivo* (O'Hanlon *et al.*, 2011). Pes3 deletion, on the other hand, increased susceptibility to voriconazole, produced shorter germlings and decreased surface β-glucan.

Following NCT treatment, there was a significant decrease in the abundance of a range of proteins involved in fumagillin and pseurotin biosynthesis (NRPS-like enzyme, fumagillin dodecapentaenoate synthase, pseurotin biosynthesis protein B, fumagillin biosynthesis methyltransferase, fumagillin biosynthesis acyltransferase, pseurotin biosynthesis protein C, NRP synthetase 14, fumagillin biosynthesis cluster P450 monooxygenase, pseurotin biosynthesis protein F). Fumagillin is a toxin produced during hyphal development in *A. fumigatus*. The toxin has well characterised amoebicidal activity, can retard the ciliary beat frequency of pulmonary epithelial cells, and can inhibit angiogenesis and microbicidal activity of human neutrophils and insect hemocytes (McCowen *et al.,* 1951; Amitani *et al.*, 1995; Fallon *et al.,* 2010, 2011).

The results presented in this Chapter indicate that NCT reduces the expression of a number of virulence factors of *A. fumigatus* similar to *Candida spp.* (Nagl *et al.*, 2002), before the killing of the fungus occurs. This may be caused by several pathways. Direct chlorination and oxidation reactions leading to abrogation

of synthesis pathways are possible as well as consumption of most of the energy of the fungus by activation of anti-oxidative pathways. There was also a significant decrease in the azole target protein 14-α sterol demethylase (*erg*11, gene product of cyp51A) which is implicated amongst 50-80% of *A. fumigatus* resistant isolates.

The decreased abundance of 14-α sterol demethylase in response to NCT was investigated by supplementing a culture of *A. fumigatus* mycelium with NCT (0.68 mM; sub-inhibitory dose), itraconazole or NCT in addition to itraconazole. Itraconazole treatment alone resulted in decreased growth of mycelium but NCT with itraconazole resulted in a significant decrease in *A. fumigatus* mycelium relative to the itraconazole alone. This indicates that NCT may induce increased susceptibility to azole treatment and this may be important to treat superficial mycoses that may be resistant to azole therapy (Nagl *et al.,* 2018).

The *in vivo* toxicity of NCT was assessed using *G. mellonella* larvae. Only a dose of 68 mM resulted in decreased survival of larvae. Larvae are a good model to assess the toxicity inside the organism, however NCT is only indicated for superficial use. The post antibiotic effect of NCT on *A. fumigatus* was also assessed and tested *in vivo.* Incubation of *A. fumigatus* conidia in NCT for 4 and 24 h resulted in increased survival of larvae relative to conidia incubated in PBS at the same timepoints. This effect could be due to decreased virulence proteins as evident from the proteomic data and reported elsewhere (Nagl *et al.,* 1999, 2002).

The results presented in this Chapter demonstrate that NCT is active against *A. fumigatus* and reduces growth, biomass formation and conidial viability. Understanding the mode of action of NCT is a good basis for both further elucidating its role in the human defence system and its potential clinical application for treatment of drug resistant *A. fumigatus* infections.

Chapter 11

Discussion

11.1 General Discussion

Murine infection models are considered to be the gold standard due to their high similarity to humans in terms of metabolism, body temperature, and immune system functions (Brunke *et al.*, 2015). Infection models have also been developed in primates, rabbits, guinea pigs, rats, hamsters, birds and canines (Hohl, 2014). Working with mammalian infection models requires specialised personnel, poses many practical difficulties, is often expensive and time consuming, and involves specific legal and ethical considerations. For these reasons alternative *in vivo* infection models have been developed (Brunke *et al.*, 2015). For pathogenic fungi, for example, these include: the vertebrate zebrafish model (Chao *et al.*, 2010; Tobin *et al.*, 2012), the embryonated chicken egg model (Jacobsen *et al.*, 2010; Jacobsen *et al.*, 2011), the nematode *C. elegans* (Breger *et al*., 2007), the insects *G. mellonella* larvae (Cotter *et al.*, 2000; Jander *et al.*, 2000) and *D. melanogaster* (Alarco *et al.*, 2004; London *et al.*, 2006), and specialised models such as *Acanthamoeba* spp. or *Dictyostelium discoideum* (Mylonakis *et al.*, 2007; Steenbergen *et al.,* 2001). Many experimental *in vivo* systems to characterise bacterial (e.g. *S. aureus*) infection dynamics have been developed and include cutaneous (Bunce *et al.*, 1992), renal (Weiss *et al.*, 2004) sepsis in mice (Tarkowski *et al.*, 2001) and endocarditis in rats (Santoro and Levison, 1978). Alternative systems are also used and include models to study bloodstream infection and pathogenesis using zebrafish embryos (Prajsnar *et al.*, 2008), digestive tract infection in *C. elegans* (Sifri *et al.*, 2003), *D. melanogaster* (Dionne and Schneider, 2008) and *G. mellonella* larvae (Tsai *et al.*, 2016).

This project aimed to analyse the pathogenicity of fungi and bacteria by detailing the cellular and humoral immune response of *G. mellonella* larvae to disseminated disease and determine the proteomic responses of fungal pathogen *A. fumigatus* to antimicrobial effectors of the innate immune response. Larvae have been utilised to assess the virulence of a range of medically important pathogens, and to determine the toxicity and efficacy of a range of empirical and novel antimicrobial agents (Slater *et al.*, 2011; Sangalli-Leite *et al.*, 2016). Larvae have advantages over conventional systems as they are easy to use, lack legal and ethical restrictions associated with mammalian testing, are low cost, easy to use and easy to establish in the laboratory, they may be incubated 37 ^{o}C and possess a large volume of

hemolymph with a high density of immune cells which can be used in a range of *ex vivo* assays using techniques already established with mammalian granulocytes (Kavanagh and Reeves, 2004; Tsai *et al.*, 2016). Infection of larvae can be assessed by many end points including survival, extent of melanization, variations in hemocyte density and microbial load, histopathology, nodule formation and alterations in proteome (Bergin *et al.*, 2003; Fuchs *et al.*, 2010; Maurer *et al.*, 2015).

The immune system of insects shares many similarities with the innate immune response of mammals and as a consequence insects may be used to assess the virulence of microbial pathogens and produce results comparable to those obtained using mammalian systems (Jander *et al.*, 2000; Brennan *et al.*, 2002). Larvae have been used to study the relative virulence of *C. albicans* (Cotter *et al.*, 2000; Brennan *et al.*, 2002), *A. fumigatus* (Reeves *et al.*, 2004a; O'Hanlon *et al.*, 2011; Slater *et al.*, 2011), and *C. neoformans* (Mylonakis *et al.*, 2005; Eisenman *et al.*, 2014), Gram positive bacteria such as *S. pyogenes* (Olsen *et al.*, 2011), *S. pneumoniae* (Evans and Rozen, 2012), *E. faecium* (Lebreton *et al.*, 2012; Chibebe Junior *et al.*, 2013), *S. aureus* (Peleg *et al.*, 2009b; Desbois and Coote, 2011), *L. monocytogenes* (Joyce and Gahan, 2010; Mukherjee *et al.*, 2010) and Gram negative bacteria such as *P. aeruginosa* (Andrejko *et al.*, 2005; Andrejko and Mizerska-Dudka, 2011), *E. coli* (Riza and Madamopoulos, 1997; Ciesielczuk *et al.*, 2015), *K. pneumonia* (Wand *et al.*, 2013; Diago-Navarro *et al.*, 2014), *L. pneumophila* (Harding *et al.*, 2012; Harding *et al.*, 2013) and *A. baumanii* (Peleg *et al.*, 2009a; Jacobs *et al.*, 2014). Larvae have been employed to study Tipula iridescent virus (TIV) (Jafri and Chaudhry, 1971), Nodamura virus (Garzon *et al.*, 1978), densonucleosis virus and iridovirus (Lebedinets *et al.*, 1978), invertebrate iridescent virus 6 (Constantino *et al.*, 2001), bovine herpes simplex virus-1 (BHSV-1) (Büyükgüzel *et al.*, 2007), and *A. fumigatus* mycovirus (Özkan and Coutts, 2015). Larvae have also been utilised to evaluate the toxicity of novel antimicrobial agents such as phenanthroline chelators (McCann *et al.*, 2012a), the efficacy of new antimicrobial agents (Jia *et al.*, 2016; Allegra *et al.*, 2018), the repurposing of antimicrobial agents (Nile *et al.*, 2019) and also in the evaluation of novel drug combination therapy (Krezdorn *et al.*, 2014).

Although insect model organisms do overcome the financial and ethical considerations associated with mammalian testing, their use possess a range of drawbacks associated with the differences between insects and vertebrates model systems. Insects engage in respiration by a network of tubes called tracheae and tracheoles, they do not possess a lymphatic system or an adaptive immune response made up on antibodies and long lived memory cells. The insect hemolymph is made up of different carbohydrates, lipids, immune effectors and cells to mammalian blood and there is a lack of analogous organs e.g. kidney, heart and liver, where disseminated fungal infections are commonly located (Ramarao *et al.*, 2012; López Hernández *et al.*, 2015). However, despite these differences, insects remain an excellent model to study virulence and more recently to study microbial pathogenesis (Mukherjee *et al.*, 2013). Larvae infected with *Listeria* showed neural pathologies similar to those in mammals thus opening the possibility of examining neural disease and repair mechanisms in insects (Mukherjee *et al.*, 2013). This finding could enable the use of *G. mellonella* larvae for studying brain development and for rapidly evaluating the efficacy of novel drugs designed to treat neural diseases or malfunction. Further to this, the central hypothesis of this project was to assess whether larvae could be used to assess microbial pathogenesis and interaction with the innate immune response.

This project focused on fungal pathogens *C. albicans, A. fumigatus* and *M. mycetomatis* and bacterial pathogen *S. aureus*. As outlined in Chapter 3, *G. mellonella* larvae are a good model to study pathogenicity and host – pathogen interactions. However, larvae are unsuitable to study superficial infections, oral or vaginal candidiasis, and chronic mucocutaneous candidiasis which can be studied using various murine infection models (Kirkpatrick and Hill, 2001; Donders *et al.*, 2018). A good animal model must be reproducible, easy to set up, cost effective and should replicate the major clinical symptoms observed during the human disease. Larvae satisfy each of these criteria however, the latter depends on the use of larvae to study invasive and disseminated disease. Relative to the human infection, which most likely originates from the GI tract, introduction of *C. albicans* cells into larvae grow and disseminate throughout the host (Berenguer *et al.*, 1993). In human infection, the lungs and kidneys are most commonly affected but also the heart, liver and spleen, while larvae possess an open circulatory system and because of their size

cannot be accurately used to study invasive infection associated with a catheter (Berenguer *et al.*, 1993; Nett *et al.*, 2014). Many of the murine models available are assessed via analysis of survival, fungal burden and histopathology which is true also for the use of *G. mellonella* larvae (MacCallum, 2012). Larvae were the first mini-host model developed to assess *Candida* virulence (Cotter *et al.*, 2000) and this is because larvae are amenable to 37 ºC unlike *D. melanogaster* and the zebrafish infection model. Furthermore, the importance of the innate immune response in curtailing the acute stages of fungal establishment has been widely documented (Margalit and Kavanagh, 2015) and the lack of an adaptive immune response in insects can been seen as an advantage so it allows the study of the innate response without interference from the adaptive response. The results presented in Chapter 3 indicate that larvae may be used to model initial stages of infection processes in mammals, to detail the dissemination of *C. albicans* during acute infection, and to assess the efficacy of antifungal therapy on survival of larvae and reduction of symptoms using cryo-imaging.

The results presented in Chapter 4 characterised disseminated *S. aureus* infection and the immune response to septicaemia. Mouse models for many important staphylococcal clinical diseases have been developed, including: peritonitis, pneumonia, sepsis, skin and soft tissue infection, endocarditis, abscesses, osteomyelitis, arthritis, and nasal colonization (Parker, 2017). Although mice are have similar immune, nervous, cardiovascular, and endocrine systems to humans, many features of mice are significantly different from humans, such as their small size, altered metabolic rate, fatty acid composition of cells, higher rates of ROS generation and thus oxidative damage, different diet, microbiome, and typically being inbred (Xiao *et al.*, 2015; Parker, 2017). *G. mellonella* larvae could be a good system to assess the effect of a live attenuated *S. aureus* vaccine on the innate immune response or to screen for novel antimicrobial especially considering the high prevalence of MRSA (Dulon *et al.*, 2011). The results presented in Chapter 4 indicate how *S. aureus* interacts with the larval immune response, induces the expression of a variety of immune related peptides and also forms nodules which are a hallmark of soft tissue infections during human infection.

Chapter 5 demonstrated that the processes of polymicrobial co-infection by *C. albicans* and *S. aureus* in *G. mellonella* are comparable to results obtained using a murine model of co-infection (Peters and Noverra, 2013). Larvae provide an easy to use and ethically acceptable *in vivo* system to assess polymicrobial interactions with their host and the efficacy of combination antimicrobial therapy on increasing larval survival. Currently, there are no well characterised animal models to study polymicrobial infection, only a few studies have detailed co-infection in peritonitis using rodents (Kesavalu *et al.*, 2007; Schabbauer, 2012; Peters and Noverra, 2013). The results generated in this Chapter matched those from Peters and Noverra (2013). *C. albicans* increased the pathogenicity of *S. aureus* and the larval humoral immune response to co-infection was comparable to infection by *C. albicans* or *S. aureus* during mono infection. Larvae could be used as a useful and ethical model to study the interactome and pathogenicity of range of microbes which would normally interact as part of the human microbiome.

In Chapter 6, the infection processes of *A. fumigatus* and the immune responses of *G. mellonella* larvae were characterised. The spectrum of aspergillosis in humans depends upon the patient's immune status and presents on a spectrum ranging from saprophytic to invasive disease. Larvae are not susceptible to saprophytic or allergic disease as the insect immune system responds to invading fungal cells with a strong antimicrobial effector arsenal and because of this when using the model to study invasive disease, a large inoculum (10^6/ larva; approximate weight ~0.2 g) must be used relative to the immunocompromised mouse (10^7 - 10^8 approximate weight ~25 g) (Ratcliffe, 1985a). Furthermore, the former disease occurs in the background of immune malfunction (i.e. CF) and it is not yet possible to delete larval genes, unlike in *D. melanogaster* which has been extensively used to study the immunopathogenesis of *A. fumigatus* (Chamilos *et al.*, 2008). The obvious hinderance associated with the use of larvae to model is the lack of an anatomically similar respiratory system, which is the primary route of infection for human patients and larvae cannot be used to study chronic infections such as ABPA because of their short lifecycle (Jorjão *et al.*, 2018). This also has an impact on the route of inoculation, where many different routes of administration of fungal conidia are available in mice models (intravenous, intraperitoneal injection, intranasal deposition, intra-tracheal/intra-bronchial instillation, inhalation in chamber etc.)

whereas only three exist in *G. mellonella* (intra-hemocoel injection, force-feeding, absorption through cuticle) (Desoubeaux and Cray, 2017). However, *A. fumigatus* disseminated infection in larvae results in the formation of granuloma type structures as a result of the insect nodulation response, however, granuloma is a common feature of $p47^{phox-/-}$ mouse model for experimental aspergillosis (Dennis *et al.*, 2006). Other animal models of aspergillosis include several avian models, guinea pigs, rabbits and rodents, with the rodent model prevailing as the model of choice. *G. mellonella* larvae can be used to study disseminated infection by *A. fumigatus* and the use of cryo-imaging allows the generation of results within 2 days. The results presented in Chapter 6 indicate that *G. mellonella* larvae may be a convenient model for studying the stages in the development of invasive aspergillosis and may offer an insight into how this process develops in mammals.

In Chapter 7 the host – pathogen interactome between *M. mycetomatis* and *G. mellonella* larvae was characterised. The larvae model for *M. mycetomatis* was developed by the Van de Sande group in 2015 and can be used to generate *M. mycetomatis* grains within a few days, although growth of the fungus on agar takes up to 1 month (Kloezen *et al.,* 2013). Interestingly, in the murine model, an adjuvant is necessary for grain formation, however in the larval model this is not needed (Ahmed *et al.,* 2003; Kloezen *et al.,* 2013). Previously, there have been attempts to establish a murine model of eumycetoma, however reproducibility was poor (Murray *et al.*, 1960). Eumycetoma is still a neglected disease and prevention is paramount, however the development of novel antifungal approaches in treating eumycetoma is important in treating established disease (Ahmed *et al.*, 2004). These results indicate that *G. mellonella* larvae are an excellent model to assess the interaction of *M. mycetomatis* with the host immune response and could be easily adapted to study toxin production. As the model is easy to use, cheap and amenable to high temperatures, larvae could be established in laboratories in endemic countries (e.g. India, Brazil, Venezuela or Sudan) to conduct *in vivo* research. The results presented in this Chapter identify similarities between the immune response to and the infection processes of *M. mycetomatis* in *G. mellonella* larvae and humans, and identified novel proteins from *M. mycetomatis* (e.g. extracellular vesicle formation, host extracellular matrix binding, extracellular material biosynthesis, response to stress/ host) which play a crucial role in grain development.

Infection by fungal pathogens *C. albicans* and *A. fumigatus* produced pathologies similar to invasive candidiasis and invasive aspergillosis, respectively, during human infection. Infection of larvae with *M. mycetomatis* produces grains which were found during human infection (Kloezen *et al.*, 2015) and the proteomic date generated demonstrated larvae are an excellent model to study grain development, the acute immune response to the grain and the stress responses of *M. mycetomatis* to the host immune response. Polymicrobial infections are vastly underestimated and research which examines infection dynamics are dominated by mono-microbial interactions. The results presented in Chapter 5 provide the evidence for larvae as an *in vivo* system to study trans-kingdom polymicrobial co-infection which could be easily adapted to study Cis- kingdom dual infection or infection caused by more than two microbes. These Chapters also utilise quantitative mass spectrometry (summarised in **Table 11.1**), which is a relatively new technology, especially considering research related to insects is dominated by genomics, however these results should provide the rationale for studying the immune response at 1) the protein level and 2) the whole cell or whole hemolymph level in future work.

Table 11.1: Summary of the key proteins identified during infection by different pathogens in *G. mellonella* larvae at 24 h post infection relative to the relevant 0 h control (ND: not detected).

	C. albicans	***S. aureus***	***C. albicans / S. aureus***	***A. fumigatus***	***M. mycetomatis***
Invasion					
Muscle protein 20 like protein	+173.3 fold	ND	+8.6 fold	+11.84 fold	+190.84 fold
Nodulation					
Hdd11	+49.4 fold	+7.24 fold	+33.3 fold	+3.66 fold	+47.19 fold
Antimicrobial peptide					
Gloverin	+52.5 fold	+121 fold	+19.3 fold	+5.16 fold	+6.38 fold
Cecropin-D	+22.8 fold	+73.7 fold	+37.8 fold	+6.54 fold	+33.46 fold
Detoxification					
Glutathione-s-transferase	+114.1 fold	ND	ND	ND	+9.93 fold
Thioredoxin	+3.2 fold	-3.94 fold	ND	+2.2 fold	+15.53 fold
Insect metalloproteinase inhibitor	ND	ND	ND	+8.2 fold	+9.30 fold
Microbial Recognition					
PG-RP LB	+71.6 fold	+9.53 fold	+14 fold	+5.90 fold	+16.91 fold
PG-RP B	+7.5 fold	+17.3 fold	ND	+5.61 fold	+12.21 fold
β-glucan recognition protein	-28.6 fold	+2.16 fold	ND at 24 h	-4.06 fold	-7.7 fold

Although insects do not have an adaptive arm of the immune system, their immune response can be primed via prior exposure to a microbe which can protect them from a subsequent lethal infection. The general belief was that immune priming was broad and unspecific. However, the results presented in Chapter 8 demonstrated the humoral immune response to fungal infection is specific and regulated and the response to bacteria is broad and non-specific. In nature, entomopathogenic fungi can penetrate the insect cuticle, multiply and disseminate throughout the host and frequently emerge from the host and produce spores which are spread by wind etc., ready to infect another suitable host (Joop and Vilcinskas, 2016). It is logical that the immune response which is activated to an infection which can penetrate through the insect cuticle is one that is robust and specific. In contrast, infection by bacteria, probably occurs most frequently through injury to the cuticle and introduction of the bacterial pathogen into the hemocoel, in this case, it is possible the immune response

must be rapid and broad in order to protect against the possibility of both bacterial and fungal infection. These results provide evidence of the specificity of immune priming to a fungal pathogen in *G. mellonella* larvae.

Chapter 9 and 10 focused on the responses of *A. fumigatus* to antimicrobial agents from the vertebrate innate immune response. In Chapter 9, the effect of the antimicrobial peptide LL-37 (which is elevated in pulmonary mucus of CF patients) on *A. fumigatus*; a common pathogen of CF patients was examined. LL-37 is possibly the most widely studied AMP and the most unique, as it has been implicated in many diseases such as atopic dermatitis, rosacea and psoriasis, has several immunomodulatory activities, induces wound healing and angiogenesis, is chemotactic to human neutrophils and displays potent antimicrobial activity (Dürr *et al.*, 2006). However, this Chapter demonstrated the growth stimulatory activity of LL-37 on *A. fumigatus*. LL-37 also promotes the growth of lung cancer and was found to be a putative growth factor for epithelial cells and increased cell proliferation in breast cancer (Heilborn *et al.*, 2005; Ji *et al.*, 2019). It is likely the growth promoting effects of LL-37 on *A. fumigatus* are due to interactions with the cell membrane through either transactivation or by direct binding of growth promoting receptors. These results indicate that LL-37 stimulates *A. fumigatus* growth and this may result in increased fungal growth and secretion of toxins in the lungs of CF patients.

The work presented in Chapter 10 aimed to characterise the response of the pulmonary pathogen *Aspergillus fumigatus* to NCT; a neutrophil-derived oxidant with remarkable *in vivo* tolerability and efficacy against a range of pathogens. NCT possesses broad spectrum antimicrobial activity against a range of clinically relevant microbes (bacterial, fungal, viral, helminth) and is non-toxic following superficial application. Inhalation of NCT to target infections of the bronchopulmonary system would provide a suitable application, and currently, inhalative antibiotics are only licensed for CF patients with decreased lung function with *P. aeruginosa* infection (Nagl *et al.,* 2013). NCT may be more advantageous than antibiotics which may have indications with immunosuppression regiments etc., in mice, NCT was comparable to saline after inhalation, and in humans, NCT only moderately decreased ciliary beat frequency of epithelial cells of the nasal mucosa (a sensitive

parameter for toxicity) (Hofer *et al.,* 2003). Furthermore, inhalation of NCT results in no systemic absorption, meaning is has no off-target effects and it displays a very short half-life in bronchial lavages from pigs and mice (Geiger *et al.,* 2009; Nagl *et al.,* 2013). NCT has some limitations such as it can only be used superficially, the efficacy of NCT against fungal infections remains to be proven in controlled, randomised clinical studies, its fungicidal activity is lower than its bactericidal activity, and it must be stored at low temperatures to maintain its activity (i.e. for a 1% solution, loss of 10% of activity at 2-4 ºC after 1 year) (Nagl *et al.,* 2018). The results in this Chapter indicate that NCT induces an oxidative stress response in *A. fumigatus* as evidenced by alterations in the proteome and inhibits conidial and mycelial growth. Clinical investigations of topical application of NCT to treat *Aspergillus* infections are encouraged.

11.2 Future research

The research presented in this thesis is primarily proteomic based and performing transcriptomic analysis of infected larval hemolymph and comparing this to the proteomic data would generate a greater understanding of the host – pathogen interactome at the molecular level. *G. mellonella* larvae were the animal model at the centre of this project, however to compare the humoral immune system of larvae to the humoral immune response of infected mice or patients with the fungal or bacterial pathogens in this project using LC-MS/MS would generate very interesting data. This may allow the identification of overlapping mediators involved of each. Proteomic analysis of human neutrophil and insect granulocyte cell lysates (± infected) could allow the identification of orthologous proteins to focus future studies and further validate the larval model.

It would also be interesting to use larvae to identify novel combination therapies against multidrug resistance in bacteria e.g. *K. pneumoniae.* To generate a new endpoint of infection it may be possible to infect larvae with a pathogen and treat them with a relevant antimicrobial agent and look at the proteome of infected and treated larvae to determine the effect of antimicrobial chemotherapy on the proteome of infected larvae. Future research should utilise the recently sequenced *G. mellonella* genome (Lange *et al.*, 2018) to 1) to knockout immune relevant genes in order to identify their function during the immune response and 2) generate a more accurate and annotated proteome for *G. mellonella*. To determine the *in vitro* proteome of *M. mycetomatis* grains and identify the role of extracellular vesicles in infection and grain development which may reveal the factors responsible for the analgesic effect of eumycetoma. The growth promoting effects of LL-37 should be studied *in vivo* by generating a CF- mouse model over expressing LL-37, which should be infected with *A. fumigatus* and survival, fungal burden, histopathology should be determined.

Chapter 12

Bibliography

12.0 Bibliography

Abad, A., Fernández-Molina, J.V., Bikandi, J., Ramírez, A., Margareto, J., Sendino, J., *et al.* (2010) What makes *Aspergillus fumigatus* a successful pathogen? Genes and molecules involved in invasive aspergillosis. *Rev Iberoam Micol* **27**: 155–182.

Acta, B.B. (2016) HHS Public Access. **1849**: 836–844.

Ahmed, A.O.A., Leeuwen, W. Van, Fahal, A., Sande, W. Van De, Verbrugh, H., and Belkum, A. Van (2004) Mycetoma caused by *Madurella mycetomatis*: A neglected infectious burden. *Lancet Infect Dis* **4**: 566–574.

Aimanianda, V., Bayry, J., Bozza, S., Kniemeyer, O., Perruccio, K., Elluru, S.R., *et al.* (2009) Surface hydrophobin prevents immune recognition of airborne fungal spores. *Nature* **460**: 1117–1121.

Akira, S., and Hemmi, H. (2003) Recognition of pathogen-associated molecular patterns by TLR family. *Immunol Lett* **85**: 85–95.

Alarco, A.-M., Marcil, A., Chen, J., Suter, B., Thomas, D., and Whiteway, M. (2004) Immune-Deficient *Drosophila melanogaster*: A Model for the Innate Immune Response to Human Fungal Pathogens. *J Immunol* **172**: 5622–5628.

Alcazar-Fuoli, L., Buitrago, M., Gomez-Lopez, A., and Mellado, E. (2015) An alternative host model of a mixed fungal infection by azole susceptible and resistant *Aspergillus* spp strains. *Virulence* **6**: 376–384.

Alekseeva, L., Huet, D., Féménia, F., Mouyna, I., Abdelouahab, M., Cagna, A., *et al.* (2009) Inducible expression of β defensins by human respiratory epithelial cells exposed to *Aspergillus fumigatus* organisms. *BMC Microbiol* **9**: 33.

Allameh, A., Farahani, M., and Zarghi, A. (2000) Kinetic studies of aflatoxin B1-glutathione conjugate formation in liver and kidneys of adult and weanling rats. *Mech Ageing Dev* **115**: 73–83.

Allegra, E., Titball, R.W., Carter, J., and Champion, O.L. (2018) *Galleria mellonella* larvae allow the discrimination of toxic and non-toxic chemicals. *Chemosphere* **198**: 469–472.

Allen, U.D. (2010) Antifungal agents for the treatment of systemic fungal infections in children. *Paediatr Child Health (Oxford)* **15**: 603–608.

Ames, L., Duxbury, S., Pawlowska, B., Ho, H. lui, Haynes, K., and Bates, S. (2017) *Galleria mellonella* as a host model to study *Candida glabrata* virulence and antifungal efficacy. *Virulence* **8**: 1909–1917.

Amitani, R., Murayama, T., Nawada, R., Lee, W.J., Niimi, A., Suzuki, K., *et al.* (1995a) *Aspergillus* culture filtrates and sputum sols from patients with pulmonary aspergillosis cause damage to human respiratory ciliated epithelium *in vitro*. *Eur Respir J* **8**: 1681–1687.

Amitani, R., Taylor, G., Elezis, E., Llewellyn-jones, C., Mitchell, J., Kuze, F., *et al.* (1995b) Purification and Characterization of Factors Produced by *Aspergillus fumigatus* Which Affect Human Ciliated Respiratory Epithelium. **63**: 3266–3271.

Andrä, J., Berninghausen, O., and Leippe, M. (2000) Cecropins, antibacterial peptides from insects and mammals, are potently fungicidal against *Candida albicans*. *Med Microbiol Immunol* **189**: 169–173.

Andrejko, M., Cytryńska, M., and Jakubowicz, T. (2005) Apolipophorin III is a substrate for protease IV from *Pseudomonas aeruginosa*. *FEMS Microbiol Lett* **243**: 331–337.

Andrejko, M., and Mizerska-Dudka, M. (2011) Elastase B of *Pseudomonas aeruginosa* stimulates the humoral immune response in the greater wax moth, *Galleria mellonella*. *J Invertebr Pathol* **107**: 16–26.

Aneja, B., Irfan, M., Kapil, C., Jairajpuri, M.A., Maguire, R., Kavanagh, K., *et al.* (2016) Effect of novel triazole–amino acid hybrids on growth and virulence of *Candida* species: *in vitro* and *in vivo* studies. *Org Biomol Chem* **14**: 10599–10619.

Arteaga Blanco, L.A., Crispim, J.S., Fernandes, K.M., Oliveira, L.L. de, Pereira, M.F., Bazzolli, D.M.S., and Martins, G.F. (2017) Differential cellular immune response of *Galleria mellonella* to Actinobacillus pleuropneumoniae. *Cell Tissue Res* **370**: 153–168.

Astvad, K.M.T., Meletiadis, J., Whalley, S., and Arendrup, M.C. (2017) Fluconazole pharmacokinetics in *Galleria mellonella* larvae and performance evaluation of a bioassay compared to liquid chromatography-tandem mass spectrometry for hemolymph specimens. *Antimicrob Agents Chemother* **61**.

Banerjee, B., Greenberger, P.A., Fink, J.N., and Kurup, V.P. (1998) Immunological characterization of Asp f 2, a major allergen from *Aspergillus fumigatus* associated with allergic bronchopulmonary *aspergillosis*. *Infect Immun* **66**: 5175–5182.

Banville, N., Fallon, J., McLoughlin, K., and Kavanagh, K. (2011) Disruption of haemocyte function by exposure to cytochalasin b or nocodazole increases the susceptibility of *Galleria mellonella* larvae to infection. *Microbes Infect* **13**: 1191–1198.

Barbosa, M.S., Báo, S.N., Andreotti, P.F., Faria, F.P. De, Felipe, M.S.S., Feitosa, L.D.S., *et al.* (2006) Glyceraldehyde-3-phosphate dehydrogenase of *Paracoccidioides brasiliensis* is a cell surface protein involved in fungal adhesion to extracellular matrix proteins and interaction with cells. *Infect Immun* **74**: 382–389.

Bastidas, R.J., Shertz, C.A., Lee, S.C., Heitman, J., and Cardenas, M.E. (2012) Rapamycin exerts antifungal activity *in vitro* and *in vivo* against mucor circinelloides via FKBP12-dependent inhibition of tor. *Eukaryot Cell* **11**: 270–281.

Becher, M.A., and Moritz, R.F.A. (2009) A new device for continuous temperature measurement in brood cells of honeybees (*Apis mellifera*). *Apidologie* **40**: 577–584.

Beekman, C., Meckler, L., Kim, E., and Bennett, R.J. (2018) *Galleria mellonella* as an Insect Model for *P. destructans*, the Cause of White-Nose Syndrome in Bats. 1–32.

Bellocchio, S., Moretti, S., Perruccio, K., Fallarino, F., Bozza, S., Montagnoli, C., *et al.* (2004) TLRs govern neutrophil activity in *Aspergillosis*. *J Immunol* **173**: 7406–7415.

Ben-Ami, R., Lewis, R.E., and Kontoyiannis, D.P. (2010) Enemy of the (immunosuppressed) state: An update on the pathogenesis of A*spergillus fumigatus* infection. *Br J Haematol* **150**: 406–417.

Ben-Dov, Y. (1993) A systematic catalogue of the soft scale insects of the world (Homoptera:Coccoidea:Coccidae) : with data on geographical distribution, host plants, biology, and economics importance. *Annals of the Entomological Society of America* **6**: 578–585.

Bera, A., Herbert, S., Jakob, A., Vollmer, W., and Götz, F. (2005) Why are pathogenic staphylococci so lysozyme resistant? The peptidoglycan O-acetyltransferase OatA is the major determinant for lysozyme resistance of *Staphylococcus aureus*. *Mol Microbiol* **55**: 778–787.

Berenguer, J., Buck, M., Witebsky, F., Stock, F., Pizzo, P.A., and Walsh, T.J. (1993) Lysis-centrifugation blood cultures in the detection of tissue-proven invasive candidiasis disseminated versus single-organ infection. *Diagn Microbiol Infect Dis* **17:** 103–109.

Bergin, D., Brennan, M., and Kavanagh, K. (2003) Fluctuations in haemocyte density and microbial load may be used as indicators of fungal pathogenicity in larvae of *Galleria mellonella*. *Microbes Infect* **5**: 1389–1395.

Bergin, D., Murphy, L., Keenan, J., Clynes, M., and Kavanagh, K. (2006) Pre-exposure to yeast protects larvae of *Galleria mellonella* from a

subsequent lethal infection by *Candida albicans* and is mediated by the increased expression of antimicrobial peptides. *Microbes Infect* **8**: 2105–2112.

Bergin, D., Reeves, E.P., Renwick, J., Frans, B., Kavanagh, K., and Wientjes, F.B. (2005) Superoxide Production in *Galleria mellonella* Hemocytes : Identification of Proteins Homologous to the NADPH Oxidase Complex of Human Neutrophils Superoxide Production in *Galleria mellonella* Hemocytes. *Infect Immun* **73**: 4161–4170.

Bergsson, G., Reeves, E.P., McNally, P., Chotirmall, S.H., Greene, C.M., Greally, P., *et al.* (2009) LL-37 complexation with glycosaminoglycans in cystic fibrosis lungs inhibits antimicrobial activity, which can be restored by hypertonic saline. *J Immunol* **183**: 543–551.

Bhakdi, S., and Tranum-Jensen, J. (1991) Alpha-toxin of *Staphylococcus aureus. Microbiol Rev* **55**: 733–51.

Bielska, E., and May, R.C. (2019) Extracellular vesicles of human pathogenic fungi. *Curr Opin Microbiol* **52**: 90–99.

Bolouri Moghaddam, M.R., Tonk, M., Schreiber, C., Salzig, D., Czermak, P., Vilcinskas, A., and Rahnamaeian, M. (2016) The potential of the *Galleria mellonella* innate immune system is maximized by the co-presentation of diverse antimicrobial peptides. *Biol Chem* **397**: 939–945.

Bongomin, F., Gago, S., Oladele, R., and Denning, D. (2017) Global and Multi-National Prevalence of Fungal Diseases—Estimate Precision. *J Fungi*. **4**: 57–76.

Borman, A.M., Szekely, A., and Johnson, E.M. (2016) Comparative Pathogenicity of United Kingdom Isolates of the Emerging Pathogen *Candida auris* and Other Key Pathogenic *Candida* Species. *mSphere* **1**: e00189-16.

Bowdish, D., Davidson, J., Lau, E., Lee, K., Scott, M., and Hancock, E. (2005) Impact of LL-37 on anti-infective immunity. *J Leukoc Biol* **77**: 451–459.

Braun, B.R., Head, W.S., Wang, M.X., and Johnson, A.D. (2000) Identification and characterization of TUP1-regulated genes in *Candida albicans*. *Genetics* **156(1)**: 31–44.

Brennan, M., Thomas, D.Y., Whiteway, M., and Kavanagh, K. (2002) Correlation between virulence of *Candida albicans* mutants in mice and *Galleria mellonella* larvae. *FEMS Immunol Med Microbiol* **34**: 153–157.

Brenner, M., and Hearing, V.J. (2008) The protective role of melanin against UV damage in human skin. *Photochem Photobiol* **84**: 539–549.

Brown, A.F., Leech, J.M., Rogers, T.R., and McLoughlin, R.M. (2014) *Staphylococcus aureus* colonization: Modulation of host immune response and impact on human vaccine design. *Front Immunol* **8;4**: doi: 10.3389/fimmu.2013.00507.

Brown, G.D., Denning, D.W., Gow, N.A.R., Levitz, S.M., Netea, M.G., and White, T.C. (2012) Hidden Killers: Human Fungal Infections. *Sci Transl Med* **4**: 1–9.

Brown, S.E., Howard, A., Kasprzak, A.B., Gordon, K.H., and East, P.D. (2008) The discovery and analysis of a diverged family of novel antifungal moricin-like peptides in the wax moth *Galleria mellonella*. *Insect Biochem Mol Biol* **38**: 201–212.

Brown, S.E., Howard, A., Kasprzak, A.B., Gordon, K.H., and East, P.D. (2009) A peptidomics study reveals the impressive antimicrobial peptide arsenal of the wax moth *Galleria mellonella. Insect Biochem Mol Biol* **39**: 792–800.

Browne, N., Hackenberg, F., Streciwilk, W., Tacke, M., and Kavanagh, K. (2014) Assessment of *in vivo* antimicrobial activity of the carbene silver(I) acetate derivative SBC3 using *Galleria mellonella* larvae. *BioMetals* **27**: 745–752.

Browne, N., Heelan, M., and Kavanagh, K. (2013) An analysis of the structural and functional similarities of insect hemocytes and mammalian phagocytes. *Virulence* **4**: 597–603.

Browne, N., Surlis, C., Maher, A., Gallagher, C., Carolan, J.C., Clynes, M., and Kavanagh, K. (2015) Prolonged pre-incubation increases the susceptibility of *Galleria mellonella* larvae to bacterial and fungal infection. *Virulence* **6**: 37–41.

Brunke, S., Quintin, J., Kasper, L., Jacobsen, I.D., Richter, M.E., Hiller, E., *et al.* (2015) Of mice, flies - and men? Comparing fungal infection models for large-scale screening efforts. *Dis Model Mech* **8**: 473–486.

Bulet, P., Hetru, C., Dimarcq, J.L., and Hoffmann, D. (1999) Antimicrobial peptides in insects; structure and function. *Dev Comp Immunol* **23**: 329–344.

Bunce, C., Wheeler, L., Reed, G., Musser, J., and Barg, N. (1992) Murine model of cutaneous infection with gram-positive cocci. *Infect Immun* **60**: 2636–2640.

Burman, J.D., Leung, E., Atkins, K.L., O'Seaghdha, M.N., Lango, L., Bernado, P., *et al.* (2008) Interaction of human complement with Sbi, a staphylococcal immunoglobulin-binding protein: Indications of a novel mechanism of complement evasion by *Staphylococcus aureus*. *J Biol Chem* **283**: 17579–17593.

Buskirk, A.D., Green, B.J., Lemons, A.R., Nayak, A.P., Goldsmith, W.T., Kashon, M.L., *et al.* (2014) A murine inhalation model to characterize pulmonary exposure to dry *Aspergillus fumigatus* conidia. *PLoS One* **9(10)**: e109855.

Büyükgüzel, E., Tunaz, H., Stanley, D., and Büyükgüzel, K. (2007) Eicosanoids mediate *Galleria mellonella* cellular immune response to viral infection. *J Insect Physiol* **53**: 99–105.

Byfield, F.J., Kowalski, M., Cruz, K., Leszczynska, K., Namiot, A., Savage, P.B., *et al.* (2017) Cathelicidin LL-37 Increases Lung Epithelial Cell Stiffness, Decreases Transepithelial Permeability, and Prevents Epithelial Invasion by *Pseudomonas aeruginosa*. *J Immunol* **187**: 6402–6409.

Calderone, R.A., and Fonzi, W.A. (2001) Virulence factors of *Candida albicans. Trends Microbiol* **9**: 327–335.

Capparelli, R., Parlato, M., Borriello, G., Salvatore, P., and Iannelli, D. (2007) Experimental phage therapy against *Staphylococcus aureus* in mice. *Antimicrob Agents Chemother* **51**: 2765–2773.

Carvalho Dias, K. De, Barbugli, P.A., Patto, F. De, Lordello, V.B., Aquino Penteado, L. De, Medeiros, A.I., and Vergani, C.E. (2017) Soluble factors from biofilm of *Candida albicans* and *Staphylococcus aureus* promote cell death and inflammatory response. *BMC Microbiol* **17**: 146.

Cerenius, L., Kawabata, S. ichiro, Lee, B.L., Nonaka, M., and Söderhäll, K. (2010) Proteolytic cascades and their involvement in invertebrate immunity. *Trends Biochem Sci* **35**: 575–583.

Cerenius, L., Lee, B.L., and Söderhäll, K. (2008) The proPO-system: pros and cons for its role in invertebrate immunity. *Trends Immunol* **29**: 263–271.

Cerenius, L., and Söderhäll, K. (2011) Coagulation in invertebrates. *J Innate Immun* **3**: 3–8.

Chain, B.M., and Anderson, R.S. (1983) Inflammation in insects: The release of a plasmatocyte depletion factor following interaction between bacteria and haemocytes. *J Insect Physiol* **29**: 1–4.

Chamilos, G., Lewis, R.E., Hu, J., Xiao, L., Zal, T., Gilliet, M., *et al.* (2008) *Drosophila melanogaster* as a model host to dissect the immunopathogenesis of zygomycosis. *Proc Natl Acad Sci* **105**: 9367–9372

Chamilos, G., Samonis, G., and P. Kontoyiannis, D. (2011) *Drosophila melanogaster* As a Model Host for the Study of Microbial Pathogenicity And the Discovery of Novel Antimicrobial Compounds. *Curr Pharm Des* **17**: 1246–1253.

Champer, J., Ito, J.I., Clemons, K. V, Stevens, D.A., and Kalkum, M. (2016) Proteomic Analysis of Pathogenic Fungi Reveals Highly Expressed Conserved Cell Wall Proteins. *J fungi* **2**: 6.

Champion, O.L., Wagley, S., and Titball, R.W. (2016) *Galleria mellonella* as a model host for microbiological and toxin research. *Virulence* **7**: 840–845.

Chao, C.C., Hsu, P.C., Jen, C.F., Chen, I.H., Wang, C.H., Chan, H.C., *et al.* (2010) Zebrafish as a model host for *Candida albicans* infection. *Infect Immun* **78**: 2512–2521.

Chapman, R.F. (2003) Contact chemoreception in feeding by phytophagous insects. *Annu Rev Entomol* **48**: 455–84.

Chen, C.I.-U., Schaller-Bals, S., Paul, K.P., Wahn, U., and Bals, R. (2004) B-defensins and LL-37 in bronchoalveolar lavage fluid of patients with cystic fibrosis. *J Cyst Fibros* **3**: 45–50.

Chen, X., Niyonsaba, F., Ushio, H., Okuda, D., Nagaoka, I., Ikeda, S., *et al.* (2005) Synergistic effect of antibacterial agents human β-defensins, cathelicidin LL-37 and lysozyme against *Staphylococcus aureus* and *Escherichia coli*. *J Dermatol Sci* **40**: 123–132.

Chen, Y.Y., Chen, J.C., Lin, Y.C., Kitikiew, S., Li, H.F., Bai, J.C., *et al.* (2014) Endogenous molecules induced by a Pathogen-Associated Molecular Pattern (PAMP) elicit innate immunity in shrimp. *PLoS One* **9**.

Cheng, A.G., Kim, H.K., Burts, M.L., Krausz, T., Schneewind, O., and Missiakas, D.M. (2009) Genetic requirements for *Staphylococcus aureus* abscess formation and persistence in host tissues. *FASEB J* **23**: 3393–3404.

Chibebe Junior, J., Fuchs, B.B., Sabino, C.P., Junqueira, J.C., Jorge, A.O.C., Ribeiro, M.S., *et al.* (2013) Photodynamic and Antibiotic Therapy Impair the Pathogenesis of *Enterococcus faecium* in a Whole Animal Insect Model. *PLoS One* **8**.

Chinen, J., Fleisher, T.A., and Shearer, W.T. (2013) Adaptive Immunity. In *Middleton's Allergy: Principles and Practice: Eighth Edition*. pp. 20–29.

Cho, T., Toyoda, M., Sudoh, M., Nakashima, Y., Calderone, R.A., and Kaminishi, H. (2003) Isolation and sequencing of the *Candida albicans* MS13, a putative novel member of the HSP70 family. *Yeast* **20**: 149–156.

Chotirmall, S.H., Al-Alawi, M., Mirkovic, B., Lavelle, G., Logan, P.M., Greene, C.M., and McElvaney, N.G. (2013) *Aspergillus*-associated airway disease, inflammation, and the innate immune response. *Biomed Res Int* **2013**: 723129.

Ciesielczuk, H., Betts, J., Phee, L., Doumith, M., Hope, R., Woodford, N., and Wareham, D.W. (2015) Comparative virulence of urinary and bloodstream isolates of extra-intestinal pathogenic *Escherichia coli* in a *Galleria mellonella* model. *Virulence* **6**: 145–151.

Citiulo, F., Jacobsen, I.D., Miramón, P., Schild, L., Brunke, S., Zipfel, P., *et al.* (2012) *Candida albicans* scavenges host zinc via Pra1 during endothelial invasion. *PLoS Pathog* **8**.

Clow, L., Raftos, D., Gross, P.S., and Smith, L.C. (2004) The sea urchin complement homologue, SpC3, functions as an opsonin. *J Exp Biol* **207**: 2147–2155.

Coffelt, S.B., Waterman, R.S., Florez, L., Zu Bentrup, K.H., Zwezdaryk, K.J., Tomchuck, S.L., *et al.* (2008) Ovarian cancers overexpress the antimicrobial protein hCAP-18 and its derivative LL-37 increases ovarian cancer cell proliferation and invasion. *Int J Cancer* **122**: 1030–1039.

Coleman, J.J., Muhammed, M., Kasperkovitz, P. V., Vyas, J.M., and Mylonakis, E. (2011) Fusarium pathogenesis investigated using *Galleria mellonella* as a heterologous host. *Fungal Biol* **115**: 1279–1289.

Collins, C., Hurley, R., Almutlaqah, N., O'Keeffe, G., Keane, T.M., Fitzpatrick, D.A., and Owens, R.A. (2017) Proteomic Characterization of *Armillaria mellea* Reveals Oxidative Stress Response Mechanisms and Altered Secondary Metabolism Profiles. *Microorganisms* **5**: E60.

Colombo, A.L., Padovan, A.C.B., and Chaves, G.M. (2011) Current knowledge of *trichosporon* spp. and trichosporonosis. *Clin Microbiol Rev* **24**: 682–700.

Coméra, C., André, K., Laffitte, J., Collet, X., Galtier, P., and Maridonneau-Parini, I. (2007) Gliotoxin from *Aspergillus fumigatus* affects phagocytosis and the organization of the actin cytoskeleton by distinct signalling pathways in human neutrophils. *Microbes Infect* **9**: 47–54.

Constantino, M., Christian, P., Marina, C.F., and Williams, T. (2001) A comparison of techniques for detecting Invertebrate iridescent virus 6. *J Virol Methods* **98**: 109–118.

Cook, S.M., and McArthur, J.D. (2013) Developing *Galleria mellonella* as a model host for human pathogens. *Virulence* **4**: 350–3.

Cooper, D., and Eleftherianos, I. (2017b) Memory and specificity in the insect immune system: Current perspectives and future challenges. *Front Immunol* **8**: 539.

Cooper, M.D., and Alder, M.N. (2006) The evolution of adaptive immune systems. *Cell* **124**: 815–822.

Cornely, O.A., Bassetti, M., Calandra, T., Garbino, J., Kullberg, B.J., Lortholary, O., *et al.* (2012) ESCMID guideline for the diagnosis and management of *Candida* diseases 2012: Non-neutropenic adult patients. *Clin Microbiol Infect* **18**: 19–37.

Côté, R.G., Griss, J., Dianes, J.A., Wang, R., Wright, J.C., Toorn, H.W.P. van den, *et al.* (2012) The PRoteomics IDEntification (PRIDE) Converter 2 Framework: An Improved Suite of Tools to Facilitate Data Submission to the PRIDE Database and the ProteomeXchange Consortium. *Mol Cell Proteomics* **11**: 1682–1689.

Cotter, G., Doyle, S., and Kavanagh, K. (2000) Development of an insect model for the *in vivo* pathogenicity testing of yeasts. *FEMS Immunol Med Microbiol* **27**: 163–169.

Coughlan, C.A., Chotirmall, S.H., Renwick, J., Hassan, T., Low, T.B., Bergsson, G., *et al.* (2012) The Effect of *Aspergillus fumigatus* Infection on Vitamin D Receptor Expression in Cystic Fibrosis. *Am J Respir Crit Care Med* **186**: 999–1007.

Cox, J., Neuhauser, N., Michalski, A., Scheltema, R.A., Olsen, J. V., and Mann, M. (2011) Andromeda: A peptide search engine integrated into the MaxQuant environment. *J Proteome Res* **10**: 1794–1805.

Cytryńska, M., Mak, P., Zdybicka-Barabas, A., Suder, P., and Jakubowicz, T. (2007) Purification and characterization of eight peptides from *Galleria mellonella* immune hemolymph. *Peptides* **28**: 533–546.

D'Arcangelo, J.G., Stahmer, K.R., and Miller, E.A. (2013) Vesicle-mediated export from the ER: COPII coat function and regulation. *Biochim Biophys Acta - Mol Cell Res* **1833**: 2464–2472.

Dagenais, T.R.T., and Keller, N.P. (2009) Pathogenesis of *Aspergillus fumigatus* in invasive aspergillosis. *Clin Microbiol Rev* **22**: 447–465.

Dean, S.N., Bishop, B.M., and Hoek, M.L. Van (2011) Susceptibility of *Pseudomonas aeruginosa* biofilm to alpha-helical peptides: D-

enantiomer of LL-37. *Front Microbiol* **2**: 128–135.

Dennis, C.G., Greco, W.R., Brun, Y., Youn, R., Slocum, H.K., Bernacki, R.J., *et al.* (2006) Effect of amphotericin B and micafungin combination on survival, histopathology, and fungal burden in experimental aspergillosis in the p47 phox-/- mouse model of chronic granulomatous disease. *Antimicrob Agents Chemother* **50**: 422–427.

Desbois, A.P., and Coote, P.J. (2011) Wax moth larva (*Galleria mellonella*): An *in vivo* model for assessing the efficacy of antistaphylococcal agents. *J Antimicrob Chemother* **66**: 1785–1790.

Desbois, A.P., and Coote, P.J. (2012) Utility of greater wax moth larva (*Galleria mellonella*) for evaluating the toxicity and efficacy of new antimicrobial agents. *Adv Appl Microbiol* **78**: 25–53.

Deslyper, G., Colgan, T.J., Cooper, A.J.R., Holland, C. V., and Carolan, J.C. (2016) A Proteomic Investigation of Hepatic Resistance to Ascaris in a Murine Model. *PLoS Negl Trop Dis* **10**: e0004837.

Desoubeaux, G., and Cray, C. (2017) Rodent models of invasive aspergillosis due to *Aspergillus fumigatus*: Still a long path toward standardization. *Front Microbiol* **8**: 841-847.

Diago-Navarro, E., Chen, L., Passet, V., Burack, S., Ulacia-Hernando, A., Kodiyanplakkal, R.P., *et al.* (2014) Carbapenem-resistant *Klebsiella pneumoniae* exhibit variability in capsular polysaccharide and capsule associated virulence traits. *J Infect Dis* **210**: 803–813.

Dionne, M.S., and Schneider, D.S. (2008) Models of infectious diseases in the fruit fly *Drosophila melanogaster. Dis Model Mech* **1**: 43–49.

Donders, G.G.G., Ruban, K.S., Bellen, G., and Grinceviciene, S. (2018) Vulvovaginal candidosis. In *Diagnostics to Pathogenomics of Sexually Transmitted Infections* **4**: 232–249.

Doyle, S. (2011) Fungal proteomics: From identification to function. *FEMS Microbiol Lett* **321**: 1–9.

Dubovskiy, I., Kryukova, N., Glupov, V., and Ratcliffe, N. (2016) Encapsulation and nodulation in insects. *ISJ* **13**: 229–246.

Dubovskiy, I.M., Martemyanov, V. V., Vorontsova, Y.L., Rantala, M.J., Gryzanova, E. V., and Glupov, V. V. (2008) Effect of bacterial infection on antioxidant activity and lipid peroxidation in the midgut of *Galleria mellonella* L. larvae (Lepidoptera, Pyralidae). *Comp Biochem Physiol - C Toxicol Pharmacol* **148**: 1–5.

Dubuffet, A., Zanchi, C., Boutet, G., Moreau, J., Teixeira, M., and Moret, Y. (2015) Trans-generational Immune Priming Protects the Eggs Only against Gram-Positive Bacteria in the Mealworm Beetle. *PLoS Pathog* **11**: e1005178.

Dulon, M., Haamann, F., Peters, C., Schablon, A., and Nienhaus, A. (2011) Mrsa prevalence in european healthcare settings: A review. *BMC Infect Dis* **11**: 138.

Dürr, U.H.N., Sudheendra, U.S., and Ramamoorthy, A. (2006) LL-37, the only human member of the cathelicidin family of antimicrobial peptides. *Biochim Biophys Acta - Biomembr* .

Dziarski, R. (2004) Peptidoglycan recognition proteins (PGRPs). *Mol Immunol* **40**: 877–886.

Eisenman, H.C., and Casadevall, A. (2012) Synthesis and assembly of fungal melanin. *Appl Microbiol Biotechnol* **93**: 931–940.

Eisenman, H.C., Duong, R., Chan, H., Tsue, R., and McClelland, E.E. (2014) Reduced virulence of melanized *Cryptococcus neoformans* in *Galleria mellonella*. *Virulence* **5**:611–618.

Eissa, A., Amodeo, V., Smith, C.R., and Diamandis, E.P. (2011) Kallikrein-related Peptidase-8 (KLK8) Is an Active Serine Protease in Human Epidermis and Sweat and Is Involved in a Skin Barrier Proteolytic Cascade. **286**: 687–706.

Eleftherianos, I., and Revenis, C. (2011) Role and importance of phenoloxidase in insect hemostasis. *J Innate Immun* **3**: 28–33.

Elkon, K.B., and Rhiannon, J.J. (2012) Innate immunity. In *Scleroderma:* From Pathogenesis to Comprehensive Management. pp. 191–197.

Epstein, F.H., and Weiss, S.J. (1989) Tissue Destruction by Neutrophils. *N Engl J Med* **320**: 365–376.

Ertürk-Hasdemir, D., Broemer, M., Leulier, F., Lane, W.S., Paquette, N., Hwang, D., *et al.* (2009) Two roles for the *Drosophila* IKK complex in the activation of Relish and the induction of antimicrobial peptide genes. *Proc Natl Acad Sci U S A* **106**: 9779–84.

Eshwika, A., Kelly, J., Fallon, J.P., and Kavanagh, K. (2013) Exposure of *Aspergillus fumigatus* to caspofungin results in the release, and de novo biosynthesis, of gliotoxin. *Med Mycol* **51**: 121–7.

Evans, B.A., and Rozen, D.E. (2012) A *Streptococcus pneumoniae* infection model in larvae of the wax moth *Galleria mellonella*. *Eur J Clin Microbiol Infect Dis* **31**: 2653–2660.

Evans, E.W., and Harmon, B.G. (1995) A Review of Antimicrobial Peptides: Defensins and Related Cationic Peptides. *Vet Clin Pathol* **24**: 109–116.

Fahal, A., Suliman, S., and Hay, R. (2018) Mycetoma: The Spectrum of Clinical Presentation. *Trop Med Infect Dis* **3**: 97.

Di Falco, M.R. (2018) Mass spectrometry-based proteomics. In *Methods in Molecular Biology* **1775**: 93–106.

Fallon, J.P., Reeves, E.P., and Kavanagh, K. (2010) Inhibition of neutrophil function following exposure to the *Aspergillus fumigatus* toxin fumagillin. *J Med Microbiol* **59**: 625–633.

Fallon, J.P., Reeves, E.P., and Kavanagh, K. (2011a) The *Aspergillus fumigatus* toxin fumagillin suppresses the immune response of *Galleria mellonella* larvae by inhibiting the action of haemocytes. *Microbiology* **157**: 1481–1488.

Fallon, J.P., Troy, N., and Kavanagh, K. (2011b) Pre-exposure of *Galleria mellonella* larvae to different doses of *Aspergillus fumigatus* conidia causes differential activation of cellular and humoral immune responses. *Virulence* **2**: 413–421.

Fanos, V., and Cataldi, L. (2014) Amphotericin B-Induced Nephrotoxicity: A Review. *J Chemother* **12**: 463–470.

Faruck, M.O., Yusof, F., and Chowdhury, S. (2016) An overview of antifungal peptides derived from insect. *Peptides* **80**: 80–88.

Findlay, G.H., and Vismer, H.F. (1974) Black grain mycetoma. A study of the chemistry, formation and significance of the tissue grain in *Madurella mycetomi* infection. *Br J Dermatol* **91(3):** 297–303.

Flajnik, M.F., and Kasahara, M. (2010) Origin and evolution of the adaptive immune system: Genetic events and selective pressures. *Nat Rev Genet* **11**: 47–59.

Forastiero, A., Mesa-Arango, A.C., Alastruey-Izquierdo, A., Alcazar-Fuoli, L., Bernal-Martinez, L., Pelaez, T., *et al.* (2013) *Candida tropicalis* antifungal cross-resistance is related to different azole target (Erg11p) modifications. *Antimicrob Agents Chemother* **57**: 4760–4781.

Fraczek, M.G., Bromley, M., and Bowyer, P. (2011) An improved model of the *Aspergillus fumigatus* CYP51A protein. *Antimicrob Agents Chemother* **55**: 2483–2486.

Fradin, C., Kretschmar, M., Nichterlein, T., Gaillardin, C., D'Enfert, C., and Hube, B. (2003) Stage-specific gene expression of *Candida albicans* in human blood. *Mol Microbiol* **47**: 1523–1543.

Fuchs, B.B., Li, Y., Li, D., Johnston, T., Hendricks, G., Li, G., *et al.* (2016) Micafungin Elicits an Immunomodulatory Effect in *Galleria mellonella* and Mice. *Mycopathologia* **181**: 17–25.

Fuchs, B.B., O'Brien, E., Khoury, J.B. El, and Mylonakis, E. (2010) Methods for using *Galleria mellonella* as a model host to study fungal pathogenesis. *Virulence* **1**: 475–482.

Funk, J., Schaarschmidt, B., Slesiona, S., Hallström, T., Horn, U., and Brock, M. (2016) The glycolytic enzyme enolase represents a plasminogen-binding protein on the surface of a wide variety of medically important fungal species. *Int J Med Microbiol* **306**: 59–68.

G, Putsep. H.G, Boman. M, Andersson. M., Carlsson, K. (2002) Deficiency of Antibacterial Peptides in Patients With Morbus Kotsmann: an Observation Study. *Lancet* **360**: 1144–1149.

Gago, S., García-Rodas, R., Cuesta, I., Mellado, E., and Alastruey-Izquierdo, A. (2014) *Candida parapsilosis*, *Candida orthopsilosis*,and *Candida metapsilosis* virulence in the non-conventional host *Galleria mellonella*. *Virulence* **5**: 1–8.

Gallagher, L., Owens, R.A., Dolan, S.K., O'Keeffe, G., Schrettl, M., Kavanagh, K., *et al.* (2012) The *Aspergillus fumigatus* protein gliK protects against oxidative stress and is essential for gliotoxin biosynthesis. *Eukaryot Cell* **11**: 1226–1238.

Gallo, R.L., Murakami, M., Ohtake, T., and Zaiou, M. (2002) Biology and clinical relevance of naturally occurring antimicrobial peptides. *J Allergy Clin Immunol* **110**: 823–831.

Gandhe, A.S., Janardhan, G., and Nagaraju, J. (2007a) Immune upregulation of novel antibacterial proteins from silkmoths (Lepidoptera) that resemble lysozymes but lack muramidase activity. *Insect Biochem Mol Biol* **37**: 655–666.

Gandhe, A.S., John, S.H., and Nagaraju, J. (2007b) Noduler, a novel immune up-regulated protein mediates nodulation response in insects. *J Immunol* **179**: 6943–51.

Ganesan, S., Aggarwal, K., Paquette, N., and Silverman, N. (2011) Nf-κB/Rel proteins and the humoral immune responses of *Drosophila melanogaster. Curr Top Microbiol Immunol* **349**: 25–60.

Gangneux, J.P., Camus, C., and Philippe, B. (2010) Epidemiology of invasive aspergillosis and risk factors in non neutropaenic patients. *Rev Mal Respir* **27**.

Ganz, T. (2003) Defensins: Antimicrobial peptides of innate immunity. *Nat Rev Immunol* **3**: 710–720.

Garzon, S., Charpentier, G., and Kurstak, E. (1978) Morphogenesis of the Nodamura virus in the larvae of the lepidopteran *Galleria mellonella* (L.). *Arch Virol* **56**: 61–76.

Geraghty, P., and Kavanagh, K. (2003) Disruption of mitochondrial function in *Candida albicans* leads to reduced cellular ergosterol levels and elevated growth in the presence of amphotericin B. *Arch Microbiol* .

Gil-Navarro, I., Gil, M.L., Casanova, M., O'Connor, J.E., Martínez, J.P., and Gozalbo, D. (1997) The glycolytic enzyme glyceraldehyde-3-phosphate dehydrogenase of *Candida albicans* is a surface antigen. *J Bacteriol* **179**: 4992–4999.

Gillespie and, J.P., Kanost, M.R., and Trenczek, T. (1997) Biological Mediators Of Insect Immunity. *Annu Rev Entomol* **42**: 611–643.

Gillespie, J.P., Bailey, A.M., Cobb, B., and Vilcinskas, A. (2000) Fungi as elicitors of insect immune responses. *Arch Insect Biochem Physiol* **44**: 49–68.

Gomez-Lopez, A., Forastiero, A., Cendejas-Bueno, E., Gregson, L., Mellado, E., Howard, S.J., *et al.* (2014) An invertebrate model to evaluate virulence in *Aspergillus fumigatus*: The role of azole resistance. *Med Mycol* **52**: 311–319.

Gonzales, P.R., Pesesky, M.W., Bouley, R., Ballard, A., Biddy, B.A., Suckow, M.A., *et al.* (2015) Synergistic, collaterally sensitive β-lactam combinations suppress resistance in MRSA. *Nat Chem Biol* **11**: 855–861.

Gottardi, W., Debabov, D., and Nagl, M. (2013) N-chloramines, A promising class of well-tolerated topical anti-infectives. *Antimicrob Agents Chemother* **57**: 1107–1114.

Gottardi, W., and Nagl, M. (2005) Chlorine covers on living bacteria: The initial step in antimicrobial action of active chlorine compounds. *J Antimicrob Chemother* **55**: 475–482.

Gottardi, W., and Nagl, M. (2010) N-chlorotaurine, a natural antiseptic with outstanding tolerability. *J Antimicrob Chemother* **65**: 399–409.

Gottardi, W., and Nagl, M. (2013) Active halogen compounds and proteinaceous material: Loss of activity of topical anti-infectives by halogen consumption. *J Pharm Pharmacol* **65**: 213–218.

Govind, S. (2008) Innate immunity in *Drosophila*: Pathogens and pathways. *Insect Sci* **15**: 29–43.

Grabińska, K., and Palamarczyk, G. (2002) Dolichol biosynthesis in the yeast *Saccharomyces cerevisiae:* An insight into the regulatory role of farnesyl diphosphate synthase. *FEMS Yeast Res* **2**: 259–265.

Green, D.S., Colgan, T.J., Thompson, R.C., and Carolan, J.C. (2019) Exposure to microplastics reduces attachment strength and alters the haemolymph proteome of blue mussels (Mytilus edulis). *Environ Pollut* 423–434.

Griesch, J., Wedde, M., and Vilcinskas, A. (2000) Recognition and regulation of metalloproteinase activity in the haemolymph of *Galleria mellonella*: A new pathway mediating induction of humoral immune responses. *Insect Biochem Mol Biol* **30**: 461–472.

Grisham, M.B., Jefferson, M.M., Melton, D.F., and Thomas, E.L. (1984) Chlorination of endogenous amines by isolated neutrophils. Ammonia-dependent bactericidal, cytotoxic, and cytolytic activities of the chloramines. *J Biol Chem* **259**: 10404–10413.

Gruber, M., Moser, I., Nagl, M., and Lackner, M. (2017) Bactericidal and fungicidal activity of N-Chlorotaurine is enhanced in cystic fibrosis sputum medium. *Antimicrob Agents Chemother* **61**: e02527-16.

Gu, W., Yu, Q., Yu, C., and Sun, S. (2018) *In vivo* activity of fluconazole/tetracycline combinations in *Galleria mellonella* with resistant *Candida albicans* infection. *J Glob Antimicrob Resist* **13**: 74–80.

Guerra, F.E., Borgogna, T.R., Patel, D.M., Sward, E.W., and Voyich, J.M. (2017) Epic Immune Battles of History: Neutrophils vs. *Staphylococcus aureus*. *Front Cell Infect Microbiol* **7**: 286.

Gyurko, C., Lendenmann, U., Troxler, R.F., and Oppenheim, F.G. (2000) *Candida albicans* mutants deficient in respiration are resistant to the small cationic salivary antimicrobial peptide histatin 5. *Antimicrob Agents Chemother* **44**: 348–354.

Halwani, A.E., Niven, D.F., and Dunphy, G.B. (2000) Apolipophorin-III and the interactions of lipoteichoic acids with the immediate immune responses of *Galleria mellonella*. *J Invertebr Pathol* **76**: 233–241.

Hamamoto, H., Tonoike, A., Narushima, K., Horie, R., and Sekimizu, K. (2009) Silkworm as a model animal to evaluate drug candidate toxicity and metabolism. *Comp Biochem Physiol - C Toxicol Pharmacol* **149**: 334–339.

Hara, S., and Yamakawa, M. (1995) Moricin, a novel type of antibacterial peptide isolated from the silkworm, *Bombyx mori*. *J Biol Chem* **270**: 29923–29927.

Harding, C.R., Schroeder, G.N., Reynolds, S., Kosta, A., Collins, J.W., Mousnier, A., and Frankel, G. (2012) *Legionella pneumophila* pathogenesis in the *Galleria mellonella* infection model. *Infect Immun* **80**: 2780–2790.

Harding, C.R., Stoneham, C.A., Schuelein, R., Newton, H., Oates, C. V., Hartland, E.L., *et al.* (2013) The Dot/Icm Effector SdhA Is Necessary for Virulence of *Legionella pneumophila* in *Galleria mellonella* and A/J Mice. *Infect Immun* **81**: 2598–2605.

Harriott, M.M., and Noverr, M.C. (2009) *Candida albicans* and *Staphylococcus aureus* form polymicrobial biofilms: Effects on antimicrobial resistance. *Antimicrob Agents Chemother* **53**: 3914–3922.

Hartleib, R.J., Kö, N., Dickinson, R.B., Chhatwal, G.S., Sixma, J.J., Hartford, O.M., *et al.* (2000) Protein A is the von Willebrand factor binding protein on *Staphylococcus aureus*. *Blood* **96**: 2149–56.

Haussen, J. Von, Koczulla, R., Shaykhiev, R., Herr, C., Pinkenburg, O., Reimer, D., *et al.* (2008) The host defence peptide LL-37/hCAP-18 is a growth factor for lung cancer cells. *Lung Cancer* **59**: 12–23.

Hawkey, P.M., and Livermore, D.M. (2012) Carbapenem antibiotics for serious infections. *BMJ* **344**: e3236.

Hebecker, B., Naglik, J.R., Hube, B., and Jacobsen, I.D. (2014) Pathogenicity mechanisms and host response during oral *Candida albicans* infections. *Expert Rev Anti Infect Ther* **12**: 867–879.

Hedayati, M.T., Pasqualotto, A.C., Warn, P.A., Bowyer, P., and Denning, D.W. *Aspergillus flavus*: Human pathogen, allergen and mycotoxin producer. *Microbiology* **153**: 1677–1692.

Heilborn, J.D., Nilsson, M.F., Chamorro Jimenez, C.I., Sandstedt, B., Borregaard, N., Tham, E., *et al.* (2005) Antimicrobial protein hCAP18/LL-37 is highly expressed in breast cancer and is a putative growth factor for epithelial cells. *Int J Cancer* **114**: 713–719.

Heitmueller, M., Billion, A., Dobrindt, U., Vilcinskas, A., and Mukherjee, K. (2017) Epigenetic mechanisms regulate innate immunity against uropathogenic and commensal-like *Escherichia coli* in the surrogate insect model *Galleria mellonella*. *Infect Immun* **85**.

Hertog, A.L. Den, Marle, J. Van, Veerman, E.C.I., Valentijn-Benz, M., Nazmi, K., Kalay, H., *et al.* (2006) The human cathelicidin peptide LL-37 and truncated variants induce segregation of lipids and proteins in the plasma membrane of *Candida albicans*. In *Biological Chemistry*. pp. 1495–1502.

Hoffmann, J.A. (1995) Innate immunity of insects. *Curr Opin Immunol* **7**: 4–10.

Hohl, T.M. (2014) Overview of vertebrate animal models of fungal infection. *J Immunol Methods* **410**: 100–112.

Hohl, T.M., Epps, H.L. Van, Rivera, A., Morgan, L.A., Chen, P.L., Feldmesser, M., and Pamer, E.G. (2005) *Aspergillus fumigatus* triggers inflammatory responses by stage-specific β-glucan display. *PLoS Pathog* **1**: 0232–0240.

Hornbach, A., Heyken, A., Schild, L., Hube, B., Löffler, J., and Kurzai, O. (2009) The glycosylphosphatidylinositol-anchored protease Sap9 modulates the interaction of *Candida albicans* with human neutrophils. *Infect Immun* **77**: 5216–5224.

Hornsey, M., and Wareham, D.W. (2011) *In vivo* efficacy of glycopeptide-colistin combination therapies in a *Galleria mellonella* model of *Acinetobacter baumannii* infection. *Antimicrob Agents Chemother* **55**: 3534–3537.

Hultmark, D. (1996) Insect lysozymes. *EXS* **75**: 87–102.

Hynes, R.O., and Zhao, Q. (2000) The evolution of cell adhesion. *J Cell Biol* **150**: F89-96.

Ibrahim, A.I., Hassan, A.M. El, Fahal, A., and Sande, W.W. van de (2013) A Histopathological Exploration of the *Madurella mycetomatis* Grain. *PLoS One* **8**.

Imler, J.-L. (2003) Biology of Toll receptors: lessons from insects and mammals. *J Leukoc Biol* **75**: 18–26.

Ishii, M., Matsumoto, Y., and Sekimizu, K. (2015) Usefulness of silkworm as a model animal for understanding the molecular mechanisms of fungal pathogenicity. *Drug Discov Ther* **9**: 234–237.

Ito, Y., Nakamura, M., Hotani, T., and Imoto, T. (1995) Insect lysozyme from house fly (*Musca domestica*) larvae: Possible digestive function based on sequence and enzymatic properties. *J Biochem* **118**: 546–551.

Jackson, J.C., Higgins, L.A., and Lin, X. (2009) Conidiation color mutants of *Aspergillus fumigatus* are highly pathogenic to the heterologous insect host *Galleria mellonella*. *PLoS One* **4(1)**: e4224.

Jacobs, A.C., Thompson, M.G., Black, C.C., Kessler, J.L., Clark, L.P., McQueary, C.N., *et al.* (2014) AB5075, a highly virulent isolate of *Acinetobacter baumannii*, as a model strain for the evaluation of pathogenesis and antimicrobial treatments. *MBio* **5**: e01076-14.

Jacobsen, I.D. (2014) *Galleria mellonella* as a model host to study virulence of *Candida. Virulence* **5**: 237–9.

Jacobsen, I.D., Große, K., Berndt, A., and Hube, B. (2011) Pathogenesis of *candida albicans* infections in the alternative chorio-allantoic membrane chicken embryo model resembles systemic murine infections. *PLoS One* **6**: e19741.

Jacobsen, I.D., Große, K., Slesiona, S., Hube, B., Berndt, A., and Brock, M. (2010) Embryonated eggs as an alternative infection model to investigate *Aspergillus fumigatus* virulence. *Infect Immun* **78**: 2995–3006.

Jafri, R.H., and Chaudhry, M.B. (1971) Development of Tipula iridescent virus (TIV) in *Galleria mellonella* larvae exposed to gamma radiation. *J Invertebr Pathol* **18**: 46–50.

Jander, G., Rahme, L.G., and Ausubel, F.M. (2000) Positive correlation between virulence of *Pseudomonas aeruginosa* mutants in mice and insects. *J Bacteriol* **182**: 3843–3845.

Jensen, J.U.S., Hein, L.H., Lundgren, B., Bestle, M.H., Mohr, T., Andersen, M.H., *et al.* (2015) Invasive *Candida* infections and the harm from antibacterial drugs in critically ill patients: Data from a randomized, controlled trial to determine the role of ciprofloxacin, piperacillin-tazobactam, meropenem, and cefuroxime. *Crit Care Med* **43**: 594–602.

Jensen, L.J., Kuhn, M., Stark, M., Chaffron, S., Creevey, C., Muller, J., *et al.* (2009) STRING 8 - A global view on proteins and their functional interactions in 630 organisms. *Nucleic Acids Res* **37**: D412–416.

Ji, P., Zhou, Y., Yang, Y., Wu, J., Zhou, H., Quan, W., *et al.* (2019) Myeloid cell-derived LL-37 promotes lung cancer growth by activating Wnt/β-catenin signaling. *Theranostics* **9(8)**: 2209–2223.

Jia, C., Tsai, -Yun, Mei, J., Loh, S., and Proft, T. (2016) *Galleria mellonella* infection models for the study of bacterial diseases and for antimicrobial drug testing. *Virulence* **7**: 214–29.

Jiao, D., Wong, C., Tsang, M.S., Chu, I.M., Liu, D., Zhu, J., *et al.* (2017) Activation of Eosinophils Interacting with Bronchial Epithelial Cells by Antimicrobial Peptide LL-37 : Implications in Allergic Asthma. *Sci Rep* **4:** 1–13.

Johnson, M.D., and Perfect, J.R. (2010) Use of antifungal combination therapy: Agents, order, and timing. *Curr Fungal Infect Rep* **4**: 87–95.

Johnston, M.D., Hanlon, G.W., Denyer, S.P., and Lambert, R.J.W. (2003) Membrane damage to bacteria caused by single and combined biocides. *J Appl Microbiol* **94**: 1015–1023.

Jong, A.Y., Chen, S.H.M., Stins, M.F., Kim, K.S., Tuan, T.L., and Huang, S.H. (2003) Binding of *Candida albicans* enolase to plasmin(ogen) results in enhanced invasion of human brain microvascular endothelial cells. *J Med Microbiol* **52**: 615–622.

Jongerius, I., Köhl, J., Pandey, M.K., Ruyken, M., Kessel, K.P.M. van, Strijp, J.A.G. van, and Rooijakkers, S.H.M. (2007) Staphylococcal complement evasion by various convertase-blocking molecules. *J Exp Med* **204**: 2461–2471.

Joop, G., and Vilcinskas, A. (2016) Coevolution of parasitic fungi and insect hosts. *Zoology* **119(4)**:350–358.

Jorjão, A.L., Oliveira, L.D., Scorzoni, L., Figueiredo-Godoi, L.M.A., Prata, M.C.A., Jorge, A.O.C., and Junqueira, J.C. (2018) From moths to caterpillars: Ideal conditions for *Galleria mellonella* rearing for *in vivo* microbiological studies. *Virulence* 9(1): 383–389.

Joyce, S.A., and Gahan, C.G.M. (2010) Molecular pathogenesis of Listeria monocytogenes in the alternative model host *Galleria mellonella*. *Microbiology* **156**: 3456–3468.

Kaito, C., Akimitsu, N., Watanabe, H., and Sekimizu, K. (2002) Silkworm larvae as an animal model of bacterial infection pathogenic to humans. *Microb Pathog* **32**: 183–190.

Kanost, M.R. (1999) Serine proteinase inhibitors in arthropod immunity. *Dev Comp Immunol* **23**: 291–301.

Kanost, M.R., Jiang, H., and Yu, X.Q. (2004) Innate immune responses of a lepidopteran insect, *Manduca sexta*. *Immunol Rev* **198**: 97–105.

Kavanagh, K., and Reeves, E.P. (2004) Exploiting the potential of insects for *in vivo* pathogenicity testing of microbial pathogens. *FEMS Microbiol Rev* **28**: 101–112.

Kean, R., Rajendran, R., Haggarty, J., Townsend, E.M., Short, B., Burgess, K.E., *et al.* (2017) *Candida albicans* mycofilms support *Staphylococcus aureus* colonization and enhances miconazole resistance in dual-species interactions. *Front Microbiol* **8**: 258.

Kelly, J., and Kavanagh, K. (2010) Proteomic analysis of proteins released from growth-arrested *Candida albicans* following exposure to caspofungin. *Med Mycol* **48**: 598–605.

Kelly, J., and Kavanagh, K. (2011) Caspofungin primes the immune response of the larvae of *Galleria mellonella* and induces a non-specific antimicrobial response. *J Med Microbiol* **60**: 189–196.

Kemp, M.W., and Massey, R.C. (2007) The use of insect models to study human pathogens. *Drug Discov Today Dis Model* **4**: 105–110.

Kesavalu, L., Sathishkumar, S., Bakthavatchalu, V., Matthews, C., Dawson, D., Steffen, M., and Ebersole, J.L. (2007) Rat model of polymicrobial infection, immunity, and alveolar bone resorption in periodontal disease. *Infect Immun* **4**: 1704–1712.

Kim, C.H., Lee, J.H., Kim, I., Seo, S.J., Son, M.S., Lee, K.Y., and Lee, I.H. (2004) Purfication and cDNA Cloning of a Cecropin-like Peptide from the Great Wax Moth, *Galleria mellonella. Mol Cells* **17**: 262–266.

Kirkpatrick, C.H., and Hill, H.R. (2001) Chronic mucocutaneous candidiasis. *Pediatr Infect Dis J* **20(2)**:197–206.

Klebanoff, S.J. (2005) Myeloperoxidase: friend and foe. *J Leukoc Biol* **77**: 598–625.

Kleino, A., and Silverman, N. (2014) The *Drosophila* IMD pathway in the activation of the humoral immune response. *Dev Comp Immunol* **42**: 25–35.

Klerk, N. De, Vogel, C. De, Fahal, A., Belkum, A. Van, and Sande, W.W.J. Van De (2012) Fructose-bisphosphate aldolase and pyruvate kinase, two novel immunogens in *Madurella mycetomatis. Med Mycol* **50**: 143–151.

Kloezen, W., Helvert-van Poppel, M. van, Fahal, A.H., and Sande, W.W.J. van de (2015) A *madurella mycetomatis* grain model in *Galleria mellonella* larvae. *PLoS Negl Trop Dis* **9**: 1–14.

Kloezen, W., Parel, F., Brüggemann, R., Asouit, K., Helvert-van Poppel, M., Fahal, A., *et al.* (2017) Amphotericin B and terbinafine but not the azoles prolong survival in *Galleria mellonella* larvae infected with *Madurella mycetomatis*. *Med Mycol* **1**: 469–478.

Klotz, S.A., Chasin, B.S., Powell, B., Gaur, N.K., and Lipke, P.N. (2007) Polymicrobial bloodstream infections involving *Candida* species: analysis of patients and review of the literature. *Diagn Microbiol Infect Dis* **59**: 401–406.

Kobayashi, S.D., Malachowa, N., and Deleo, F.R. (2015) Pathogenesis of *Staphylococcus aureus* abscesses. *Am J Pathol* **185**: 1518–1527.

Koczulla, R., Degenfeld, G. Von, Kupatt, C., Krötz, F., Zahler, S., Gloe, T., *et al.* (2003) An angiogenic role for the human peptide antibiotic LL-37 / hCAP-18. **111**: 1665–1672.

Kong, E.F., Tsui, C., Kucharíková, S., Andes, D., Dijck, P. Van, and Jabra-Rizk, M.A. (2016) Commensal Protection of *Staphylococcus aureus* against Antimicrobials by *Candida albicans* Biofilm Matrix. *MBio* **7**: e01365-16

Kong, E.F., Tsui, C., Kucharíková, S., Dijck, P. Van, and Jabra-Rizk, M.A. (2017) Modulation of *Staphylococcus aureus* Response to Antimicrobials by the *Candida albicans* Quorum Sensing Molecule Farnesol. *Antimicrob Agents Chemother* **61**: e01573-17.

Krezdorn, J., Adams, S., and Coote, P.J. (2014) A *Galleria mellonella* infection model reveals double and triple antibiotic combination therapies with enhanced efficacy versus a multidrug-resistant strain of *Pseudomonas aeruginosa*. *J Med Microbiol* **63**: 945–955.

Kronenberg, F., and Heller, H.C. (1982) Colonial thermoregulation in honey bees (Apis mellifera). *J Comp Physiol B* **148**: 65–76.

Krüger, W., Vielreicher, S., Kapitan, M., Jacobsen, I.D., and Niemiec, M.J. (2019) Fungal-Bacterial Interactions in Health and Disease. *Pathogens* **8:** E70.

Kumagai, T., Nagata, T., Kudo, Y., Fukuchi, Y., Ebina, K. & Yokota, K. (1999) Cytotoxic activity and cytokine gene induction of Asp-hemolysin to murine macrophages. *Japanese J Med Mycol* **40**: 217–222.

Kumar, R., Breindel, C., Saraswat, D., Cullen, P.J., and Edgerton, M. (2017) *Candida albicans* Sap6 amyloid regions function in cellular aggregation and zinc binding, and contribute to zinc acquisition. *Sci Rep* **7**: 2908.

Lackner, M., Binder, U., Reindl, M., Gönül, B., Fankhauser, H., Mair, C., and Nagl, M. (2015) N-Chlorotaurine exhibits fungicidal activity against therapy-refractory *Scedosporium* species and *Lomentospora prolificans. Antimicrob Agents Chemother* **59**: 6454–6462.

Lacorte Singulani, J. de, Scorzoni, L., Paula e Silva, A.C.A. de, Fusco-Almeida, A.M., and Mendes-Giannini, M.J.S. (2016) Evaluation of the efficacy of antifungal drugs against *Paracoccidioides brasiliensis* and *Paracoccidioides lutzii* in a *Galleria mellonella* model. *Int J Antimicrob Agents* **48**: 292–297.

Lai, Y., and Gallo, R.L. (2009) AMPed up immunity: how antimicrobial peptides have multiple roles in immune defense. *Trends Immunol* **30**: 131–141.

Lange, A., Beier, S., Huson, D.H., Parusel, R., Iglauer, F., and Frick, J.-S. (2018) Genome Sequence of *Galleria mellonella* (Greater Wax Moth). *Genome Announc* **6**: e01220-17.

Larrick, J.W., Lee, J., Ma, S., Li, X., Francke, U., and Wright, S.C. (1996) Structural, functional analysis and localization of the human CAP18 gene. **398**: 74–80.

Lazzarini, C., Esposto, M.C., Prigitano, A., Cogliati, M., Lorenzis, G. De, and Tortorano, A.M. (2016) Azole resistance in *Aspergillus*

fumigatus clinical isolates from an italian culture collection. *Antimicrob Agents Chemother* **60**: 682–685.

Lebedinets, N.N., Tsarichkova, D.B., Karpenko, L. V, Kononko, A.G., and Buchatskii, L.P. (1978) Analysis Of The Effects Of The Mosquito *Aedes-Aegypti Densonucleosis* Virus On Pre Imaginal Stages Of Different Species Of Blood Sucking Mosquitoes. *Mikrobiol Zhurnal* **40**: 352–356.

Lebreton, F., Bras, F. Le, Reffuveille, F., Ladjouzi, R., Giard, J.C., Leclercq, R., and Cattoir, V. (2012) *Galleria mellonella* as a-Model for studying *Enterococcus faecium* host persistence. *J Mol Microbiol Biotechnol* **21**: 191–196.

Lee, C., Sun, Y., Qian, S., and Huang, H.W. (2011) Transmembrane Pores Formed by Human Antimicrobial Peptide LL-37. *Biophysj* **100**: 1688–1696.

Lee, E., Jeong, K.W., Lee, J., Shin, A., Kim, J.K., Lee, J., *et al.* (2013) Structure-activity relationships of cecropin-like peptides and their interactions with phospholipid membrane. *BMB Rep* **46**: 282–287.

Lee, E., Shin, A., and Kim, Y. (2015) Anti-inflammatory activities of cecropin A and its mechanism of action. *Arch Insect Biochem Physiol* **88**: 31–44.

Lee, J., and Lee, D.G. (2014) Antimicrobial peptides (AMPs) with dual mechanisms: Membrane disruption and apoptosis. *J Microbiol Biotechnol* **25**: 759–764.

Lee, J.D., and Kolattukudy, P.E. (1995) Molecular Cloning of the cDNA and Gene for an Elastinolytic Aspartic Proteinase from *Aspergillus fumigatus* and Evidence of Its Secretion by the Fungus during Invasion of the Host Lung. *Infect Immun* **63**: 3796–3803.

Lee, L.Y.L., Höök, M., Haviland, D., Wetsel, R.A., Yonter, E.O., Syribeys, P., *et al.* (2004a) Inhibition of Complement Activation by a Secreted *Staphylococcus aureus* Protein. *J Infect Dis* **190**: 571–579.

Lee, Y.S., Yun, E.K., Jang, W.S., Kim, I., Lee, J.H., Park, S.Y., *et al.* (2004b) Purification, cDNA cloning and expression of an insect defensin from the great wax moth, *Galleria mellonella*. *Insect Mol Biol* **13**: 65–72.

Leger, R.J. St., Screen, S.E., and Shams-Pirzadeh, B. (2000) Lack of host specialization in *Aspergillus flavus*. *Appl Environ Microbiol* **66**: 320–324.

Lemaitre, B., and Hoffmann, J. (2007) The Host Defense of *Drosophila melanogaster. Annu Rev Immunol* **25**: 697–743.

Leonardi, M.S., Crespo, E.A., Raga, J.A., and Fernández, M. (2012) Scanning electron microscopy of *Antarctophthirus microchir* (*Phthiraptera: Anoplura: Echinophthiriidae*): Studying morphological adaptations to aquatic life. *Micron* **43**: 929–936.

Lessing, F., Kniemeyer, O., Wozniok, I., Loeffler, J., Kurzai, O., Haertl, A., and Brakhage, A.A. (2007) The *Aspergillus fumigatus* Transcriptional Regulator AfYap1 Represents the Major Regulator for Defense against Reactive Oxygen Intermediates but Is Dispensable for Pathogenicity in an Intranasal Mouse Infection Model. *Eukaryot Cell* **6**: 2290–2302.

Levitz, S.M., and Diamond, R.D. (1985) Mechanisms of resistance of *Aspergillus fumigatus* conidia to killing by neutrophils *in vitro*. *J Infect Dis* **152**: 33–42.

Lewis, J.G., Learmonth, R.P., and Watson, K. (1995) Induction of heat, freezing and salt tolerance by heat and salt shock in *Saccharomyces cerevisiae*. *Microbiology* **141**: 687–694.

Li, D., Scherfer, C., Korayem, A.M., Zhao, Z., Schmidt, O., and Theopold, U. (2002a) Insect hemolymph clotting: Evidence for interaction between the coagulation system and the prophenoloxidase activating cascade. *Insect Biochem Mol Biol* **32**: 919–928.

Li, N., Yamasaki, K., Saito, R., Shimada-omori, R., Aiba, S., and Alerts, E. (2014) Alarmin Function of Cathelicidin Antimicrobial Peptide LL37 through IL-36 γ Induction in Human Epidermal Keratinocytes. *J Immunol* **193**: 5140–5148.

Li, X.S., Reddy, M.S., Baev, D., and Edgerton, M. (2003) *Candida albicans* Ssa1/2p is the cell envelope binding protein for human salivary histatin 5. *J Biol Chem* **278**: 28553–28561.

Li, Y. (2005) Structure-based Functional Analysis Reveals a Role for the SM Protein Sly1p in Retrograde Transport to the Endoplasmic Reticulum. *Mol Biol Cell* **16**: 3951–3962.

Li, Y., Karlin, A., Loike, J.D., and Silverstein, S.C. (2002b) A critical concentration of neutrophils is required for effective bacterial killing in suspension. *Proc Natl Acad Sci* **99**: 8289–8294.

Lillie, S.H., and Pringle, J.R. (1980) Reserve carbohydrate metabolism in *Saccharomyces cerevisiae*: responses to nutrient limitation. *J Bacteriol* **143**: 1384–1394.

Lim, W., Melse, Y., Konings, M., Phat Duong, H., Eadie, K., Laleu, B., *et al.* (2018) Addressing the most neglected diseases through an open research model: The discovery of fenarimols as novel drug candidates for eumycetoma. *PLoS Negl Trop Dis* **12**: e0006437.

Lindgren, M., Riazi, R., Lesch, C., Wilhelmsson, C., Theopold, U., and Dushay, M.S. (2008) Fondue and transglutaminase in the *Drosophila* larval clot. *J Insect Physiol* **54**: 586–592.

Lionakis, M.S., Lim, J.K., Lee, C.-C.R., and Murphy, P.M. (2011) Organ-Specific Innate Immune Responses in a Mouse Model of Invasive Candidiasis. *J Innate Immun* **3**: 180–199.

Liu, Z.G. (2005) Molecular mechanism of TNF signaling and beyond. *Cell Res* **15**: 24–27.

Loeb, J.M., Hendee, W.R., Smith, S.J., and Schwarz, M.R. (1989) Human vs Animal Rights. *JAMA* **262**: 2716.

London, R., Orozco, B.S., and Mylonakis, E. (2006) The pursuit of cryptococcal pathogenesis: Heterologous hosts and the study of cryptococcal host-pathogen interactions. *FEMS Yeast Res* **6**: 567–573.

López Hernández, Y., Yero, D., Pinos-Rodríguez, J.M., and Gibert, I. (2015) Animals devoid of pulmonary system as infection models in the study of lung bacterial pathogens. *Front Microbiol* **6**.

Lowy, F.D. (1998) *Staphylococcus aureus* Infections. *N Engl J Med* **339**: 520–532.

Lu, A., Zhang, Q., Zhang, J., Yang, B., Wu, K., Xie, W., *et al.* (2014) Insect prophenoloxidase: The view beyond immunity. *Front Physiol* **11;5:252.**: 5.

Lu, X.M., Jin, X.B., Zhu, J.Y., Mei, H.F., Ma, Y., Chu, F.J., *et al.* (2010) Expression of the antimicrobial peptide cecropin fused with human lysozyme in *Escherichia coli*. *Appl Microbiol Biotechnol* **87**: 2169–2176.

Luo, X.L., Li, J.X., Huang, H.R., Duan, J.L., Dai, R.X., Tao, R.J., *et al.* (2019) LL37 Inhibits *Aspergillus fumigatus* Infection via Directly Binding to the Fungus and Preventing Excessive Inflammation. *Front Immunol* **10**: 283.

MacCallum, D.M. (2009) Massive induction of innate immune response to *Candida albicans* in the kidney in a murine intravenous challenge model. *FEMS Yeast Res* **9**: 1111–1122.

MacCallum, D.M. (2012) Hosting infection: Experimental models to assay *Candida* virulence. *Int J Microbiol* **2012**: e363764.

MacCallum, D.M., Desbois, A.P., and Coote, P.J. (2013) Enhanced efficacy of synergistic combinations of antimicrobial peptides with caspofungin versus *Candida albicans* in insect and murine models of systemic infection. *Eur J Clin Microbiol Infect Dis* **32**: 1055–1062.

Maguire, R., Duggan, O., and Kavanagh, K. (2016) Evaluation of *Galleria mellonella* larvae as an in vivo model for assessing the relative toxicity of food preservative agents. *Cell Biol Toxicol* **32**: 209–216.

Maguire, R., Kunc, M., Hyrsl, P., and Kavanagh, K. (2017a) Analysis of the acute response of *Galleria mellonella* larvae to potassium nitrate. *Comp Biochem Physiol Part C Toxicol Pharmacol* **195**: 44–51.

Maguire, R., Kunc, M., Hyrsl, P., and Kavanagh, K. (2017b) Caffeine administration alters the behaviour and development of *Galleria mellonella* larvae. *Neurotoxicol Teratol* **64**: 37–44.

Maher, A., Staunton, K., and Kavanagh, K. (2018) Analysis of the effect of temperature on protein abundance in Demodex-associated *Bacillus oleronius*. *Pathog Dis* **76**.

Mahgoub, E.S., and el-Hassan, A.M. (1972) Pulmonary aspergillosis caused by *Aspergillus flavus. Thorax* **27**: 33–37.

Mak, P., Chmiel, D., and Gacek, G.J. (2001) Antibacterial peptides of the moth *Galleria mellonella*. *Acta Biochim Pol* **48**: 1191–1195.

Mak, P., Zdybicka-Barabas, A., and Cytryńska, M. (2010) A different repertoire of *Galleria mellonella* antimicrobial peptides in larvae challenged with bacteria and fungi. *Dev Comp Immunol* **34**: 1129–1136.

Mallick, P., and Kuster, B. (2010) Proteomics: A pragmatic perspective. *Nat Biotechnol* **28**: 695–709.

Marcinkiewicz, J., Czajkowska, B., Grabowska, A., Kasprowicz, A., and Kociszewska, B. (1994) Differential effects of chlorination of bacteria on their capacity to generate NO, TNF-alpha and IL-6 in macrophages. *Immunology* **83**: 611–616.

Marcinkiewicz, J., and Kontny, E. (2014) Taurine and inflammatory diseases. *Amino Acids* **46**: 7–20.

Margalit, A., and Kavanagh, K. (2015) The innate immune response to *Aspergillus fumigatus* at the alveolar surface. *FEMS Microbiol Rev* **39**: 670–687.

Mariné, M., Bom, V.L.P., Castro, P.A. de, Winkelstroter, L.K., Ramalho, L.N., Brown, N.A., and Goldman, G.H. (2015) The development of animal infection models and antifungal efficacy assays against clinical isolates of Trichosporon asahii, T. asteroides and T. inkin. *Virulence* **6**: 476–486.

Maróti Gergely, G., Kereszt, A., Kondorosi, É., and Mergaert, P. (2011) Natural roles of antimicrobial peptides in microbes, plants and animals. *Res Microbiol* **162**: 363–374.

Marques, L.M. (2015) Sepsis Induced by *Staphylococcus aureus*: Participation of Biomarkers in a Murine Model. *Med Sci Monit* **21**: 345–355.

Martínez-Solano, L., Reales-Calderón, J.A., Nombela, C., Molero, G., and Gil, C. (2009) Proteomics of RAW 264.7 macrophages upon interaction with heat-inactivated *Candida albicans* cells unravel an anti-inflammatory response. *Proteomics* **9**: 2995–3010.

Stanzani, M., Orciuolo, E., Lewis, R., Kontoyiannis, D.P., Martins, S.L., St John, L.S., Komanduri, K.V. (2017) *Aspergillus fumigatus* suppresses the human cellular immune response via gliotoxin-mediated apoptosis of monocytes. *Blood* **105**: 2258-2265.

Matsumoto, Y., Miyazaki, S., Fukunaga, D.H., Shimizu, K., Kawamoto, S., and Sekimizu, K. (2012) Quantitative evaluation of cryptococcal pathogenesis and antifungal drugs using a silkworm infection model with *Cryptococcus neoformans*. *J Appl Microbiol* **112**: 138–146.

Maurer, E., Browne, N., Surlis, C., Jukic, E., Moser, P., Kavanagh, K., and Binder, U. (2015) *Galleria mellonella* as a host model to study *Aspergillus terreus* virulence and amphotericin B resistance. *Virulence* **6(6)**: 1–8.

Maurer, E., Hörtnagl, C., Lackner, M., Grässle, D., Naschberger, V., Moser, P., *et al.* (2019) *Galleria mellonella* as a model system to study virulence potential of mucormycetes and evaluation of antifungal treatment. *Med Mycol* **57**: 351–362.

Mc Namara, L., Carolan, J.C., Griffin, C.T., Fitzpatrick, D., and Kavanagh, K. (2017) The effect of entomopathogenic fungal culture filtrate on the immune response of the greater wax moth, *Galleria mellonella*. *J Insect Physiol* **100**: 82–92.

McCann, M., Kellett, A., Kavanagh, K., Devereux, M., and L.S. Santos, A. (2012a) Deciphering the Antimicrobial Activity of Phenanthroline Chelators. *Curr Med Chem* **19**: 2703–2714.

McCann, M., Santos, A.L.S., Silva, B.A. Da, Romanos, M.T. V, Pyrrho, A.S., Devereux, M., *et al.* (2012b) *In vitro* and *in vivo* studies into the biological activities of 1,10-phenanthroline, 1,10-phenanthroline-5,6-dione and its copper(ii) and silver(i) complexes. *Toxicol Res (Camb)* **1**: 47–54.

McCloskey, A.P., Lee, M., Megaw, J., McEvoy, J., Coulter, S.M., Pentlavalli, S., and Laverty, G. (2019) Investigating the *in vivo* Antimicrobial Activity of a Self-Assembling Peptide Hydrogel Using a *Galleria mellonella* Infection Model. *ACS Omega* **4**: 2584–2589.

McCowen, M.C., Callender, M.E., and Lawlis, J.F. (1951) Fumagillin (H-3), a new antibiotic with amebicidal properties. *Science (80-)* **113**: 202–203.

Mcgee, D.J., George, A.E., Trainor, E.A., Horton, K.E., Hildebrandt, E., and Testerman, T.L. (2011) Cholesterol Enhances *Helicobacter pylori* Resistance to Antibiotics and LL-37. **55**: 2897–2904.

Medzhitov R, Preston-Hurlburt P, and Janeway CA Jr (1997) A human homologue of the *Drosophila* Toll protein signals activation of adaptive immunity. *Nature* **388**: 394–397.

Mesa-Arango, A.C., Forastiero, A., Bernal-Martínez, L., Cuenca-Estrella, M., Mellado, E., and Zaragoza, O. (2013) The non-mammalian host *Galleria mellonella* can be used to study the virulence of the fungal pathogen *Candida tropicalis* and the efficacy of antifungal drugs during infection by this pathogenic yeast. *Med Mycol* **51**: 461–72.

Midorikawa, K., Ouhara, K., Komatsuzawa, H., Kawai, T., Yamada, S., Fujiwara, T., *et al.* (2003) *Staphylococcus aureus* susceptibility to innate antimicrobial peptides, β-defensins and CAP18, expressed by human keratinocytes. *Infect Immun* **71**: 3730–3739.

Misme-Aucouturier, B., Albassier, M., Alvarez-Rueda, N., and Pape, P. Le (2017) Specific human and *Candida* cellular interactions lead to controlled or persistent infection outcomes during granuloma-like formation. *Infect Immun* **85**: e00807-16.

Molne, L., Verdrengh, M., and Tarkowski, A. (2000) Role of neutrophil leukocytes in cutaneous infection caused by *Staphylococcus aureus*. *Infect Immun* **68**: 6162–6167.

Moloney, N.M., Owens, R.A., Meleady, P., Henry, M., Dolan, S.K., Mulvihill, E., *et al.* (2016) The iron-responsive microsomal proteome of *Aspergillus fumigatus*. *J Proteomics* **136**: 99–111.

Moore, A.J., Beazley, W.D., Bibby, M.C., and Devine, D.A. (1996) Antimicrobial activity of cecropins. *J Antimicrob Chemother* **37**: 1077–1089.

Moreillon, P., Entenza, J.M., Francioli, P., McDevitt, D., Foster, T.J., Francois, P., and Vaudaux, P. (1995) Role of *Staphylococcus aureus* coagulase and clumping factor in pathogenesis of experimental endocarditis. *Infect Immun* **63**: 4738–4743.

Mouyna, I., Fontaine, T., Vai, M., Monod, M., Fonzi, W.A., Diaquin, M., *et al.* (2000) Play an Active Role in the Biosynthesis of the Fungal Cell Wall *. *J Biol Chem* **275**: 14882–14889.

Mowlds, P., Barron, A., and Kavanagh, K. (2008) Physical stress primes the immune response of *Galleria mellonella* larvae to infection by *Candida albicans*. *Microbes Infect* **10**: 628–634.

Mowlds, P., Coates, C., Renwick, J., and Kavanagh, K. (2010) Dose-dependent cellular and humoral responses in *Galleria mellonella* larvae following β-glucan inoculation. *Microbes Infect* **12**: 146–153.

Mowlds, P., and Kavanagh, K. (2008) Effect of pre-incubation temperature on susceptibility of *Galleria mellonella* larvae to infection by *Candida albicans*. *Mycopathologia* **165**: 5–12.

Mukherjee, K., Altincicek, B., Hain, T., Domann, E., Vilcinskas, A., and Chakraborty, T. (2010) *Galleria mellonella* as a model system for studying Listeria pathogenesis. *Appl Environ Microbiol* **76**: 310–317.

Mukherjee, K., Hain, T., Fischer, R., Chakraborty, T., and Vilcinskas, A. (2013) Brain infection and activation of neuronal repair mechanisms by the human pathogen Listeria monocytogenes in the lepidopteran model host *Galleria mellonella*. *Virulence* **4**: 324–32.

Mukherjee, K., Mraheil, M.A., Silva, S., Müller, D., Cemic, F., Hemberger, J., *et al.* (2011) Anti-Listeria activities of *Galleria mellonella* hemolymph proteins. *Appl Environ Microbiol* **77**: 4237–4240.

Mukherjee, K., and Vilcinskas, A. (2014) Development and immunity-related microRNAs of the lepidopteran model host *Galleria mellonella. BMC Genomics* **15**.

Murakami, M., Lopez-garcia, B., Braff, M., Dorschner, R.A., Gallo, R.L., Murakami, M., *et al.* (2004) Postsecretory Processing Generates Multiple Cathelicidins for Enhanced Topical Antimicrobial Defense. *J Immunol* **172**: 3070–3077.

Murray, I.G., Spooner, E.T.C., and Walker, J. (1960) Experimental infection of mice with *Madurella mycetomi*. *Trans R Soc Trop Med Hyg* **54**: 335–341.

Mustedanagic, J., Ximenes, V.F., and Nagl, M. (2017) Microbicidal activity of N-chlorotaurine in combination with hydrogen peroxide. *AMB Express* **7**: 102.

Myllymäki, H., and Rämet, M. (2014) JAK/STAT Pathway in *Drosophila* Immunity. *Scand J Immunol* **79**: 377–385.

Mylonakis, E., Moreno, R., E Khoury, J.B., Idnurm, A., Heitman, J., Calderwood, S.B., *et al.* (2005) *Galleria mellonella* as a model system to study *Cryptococcus neoformans* pathogenesis. *Infect Immun* **73**: 3842–3850.

Nagao, J.I., Cho, T., Uno, J., Ueno, K., Imayoshi, R., Nakayama, H., *et al.* (2012) *Candida albicans* Msi3p, a homolog of the *Saccharomyces cerevisiae* Sse1p of the Hsp70 family, is involved in cell growth and fluconazole tolerance. *FEMS Yeast Res* **12**: 728–737.

Nagl, M., Arnitz, R., and Lackner, M. (2018) N-Chlorotaurine, a Promising Future Candidate for Topical Therapy of Fungal Infections. *Mycopathologia* **183**: 161–170.

Nagl, M., Gruber, A., Fuchs, A., Lell, C.P., Lemberger, E.M., Borg-Von Zepelin, M., and Würzner, R. (2002) Impact of N-chlorotaurine on viability and production of secreted aspartyl proteinases of *Candida* spp. *Antimicrob Agents Chemother* **46**: 1996–1999.

Nagl, M., Hengster, P., Semenitz, E., and Gottardi, W. (1999) The postantibiotic effect of N-chlorotaurine on *Staphylococcus aureus*. Application in the mouse peritonitis model. *J Antimicrob Chemother* **43**: 805–809.

Nagl, M., Hess, M.W., Pfaller, K., Hengster, P., and Gottardi, W. (2000a) Bactericidal activity of micromolar N-Chlorotaurine: Evidence for its antimicrobial function in the human defense system. *Antimicrob Agents Chemother* **44**: 2507–2513.

Nagl, M., Lass-Flörl, C., Neher, a, Gunkel, a, and Gottardi, W. (2001) Enhanced fungicidal activity of N-chlorotaurine in nasal secretion. *J Antimicrob Chemother* **47**: 871–4.

Nagl, M., Teuchner, B., Pöttinger, E., Ulmer, H., and Gottardi, W. (2000b) Tolerance of N-chlorotaurine, a new antimicrobial agent, in infectious conjunctivitis - A phase II pilot study. *Ophthalmologica* **214**: 111–114.

Nakamura, T., Maeda, Y., Tanoue, N., Makita, T., Kato, M., and Kobayashi, T. (2006) Expression Profile of Amylolytic Genes in *Aspergillus nidulans*. *Biosci Biotechnol Biochem* **70**: 2363–2370.

Nakatsuji, T., Cogen, A.L., and Gallo, R.L. (2011) TLR2 Expression Is Increased in Rosacea and Stimulates Enhanced Serine Protease Production by Keratinocytes. *J Invest Dermatol* **131**: 688–697.

Namvar, S., Warn, P., Farnell, E., Bromley, M., Fraczek, M., Bowyer, P., and Herrick, S. (2015) *Aspergillus fumigatus* proteases, Asp f 5 and Asp f 13, are essential for airway inflammation and remodelling in a murine inhalation model. *Clin Exp Allergy* **45**: 982–993.

Navarro-Velasco, G.Y., Prados-Rosales, R.C., Ortíz-Urquiza, A., Quesada-Moraga, E., and Pietro, A. Di (2011) *Galleria mellonella* as model host for the trans-kingdom pathogen *Fusarium oxysporum*. *Fungal Genet Biol* **48**: 1124–1129.

Neher, A., Nagl, M., Appenroth, E., Gstöttner, M., Wischatta, M., Reisigl, F., *et al.* (2004) Acute Otitis Externa: Efficacy and Tolerability of N-Chlorotaurine, a Novel Endogenous Antiseptic Agent. *Laryngoscope* **114**: 850–854.

Nett, J.E., Brooks, E.G., Cabezas-Olcoz, J., Sanchez, H., Zarnowski, R., Marchillo, K., and Andes, D.R. (2014) Rat indwelling urinary catheter model of *Candida albicans* biofilm infection. *Infect Immun* **82(12)**: 4931–4940.

Neuwirth, M. (1973) The structure of the hemocytes of *Galleria mellonella* (Lepidoptera). *J Morphol* **139**: 105–123.

Ngamskulrungroj, P., Himmelreich, U., Breger, J.A., Wilson, C., Chayakulkeeree, M., Krockenberger, M.B., *et al.* (2009) The trehalose synthesis pathway is an integral part of the virulence composite for *Cryptococcus gattii*. *Infect Immun* **77**: 4584–4596.

Nielsen, M.S., Madsen, P., Christensen, E.I., Nykjær, A., Gliemann, J., Kasper, D., *et al.* (2001) The sortilin cytoplasmic tail conveys Golgi-endosome transport and binds the VHS domain of the GGA2 sorting protein. *EMBO J* **20**: 2180–2190.

Niere, M., Dettloff, M., Maier, T., Ziegler, M., and Wiesner, A. (2001) Insect immune activation by apolipophorin III is correlated with the lipid-binding properties of this protein. *Biochemistry* **40**: 11502–11508.

Niere, M., Meißlitzer, C., Dettloff, M., Weise, C., Ziegler, M., and Wiesner, A. (1999) Insect immune activation by recombinant *Galleria mellonella* apolipophorin III. *Biochim Biophys Acta - Protein Struct Mol Enzymol* **1433**: 16–26.

Nile, C., Falleni, M., Cirasola, D., Alghamdi, A., Anderson, O.F., Delaney, C., *et al.* (2019) Repurposing Pilocarpine Hydrochloride for Treatment of *Candida albicans* Infections. *mSphere* **4**: e00689-18

Noore, J., Noore, A., and Li, B. (2013) Cationic antimicrobial peptide LL-37 is effective against both extra- and intracellular *Staphylococcus aureus*. *Antimicrob Agents Chemother* **57**: 1283–90.

O'Hanlon, K.A., Cairns, T., Stack, D., Schrettl, M., Bignell, E.M., Kavanagh, K., *et al.* (2011) Targeted disruption of nonribosomal peptide synthetase Pes3 augments the virulence of *Aspergillus fumigatus. Infect Immun* **79**: 3978–3992.

Olsen, R.J., Ebru Watkins, M., Cantu, C.C., Beres, S.B., and Musser, J.M. (2011) Virulence of serotype M3 group A *streptococcus* strains in

wax worms (*Galleria mellonella* larvae). *Virulence* **2**: 111–9.

Ommori, R., Ouji, N., Mizuno, F., Kita, E., Ikada, Y., and Asada, H. (2013) Selective induction of antimicrobial peptides from keratinocytes by staphylococcal bacteria. *Microb Pathog* **56**: 35–39.

Ordonez, S.R., Amarullah, I.H., Wubbolts, R.W., Veldhuizen, E.J.A., and Haagsman, P. (2014) Fungicidal Mechanisms of Cathelicidins LL-37 and CATH-2 Revealed by Live-Cell Imaging. **58**: 2240–2248.

Otto, M. (2008) Staphylococcal biofilms. *Curr Top Microbiol Immunol* **322**: 207–228.

Owens, R.A., Hammel, S., Sheridan, K.J., Jones, G.W., and Doyle, S. (2014) A proteomic approach to investigating gene cluster expression and secondary metabolite functionality in *Aspergillus fumigatus*. *PLoS One* **9**.

Özkan, S., and Coutts, R.H.A. (2015) *Aspergillus fumigatus* mycovirus causes mild hypervirulent effect on pathogenicity when tested on *Galleria mellonella. Fungal Genet Biol* **76**: 20–26.

Panthee, S., Paudel, A., Hamamoto, H., and Sekimizu, K. (2017) Advantages of the silkworm as an animal model for developing novel antimicrobial agents. *Front Microbiol* **8**: 373.

Park, S.Y., Kim, C.H., Jeong, W.H., Lee, J.H., Seo, S.J., Han, Y.S., and Lee, I.H. (2005) Effects of two hemolymph proteins on humoral defense reactions in the wax moth, *Galleria mellonella*. *Dev Comp Immunol* **29**: 43–51.

Parker, D. (2017) Humanized mouse models of *Staphylococcus aureus* infection. *Front Immunol* **4**: 512.

Pazgier, M., Hoover, D.M., Yang, D., Lu, W., and Lubkowski, J. (2006) Human β-defensins. *Cell Mol Life Sci* **63**: 1294–1313.

Pea, F., and Lewis, R.E. (2018) Overview of antifungal dosing in invasive candidiasis. *J Antimicrob Chemother* **73**: i33–i43.

Pech M. R., L.L.. S. (1996) Granular cells are required for encapsulation of foreign targets by insect haemocytes. *J Cell Sci* **109**: 2053–2060.

Peleg, A.Y., Jara, S., Monga, D., Eliopoulos, G.M., Moellering, R.C., and Mylonakis, E. (2009a) *Galleria mellonella* as a model system to study *Acinetobacter baumannii* pathogenesis and therapeutics. *Antimicrob Agents Chemother* **53**: 2605–2609.

Peleg, A.Y., Monga, D., Pillai, S., Mylonakis, E., Moellering, Jr., R.C., and Eliopoulos, G.M. (2009b) Reduced Susceptibility to Vancomycin Influences Pathogenicity in *Staphylococcus aureus* Infection. *J Infect Dis* **199**: 532–536.

Pérez, A., Pedrós, B., Murgui, A., Casanova, M., López-Ribot, J.L., and Martínez, J.P. (2006) Biofilm formation by *Candida albicans* mutants for genes coding fungal proteins exhibiting the eight-cysteine-containing CFEM domain. *FEMS Yeast Res* **6**: 1074–1084.

Perfect, J.R., Tenor, J.L., Miao, Y., and Brennan, R.G. (2017) Trehalose pathway as an antifungal target. *Virulence* **8**: 143–149.

Peters, B.M., and Noverra, M.C. (2013) *Candida albicans-staphylococcus aureus* polymicrobial peritonitis modulates host innate immunity. *Infect Immun* **81**: 2178–2189.

Petitjean, M., Teste, M.A., François, J.M., and Parrou, J.L. (2015) Yeast tolerance to various stresses relies on the trehalose-6P synthase (Tps1) protein, not on trehalose. *J Biol Chem* **290**: 16177–16190.

Petraitiene, R., Petraitis, V., Groll, A.H., Sein, T., Schaufele, R.L., Francesconi, A., *et al.* (2002) Antifungal efficacy of caspofungin (MK-0991) in experimental pulmonary aspergillosis in persistently neutropenic rabbits: Pharmacokinetics, drug disposition, and relationship to galactomannan antigenemia. *Antimicrob Agents Chemother* **46**: 12–23.

Philippe, B., Ibrahim-Granet, O., Prévost, M.C., Gougerot-Pocidalo, M.A., Perez, M.S., Meeren, A. Van der, and Latgé, J.P. (2003) Killing of *Aspergillus fumigatus* by alveolar macrophages is mediated by reactive oxidant intermediates. *Infect Immun* **71**: 3034–3042.

Pietrella, D., Bistoni, G., Corbucci, C., Perito, S., and Vecchiarelli, A. (2006) *Candida albicans* mannoprotein influences the biological function of dendritic cells. *Cell Microbiol* **8**: 602–612.

Prajsnar, T.K., Cunliffe, V.T., Foster, S.J., and Renshaw, S.A. (2008) A novel vertebrate model of *Staphylococcus aureus* infection reveals phagocyte-dependent resistance of zebrafish to non-host specialized pathogens. *Cell Microbiol* **10**: 2312–2325.

Price, C.D., and Ratcliffe, N.A. (1974) A reappraisal of insect haemocyte classification by the examination of blood from fifteen insect orders. *Zeitschrift für Zellforsch und mikroskopische Anat* **147**: 537–549.

Priebe, S., Linde, J., Albrecht, D., Guthke, R., and Brakhage, A.A. (2011) FungiFun: A web-based application for functional categorization of fungal genes and proteins. *Fungal Genet Biol* **48(4)**: 353–8.

Qiao, C., Cui, F., and Yan, S. (2009) Structure, Function and Applications of Carboxylesterases from Insects for Insecticide Resistance. *Protein Pept Lett* **16**: 1181–1188.

Qu, X. M, Steiner, H., Engström, Å., Bennich, H., And Boman, H.G. (1982) Insect Immunity: Isolation and Structure of Cecropins B and D from Pupae of the Chinese Oak Silk Moth, Antheraea pernyi. *Eur J Biochem* **127**: 219–224.

Ragland, S.A., and Criss, A.K. (2017) From bacterial killing to immune modulation: Recent insights into the functions of lysozyme. *PLoS Pathog* **13**. e1006512.

Ramarao, N., Nielsen-Leroux, C., and Lereclus, D. (2012) The insect *Galleria mellonella* as a powerful infection model to investigate bacterial pathogenesis. *J Vis Exp* e4392.

Rambach, G., Dum, D., Mohsenipour, I., Hagleitner, M., Würzner, R., Lass-flörl, C., and Speth, C. (2010) Secretion of a fungal protease represents a complement evasion mechanism in cerebral aspergillosis. **47**: 1438–1449.

Ramos, R., Pedro, J., Cristina, A., Costa, R., Guardão, L., Schmitt, F., *et al.* (2011) Peptides Wound healing activity of the human antimicrobial peptide LL37. *Peptides* **32**: 1469–1476.

Rapala-Kozik, M., Bochenska, O., Zawrotniak, M., Wolak, N., Trebacz, G., Gogol, M., *et al.* (2015) Inactivation of the antifungal and immunomodulatory properties of human cathelicidin LL-37 by aspartic proteases produced by the pathogenic yeast *Candida albicans. Infect Immun* **83**: 2518–2530.

Ratcliffe, N.A. (1985a) Invertebrate immunity — A primer for the non-specialist. *Immunol Lett* **10**: 253–270.

Ratcliffe, N.A., and Gagen, S.J. (1977) Studies on the *in vivo* cellular reactions of insects: An ultrastructural analysis of nodule formation in *Galleria mellonella*. *Tissue Cell* **9**: 73–85.

Reales-Calderón, J.A., Martínez-Solano, L., Martínez-Gomariz, M., Nombela, C., Molero, G., and Gil, C. (2012) Sub-proteomic study on macrophage response to *Candida albicans* unravels new proteins involved in the host defense against the fungus. *J Proteomics* **75**: 4734–4746.

Reece, E., Segurado, R., Jackson, A., Mcclean, S., Renwick, J., and Greally, P. (2017) Co-colonisation with *Aspergillus fumigatus* and *Pseudomonas aeruginosa* is associated with poorer health in cystic fibrosis patients : an Irish registry analysis. 1–8.

Reeves, E.P., Messina, C.G.. M., Doyle, S., and Kavanagh, K. (2004a) Correlation between gliotoxin production and virulence of *Aspergillus fumigatus* in *Galleria mellonella*. *Mycopathologia* **158**: 73–79.

Reeves, E.P., Murphy, T., Daly, P., and Kavanagh, K. (2004b) Amphotericin B enhances the synthesis and release of the immunosuppressive agent gliotoxin from the pulmonary pathogen *Aspergillus fumigatus*. *J Med Microbiol* **53**: 719–725.

Reeves, E.P., Nagl, M., O'Keeffe, J., Kelly, J., and Kavanagh, K. (2006a) Effect of N-chlorotaurine on Aspergillus, with particular reference to destruction of secreted gliotoxin. *J Med Microbiol* **55**: 913–918.

Reeves, E.P., Reiber, K., Neville, C., Scheibner, O., Kavanagh, K., and Doyle, S. (2006b) A nonribosomal peptide synthetase (Pes1) confers protection against oxidative stress in *Aspergillus fumigatus*. *FEBS J* **273**: 3038–53.

Reno, J., Doshi, S., Tunali, A.K., Stein, B., Farley, M.M., Ray, S.M., and Jacob, J.T. (2015) Epidemiology of Methicillin-Resistant *staphylococcus aureus* bloodstream coinfection among adults with candidemia in Atlanta, GA, 2008–2012. *Infect Control Hosp Epidemiol* **36**: 1298–1304.

Renwick, J., Daly, P., Reeves, E.P., and Kavanagh, K. (2006) Susceptibility of larvae of *Galleria mellonella* to infection by *Aspergillus fumigatus* is dependent upon stage of conidial germination. *Mycopathologia* **161**: 377–384.

Renwick, J., Reeves, E.P., Wientjes, F.B., and Kavanagh, K. (2007) Translocation of proteins homologous to human neutrophil p47phox and p67phox to the cell membrane in activated hemocytes of *Galleria mellonella. Dev Comp Immunol* **31**: 347–359.

Ribeiro, M.A., Alastruey-Izquierdo, A., Gomez-Lopez, A., Rodriguez-Tudela, J.L., and Cuenca-Estrella, M. (2008) Molecular identification and susceptibility testing of Trichosporon isolates from a Brazilian hospital. *Rev Iberoam Micol* **25**: 221–225.

Riera Romo, M., Pérez-Martínez, D., and Castillo Ferrer, C. (2016) Innate immunity in vertebrates: An overview. *Immunology* **148**: 125–139.

Riza, N.A., and Madamopoulos, N. (1997) All-fiber connectorized fiber-optic delay module using 3-D polarization optics. *Conf Proc - Lasers Electro-Optics Soc Annu Meet* **2**: 472–473.

Robert, B., Xiaorong, W., Zasloff, M., and James, M, W. (1998) The peptide antibiotic LL-37 ¯hCAP-18 is expressed in epithelia of the human lung where it has broad antimicrobial activity at the airway surface. **95**: 9541–9546.

Robertson, C.M., Perrone, E.E., McConnell, K.W., Dunne, W.M., Boody, B., Brahmbhatt, T., *et al.* (2008) Neutrophil Depletion Causes a Fatal Defect in Murine Pulmonary *Staphylococcus aureus* clearance. *J Surg Res* **150**: 278–285.

Rochford, G., Molphy, Z., Browne, N., Surlis, C., Devereux, M., McCann, M., *et al.* (2018) *In-vivo* evaluation of the response of *Galleria mellonella* larvae to novel copper(II) phenanthroline-phenazine complexes. *J Inorg Biochem* **186**: 135–146.

Rodrigues, M.L., Nosanchuk, J.D., Schrank, A., Vainstein, M.H., Casadevall, A., and Nimrichter, L. (2011) Vesicular transport systems in fungi. *Future Microbiol* **6**: 1371–1381.

Rogers, T.R. (2008) Treatment of zygomycosis: Current and new options. *J Antimicrob Chemother* **61**: 35–40.

Rollin, B.E. (2009) Scientific autonomy and the 3Rs. *Am J Bioeth* **9**: 62–64.

Roncero, C., and Duran, A. (1985) Effect of Calcofluor white and Congo red on fungal cell wall morphogenesis : in vivo activation of chitin polymerization . Effect of Calcofluor White and Congo Red on Fungal Cell Wall Morphogenesis : *In Vivo* Activation of Chitin Polymerization. *J Bacteriol* **163**: 1180–1185.

Rosen, H. (1957) A modified ninhydrin colorimetric analysis for amino acids. *Arch Biochem Biophys* **67**: 10–15.

Rossi, D., Silveira, S., Valentini, S.R., and Zanelli, F. (2013) The Deoxyhypusine Synthase Mutant dys1-1 Reveals the Association of eIF5A and Asc1 with Cell Wall Integrity. *PLoS One* **8**: e60140.

Rowley, A.F., and Ratcliffe, N.A. (1976) The granular cells of *Galleria mellonella* during clotting and phagocytic reactions in vitro. *Tissue Cell* **8**: 437–446.

Ruiz-Herrera, J., Victoria Elorza, M., Valentín, E., and Sentandreu, R. (2006) Molecular organization of the cell wall of *Candida albicans* and its relation to pathogenicity. *FEMS Yeast Res* **6**: 14–29.

Sande, W.W.J. van de, Janse, D.-J., Hira, V., Goedhart, H., Zee, R. van der, Ahmed, A.O.A., *et al.* (2006) Translationally Controlled Tumor Protein from *Madurella mycetomatis* , a Marker for Tumorous Mycetoma Progression. *J Immunol* **177**: 1997–2005.

Sande, W.W.J. Van De, Vianen, W. Van, Kate, M. Ten, Fahal, A., and Bakker-Woudenberg, I. (2015) Amphotericin B but not itraconazole is able to prevent grain formation in experimental *Madurella mycetomatis* mycetoma in mice. *Br J Dermatol* **173**: 1561–1562.

Sanders, K.L., and Lee, M.S.Y. (2010) Arthropod molecular divergence times and the Cambrian origin of pentastomids. *Syst Biodivers* **8**: 63–74.

Sandini, S., Stringaro, A., Arancia, S., Colone, M., Mondello, F., Murtas, S., *et al.* (2011) The MP65 gene is required for cell wall integrity, adherence to epithelial cells and biofilm formation in *Candida albicans*. *BMC Microbiol* **11**.

Sangalli-Leite, F., Scorzoni, L., Alves de Paula e Silva, A.C., Silva, J. de F. da, Oliveira, H.C. de, Lacorte Singulani, J. de, *et al.* (2016) Synergistic effect of pedalitin and amphotericin B against *Cryptococcus neoformans* by *in vitro* and *in vivo* evaluation. *Int J Antimicrob Agents* **48**: 504–511.

Santoro, J., and Levison, M.E. (1978) Rat model of experimental endocarditis. *Infect Immun* **19**: 915–918.

Sarauer, B.L., Gillott, C., and Hegedus, D. (2003) Characterization of an intestinal mucin from the peritrophic matrix of the diamondback moth, *Plutella xylostella*. *Insect Mol Biol* **12**: 333–343.

Satyavathi, V. V., Minz, A., and Nagaraju, J. (2014) Nodulation: An unexplored cellular defense mechanism in insects. *Cell Signal* **26**: 1753–1763.

Schaaf, G.J., Nijmeijer, S.M., Maas, R.F.M., Roestenberg, P., Groene, E.M. De, and Fink-Gremmels, J. (2002) The role of oxidative stress in the ochratoxin A-mediated toxicity in proximal tubular cells. *Biochim Biophys Acta - Mol Basis Dis* **1588**: 149–158.

Schabbauer, G. (2012) Polymicrobial sepsis models: CLP versus CASP. *Drug Discov Today Dis Model* **9**: e17–e21.

Scherfer, C., Karlsson, C., Loseva, O., Bidla, G., Goto, A., Havemann, J., *et al.* (2004) Isolation and characterization of hemolymph clotting factors in *Drosophila melanogaster* by a pullout method. *Curr Biol* **14**: 625–629.

Schlecht, L.M., Peters, B.M., Krom, B.P., Freiberg, J.A., Hänsch, G.M., Filler, S.G., *et al.* (2015) Systemic *Staphylococcus aureus* infection mediated by *Candida albicans* hyphal invasion of mucosal tissue. *Microbiol (United Kingdom)* **161**: 168–181.

Schmit, A.R., and Ratcliffe, N.A. (1977) The encapsulation of foreign tissue implants in G*alleria mellonella* larvae. *J Insect Physiol* **23**: 175–184.

Schmit, A.R., and Ratcliffe, N.A. (1978) The encapsulation of Araldite implants and recognition of foreignness in *Clitumnus extradentatus. J*

Insect Physiol **24**. 511–521.

Schmolz, E., and Schulz, O. (1995) Calorimetric investigations on thermoregulation and growth of wax moth larvae *Galleria mellonella. Thermochim Acta* **251**: 241–245.

Schuhmann, B., Seitz, V., Vilcinskas, A., and Podsiadlowski, L. (2003) Cloning and expression of gallerimycin, an antifungal peptide expressed in immune response of greater wax moth larvae, *Galleria mellonella*. *Arch Insect Biochem Physiol* **53**: 125–133.

Schultzhaus, Z., Johnson, T.B., and Shaw, B.D. (2017) Clathrin localization and dynamics in *Aspergillus nidulans*. *Mol Microbiol* **103**: 299–318.

Segal, B.H., and Romani, L.R. (2009) Invasive aspergillosis in chronic granulomatous disease. *Med Mycol* **47**: S282–S290.

Seitz, V., Clermont, A., Wedde, M., Hummel, M., Vilcinskas, A., Schlatterer, K., and Podsiadlowski, L. (2003) Identification of immunorelevant genes from greater wax moth (*Galleria mellonella*) by a subtractive hybridization approach. *Dev Comp Immunol* **27**: 207–215.

Selisko, B., Garcia, C., Becerril, B., Gómez-Lagunas, F., Garay, C., and Possani, L.D. (1998) Cobatoxins 1 and 2 from Centruroides noxius Hoffmann constitute a subfamily of potassium-channel-blocking scorpion toxins. *Eur J Biochem* **254**: 468–479.

Sentandreu, M., Elorza, M.V., Sentandreu, R., and Fonzi, W.A. (1998) Cloning and characterization of PRA1, a gene encoding a novel pH-regulated antigen of *Candida albicans. J Bacteriol* **180**: 282–289.

Shahmiri, M., Enciso, M., Adda, C.G., Smith, B.J., Perugini, M. a., and Mechler, A. (2016) Membrane Core-Specific Antimicrobial Action of Cathelicidin LL-37 Peptide Switches Between Pore and Nanofibre Formation. *Sci Rep* **6**: 38184.

Shaik, H.A., and Sehnal, F. (2009) Hemolin expression in the silk glands of *Galleria mellonella* in response to bacterial challenge and prior to cell disintegration. *J Insect Physiol* **55**: 781–787.

Shenton, D., Smirnova, J.B., Selley, J.N., Carroll, K., Hubbard, S.J., Pavitt, G.D., *et al.* (2006) Global translational responses to oxidative stress impact upon multiple levels of protein synthesis. *J Biol Chem* **281**: 29011–29021.

Shinji, H., Yosizawa, Y., Tajima, A., Iwase, T., Sugimoto, S., Seki, K., and Mizunoe, Y. (2011) Role of fibronectin-binding proteins A and B in *in vitro* cellular infections and *in vivo* septic infections by *Staphylococcus aureus*. *Infect Immun* **79**: 2215–2223.

Shirtliff, M.E., Peters, B.M., and Jabra-Rizk, M.A. (2009) Cross-kingdom interactions: *Candida albicans* and bacteria. *FEMS Microbiol Lett* **299**: 1–8.

Shoham, S., and Levitz, S.M. (2005) The immune response to fungal infections. *Br J Haematol* **129**: 569–582.

Shokal, U., and Eleftherianos, I. (2017) Evolution and function of thioester-containing proteins and the complement system in the innate immune response. *Front Immunol* **8**.

Sifri, C.D., Begun, J., Ausubel, F.M., and Calderwood, S.B. (2003) *Caenorhabditis elegans* as a model host for *Staphylococcus aureus* pathogenesis. *Infect Immun* **71**: 2208–2217.

Sigel, H.C., Thewes, S., Niewerth, M., Korting, H.C., Schäder-Korting, M., and Hube, B. (2005) Oxygen accessibility and iron levels are critical factors for the antifungal action of ciclopirox against *Candida albicans*. *J Antimicrob Chemother* **55**: 663–673.

Silva, L.N., Campos-Silva, R., Ramos, L.S., Trentin, D.S., Macedo, A.J., Branquinha, M.H., and Santos, A.L.S. (2018) Virulence of *Candida haemulonii* complex in *Galleria mellonella* and efficacy of classical antifungal drugs: a comparative study with other clinically relevant non-albicans *Candida* species. *FEMS Yeast Res* **18**: foy082.

Silverman, N., and Maniatis, T. (2001) NF-κB signaling pathways in mammalian and insect innate immunity. *Genes Dev* **15**: 2321–2342.

Singh, B., Fleury, C., Jalalvand, F., and Riesbeck, K. (2012) Human pathogens utilize host extracellular matrix proteins laminin and collagen for adhesion and invasion of the host. *FEMS Microbiol Rev* **36**: 1122–1180.

Slater, J.L., Gregson, L., Denning, D.W., and Warn, P.A. (2011) Pathogenicity of *Aspergillus fumigatus* mutants assessed in *Galleria mellonella* matches that in mice. *Med Mycol* **49**: S107–S113.

Smagur, J., Guzik, K., Bzowska, M., Kuzak, M., Zarebski, M., Kantyka, T., *et al.* (2009) Staphylococcal cysteine protease staphopain B (SspB) induces rapid engulfment of human neutrophils and monocytes by macrophages. *Biol Chem* **390**: 361–371.

Snelders, E., Huis In 't Veld, R.A.G., Rijs, A.J.M.M., Kema, G.H.J., Melchers, W.J.G., and Verweij, P.E. (2009) Possible environmental origin of resistance of *Aspergillus fumigatus* to medical triazoles. *Appl Environ Microbiol* **75**: 4053–4057.

Söderhäll, K., and Cerenius, L. (1998) Role of the prophenoloxidase-activating system in invertebrate immunity. *Curr Opin Immunol* **10**: 23–28.

Solano, F. (2014) Melanins: Skin Pigments and Much More—Types, Structural Models, Biological Functions, and Formation Routes. *New J Sci* **2014**: 1–28.

Sørensen, O.E., Follin, P., Johnsen, A.H., Calafat, J., Tjabringa, G.S., Hiemstra, P.S., and Borregaard, N. (2017) Human cathelicidin , hCAP-18 , is processed to the antimicrobial peptide LL-37 by extracellular cleavage with proteinase 3. **97**: 3951–3960.

Sowa-Jasiłek, A., Zdybicka-Barabas, A., Stączek, S., Wydrych, J., Skrzypiec, K., Mak, P., *et al.* (2016) *Galleria mellonella* lysozyme induces apoptotic changes in *Candida albicans* cells. *Microbiol Res* **193**: 121–131.

Spaulding, A.R., Salgado-Pabón, W., Kohler, P.L., Horswill, A.R., Leung, D.Y.M., and Schlievert, P.M. (2013) Staphylococcal and streptococcal superantigen exotoxins. *Clin Microbiol Rev* **26**: 422–447.

Srivastava, P. (2002) Roles of heat-shock proteins in innate and adaptive immunity. *Nat Rev Immunol* **2**: 185–194.

Stevens, D.A., Moss, R.B., Kurup, V.P., Knutsen, A.P., Greenberger, P., Judson, M.A., *et al.* (2003) Allergic Bronchopulmonary Aspergillosis in Cystic Fibrosis — State of the Art : Cystic Fibrosis Foundation Consensus Conference Encounters And Allergic. *Clin Infect Dis* **37**: S225-64.

Strand, M.R. (2008) Insect Hemocytes and Their Role in Immunity. *Insect Immunol* **32**: 25–47.

Sun, J.N., Solis, N. V., Phan, Q.T., Bajwa, J.S., Kashleva, H., Thompson, A., *et al.* (2010) Host cell invasion and virulence mediated by *Candida albicans* Ssa1. *PLoS Pathog* **6**: e1001181.

Surlis, C., Carolan, J.C., Coffey, M., and Kavanagh, K. (2018) Quantitative proteomics reveals divergent responses in *Apis mellifera* worker and drone pupae to parasitization by Varroa destructor. *J Insect Physiol* **107**: 291–301.

Tarkowski, A., Collins, L., Gjertsson, I., Hultgren, O.H., Jonsson, I.M., Sakiniene, E., and Verdrengh, M. (2001) Model systems: Modeling human staphylococcal arthritis and sepsis in the mouse. *Trends Microbiol* **9**: 321–326.

Taszlow, P., and Wojda, I. (2015) Changes in the hemolymph protein profiles in *Galleria mellonella* infected with *Bacillus thuringiensis* involve apolipophorin III. The effect of heat shock. *Arch Insect Biochem Physiol* **88**: 123–143.

Test, S.T., Lampert, M.B., Ossanna, P.J., Thoene, J.G., and Weiss, S.J. (1984) Generation of nitrogen-chlorine oxidants by human phagocytes. *J Clin Invest* **74**: 1341–1349.

Thati, B., Noble, A., Rowan, R., Creaven, B.S., Walsh, M., McCann, M., *et al.* (2007) Mechanism of action of coumarin and silver(I)-coumarin complexes against the pathogenic yeast *Candida albicans*. *Toxicol Vitr* **21**: 801–808.

Thennarasu, S., Tan, A., Penumatchu, R., Shelburne, C.E., Heyl, D.L., and Ramamoorthy, A. (2010) Antimicrobial and Membrane Disrupting Activities of a Peptide Derived from the Human Cathelicidin Antimicrobial Peptide LL37. *Biophysj* **98**: 248–257.

Thomaz, L., García-Rodas, R., Guimarães, A.J., Taborda, C.P., Zaragoza, O., and Nosanchuk, J.D. (2013) *Galleria mellonella* as a model host to study *Paracoccidioides Lutzii* and *Histoplasma Capsulatum. Virulence* **4**: 139–146.

Thomer, L., Schneewind, O., and Missiakas, D. (2016) Pathogenesis of *Staphylococcus aureus* Bloodstream Infections. *Annu Rev Pathol Mech Dis* **11**: 343–364.

Ting, A.T., and Bertrand, M.J.M. (2016) More to Life than NF-κB in TNFR1 Signaling. *Trends Immunol* **37**: 535–545.

Tobin, D.M., May, R.C., and Wheeler, R.T. (2012) Zebrafish: A see-through host and a fluorescent toolbox to probe host-pathogen interaction. *PLoS Pathog* **8**: e1002349.

Tomasinsig, L., and Zanetti, M. (2005) The Cathelicidins – Structure , Function and Evolution. *Curr Protein Pept Sci* **6**: 23–34.

Tong, S.Y.C., Davis, J.S., Eichenberger, E., Holland, T.L., and Fowler, V.G. (2015) *Staphylococcus aureus* infections: Epidemiology, pathophysiology, clinical manifestations, and management. *Clin Microbiol Rev* **28**: 603–661.

Tournu, H., Fiori, A., and Dijck, P. Van (2013) Relevance of Trehalose in Pathogenicity: Some General Rules, Yet Many Exceptions. *PLoS Pathog* **9**: e1003447.

Trevijano-Contador, N., Herrero-Fernández, I., García-Barbazán, I., Scorzoni, L., Rueda, C., Rossi, S.A., *et al.* (2014) *Cryptococcus neoformans* induces antimicrobial responses and behaves as a facultative intracellular pathogen in the non mammalian model *Galleria mellonella*. *Virulence* **6**: 66–74.

Tsai, C.J.-Y., Loh, J.M.S., Proft, T., Jia, C., Tsai, -Yun, Mei, J., *et al.* (2016) *Galleria mellonella* infection models for the study of bacterial diseases and for antimicrobial drug testing. *Virulence* **7**: 214–29.

Tsai, P.W., Cheng, Y.L., Hsieh, W.P., and Lan, C.Y. (2014) Responses of *Candida albicans* to the human antimicrobial peptide LL-37. *J Microbiol* **52**: 581–589.

Tsai, P.W., Yang, C.Y., Chang, H.T., and Lan, C.Y. (2011) Human antimicrobial peptide LL-37 inhibits adhesion of *Candida albicans* by interacting with yeast cell-wall carbohydrates. *PLoS One* **6**.

Tsoni, S.V., Kerrigan, A.M., Marakalala, M.J., Srinivasan, N., Duffield, M., Taylor, P.R., *et al.* (2009) Complement C3 plays an essential role in the control of opportunistic fungal infections. *Infect Immun* **77**: 3679–3685.

Tuli, L., and W. Ressom, H. (2009) LC–MS Based Detection of Differential Protein Expression. *J Proteomics Bioinform* **2**: 416–438.

Turner, J., Cho, Y., Dinh, N.N., Waring, A.J., and Lehrer, R.I. (1998) Activities of LL-37, a cathelin-associated antimicrobial peptide of human neutrophils. *Antimicrob Agents Chemother* **42**: 2206–2214.

Uchida, R., Namiguchi, S., Ishijima, H., and Tomoda, H. (2016) Therapeutic effects of three trichothecenes in the silkworm infection assay with *Candida albicans*. *Drug Discov Ther* **10**: 44–48.

Upadhyay, S.K., Gautam, P., Pandit, H., Singh, Y., Basir, S.F., and Madan, T. (2012) Identification of fibrinogen-binding proteins of *Aspergillus fumigatus* using proteomic approach. *Mycopathologia* **173**: 73–82.

Upadhyay, S.K., Mahajan, L., Ramjee, S., Singh, Y., Basir, S.F., and Madan, T. (2009) Identification and characterization of a laminin-binding protein of *Aspergillus fumigatus*: Extracellular thaumatin domain protein (AfCalAp). *J Med Microbiol* **58**: 714–722.

Urban, C., Xiong, X., Sohn, K., Schröppel, K., Brunner, H., and Rupp, S. (2005) The moonlighting protein Tsa1p is implicated in oxidative stress response and in cell wall biogenesis in *Candida albicans*. *Mol Microbiol* **57**: 1318–1341.

Valanne, S., Wang, J.-H., and Ramet, M. (2011) The Drosophila Toll Signaling Pathway. *J Immunol* **186**: 649–656.

Vasco, P., Herriko, E., Rementeria, A., López-molina, N., and Ludwig, A. (2005) Genes and molecules involved in *Aspergillus fumigatus* virulence Genes and molecules involved in *Aspergillus fumigatus* virulence. *Rev Iberoam Micol* **22(1)**: 1–23.

Veerdonk, F.L. van de, Gresnigt, M.S., Romani, L., Netea, M.G., and Latgé, J.-P. (2017) *Aspergillus fumigatus* morphology and dynamic host interactions. *Nat Rev Microbiol* **15**: 661–674.

Veerman, E.C.I., and Amerongen, A.V.N. (2005) Candidacidal effects of two antimicrobial peptides : histatin 5 causes small membrane defects , but LL-37 causes massive disruption of the cell membrane. **695**: 689–695.

Velagapudi, R., Hsueh, Y.P., Geunes-Boyer, S., Wright, J.R., and Heitman, J. (2009) Spores as infectious propagules of *Cryptococcus neoformans*. *Infect Immun* **77**: 4345–4355.

Vertyporokh, L., Taszłow, P., Samorek-Pieróg, M., and Wojda, I. (2015) Short-term heat shock affects the course of immune response in *Galleria mellonella* naturally infected with the entomopathogenic fungus Beauveria bassiana. *J Invertebr Pathol* **130**: 42–51.

Vertyporokh, L., and Wojda, I. (2017) Expression of the insect metalloproteinase inhibitor IMPI in the fat body of *Galleria mellonella* exposed to infection with *Beauveria bassiana*. *Acta Biochim Pol* **64**: 273–278.

Vilcinskas, A., and Wedde, M. (2002) Insect inhibitors of metalloproteinases. *IUBMB Life* **54**: 339–343.

Vilmos, P., and Kurucz, É. (1998) Insect immunity: Evolutionary roots of the mammalian innate immune system. *Immunol Lett* **62**: 59–66.

Vödisch, M., Scherlach, K., Winkler, R., Hertweck, C., Braun, H.P., Roth, M., *et al.* (2011) Analysis of the *Aspergillus fumigatus* proteome reveals metabolic changes and the activation of the pseurotin A biosynthesis gene cluster in response to hypoxia. *J Proteome Res* **10**: 2508–2524.

Vogel, H., Altincicek, B., Glöckner, G., and Vilcinskas, A. (2011) A comprehensive transcriptome and immune- gene repertoire of the lepidopteran model host *Galleria mellonella*. *BMC Genomics* **12**: 308.

Walther, T.C., and Mann, M. (2010) Mass spectrometry-based proteomics in cell biology. *J Cell Biol* **190**: 491–500.

Wand, M.E., McCowen, J.W.I., Nugent, P.G., and Sutton, J.M. (2013) Complex interactions of *Klebsiella pneumoniae* with the host immune system in a *Galleria mellonella* infection model. *J Med Microbiol* **62**: 1790–1798.

Wang, G., Li, X., and Wang, Z. (2016) APD3: The antimicrobial peptide database as a tool for research and education. *Nucleic Acids Res* **44**: D1087–D1093.

Wang, Q., Liu, Y., He, H.J., Zhao, X.F., and Wang, J.X. (2010) Immune responses of *Helicoverpa armigera* to different kinds of pathogens.

BMC Immunol **11**.

Wartenberg, D., Lapp, K., Jacobsen, I.D., Dahse, H.M., Kniemeyer, O., Heinekamp, T., and Brakhage, A.A. (2011) Secretome analysis of *Aspergillus fumigatus* reveals Asp-hemolysin as a major secreted protein. *Int J Med Microbiol* **301**: 602–611.

Wedde, M., Weise, C., Nuck, R., Altincicek, B., and Vilcinskas, A. (2007) The insect metalloproteinase inhibitor gene of the lepidopteran *Galleria mellonella* encodes two distinct inhibitors. *Biol Chem* **388**: 119–127.

Weerden, N.L. Van Der, Bleackley, M.R., and Anderson, M.A. (2013) Properties and mechanisms of action of naturally occurring antifungal peptides. *Cell Mol Life Sci* **70**: 3545–3570.

Weig, M., Frosch, M., Tintelnot, K., and Haas, A. (2001) Use of Recombinant Mitogillin for Improved Serodiagnosis of *Aspergillus fumigatus* -Associated Diseases. **39**: 1721–1730.

Weiss, S.J., Klein, R., Slivka, A., and Wei, M. (1982) Chlorination of taurine by human neutrophils. *J Clin Invest* **70**: 598–607.

Weiss, W.J., Lenoy, E., Murphy, T., Tardio, L.A., Burgio, P., Projan, S.J., *et al.* (2004) Effect of srtA and srtB gene expression on the virulence of *Staphylococcus aureus* in animal models of infection. *J Antimicrob Chemother* **53**: 480–486.

Weissman, Z., and Kornitzer, D. (2004) A family of *Candida* cell surface haem-binding proteins involved in haemin and haemoglobin-iron utilization. *Mol Microbiol* **53**: 1209–1220.

Whitten, M.M.A., Tew, I.F., Lee, B.L., and Ratcliffe, N.A. (2004) A Novel Role for an Insect Apolipoprotein (Apolipophorin III) in B-1,3-Glucan Pattern Recognition and Cellular Encapsulation Reactions. *J Immunol* **172**: 2177–2185.

Wiemken, A. (1990) Trehalose in yeast, stress protectant rather than reserve carbohydrate. *Antonie Van Leeuwenhoek* **58**: 209–217.

Wiesner, J., and Vilcinskas, A. (2010) Antimicrobial peptides: The ancient arm of the human immune system. *Virulence* **1**: 440–464.

Williams, D., Kadaria, D., Sodhi, A., Fox, R., Williams, G., and Threlkeld, S. (2017) Chronic Granulomatous Disease Presenting as *Aspergillus Fumigatus* Pneumonia in a Previously Healthy Young Woman. *Am J Case Rep* **18**: 351–354.

Witko-Sarsat, V., Delacourt, C., Rabier, D., Bardet, J., Nguyen, A.T., and Descamps-Latscha, B. (1995) Neutrophil-derived long-lived oxidants in cystic fibrosis sputum. *Am J Respir Crit Care Med* **152**: 1910–1916.

Wojda, I. (2017) Immunity of the greater wax moth *Galleria mellonella. Insect Sci* **24**: 342–357.

Wojda, I., and Jakubowicz, T. (2007) Humoral immune response upon mild heat-shock conditions in *Galleria mellonella* larvae. *J Insect Physiol* **53**: 1134–1144.

Wojda, I., Kowalski, P., and Jakubowicz, T. (2009) Humoral immune response of *Galleria mellonella* larvae after infection by *Beauveria bassiana* under optimal and heat-shock conditions. *J Insect Physiol* .

Wojda, I., and Taszłow, P. (2013) Heat shock affects host-pathogen interaction in *Galleria mellonella* infected with *Bacillus thuringiensis*. *J Insect Physiol* **59**: 894–905.

Woods, C.M., Hooper, D.N., Ooi, E.H., Tan, L.W., and Carney, A.S. (2011) Human lysozyme has fungicidal activity against nasal fungi. *Am J Rhinol Allergy* **25**: 236–240.

Woon Shin, S., Park, S.S., Park, D.S., Gwang Kim, M., Sun Chang Kim, Brey, P.T., and Park, H.Y. (1998) Isolation and characterization of immune-related genes from the fall webworm, *Hyphantria cunea*, using PCR-based differential display and subtractive cloning. *Insect Biochem Mol Biol* **28**: 827–837.

Wu, G., Yi, Y., Lv, Y., Li, M., Wang, J., and Qiu, L. (2015) The lipopolysaccharide (LPS) of *Photorhabdus luminescens* TT01 can elicit dose- and time-dependent immune priming in *Galleria mellonella* larvae. *J Invertebr Pathol* **127**: 63–72.

Wu, T., Samaranayake, L.P., Leung, W.K., and Sullivan, P.A. (1999) Inhibition of growth and secreted aspartyl proteinase production in *Candida albicans* by lysozyme. *J Med Microbiol* **48**: 721–730.

Xhindoli, D., Pacor, S., Benincasa, M., Scocchi, M., Gennaro, R., and Tossi, A. (2016) The human cathelicidin LL-37 - A pore-forming antibacterial peptide and host-cell modulator. *Biochim Biophys Acta - Biomembr* **1858**: 546–566.

Xiao, L., Feng, Q., Liang, S., Sonne, S.B., Xia, Z., Qiu, X., *et al.* (2015) A catalog of the mouse gut metagenome. *Nat Biotechnol* **33**: 1103–1108.

Xiao, W., Hsu, Y.P., Ishizaka, A., Kirikae, T., and Moss, R.B. (2005) Sputum cathelicidin, urokinase plasminogen activation system components, and cytokines discriminate cystic fibrosis, COPD, and asthma inflammation. *Chest* **128**: 2316–2326.

Xu, X.X., Zhong, X., Yi, H.Y., and Yu, X.Q. (2012) *Manduca sexta* gloverin binds microbial components and is active against bacteria and fungi. *Dev Comp Immunol* **38**: 275–284.

Yaakov, D. Ben, Rivkin, A., Mircus, G., Albert, N., Dietl, A.M., Kovalerchick, D., *et al.* (2016) Identification and characterization of haemofungin, a novel antifungal compound that inhibits the final step of haem biosynthesis. *J Antimicrob Chemother* **71**: 946–952.

Yamasaki, K. Nardo, DA. Antonella Bardan, A. Gallo, G. et al. (2007) Increased serine protease activity and cathelicidin promotes skin inflammation in rosacea. *Nat Med* **13**: 975–980.

Yanay, C., Morpurgo, N., and Linial, M. (2008) Evolution of insect proteomes: Insights into synapse organization and synaptic vesicle life cycle. *Genome Biol* **9**.

Yang, C., Zhang, Y., Jacob, M.R., Shabana, I., Yang, C., Zhang, Y., *et al.* (2006) Antifungal Activity of C-27 Steroidal Saponins Antifungal Activity of C-27 Steroidal Saponins. **50**: 2–7.

Yang, De, Chen, Q., Schmidt, A.P., Anderson, G.M., Wang, J.M., Wooters, J., *et al.* (2000) Ll-37, the Neutrophil Granule–And Epithelial Cell–Derived Cathelicidin, Utilizes Formyl Peptide Receptor–Like 1 (Fprl1) as a Receptor to Chemoattract Human Peripheral Blood Neutrophils, Monocytes, and T Cells. *J Exp Med* **192**: 1069–1074.

Yasmin, S., Alcazar-Fuoli, L., Grundlinger, M., Puempel, T., Cairns, T., Blatzer, M., *et al.* (2012) Mevalonate governs interdependency of ergosterol and siderophore biosyntheses in the fungal pathogen *Aspergillus fumigatus*. *Proc Natl Acad Sci* **109**: E497–E504.

Yi, H.-Y., Chowdhury, M., Huang, Y.-D., and Yu, X.-Q. (2014) Insect Antimicrobial Peptides and Their Applications. *Appl Microbiol Biotechnol* **98**: 5807–5822.

Yi, H.-Y., Deng, X.-J., Yang, W.-Y., Zhou, C.-Z., Cao, Y., Yu, X.-Q., *et al.* (2013) Gloverins of the silkworm *Bombyx mori:* Structural and binding properties and activities. *Insect Biochem Mol Biol* **43**: 612–625.

Yu, X.Q., and Kanost, M.R. (2002) Binding of hemolin to bacterial lipopolysaccharide and lipoteichoic acid: An immunoglobulin superfamily member from insects as a pattern-recognition receptor. *Eur J Biochem* **269**: 1827–1834.

Yun, J.E., and Lee, D.G. (2016) Cecropin A-induced apoptosis is regulated by ion balance and glutathione antioxidant system in *Candida albicans*. *IUBMB Life* 652–662.

Zarnowski, R., Sanchez, H., Covelli, A.S., Dominguez, E., Jaromin, A., Bernhardt, J., *et al.* (2018) *Candida albicans* biofilm-induced vesicles confer drug resistance through matrix biogenesis. *PLoS Biol* **16**: e2006872.

Zdybicka-Barabas, A., and Cytryńska, M. (2011) Involvement of apolipophorin III in antibacterial defense of *Galleria mellonella* larvae. *Comp Biochem Physiol - B Biochem Mol Biol* **158**: 90–98.

Zdybicka-Barabas, A., and Cytryñska, M. (2013) Apolipophorins and insects immune response. *ISJ - Invertebr Surviv J* **10**: 58–68.

Zdybicka-Barabas, A., Mak, P., Jakubowicz, T., and Cytryńska, M. (2014) Lysozyme and defense peptides as suppressors of phenoloxidase activity in *Galleria mellonella. Arch Insect Biochem Physiol* **87**: 1–12.

Zdybicka-Barabas, A., Stączek, S., Mak, P., Skrzypiec, K., Mendyk, E., and Cytryńska, M. (2013) Synergistic action of *Galleria mellonella* apolipophorin III and lysozyme against Gram-negative bacteria. *Biochim Biophys Acta - Biomembr* **1828**: 1449–1456.

Zgliczyński, J.M., Stelmaszyńska, T., Domański, J., and Ostrowski, W. (1971) Chloramines as intermediates of oxidation reaction of amino acids by myeloperoxidase. *BBA - Enzymol* **235**: 419–424.

Zhang, G., and Ghosh, S. (2001) Toll-like receptor-mediated NF-κB activation: A phylogenetically conserved paradigm in innate immunity. *J Clin Invest* **107**: 13–19.

Zhang, J., Li, Q., Wei, G., Wang, L., Qian, C., Sun, Y., *et al.* (2019) Identification and function of a lebocin-like gene from the Chinese oak silkworm, *Antheraea pernyi*. *J Invertebr Pathol* **166**: 107207.

Zhang, L.J., and Gallo, R.L. (2016) Antimicrobial peptides. *Curr Biol* **26**: R14–R19.

Zhang, Y., Wu, J., Xin, Z., and Wu, X. (2014) *Aspergillus fumigatus* triggers innate immune response via NOD1 signaling in human corneal epithelial cells. *Exp Eye Res* **127**: 170–178.

Zhao, P., Li, J., Wang, Y., and Jiang, H. (2007) Broad-spectrum antimicrobial activity of the reactive compounds generated *in vitro* by *Manduca sexta* phenoloxidase. *Insect Biochem Mol Biol* **37**: 952–959.

Zou, Z., Wang, Y., and Jiang, H. (2005) *Manduca sexta* prophenoloxidase activating proteinase-1 (PAP-1) gene: Organization, expression, and regulation by immune and hormonal signals. *Insect Biochem Mol Biol* **35**: 627–636.

Chapter 13

Appendices

The following Appendices are located on the disc provided or at the link below:

- https://drive.google.com/file/d/1JLotXQzNa4DBsbTkTbg6aNQeWn9YJTUi/view?usp=sharing
- https://tinyurl.com/AppendixGS

Appendices: List of Tables

Table No.	Table Title
Table A3.1	Proteins which were found to be increased (A) and decreased (B) in 6 h *C. albicans* infection larvae relative to 0 h infected larvae.
Table A3.2	Proteins which were found to be increased (A) and decreased (B) in 24 h *C. albicans* infection larvae relative to 0 h infected larvae.
Table A3.3	Functional enrichment of *C. albicans* proteins released during infection of *G. mellonella* larvae.
Table A3.4	List of proteins detected in *G. mellonella* larval hemolymph after 24 h infection with *C. albicans* at 30 ºC.
Table A3.5	Functional enrichment of proteins differentially abundant proteins from *C. albicans* exposed to *G. mellonella* larvae hemolymph
Table A3.5	List of proteins detected which were statistically significant and differentially in *C. albicans* incubated in *G. mellonella* hemolymph as compared to PBS after 6 h incubated at 30 ºC
Table A4.1	Proteins increased (Red) and decreased (Green) in abundance in *G. mellonella* larvae hemolymph infected with *S. aureus* for 6 h as compared to 0 h
Table A4.2	Proteins increased (Red) and decreased (Green) in abundance in *G. mellonella* larvae hemolymph infected with *S. aureus* for 24 h as compared to 0 h
Table A5.1	Proteins changed (increased [+] and decreased [-]) in abundance in *G. mellonella* larvae co-infected with *C. albicans* [1×10^5 $larva^{-1}$] *S. aureus* [2×10^4 $larva^{-1}$]) at 6 h relative to control larvae
Table A5.2	Proteins changed (increased [+] and decreased [-]) in abundance in *G. mellonella* larvae co-infected with *C. albicans* [1×10^5 $larva^{-1}$] *S. aureus* [2×10^4 $larva^{-1}$]) at 24 h relative to control larvae
Table A5.3	List of *C. albicans* proteins detected in *G. mellonella* larval hemolymph at 24 h post co-infection with *C. albicans* [1×10^5 $larva^{-1}$] *S. aureus* [2×10^4 $larva^{-1}$]).
Table A5.4	List of *S. aureus* proteins detected in *G. mellonella* larval hemolymph at 24 h post co-infection with *C. albicans* [1×10^5 $larva^{-1}$] *S. aureus* [2×10^4 $larva^{-1}$]).
Table A6.1	Proteins which are changed (increased [+] and decreased [-]) in *G. mellonella* larval hemolymph in response to infection to *A. fumigatus* 6 h post infection.
Table A6.2	Proteins which are changed (increased [+] and decreased [-]) in *G. mellonella* larval hemolymph in response to infection to *A. fumigatus* 24 h post infection.
Table A7.1	Proteins from *M. mycetomatis* identified within grains extracted from infected *G. mellonella* larvae.
Table A7.2A	*G. mellonella* larval proteins increased in abundance in grains isolated from larvae infected with *M. mycetomatis* for 24 h as compared to control larval hemolymph proteome.
Table A7.2B	*G. mellonella* larval proteins decreased in abundance in nodules isolated from larvae infected with *M. mycetomatis* for 24 h as compared to control larval hemolymph proteome.
Table A7.3	*M. mycetomatis* proteins identified in *G. mellonella* larvae hemolymph during infection.

Table A7.4A *G. mellonella* larval proteins increased in abundance in 24 h *M. mycetomatis* infected *G. mellonella* larval hemolymph as compared to 0 h hemolymph.

Table 7.4B *G. mellonella* larval proteins decreased in abundance in 24 h *M. mycetomatis* infected *G. mellonella* larval hemolymph as compared to 0 h hemolymph.

Table A7.5 Enrichment for GO terms (Biological Process [A], Molecular Function [B] and Cellular Component [C]) from the total SSDA hemolymph proteins from *G. mellonella* larvae infected with *M. mycetomatis* (24 h relative to 0 h hemolymph proteome).

Table A7.6A *G. mellonella* larval proteins increased in abundance in grains isolated from larvae infected with *M. mycetomatis* for 72 h as compared to grains extracted from larvae infected with *M. mycetomatis* for 24 h.

Table A7.6B *G. mellonella* larval proteins decreased in abundance in grains isolated from larvae infected with *M. mycetomatis* for 72 h as compared to grains extracted from larvae infected with *M. mycetomatis* for 24 h.

Table A7.7A *G. mellonella* larval proteins increased in abundance in 72 h *M. mycetomatis* infected *G. mellonella* larval hemolymph as compared to 0 h hemolymph.

Table A7.7B *G. mellonella* larval proteins decreased in abundance in 72 h *M. mycetomatis* infected *G. mellonella* larval hemolymph as compared to 0 h hemolymph.

Table A7.8 Enrichment for GO terms (Biological Process [A], Molecular Function [B] and Cellular Component [C]) from the total SSDA hemolymph proteins from larvae infected with *M. mycetomatis* (3 days relative to 0 h hemolymph proteome).

Table A7.9A *G. mellonella* larval proteins increased in abundance in grains isolated from larvae infected with *M. mycetomatis* for 7 day as compared to grains extracted from larvae infected with *M. mycetomatis* for 72 h.

Table A7.9B *G. mellonella* larval proteins decreased in abundance in grains isolated from larvae infected with *M. mycetomatis* for 7 day as compared to grains extracted from larvae infected with *M. mycetomatis* for 72 h.

Table A7.10A *G. mellonella* larval proteins increased in abundance in 7 day *M. mycetomatis* infected *G. mellonella* larval hemolymph as compared to 0 h hemolymph.

Table A7.10B *G. mellonella* larval proteins decreased in abundance in 7 day *M. mycetomatis* infected *G. mellonella* larval hemolymph as compared to 0 h hemolymph.

Table A7.11 Enrichment for GO terms (Biological Process [A], Molecular Function [B] and Cellular Component [C]) from the total SSDA hemolymph proteins from larvae infected with *M. mycetomatis* (7 day relative to 0 h hemolymph proteome).

Table A8.1 *G. mellonella* larval hemolymph proteins altered in abundance (increased [red] and decreased [green] in larvae injected with 20 µl of heat killed *C. albicans* (1×10^6 20 μl^{-1}) and incubated at 30 ºC for 24 h as compared to control (30 ºC for 24 h).

Table A8.2 *G. mellonella* larval hemolymph proteins altered in abundance (increased [red] and decreased [green] in larvae injected with 20 µl of heat killed *Staphylococcus aureus* (OD 0.1) and incubated at 30 ºC for 24 h as compared to larvae injected with 20 µl and incubated at 30 ºC for 24 h.

Table A8.3 *G. mellonella* larval hemolymph proteins altered in abundance (increased [red] and decreased [green] in larvae injected with 20 µl of PBS and incubated at 37 ºC for 24 h as compared to larvae injected with 20 µl and incubated at 30 ºC for 24 h.

Table A9.1 Proteins changed (increased [+] and decreased [-]) in abundance in *A. fumigatus* mycelium exposed to LL-37 (5 µg/ml) for 24 h.

Table A9.2 Proteins changed (increased [+] and decreased [-]) in abundance in *A. fumigatus* mycelium exposed to LL-37 (5 µg/ml) for 48 h.

Table A10.1 List of proteins which are decreased in abundance in N-Chlorotaurine (6.8 mM) treated *A. fumigatus* (ATCC 26933) mycelium as compared to untreated mycelium.

Table A3.1. Proteins which were found to be increased (A) and decreased (B) in 6 h *C. albicans* infection larvae relative to 0 h infected larvae.

A

P - value	Fold Change (+)	Uniprot Identifier	Protein Name	Peptides
0.047214	3.3	Q2F5Y9	Mitochondrial aldehyde dehydrogenase	19
0.027488	3.1	B2DBM1	muscle protein 20-like protein	18
0.032262	2.4	Q5DI99	Prophenoloxidase activating protease I (Prophenoloxidase-activating proteinase-1)	3
0.02558	2.2	C0M4Z1	Tubulin alpha chain (Fragment)	3
0.033036	2.2	P01507	Cecropin-A (Cecropin-C)	2
0.014568	2.0	O96381	Immune-related Hdd1	21
0.003371	1.2	Q8ITT1	Peptidoglycan recognition-like protein B (Fragment)	13
0.047858	1.6	B4KSC6	Uncharacterized protein	8
0.022133	1.5	B0ZT34	Heat shock protein 25.4	15

B

P - value	Fold Change (-)	Uniprot Identifier	Protein Name	Peptides
0.039799	5.6	Q7KTW1	HDC11369 (IP19829p) (IP19929p)	3
0.008267	4.8	B2ZDZ0	Carboxylic ester hydrolase (EC 3.1.1.-)	7
0.014685	4.6	Q3LB95	Chemosensory protein 7; Chemosensory protein11	4
0.029352	2.9	A2TK65	Translationally controlled tumor protein	4
0.001736	2.1	D6WFH1	Glutamine synthetase (EC 6.3.1.2)	5
0.002121	1.8	Q75PQ3	Fructose-bisphosphate aldolase (EC 4.1.2.13)	4
0.007346	1.8	A1DYI5	Cathepsin B-like cysteine proteinase	6
0.026155	1.7	XP_970725	succinyl-CoA ligase	6
0.00076	1.7	B2DBI9	Uncharacterized protein	39
0.013062	1.6	Q1EPM0	Glyceraldehyde-3-phosphate dehydrogenase (EC 1.2.1.12)	14

Table A3.2: Proteins which were found to be increased (A) and decreased (B) in 24 h *C. albicans* infection larvae relative to 0 h infected larvae.

A

P - value	Fold Change (+)	Uniprot Identifier	Protein Name	Peptides
0.000932	174.3	B2DBM1	Transgelin	18
5.12E-05	141.3	B2DBI0	Tropomyosin 2	12
9.28E-05	121.4	A2AX87	Gustatory receptor	7
1.13E-05	114.1	Q964D6	Glutathione-S-transferase-like protein	13
0.001338	103.6	Q8T8B0	Tubulin beta chain	13
0.000189	101.2	D6WGB6	Selenium-binding protein 1-like Protein	19
2.62E-05	71.6	Q0P6N3	Peptidoglycan-recognition protein-LB (Fragment)	5
0.003558	66.2	Q16Z50	Calponin	11
0.000555	61.6	B0FMT1	Troponin I	10
5.33E-05	61.3	B2DBH9	Troponin T	8
0.00192	54.4	Q2F5Y9	Mitochondrial aldehyde dehydrogenase	19
0.001557	52.5	Q0VJV0	Gloverin	2
0.00368	49.4	O96382	Putative defense protein Hdd11 (Hyphantria differentially displayed gene 11)	9
0.009493	47.2	Q5R1P5	Heat shock protein hsp21.4	11
0.000103	45.1	Q1HPK1	Troponin C	11
0.009912	34.8	Q6Q2D7	Serpin-4B	4
1.8E-05	33.6	B0LF73	Beta actin	10
0.001766	30.6	C4P3Q0	Heat shock protein 90	18
0.000382	29.9	A5Z1R7	Superoxide dismutase (EC 1.15.1.1)	6
2.85E-05	28.7	B4KSC6	Uncharacterized protein	8
0.001798	27.4	C0LZ14	Troponin T transcript variant B (Fragment)	3
0.000109	26.3	K7IVY6	Uncharacterized protein	11
0.005037	26.1	B2DBL0	Elongation factor 1-alpha	13
0.002367	22.8	P85210	Cecropin-D-like peptide	2
0.038713	22.5	B2ZDZ0	Carboxylic ester hydrolase (EC 3.1.1.-)	1
0.003462	22.1	C0M4Z1	Tubulin alpha chain (Fragment)	3
2.86E-05	20.8	D6WME9	N-acetylneuraminate lyase-like Protein	7
0.005541	20.6	A5JSU6	Moricin-like peptide B	1
0.000508	20.1	A7BIV1	Peptidoglycan recognition protein-D	5
0.004394	19.8	Q1HPX6	Alcohol dehydrogenase	9
0.000451	19.1	D6WJ70	C-terminal-binding protein-like Protein	10
0.012853	16.5	Q2VG86	CLIP domain-containing serine protease 2 (EC 3.4.21.-) (BzArgOEtase) (BAEEase) [Cleaved into: CLIP domain-containing serine protease 2 light chain; CLIP domain-containing serine protease 2 heavy chain]	7
2.83E-05	15.4	Q5XUN5	Triosephosphate isomerase (EC 5.3.1.1)	16

0.004712	15.3	Q1G151	Putative alcohol dehydrogenase	5
0.01807	14.7	B2X122	Serpin-2	12
0.000223	14.6	Q17B70	AAEL005062-PA (AMP dependent coa ligase)	3
0.024649	13.8	A8QWQ4	Chemosensory protein	8
0.001428	13.5	O96381	Immune-related Hdd1	21
0.001373	13.0	B3NNF9	Uncharacterized protein, isoform A (Uncharacterized protein, isoform B)	5
0.001189	12.4	Q1HPR4	NADP-dependent oxidoreductase	8
0.048496	12.4	Q0Q011	Protease inhibitor-like protein	1
0.00206	12.3	D6W6F9	Electron transfer flavoprotein subunit alpha, mitochondrial-like Protein	6
0.010548	12.3	E0VZK1	High affinity nuclear juvenile hormone binding protein, putative	10
0.000934	12.2	A2FD36	Viral A-type inclusion protein, putative	4
0.009823	11.3	Q9BLL3	Serpin-like protein (SEP-LP)	8
0.016156	9.7	B5AFH2	Mitochondrial cytochrome c	5
0.006382	9.2	Q9U4X1	Glutathione S-transferase (EC 2.5.1.18)	7
0.034363	9.0	E0VRD9	10 kDa heat shock protein, putative	8
0.008303	8.0	Q5CCL3	Peptidyl-prolyl cis-trans isomerase (PPIase) (EC 5.2.1.8)	7
0.002343	7.8	Q3S2I9	Phosphoglycerate mutase (EC 5.4.2.11) (EC 5.4.2.4)	11
0.001791	7.6	B4NZC0	Uncharacterized protein (EC 3.4.13.-)	8
0.002666	7.5	A1E8I8	Profilin	6
0.00027	7.5	Q8ITT1	Peptidoglycan recognition-like protein B (Fragment)	13
0.004235	7.1	A6YPQ5	Ubiquitin carboxyl-terminal hydrolase (EC 3.4.19.12)	4
0.001176	6.8	B8XE47	Arginine kinase (Fragment)	11
0.024256	6.4	Q22TN9	Uncharacterized protein	6
0.003036	6.3	A2TK65	Translationally controlled tumor protein	4
0.003877	6.1	Q5F320	Annexin	9
0.008769	5.9	Q5MGP0	Heat shock protein 1	8
0.034761	5.6	Q5MGF8	Uncharacterized protein (Fragment)	9
1.22E-05	5.1	A8QWQ6	Chemosensory protein	6
0.001586	4.9	D6WFH1	Glutamine synthetase (EC 6.3.1.2)	5
0.006518	4.5	B7PIM5	CNDP dipeptidase, putative (EC 3.5.1.18) (CNDP dipeptidase, putative (Fragment) (Fragment)) (Fragment)	6
0.00378	4.0	Q8MUB0	Dihydrolipoyl dehydrogenase (EC 1.8.1.4)	8
0.002149	3.7	B1NLD7	Uncharacterized protein (Fragment)	17
0.026476	3.7	Q2F5I4	Protease inhibitor 1	3
0.044067	3.4	Q1HQD0	S-(hydroxymethyl)glutathione dehydrogenase (EC 1.1.1.284)	5
0.000631	3.2	Q1HQ86	Mobility group protein 1B	4
0.0468	3.2	A0FDR1	Thioredoxin	7
0.036249	3.1	B0WPV2	Uncharacterized protein	3

0.000178	3.0	Q6F440	Cellular retinoic acid binding protein	17
0.048097	2.9	Q402D8	Juvenile hormone binding protein	2
0.033825	2.8	Q8ITS7	Heat shock-like protein (Fragment)	5
0.002924	2.7	Q0KKW8	Multi-binding protein	3
0.008025	2.5	A0CJH0	Uncharacterized protein	6
0.025499	2.5	Q6F456	Diazepam binding inhibitor-like protein	5
0.003599	2.4	A1YQ87	Enolase	25
0.001967	2.2	Q75PQ3	Fructose-bisphosphate aldolase (EC 4.1.2.13)	4
0.038818	2.0	Q867T1	Serpin 3a (Serpin 3b)	9
0.020851	1.9	Q5U9P8	Hemolin (Fragment)	14
0.002043	1.9	Q1HPY5	Scolexin	16
0.010164	1.9	Q9XTN0	Peptidoglycan recognition protein	11
0.013215	1.8	Q49QW0	Prophenol oxidase activating enzyme 3	16
0.011678	1.7	A9LS22	Carboxylic ester hydrolase (EC 3.1.1.-)	7
0.01476	1.6	Q1EPM0	Glyceraldehyde-3-phosphate dehydrogenase (EC 1.2.1.12)	14

B

P - value	Fold Change (-)	Uniprot Identifier	Protein Name	Peptides
0.00183	28.6	Q0E666	Beta-1,3-glucan recognition protein	17
0.000269	25.4	A9NVX2	Uncharacterized protein	5
0.019678	25.2	34556399	prophenoloxidase subunit 2	2
0.006403	6.4	B4MSH8	Uncharacterized protein (EC 3.1.-.-)	7
0.008236	5.2	Q68AP5	Catalase (EC 1.11.1.6)	16
0.018832	5.2	Q8IT91	Kunitz-like protease inhibitor	2
0.007029	4.9	A5A142	Lysozyme-like protein 1	5
0.019072	4.5	B6CMG2	Putative gram negative bacteria-binding protein	7
0.025951	4.4	Q6XD83	Spodoptericin (Fragment)	6
0.04556	3.4	Q8WRW9	Twelve cysteine protein 1	12
0.000169	3.3	A1DYI5	Cathepsin B-like cysteine proteinase	6
0.01041	3.0	A0NAZ8	General odorant-binding protein 68	10
0.009656	2.4	Q1HQ57	Fructose-1,6-bisphosphatase	3
5.48E-06	2.1	Q0QJJ5	Imaginal disc growth factor-like protein	14
0.004003	2.1	B2DBI9	Uncharacterized protein	39
0.000871	2.0	Q95P97	Bombyrin	10
0.012345	2.0	A4LA63	Cationic peptide CP8	5
0.001245	1.9	Q6IWP3	Imaginal disc growth factor	17
0.035453	1.9	B2DBM2	Similar to CG10638-PA	3
0.009591	1.9	Q68YP1	Apolipophorin (Fragment)	16
0.040119	1.9	Q3ZVJ0	Adhesion related protein, transmembrane	9
0.00857	1.9	D2A5L9	Apolipoprotein D-like Protein	18
0.004094	1.8	Q00630	Insecticyanin-B (INS-b) (Blue biliprotein)	14

0.017802	1.8	Q6UEH6	Prophenoloxidase subunit 2	4
0.004946	1.8	C1PIJ1	Uncharacterized protein (Fragment)	10
0.003084	1.8	C1PIJ1	Uncharacterized protein (Fragment)	4
0.031404	1.6	Q3LB46	Uncharacterized protein	15
0.038309	1.6	A9NZP3	Uncharacterized protein	27
0.015773	1.6	Q25490	Apolipophorins [Cleaved into: Apolipophorin-2 (Apolipophorin II) (apoLp-2); Apolipophorin-1 (Apolipophorin I) (apoLp-1)]	10

Table A3.3. Functional enrichment of *C. albicans* proteins released during infection of *G. mellonella* larvae. *C. albicans* proteins found during in hemolymph during infection of *G. mellonella* larvae were grouped into functional categories based on the GO (Gene Ontology) annotations, using the FungiFun application.

Biological Processes

GO name	Exact p-value	Adjusted p-value	# genes / input
interaction with host	1.40E-08	6.8596e-7	6 / 101
cellular response to heat	0.011762	0.040686	3 / 101
tricarboxylic acid cycle	0.0111	0.039035	2 / 101
translational frameshifting	0.0090044	0.032202	1 / 101
intracellular steroid hormone receptor signaling pathway	0.0090044	0.032202	1 / 101
carbohydrate metabolic process	0.0063708	0.032202	4 / 101
cell wall organization	0.0061783	0.032202	3 / 101
filamentous growth of a population of unicellular organisms in response to neutral pH	0.0048813	0.032202	4 / 101
response to stress	0.004316	0.032202	3 / 101
pathogenesis	0.0036173	0.032202	9 / 101

Molecular Function

GO name	Exact p-value	Adjusted p-value	# genes / input
protein binding	1.9506e-8	6.8596e-7	6 / 101
voltage-gated anion channel activity	0.0090044	0.032202	1 / 101
phosphoglycerate kinase activity	0.0090044	0.032202	1 / 101
protein domain specific binding	0.0090044	0.032202	1 / 101
[acyl-carrier-protein] S-acetyltransferase activity	0.0090044	0.032202	1 / 101
[acyl-carrier-protein] S-malonyltransferase activity	0.0090044	0.032202	1 / 101
glucan endo-1,3-beta-D-glucosidase activity	0.0090044	0.032202	1 / 101
tripeptidase activity	0.0090044	0.032202	1 / 101
GTP binding	0.0063708	0.032202	4 / 101
nucleotide binding	0.0036272	0.032202	11 / 101

Cellular Component

GO name	Exact p-value	Adjusted p-value	# genes / input
cytoplasm	2.5692e-8	7.7444e-7	17 / 101
hyphal cell wall	1.0846e-10	7.6282e-9	10 / 101
fungal-type cell wall	7.0681e-12	7.4568e-10	12 / 101
extracellular region	1.9038e-8	6.8596e-7	11 / 101

Table A3.4. List of proteins detected in *G. mellonella* larval hemolymph after 24 h infection with *C. albicans* at 30 ºC.

cell surface	8.2643e-15	1.7438e-12	16 / 101

Uniprot ID	Protein Name	Score
Q59LF8	Uncharacterized protein	7.7409
A0A1D8PDX7	Uncharacterized protein	5.6692
A0A1D8PF42	Uncharacterized protein	5.9446
A0A1D8PST6	Uncharacterized protein	5.6758
Q59Q31	Uncharacterized protein	5.6966
Q59W37	Uncharacterized protein	5.6725
A0A1D8PGR8	Uncharacterized protein	7.9593
A0A1D8PL12	Uncharacterized protein	5.6592
A0A1D8PQF9	Uncharacterized protein	26.633
Q59WF2	Uncharacterized protein	5.6608
Q59WE9	Uncharacterized protein	6.1614
A0A1D8PMI5	Uncharacterized protein	5.6584
Q5A881	Uncharacterized protein	7.9593
Q5ANL8	Uncharacterized protein	5.6593
A0A1D8PI28	Uncharacterized protein	5.6614
A0A1D8PDN5	Uncharacterized protein	5.9529
A0A1D8PEH4	Uncharacterized protein	5.9325
A0A1D8PKC4	Ubiquitin-specific protease	6.8759
Q5A109	Ubiquitin-ribosomal 40S subunit protein S31 fusion protein	27.124
A0A1D8PC97	Tubulin beta chain	323.31
Q5ADR6	Translation initiation factor eIF2B subunit delta	5.6603
Q59P53	Translation factor GUF1, mitochondrial (EC 3.6.5.-) (Elongation factor 4 homolog) (EF-4) (GTPase GUF1) (Ribosomal back-translocase)	5.8389
A0A1D8PM35	Translation elongation factor 1 subunit beta	25.804
Q59N20	Transcription activator MSS11	6.1961
A0A1D8PJA8	Tos1p	164.21
A0A1D8PU69	Thioredoxin	44.721
Q5A4W7	Tetrafunctional fatty acid synthase subunit	5.9325
Q5A0X8	Surface antigen protein 2	39.745
Q5A2A1	Succinate dehydrogenase [ubiquinone] flavoprotein subunit, mitochondrial (EC 1.3.5.1)	192.87
Q59M48	Ste13p	5.8699
A0A1D8PSJ3	Sgd1p	7.9593
A0A1D8PQA	Serine/threonine-protein phosphatase (EC 3.1.3.16)	6.2985

0		
Q5AKV0	Serine C-palmitoyltransferase	5.7159
Q5AB48	Secreted protein RBT4 (PRY family protein 4) (Repressed by TUP1 protein 4)	260.77
Q59NP5	Secreted beta-glucosidase SUN41 (EC 3.2.1.-)	50.289
A0A1D8PQE5	RNA export factor	5.7826
A0A1D8PQ43	Ribonuclease H (RNase H) (EC 3.1.26.4)	6.2477
Q5ACL4	Restriction of telomere capping protein 1	5.9325
A0A1D8PTI2	Rab family GTPase	6.0995
P83775	Putative NADPH-dependent methylglyoxal reductase GRP2 (EC 1.1.1.283) (Cytoplasmic antigenic protein 2)	177.62
A0A1D8PJ20	Proteasome endopeptidase complex (EC 3.4.25.1)	5.7313
P46273	Phosphoglycerate kinase (EC 2.7.2.3)	8.9416
A0A1D8PRM7	Phosphoenolpyruvate carboxykinase	23.656
A0A1D8PEF9	Pfk26p	11.519
Q9Y7F0	Peroxiredoxin TSA1-A (EC 1.11.1.15) (Thiol-specific antioxidant protein) (Thioredoxin peroxidase)	7.4149
A0A1D8PS61	Opt3p	5.9325
Q59UZ4	Opt2p	5.9325
Q5AG68	Nucleoside diphosphate kinase (EC 2.7.4.6)	29.991
P83781	Mitochondrial outer membrane protein porin (Cytoplasmic antigenic protein 4)	6.7964
P83778	Malate dehydrogenase, cytoplasmic (EC 1.1.1.37)	40.507
A0A1D8PCJ7	Mak32p	5.6759
A0A1D8PS79	Isocitrate dehydrogenase [NADP] (EC 1.1.1.42)	12.734
P83777	Inorganic pyrophosphatase (EC 3.6.1.1) (Pyrophosphate phospho-hydrolase) (PPase)	7.022
A0A1D8PSZ0	Ife2p	5.9325
A0A1D8PG96	Hsp70 family ATPase	201.87
Q5A397	Hsp70 family ATPase	11.766
Q59VP1	Histone H2B.2	323.31
Q59VP2	Histone H2A.2	6.2119
A0A1D8PSA6	Histone deacetylase (EC 3.5.1.98)	5.6685
Q59VZ0	Hgt2p	8.0582
P46587	Heat shock protein SSA2	60.755
Q96VB9	Heat shock protein homolog SSE1 (Chaperone protein MSI3)	7.9593
P46598	Heat shock protein 90 homolog	55.408
Q59P43	GTP-binding nuclear protein	8.2306
Q5ADM7	Glyceraldehyde-3-phosphate dehydrogenase (EC 1.2.1.12)	55.376
Q9URB4	Fructose-bisphosphate aldolase (FBP aldolase) (FBPA) (EC	35.783

	4.1.2.13) (37 kDa major allergen) (Fructose-1,6-bisphosphate aldolase) (IgE-binding allergen)	
A0A1D8PT02	Flavodoxin-like fold family protein	74.887
P30575	Enolase 1 (EC 4.2.1.11) (2-phospho-D-glycerate hydro-lyase) (2-phosphoglycerate dehydratase)	100.19
Q5A0M4	Elongation factor 2 (EF-2)	30.184
Q59QD6	Elongation factor 1-alpha 2 (EF-1-alpha 2)	20.337
Q59UP3	Dur4p	5.9325
A0A1D8PME5	DNA-binding E3 ubiquitin-protein ligase	5.659
Q5AGX1	DNA repair protein	5.7247
A0A1D8PML0	DNA primase large subunit (EC 2.7.7.-)	5.7479
Q5AKA5	Cys-Gly metallodipeptidase DUG1 (EC 3.4.13.-) (Deficient in utilization of glutathione protein 1) (GSH degradosomal complex subunit DUG1)	6.7964
Q59M50	Cwt1p	5.7175
A0A1D8PSH3	Citrate synthase	6.126
A0A1D8PFK5	Chitin synthase	5.6786
Q5AF39	Cell wall protein PGA59 (GPI-anchored protein 59)	6.7964
Q5A1E0	Cell wall protein IFF5 (Adhesin-like protein IFF5)	6.7964
G1UB63	Cell wall protein 1 (Surface antigen protein 1) (Wall protein 1)	6.2214
Q59XX2	Cell surface mannoprotein MP65 (EC 3.2.1.-) (Mannoprotein of 65 kDa) (Soluble cell wall protein 10)	323.31
A0A1D8PM94	Ald6p	5.8108
A0A1D8PP43	Adh1p	6.6413
A0A1D8PFR4	Actin	323.31
Q59WG3	AAA family ATPase	31.856
A0A1D8PFG4	60S ribosomal protein L27	6.1451
A0A1D8PFS4	6-phosphogluconate dehydrogenase, decarboxylating (EC 1.1.1.44)	22.893
O42766	14-3-3 protein homolog	31.898

Table A3.5. Functional enrichment of proteins differentially abundant proteins from *C. albicans* exposed to *G. mellonella* larvae hemolymph. Proteins that were found statistically significant and differentially abundance in *C. albicans* exposed to 100% hemolymph were grouped into functional categories based on the GO (Gene Ontology) annotations, using the FungiFun application.

Biological process

GO name	Exact p-value	# genes / category
translation	6.6882e-35	58 / 128
formation of translation preinitiation complex	6.3724e-9	7 / 7
regulation of translational initiation	4.7997e-8	7 / 8
translational initiation	9.2525e-8	12 / 28
glycolytic process	1.8762e-7	10 / 20
protein folding	1.1493E-06	14 / 46
carbohydrate metabolic process	1.8874E-06	19 / 83
translational elongation	3.3663E-06	8 / 16
oxidation-reduction process	9.7092E-06	51 / 407
methionine biosynthetic process	0.000014358	7 / 14
GDP-mannose biosynthetic process	0.000021031	4 / 4
malate metabolic process	0.000021031	4 / 4
pyrimidine nucleotide biosynthetic process	0.000099493	4 / 5
tricarboxylic acid cycle	0.00010481	7 / 18
cellular amino acid biosynthetic process	0.00012384	10 / 37
interaction with host	0.00022661	7 / 20
sulfate assimilation	0.00031166	3 / 3
carbohydrate phosphorylation	0.0011525	5 / 13
fatty acid beta-oxidation	0.0011807	4 / 8
glutamine metabolic process	0.0011835	3 / 4
'de novo' pyrimidine nucleobase biosynthetic process	0.0011835	3 / 4
glyoxylate cycle	0.0011835	3 / 4
UDP-N-acetylglucosamine biosynthetic process	0.0011835	3 / 4
glycogen biosynthetic process	0.0011835	3 / 4
trehalose biosynthetic process	0.0011835	3 / 4
cellular carbohydrate metabolic process	0.0011835	3 / 4
cellular response to drug	0.0013596	37 / 328
L-methionine biosynthetic process from methylthioadenosine	0.0028096	3 / 5
cellular protein metabolic process	0.0031744	4 / 10
protein peptidyl-prolyl isomerization	0.0031744	4 / 10
phosphorylation	0.0034577	15 / 102
rRNA processing	0.0034921	11 / 64
ribosome biogenesis	0.0034921	11 / 64
induction by symbiont of host defense response	0.0044638	6 / 24

hydrogen sulfide biosynthetic process	0.0046075	2 / 2
mitochondrial electron transport, ubiquinol to cytochrome c	0.0046075	2 / 2
'de novo' UMP biosynthetic process	0.0046075	2 / 2
acetyl-CoA biosynthetic process	0.0046075	2 / 2
fructose 6-phosphate metabolic process	0.0046075	2 / 2
acetyl-CoA biosynthetic process from acetate	0.0046075	2 / 2
hydrogen ion transmembrane transport	0.0047234	4 / 11
response to toxic substance	0.0053367	3 / 6
regulation of actin filament polymerization	0.0053367	3 / 6

Molecular function

GO name	Exact p-value	Adjusted p-value	# genes / category
structural constituent of ribosome	1.5601e-21	3.2372e-19	36 / 81
nucleotide binding	3.8332e-9	3.977e-7	68 / 490
lyase activity	5.7546e-8	2.9852E-06	13 / 32
RNA binding	7.1461e-8	3.489E-06	30 / 152
translation initiation factor activity	9.2525e-8	4.0419E-06	12 / 28
catalytic activity	5.7322e-7	2.2656E-05	46 / 319
isomerase activity	6.1527E-06	0.00018238	11 / 33
translation elongation factor activity	6.1685E-05	0.0015515	6 / 12
transferase activity	6.4532E-05	0.0015753	36 / 271
ATP binding	0.00014516	0.0030893	53 / 473
L-malate dehydrogenase activity	0.00031166	0.0056234	3 / 3
malate dehydrogenase activity	0.00031166	0.0056234	3 / 3
unfolded protein binding	0.00039326	0.0068002	8 / 28
peptidyl-prolyl cis-trans isomerase activity	0.00046366	0.0078539	5 / 11
cytochrome-c oxidase activity	0.00062369	0.010353	4 / 7
metallopeptidase activity	0.00087226	0.013756	6 / 18
oxidoreductase activity	0.0008784	0.013756	36 / 309
metal ion binding	0.00092029	0.014145	45 / 414
kinase activity	0.00097425	0.014702	14 / 81
oxidoreductase activity, acting on the CH-OH group of donors, NAD or NADP as acceptor	0.0010464	0.014884	8 / 32
succinate dehydrogenase activity	0.0011835	0.014884	3 / 4
GTP binding	0.0012476	0.015456	14 / 83
protein binding	0.0021413	0.024684	6 / 21
ligase activity	0.0030085	0.033294	10 / 54
ATP-dependent helicase activity	0.0032905	0.034571	7 / 30
flavin adenine dinucleotide binding	0.0040265	0.037128	8 / 39
trehalose-phosphatase activity	0.0046075	0.037128	2 / 2
cytochrome-b5 reductase activity, acting on NAD(P)H	0.0046075	0.037128	2 / 2

AMP binding	0.0046075	0.037128	2 / 2
6-phosphofructokinase activity	0.0046075	0.037128	2 / 2
mannose-1-phosphate guanylyltransferase activity	0.0046075	0.037128	2 / 2
acetate-CoA ligase activity	0.0046075	0.037128	2 / 2
FK506 binding	0.0046075	0.037128	2 / 2
oxidoreductase activity, acting on a sulfur group of donors, NAD(P) as acceptor	0.0046075	0.037128	2 / 2
pyruvate dehydrogenase (acetyl-transferring) activity	0.0046075	0.037128	2 / 2
3-dehydroquinate dehydratase activity	0.0046075	0.037128	2 / 2
NAD binding	0.0048362	0.038229	7 / 32
peptidase activity	0.005024	0.039339	11 / 67
hydrolase activity	0.0053339	0.040268	35 / 331
peptide binding	0.0053367	0.040268	3 / 6
GTPase activity	0.0064613	0.048314	8 / 42
aminopeptidase activity	0.0067097	0.049724	4 / 12

Cellular Component

GO name	Exact p-value	Adjusted p-value	# genes / category
cytoplasm	3.3477e-39	2.7786e-36	106 / 393
ribosome	6.1521e-22	1.7021e-19	37 / 84
ribonucleoprotein complex	3.7798e-15	6.2745e-13	28 / 72
cell surface	1.1072e-11	1.5316e-9	33 / 129
eukaryotic translation initiation factor 3 complex	4.2598e-10	5.0509e-8	8 / 8
eukaryotic 43S preinitiation complex	6.3724e-9	4.8083e-7	7 / 7
eukaryotic 48S preinitiation complex	6.3724e-9	4.8083e-7	7 / 7
intracellular	9.5751e-9	6.6228e-7	29 / 132
yeast-form cell wall	1.0982e-8	7.0116e-7	16 / 44
cytosol	5.1594e-8	2.8549E-06	14 / 37
plasma membrane	9.0272e-7	3.4057E-05	46 / 324
hyphal cell wall	2.305E-06	7.6527E-05	16 / 62
mitochondrion	5.2393E-06	0.00016106	29 / 175
large ribosomal subunit	0.00014177	0.0030893	5 / 9
fungal-type cell wall	0.00017938	0.0037222	16 / 86
hyphal septin ring	0.00031166	0.0056234	3 / 3
cytosolic small ribosomal subunit	0.00031166	0.0056234	3 / 3
small-subunit processome	0.00039326	0.0068002	8 / 28
cytoskeleton	0.00083335	0.013562	8 / 31
peroxisome	0.001621	0.019499	6 / 20
chromosome	0.0016826	0.019951	9 / 42
nucleosome	0.0020118	0.023518	4 / 9
mitochondrial outer membrane	0.0024005	0.027294	5 / 15

small ribosomal subunit	0.0031744	0.033779	4 / 10
nucleus	0.0042815	0.037128	59 / 622
cellular bud neck septin structure	0.0046075	0.037128	2 / 2
6-phosphofructokinase complex	0.0046075	0.037128	2 / 2

Table A3.6. List of proteins detected which were statistically significant and differentially in *C. albicans* incubated in *G. mellonella* hemolymph as compared to PBS after 6 h incubated at 30 ºC

(A) Proteins increased in abundance in *C. albicans* incubated in *G. mellonella* hemolymph.

Fold Change (+)	Uniprot ID	Protein Name
44.4	A0A1D8PL15	D-arabinose 1-dehydrogenase
12.1	Q59VX7	Karyopherin beta
11.6	A0A1D8PEW7	Uncharacterized protein
8.3	Q5AND9	Arf family GTPase
8.0	A0A1D8PGR6	5-oxoprolinase
7.9	A0A1D8PLT4	Karyopherin
7.8	Q5AI87	Carboxymethylenebutenolidase
7.7	Q59M69	ATP-dependent
7.6	Q59K86	3-hydroxyanthranilate 3,4-dioxygenase
7.5	A0A1D8PIF8	Leu42p
7.4	Q59SI4	Nmd5p
7.2	A0A1D8PTB8	Copper metallochaperone
7.0	A0A1D8PR39	Ahp2p
6.8	A0A1D8PSW2	Threonine aldolase
5.9	A0A1D8PMF7	Uncharacterized protein
5.8	A0A1D8PC97	Tubulin beta chain
5.8	Q5ALW6	Glutamine-dependent NAD+) synthetase
5.7	A0A1D8PN39	Uncharacterized protein
5.6	A0A1D8PNJ2	Uncharacterized protein
5.2	A0A1D8PHY7	Uncharacterized protein
5.2	A0A1D8PGP5	Uncharacterized protein
4.9	A0A1D8PDB0	Proteasome regulatory particle lid subunit
4.9	A0A1D8PE84	Cdr4p
4.7	A0A1D8PJF0	Uncharacterized protein
4.7	Q5A015	Riboflavin kinase
4.6	A0A1D8PLD7	Uncharacterized protein
4.5	A0A1D8PU69	Thioredoxin
4.3	Q5A8A6	Carbamoyl-phosphate synthase Glutamine-hydrolyzing)
4.2	A0A1D8PE78	Importin-alpha export receptor
4.1	Q5ADN1	Protein phosphatase 2A structural subunit
4.0	A0A1D8PLE6	Uncharacterized protein
3.9	A0A1D8PI19	Phm7p

3.8	A0A1D8PH17	V-type proton ATPase subunit F
3.7	Q5AM80	Enolase-phosphatase E1
3.7	A0A1D8PRI0	Nicotinate phosphoribosyltransferase
3.7	Q5AG73	Methylthioribulose-1-phosphate dehydratase MTRu-1-P dehydratase
3.6	A0A1D8PPX6	Uncharacterized protein
3.6	Q59RH5	Histone acetyltransferase type B subunit 2
3.5	Q59PE7	Protein BCP1
3.4	Q92209	Homoserine kinase
3.4	A0A1D8PDA4	Fma1p
3.4	A0A1D8PNK0	Dap2p
3.3	A0A1D8PHR5	Pst1p
3.3	A0A1D8PHQ6	Gre2p
3.3	A0A1D8PTY0	Uncharacterized protein
3.3	Q59NN8	Hsp70 nucleotide exchange factor FES1
3.2	A0A1D8PTV7	Putative cystathionine beta-lyase
3.2	A0A1D8PQ94	Hsp90 cochaperone
3.2	Q5A5B2	Uncharacterized protein
3.1	A0A1D8PCY4	Ecm33p
3.1	Q5AH60	tRNA (guanine-N7)-)-methyltransferase non-catalytic subunit TRM82
3.1	Q5AMR6	Uncharacterized protein
3.0	A0A1D8PQD4	E2 ubiquitin-conjugating protein
3.0	P56553	Cell growth-regulated gene 1 protein
3.0	Q5AF44	Thioredoxin peroxidase
3.0	A0A1D8PDL7	Uncharacterized protein
3.0	A0A1D8PFI3	Ribokinase
2.9	A0A1D8PGI9	Ubiquitinyl hydrolase 1
2.9	A0A1D8PT84	Uncharacterized protein
2.9	Q59Z17	Catabolic 3-dehydroquinase (cDHQase)
2.8	Q5A786	Profilin
2.7	Q59Z50	Spermidine synthase
2.7	A0A1D8PFU8	Uncharacterized protein
2.7	A0A1D8PFV6	Uncharacterized protein
2.7	A0A1D8PPB1	Ardp
2.7	A0A1D8PE63	Glutamate--cysteine ligase
2.7	G1UAZ9	Uncharacterized protein
2.5	A0A1D8PRF3	Uncharacterized protein
2.5	A0A1D8PNZ4	Cup1p
2.5	P0CY19	Deoxyuridine 5'-triphosphate nucleotidohydrolase
2.5	Q5A362	Cystathionine gamma-lyase
2.5	A0A1D8PJD2	Deoxyhypusine synthase
2.5	P87219	Sorbose reductase SOU1
2.5	Q59US5	Bifunctional cysteine synthase/O-acetylhomoserine aminocarboxypropyltransferase
2.4	A0A1D8PLH0	Phosphomevalonate kinase

2.4	A0A1D8PJD7	GTPase-activating protein
2.4	Q59Z55	Uncharacterized protein
2.4	Q59S63	tRNA pseudouridine synthase 1
2.4	Q59U89	Uncharacterized protein
2.4	Q5AHF9	Glucosamine 6-phosphate N-acetyltransferase
2.4	Q59P52	Phosphoserine aminotransferase
2.4	P43075	tRNA ligase
2.4	Q5ACY8	4a-hydroxytetrahydrobiopterin dehydratase
2.4	P28870	FK506-binding protein 1
2.3	A0A1D8PHW0	Sedoheptulose-bisphosphatase
2.3	A0A1D8PE37	Amidophosphoribosyltransferase
2.3	Q5AK98	Nucleotidase
2.3	A0A1D8PFF9	E2 ubiquitin-conjugating protein
2.3	A0A1D8PFS4	6-phosphogluconate dehydrogenase, decarboxylating
2.3	A0A1D8PKJ3	E1 ubiquitin-activating protein
2.3	Q5ABB2	Lactoylglutathione lyase
2.3	Q5ALX8	Adenine phosphoribosyltransferase
2.3	Q59N80	Inosine triphosphate pyrophosphatase
2.3	Q5A0L4	Plc2p
2.2	A0A1D8PKW2	Fructose 1,6-bisphosphate 1-phosphatase
2.2	A0A1D8PP67	Riboflavin synthase
2.2	A0A1D8PH39	Uncharacterized protein
2.2	A0A1D8PLI2	Isopentenyl-diphosphate delta-isomerase
2.2	P46587	Heat shock protein SSA2
2.1	Q59X24	Exopolyphosphatase
2.1	Q5AA13	Gim5p
2.1	Q59R27	Uncharacterized protein
2.1	A0A1D8PPG2	Uncharacterized protein
2.1	A0A1D8PHE5	Uncharacterized protein
2.1	Q5AMP4	Malate dehydrogenase
2.1	Q59MN2	Bifunctional 4-alpha-glucanotransferase/amylo-alpha-1,6-glucosidase
2.1	Q59VY8	Galactokinase
2.1	A0A1D8PJK5	D-lactate dehydrogenase
2.1	Q59T95	Cystathionine beta-synthase
2.1	Q5A934	Zinc finger-containing protein
2.1	A0A1D8PCS7	Putative pyridoxal 5'-phosphate synthase
2.1	P31225	Corticosteroid-binding protein
2.1	A0A1D8PNS0	Guanylate kinase
2.1	A0A1D8PH42	Branched-chain-amino-acid aminotransferase
2.1	A0A1D8PSA9	Phosphoglucomutase
2.0	Q5ANE2	Uncharacterized protein
2.0	Q59WC5	4-nitrophenylphosphatase

2.0	A0A1D8PD11	Uncharacterized protein
2.0	Q5ABA2	Survival factor 1
2.0	A0A1D8PU04	S-formylglutathione hydrolase
2.0	Q5A1M1	Tfs1p
2.0	A0A1D8PKY7	Histidine biosynthesis trifunctional protein
2.0	Q59NB8	Leukotriene A-4 hydrolase homolog
2.0	P0CH96	Adenylosuccinate synthetase
2.0	A0A1D8PSE7	Ifr2p
2.0	Q5A8Z4	Superoxide dismutase
2.0	Q96VB9	Heat shock protein homolog SSE1
2.0	A0A1D8PH55	4-aminobutyrate transaminase
2.0	P0CY20	3'2'),5'-bisphosphate nucleotidase 1
2.0	P83778	Malate dehydrogenase, cytoplasmic
2.0	A0A1D8PT02	Flavodoxin-like fold family protein
2.0	A0A1D8PQB4	Dipeptidyl peptidase 3
2.0	A0A1D8PKV4	Fum12p
2.0	Q5APF2	GMP synthase [glutamine-hydrolyzing]
2.0	A0A1D8PPK1	Ebp1p
1.9	Q59MZ5	Phosphoribosylformylglycinamidine synthase
1.9	Q5AKA5	Cys-Gly metallodipeptidase DUG1
1.9	P46598	Heat shock protein 90 homolog
1.9	Q5AIA6	Pyridoxine biosynthesis protein
1.9	Q5ANE7	Pin3p
1.9	P22011	Peptidyl-prolyl cis-trans isomerase
1.9	A0A1D8PMP0	Oye32p
1.9	P43076	pH-responsive protein 1
1.9	A0A1D8PQ57	Bifunctional AP-4-A phosphorylase/ADP sulfurylase
1.9	A0A1D8PLC6	Putative methyltransferase
1.9	P41797	Heat shock protein SSA1
1.9	A0A1D8PFY5	Putative Xaa-Pro dipeptidase
1.9	P83780	Glucose-6-phosphate isomerase
1.9	A0A1D8PPR2	2-deoxyglucose-6-phosphatase
1.9	A0A1D8PIB2	Asparagine synthase
1.9	Q5ADN2	Putative phosphomutase
1.9	Q5A4M2	Malate dehydrogenase
1.9	A0A1D8PRQ4	Uncharacterized protein
1.8	P83775	Putative NADPH-dependent methylglyoxal reductase GRP2
1.8	A0A1D8PHE6	Uncharacterized protein
1.8	A0A1D8PQN3	Long-chain fatty acid transporter
1.8	A0A1D8PQH5	Superoxide dismutase
1.8	Q59SU1	Candidapepsin-9
1.8	A0A1D8PQI4	Ribulose-phosphate 3-epimerase
1.8	Q59T35	Osm1p

1.8	Q59T45	Putative amidotransferase
1.8	Q5AG68	Nucleoside diphosphate kinase
1.8	A0A1D8PTD8	Thiosulfate sulfurtransferase
1.8	A0A1D8PHU6	Putative phosphoric monoester hydrolase
1.8	A0A1D8PQE6	Uncharacterized protein
1.8	O42766	14-3-3 protein homolog
1.8	A0A1D8PCD2	Nma111p
1.8	A0A1D8PIF6	Sulfite reductase subunit alpha
1.8	A0A1D8PRJ1	Uncharacterized protein
1.8	Q5ALM6	Peptidyl-prolyl cis-trans isomerase
1.8	Q5A500	Adenylyl-sulfate kinase
1.8	A0A1D8PNG6	UDP-N-acetylglucosamine diphosphorylase
1.8	Q5AND4	Rdi1p
1.7	P30575	Enolase 1
1.7	Q5APD5	Uncharacterized protein
1.7	P82612	Phosphoglycerate mutase
1.7	Q59MR4	Coproporphyrinogen oxidase
1.7	P46273	Phosphoglycerate kinase
1.7	P82610	5-methyltetrahydropteroyltriglutamate--homocysteine methyltransferase
1.7	A0A1D8PGS7	Phosphoribosylglycinamide formyltransferase
1.7	Q9P975	Eukaryotic translation initiation factor 4E
1.7	A0A1D8PI24	D-arabinose 1-dehydrogenase
1.7	A0A1D8PL85	Aspartate aminotransferase
1.7	Q9URB4	Fructose-bisphosphate aldolase
1.7	A0A1D8PP00	Arginase
1.7	A0A1D8PGN7	Hypoxanthine phosphoribosyltransferase
1.7	Q59US8	Uncharacterized protein
1.7	Q5ABA5	Uncharacterized protein
1.7	Q5AK88	Uncharacterized protein
1.7	P83784	Heat shock protein SSC1, mitochondrial
1.7	Q5ABP8	Protein ROT1
1.7	P83776	Hexokinase-2
1.7	A0A1D8PKZ7	Pyrroline-5-carboxylate reductase
1.7	A0A1D8PGT5	Aldehyde dehydrogenase
1.7	Q5A784	Ofr1p
1.7	A0A1D8PMB3	Xylulokinase
1.7	Q59PZ6	6-phosphogluconolactonase
1.7	Q5A860	Translationally-controlled tumor protein homolog
1.7	O13318	pH-responsive protein 2
1.7	Q59KZ1	Aminopeptidase 2
1.7	A0A1D8PM15	Uncharacterized protein
1.6	P13649	Orotidine 5'-phosphate decarboxylase
1.6	Q59R31	Argininosuccinate lyase

1.6	A0A1D8PLY4	Pyruvate carboxylase
1.6	A0A1D8PEM3	Doa1p
1.6	Q5A2A7	Metalloendopeptidase
1.6	Q5AG89	Thioredoxin reductase
1.6	Q5A6L1	Fumarase
1.6	A0A1D8PF30	Tubulin-binding prefolding complex subunit
1.6	A0A1D8PPI6	Cip1p
1.6	P31353	Phosphomannomutase
1.6	Q5ADP5	ADP-ribose diphosphatase
1.6	Q5AKW4	Phosphoacetylglucosamine mutase
1.6	Q9Y7F0	Peroxiredoxin TSA1-A
1.6	A0A1D8PS11	Orotate phosphoribosyltransferase
1.6	Q5A750	Transketolase
1.6	A0A1D8PKJ4	Saccharopine dehydrogenase
1.6	Q5ADT4	Glycerol 2-dehydrogenase
1.6	A0A1D8PH00	Asr3p
1.6	A0A1D8PQK5	3-isopropylmalate dehydrogenase
1.6	A0A1D8PL14	Ornithine-oxo-acid transaminase
1.6	P34948	Mannose-6-phosphate isomerase
1.6	A0A1D8PCV7	L-aminoadipate-semialdehyde dehydrogenase
1.6	A0A1D8PPG7	Ketol-acid reductoisomerase, mitochondrial
1.6	Q59NQ5	Glutathione-disulfide reductase
1.6	Q5A7S3	Uncharacterized protein
1.6	Q59WG6	Aspartyl aminopeptidase
1.6	A0A1D8PQ26	Adenosine kinase
1.6	P83773	Acetyl-CoA hydrolase
1.6	P83783	Adenosylhomocysteinase
1.6	A0A1D8PNG9	Threonine synthase
1.6	A0A1D8PEI2	Dihydroxyacetone kinase
1.6	P83779	Pyruvate decarboxylase
1.6	A0A1D8PES3	Ran GTPase-binding protein
1.6	P83777	Inorganic pyrophosphatase
1.6	Q59Z14	Deoxyhypusine hydroxylase
1.6	A0A1D8PLJ3	Superoxide dismutase [Cu-Zn]
1.6	Q5A435	Prefoldin subunit 4
1.6	A0A1D8PCN0	Bifunctional UDP-glucose 4-epimerase/aldose 1-epimerase
1.6	Q5A1Q0	Glucose-6-phosphate 1-epimerase
1.5	A0A1D8PSU2	Pyridoxamine-phosphate oxidase
1.5	A0A1D8PMF8	Calmodulin
1.5	Q59TZ8	Phosphotransferase
1.5	A0A1D8PTR7	Tropomyosin
1.5	Q5A017	Transaldolase
1.5	A0A1D8PGS5	Isocitrate dehydrogenase [NAD] subunit, mitochondrial

1.5	Q59WG0	Adenosine 5'-monophosphoramidase
1.5	Q5A330	Pex19p
1.5	A0A1D8PNP4	Uncharacterized protein
1.5	A0A1D8PRM7	Phosphoenolpyruvate carboxykinase
1.5	A0A1D8PRR5	Argininosuccinate synthase
1.5	Q5AL34	Psa2p
1.5	A0A1D8PHC9	Aspartate transaminase
1.5	A0A1D8PFX8	Rab GDP dissociation inhibitor
1.5	P79023	Phospho-2-dehydro-3-deoxyheptonate aldolase, tyrosine-inhibited
1.5	A0A1D8PE67	Bifunctional aminoimidazole ribotide synthase/glycinamide ribotide synthase
1.5	A0A1D8PP43	Adh1p
1.5	Q59QN6	Formate dehydrogenase
1.5	A0A1D8PHS4	Uncharacterized protein
1.5	A0A1D8PSH3	Citrate synthase

(B) Proteins decreased in abundance in *C. albicans* incubated in *G. mellonella* hemolymph.

Fold Change (-)	**Uniprot ID**	**Protein Name**
374.0	A0A1D8PF90	Uncharacterized protein
259.6	Q5AB84	Uncharacterized protein
235.3	Q5AB87	Ribosomal 60S subunit protein L16A
201.5	A0A1D8PPS1	Ribosomal 60S subunit protein L25
187.2	Q5A0Z9	Pyruvate dehydrogenase E1 component subunit alpha (EC 1.2.4.1)
184.3	Q5AMT7	Bfr1p
177.0	A0A1D8PDZ1	Ribosomal 60S subunit protein L34B
155.7	Q5A0V9	rRNA methyltransferase
151.9	A0A1D8PF79	Glutamate decarboxylase (EC 4.1.1.15)
147.9	A0A1D8PN83	Ribosomal 40S subunit protein S11A
133.9	A0A1D8PDT4	Ribosomal 60S subunit protein L39
126.4	A0A1D8PCQ5	Ribosomal 60S subunit protein L26B
115.5	A0A1D8PRR7	Acetyl-CoA carboxylase
109.8	Q59TE0	Ribosomal 60S subunit protein L17B
106.9	Q59LS1	Ribosomal 60S subunit protein L3
105.3	Q5AML3	Oxidoreductase
103.3	O59931	60S ribosomal protein L13
98.4	A0A1D8PHH4	Ribosomal 60S subunit protein L33A

81.6	Q5AK53	ATP-dependent 6-phosphofructokinase (ATP-PFK) (Phosphofructokinase) (EC 2.7.1.11) (Phosphohexokinase)
80.7	Q5AGX8	Acetyltransferase component of pyruvate dehydrogenase complex (EC 2.3.1.12)
75.6	A0A1D8PLC9	60S ribosomal protein L20
71.5	A0A1D8PMV9	Threonine--tRNA ligase
70.1	A0A1D8PNQ6	Ribosomal 40S subunit protein S25B
68.3	O43101	Centromere/microtubule-binding protein CBF5 (Centromere-binding factor 5) (H/ACA snoRNP protein CBF5) (Small nucleolar RNP protein CBF5)
68.2	A0A1D8PMH8	Glutamate dehydrogenase
67.6	A0A1D8PR93	Histone
67.5	A0A1D8PF56	H/ACA ribonucleoprotein complex subunit
65.6	Q59S06	Nucleolar protein 58
63.2	Q5A6R1	Ribosomal protein L15
62.7	Q5AKV6	Pdx1p
62.6	A0A1D8PF08	Ribosomal 60S subunit protein L2A
62.4	A0A1D8PH21	60S ribosomal protein L36
58.0	A0A1D8PI15	Ribosomal 40S subunit protein S10A
57.4	A0A1D8PPE0	Ribosomal 40S subunit protein S13
56.7	A0A1D8PCX8	60S ribosomal protein L6
56.2	Q5A782	Translation initiation factor eIF5B
56.1	Q59PR9	Transcriptional regulator HMO1 (High mobility group protein 1)
54.0	A0A1D8PK43	Ribosomal 60S subunit protein L18A
53.6	Q5AMQ5	Carnitine O-acetyltransferase
53.3	Q59VN2	Histone H3.1/H3.2
51.3	Q59VN4	Histone H4
48.1	Q5A5V6	Pyruvate dehydrogenase E1 component subunit beta (EC 1.2.4.1)
47.9	Q5A4E2	ATP-dependent RNA helicase DED1 (EC 3.6.4.13)
47.2	Q9Y872	Sulfate adenylyltransferase (EC 2.7.7.4) (ATP-sulfurylase) (Sulfate adenylate transferase) (SAT)
45.2	A0A1D8PF11	Rpl82p
44.9	A0A1D8PK40	Ribosomal protein L19
44.0	A0A1D8PM75	Ribosomal 60S subunit protein L30
43.6	Q59QB8	Gcf1p
43.3	Q59T44	40S ribosomal protein S8
41.6	Q5ANA1	Ribosomal 60S subunit protein L8B
40.5	A0A1D8PCQ3	Eukaryotic translation initiation factor 2A (eIF-2A)
40.4	Q5A940	Multiprotein-bridging factor 1

40.2	A0A1D8PFL9	Ribosomal 60S subunit protein L14B
40.2	Q5AI86	Eukaryotic translation initiation factor 3 subunit I (eIF3i) (Eukaryotic translation initiation factor 3 39 kDa subunit homolog) (eIF-3 39 kDa subunit homolog)
40.0	Q5A5P8	Tif11p
39.1	A0A1D8PK11	RNA-binding protein
39.1	A0A1D8PCW6	Ribosomal 40S subunit protein S16A
38.9	Q5AIB8	Ribosomal 60S subunit protein L10
38.6	A0A1D8PTZ1	Uncharacterized protein
38.2	A0A1D8PGY0	Ribosomal 60S subunit protein L21A
37.8	Q59KI0	UTP--glucose-1-phosphate uridylyltransferase (EC 2.7.7.9) (UDP-glucose pyrophosphorylase) (UDPGP) (UGPase)
37.0	Q5ACM9	Eukaryotic translation initiation factor 3 subunit J (eIF3j) (Eukaryotic translation initiation factor 3 30 kDa subunit) (eIF-3 30 kDa)
36.4	A0A1D8PP59	Ubiquinol--cytochrome-c reductase subunit
36.1	Q5ALV6	40S ribosomal protein S26
35.7	A0A1D8PHG1	Oxysterol-binding protein
35.2	A0A1D8PFG4	60S ribosomal protein L27
35.2	Q59LU0	ATP-dependent RNA helicase DBP2 (EC 3.6.4.13)
35.1	Q5AGZ8	ATP-dependent 6-phosphofructokinase (ATP-PFK) (Phosphofructokinase) (EC 2.7.1.11) (Phosphohexokinase)
34.9	Q9UVJ4	60S ribosomal protein L10a
34.9	A0A1D8PPN6	Ribosomal 60S subunit protein L32
33.9	Q5AGV4	Eukaryotic translation initiation factor 3 subunit B (eIF3b) (Eukaryotic translation initiation factor 3 90 kDa subunit homolog) (eIF3 p90) (Translation initiation factor eIF3 p90 subunit homolog)
33.5	Q5AJD9	Acyl-coenzyme A oxidase
32.5	A0A1D8PP14	Ribosomal 60S subunit protein L43A
32.2	Q5AI20	Fe-S cluster-binding ribosome biosynthesis protein
32.0	A0A1D8PTR4	Ribosomal 40S subunit protein S29A
31.7	A0A1D8PU46	snoRNP complex protein
30.9	Q59TB4	Uncharacterized protein
30.8	Q96W54	40S ribosomal protein S22-A
30.5	Q5A900	Ribosomal 40S subunit protein S2
29.7	Q59ZE0	F1F0 ATP synthase subunit 4
29.5	A0A1D8PSZ0	Ife2p
29.4	Q59XW4	Acetyl-coenzyme A synthetase (EC 6.2.1.1)
29.3	A0A1D8PJ13	Bifunctional hydroxyacyl-CoA dehydrogenase/enoyl-CoA hydratase
29.3	Q5AME2	Pentafunctional AROM polypeptide [Includes: 3-dehydroquinate synthase (DHQS) (EC 4.2.3.4); 3-

		phosphoshikimate 1-carboxyvinyltransferase (EC 2.5.1.19) (5-enolpyruvylshikimate-3-phosphate synthase) (EPSP synthase) (EPSPS); Shikimate kinase (SK) (EC 2.7.1.71); 3-dehydroquinate dehydratase (3-dehydroquinase) (EC 4.2.1.10); Shikimate dehydrogenase (EC 1.1.1.25)]
28.5	A0A1D8PFV4	mRNA-binding protein
28.3	A0A1D8PHW1	Ribosomal 60S subunit protein L11B
27.8	Q59VR3	FK506-binding protein 3 (EC 5.2.1.8) (Peptidyl-prolyl cis-trans isomerase) (PPIase) (Rotamase)
27.5	Q59ZV5	Eukaryotic translation initiation factor 3 subunit G (eIF3g) (Eukaryotic translation initiation factor 3 RNA-binding subunit) (eIF-3 RNA-binding subunit) (Translation initiation factor eIF3 p33 subunit homolog) (eIF3 p33 homolog)
26.4	Q59PV8	ATP synthase subunit d, mitochondrial
26.4	Q5AML1	Eukaryotic translation initiation factor 3 subunit C (eIF3c) (Eukaryotic translation initiation factor 3 93 kDa subunit homolog) (eIF3 p93) (Translation initiation factor eIF3, p93 subunit homolog)
26.1	A0A1D8PRG0	Mitochondrial 54S ribosomal protein YmL2
25.6	Q5A389	Ribosomal 40S subunit protein S20
24.6	A0A1D8PSK2	40S ribosomal protein S30
24.4	A0A1D8PSV5	Ribosomal 40S subunit protein S3
24.4	A0A1D8PDL6	Ribosomal 60S subunit protein L7A
23.3	A0A1D8PGY8	Ribosomal 40S subunit protein S9B
22.7	Q5A7K0	40S ribosomal protein S24
22.5	A0A1D8PIF0	Uncharacterized protein
22.4	Q5A5Q8	40S ribosomal protein S4
22.2	A0A1D8PD83	Septin
22.0	A0A1D8PD02	Uncharacterized protein
21.2	A0A1D8PEV4	Ribosomal 60S subunit protein L42A
21.0	A0A1D8PSQ3	Type I HSP40 co-chaperone
20.8	A0A1D8PK30	Ribosomal 60S subunit protein L35A
20.6	Q5AI37	Probable metalloprotease ARX1 (EC 3.-.-.-) (Associated with ribosomal export complex protein 1)
20.6	Q5AJF7	Ribosomal 60S subunit protein L12A
20.6	A0A1D8PTH3	Alpha-ketoglutarate dehydrogenase
20.5	A0A1D8PIP0	Slr1p
20.1	Q5A7P7	F1F0 ATP synthase subunit 5
20.0	A0A1D8PEX3	DNA-directed RNA polymerase subunit (EC 2.7.7.6)
20.0	Q59YH4	Chaperonin-containing T-complex subunit
19.8	A0A1D8PL99	40S ribosomal protein S6
19.7	Q5A8Y5	DNA-directed RNA polymerase subunit beta (EC 2.7.7.6)

19.5	Q59LF9	Methionine aminopeptidase 2 (MAP 2) (MetAP 2) (EC 3.4.11.18) (Peptidase M)
19.4	A0A1D8PF45	Ribosomal protein L37
19.3	A0A1D8PE45	Nicotinate-nucleotide pyrophosphorylase [carboxylating] (EC 2.4.2.19) (Quinolinate phosphoribosyltransferase [decarboxylating])
19.0	A0A1D8PK22	Ribosomal 40S subunit protein S15
18.7	A0A1D8PKZ3	ATP-dependent RNA helicase
18.6	Q5ALV9	Cytochrome c oxidase subunit 6A, mitochondrial (Cytochrome c oxidase polypeptide VIa)
18.6	A0A1D8PQS0	60S acidic ribosomal protein P0
18.6	Q59P08	Glyoxylate reductase
18.5	Q59LZ9	Tom22p
18.5	A0A1D8PJF9	Acetolactate synthase (EC 2.2.1.6)
18.3	A0A1D8PHA3	Ubiquinol--cytochrome-c reductase catalytic subunit
18.3	Q59N40	Aspartate aminotransferase (EC 2.6.1.1)
18.0	Q5AJD0	ATP-dependent RNA helicase DBP5 (EC 3.6.4.13)
17.7	Q5AAU3	Protein transport protein SEC31
17.6	Q59U72	Ferrochelatase (EC 4.99.1.1)
17.4	A0A1D8PQQ5	Ribosomal 40S subunit protein S18B
17.4	Q9HFQ7	60S acidic ribosomal protein P1-A (CaRP1A)
17.3	Q59YC4	Chaperonin-containing T-complex subunit
17.3	Q59PL9	Eukaryotic translation initiation factor 3 subunit A (eIF3a) (Eukaryotic translation initiation factor 3 110 kDa subunit homolog) (eIF3 p110) (Translation initiation factor eIF3, p110 subunit homolog)
17.2	A0A1D8PP21	Methionine--tRNA ligase
17.0	Q5A3P4	Tryptophan--tRNA ligase
16.6	Q5A8X7	Protein FYV4, mitochondrial
16.2	A0A1D8PHD8	DNA-directed RNA polymerase core subunit
16.1	A0A1D8PQM4	DNA-directed RNA polymerase subunit beta (EC 2.7.7.6)
15.7	Q59MA9	Clustered mitochondria protein homolog (Protein TIF31 homolog)
15.6	A0A1D8PGM4	U3 small nucleolar RNA-associated protein 22
15.4	A0A1D8PCC8	Rrs1p
15.4	Q5AK00	Uncharacterized protein
15.3	A0A1D8PFV1	Ribosomal 60S subunit protein L4B
15.3	A0A1D8PDU3	Ribosomal 40S subunit protein S23B
15.3	Q5AHD3	Mitochondrial 54S ribosomal protein YmL35
15.1	A0A1D8PSI3	Uncharacterized protein
15.1	A0A1D8PQM1	Single-stranded telomeric DNA-binding/mRNA-binding protein
14.8	A0A1D8PCY	Septin

	5	
14.4	A0A1D8PDK6	6,7-dimethyl-8-ribityllumazine synthase (DMRL synthase) (EC 2.5.1.78)
14.2	A0A1D8PEZ0	Asr1p
14.2	A0A1D8PTK1	Chorismate synthase (EC 4.2.3.5)
14.0	P39827	Cell division control protein 10
14.0	Q5APD2	Malate synthase (EC 2.3.3.9)
13.9	Q5A6A1	Ribosomal 60S subunit protein L24A
13.6	A0A1D8PTM0	Uncharacterized protein
13.3	A0A1D8PRK7	Uncharacterized protein
13.0	Q5AGZ7	Ribosomal 60S subunit protein L5
12.9	A0A1D8PSB9	Srp40p
12.9	A0A1D8PLA3	rRNA-processing protein
12.9	P40910	40S ribosomal protein S1 (S3aE)
12.8	A0A1D8PR11	Uncharacterized protein
12.7	A0A1D8PU51	Uncharacterized protein
12.6	Q5A1D5	FACT complex subunit SPT16 (CaCDC68) (Cell division control protein 68) (Facilitates chromatin transcription complex subunit SPT16)
12.4	A0A1D8PET7	Uncharacterized protein
12.3	A0A1D8PUA6	DNA-directed RNA polymerase subunit (EC 2.7.7.6)
12.2	Q59YH5	Mitochondrial 54S ribosomal protein YmL36
12.2	A0A1D8PJF3	Uncharacterized protein
12.1	P53704	Glutamine--fructose-6-phosphate aminotransferase [isomerizing] (GFAT) (EC 2.6.1.16) (D-fructose-6-phosphate amidotransferase) (Hexosephosphate aminotransferase)
12.0	A0A1D8PCH2	mRNA-binding protein
11.8	Q5A6S0	Mitochondrial 54S ribosomal protein YmL40
11.7	A0A1D8PMD5	Uncharacterized protein
11.6	Q59R18	Asparagine--tRNA ligase
11.5	Q5AKX2	Fumarate reductase
11.5	Q5A1Z1	Mitochondrial 37S ribosomal protein MRP21
11.4	Q5AEN2	Ribosomal 60S subunit protein L9B
11.3	Q59M32	Mitochondrial 54S ribosomal protein YmL15
11.3	Q5A678	Ssz1p
11.3	A0A1D8PKK1	Translocon subunit
11.2	Q5AF38	Alpha-mannosidase (EC 3.2.1.-)
11.2	A0A1D8PDE3	Coatomer subunit gamma
11.2	Q59NG6	Mitochondrial 37S ribosomal protein PET123
11.2	Q5A0W7	RuvB-like helicase 1 (EC 3.6.4.12)
10.9	A0A1D8PRJ6	Translation initiation factor eIF2 subunit beta

10.9	Q5ADQ6	40S ribosomal protein S12
10.8	Q5AAS9	Mitochondrial 54S ribosomal protein YmL19
10.8	Q5AQ76	Protein transport protein SEC24
10.7	Q9B8D8	Cytochrome c oxidase subunit 2 (EC 1.9.3.1) (Cytochrome c oxidase polypeptide II)
10.6	A0A1D8PSC5	Ribosomal 60S subunit protein L28
10.6	Q5AJ93	40S ribosomal protein S7
10.3	Q59ZE2	2-methoxy-6-polyprenyl-1,4-benzoquinol methylase, mitochondrial (EC 2.1.1.201) (Ubiquinone biosynthesis methyltransferase COQ5)
10.1	Q5AGZ9	RuvB-like helicase 2 (EC 3.6.4.12)
9.9	A0A1D8PQH1	Uncharacterized protein
9.8	Q5AK02	Mitochondrial 37S ribosomal protein RSM7
9.8	Q5AF98	Zuotin
9.8	A0A1D8PPT5	Ribosomal 60S subunit protein L23B
9.7	A0A1D8PHF5	Ribosomal 60S subunit protein L31B
9.7	A0A1D8PND4	Mitochondrial 37S ribosomal protein YMR31
9.7	A0A1D8PMK0	Ago1p
9.6	Q5A779	GTP-binding protein
9.6	A0A1D8PDT3	Ribosomal 40S subunit protein S14B
9.6	Q5A3N5	Mitochondrial 54S ribosomal protein YmL13
9.4	Q59YE8	Translation termination factor GTPase eRF3
9.3	Q5ADU3	Eukaryotic translation initiation factor 3 subunit H (eIF3h)
9.2	O74161	Chitin biosynthesis protein CHS5
9.1	Q5AK16	T-complex protein 1 subunit gamma
9.1	Q5A798	Mitochondrial 54S ribosomal protein YmL3
9.1	A0A1D8PJB0	Coatomer subunit alpha
9.1	A0A1D8PNC8	Proteasome subunit beta (EC 3.4.25.1)
9.1	Q59UQ4	Chromatin-binding transcription coactivator
9.0	A0A1D8PHP8	Putative ammonium permease
9.0	A0A1D8PRF5	Sla2p
9.0	A0A1D8PJA6	Uncharacterized protein
8.9	A0A1D8PTP9	Chaperone ATPase
8.9	Q5AEF2	Protein transport protein SEC13
8.7	Q5A1E3	Transcriptional regulator CBF1
8.6	A0A1D8PTY4	Elf1p
8.5	Q5AK42	rRNA-processing protein EFG1
8.5	Q59ZH8	Translation termination factor eRF1
8.4	Q5A455	Protein transport protein SEC23
8.4	Q5ALL8	FACT complex subunit POB3 (Facilitates chromatin transcription complex subunit POB3)
8.4	Q5ANB2	ATP-dependent RNA helicase DBP10 (EC 3.6.4.13)

8.4	Q59VP1	Histone H2B.2
8.4	A0A1D8PMN9	Chaperonin-containing T-complex subunit
8.3	Q59ZI7	Mitochondrial 54S ribosomal protein YmL10/YmL18
8.2	Q5A6M9	SnoRNA-binding protein
8.2	A0A1D8PR73	Uncharacterized protein
8.1	Q5AP79	Mir1p
8.1	Q5A2T2	ATP-binding cassette family ATPase
8.1	O94150	37S ribosomal protein S9, mitochondrial
8.0	P83781	Mitochondrial outer membrane protein porin (Cytoplasmic antigenic protein 4)
8.0	Q5A516	ADP/ATP carrier protein
7.9	A0A1D8PN45	Dynamin-like GTPase
7.8	A0A1D8PG09	Stf2p
7.7	A0A1D8PPV5	Coatomer subunit beta'
7.7	A0A1D8PH91	Mitochondrial 37S ribosomal protein MRP51
7.5	Q5AK79	CTP synthase (EC 6.3.4.2) (UTP--ammonia ligase)
7.5	Q5ALN3	Uncharacterized protein
7.4	Q5A4Y4	Uncharacterized protein
7.4	Q59X93	Mitochondrial 54S ribosomal protein YmL17/YmL30
7.4	A0A1D8PK61	Ribosomal 40S subunit protein S19A
7.3	Q59P03	NADH-cytochrome b5 reductase 1 (EC 1.6.2.2) (Microsomal cytochrome b reductase)
7.3	A0A1D8PP33	Uncharacterized protein
7.3	A0A1D8PQC8	Uncharacterized protein
7.2	Q59QD6	Elongation factor 1-alpha 2 (EF-1-alpha 2)
7.1	Q5ABD0	Vacuolar-sorting protein SNF7 (Vacuolar protein-sorting-associated protein 32)
7.1	Q5A4L1	Uncharacterized protein
7.0	Q5AJU7	AP-1-like transcription factor CAP1
7.0	A0A1D8PSW1	Pex14p
7.0	Q5A7M1	ADP-ribosylation factor GTPase-activating protein
7.0	A0A1D8PGA2	Protein phosphatase regulator
6.9	Q59MZ8	DNA-directed RNA polymerase core subunit
6.9	Q5ACU9	Transcription factor
6.8	Q5A0M4	Elongation factor 2 (EF-2)
6.7	A0A1D8PK85	Proteasome core particle subunit beta 1
6.7	Q5A4L3	Uncharacterized protein
6.7	Q5A7K7	Uncharacterized protein
6.7	Q59LZ5	Protein channel
6.7	A0A1D8PJ76	Uncharacterized protein
6.6	Q59YF4	Increased recombination centers protein 22-1
6.6	Q59QN7	Succinate dehydrogenase [ubiquinone] iron-sulfur

		subunit, mitochondrial (EC 1.3.5.1)
6.6	A0A1D8PJ20	Proteasome endopeptidase complex (EC 3.4.25.1)
6.6	A0A1D8PEY9	Ribosomal 40S subunit protein S17B
6.5	A0A1D8PH72	Uncharacterized protein
6.5	A0A1D8PFZ9	U3 small nucleolar ribonucleoprotein protein MPP10
6.4	Q5AA47	Arp2/3 complex 34 kDa subunit
6.4	A0A1D8PGR5	Uncharacterized protein
6.4	A0A1D8PRM5	F1F0 ATP synthase subunit f
6.4	A0A1D8PL86	Mlp1p
6.3	Q5A6R2	Bifunctional phosphoribosylaminoimidazolecarboxamide formyltransferase/IMP cyclohydrolase
6.3	Q59Y36	Uncharacterized protein
6.3	P12461	Thymidylate synthase (TS) (TSase) (EC 2.1.1.45)
6.3	Q5AEI1	Nuo2p
6.2	Q5AI14	Trehalose-phosphatase
6.2	Q59RP7	54S ribosomal protein L4, mitochondrial
6.2	Q5AFG1	Ribosome biogenesis protein ALB1
6.1	Q5AHA6	AMP deaminase
6.1	A0A1D8PQJ8	Uncharacterized protein
6.1	A0A1D8PRA6	Uncharacterized protein
6.1	Q5ABS1	Cytochrome b-c1 complex subunit 7
6.0	Q59Z11	Actin-related protein 3
6.0	A0A1D8PQN0	Ribosomal 40S subunit protein S28B
6.0	Q5ABZ2	Transcription factor RBF1 (RPG-box-binding factor 1)
5.9	Q59Z65	Proteasome core particle subunit beta 5
5.9	Q9UVL1	Non-histone chromosomal protein 6
5.9	Q5A5V8	Uncharacterized protein
5.8	Q5ALV5	Cytochrome c oxidase subunit IV
5.8	A0A1D8PFH2	Ribosome biosynthesis protein
5.7	Q5ANL6	13 kDa ribonucleoprotein-associated protein
5.7	A0A1D8PLR7	NADPH--cytochrome P450 reductase (CPR) (p450R) (EC 1.6.2.4)
5.6	A0A1D8PTY6	Proteasome endopeptidase complex (EC 3.4.25.1)
5.6	A0A1D8PDE2	Aldo-keto reductase superfamily protein
5.5	Q5ALL3	tRNA-dihydrouridine(47) synthase [NAD(P)(+)] (EC 1.3.1.89) (tRNA-dihydrouridine synthase 3)
5.5	Q5AAW3	ATP-dependent RNA helicase DHH1 (EC 3.6.4.13)
5.4	A0A1D8PTD1	Bifunctional carbamoylphosphate synthetase/aspartate transcarbamylase
5.4	A0A1D8PNY3	Uncharacterized protein

5.4	P53698	Cytochrome c
5.4	A0A1D8PLW8	Proteasome regulatory particle lid subunit
5.4	A0A1D8PMJ1	RNA-binding GTPase
5.3	A0A1D8PCU5	Uncharacterized protein
5.3	A0A1D8PDC7	Uncharacterized protein
5.2	A0A1D8PFP3	5'-3' exoribonuclease 1 (EC 3.1.13.-)
5.1	Q874I4	Dihydroorotate dehydrogenase (quinone), mitochondrial (DHOD) (DHODase) (DHOdehase) (EC 1.3.5.2) (Dihydroorotate oxidase)
5.1	A0A1D8PMP9	Methionine aminopeptidase (EC 3.4.11.18)
5.1	Q59YJ9	mRNA-binding translational activator
5.0	A0A1D8PRA1	Mitochondrial 54S ribosomal protein YmL49
5.0	Q5AK59	ATP-dependent RNA helicase HAS1 (EC 3.6.4.13)
5.0	A0A1D8PNN8	Cam1-1p
4.9	Q59QC1	Mitochondrial 54S ribosomal protein YmL28
4.9	Q8NJN3	Acetyl-coenzyme A synthetase 2 (EC 6.2.1.1) (Acetate--CoA ligase 2) (Acyl-activating enzyme 2)
4.9	A0A1D8PU67	Proteasome core particle subunit beta 2
4.9	Q59K70	Uncharacterized protein
4.8	A0A1D8PQ03	Uncharacterized protein
4.8	Q3MNT0	Transcription elongation factor SPT6 (Chromatin elongation factor SPT6)
4.8	Q59RQ6	Dihydrolipoyl dehydrogenase (EC 1.8.1.4)
4.8	Q5A501	ESCRT-III subunit protein
4.7	Q59SM8	Trifunctional formate-tetrahydrofolate ligase/methenyltetrahydrofolate cyclohydrolase/methylenetetrahydrofolate dehydrogenase
4.7	Q5A8Y6	Mitochondrial 54S ribosomal protein YmL23
4.7	A0A1D8PJA9	Uncharacterized protein
4.7	A0A1D8PM44	Methylenetetrahydrofolate dehydrogenase (NAD(+))
4.7	A0A1D8PPJ1	Cic1p
4.6	A0A1D8PQJ1	Uncharacterized protein
4.6	A0A1D8PEV9	Mitochondrial 37S ribosomal protein MRPS5
4.6	A0A1D8PIF1	Uncharacterized protein
4.6	A0A1D8PHT4	Uncharacterized protein
4.6	Q59N42	Serine/threonine-protein phosphatase (EC 3.1.3.16)
4.6	A0A1D8PLQ3	Gly-Xaa carboxypeptidase
4.6	A0A1D8PG96	Hsp70 family ATPase
4.6	Q5A8Z9	Uncharacterized protein
4.5	A0A1D8PND9	Coatomer subunit delta

4.5	Q59XP0	Protein transport protein SEC9
4.5	Q92206	Squalene monooxygenase (EC 1.14.14.17) (Squalene epoxidase) (SE)
4.5	Q5A6P2	RNA cytidine acetyltransferase (EC 2.3.1.-) (18S rRNA cytosine acetyltransferase)
4.4	A0A1D8PKD3	Nucleolar GTP-binding protein 1
4.4	A0A1D8PPQ1	Tif3p
4.4	A0A1D8PHY2	Mitochondrial 54S ribosomal protein YmL7/YmL5
4.4	Q5AG43	Ribosomal 40S subunit protein S5
4.4	Q92410	Alpha,alpha-trehalose-phosphate synthase [UDP-forming] (EC 2.4.1.15) (Trehalose-6-phosphate synthase) (UDP-glucose-glucosephosphate glucosyltransferase)
4.3	A0A1D8PRL4	Mis12p
4.3	Q5APB9	Uncharacterized protein
4.3	Q59Y40	SnoRNA-binding rRNA-processing protein
4.3	Q5A222	NADH-ubiquinone oxidoreductase
4.3	Q5A397	Hsp70 family ATPase
4.3	Q5A302	Endoplasmic reticulum vesicle protein 25
4.3	Q5A3P1	Exosome catalytic subunit
4.2	A0A1D8PRU4	Actin-related protein 2/3 complex subunit 4
4.2	A0A1D8PI73	Translation initiation factor eIF4G
4.2	Q5A4X9	Ribonuclease
4.2	A0A1D8PHI0	Replication factor C subunit 1
4.2	A0A1D8PF50	18S rRNA pseudouridine methyltransferase
4.1	A0A1D8PE97	Glycine cleavage system P protein (EC 1.4.4.2)
4.1	A0A1D8PSN8	rRNA (Cytosine-C5-)-methyltransferase
4.1	A0A1D8PJ73	Ali1p
4.1	Q5AJA5	DEAH-box ATP-dependent RNA helicase
4.1	A0A1D8PFJ8	DNA-directed RNA polymerase core subunit
4.1	A0A1D8PK71	Uncharacterized protein
4.1	Q59LF3	Regulator of cytoskeleton and endocytosis RVS167
4.0	Q59KZ3	Uridylate kinase (UK) (EC 2.7.4.14) (ATP:UMP phosphotransferase) (Deoxycytidylate kinase) (CK) (dCMP kinase) (Uridine monophosphate kinase) (UMP kinase) (UMPK)
4.0	Q59PZ1	Proteasome endopeptidase complex (EC 3.4.25.1)
4.0	Q5AI30	Mitochondrial 37S ribosomal protein RSM24
4.0	Q5AH14	Tom40p
4.0	P10613	Lanosterol 14-alpha demethylase (EC 1.14.13.70) (CYPLI) (Cytochrome P450 51) (Cytochrome P450-14DM) (Cytochrome P450-LIA1) (Sterol 14-alpha demethylase)
4.0	A0A1D8PT60	Arc40p
3.9	A0A1D8PCP4	Uncharacterized protein

3.9	A0A1D8PU27	Uncharacterized protein
3.9	A0A1D8PQQ7	mRNA-binding protein
3.9	A0A1D8PG16	Ribosomal 60S subunit protein L38
3.9	Q5ADP3	Transcription regulator
3.9	Q5A1E8	Succinate dehydrogenase [ubiquinone] flavoprotein subunit, mitochondrial (EC 1.3.5.1)
3.9	Q5AEE1	Histone H2A.Z
3.9	A0A1D8PIS4	Trehalose 6-phosphate synthase/phosphatase complex subunit
3.9	Q5AK62	Virulence protein SSD1
3.8	A0A1D8PMA9	Uncharacterized protein
3.8	Q5ADR2	Glutamate-5-semialdehyde dehydrogenase
3.8	Q5ALK3	Ribose phosphate diphosphokinase subunit
3.8	Q59QB7	Chaperonin-containing T-complex alpha subunit
3.8	Q59KY7	Mitochondrial 37S ribosomal protein RSM18
3.7	Q5A9A9	RNA-binding signal recognition particle subunit
3.7	A0A1D8PUB4	L-iditol 2-dehydrogenase
3.7	Q59RN2	Actin-related protein 2/3 complex subunit 5
3.7	A0A1D8PRR4	Trans-hexaprenyltranstransferase
3.7	A0A1D8PEA2	Dolichyl-phosphate beta-D-mannosyltransferase
3.7	A0A1D8PGL1	Uncharacterized protein
3.7	A0A1D8PHC4	Uncharacterized protein
3.7	Q5A0N3	Ribonucleoside-diphosphate reductase (EC 1.17.4.1)
3.6	A0A1D8PR80	Ran guanyl-nucleotide exchange factor
3.6	Q5APD0	Uncharacterized protein
3.5	A0A1D8PEY6	Tricalbin
3.5	A0A1D8PQE5	RNA export factor
3.5	A0A1D8PHE0	Mitochondrial 37S ribosomal protein MRPS35
3.5	Q5A8H8	Pbp2p
3.5	Q5AFE4	Regulator of cytoskeleton and endocytosis RVS161
3.5	A0A1D8PMK4	Uncharacterized protein
3.5	Q5AL45	Elongation factor G, mitochondrial (EF-Gmt) (Elongation factor G 1, mitochondrial) (mEF-G 1) (Elongation factor G1)
3.5	A0A1D8PH93	Uncharacterized protein
3.5	A0A1D8PMT6	Coatomer subunit epsilon
3.5	A0A1D8PCC3	Transcriptional regulator
3.5	A0A1D8PNA3	Peptide alpha-N-acetyltransferase complex A subunit
3.5	A0A1D8PJX3	Cytochrome b-c1 complex subunit Rieske, mitochondrial (EC 1.10.2.2)
3.4	A0A1D8PE03	Uncharacterized protein

3.4	Q59UF7	Aspartate--tRNA ligase
3.4	Q5AH35	Mitochondrial 54S ribosomal protein MRP49
3.4	Q59WV9	Uncharacterized protein
3.4	A0A1D8PIR2	Gcn1p
3.3	A0A1D8PE79	Oxysterol-binding protein related protein
3.3	A0A1D8PDD1	Lipid-binding protein
3.3	Q5ABC3	Elongation factor Tu
3.3	A0A1D8PLU5	Csh3p
3.2	A0A1D8PG50	F1F0 ATP synthase subunit i
3.2	A0A1D8PQQ9	Mitochondrial 54S ribosomal protein YmL6
3.2	O94083	Eukaryotic translation initiation factor 5A (eIF-5A) (eIF-4D)
3.2	Q5A006	Coatomer subunit zeta
3.2	Q5AAR2	Uncharacterized protein
3.2	Q8TGH6	Guanosine-diphosphatase (GDPase) (EC 3.6.1.42)
3.1	A0A1D8PMP1	Glycerol-3-phosphate dehydrogenase (EC 1.1.5.3)
3.1	Q59T87	Uncharacterized protein
3.1	A0A1D8PFX2	DNA-directed RNA polymerase core subunit
3.1	Q5A8X6	Succinate--CoA ligase [ADP-forming] subunit alpha, mitochondrial (EC 6.2.1.5) (Succinyl-CoA synthetase subunit alpha) (SCS-alpha)
3.1	A0A1D8PC73	Uncharacterized protein
3.0	A0A1D8PL02	F1F0 ATP synthase subunit e
3.0	Q5A6Q4	tRNA (adenine(58)-N(1))-methyltransferase non-catalytic subunit TRM6 (tRNA(m1A58)-methyltransferase subunit TRM6) (tRNA(m1A58)MTase subunit TRM6)
3.0	Q59KV8	Lipid-binding protein
3.0	A0A1D8PLN1	rRNA-processing protein
3.0	A0A1D8PTN4	snoRNP complex protein
3.0	Q59Z25	Mitochondrial nucleoid protein
3.0	Q5ADP0	Histone deacetylase (EC 3.5.1.98)
3.0	A0A1D8PQ55	Uncharacterized protein
3.0	A0A1D8PG26	Uncharacterized protein
3.0	A0A1D8PRH3	Ume1p
3.0	Q5AF71	Putative phosphotransferase
2.9	Q59VX8	Septation protein 7 (Seventh homolog of septin 1)
2.9	A0A1D8PM35	Translation elongation factor 1 subunit beta
2.9	Q5ADT9	37S ribosomal protein S10, mitochondrial (Mitochondrial ribosomal small subunit protein 10)
2.9	Q59TD5	NADH dehydrogenase [ubiquinone] flavoprotein 1, mitochondrial (EC 1.6.5.3) (EC 1.6.99.3)
2.9	A0A1D8PHH2	Png2p

2.9	A0A1D8PSC8	Arc1p
2.8	Q59RB8	Isocitrate lyase
2.8	P25997	Elongation factor 3 (EF-3)
2.8	A0A1D8PLK1	Proteasome core particle subunit beta 6
2.8	A0A1D8PPW9	Aminomethyltransferase (EC 2.1.2.10) (Glycine cleavage system T protein)
2.8	Q5APK5	Cytochrome c oxidase subunit Va
2.8	A0A1D8PTX1	Actin-related protein 2
2.8	A0A1D8PND7	Uncharacterized protein
2.8	Q59RK3	Putative serine--tRNA ligase
2.7	Q5ANH5	Ribosomal protein P2B
2.7	A0A1D8PU56	Long-chain fatty acid-CoA ligase
2.7	Q5AJZ5	Proteasome core particle subunit beta 4
2.7	A0A1D8PQL8	Glutamate--tRNA ligase
2.7	Q5A6S7	Uncharacterized protein
2.7	A0A1D8PRH6	Proteasome endopeptidase complex (EC 3.4.25.1)
2.7	Q5A5S6	Malate dehydrogenase (EC 1.1.1.37)
2.7	A0A1D8PSE0	Uncharacterized protein
2.6	Q5A7P6	Mitochondrial 54S ribosomal protein RML2
2.6	Q5A2A2	Mitochondrial homologous recombination protein 1
2.6	Q59XV1	Calmodulin-dependent protein kinase
2.6	Q5AAI8	Nucleosome assembly protein 1
2.6	P83782	Cytochrome b-c1 complex subunit 2, mitochondrial (Complex III subunit 2) (Core protein II) (Cytoplasmic antigenic protein 5) (Ubiquinol-cytochrome-c reductase complex core protein 2)
2.6	Q59Z24	DNA-directed RNA polymerase subunit
2.6	A0A1D8PTI9	Rgd3p
2.6	Q5ANP6	Sbp1p
2.6	Q59X67	Enhanced filamentous growth protein 1
2.6	A0A1D8PJK2	D-aminoacyl-tRNA deacylase (EC 3.1.1.-) (EC 3.1.1.96)
2.6	A0A1D8PQD5	Cytochrome c oxidase subunit
2.5	A0A1D8PE54	Bbc1p
2.5	A0A1D8PKC3	Translation elongation factor EF1B gamma
2.5	O42817	40S ribosomal protein S0
2.5	Q5ADU2	Lysine--tRNA ligase (EC 6.1.1.6) (Lysyl-tRNA synthetase)
2.5	O93827	Mannose-1-phosphate guanyltransferase (EC 2.7.7.13) (ATP-mannose-1-phosphate guanylyltransferase) (CASRB1) (GDP-mannose pyrophosphorylase)
2.5	Q5A4Q1	Adenylate kinase (EC 2.7.4.3) (ATP-AMP transphosphorylase) (ATP:AMP phosphotransferase) (Adenylate kinase cytosolic

		and mitochondrial) (Adenylate monophosphate kinase)
2.4	A0A1D8PTS0	Ribosomal protein P2A
2.4	Q59M49	mRNA-binding ribosome synthesis protein
2.4	Q5A473	Gvp36p
2.3	Q59XU9	Glycerol-3-phosphate dehydrogenase [NAD(+)] (EC 1.1.1.8)
2.3	A0A1D8PQ38	Uncharacterized protein
2.3	A0A1D8PD15	Proteasome regulatory particle lid subunit
2.3	A0A1D8PD99	mRNA-binding ribosome biosynthesis protein
2.3	Q59QT0	DNA-directed RNA polymerase core subunit
2.2	Q5AMR4	Exosome non-catalytic core subunit
2.2	Q59SI1	ATPase-activating ribosome biosynthesis protein
2.2	A0A1D8PFS0	SNAP receptor
2.1	Q00310	Glycolipid 2-alpha-mannosyltransferase 1 (EC 2.4.1.-) (Alpha-1,2-mannosyltransferase 1)
2.1	A0A1D8PDC4	ATP synthase subunit alpha
2.1	A0A1D8PQP7	Cyb5p
2.1	Q5A850	Glycogen [starch] synthase (EC 2.4.1.11)
2.1	A0A1D8PGU0	Hsp70 family chaperone
2.0	A0A1D8PTI7	40S ribosomal protein S27
2.0	O93852	D-arabinono-1,4-lactone oxidase (ALO) (EC 1.1.3.37) (L-galactono-gamma-lactone oxidase)
2.0	A0A1D8PTG5	U4/U6-U5 snRNP complex subunit
2.0	G1UB61	Septin CDC11 (Cell division control protein 11)
2.0	P0CT51	Blood-induced peptide 1
2.0	A0A1D8PL12	Uncharacterized protein
2.0	Q5A109	Ubiquitin-ribosomal 40S subunit protein S31 fusion protein
2.0	Q59M70	NADH-cytochrome b5 reductase 2 (EC 1.6.2.2) (Mitochondrial cytochrome b reductase)
2.0	A0A1D8PRY3	ATP synthase subunit gamma
2.0	A0A1D8PCT4	Phenylalanine--tRNA ligase subunit alpha
1.9	A0A1D8PDI5	Ubiquitin-binding protein
1.9	Q5AFA8	Abp1p
1.9	Q5AHY9	DNA polymerase epsilon noncatalytic subunit
1.9	A0A1D8PDE8	Obg-like ATPase 1
1.9	A0A1D8PGX7	Uncharacterized protein
1.8	A0A1D8PC43	Diphosphomevalonate decarboxylase (EC 4.1.1.33) (Mevalonate pyrophosphate decarboxylase)
1.8	Q5ACI8	Peptidyl-prolyl cis-trans isomerase D (PPIase D) (EC 5.2.1.8) (Rotamase D)
1.8	Q5AHB1	Actin cytoskeleton-regulatory complex protein PAN1
1.8	Q59Y38	Uncharacterized protein

1.8	A0A1D8PKZ9	ATP synthase subunit beta (EC 3.6.3.14)
1.7	A0A1D8PRP0	U4/U6-U5 snRNP complex subunit
1.7	A0A1D8PS79	Isocitrate dehydrogenase [NADP] (EC 1.1.1.42)
1.7	P0CY34	Transcriptional repressor TUP1
1.7	Q5A7P9	Thioredoxin peroxidase
1.7	A0A1D8PR99	Protein disulfide isomerase
1.7	A0A1D8PMH6	Tryptophan synthase (EC 4.2.1.20)
1.7	Q5A9D9	Homoisocitrate dehydrogenase
1.7	A0A1D8PJ67	Uncharacterized protein
1.7	A0A1D8PHU0	Mitochondrial 54S ribosomal protein MRPL50
1.6	Q5AMQ2	Clathrin light chain
1.6	Q5A893	F-actin-capping protein subunit alpha
1.6	Q5A3K7	Phosphoglycerate dehydrogenase
1.6	A0A1D8PKE2	Mitogen-activated protein kinase kinase
1.6	A0A1D8PPH3	Uncharacterized protein
1.6	A0A1D8PHF8	Wh11p
1.6	A0A1D8PTZ6	Uncharacterized protein
1.6	Q5ADT0	Slk19p
1.6	Q59NP1	Copper transport protein CTR1
1.6	Q59TU0	Nascent polypeptide-associated complex subunit beta (NAC-beta) (Beta-NAC)
1.6	A0A1D8PKD0	Uncharacterized protein
1.5	A0A1D8PG81	Hgt7p
1.5	O13426	Serine hydroxymethyltransferase, cytosolic (SHMT) (EC 2.1.2.1) (Glycine hydroxymethyltransferase) (SHMII) (Serine methylase)
1.5	P83774	Guanine nucleotide-binding protein subunit beta-like protein (Cytoplasmic antigenic protein 1)

Table A4.1. Proteins increased (Red) and decreased (Green) in abundance in *G. mellonella* larvae hemolymph infected with *S. aureus* for 6 h as compared to 0 h

Protein Name	Number of Peptides	Sequence coverage [%]	Score	p value	Fold Change
Gloverin	3	46.2	42.566	5.269E-05	20.06
Gustatory receptor	6	40.9	62.929	0.0002057	18.14
Uncharacterized protein	6	22.7	100.94	0.0115559	16.19
Serpin-4B	5	78.8	41.117	0.007772	6.63
Peptidoglycan-recognition protein-LB	3	72.4	39.312	0.024767	5.97
Peptidoglycan recognition-like protein B	13	34	296.93	0.0013876	5.41
Uncharacterized protein	3	19	75.959	0.0154921	4.76
Beta actin	9	52	261.97	0.0024351	4.61
AGAP011516-PA	5	14.5	38.671	0.0316638	3.99
Prophenol oxidase activating enzyme 3	5	44.4	55.786	0.0316365	2.85
Protease inhibitor 1	15	37	169.5	0.0313505	2.56
Uncharacterized protein	3	21.2	183.66	0.0427484	2.10
Serine protease inhibitor dipetalogastin	3	15.5	40.032	0.0185339	1.98
Fructose-1,6-bisphosphatase	12	28	323.31	0.0083192	1.92
Arginine kinase	2	29.1	53.86	0.0300812	1.82
Putative hydroxypyruvate isomerase	10	71.1	224.42	0.0128579	1.68
Carboxylic ester hydrolase	11	31.5	103.82	0.0202315	1.63
alpha-esterase 45	5	8.5	48.709	0.002778	-1.63

Table A4.2. Proteins increased (Red) and decreased (Green) in abundance in *G. mellonella* larvae hemolymph infected with *S. aureus* for 24 h as compared to 0 h

Protein Name	Number of Peptides	Sequence coverage [%]	Score	p value	Fold Change
Gloverin	3	46.2	42.566	2.05E-05	121.69
Cecropin-D-like peptide	2	14.5	81.412	4.4E-05	73.70
Lysozyme	6	19.1	45.237	4.73E-05	31.38
Moricin-like peptide B	1	13.3	14.208	0.001982	20.81
Peptidoglycan recognition-like protein B	13	34	296.93	2.12E-05	17.35
Uncharacterized protein	6	22.7	100.94	0.009474	17.23
Inducible metalloproteinase inhibitor protein	7	35.1	99.811	0.001234	14.61
Gustatory receptor	6	40.9	62.929	0.000171	13.30
Cecropin-A (Cecropin-C)	1	8.5	9.4615	0.005058	10.56

Uncharacterized protein	3	19	75.959	2.23E-05	9.88
Peptidoglycan-recognition protein-LB	3	72.4	39.312	0.014231	9.53
Hemolin	5	53.6	106.13	0.002471	9.23
Hemolin	16	51.5	323.31	0.001797	8.39
Putative defense protein Hdd11	6	34.2	53.851	0.024342	7.24
Serpin-4B	5	78.8	41.117	0.007182	7.03
Yellow-d	12	26.6	196.65	0.016128	6.96
Protease inhibitor 1	3	21.2	183.66	0.000272	5.81
Prophenol oxidase activating enzyme 3	15	37	169.5	0.007552	4.97
Peptidoglycan recognition protein	11	56	313.13	0.0015	4.64
Chemosensory protein 7	4	21	181.63	0.012462	4.50
Gloverin	2	14.8	13.135	0.005864	3.83
sulfhydryl oxidase 1	5	26.2	105.27	0.002125	3.54
Prophenoloxidase activating protease I	2	57.7	21.028	0.006467	3.46
Serine protease inhibitor dipetalogastin	12	28	323.31	0.012544	2.68
Beta-1,3-glucan recognition protein	19	41.4	315.64	0.001665	2.16
Inducible serine protease inhibitor 2	3	9.8	111.22	0.00849	1.72
Hemolymph proteinase 16	10	38.2	146.66	0.0024	1.57
Serine proteinase	14	34	323.31	0.019384	-2.70
Uncharacterized protein	2	5.6	58.117	0.014143	-2.71
Cathepsin B-like cysteine proteinase	4	13.8	41.669	0.017993	-2.79
Heat shock protein 25.4	13	48	323.31	0.016116	-2.93
BmP109	7	23.4	60.397	0.019927	-3.72
Thioredoxin	3	13.6	35.124	0.014066	-3.94

Table A5.1. Proteins changed (increased [+] and decreased [-]) in abundance in *G. mellonella* larvae co-infected with *C. albicans* [1×10^5 larva^{-1}] *S. aureus* [2×10^4 larva^{-1}]) at 6 h relative to control larvae

Protein name	Number of peptides	Sequence coverage [%]	Score	P-value	Fold Change
gustatory receptor candidate 25	5	34	79.852	0.000299	+10.5
gloverin-like protein, partial	3	16.9	162.16	4.77E-05	+7.9
Putative defense protein Hdd11	8	60.7	131.58	0.001001	+7.1
actin 3	8	30.9	148.38	0.000381	+6.6
paramyosin, putative	5	21.3	44.51	0.010233	+5.0
odorant-binding protein	3	8.9	24.256	0.01226	+4.9
integument esterase 2 precursor	7	33.6	54.189	0.002835	+4.6
prophenoloxidase activating factor 3	8	45.5	99.646	0.006993	+4.2
Kunitz-type serine protease inhibitor vestiginin-1	3	17	23.033	0.00659	+4.0
putative protease inhibitor 4	7	24.3	239.81	0.00084	+3.7
serine protease inhibitor 5 precursor	6	17.2	58.799	0.01111	+3.6
cobatoxin-like protein	2	15.8	63.982	0.011142	+3.2
serine proteinase-like protein 2	3	40.2	52.672	0.010279	+3.1
peptidoglycan recognition-like protein B, partial	13	34	135.36	0.000185	+3.0
thymosin isoform 1	5	42.7	64.28	0.038421	+3.0
Serine protease inhibitor dipetalogastin	14	28.8	323.31	0.000475	+2.9
nimrod B precursor	2	21.7	134.44	0.000309	+2.7
GI17397	4	53.2	92.275	0.003409	+2.6
conserved hypothetical protein	4	22.6	33.183	0.034018	+2.5
beta actin	12	54.1	323.31	0.015716	+2.4
kazal-type proteinase inhibitor precursor	6	21.4	155.94	0.000117	+2.4
paramyosin, putative	19	43	323.31	0.000521	+2.3
cellular retinoic acid binding protein	15	35.6	179.65	0.004901	+2.3
prophenol oxidase activating enzyme 3	16	41.6	171.68	0.047205	+2.2
chemosensory protein	4	24.8	35.034	0.039315	+2.0
spodoptericin, partial	4	33.5	145.34	0.013664	+1.9
cationic peptide CP8 precursor	8	29.2	323.31	0.007608	+1.9
diapause bioclock protein	4	62.6	234.71	0.004356	+1.8
chemosensory protein	5	16.7	63.037	0.027691	+1.7
Inducible serine protease inhibitor 2	4	13.2	112.66	0.006884	+1.6
AGAP011516-PA, partial	7	44.4	79.314	0.046237	+1.6
Gelsolin	24	36.9	323.31	0.037978	-1.5
juvenile hormone binding protein	15	44.5	323.31	0.000451	-1.6
arylphorin	81	78.6	323.31	0.001997	-1.7

uncharacterized protein Dmel_CG33290	2	11.9	33.278	0.027253	-1.7
arylphorin	55	79.8	323.31	0.001283	-1.7
hypothetical protein	16	37.1	323.31	0.003286	-1.8
Apolipophorins	9	53	254.29	0.000104	-1.9
adhesion related protein, transmembrane (plasmid)	9	37.2	129.75	0.001665	-1.9
unknown [Picea sitchensis]	11	29.8	216.69	0.003057	-2.0
hypothetical protein, partial	5	13.3	81.426	0.000517	-2.0
beta-1,3-glucan recognition protein precursor	17	32.3	175.69	0.000531	-2.0
methionine-rich storage protein	18	81.4	323.31	0.018393	-2.2
Beta-1,3-glucan-binding protein	2	14.5	53.396	0.005218	-2.3
Apolipophorins	1	13.8	18.495	0.001219	-2.4
unknown [Picea sitchensis]	5	13.2	45.134	0.00831	-3.8
cathepsin B-like cysteine proteinase	7	24.3	60.827	0.003242	-4.9
unknown [Picea sitchensis]	3	23.3	42.505	0.03811	-14.2

Table A5.2. Proteins changed (increased [+] and decreased [-]) in abundance in *G. mellonella* larvae co-infected with *C. albicans* [1×10^5 larva^{-1}] *S. aureus* [2×10^4 larva^{-1}]) at 24 h relative to control larvae

Protein name	**Number of peptides**	**Sequence coverage [%]**	**Score**	**P-value**	**Fold change**
Cecropin-A	2	12.7	18.93	9.31E-05	+45.4
gustatory receptor candidate 25	5	34	79.852	2.5E-05	+41.7
Cecropin-D-like peptide	2	14.5	45.092	7.27E-05	+37.8
Putative defense protein Hdd11	8	60.7	131.58	3.34E-05	+33.3
gloverin	4	59.6	36.145	0.043792	+19.3
gloverin-like protein	3	16.9	162.16	0.000207	+15.3
peptidoglycan-recognition protein-LB	3	72.4	31.878	0.001428	+14.0
serpin-4B	5	78.8	51.837	0.001239	+12.9
salivary cysteine-rich peptide precursor	3	13.5	37.275	0.020182	+12.6
hypothetical protein TTHERM_00163900	4	21.7	40.212	0.002905	+10.1
DNA-directed RNA polymerase II subunit RPB1	3	15.5	59.002	0.000532	+10.0
muscle protein 20-like protein	7	32.5	184.74	0.016145	+8.6
peptidoglycan recognition-like protein B	13	34	135.36	1.28E-05	+8.5
Inducible metalloproteinase inhibitor protein	7	33.2	78.171	9.47E-05	+7.1
hypothetical protein (macronuclear)	7	31	100.56	0.019526	+6.8

protease inhibitor 1 precursor	3	21.2	175.06	1.04E-05	+6.0
heat shock protein hsp21.4	8	18.6	94.178	0.00975	+5.4
Serine protease inhibitor dipetalogastin	14	28.8	323.31	5.01E-05	+5.3
cobatoxin-like protein	2	15.8	63.982	0.002108	+5.0
prophenoloxidase activating factor 3	8	45.5	99.646	0.005944	+4.8
actin 3	8	30.9	148.38	0.001451	+4.5
paramyosin, putative	5	21.3	44.51	0.019479	+4.3
chemosensory protein 7 precursor	8	30.8	124.29	0.006951	+4.3
beta actin	12	54.1	323.31	0.000762	+4.1
serpin 3a	9	13.2	122.9	0.041815	+4.1
integument esterase 2 precursor	7	33.6	54.189	0.004394	+4.0
Kunitz-type serine protease inhibitor vestiginin-1	3	17	23.033	0.014824	+3.8
hemolin, partial	17	66	306.28	0.005263	+3.7
prophenol oxidase activating enzyme 3	16	41.6	171.68	0.006246	+3.5
chemosensory protein	4	24.8	35.034	0.005067	+3.5
thymosin isoform 1	5	42.7	64.28	0.019699	+3.2
peptidoglycan recognition protein precursor	12	53	272.37	0.000495	+3.2
hemolin	7	56.4	228.83	0.000336	+3.1
putative protease inhibitor 4	7	24.3	239.81	0.012987	+3.0
serine proteinase-like protein 2	3	40.2	52.672	0.021263	+2.7
AGAP011516-PA, partial	7	44.4	79.314	0.007866	+2.7
kazal-type proteinase inhibitor precursor	6	21.4	155.94	0.001432	+2.4
nimrod B precursor	2	21.7	134.44	0.001901	+2.4
GI17397	4	53.2	92.275	0.003949	+2.3
myophilin	5	18.9	50.592	0.004987	+2.0
hypothetical protein 29, partial	7	32.2	60.846	0.043305	+1.9
cationic peptide CP8 precursor	8	29.2	323.31	0.018288	+1.9
hypothetical protein	37	67.5	323.31	0.025558	+1.9
paramyosin, putative	19	43	323.31	0.014214	+1.8
serine protease inhibitor 11 precursor	10	23.1	116.7	0.027161	+1.8
Inducible serine protease inhibitor 2	4	13.2	112.66	0.013159	+1.8
unknown, partial [Helicoverpa armigera]	20	36.6	274.94	0.000967	+1.7
diapause bioclock protein	4	62.6	234.71	0.014342	+1.7
Gelsolin	24	36.9	323.31	0.022655	+1.6
uncharacterized protein LOC661483	6	13.9	120.98	0.014646	+1.5
unknown [Picea sitchensis]	21	48.5	323.31	0.00011	-1.6
Anionic antimicrobial	10	32.9	312.43	0.023877	-1.7

peptide 2					
beta-galactosidase	23	35.2	297.16	0.00048	-1.7
aminoacylase	9	24.5	89.608	0.02118	-1.7
Apolipophorins	12	85.9	323.31	0.00049	-1.8
carboxylesterase clade H, member 1 precursor	25	69.1	323.31	0.000112	-1.8
heat shock protein 25.4 precursor	14	40.5	323.31	0.040029	-1.8
C-type lectin 21 precursor	11	31.2	161.97	0.017307	-1.8
juvenile hormone binding protein	15	44.5	323.31	0.003041	-1.8
apolipophorin, partial	16	47.9	323.31	7.37E-05	-1.8
adhesion related protein, transmembrane (plasmid)	9	37.2	129.75	0.001229	-1.8
putative serine protease-like protein 2	20	71	323.31	0.000156	-1.9
hypothetical protein, partial	5	13.3	81.426	0.000798	-1.9
unknown [Picea sitchensis]	11	29.8	216.69	0.007533	-2.0
similar to CG10638-PA	4	28.8	205.96	0.00011	-2.0
Apolipophorins	9	53	254.29	8.95E-05	-2.1
carboxylesterase clade H, member 1 precursor	10	39.3	209.21	0.012125	-2.1
arylphorin	81	78.6	323.31	0.000548	-2.2
arylphorin	55	79.8	323.31	0.000218	-2.2
juvenile hormone binding protein	17	56.4	323.31	0.016559	-2.6
abnormal wing disc-like protein	10	52.6	120.66	0.00805	-2.8
Fibrohexamerin	14	18	323.31	0.03681	-2.8
methionine-rich storage protein	18	81.4	323.31	0.001717	-2.9
hypothetical protein	16	37.1	323.31	0.000316	-3.1
unknown [Picea sitchensis]	7	20.1	70.525	0.044628	-3.2
unknown [Picea sitchensis]	5	13.2	45.134	0.019255	-3.7
cathepsin B-like cysteine proteinase	7	24.3	60.827	0.007651	-4.0
hypothetical protein, partial	3	7.7	21.784	0.034442	-5.2
carboxylesterase CarE-11 precursor	4	33.1	65.687	0.025218	-5.6
saposin-related precursor	10	31.4	78.529	0.011407	-5.8
serine proteinase	15	35.8	323.31	0.004564	-6.2
alpha-esterase 45	14	52.9	285.29	0.044877	-7.7
Apolipophorin	1	13.8	18.495	0.000172	-62.4

Table A5.3. List of *C. albicans* proteins detected in *G. mellonella* larval hemolymph at 24 h post co infection with *C. albicans* [1×10^5 larva^{-1}] *S. aureus* [2×10^4 larva^{-1}]).

Uniprot ID	Protein IDs
A0A1D8PEV2	Alkaline phosphatase (EC 3.1.3.1)
A0A1D8PFM7	Uncharacterized protein
A0A1D8PG96	Hsp70 family ATPase
A0A1D8PGY6	Uncharacterized protein
A0A1D8PS79	Isocitrate dehydrogenase [NADP] (EC 1.1.1.42)
A0A1D8PI81	Ifm3p
A0A1D8PIA8	Uncharacterized protein
A0A1D8PKC4	Ubiquitin-specific protease
A0A1D8PKJ3	E1 ubiquitin-activating protein
A0A1D8PKJ4	Saccharopine dehydrogenase (NADP+, L-glutamate-forming)
A0A1D8PL61	Midasin
A0A1D8PRP3	Mms22p
A0A1D8PT92	Uncharacterized protein
A0A1D8PU73	Uncharacterized protein
Q9Y7F0	Peroxiredoxin TSA1-A (EC 1.11.1.15) (Thiol-specific antioxidant protein) (Thioredoxin)
Q59QD6	Elongation factor 1-alpha 2 (EF-1-alpha 2)
P25997	Elongation factor 3 (EF-3)
P46587	Heat shock protein SSA2
Q59KI4	Chromatin-remodeling ATPase INO80 (EC 3.6.4.-)
Q59LZ4	Uncharacterized protein
Q59VP2	Histone H2A.2
Q5AAT3	Uncharacterized protein
Q5AG31	Mediator of RNA polymerase II transcription subunit 14 (Mediator complex subunit 14)

Table A5.4. List of *S. aureus* proteins detected in *G. mellonella* larval hemolymph at 24 h post co infection with *C. albicans* [1×10^5 $larva^{-1}$] *S. aureus* [2×10^4 $larva^{-1}$]).

Uniprot ID	Protein IDs
P69848	GTP 3',8-cyclase (EC 4.1.99.22) (Molybdenum cofactor biosynthesis protein A)
Q2FUW0	Uncharacterized protein
Q2FVC2	Pyrophosphohydrolase, putative
Q2FVF4	Glutamate synthase alpha subunit, putative (EC 1.4.1.13)
Q2FWP8	Phi PVL orf 32-like protein
Q2FX03	UPF0421 protein SAOUHSC_02103
Q2FX51	Phage terminase, large subunit, PBSX family
Q2FX65	Phage tape measure protein
Q2FY35	Probable glycine dehydrogenase (decarboxylating) subunit 2 (EC 1.4.4.2) (Glycine cleavage system P-protein subunit 2) (Glycine decarboxylase subunit 2) (Glycine dehydrogenase (aminomethyl-transferring) subunit 2)
Q2FZ20	Polyribonucleotide nucleotidyltransferase (EC 2.7.7.8) (Polynucleotide phosphorylase) (PNPase)
Q2FZF9	Glycerophosphoryl diester phosphodiesterase, putative (EC 3.1.4.46)
Q2FZL3	Staphopain B (EC 3.4.22.-) (Staphylococcal cysteine proteinase B) (Staphylopain B)
Q2FZS6	2-isopropylmalate synthase, putative (EC 2.3.3.13)
Q2G012	Extracellular matrix protein-binding protein emp
Q2G146	Uncharacterized protein
Q2G1H6	Acetylglutamate kinase (EC 2.7.2.8) (N-acetyl-L-glutamate 5-phosphotransferase) (NAG kinase) (NAGK)
Q2G1S8	Uncharacterized protein
Q2G2A7	Spermidine/putrescine import ATP-binding protein PotA (EC 3.6.3.31)
Q2G2D3	Ribosome maturation factor RimP
Q9F0R1	HTH-type transcriptional regulator SarR (Staphylococcal accessory regulator R)

Table A6.1. Proteins which are changed (increased [+] and decreased [-]) in *G. mellonella* larval hemolymph in response to infection to *A. fumigatus* 6 h post infection.

Fold Change	GI Number	Protein Name	Peptide Number	Sequence coverage [%]	Score
+37.22	1.26E+08	gustatory receptor candidate 25	7	40.9	130.55
+13.69	23208538	gloverin-like protein, partial	2	14.3	33.27
+11.48	116087	Cecropin-C	1	8.5	4.8467
+5.06	15214063	Lysozyme	3	7.4	13.762
+4.12	1.46E+08	hypothetical protein	10	21.4	323.31
+3.92	1.47E+08	moricin-like peptide B	1	13.3	19.402
+3.42	1.18E+08	hypothetical protein TTHERM_00163900	7	30.9	323.31
+3.41	1.46E+08	hypothetical protein (macronuclear)	15	42.4	281.15
+3.34	1.7E+08	peroxisomal multifunctional enzyme type 2	4	21.2	28.098
+2.88	1.58E+08	beta actin	9	47.7	323.31
+2.77	1.84E+08	muscle protein 20-like protein	10	34.7	93.758
+2.68	23208535	peptidoglycan recognition-like protein B	13	34	207.89
+2.42	23208544	cobatoxin-like protein	2	15.8	107.8
+2.25	1.95E+08	uncharacterized protein Dmoj_GI19595	6	63.5	75.787
+1.58	56718390	prophenol oxidase activating enzyme 3	18	42.1	194.33
+1.53	1.84E+08	hypothetical protein	41	68.9	323.31
+1.53	45594226	serpin-4B	5	78.8	56.476
+1.51	25989211	prophenoloxidase activating factor 3	7	53.6	78.263
+1.51	1.13E+08	serine protease inhibitor 5 precursor	11	21.9	76.78
-1.64	91084741	PREDICTED: apolipoprotein D	15	40.9	323.31
-2.10	1.62E+08	alpha-esterase 45	15	55.3	323.31
-2.22	1.62E+08	alpha-esterase 45	10	47.7	323.31
-2.44	27733415	serpin 3a	12	14.3	227.73
-3.17	2.42E+08	conserved hypothetical protein	6	34.4	71.983
-3.69	91082037	PREDICTED: succinyl-CoA ligase	5	7	14.315
-18.23	1.59E+08	juvenile hormone binding protein	15	56.4	323.31

Table A6.2. Proteins which are changed (increased [+] and decreased [-]) in *G. mellonella* larval hemolymph in response to infection to *A. fumigatus* 24 h post infection.

Fold Change	GI Number	Protein Name	Peptide Number	Sequence coverage [%]	Score
+126.19	125629089	gustatory receptor candidate 25	7	40.9	130.55
+22.71	189234613	DNA-directed RNA polymerase II subunit RPB1	4	15.5	55.252
+17.11	60592747	cyclophilin-like protein	5	24.7	54.996
+16.43	238915964	growth-blocking peptide	2	9.4	31.768
+15.84	146737994	moricin-like peptide C1	2	15.4	35.328
+13.59	145504735	hypothetical protein (macronuclear)	10	21.4	323.31
+11.84	183979237	muscle protein 20-like protein	10	34.7	93.758
+11.66	114053193	protease inhibitor 1 precursor	5	36	292.17
+11.60	145504735	hypothetical protein (macronuclear)	15	42.4	281.15
+11.07	195022411	GH17138	2	51.5	48.976
+10.89	158962505	chemosensory protein	3	11.3	68.332
+9.97	170578347	Immunoglobulin I-set domain containing protein	2	35.2	13.266
+9.91	170027588	chitinase A1	6	15.9	83.773
+9.25	112983872	serine protease inhibitor 12	13	32	168.88
+9.10	183979284	elongation factor 1 alpha	6	26.6	31.825
+8.63	157132177	lipase 3 isoform X2	13	26.1	76.264
+8.41	23208526	6tox	8	22.4	23.124
+8.25	157927723	beta actin	9	47.7	323.31
+8.20	33860163	Inducible metalloproteinase inhibitor protein	6	30.2	71.715
+7.98	116087	Cecropin-A	1	8.5	4.8467
+7.97	118350731	hypothetical protein TTHERM_00163900	7	30.9	323.31
+7.60	91076018	uncharacterized protein LOC660215	3	2.7	56.019
+6.54	156630481	Cecropin-D-like peptide	2	14.5	61.768
+6.28	195119912	uncharacterized protein Dmoj_GI19595	6	63.5	75.787
+6.19	112983342	beta-tubulin	10	23.8	82.248
+5.90	112702923	peptidoglycan-recognition protein-LB, partial	4	72.4	58.788
+5.78	45594226	serpin-4B	5	78.8	56.476
+5.73	170030366	peroxisomal multifunctional enzyme type 2	4	21.2	28.098
+5.61	23208535	peptidoglycan recognition-like protein B, partial	13	34	207.89
+5.41	158292087	chemosensory protein	7	22.5	58.212
+5.36	158962507	chemosensory protein	7	23.3	93.247

+5.16	23208538	gloverin-like protein, partial	2	14.3	33.27
+4.80	186703381	hemolin	5	47.9	302.52
+4.27	242005732	hemicentin, putative	3	12.3	8.4233
+4.21	167736344	spatzle-1 precursor	4	11.3	94.55
+3.99	170070131	pancreatic triacylglycerol lipase	7	13.1	58.822
+3.79	4090964	immune-related Hdd1	19	30	183.41
+3.66	74873244	Hdd11	8	57.1	147.94
+3.53	58864722	putative annexin IX-B	6	29.2	50.04
+3.36	23208544	cobatoxin-like protein	2	15.8	107.8
+3.06	55139149	hemolin, partial	15	56.1	323.31
+2.95	157704337	Hdd1-like protein	5	56.9	98.542
+2.81	112983414	heat shock protein hsp21.4	5	15	110.34
+2.73	22901764	Kunitz-like protease inhibitor precursor	5	31.1	63.67
+2.73	112983994	peptidoglycan recognition protein precursor	12	56.4	234.84
+2.63	112984054	yellow-d precursor	17	40.8	280.59
+2.51	154707830	triosephosphate isomerase	13	28.2	119.12
+2.44	56718390	prophenol oxidase activating enzyme 3	18	42.1	194.33
+2.42	56462318	hypothetical protein 29, partial	7	32.2	52.237
+2.40	83583693	hemicentin-like protein 1, partial	6	13.2	58.056
+2.28	219552448	arginine kinase, partial	9	71.1	215.81
+2.20	148298796	thioredoxin-like protein	4	13.6	41.607
+2.14	34921426	Serine protease inhibitor dipetalogastin	12	28	323.31
+2.07	112983052	chemosensory protein 7 precursor	5	25.6	307.77
+2.05	195456798	uncharacterized protein Dwil_GK17235	4	44.8	64.811
+2.00	192763882	actin 3	7	29.4	213.63
+1.92	25989211	prophenoloxidase activating factor 3	7	53.6	78.263
+1.74	116780375	unknown	4	15.6	66.6
+1.73	183979392	hypothetical protein	41	68.9	323.31
+1.64	110347843	protease inhibitor-like protein	2	40	79.649
+1.51	156630460	Anionic antimicrobial peptide 2	8	32.9	323.31
+1.51	183979239	similar to CG10638-PA	8	27.4	163.58
-1.52	237874122	Cystatin manduca sexta	9	55.8	211.57
-1.53	229002332	hypothetical protein	8	50.7	323.31
-1.53	33439712	spodoptericin	6	33.5	205.8
-1.55	193624668	acid phosphatase type 7	4	9.2	11.202
-1.56	169646838	heat shock protein 25.4 precursor	13	48	323.31
-1.56	114649525	beta-1,3-glucan recognition protein precursor	23	46.1	314.84
-1.56	114052150	triacylglycerol lipase	17	37.7	228.57
-1.61	195432134	poly(U)-specific endoribonuclease homolog	16	33.4	173.04

-1.61	112984026	saposin-related precursor	11	35.9	98.091
-1.62	183979239	similar to CG10638-PA	3	28.8	323.31
-1.68	229556834	NADPH:quinone reductase	7	21.7	72.342
-1.71	134252572	beta-hexosaminidase	10	19.7	43.428
-1.71	46396271	27 kDa hemolymph protein	11	31.6	283.22
-1.72	116791778	unknown	24	55.6	323.31
-1.74	162462783	alpha-esterase 45	19	32.4	323.31
-1.74	162462783	alpha-esterase 45	5	8.5	41.692
-1.78	145286562	lysozyme-like protein 1	8	16.9	116.69
-1.78	77415676	hypothetical protein	13	33.1	323.31
-1.98	3182995	Ecdysteroid-regulated 16 kDa protein	4	47.9	103.48
-2.00	208972535	beta-1,3-glucan recognition protein 3	7	28.1	65.459
-2.12	162462783	alpha-esterase 45	10	47.7	323.31
-2.25	148298818	C-type lectin 10 precursor	7	16	25.036
-2.27	162462783	alpha-esterase 45	15	55.3	323.31
-2.28	121308868	serine proteinase	14	42.6	323.31
-2.67	240129600	cold-related protein	1	11.6	95.835
-2.84	4753912	3-dehydroecdysone 3beta-reductase	10	25.5	230.53
-3.00	112984548	serine protease inhibitor 5 precursor	11	21.9	76.78
-3.03	182509208	carboxylesterase CarE-11 precursor	2	29.5	5.5189
-3.31	116326818	hypothetical protein TNAV2c_gp132	4	27.3	76.529
-3.42	112984526	promoting protein precursor	6	27.3	24.834
-3.45	195375235	Uncharacterized protein	9	25.8	323.31
-3.91	226342886	serine protease inhibitor 13 precursor	10	24.5	117.27
-4.06	52782700	Beta-1,3-glucan-binding protein	4	40.1	62.87
-4.21	112984088	yellow-fb precursor	6	21.8	98.511
-4.23	156543790	similar to RE14504p	2	45	35.333
-4.29	91082037	succinyl-CoA ligase	5	7	14.315
-6.37	112983816	glyceraldehyde-3-phosphate dehydrogenase	11	36.7	66.846
-7.04	229002332	hypothetical protein, partial	3	14.5	146.95
-8.30	242014152	conserved hypothetical protein	6	34.4	71.983
-8.37	170058562	dimeric dihydrodiol dehydrogenase	7	20.1	55.213
-13.31	9087198	Fibrohexamerin	12	17.2	323.31

Table A7.1. Proteins from *M. mycetomatis* identified within grains extracted from infected *G. mellonella* larvae.

Uniprot ID	Protein Name
A0A150AS49	Annexin
A0A150ASS0	78 kDa glucose-regulated protein
A0A150ASS5	Putative cytochrome b5
A0A175VMY6	Uncharacterized protein
A0A175VN17	Ribosomal protein
A0A175VN81	Protein SET (Fragment)
A0A175VP10	Pectate lyase A (Fragment)
A0A175VPL2	Woronin body major protein
A0A175VPT8	Malate dehydrogenase
A0A175VPZ3	UTP--glucose-1-phosphate uridylyltransferase
A0A175VQT4	T-complex protein 1 subunit gamma
A0A175VR56	ATP-dependent RNA helicase eIF4A
A0A175VRA2	Histone H4
A0A175VRB1	Putative 5-methyltetrahydropteroyltriglutamate--homocysteine methyltransferase
A0A175VRU2	ATP synthase subunit alpha
A0A175VS81	Phosphoenolpyruvate carboxykinase [ATP]
A0A175VSD8	Peptidylprolyl isomerase
A0A175VSG5	Guanine nucleotide-binding protein alpha-2 subunit
A0A175VSH5	Protein disulfide-isomerase
A0A175VSK1	Uncharacterized protein
A0A175VSM5	Uncharacterized protein
A0A175VT02	Heat shock protein 90
A0A175VTM6	Histone H2A
A0A175VTP0	Mitochondrial acidic protein mam33
A0A175VTQ2	Putative T-complex protein 1 subunit beta
A0A175WC99	Catalase-peroxidase (CP)
A0A175VUG0	Histone H2B
A0A175VUL2	ATP synthase subunit 5, mitochondrial
A0A175VUN5	GTP-binding nuclear protein
A0A175VUP0	Uncharacterized protein
A0A175VUU8	ATP synthase subunit d, mitochondrial
A0A175VUV3	Mitochondrial-processing peptidase subunit beta
A0A175VUW6	Uncharacterized protein
A0A175VV65	Uncharacterized protein
A0A175VVD3	Mitochondrial phosphate carrier protein
A0A175VVR6	Major allergen Asp f 2
A0A175VW03	Transaldolase
A0A175VW48	Putative fungistatic metabolite
A0A175VWI6	Cyanovirin-N

A0A175VWJ3	3-isopropylmalate dehydrogenase
A0A175VWW7	Mitochondrial outer membrane protein porin
A0A175VXC6	Putative alpha/beta-glucosidase agdC
A0A175VXH0	Uncharacterized protein
A0A175VXJ7	60S acidic ribosomal protein P0
A0A175VXN5	Uncharacterized protein
A0A175VXP6	Citrate synthase
A0A175VXW8	Glutamine--fructose-6-phosphate aminotransferase [isomerizing]
A0A175VXZ6	Uncharacterized protein
A0A175W852	ATP-dependent RNA helicase DBP2
A0A175VY89	Phospholipase
A0A175VY99	Uncharacterized protein
A0A175VYF7	Putative aspartate-semialdehyde dehydrogenase (Fragment)
A0A175VYV0	Cell division control protein 48
A0A175VZ06	Small COPII coat GTPase SAR1
A0A175VZ89	Nucleoside diphosphate kinase
A0A175VZY6	Isocitrate lyase
A0A175W089	Uncharacterized protein
A0A175W0E4	Uncharacterized protein
A0A175W120	Tubulin alpha chain
A0A175W1E5	Actin
A0A175W1F8	Tubulin beta chain
A0A175W1H7	Uncharacterized protein
A0A175W1R3	60S ribosomal protein L27
A0A175W1R6	Uncharacterized protein
A0A175W1S4	Serine/threonine-protein kinase nrc-2
A0A175W1X2	Flavohemoprotein
A0A175W1X3	Glutamate dehydrogenase
A0A175W2C0	Uncharacterized protein
A0A175W2D6	DNA damage checkpoint protein rad24
A0A175W2K5	Tropomyosin-1
A0A175W3F4	Enolase
A0A175W3X8	Phosphoglycerate kinase
A0A175W3Y7	Heme-responsive zinc finger transcription factor HAP1
A0A175W4W0	Superoxide dismutase
A0A175W5H5	Uncharacterized protein
A0A175W6A8	Putative Ras-related protein Rab7
A0A175W703	Peptidyl-prolyl cis-trans isomerase (PPIase)
A0A175W7C5	Elongation factor 1-gamma 1
A0A175W7X9	Superoxide dismutase
A0A175W804	Elongation factor 1-beta
A0A175W860	Proteasome subunit alpha type
A0A175W8E2	Elongation factor 2
A0A175W8L2	ADP,ATP carrier protein

A0A175W8P0	Tubulin alpha chain
A0A175W8P5	Mitochondrial peroxiredoxin PRX1
A0A175W8X0	Uncharacterized protein
A0A175W9A6	6-phosphogluconate dehydrogenase, decarboxylating
A0A175W9B3	Uncharacterized protein
A0A175W9U5	Peroxisomal hydratase-dehydrogenase-epimerase
A0A175WA11	Heat shock 70 kDa protein
A0A175WA79	Uncharacterized protein
A0A175WAC4	Putative voltage-gated potassium channel subunit beta
A0A175WAT4	Clathrin heavy chain
A0A175WB24	Ras-related protein YPTC6
A0A175WBA2	Uncharacterized protein
A0A175WBA6	Uncharacterized protein
A0A175WBG9	Iron-sulfur cluster assembly protein
A0A175WC19	Putative argininosuccinate lyase
A0A175WCF3	Isocitrate dehydrogenase [NADP]
A0A175WCH5	Cytochrome c oxidase subunit 6, mitochondrial
A0A175WCI9	Heat shock protein 60
A0A175WCN7	Uncharacterized protein
A0A175WCP3	Putative beta-glucosidase A
A0A175WCT4	Trehalose-phosphatase
A0A175WCW2	Putative pyridoxal 5'-phosphate synthase subunit pdx-1
A0A175WCZ7	Pyruvate carboxylase
A0A175WDA3	Cytochrome b-c1 complex subunit 2, mitochondrial
A0A175WDC7	Heat shock 70 kDa protein
A0A175WDG0	30 kDa heat shock protein
A0A175WDI2	Cytochrome b-c1 complex subunit 6
A0A175WE26	Protein ecm33
A0A175WE38	Ketol-acid reductoisomerase, mitochondrial
A0A175WE75	Uncharacterized protein
A0A175WEH6	Uncharacterized protein
A0A175WF15	10 kDa heat shock protein, mitochondrial
A0A175WFJ6	Trehalase
A0A175WFQ0	Nucleosome assembly protein 1
A0A175WFT1	D-3-phosphoglycerate dehydrogenase 1
A0A175WGJ7	Sulfate adenylyltransferase
A0A175WGL9	Malate dehydrogenase
A0A175WGS8	GTP-binding protein ypt1
A0A175WH58	Beta-hexosaminidase
A0A175WHE8	Uncharacterized protein
A0A175WHN2	40S ribosomal protein S4
A0A175WHS9	Transketolase
A0A175WI88	V-type proton ATPase subunit B
A0A175WIJ7	Uncharacterized protein

G0Z837	Fructose-bisphosphate aldolase
G0Z838	Glyceraldehyde-3-phosphate dehydrogenase

Table A7.2A. *G. mellonella* larval proteins increased in abundance in grains isolated from larvae infected with *M. mycetomatis* for 24 hour as compared to control larval hemolymph proteome.

P value	Fold Change (+)	GI Number	Protein Name	Peptides	Sequence coverage [%]	Score
3.92E-05	1112.00	114052072	ATP synthase subunit beta (EC 7.1.2.2)	38	72.8	323.31
3.39E-06	810.38	17826933	Calreticulin	18	28	323.31
1.61E-05	673.62	23208546	Heat shock-like protein (Fragment)	13	37.8	313.77
1.45E-04	593.13	112983414	Heat shock protein hsp21.4	8	19.4	323.31
3.26E-04	567.07	223671147	putative cuticle protein	5	33.8	323.31
9.72E-04	491.47	158292666	AGAP005155-PA	3	9.1	278.2
3.36E-05	423.59	158298459	AGAP009604-PA	8	60.2	323.31
8.25E-04	318.32	3913261	Larval cuticle protein 1	4	26	323.31
5.54E-04	289.09	62241290	Protein disulfide-isomerase (EC 5.3.4.1)	40	57.2	323.31
1.40E-03	284.98	183979347	Cuticular protein CPR3	7	28.8	323.31
6.33E-05	276.22	91076018	Uncharacterized protein	3	14.3	98.229
1.65E-05	265.96	171740905	Inactive lipase	9	31.2	137.84
1.41E-04	265.68	189234613	Uncharacterized protein	6	21.8	223.02
1.70E-04	263.09	125629089	Gustatory receptor	7	43	190.57
1.08E-04	260.96	112984454	Protein disulfide-isomerase (EC 5.3.4.1)	8	41.7	161.43
7.17E-06	254.43	148298673	Mitochondrial ATP synthase coupling factor 6	7	28.6	99.647
6.05E-06	241.38	58391242	60 kDa heat shock protein, mitochondrial precursor	20	33.6	323.31

			(AGAP004002-PA)			
1.04E-02	237.66	112983342	Tubulin beta chain	23	47.1	323.31
1.33E-04	233.62	114051966	Mitochondrial aldehyde dehydrogenase	26	54.8	323.31
5.71E-05	197.92	151301059	H+ transporting ATP synthase delta subunit	9	42.6	210.09
2.52E-03	178.79	192763882	Actin 3	12	36.9	323.31
2.10E-03	178.09	223671186	putative cuticle protein	4	21.9	99.666
1.01E-05	175.74	156630481	Cecropin-D-like peptide	2	14.5	137.98
9.38E-04	172.27	157927723	Beta actin	11	54.1	323.31
9.23E-04	163.19	91088621	similar to voltage-dependent anion-selective channel isoform 1	18	47.4	323.31
7.34E-04	157.40	183979237	Transgelin	16	43.8	282.76
9.35E-04	156.78	189238710	Peptidyl-prolyl cis-trans isomerase (PPIase) (EC 5.2.1.8)	28	36.1	323.31
1.87E-05	152.31	60592747	cyclophilin-like protein	8	33.3	238.43
5.81E-04	150.55	148298818	Multi-binding protein	10	13.9	188.05
2.34E-04	147.04	74873244	Putative defense protein Hdd11 (Hyphantria differentially displayed gene 11)	10	60.7	246.4
1.14E-04	144.27	229562186	Heat shock protein 90	37	48.4	323.31
7.13E-04	130.57	153791739	ATP synthase subunit d, mitochondrial	15	49.1	289.07
6.29E-04	129.92	23208544	Cobatoxin-like protein	3	19.5	115.72
1.48E-04	128.43	148298796	Thioredoxin	6	20.7	129.74
1.20E-05	122.01	58864722	Annexin	21	57.7	323.31
4.77E-04	119.80	27260894	Heat shock cognate 70 protein	4	14.8	59.95
1.93E-05	118.13	112984012	Heat shock 70 kD protein cognate (Heat shock protein 70)	5	84.1	131.23

6.57E-04	115.62	148719710	Superoxide dismutase (EC 1.15.1.1)	10	54.8	307.21
6.57E-04	114.80	110649240	Gloverin	2	28.8	71.375
7.65E-04	114.44	183979278	Cuticular protein CPR2	6	56.3	137.87
9.93E-04	114.06	183979284	Elongation factor 1-alpha	16	56.4	313.03
2.04E-04	110.99	113208389	Heat shock protein 20.7	13	49.8	224.91
2.69E-03	109.48	189237651	N-acetylneuraminate lyase-like Protein	8	25	157.48
2.25E-04	104.65	225031010	Tubulin alpha chain (Fragment)	4	47.2	228
1.73E-04	100.49	112983096	Dihydrolipoyl dehydrogenase (EC 1.8.1.4)	25	51.6	323.31
3.65E-04	98.51	17901818	32 kDa ferritin subunit	6	17.8	121.01
5.95E-05	97.91	11890404	26kDa ferritin subunit	10	29.6	198.67
3.13E-05	97.63	112982865	Profilin	6	24.8	137.05
5.38E-05	96.21	112982880	Translationally controlled tumor protein	10	48	179.58
4.13E-03	96.16	154707830	Triosephosphate isomerase (EC 5.3.1.1)	17	29.5	300.18
3.78E-03	94.42	183979372	Troponin T	10	42.5	142.31
2.21E-05	93.54	7576710	CALNUC	11	49	185.05
3.76E-03	92.34	114053181	Histone H2A	6	18.5	57.209
1.88E-03	90.12	156537163	Cytochrome c oxidase subunit Va	17	48.7	323.31
1.38E-03	85.40	164448662	Larval cuticle protein (Putative cuticle protein)	6	13.7	123.81
4.51E-03	81.25	112984038	Larval cuticle protein LCP-22	4	28.9	105.28
1.09E-03	77.95	112984376	Ribosomal protein L14	9	34.4	105.93
9.58E-05	77.27	112983487	Ribosomal protein L8	15	38.6	260.73
1.80E-04	75.80	148298770	ATPase inhibitor-like protein	6	15.9	120.73
3.77E-04	70.74	242016119	10 kDa heat shock protein, putative	10	30.8	127.63
1.00E-03	69.18	91092064	Selenium-binding protein 1-like	20	49.5	323.31

			Protein			
2.88E-05	68.44	195119912	Uncharacterized protein	7	63.5	142.79
3.83E-05	66.60	157109957	mitochondrial processing peptidase beta subunit	23	60.9	323.31
5.42E-04	65.69	61744169	16 kDa salivary protein	5	28.6	165.99
1.77E-03	65.18	114052615	Myosin II essential light chain (Nonmuscle myosin essential light chain)	9	33.2	144.9
1.15E-03	64.42	15213812	40S ribosomal protein S12	9	53.7	80.075
4.41E-04	62.41	112982743	Elongation factor 1-beta'	10	50	181.65
4.62E-04	61.24	114053193	Protease inhibitor 1	5	36	323.31
3.66E-04	60.95	91075966	Electron transfer flavoprotein subunit alpha, mitochondrial-like Protein	16	47.5	232.03
2.16E-04	59.72	193713737	Uncharacterized protein	7	21.3	164.09
1.46E-04	58.17	15213770	Ribosomal protein L22 (SFRICE_023778)	4	32	66.978
4.24E-04	55.96	156548621	hypothetical protein	5	19	80.519
8.40E-04	53.50	183979374	Tropomyosin 2	10	32.5	323.31
1.29E-04	52.60	91078412	cytochrome c oxidase subunit 6B2 isoform X2	5	29.7	73.817
4.10E-04	52.57	54039568	40S ribosomal protein S8	12	50.7	224.23
2.03E-04	52.17	58376764	NADH dehydrogenase [ubiquinone] 1 alpha subcomplex subunit 8	8	22.1	213.93
1.19E-04	50.80	134948671	Small nuclear ribonucleoprotein Sm D2 (Sm-D2) (snRNP core protein D2)	6	21.4	102.58
4.37E-05	50.31	112984026	BmP109	23	53.8	323.31
5.20E-05	49.01	169234934	FK506-binding protein precursor	12	28.8	269.85

2.73E-03	48.48	112984352	Ribosomal protein S15	5	44.8	119.01
5.37E-04	47.64	164448660	Cytochrome c oxidase polypeptide Vb	7	28.2	99.694
1.57E-04	47.49	114053221	Prohibitin protein WPH	13	47.6	187.94
1.85E-04	47.46	23208526	6tox	16	31.4	202.03
1.57E-04	47.28	56718390	Prophenol oxidase activating enzyme 3	26	45	323.31
1.20E-03	46.79	112983872	Serpin-like protein (SEP-LP)	9	22.4	163.11
7.06E-04	45.29	21759389	60S ribosomal protein L13	10	37.5	145.88
5.02E-04	44.90	90025232	Epoxide hydrolase (EC 3.3.2.9)	12	35.1	167.32
3.45E-05	44.78	91079628	Glutamine synthetase (EC 6.3.1.2)	11	23.1	246.17
2.14E-03	43.49	112702923	Peptidoglycan-recognition protein-LB (Fragment)	6	81.6	50.387
7.48E-05	43.45	183979309	Ribosomal protein L23A	10	25.9	108.05
2.14E-03	43.18	164451507	Troponin I	8	25.8	144.07
1.23E-04	42.52	114052230	Hydroxyacyl-coenzyme A dehydrogenase	32	52.3	323.31
1.17E-03	42.39	114051800	Eukaryotic translation initiation factor 3 subunit I (eIF3i)	15	56.4	312.82
8.46E-04	41.53	112983086	Troponin C	11	34.2	162.39
4.19E-03	41.26	114051191	Peroxiredoxin	13	34.9	274.81
2.20E-03	38.87	206725499	Cathepsin L like protein	9	16.7	165.77
9.26E-06	38.85	169646838	Heat shock protein 25.4	19	55.2	323.31
1.41E-03	38.57	118350731	Uncharacterized protein	7	30.3	119.42
4.04E-05	38.32	91082963	DnaJ homolog subfamily B member 11-like Protein	9	32.6	168.69
3.61E-03	37.98	27461086	Cytochrome b-c1 complex subunit 6	4	29.1	102.68
8.04E-03	36.61	223671107	putative cuticle protein	6	29.9	26.941
1.24E-	36.56	24201728	Tubulin alpha chain	4	46	90.77

04		3				
3.41E-05	36.34	112982661	40S ribosomal protein S6	8	32	177.69
2.18E-04	36.16	112984008	Ribosomal protein S17	7	58.9	118.32
4.70E-04	34.92	148298695	Polyadenylate-binding protein (PABP)	16	28.9	200.66
4.36E-03	33.91	16226511	Larval cuticle protein	1	30.9	65.324
8.25E-04	33.73	114050993	Proteasome subunit alpha type (EC 3.4.25.1)	7	21.8	122.04
2.18E-03	33.69	82941226	Heat shock protein 19.5	13	54.9	272.36
5.01E-04	33.40	158284547	AGAP012577-PA	4	90	51.969
4.98E-05	32.75	170038659	Uncharacterized protein	4	11.4	49.459
2.49E-05	32.46	112982910	Ribosomal protein S28	3	18.9	60.926
2.02E-04	32.45	195110195	Uncharacterized protein	11	33.6	138.63
1.11E-03	32.11	112984274	40S ribosomal protein S28	6	34.5	95.807
1.16E-02	31.84	15072548	Mesencephalic astrocyte-derived neurotrophic factor homolog (MANF/CDNF-like protein)	2	70.5	152.06
9.89E-04	31.29	170051146	Ribosomal protein L23	5	12.7	37.755
2.87E-03	30.66	112983495	Trypsin-like protein	8	47.5	115.03
1.42E-05	30.31	114052210	Peroxiredoxin-4	8	27.3	134.05
7.64E-03	30.09	110756487	Ribosomal protein L9	5	20.5	47.373
2.90E-04	29.90	193704761	Thioredoxin peroxidase	6	47.6	97.18
7.52E-06	29.58	189234578	Uncharacterized protein	14	34.9	259.27
5.11E-04	29.17	194752327	Delta-1-pyrroline-5-carboxylate synthase	22	36.5	277.8
4.17E-04	28.92	238667031	tubulin alpha chain	5	65.4	66.714
1.02E-02	28.75	56462154	Heat shock protein 1	17	54.2	323.31
9.56E-04	28.71	226903593	Myofilin variant A	5	19.9	63.981
3.54E-03	28.51	23208535	Peptidoglycan recognition-like	13	32.1	323.31

			protein B (Fragment)			
4.40E-04	28.01	153791621	Acetoacetyl-CoA thiolase (EC 2.3.1.9)	20	50.6	227.07
9.12E-05	27.21	87248109	Enoyl-CoA hydratase 1	11	34.4	239.67
1.30E-05	27.09	87248535	Mitochondrial matrix protein p32	13	47.1	236.52
4.52E-03	26.35	91076494	Protein CREG1-like Protein	6	23.9	93.79
1.39E-03	26.27	160333484	Myosin light polypeptide 9 isoform 1	13	37.8	323.31
1.02E-03	26.04	4090964	Immune-related Hdd1	17	25.3	194.38
6.04E-04	25.05	156547257	Uncharacterized protein	7	14.7	59.012
1.01E-02	25.00	171740915	Putative gram negative bacteria-binding protein	9	30.5	168.58
6.73E-05	24.46	91088191	Ribonuclease UK114-like Protein	5	35.2	60.072
1.55E-03	23.72	91077606	LDLR chaperone boca-like Protein	13	44.5	276.81
9.45E-05	23.64	49532918	Cellular retinoic acid binding protein	13	34.8	228.51
3.45E-03	23.55	14517793	Glutathione-S-transferase-like protein	10	44.9	236.31
3.25E-02	23.37	114051738	Alcohol dehydrogenase	9	31.2	101.43
9.47E-04	21.98	62002225	Carboxylic ester hydrolase (EC 3.1.1.-)	7	48.7	93.062
3.65E-03	21.90	112984000	Ribosomal protein S18	11	40.4	80.396
1.29E-03	21.18	112984306	Ribosomal protein L19	7	26.2	203.3
3.26E-07	21.03	4090970	Immune-related Hdd23	5	24.7	165.52
7.06E-04	20.53	91082581	Multiple coagulation factor deficiency protein 2 homolog-like Protein	3	23.7	39.338
3.00E-03	19.94	112983062	Lipopolysaccharide binding protein	17	40.6	323.31
6.58E-03	19.59	25989211	CLIP domain-containing serine protease 2	10	61.8	186.29
2.92E-03	19.58	158635929	Translocase of inner mitochondrial	5	22.3	53.837

			membrane 8 homolog b			
2.91E-04	19.57	242015614	Glucosidase 2 subunit beta precursor, putative (Glucosidase 2 subunit beta, putative)	3	6.1	98.6
2.09E-03	19.22	2459696	Alpha-crystallin cognate protein 25	8	37.8	93.687
1.50E-03	19.04	186703381	Hemolin	7	59.3	192.54
7.21E-04	18.82	225733991	Polyubiquitin-C [Cleaved into: Ubiquitin]	4	52.8	49.899
1.63E-05	18.73	91089799	Transcription factor BTF3	6	21.2	162.9
2.80E-03	18.62	157704337	Hdd1-like protein	7	56.9	272.49
1.99E-03	18.47	18140733	Twelve cysteine protein 1	17	37.3	237.4
4.16E-03	18.46	6671050	Glutathione S-transferase (EC 2.5.1.18)	9	39.4	117.18
1.83E-03	18.39	170075163	Membrane associated progesterone receptor	8	42.5	108.04
2.67E-03	18.27	118795183	AGAP001177-PA (Ca2+-triggered coelenterazine-binding protein 1)	5	11.7	96.246
3.41E-03	17.99	15214063	Lysozyme (EC 3.2.1.17) (1,4-beta-N-acetylmuramidase)	7	16.7	132.63
1.45E-03	17.71	242011684	Endoplasmic reticulum protein ERp29, putative	14	27.9	118.44
3.98E-03	17.34	112982861	Ribosomal protein S11-2	7	37.6	66.981
5.31E-05	16.96	112983886	Elongation factor 1 delta	4	26.2	37.615
8.03E-03	16.67	114052765	Stromal cell-derived factor 2	4	10.5	98.283
8.19E-05	16.37	58396343	AGAP001312-PA	10	21.4	127.74
3.08E-03	16.21	158292087	Succinate--CoA ligase [ADP/GDP-forming] subunit alpha, mitochondrial (EC 6.2.1.4) (EC 6.2.1.5) (Succinyl-	10	32	96.631

			CoA synthetase subunit alpha) (SCS-alpha)			
4.33E-03	15.99	112984422	60S ribosomal protein L17	7	22.1	87.256
3.69E-04	15.94	91092424	Prefoldin subunit 1-like Protein	5	20.5	67.747
7.07E-04	15.80	91078330	15 kDa selenoprotein-like Protein	6	36.5	53.208
7.68E-03	15.78	21630233	Serine proteinase-like protein 2	3	40.2	118.94
7.31E-04	15.77	148298648	Ribosomal protein S13	7	31.1	75.464
9.98E-04	15.48	112984248	Ribosomal protein L24	5	41.7	32.859
1.01E-02	15.41	114052645	Thymosin isoform 1	4	40.9	77.676
1.31E-02	15.36	157108606	AAEL005062-PA (AMP dependent coa ligase)	8	28.3	64.622
9.41E-04	15.08	157118472	Calponin	7	18.9	103.62
2.93E-03	14.95	16566722	40S ribosomal protein S3a	8	23.7	102.8
1.60E-03	14.72	195022411	GH17138	2	51.5	83.817
4.09E-04	14.64	74904844	40S ribosomal protein S14	8	52.6	104.12
4.48E-04	14.48	91089541	Protein canopy 4-like Protein	6	23.8	86.758
1.89E-03	14.43	160425427	Single domain major allergen 1 protein (Fragment)	5	30.1	74.43
6.30E-03	14.23	114053277	H+ transporting ATP synthase O subunit isoform 1	13	36.3	166.38
1.67E-03	14.23	148298667	Signal sequence receptor	5	22	76.523
3.68E-04	14.14	242019202	Spectrin beta chain, putative	7	26.8	152.42
1.08E-03	13.99	112984100	Yellow-b	11	20.5	208.52
2.90E-03	13.90	114051357	Transgelin	5	76.3	164.29
1.58E-02	13.83	56462126	Cuticle protein 1	2	16.7	67.986
2.38E-02	13.68	157168007	Dolichyl-diphosphooligosaccharide--protein glycosyltransferase subunit 1	20	57.3	191.04
3.32E-04	13.21	114053151	Electron-transfer-flavoprotein beta	12	38.6	120.95

			polypeptide			
8.07E-03	13.15	112983980	Ribosomal protein S19	7	29.9	54.261
1.68E-04	13.15	183979300	Similar to CG6803-PB	10	34.5	89.291
1.07E-03	13.13	9624379	Tetraspanin	3	5.9	35.267
5.25E-03	13.09	114053311	26S protease regulatory subunit 6B	13	40	156.12
4.03E-03	13.05	91080053	ADP,ATP carrier protein-like Protein	2	33.3	13.018
1.25E-02	12.95	71913231	40S ribosomal protein S7	9	40.9	88.839
5.21E-03	12.83	170062088	26S protease regulatory subunit 6A	17	47.1	205.95
1.68E-03	12.73	114050793	Small nuclear ribonucleoprotein G (snRNP-G)	3	22.6	42.292
6.27E-03	12.55	91091394	Hypothetical protein	3	20.7	106.8
3.50E-02	12.46	51701794	60S ribosomal protein L31	3	21.5	21.606
2.46E-02	12.46	114052711	transmembrane emp24 protein transport domain containing 9 precursor	6	21.3	69.189
3.44E-03	12.19	55139149	Hemolin (Fragment)	14	47.3	323.31
6.56E-03	12.05	194911336	Uncharacterized protein	9	29.7	103.11
9.06E-03	12.02	219472060	Uncharacterized protein	6	23.8	104.55
9.43E-03	11.62	91080019	MICOS complex subunit Mic25 isoform X1	8	19.2	88.479
1.11E-02	11.52	112983184	Eukaryotic translation initiation factor 3 subunit B	4	6.1	34.366
2.10E-02	11.51	34556399	Prophenoloxidase subunit 2	2	35.7	63.214
1.97E-02	11.36	187884602	Chitin deacetylase 1	5	47.8	76.273
1.02E-02	11.25	223671103	putative cuticle protein	8	29.7	192.05
1.54E-03	11.17	2499773	46 kDa FK506-binding nuclear protein	6	12	49.619
8.52E-03	11.13	163716794	Gustatory receptor	6	12.2	164.32

4.03E-02	11.08	154091250	Ribosomal protein S25	4	32.6	32.87
1.38E-03	10.85	157106230	AAEL004460-PA	9	20.6	76.158
7.92E-04	10.84	110347794	Gloverin-like protein	7	27.6	152.26
2.75E-02	10.72	49532840	Ribosomal protein L27A2	6	29.6	76.82
6.55E-03	10.68	112984404	Ribosomal protein L15	7	27	65.93
4.28E-02	10.42	112982735	60S acidic ribosomal protein P0	2	61.3	73.494
9.14E-03	10.38	399471	Fatty acid-binding protein 1 (FABP 1)	8	45.5	90.976
4.47E-04	10.27	114053275	60S ribosomal protein L7/l12	4	22	38.986
2.82E-03	10.12	56418393	Hemolymph proteinase 6	9	47.9	138.64
2.16E-02	10.10	189240992	Ubiquinol-cytochrome c reductase core protein II	19	28.7	182.68
8.83E-04	10.01	163838684	Carboxypeptidase (EC 3.4.16.-)	19	55.3	288.66
1.43E-04	9.97	170045511	vitellogenic carboxypeptidase	11	24.3	84.703
6.32E-03	9.91	154091289	60S ribosomal protein L27	5	19.9	69.439
8.88E-05	9.85	114051372	NADH dehydrogenase (Ubiquinone) Fe-S protein 8	9	33.8	139.04
4.60E-04	9.77	112982822	Phosphoglycerate mutase (EC 5.4.2.11) (EC 5.4.2.4)	8	12	79.055
3.26E-03	9.76	114053231	V-type proton ATPase subunit G	5	16.8	81.847
1.34E-02	9.74	114052242	Glutathione S-transferase omega 1	11	50.2	130.6
5.70E-03	9.71	56462370	Ribosomal protein 30	8	21.3	86.72
2.98E-03	9.59	145504735	Uncharacterized protein	6	14.3	94.061
1.34E-03	9.47	242023380	Mitochondrial import inner membrane translocase subunit TIM13, putative	5	26.1	56.699
4.01E-04	9.13	164683438	Eukaryotic initiation factor 4A	15	25.1	200.2
2.29E-03	9.12	58864724	Annexin (Fragment)	1	5.8	11.177

2.76E-02	9.12	157132602	AAEL002881-PA (Mitochondrial NADH dehydrogenase (Ubiquinone) 1 alpha subcomplex)	5	36.4	49.99
1.32E-03	8.97	112982855	Ribosomal protein S15A	6	36.3	82.265
5.21E-03	8.88	91082167	similar to Arp2/3 complex subunit ARPC5	6	36.2	68.08
3.52E-03	8.87	112984334	Ribosomal protein L11	6	34.8	110.77
9.82E-04	8.72	91089049	Protein enhancer of sevenless 2B-like Protein	6	9.8	120.65
6.68E-03	8.52	160333861	Ribosomal protein L10	7	40.8	49.242
1.52E-03	8.03	110756109	endoplasmic reticulum lectin 1 isoform X1	12	33.8	103.58
1.28E-03	7.92	189234130	peroxidase precursor	20	30.2	153.32
2.50E-04	7.64	219552448	Arginine kinase (Fragment)	9	68.4	310.24
3.88E-04	7.52	183979392	Uncharacterized protein	40	65.5	323.31
1.17E-03	7.51	112983090	Eukaryotic translation initiation factor 3 subunit J (eIF3j)	5	15.3	51.106
4.78E-02	7.45	116833131	Uncharacterized protein (Fragment)	7	23.6	83.164
2.85E-03	7.40	114051097	H+ transporting ATP synthase subunit g	3	11.9	46.248
1.73E-03	7.38	45330818	Fructose-bisphosphate aldolase (EC 4.1.2.13)	4	28.4	49.257
1.37E-04	7.35	49532886	Diazepam binding inhibitor-like protein	3	25.9	36.14
8.36E-03	7.31	113866028	Cytochrome b-c1 complex subunit 7	7	41.3	101.75
1.79E-03	7.13	114051978	Macrophage migration inhibitory factor	4	14.2	78.711
3.73E-03	7.03	112983052	Chemosensory protein 7; Chemosensory protein11	9	26.7	149.01
7.66E-03	7.02	114052561	Malate dehydrogenase (EC	11	29.6	136.45

			1.1.1.37)			
1.07E-02	6.99	112984158	Ribosomal protein L36	4	10.1	70.779
3.55E-03	6.99	124802527	hypothetical protein	4	18.5	40.152
2.68E-03	6.97	149898901	Ubiquitin carboxyl-terminal hydrolase (EC 3.4.19.12)	4	19	30.795
1.43E-02	6.90	195383286	Uncharacterized protein	3	20.3	38.161
1.82E-03	6.83	154091248	Ribosomal protein L18	6	28.5	123.74
6.67E-04	6.77	238915967	Hemicentin-like protein (Fragment)	11	22.5	80.653
4.53E-03	6.62	91081585	Protein FAM177A1-like Protein	5	16.2	66.242
7.64E-03	6.60	148298800	Enolase	15	38.1	156.91
1.21E-03	6.60	15146043	Alpha-crystallin	13	45.7	268.76
3.40E-03	6.44	112983816	Glyceraldehyde-3-phosphate dehydrogenase (EC 1.2.1.12)	15	47.6	122.8
1.71E-02	6.44	91083249	NADH dehydrogenase [ubiquinone] iron-sulfur protein 6, mitochondrial	3	19.4	42.266
3.55E-02	6.40	114052408	Mitochondrial aldehyde dehydrogenase	1	5.7	68.304
2.25E-02	6.36	52000789	40S ribosomal protein S23	6	35.4	69.823
2.91E-02	6.35	114051842	Cyclic AMP-regulated protein	7	22	81.903
1.44E-02	6.35	160333493	Mitochondrial intermembrane space translocase subunit Tim10	4	12.9	65.888
3.64E-02	6.32	53148463	Receptor for activated protein kinase C homolog	14	50.1	165.95
1.24E-02	6.30	193690653	tubulin beta-1	3	27.2	83.77
4.93E-02	6.26	114052036	V-type proton ATPase subunit F	10	39	214.27
3.39E-03	6.21	156551153	Uncharacterized protein	3	21.6	25.158
4.09E-02	6.01	195475698	Uncharacterized protein (EC 3.4.13.-)	8	43.6	77.418

7.57E-03	6.01	148298726	ADP-ribosylation factor	7	20	58.457
3.09E-02	5.82	74910327	60S ribosomal protein L38	3	21.5	19.266
1.23E-02	5.76	148298693	Heat shock protein 20.8 (Heat shock protein hsp20.8A)	5	66.7	47.429
2.91E-03	5.70	112983493	Protein kinase c inhibitor	3	10.5	32.227
4.62E-02	5.64	56462206	Ribosomal protein L1	7	35	70.276
3.95E-04	5.61	109119903	Glyceraldehyde-3-phosphate dehydrogenase (EC 1.2.1.12)	17	55.6	323.31
4.17E-02	5.42	56462288	Protease inhibitor 5 (Fragment)	4	20.2	45.447
7.62E-03	5.38	156550835	probable RISC-loading complex subunit	10	20	168.85
4.02E-02	5.16	54609197	60S ribosomal protein L5	9	38.7	104.79
4.70E-02	5.11	170033490	Kakapo	2	75	13.843
9.01E-04	5.11	229002332	Uncharacterized protein (Fragment)	6	21.4	323.31
2.04E-02	5.06	157114409	AAEL006836-PB	8	26.9	67.323
2.67E-04	5.03	45553223	HDC11369 (IP19829p) (IP19929p)	2	11.9	72.569
1.30E-02	5.03	15213774	Ribosomal protein L26	7	20.2	48.724
1.21E-02	4.90	112983974	Small ubiquitin-related modifier (SUMO)	3	11.2	27.257
4.96E-02	4.68	114051530	UMP-CMP kinase (EC 2.7.4.14) (Deoxycytidylate kinase) (CK) (dCMP kinase) (Uridine monophosphate/cytidine monophosphate kinase) (UMP/CMP kinase) (UMP/CMPK)	4	16.2	30.594
4.69E-02	4.56	157132177	AAEL012341-PA	9	19.4	94.695
8.16E-03	4.42	34921426	Serine protease inhibitor dipetalogastin (Dipetalin)	12	28	323.31

			(Fragment)			
3.45E-04	4.38	153791457	Glia maturation factor beta	6	16	75.528
3.13E-04	4.21	195442422	Uncharacterized protein, isoform A (EC 1.10.2.2) (Uncharacterized protein, isoform B) (Uncharacterized protein, isoform C)	3	15.8	24.567
4.25E-02	4.14	242023106	T-complex protein 1 subunit gamma	1	26.3	31.21
7.47E-03	4.13	158284767	AGAP009439-PA (Fragment)	3	17.3	26.417
1.58E-02	4.12	112983138	UDP-glucuronosyltransferase (EC 2.4.1.17)	3	9.3	25.917
3.51E-02	4.05	149689114	Cytochrome c oxidase	2	16	30.409
7.07E-04	3.88	112984054	Yellow-d	12	24.1	172.3
4.50E-02	3.66	114053203	DnaJ homolog subfamily A member 1 (DnaJ-2)	8	24.4	81.35
4.43E-02	3.65	112983960	BAG domain-containing protein Samui	4	18.2	31.383
5.02E-03	3.63	91082037	Uncharacterized protein (Fragment)	13	15.5	216.81
3.17E-04	3.58	56462318	Cathepsin B-like cysteine proteinase	6	31.8	49.498
1.55E-03	3.56	118424551	Programmed cell death protein 5-like protein	15	37.6	179.95
9.14E-04	3.54	148298849	programmed cell death protein 5-like protein	3	19.2	22.245
8.00E-03	3.53	114052649	Phosphohistidine phosphatase	4	24	25.152
4.03E-02	3.53	219362823	Innexin	3	17.3	60.31
3.51E-02	3.35	112983408	Protein transport protein Sec61 subunit beta	2	11.6	15.799
5.72E-03	3.33	112984164	Ribosomal protein L35	4	26.1	44.817
2.90E-03	3.06	75906185	Adhesion related protein, transmembrane	8	32.2	210.68
1.84E-02	3.02	158289729	5'-nucleotidase (EC 3.1.3.5)	6	21.7	68.283
1.95E-02	2.99	114052472	Peptidyl-prolyl cis-trans isomerase (PPIase) (EC	13	38.7	170.19

			5.2.1.8)			
5.15E-03	2.95	153792309	Pyruvate dehydrogenase E1 component subunit alpha (EC 1.2.4.1)	8	17.8	81.846
7.17E-04	2.93	219432895	hypothetical protein	4	14.2	42.156
1.93E-02	2.86	91078902	Syntaxin-7-like Protein	6	19.9	58.006
2.67E-02	2.79	156549389	Uncharacterized protein	6	14.1	73.179
5.97E-03	2.59	47607477	Imaginal disc growth factor	15	48.9	323.31
1.06E-02	2.57	242009020	Paramyosin, putative	13	31.9	204.26
6.07E-03	2.48	242005732	Hemicentin, putative	3	6.6	22.003
3.94E-02	2.40	153791847	abnormal wing disc-like protein	8	42.2	181.01
3.87E-02	2.33	112983010	Translation elongation factor 2 (EF-2)	3	37.2	48.609
3.19E-03	2.20	195115822	GI17397	3	51.9	89.497
2.36E-02	2.13	91084741	Apolipoprotein D-like Protein	15	40.9	323.31
1.22E-02	1.99	85726208	Imaginal disc growth factor-like protein	16	59.6	323.31
3.45E-02	1.95	158299186	AGAP010145-PA (Fragment)	16	39.3	254.01
3.47E-02	1.89	118789328	AGAP008115-PA	4	11.7	323.31
3.17E-03	1.89	156630460	Anionic antimicrobial peptide 2	7	32.9	247.1
4.17E-02	1.85	163838694	Cytochrome c1	5	16.6	57.966
1.54E-02	1.39	162462783	Carboxylic ester hydrolase (EC 3.1.1.-)	16	31.5	285.11

Table A7.2B. *G. mellonella* larval proteins decreased in abundance in nodules isolated from larvae infected with *M. mycetomatis* for 24 hour as compared to control larval hemolymph proteome.

P value	Fold Change (-)	GI Number	Protein Name	Peptides	Sequence coverage [%]	Score

2.82E-04	310.15	14599862	Hexamerin storage srotein PinSP1	75	76.6	323.31
1.47E-04	14.50	110743533	Methionine-rich storage protein	14	79.1	323.31
1.02E-04	13.32	114052174	Aminoacylase	7	26.9	88.164
6.18E-05	12.53	384243	Arylphorin	21	59.5	323.31
3.98E-05	11.90	56462300	Putative serine protease-like protein 2	16	67.3	323.31
5.55E-03	10.67	121308868	Serine proteinase	14	36.5	247.94
5.00E-03	9.37	114051866	Isocitrate dehydrogenase [NADP] (EC 1.1.1.42)	16	39	163.29
2.08E-04	6.95	14599864	Hexamerin storage protein PinSP2	10	63.2	149.11
1.74E-04	6.44	159528	Methionine-rich storage protein 2	77	82.2	323.31
8.35E-05	6.00	159078	Arylphorin	51	77.5	323.31
6.56E-04	5.44	134103857	Cationic peptide CP8	3	19.6	131.94
1.85E-04	5.40	70609810	Transferrin	59	55.6	323.31
1.39E-03	5.08	182509208	Carboxylic ester hydrolase (EC 3.1.1.-)	6	42.9	82.053
3.11E-02	5.07	114050871	Carboxylesterase	9	41.5	203.18
3.61E-05	4.74	158515746	juvenile hormone binding protein	12	40.8	312.16
2.04E-02	4.71	2498144	Apolipophorins [Cleaved into: Apolipophorin-2 (Apolipophorin II) (apoLp-2); Apolipophorin-1 (Apolipophorin I) (apoLp-1)]	12	85.9	323.31
1.68E-04	4.38	56418411	Hemolymph proteinase 16	8	27.5	88.118
6.19E-04	4.27	112983654	Bombyrin	9	25.8	183.58
7.20E-03	3.60	77415676	Uncharacterized protein	12	30.2	323.31
1.27E-02	3.43	50404098	Apolipophorin (Fragment)	12	45.2	323.31
2.98E-03	2.77	145286562	Lysozyme-like protein 1	5	14.3	38.045

3.99E-04	2.58	91082539	Inter-alpha-trypsin inhibitor heavy chain H4-like Protein	20	43.4	323.31
7.60E-03	2.57	46396271	27 kDa hemolymph protein (P27K) (27k)	10	59.6	323.31
3.07E-03	2.47	6919921	Inducible serine protease inhibitor 2 (ISPI-2) (Fragment)	3	9.8	43.382
3.78E-02	2.47	114052484	Kazal-type proteinase inhibitor	5	21.4	106.51
4.64E-02	2.04	183979239	Similar to CG10638-PA	6	26.4	54.027
3.55E-02	1.83	112984548	Serpin-5	10	23.6	71.201
3.96E-02	1.70	242004672	Uncharacterized protein	9	51.9	164.35
1.30E-02	1.60	116791778	Uncharacterized protein	19	56.6	323.31

Table A7.3. *M. mycetomatis* proteins identified in *G. mellonella* larvae hemolymph during infection.

Uniprot ID	**Protein Name**
A0A150ASN1	Long-chain-fatty-acid--CoA ligase 1
A0A175VN17	Ribosomal protein
A0A175VNI1	Protein kinase dsk1
A0A175VP33	Conidiation-specific protein 6
A0A175VPF9	Signal peptidase complex subunit SPC2
A0A175VPU3	Protein csh3
A0A175VPW2	Uncharacterized protein
A0A175VQA2	Uncharacterized protein
A0A175VQC4	USP6 N-terminal-like protein
A0A175VR24	GPI ethanolamine phosphate transferase 2
A0A175VR85	Kinesin-like protein KIF1A
A0A175VRA2	Histone H4
A0A175VRU2	ATP synthase subunit alpha
A0A175VRX2	5'-3' exoribonuclease
A0A175VSN9	Reticuline oxidase
A0A175VSX5	4-O-methyl-glucuronoyl methylesterase
A0A175VT02	Heat shock protein 90

A0A175VT46	Putative sterigmatocystin biosynthesis P450 monooxygenase stcF
A0A175VT53	Trans-aconitate 2-methyltransferase
A0A175VTM6	Histone H2A
A0A175VU49	High-affinity nicotinic acid transporter
A0A175VUG0	Histone H2B
A0A175VUK8	Putative flavin-containing monooxygenase 1
A0A175VUN5	GTP-binding nuclear protein
A0A175VVC8	Uncharacterized protein
A0A175VWM1	Calcium uniporter protein 6, mitochondrial
A0A175VWW4	Sortilin
A0A175VY37	Clustered mitochondria protein homolog (Protein TIF31 homolog)
A0A175VYR8	Catechol 1,2-dioxygenase
A0A175VYS3	pH-response transcription factor pacc-1
A0A175VYV0	Cell division control protein 48
A0A175VZ06	Small COPII coat GTPase SAR1
A0A175VZE3	Serine/threonine-protein kinase 32C
A0A175W0E4	Uncharacterized protein
A0A175W0F9	Chromodomain helicase hrp3
A0A175W0L4	Vegetative incompatibility protein HET-E-1
A0A175W120	Tubulin alpha chain
A0A175W1E5	Actin
A0A175W1R3	60S ribosomal protein L27
A0A175W1U0	Putative DNA helicase ino80
A0A175W1Y0	Dehydrodolichyl diphosphate syntase complex subunit NUS1
A0A175W2D6	DNA damage checkpoint protein rad24
A0A175W2D7	Uncharacterized protein
A0A175W322	Alpha-1,4 glucan phosphorylase
A0A175W3I8	Histone deacetylase complex subunit SAP18
A0A175W487	Putative N-acetylglucosamine-6-phosphate deacetylase
A0A175W509	DNA helicase
A0A175W5H5	Uncharacterized protein
A0A175W5M7	Uncharacterized protein
A0A175W6Z4	Molybdenum cofactor biosynthesis protein 1
A0A175W760	Meiotic expression up-regulated protein 26
A0A175W7B7	ADP-ribosylation factor
A0A175W7C2	Protein RTA1
A0A175W7E1	TEL2-interacting protein 1
A0A175W836	Superoxide dismutase 1 copper chaperone
A0A175W8E2	Elongation factor 2
A0A175W8P0	Tubulin alpha chain
A0A175W961	Tricalbin-3
A0A175W9B3	Uncharacterized protein

A0A175W9D4	3-dehydroshikimate dehydratase
A0A175WA11	Heat shock 70 kDa protein
A0A175WAG6	Uncharacterized protein
A0A175WAT4	Clathrin heavy chain
A0A175WB24	Ras-related protein YPTC6
A0A175WB50	Uncharacterized protein
A0A175WBB9	Protein sly1
A0A175WC71	Uncharacterized protein
A0A175WCF3	Isocitrate dehydrogenase [NADP]
A0A175WCR0	Uncharacterized protein
A0A175WDC7	Heat shock 70 kDa protein
A0A175WDF8	Putative serine racemase
A0A175WDK6	Cation-transporting ATPase
A0A175WDW4	DnaJ-related protein SCJ1
A0A175WEH0	Uncharacterized protein
A0A175WG07	Phosphoribosylaminoimidazole-succinocarboxamide synthase
A0A175WG82	Midasin
A0A175WG89	Uncharacterized protein
A0A175WGL9	Malate dehydrogenase
A0A175WGN5	Glucose-6-phosphate 1-dehydrogenase
A0A175WGS8	GTP-binding protein ypt1
A0A175WH80	Peroxisomal long-chain fatty acid import protein 2
A0A175WHD6	Arginine--tRNA ligase, cytoplasmic
A0A175WHM7	Succinyl-CoA:3-ketoacid-coenzyme A transferase
A0A175WHZ5	Uncharacterized protein
A0A175WI88	V-type proton ATPase subunit B

Table A7.4A. *G. mellonella* larval proteins increased in abundance in 24 hour *M. mycetomatis* infected *G. mellonella* larval hemolymph as compared to 0 hour hemolymph.

Protein Name	GI Number	P value	Peptides	Sequence coverage [%]	Fold Change (+)
Transgelin	183979237	5.2277E-05	17	45.1	190.84
Beta actin	157927723	0.00374135	14	55.9	161.62
Gustatory receptor	125629089	0.000375126	8	43	120.18
Putative defense protein Hdd11	74873244	0.00245946	10	60.7	47.19
Uncharacterized protein	195119912	0.000382483	9	63.5	41.05
Cecropin-D-like peptide	156630481	0.004577732	2	14.5	33.46

Uncharacterized protein	145504735	0.000523472	9	34.8	32.47
Tubulin beta chain	112983342	0.004196197	18	34	28.25
Immune-related Hdd1	4090964	0.000297776	26	37.1	26.71
Calponin	157118472	0.008064786	11	32.1	26.69
Tropomyosin 2	183979374	0.00198155	10	32.5	25.48
Protease inhibitor 1	114053193	0.019293667	4	30.6	24.45
CLIP domain-containing serine protease 2	25989211	0.001202955	2	38.6	20.97
Heat shock protein hsp21.4	112983414	0.006484677	7	18.4	20.84
Triosephosphate isomerase	154707830	0.006710254	13	28.5	19.54
Heat shock-like protein	23208546	0.000629917	10	24.8	19.40
Elongation factor 1-alpha	183979284	0.000436203	11	41.8	19.29
Serpin-like protein (SEP-LP)	112983872	0.000214189	17	35.8	18.40
Peptidoglycan-recognition protein-LB	112702923	0.001882782	7	89.5	16.91
Thioredoxin	148298796	0.000774337	6	20.7	15.53
Kunitz-like protease inhibitor	22901764	0.007523229	3	29.5	15.48
Heat shock protein 90	229562186	0.003950293	32	48.6	15.26
Uncharacterized protein, isoform A	194882165	0.007384207	9	19.9	15.16
Enolase	148298800	0.005098414	22	48.2	14.85
Hemicentin-like protein 1	83583693	0.017332286	13	25.5	14.72
Cathepsin L like protein	206725499	0.040407094	11	16.7	14.52
Troponin I	164451507	0.039318574	9	31.1	14.39
Uncharacterized protein	56462318	0.000587164	8	34.4	14.03
Peptidyl-prolyl cis-trans isomerase	60592747	0.001111881	6	26.5	13.02
AGAP004366-PA	158292087	0.003309045	12	38.8	12.75
Peptidoglycan recognition-like protein B	23208535	6.37462E-05	13	32.1	12.21
Odorant-binding protein	39579195	0.001762561	5	19.5	12.19
Serpin-4B	45594226	0.019290203	5	78.8	11.94
Actin 3	192763882	0.00320419	9	30.9	10.87
Prophenol oxidase activating enzyme 3	56718390	0.000404234	25	47.9	10.72

Peptidoglycan-recognition protein	112982725	0.003381177	4	20.5	10.71
Hemicentin, putative	242005732	0.013403009	15	60.6	10.48
Uncharacterized protein	170578347	0.006116064	3	53.4	10.37
hypothetical protein TTHERM_00163900	118350731	2.95175E-05	8	31.8	10.31
CALNUC	7576710	0.001671888	7	38.9	10.16
GH17138	195022411	0.000470466	2	51.5	10.00
Glutathione-S-transferase-like protein	14517793	0.000616739	12	50.8	9.93
Hemolin	186703381	0.001399058	7	59.3	9.47
Inducible metalloproteinase inhibitor protein	33860163	0.014309318	11	39.7	9.30
Serpin-11	226342884	0.000854124	23	54.7	8.98
Troponin T	183979372	0.031678636	9	34.7	8.77
Uncharacterized protein	145504735	0.000657432	8	18.3	8.74
DNA-directed RNA polymerase II subunit RPB1	189234613	0.007845276	4	15.5	8.73
renin receptor isoform X3	156549004	0.044153853	7	18.7	8.36
Uncharacterized protein	148906269	0.001299673	8	17.7	8.05
Tubulin alpha chain	225031010	0.008238892	4	47.2	7.81
Calreticulin	17826933	0.009241452	10	20.7	7.42
chemosensory protein	158962505	0.004827641	3	11.3	7.39
odorant-binding protein	39579195	0.009532495	9	22	6.50
Chemosensory protein	25989211	0.007725442	10	61.8	6.40
Gloverin	110649240	0.016270655	2	28.8	6.38
Hemolin	55139149	0.005144114	16	63	6.11
Prophenoloxidase activating protease 1	60299968	0.009147662	3	76.9	5.65
Yellow-d precursor	112984054	4.58945E-05	20	42.5	5.55
Chemosensory protein 7	189234130	0.013259273	19	29.5	5.48
Uncharacterized protein	112983052	0.004951208	8	26.7	5.14
uncharacterized protein LOC660215	91076018	0.002487848	5	4.4	4.90
Troponin T transcript variant B	225346689	0.046612834	4	24.8	4.84

Protease inhibitor-like protein	157927723	0.006282492	5	16.1	4.22
Serine protease inhibitor dipetalogastin	110347843	0.010683281	2	40	4.20
Peptidoglycan recognition protein	34921426	0.000750934	12	28	4.15
peptidoglycan recognition protein precursor	112983994	0.001198494	12	56.4	3.86
Arginine kinase	219552448	0.015823638	9	68.4	3.72
Dihydrolipoyl dehydrogenase	112983096	0.037775964	5	15.8	2.98
Tubulin alpha chain	238667031	0.047744816	4	64.1	2.90
Uncharacterized protein	156968291	0.023597034	23	36.6	2.81
Cecropin-A	116087	0.03590646	1	8.5	2.77
Cellular retinoic acid binding protein	49532918	0.000887879	15	36.3	2.59
Paramyosin, putative	242009020	0.020052027	16	32.1	2.57
DEAD-box RNA helicase (Fragment)	82705976	0.029221171	6	32.9	2.53
Adhesion related protein, transmembrane	75906185	0.00327163	11	51.4	2.24
AGAP010145-PA	158299186	0.049494711	8	27.6	2.13
Translationally controlled tumor protein	112982880	0.034602076	8	38.3	2.09

Table 7.4B. *G. mellonella* larval proteins decreased in abundance in 24 hour *M. mycetomatis* infected *G. mellonella* larval hemolymph as compared to 0 hour hemolymph.

Protein Name	**GI Number**	**P value**	**Peptides**	**Sequence coverage [%]**	**Fold Change (-)**
Hexamerin storage srotein PinSP1	14599862	0.004935032	78	76.6	14.77
Ecdysteroid-regulated 16 kDa protein	3182995	0.00279485	3	32.7	10.30
Beta-1,3-glucan recognition protein	114649525	0.00635458	23	49.6	7.70
Apolipophorins	2498144	0.00479854	13	85.9	6.36
Glyceraldehyde-3-phosphate dehydrogenase	112983816	0.031367829	11	38.8	6.16
Cathepsin B-like	118424551	0.008318931	8	26.4	5.71

cysteine proteinase					
Apolipophorins	50404098	0.013134045	15	46.1	5.19
Lipopolysaccharide binding protein	2498144	0.002877231	8	51	4.74
C-type lectin 21 precursor	112983062	0.020324563	14	47.7	4.28
hemicentin	242005732	0.039715574	7	21.9	3.31
GTP-binding nuclear protein	114052751	0.011660189	5	17.4	2.88
Chaperonin	120444903	0.03245724	7	11.3	2.63
Isocitrate dehydrogenase	114051866	0.001198588	17	43	2.59
carboxylesterase clade H	114050871	0.008776959	9	41.5	2.56
Putative serine protease-like protein 2	56462300	0.003119882	19	67.9	2.43
Anionic antimicrobial peptide 2	156630460	0.010225278	7	32.9	2.39
Putative hydroxypyruvate isomerase	164459610	0.007844326	12	31.5	2.37
Carboxylesterase	114050871	0.003138215	24	69.6	2.35
High affinity nuclear juvenile hormone binding protein	242022233	0.012712216	6	13.9	2.34
Cationic peptide CP8	134103857	0.004168642	4	22	2.22
Scolexin	153791206	0.037726072	17	29.9	1.94
Uncharacterized protein	229002332	0.004550935	8	50.7	1.90
3-dehydroecdysone 3beta-reductase	4753912	0.000934337	8	26	1.86
Beta-1,3-glucan-binding protein	52782700	0.005069277	3	24.3	1.82
Carboxylic ester hydrolase	189181680	0.012846866	24	50.9	1.79
Bombyrin	112983654	0.043373957	10	28.9	1.77
Aminoacylase	114052174	0.047515735	10	27.5	1.77
Peptidyl-prolyl cis-trans isomerase	114052472	0.009121992	14	38.7	1.76
juvenile hormone binding protein	158515746	0.003824964	13	40.8	1.75
Fibrillin-like protein	112983550	0.005083542	2	21.7	1.74
Apolipoprotein D-like Protein	91084741	0.014484426	17	42.7	1.53
27 kDa hemolymph protein	46396271	0.040388511	11	59.6	1.52

Table A7.5. Enrichment for GO terms (Biological Process [A], Molecular Function [B] and Cellular Component [C]) from the total SSDA hemolymph proteins from *G. mellonella* larvae infected with *M. mycetomatis* (24 hour relative to 0 hour hemolymph proteome).

A

Biological process (GO)		
Pathway description	**Count in gene set**	**False discovery rate**
Response to stress	5	1.58e-05
Organic substance metabolic process	7	1.58e-05
Innate immune response	4	3.15e-05
Primary metabolic process	6	7.4e-05
Macromolecule metabolic process	5	0.000763
Cellular metabolic process	5	0.0012
Cellular protein metabolic process	4	0.00167
Protein folding	2	0.0032
Defense response to bacterium	2	0.028
Cellular nitrogen compound metabolic process	3	0.0415

B

Molecular function (GO)		
Pathway description	**Count in gene set**	**False discovery rate**
Ion binding	6	3.55e-06
Carbohydrate derivative binding	5	3.55e-06
Purine ribonucleoside binding	4	1.98e-05
Purine ribonucleotide binding	4	1.98e-05
Purine ribonucleoside triphosphate binding	4	1.98e-05
Catalytic activity	5	2.7e-05
Hydrolase activity	4	4.16e-05
Binding	5	0.000356
Metal ion binding	2	0.043

C

Cellular component (GO)		
Pathway description	**Pathway description**	**Pathway description**

Cytoplasm	8	1.1e-08
Intracellular	8	9.57e-08
Cell	8	1.92e-07
Extracellular region	5	2.31e-05
Cytoskeleton	2	0.00684
Intracellular organelle	3	0.0187

Table S7.6A. *G. mellonella* larval proteins increased in abundance in grains isolated from larvae infected with *M. mycetomatis* for 72 hour as compared to grains extracted from larvae infected with MM for 24 h.

P value	Fold Change (+)	GI Number	Protein Name	Peptides	Sequence coverage [%]	Score
2.79E-04	39.01	158299186	AGAP010145-PA (Fragment)	16	39.3	254.01
7.02E-04	13.38	241705635	ATP synthase subunit alpha	1	22.2	42.448
6.30E-04	12.35	195488294	Transferrin	9	46.4	186.64
2.81E-02	10.40	114051710	Mitochondrial prohibitin complex protein 2	14	45.2	152.58
8.10E-03	9.46	158289729	Rab GDP dissociation inhibitor	6	21.7	68.283
3.98E-02	8.12	401332	V-type proton ATPase subunit E	10	16.9	174.14
1.27E-02	7.67	148298861	Dolichyl-diphosphooligosaccharide--protein glycosyltransferase 48 kDa subunit	14	47.7	257.5
7.56E-03	7.54	91082037	5'-nucleotidase (EC 3.1.3.5)	13	15.5	216.81
3.93E-02	7.23	195542220	Carboxylesterase 4 variant 1 (Carboxylesterase 4 variant 3)	17	32.3	234.38
3.90E-02	6.23	53148463	Receptor for activated protein kinase C homolog	14	50.1	165.95
2.24E-03	6.21	112983416	Ras protein	11	15.6	259.62
4.67E-02	5.99	91094383	Alanyl-tRNA editing protein	8	12	93.999

			Aarsd1-like Protein			
3.62E-02	5.97	18253049	Ribosomal protein L7	7	21.4	71.856
8.34E-03	5.74	158298342	AGAP010792-PA	4	18.6	57.523
2.33E-02	5.40	114052334	Transmembrane trafficking protein	3	6.6	76.02
3.85E-02	5.39	114052452	Acyl carrier protein	2	6	24.902
1.34E-02	5.11	114052605	26S proteasome regulatory ATPase subunit 10B	7	24.1	91.871
2.68E-02	4.89	114052967	elongation factor Tu	15	46.1	136.61
9.85E-03	4.72	49532894	Heterotrimeric guanine nucleotide binding protein gamma subunit-like protein	3	12.7	25.538
1.93E-02	4.43	158292674	AGAP005160-PA (AGAP005160-PB) (Ras homolog gene family, member A)	7	9.4	82.825
2.97E-02	4.37	120444903	Chaperonin	12	23.3	153.74
2.14E-02	4.37	112984100	Yellow-b	11	20.5	208.52
2.56E-03	4.33	242013531	Uncharacterized protein	7	24.4	51.659
1.06E-02	4.11	114052454	NADH dehydrogenase [ubiquinone] 1 beta subcomplex subunit 10	5	32.5	157.25
2.39E-03	4.07	74873244	Putative defense protein Hdd11 (Hyphantria differentially displayed gene 11)	10	60.7	246.4
1.54E-02	3.88	118789328	AGAP008115-PA	4	11.7	323.31
1.20E-04	3.65	194910105	GG12390	10	27.7	119.3
2.06E-02	3.64	219362823	Innexin	3	17.3	60.31
3.29E-03	3.46	114053203	DnaJ homolog subfamily A member 1 (DnaJ-2)	8	24.4	81.35
2.08E-02	3.44	193690653	tubulin beta-1	3	27.2	83.77
2.74E-02	3.42	114052408	Mitochondrial aldehyde dehydrogenase	1	5.7	68.304
1.89E-02	3.39	163838694	Cytochrome c1	5	16.6	57.966
4.28E-02	3.35	83583695	Hemicentin-like protein 2 (Fragment)	3	60.4	21.64
4.30E-02	3.27	91080053	ADP,ATP carrier protein-like Protein	2	33.3	13.018
2.32E-02	3.18	163838684	Ubiquinol-	19	55.3	288.66

			cytochrome c reductase core protein II			
1.26E-02	3.09	114052230	Hydroxyacyl-coenzyme A dehydrogenase	32	52.3	323.31
4.02E-03	3.00	195442422	40S ribosomal protein S16	3	15.8	24.567
3.74E-02	2.95	14517793	Glutathione-S-transferase-like protein	10	44.9	236.31
8.29E-03	2.87	91080775	rab GDP dissociation inhibitor alpha	3	8.7	60.566
4.23E-03	2.86	54039446	AAEL005991-PA	5	28.2	57.601
6.17E-03	2.85	31340317	60S ribosomal protein L13a	4	12	35.501
1.33E-02	2.83	154091248	Ribosomal protein L18	6	28.5	123.74
8.75E-03	2.75	193594278	dihydrolipoyllysine-residue succinyltransferase component of 2-oxoglutarate dehydrogenase complex, mitochondrial	2	12.8	29.919
4.69E-03	2.74	157111903	LDLR chaperone boca-like Protein	7	12.9	54.892
2.70E-02	2.72	9725	Ribosomal protein S27A	3	37.2	116.93
2.89E-02	2.68	225031010	Tubulin alpha chain (Fragment)	4	47.2	228
9.55E-03	2.58	114051357	Transgelin	5	76.3	164.29
9.22E-03	2.55	91081585	Protein FAM177A1-like Protein	5	16.2	66.242
3.92E-02	2.43	158292087	AGAP004366-PA	10	32	96.631
2.94E-02	2.34	112984164	Ribosomal protein L35	4	26.1	44.817
2.46E-02	2.30	238667031	tubulin alpha chain	5	65.4	66.714
3.88E-02	2.18	91078902	Syntaxin-7-like Protein	6	19.9	58.006
1.05E-02	2.17	148298648	Ribosomal protein S13	7	31.1	75.464
3.37E-03	2.15	58864722	Annexin	21	57.7	323.31
3.67E-02	2.12	114052210	Thioredoxin peroxidase	8	27.3	134.05
4.14E-02	2.10	110760247	nucleolin 1 isoform X1	3	5.2	17.648
3.78E-02	2.02	242023106	T-complex protein 1 subunit gamma	1	26.3	31.21
3.95E-02	1.73	58864724	Annexin	1	5.8	11.177

			(Fragment)			
2.65E-02	1.65	189240992	Elongation factor Tu	19	28.7	182.68
1.88E-02	1.58	17826933	Calreticulin	18	28	323.31
1.16E-02	1.49	114053275	60S ribosomal protein L7/l12	4	22	38.986
5.09E-03	1.39	91077606	LDLR chaperone boca	13	44.5	276.81
2.43E-02	1.39	91089799	Transcription factor BTF3	6	21.2	162.9
2.90E-02	1.32	27461086	Cytochrome b-c1 complex subunit 6	4	29.1	102.68
2.12E-02	1.28	225733991	Polyubiquitin-C [Cleaved into: Ubiquitin]	4	52.8	49.899
4.22E-02	1.27	189238710	Uncharacterized protein	21	27.3	323.31

Table S7.6B. *G. mellonella* larval proteins decreased in abundance in grains isolated from larvae infected with *M. mycetomatis* for 72 h as compared to grains extracted from larvae infected with MM for 24 h.

P value	Fold Change (-)	GI Number	Protein Name	Peptides	Sequence coverage [%]	Score
6.60E-04	57.58	125629089	Gustatory receptor	7	43	190.57
4.55E-02	23.32	3913261	Larval cuticle protein 1	4	26	323.31
3.37E-02	16.11	183979372	Troponin T	10	42.5	142.31
2.41E-02	14.39	23208544	Cobatoxin-like protein	3	19.5	115.72
6.08E-03	12.57	118350731	Uncharacterized protein	7	30.3	119.42
8.71E-03	10.39	206725499	Cathepsin L like protein	9	16.7	165.77
1.88E-02	8.93	148298818	Multi-binding protein	12	32.5	237.78
5.16E-03	8.46	164451507	Troponin I	8	25.8	144.07
2.47E-02	8.39	183979374	Tropomyosin 2	10	32.5	323.31
2.83E-03	8.20	183979392	Uncharacterized protein	40	65.5	323.31
1.00E-02	8.06	114053193	Protease inhibitor 1	5	36	323.31
2.45E-02	6.97	112702923	Peptidoglycan-recognition protein-LB (Fragment)	6	81.6	50.387
3.56E-02	5.63	114051966	mitochondrial aldehyde	3	6.5	12.256

			dehydrogenase			
3.06E-02	5.01	21630233	Serine proteinase-like protein 2	3	40.2	118.94
1.77E-02	4.71	34921426	Serine protease inhibitor dipetalogastin (Dipetalin) (Fragment)	12	28	323.31
1.25E-03	4.55	156630481	Cecropin-D-like peptide	2	14.5	137.98
4.10E-02	3.97	110649240	Gloverin	2	28.8	71.375
2.80E-02	3.82	56462288	Protease inhibitor 5 (Fragment)	4	20.2	45.447
2.10E-03	3.62	21630233	Serine proteinase-like protein 2	2	9	33.893
8.28E-04	3.54	114051966	Mitochondrial aldehyde dehydrogenase	26	54.8	323.31
5.87E-03	3.39	134103857	Cationic peptide CP8	3	19.6	131.94
3.96E-04	3.09	25989211	CLIP domain-containing serine protease serine protease 2	10	61.8	186.29
5.18E-03	2.94	124802527	hypothetical protein	4	18.5	40.152
4.77E-02	2.92	156630460	Anionic antimicrobial peptide 2	7	32.9	247.1
2.41E-02	2.86	56718390	Prophenol oxidase activating enzyme 3	26	45	323.31
3.90E-02	2.81	56418393	Hemolymph proteinase 6	9	47.9	138.64
1.51E-02	2.42	49532918	Cellular retinoic acid binding protein	13	34.8	228.51
1.96E-02	2.26	56462318	Uncharacterized protein (Fragment)	6	31.8	49.498
3.98E-02	2.02	148298693	Heat shock protein 20.8 (Heat shock protein hsp20.8A)	5	66.7	47.429
3.92E-03	1.99	158515746	Uncharacterized protein, isoform A	12	40.8	312.16
8.52E-03	1.96	112983816	Glyceraldehyde-3-phosphate dehydrogenase (EC 1.2.1.12)	15	47.6	122.8
2.57E-02	1.93	116791778	Uncharacterized protein	19	56.6	323.31
1.97E-03	1.86	91079628	Glutamine synthetase (EC 6.3.1.2)	11	23.1	246.17

9.13E-03	1.64	114052561	Malate dehydrogenase (EC 1.1.1.37)	11	29.6	136.45
2.77E-03	1.63	7576710	CALNUC	5	31.7	160.16
2.04E-03	1.55	70609810	Transferrin	59	55.6	323.31

Table A7.7A. *G. mellonella* larval proteins increased in abundance in 72 hour *M. mycetomatis* infected *G. mellonella* larval hemolymph as compared to 0 hour hemolymph.

Protein Name	GI Number	P value	Peptides	Sequence coverage [%]	Fold Change (+)
Hdd11	74873244	0.000594322	10	60.7	337.21
Transgelin	183979237	2.35238E-06	17	45.1	222.65
Beta actin	157927723	0.003113413	14	55.9	202.37
Heat shock-like protein	23208546	0.000211515	10	24.8	115.14
Tubulin beta chain	112983342	0.000926519	18	34	80.59
Gustatory receptor	125629089	0.000953839	8	43	76.73
Elongation factor 1-alpha	183979284	0.000222953	11	41.8	46.19
Heat shock protein 90	229562186	0.001606195	32	48.6	40.64
Uncharacterized protein	195119912	1.32688E-05	9	63.5	37.36
Annexin	58864722	0.001886163	14	54.1	36.26
CLIP domain-containing serine protease 2	25989211	0.000433882	2	38.6	33.66
Immune-related Hdd1	4090964	0.000754867	26	37.1	29.53
Heat shock protein hsp21.4	112983414	0.002292758	7	18.4	29.27
Calponin	157118472	0.006043452	11	32.1	28.77
Uncharacterized protein	145504735	9.57759E-05	9	34.8	28.31
Tubulin alpha chain	225031010	0.000618805	4	47.2	27.61
Protease inhibitor 1	114053193	0.019563436	4	30.6	27.54
Peptidyl-prolyl cis-trans isomerase	60592747	0.00037325	6	26.5	27.21
Chemosensory protein	158962507	0.006905844	11	34	25.81
Glutathione-S-transferase-like protein	14517793	0.000162632	12	50.8	25.29
Triosephosphate isomerase	154707830	0.005192371	13	28.5	24.53
ATP synthase subunit beta	114052072	0.005110881	22	56.8	23.93
Actin 3	192763882	0.00112571	9	30.9	23.91
Hemicentin, putative	242005732	0.001943675	15	60.6	23.62
Hemicentin-like protein	83583693	0.003871596	13	25.5	22.53

1					
Chemosensory protein	158962505	0.005521002	3	11.3	19.96
AGAP004366-PA	158292087	0.001335057	12	38.8	17.97
Thioredoxin	148298796	0.00085352	6	20.7	17.90
Chemosensory protein 7	112983052	0.00019556	8	26.7	17.48
Enolase	148298800	0.003878842	22	48.2	17.31
Uncharacterized protein, isoform A	194882165	0.005884123	9	19.9	15.98
Serpin-like protein (SEP-LP)	112983872	0.000181475	17	35.8	15.96
Carboxylic ester hydrolase	189181680	0.022455928	1	28.3	15.77
Profilin	112982865	0.009661286	5	24.8	15.58
Tropomyosin 2	183979374	0.000310694	10	32.5	14.47
Serpin-11	226342884	0.000493205	23	54.7	14.36
prophenoloxidase activating factor 3	25989211	0.001902085	10	61.8	14.28
hypothetical protein (macronuclear)	145504735	0.001934799	8	18.3	13.86
Uncharacterized protein	56462318	0.000807375	8	34.4	13.83
Serpin-4B	45594226	0.017386783	5	78.8	12.74
Peptidoglycan-recognition protein-LB	112702923	0.002928848	7	89.5	12.50
Prophenol oxidase activating enzyme 3	56718390	0.00160228	25	47.9	12.10
Troponin C	112983086	0.006193781	10	29.2	12.10
Protein CREG1-like Protein	91076494	0.009460809	5	23.4	11.57
Serpin-4B	45594226	0.022602168	4	42.1	10.32
Inducible metalloproteinase inhibitor protein	33860163	0.000826913	11	39.7	10.24
Putative gram negative bacteria-binding protein	171740915	0.040122557	10	27	9.88
beta actin	157927723	0.000664462	5	16.1	9.60
AGAP010145-PA	158299186	0.000543791	8	27.6	9.48
Hemolin	186703381	0.003706073	7	59.3	9.46
Superoxide dismutase	148719710	0.03402742	4	17.8	9.33
Peptidoglycan recognition-like protein B	23208535	0.001084785	13	32.1	9.01
Uncharacterized protein	189234613	0.007589168	4	15.5	8.82
Calreticulin	17826933	0.004604323	10	20.7	8.66
Odorant-binding protein	39579195	0.005973551	5	19.5	8.47
Tubulin alpha chain	238667031	0.002409628	4	64.1	7.88
Hdd1-like protein	157704337	0.043358432	7	56.9	7.70
Uncharacterized protein	91076018	0.000865144	5	4.4	7.63
Hemolin	55139149	0.001377314	16	63	7.50
CALNUC	7576710	0.004835611	7	38.9	7.35

Peptidoglycan recognition protein-D	154240658	0.006677323	5	15.7	7.33
Arginine kinase	219552448	0.000904098	9	68.4	7.25
60 kDa heat shock protein	58391242	0.012072755	8	21.1	6.93
Uncharacterized protein	118350731	0.000207835	8	31.8	6.79
Mitochondrial cytochrome c	194303591	0.000818578	4	15.9	6.68
Protease inhibitor-like protein	110347843	0.000227149	2	40	6.33
High affinity nuclear juvenile hormone binding protein	242022233	0.000952131	6	13.9	6.22
Multi-binding protein	148298818	0.003820719	6	6.9	5.88
Yellow-d precurser	112984054	0.003948699	20	42.5	5.80
Phosphoglycerate mutase	112982822	0.001085208	6	9.2	5.70
Protein disulfide-isomerase	62241290	0.000831918	12	29.1	5.41
60 kDa heat shock protein	58391242	0.007221175	9	22.7	5.35
odorant-binding protein	39579195	0.026524152	9	22	5.24
Transgelin	114051357	0.030362016	4	75	5.11
peroxidase precursor	189234130	0.027482067	19	29.5	4.81
Apyrase precursor	170041898	0.009651372	36	49.6	4.81
Fructose-bisphosphate aldolase	45330818	0.013425752	4	28.4	4.76
Troponin T	183979372	0.032236019	9	34.7	4.57
Sensory appendage protein 1	6560637	0.000266148	14	31.5	4.52
Uncharacterized protein	156968291	0.000117079	23	36.6	4.31
CNDP dipeptidase	241263211	0.004773304	5	18	3.91
Rab GDP dissociation inhibitor	91080775	0.000469167	6	14.5	3.89
Cellular retinoic acid binding protein	49532918	0.000866161	15	36.3	3.83
Glutathione S-transferase 2	112983028	0.014316296	1	16.7	3.72
Diazepam binding inhibitor-like protein	49532886	0.009983858	3	20.6	3.56
Translationally controlled tumor protein	112982880	0.008819836	8	38.3	3.50
Selenium-binding protein 1-like Protein	91092064	0.049799283	13	34.3	3.48
Proteasome subunit alpha type	114052034	0.012542154	3	15.3	3.23
Dihydrolipoyl dehydrogenase	112983096	0.00065072	5	15.8	3.21
Chemosensory protein	158962511	0.00476338	6	16.3	3.17
Peptidoglycan recognition protein	112983994	0.00090686	12	56.4	2.92

Thymosin isoform 1	114052645	0.03187832	4	34.5	2.90
BmP109	112984026	0.012459667	12	37.8	2.82
Heat shock protein 25.4	169646838	0.034979743	15	55.2	2.67
Apolipoprotein D-like Protein	91084741	0.00175404	17	42.7	2.64
integument esterase 2 precursor	189181680	0.000254182	24	50.9	2.51
Ferritin	17901818	0.012124338	3	12.3	2.48
Peptidyl-prolyl cis-trans isomerase	114052472	0.013488621	14	38.7	2.28
Nucleoside diphosphate kinase	153791847	0.000287122	13	55.9	2.17
Uncharacterized protein	242004672	0.041674985	11	51.9	1.96
Carboxylic ester hydrolase	162462783	0.032214922	19	35.5	1.87
Scolexin	153791206	0.030804846	17	29.9	1.71
Carboxylic ester hydrolase	220902980	0.038969329	10	56.7	1.69

Table A7.7B. *G. mellonella* larval proteins decreased in abundance in 72 hour *M. mycetomatis* infected *G. mellonella* larval hemolymph as compared to 0 hour hemolymph.

Protein Name	**GI Number**	**P value**	**Peptides**	**Sequence coverage [%]**	**Fold Change (-)**
Ecdysteroid-regulated 16 kDa protein	3182995	0.00023823	3	32.7	35.01
Apolipophorin	2498144	0.039545653	1	13.8	32.99
Hexamerin storage srotein PinSP1	14599862	0.045467641	78	76.6	10.44
similar to CG10638-PA	183979239	0.014799767	10	23.3	7.88
Hypothetical protein	229002332	0.031171056	3	14.5	6.65
Apolipophorin	2498144	0.003575964	13	85.9	5.48
3-dehydroecdysone 3beta-reductase	4753912	0.000114526	8	26	4.76
Apolipophorin	2498144	0.013298178	8	51	4.43
Apolipophorin	50404098	0.008854542	15	46.1	4.26
Apolipophorin	46396271	0.013402013	11	59.6	4.21
Cationic peptide CP8	134103857	0.001578319	4	22	4.13
Similar to CG10638-PA	183979239	0.047237895	7	28.4	3.89
27 kDa hemolymph protein	114050871	0.006368078	9	41.5	3.52
Hemicentin	242005732	0.026982432	7	21.9	3.35
Carboxylesterase	114050871	0.007142257	24	69.6	3.27
Putative hydroxypyruvate	164459610	0.009353299	12	31.5	3.25

isomerase					
Twelve cysteine protein 1	18140733	0.000829875	8	43.4	3.25
Uncharacterized protein	77415676	0.017283385	12	30.2	3.23
Aminoacylase	114052174	0.001987955	10	27.5	2.99
Anionic antimicrobial peptide 2	156630460	0.001355922	7	32.9	2.97
similar to CG10638-PA	183979239	0.038455245	3	28.8	2.90
Aminoacylase	114052174	0.004265983	10	31.2	2.80
juvenile hormone binding protein	158515746	0.002373486	13	40.8	2.71
Anionic antimicrobial peptide 2	34556399	0.003938115	4	75.7	2.56
Hypothetical protein	229002332	0.005614832	8	50.7	2.38
Uncharacterized protein	229002332	0.013295884	6	31.3	2.36
Isocitrate dehydrogenase	114051866	0.022624931	17	43	2.30
Prophenoloxidase subunit 2	189181680	0.010730209	3	32.6	2.13
Uncharacterized protein	195380485	0.040204123	8	35.9	2.09
Arylphorin	384243	0.005791098	21	59.5	1.98
Methionine-rich storage protein 2	159528	0.001694098	87	83.2	1.84
PREDICTED: arylsulfatase B-like isoform X1	156543790	0.019713229	2	45	1.74
Bombyrin	112983654	0.040808819	10	28.9	1.74
Putative serine protease-like protein 2	56462300	0.041229682	19	67.9	1.74
Uncharacterized protein	116782397	0.016592704	13	40.5	1.68
Methionine-rich storage protein	110743533	0.022087032	18	81.4	1.66
similar to AGAP002006-PA	189236506	0.034421158	6	8.7	1.65
General odorant-binding protein 68	116245495	0.03345177	11	40.5	1.54
Imaginal disc growth factor-like protein	85726208	0.037949895	16	57.7	1.51
Insecticyanin-B	124527	0.011660777	16	56.5	1.50
Lipopolysaccharide binding protein	112983062	0.011887194	14	40.4	1.50

Table A7.8. Enrichment for GO terms (Biological Process [A], Molecular Function [B] and Cellular Component [C]) from the total SSDA hemolymph proteins from *G. mellonella* larvae infected with *M. mycetomatis* (72 hour relative to 0 hour hemolymph proteome).

A

Biological process (GO)		
Pathway description	**Pathway description**	**Pathway description**
Organic substance metabolic process	7	8.61e-05
Primary metabolic process	6	0.000389
Response to stress	4	0.000423
Cellular metabolic process	5	0.00481
Single-organism metabolic process	3	0.00543
Organonitrogen compound metabolic process	4	0.00543
Defense response	3	0.00618
Protein folding	2	0.00678
Oxidation-reduction process	2	0.0292
Innate immune response	2	0.0468

B

Molecular function (GO)		
Pathway description	**Pathway description**	**Pathway description**
Ion binding	6	8.46e-06
Catalytic activity	5	0.000185
Carbohydrate derivative binding	4	0.0002
Binding	5	0.00153
Purine ribonucleoside binding	3	0.00153
Purine ribonucleotide binding	3	0.00153
Purine ribonucleoside triphosphate binding	3	0.00153
Nutrient reservoir activity	2	0.00207
Metal ion binding	3	0.00473
Oxidoreductase activity	2	0.0095

C

Cellular component (GO)		
Pathway description	**Pathway description**	**Pathway description**
Extracellular region	6	5.25e-06
Cytoplasm	6	2.09e-05
Intracellular	6	9.86e-05
Cell	6	0.000156
Cytoskeleton	2	0.00913
Intracellular organelle	3	0.0282

Table A7.9A. *G. mellonella* larval proteins increased in abundance in grains isolated from larvae infected with *M. mycetomatis* for 7 day as compared to grains extracted from larvae infected with *M. mycetomatis* for 72 hour.

P value	Fold Change (+)	GI Number	Protein Name	Peptides	Sequence coverage [%]	Score
3.44E-04	11.41	110760247	nucleolin 1 isoform X1	3	5.2	17.648
1.22E-03	9.35	145286562	Lysozyme-like protein 1	5	14.3	38.045
2.65E-05	9.27	56418411	Hemolymph proteinase 16	8	27.5	88.118
1.49E-04	9.15	158299186	AGAP009439-PA (Fragment)	16	39.3	254.01
4.65E-04	9.07	83583695	Hemicentin-like protein 2 (Fragment)	3	60.4	21.64
2.17E-03	8.17	242013531	Uncharacterized protein	7	24.4	51.659
2.11E-03	7.79	110760858	sulfhydryl oxidase 1	3	20.8	24.668
5.81E-04	7.68	31340317	60S ribosomal protein L13a	4	12	35.501
4.51E-04	7.27	158289729	AAEL012341-PA	6	21.7	68.283
1.19E-03	7.12	194910105	GG12390	10	27.7	119.3
6.63E-04	6.94	189233735	rab11 family-interacting protein 2 isoform X5	2	3.1	15.181
1.22E-03	6.92	170033490	Kakapo	2	75	13.843
5.44E-04	6.65	157111903	putative tricarboxylate transport protein	7	12.9	54.892
5.85E-05	6.59	158284767	AAEL005991-PA	3	17.3	26.417
4.98E-04	6.44	226342884	Serpin-11	7	14.4	65.5
9.47E-04	6.03	114051598	Leukotriene A4 hydrolase	5	31	94.784
1.29E-03	5.30	67475506	Viral A-type inclusion protein repeat, putative (Viral a-type inclusion protein repeat putative)	3	6.3	29.513
1.85E-04	5.13	148298849	Programmed cell death protein 5-like protein	3	19.2	22.245
1.96E-03	4.86	195442422	Uncharacterized protein, isoform A	3	15.8	24.567

			(EC 1.10.2.2) (Uncharacterized protein, isoform B) (Uncharacterized protein, isoform C)			
5.27E-04	4.77	91082037	Uncharacterized protein	13	15.5	216.81
3.76E-04	4.33	112983090	Eukaryotic translation initiation factor 3 subunit J (eIF3j)	5	15.3	51.106
2.16E-03	4.25	157132177	lipase 3 isoform X2	9	19.4	94.695
2.13E-03	3.96	156541662	ATP synthase subunit d, mitochondrial	5	22.8	39.427
1.41E-03	3.78	114051530	UMP-CMP kinase (EC 2.7.4.14) (Deoxycytidylate kinase) (CK) (dCMP kinase) (Uridine monophosphate/cytidine monophosphate kinase) (UMP/CMP kinase) (UMP/CMPK)	4	16.2	30.594
1.74E-03	3.65	112984164	Ribosomal protein L35	4	26.1	44.817
2.03E-03	2.98	91083881	Protein CREG1-like Protein	4	10.2	36.071

Table A7.9B. *G. mellonella* larval proteins decreased in abundance in grains isolated from larvae infected with *M. mycetomatis* for 7 day as compared to grains extracted from larvae infected with *M. mycetomatis* for 72 hour.

P value	Fold Change (-)	GI Number	Protein Name	Peptides	Sequence coverage [%]	Score
1.50E-04	358.31	169646838	Heat shock protein 25.4	19	55.2	323.31
7.84E-05	241.25	159528	Methionine-rich storage protein 2	77	82.2	323.31
8.44E-05	159.36	47607477	Imaginal disc growth factor	15	48.9	323.31
3.02E-05	98.46	183979392	Uncharacterized protein	40	65.5	323.31
1.42E-04	75.53	46396271	27 kDa hemolymph protein (P27K) (27k)	10	59.6	323.31

1.83E-04	75.17	50404098	Apolipophorin (Fragment)	12	45.2	323.31
1.06E-03	66.30	49532918	Cellular retinoic acid binding protein	13	34.8	228.51
1.75E-04	64.25	34921426	Serine protease inhibitor dipetalogastin (Dipetalin) (Fragment)	12	28	323.31
2.35E-04	62.63	159078	Arylphorin	51	77.5	323.31
9.66E-04	60.21	114053193	Protease inhibitor 1	5	36	323.31
3.58E-04	53.47	156630460	Anionic antimicrobial peptide 2	7	32.9	247.1
2.04E-04	47.34	112983414	Heat shock protein hsp21.4	8	19.4	323.31
9.96E-05	44.35	70609810	Transferrin	59	55.6	323.31
8.21E-05	43.03	23208546	Heat shock-like protein (Fragment)	13	37.8	313.77
1.24E-05	41.16	14599864	Hexamerin storage protein PinSP2	10	63.2	149.11
3.98E-04	38.17	112983342	Tubulin beta chain	23	47.1	323.31
2.32E-05	35.96	17826933	Calreticulin	18	28	323.31
1.54E-03	33.08	112983062	Lipopolysaccharide binding protein	17	40.6	323.31
1.91E-04	32.28	91084741	C-terminal-binding protein-like Protein	15	40.9	323.31
1.28E-04	32.03	124527	Insecticyanin-B (INS-b) (Blue biliprotein)	16	60.9	283.3
1.19E-03	28.51	55139149	Hemolin (Fragment)	14	47.3	323.31
1.11E-03	23.75	189181680	Carboxylic ester hydrolase (EC 3.1.1.-)	19	51.1	323.31
4.57E-04	23.60	116780375	Uncharacterized protein	4	15.6	113.1
9.61E-04	19.22	384243	Arylphorin	21	59.5	323.31
2.34E-04	18.99	242004672	Uncharacterized protein	9	51.9	164.35
1.27E-03	18.11	116791778	Uncharacterized protein	19	56.6	323.31
1.58E-03	16.19	91088621	Apolipoprotein D-like Protein	18	47.4	323.31
2.10E-04	15.89	91076018	Uncharacterized protein	3	14.3	98.229
3.73E-04	15.62	219552448	Arginine kinase (Fragment)	9	68.4	310.24

4.57E-04	15.46	195119912	Uncharacterized protein	7	63.5	142.79
1.61E-03	15.23	148298673	Mitochondrial ATP synthase coupling factor 6	7	28.6	99.647
1.16E-04	14.65	134103857	Cationic peptide CP8	3	19.6	131.94
1.00E-03	14.44	113208389	Heat shock protein 20.7	13	49.8	224.91
2.80E-04	14.11	112984454	Protein disulfide-isomerase (EC 5.3.4.1)	8	41.7	161.43
2.87E-04	14.05	110743533	Methionine-rich storage protein	14	79.1	323.31
1.87E-04	13.91	114051966	Mitochondrial aldehyde dehydrogenase	26	54.8	323.31
1.21E-03	13.32	186703381	Hemolin	7	59.3	192.54
3.23E-04	12.91	151301059	H+ transporting ATP synthase delta subunit	9	42.6	210.09
3.68E-04	12.17	242016119	10 kDa heat shock protein, putative	10	30.8	127.63
7.27E-04	11.76	15146043	Alpha-crystallin	13	45.7	268.76
1.50E-03	11.52	156630481	Cecropin-D-like peptide	2	14.5	137.98
1.32E-03	11.41	225031010	Tubulin alpha chain (Fragment)	4	47.2	228
1.49E-05	11.00	153791739	H+ transporting ATP synthase delta subunit	15	49.1	289.07
2.63E-04	9.95	171740905	Inactive lipase	9	31.2	137.84
4.62E-04	9.22	109119903	Glyceraldehyde-3-phosphate dehydrogenase (EC 1.2.1.12)	17	55.6	323.31
5.75E-04	9.20	170036627	Gelsolin precursor	8	7.7	68.148
2.12E-04	8.81	27260894	Heat shock cognate 70 protein	4	14.8	59.95
1.15E-03	8.70	58391242	60 kDa heat shock protein, mitochondrial precursor (AGAP004002-PA)	20	33.6	323.31
1.12E-03	8.69	112982865	Profilin	6	24.8	137.05
6.16E-04	8.68	74873244	Putative defense protein Hdd11	10	60.7	246.4
1.46E-03	8.52	112983070	BCP inhibitor	7	21.3	308.94

4.87E-05	8.45	158515746	5'-nucleotidase (EC 3.1.3.5)	12	40.8	312.16
6.16E-05	8.10	112982743	Elongation factor 1-beta'	10	50	181.65
4.38E-04	7.89	229002332	Uncharacterized protein (Fragment)	8	50.7	260.02
6.84E-04	7.26	157109957	mitochondrial processing peptidase beta subunit	23	60.9	323.31
1.17E-04	6.97	114051800	Eukaryotic translation initiation factor 3 subunit I (eIF3i)	15	56.4	312.82
2.34E-04	5.86	148298796	Thioredoxin	6	20.7	129.74
1.63E-03	5.82	91076494	protein CREG1	6	23.9	93.79
3.75E-04	5.56	164448660	Carboxylic ester hydrolase (EC 3.1.1.-)	7	28.2	99.694
8.77E-04	5.55	156548621	Uncharacterized protein	5	19	80.519
4.75E-04	5.31	169234934	Cytochrome c oxidase subunit Va	12	28.8	269.85
5.00E-04	4.93	189238710	uncharacterized protein	21	27.3	323.31
5.68E-04	4.82	193713737	Uncharacterized protein	7	21.3	164.09
3.06E-05	4.75	164448662	Cytochrome c oxidase polypeptide Vb	6	13.7	123.81
6.20E-05	4.65	7576710	CALNUC	5	31.7	160.16
8.08E-04	4.19	112983654	Bombyrin	9	25.8	183.58
5.58E-04	3.93	87248535	Mitochondrial matrix protein p32	13	47.1	236.52
1.26E-04	3.84	162462783	AGAP010145-PA (Fragment)	16	31.5	285.11
1.41E-03	2.91	27461086	Cytochrome b-c1 complex subunit 6	4	29.1	102.68
2.13E-04	1.85	156547257	Sulfhydryl oxidase (EC 1.8.3.2)	7	14.7	59.012

Table A7.10A. *G. mellonella* larval proteins increased in abundance in 7 day *M. mycetomatis* infected *G. mellonella* larval hemolymph as compared to 0 hour hemolymph.

Protein Name	GI Number	P value	Peptides	Sequence coverage [%]	Fold Change (+)
Hdd11	74873244	0.000202401	10	60.7	533.06
Heat shock-like protein	23208546	0.000109029	10	24.8	249.73
Tubulin beta chain	112983342	0.00119673	18	34	111.34
Transgelin	183979237	0.000952686	17	45.1	75.64
AAEL012341-PA	157132177	0.006110975	21	42.7	72.79
Hemicentin	242005732	0.001245125	15	60.6	54.14
Beta actin	157927723	0.009711739	14	55.9	53.67
Elongation factor 1-alpha	183979284	0.00017215	11	41.8	49.22
Heat shock protein 90	229562186	0.001193295	32	48.6	44.98
Tubulin alpha chain	225031010	0.000732056	4	47.2	43.79
Hemolin	186703381	0.000129288	7	59.3	43.76
Thioredoxin	148298796	0.000224403	6	20.7	41.08
Annexin	58864722	0.002479056	14	54.1	38.29
Hemicentin-like protein 1	83583693	0.003085913	13	25.5	36.94
Actin 3	192763882	0.000551846	9	30.9	31.39
Hemolin	55139149	0.000239337	16	63	30.41
Chemosensory protein	158962507	0.002929809	11	34	29.71
Uncharacterized protein	145504735	0.000413544	9	34.8	27.52
Peptidyl-prolyl cis-trans isomerase	60592747	0.000531532	6	26.5	26.43
Immunoglobulin I-set domain containing protein	170578347	0.000284667	3	53.4	25.74
ATP synthase subunit beta	114052072	0.005950119	22	56.8	24.64
Triosephosphate isomerase	154707830	0.007348444	13	28.5	23.86
Glutathione-S-transferase-like protein	14517793	0.000755433	12	50.8	21.20
AAEL003067-PA	157133952	7.50945E-06	9	27.6	20.52
Chemosensory protein 7	112983052	0.009800705	2	36.6	20.43
Uncharacterized protein	112983052	0.000816688	8	26.7	18.49
uncharacterized protein LOC660215	91076018	0.000806204	5	4.4	17.14
Carboxylic ester hydrolase	189181680	0.018846697	1	28.3	16.43

Protease inhibitor 1	114053193	0.028847728	4	30.6	16.36
Hemicentin-like protein 2	83583695	0.010368996	3	60.4	16.02
Gustatory receptor	125629089	0.00258063	8	43	15.85
Hdd1-like protein	157704337	0.008737311	7	56.9	14.93
Uncharacterized protein	195119912	0.000569522	9	63.5	14.91
Profilin	112982865	0.010418898	5	24.8	13.96
AGAP010145-PA	158299186	0.002249001	8	27.6	13.36
Serpin-11	226342884	0.000207131	23	54.7	13.29
Enolase	148298800	0.005548843	22	48.2	12.98
Putative gram negative bacteria-binding protein	171740915	0.030468408	10	27	12.94
Uncharacterized protein	170046360	0.023277291	5	19.2	12.58
Cecropin-A	116087	0.000215022	1	8.5	12.35
Juvenile hormone binding protein	112983390	0.002342686	6	23.9	12.00
tubulin alpha chain	238667031	0.001667421	4	64.1	11.46
Yellow-d precurser	112984054	0.000243267	20	42.5	10.73
60 kDa heat shock protein	58391242	0.003965227	8	21.1	10.25
Serpin-4B	45594226	0.025891403	4	42.1	10.10
14-3-3zeta	239736502	0.010847056	3	4.6	10.02
Odorant-binding protein	39579195	0.00191445	9	22	9.86
Heat shock protein hsp21.4	112983414	0.020109126	7	18.4	9.70
Protein CREG1-like Protein	91076494	0.011684611	5	23.4	9.56
Immune-related Hdd1	4090964	0.042379636	26	37.1	9.28
Uncharacterized protein	91092724	0.034638693	16	24.6	8.91
Esterase	110826028	0.022252287	6	18.3	8.56
Kunitz-like protease inhibitor	22901764	0.014733321	3	29.5	8.32
CLIP domain-containing serine protease 2	45594226	0.034814306	5	78.8	8.31
prophenoloxidase activating factor 3	25989211	0.031375159	10	61.8	8.26
Apyrase precursor	170041898	0.005953156	36	49.6	7.76
hypothetical protein	145504735	0.00138824	8	18.3	7.76
Chaperonin subunit	241998158	0.006254251	2	23.4	7.72
Transgelin	114051357	0.017459222	4	75	7.68
Inducible metalloproteinase inhibitor protein	33860163	0.000373001	11	39.7	7.65
Uncharacterized	56462318	0.014971237	8	34.4	7.44

protein					
Chemosensory protein	158962511	0.00381062	6	16.3	7.23
Twelve cysteine protein 1	18140733	0.017496536	10	21.4	7.00
Histone H2A	114053181	0.025625242	2	4.3	6.96
Calreticulin	17826933	0.01838573	10	20.7	6.52
Laminin	12657593	0.033738032	7	15.6	6.46
AGAP004002-PA	58391242	0.006757297	9	22.7	5.76
peroxidase precursor	189234130	0.009071889	19	29.5	5.61
Prophenol oxidase activating enzyme 3	56718390	0.012439478	25	47.9	5.52
Proteasome subunit beta type	66519157	0.007511291	4	20.8	5.44
Ferritin	11890404	0.017336931	5	25.9	5.38
Carboxylic ester hydrolase	162462783	0.006576822	8	10.5	5.20
Serpin-2	156254836	0.037864821	12	29.3	5.18
Serpin-like protein (SEP-LP)	112983872	0.020212537	17	35.8	5.01
odorant-binding protein	39579195	0.017000104	5	19.5	4.92
Thymosin isoform 1	114052645	0.005744765	4	34.5	4.91
Peptidoglycan recognition-like protein B	23208535	0.002190978	13	32.1	4.73
Mitochondrial cytochrome c	194303591	0.01818144	4	15.9	4.66
Fructose-bisphosphate aldolase	45330818	0.017924638	4	28.4	4.47
ADP-ribosylation factor	148298726	0.032612118	5	14.3	4.29
Heat shock protein 25.4	169646838	0.000115535	15	55.2	4.26
Diazepam binding inhibitor-like protein	49532886	0.023552014	3	20.6	4.17
Protein disulfide-isomerase	62241290	0.005303772	12	29.1	4.12
alpha-esterase 45	162462783	0.002471393	19	35.5	3.76
Proteasome subunit alpha type	114050993	0.026801865	7	21.5	3.75
Arginine kinase	219552448	0.001211592	9	68.4	3.74
BmP109	112984026	0.002478266	12	37.8	3.72
6tox	23208526	0.025331881	12	27.4	3.32
Sensory appendage protein 1	6560637	0.01376862	14	31.5	3.25
Ferritin	17901818	0.007911795	3	12.3	3.20
CNDP dipeptidase	241263211	0.003889126	5	18	3.17
Apolipoprotein D-like Protein	91084741	0.000816581	17	42.7	3.11
integument esterase 2	189181680	0.004955069	24	50.9	2.98

precursor					
Carboxylic ester hydrolase	220902980	7.46095E-05	10	56.7	2.92
Protease inhibitor 5	56462288	0.009610486	4	13.9	2.67
HDC11369 (IP19829p)	45553223	0.023406976	2	11.9	2.67
Uncharacterized protein	116326818	0.00243304	3	18.8	2.64
Serpin-5	112984548	0.001020397	17	38.3	2.58
40S ribosomal protein S12	15213812	0.030765555	3	30.2	2.51
Peptidoglycan recognition protein	112983994	0.001398249	12	56.4	2.50
Rab GDP dissociation inhibitor	91080775	0.037371827	6	14.5	2.37
Gallerin	1146408	0.006956	10	21	2.34
Spodoptericin	33439712	0.01340568	6	33.5	2.30
similar to AGAP002006-PA	189236506	0.00725586	6	8.7	2.21
Beta-galactosidase	239938036	0.048017751	25	36.1	2.21
AGAP008115-PA	118789328	0.000589549	4	11.7	2.21
Serpin 3a	27733415	0.024844403	15	19.5	2.13
Alpha-crystallin	15146043	0.007670045	10	40.8	2.00
Peptidyl-prolyl cis-trans isomerase	114052472	0.00456977	14	38.7	1.87
Nucleoside diphosphate kinase	153791847	0.007808846	13	55.9	1.71
Uncharacterized protein	156968291	0.000522628	23	36.6	1.69
alpha-esterase 45	162462783	0.017186214	19	60.8	1.53
Arylphorin	159078	0.038228816	86	80	1.53

Table A7.10B. *G. mellonella* larval proteins decreased in abundance in 7 day *M. mycetomatis* infected *G. mellonella* larval hemolymph as compared to 0 hour hemolymph.

Protein Name	**GI Number**	**P value**	**Peptides**	**Sequence coverage [%]**	**Fold Change (-)**
Hexamerin storage protein PinSP1	14599862	0.020934648	78	76.6	63.80
Putative hydroxypyruvate isomerase	164459610	0.011191902	12	31.5	49.67
Aminoacylase	114052174	0.005198641	10	31.2	33.33
Hypothetical protein	229002332	2.03203E-06	3	14.5	32.75
similar to CG10638-	183979239	4.10771E-05	10	23.3	22.93

PA					
Apolipophorin	2498144	0.022440653	1	13.8	17.63
Aminoacylase	114052174	0.01190618	10	27.5	12.55
27 kDa hemolymph protein	46396271	0.00306878	11	59.6	8.95
Carboxylesterase	114050871	0.032410608	24	69.6	8.43
Phosphoribosylaminoimidazole carboxylase	114051325	0.004975377	9	18.4	7.04
Uncharacterized protein	116791778	0.007986979	25	60.7	6.30
Cationic peptide CP8	134103857	0.003164438	4	22	6.13
Glyceraldehyde-3-phosphate dehydrogenase	112983816	0.040107093	11	38.8	6.08
Putative protease inhibitor 4	56462286	0.000551868	5	22.1	5.85
3-dehydroecdysone 3beta-reductase	4753912	0.005008371	8	26	4.85
Apolipophorin	158515746	0.000417961	13	40.8	4.09
Apolipophorin	2498144	0.004332885	13	85.9	4.05
Similar to CG10638-PA	183979239	0.000168231	3	28.8	3.74
hypothetical protein,	229002332	0.004760074	6	31.3	3.58
twelve cysteine protein 1	18140733	0.001322986	8	43.4	3.43
Prophenoloxidase subunit 2	34556399	0.000691976	4	75.7	3.33
Hexamerin storage protein PinSP2	14599864	0.021299884	10	63.2	3.30
Apolipophorin	50404098	0.002394337	15	46.1	3.29
Beta glucan binding protein	52782700	0.001364404	3	24.3	3.23
Apolipophorin	2498144	0.008369567	8	51	3.22
Kazal-type proteinase inhibitor	114052484	0.009634193	5	21.4	3.16
Arylphorin	384243	0.000230694	21	59.5	2.98
Anionic antimicrobial peptide 2	156630460	0.007088602	7	32.9	2.90
Uncharacterized protein	77415676	0.020818998	12	30.2	2.82
Isocitrate dehydrogenase	114051866	6.50571E-05	17	43	2.40
Beta-1,3-glucan-binding protein (BGBP)	52782700	0.011018849	4	22.1	2.39
Methionine-rich storage protein	110743533	0.0146823	18	81.4	2.35
Serine protease inhibitor dipetalogastin	34921426	0.005685654	12	28	2.33
Serine protease inhibitor dipetalogastin	195115822	0.00689856	3	51.9	2.30

Methionine-rich storage protein 2	159528	0.002365227	87	83.2	2.16
Putative serine protease-like protein 2	56462300	0.001756954	19	67.9	2.14
hypothetical protein	229002332	0.026325599	7	26.1	2.06
27 kDa hemolymph protein	46396271	0.040418757	11	35.3	2.04
27 kDa hemolymph protein	229002332	0.008908278	8	50.7	2.00
Uncharacterized protein	6919921	7.32451E-06	3	9.8	1.97
Inducible serine protease inhibitor 2	237874122	0.006914957	8	55.8	1.58

Table A7.11: Enrichment for GO terms (Biological Process [A], Molecular Function [B] and Cellular Component [C]) from the total SSDA hemolymph proteins from *G. mellonella* larvae infected with *M. mycetomatis* (7 day relative to 0 hour hemolymph proteome).

A

Biological process (GO)		
Pathway description	**Pathway description**	**Pathway description**
Organic substance metabolic process	7	0.000135
Response to stress	4	0.000345
Primary metabolic process	6	0.000345
Carbohydrate derivative metabolic process	3	0.000345
Organonitrogen compound metabolic process	5	0.000345
Organic substance catabolic process	3	0.000345
Macromolecule metabolic process	5	0.0021
Cellular metabolic process	5	0.00328
Defense response	3	0.00461
Innate immune response	2	0.0482

B

Molecular function (GO)		
Pathway description	**Pathway description**	**Pathway description**
Catalytic activity	5	0.000255
Ion binding	5	0.000255
Nutrient reservoir activity	2	0.00827

Carbohydrate derivative binding	3	0.00861
Hydrolase activity	3	0.00866
Metal ion binding	3	0.0143
Binding	4	0.0238

C

Cellular component (GO)		
Pathway description	**Count in gene set**	**False discovery rate**
Extracellular region	7	2.16e-07
Cytoplasm	5	0.000652
Intracellular	5	0.00209
Cell	5	0.00285

Table A8.1. *G. mellonella* larval hemolymph proteins altered in abundance (increased [red] and decreased [green] in larvae injected with 20 µl of heat killed *Candida albicans* (1×10^6 20 μl^{-1}) and incubated at 30 ºC for 24 h as compared to larvae injected with 20 µl and incubated at 30 ºC for 24 h.

Protein Name	GI Number	Peptides	Sequence coverage [%]	p value	Fold Change
Gustatory receptor	125629089	5	36.2	0.00047825	+32.73
Putative defense protein Hdd11	74873244	9	60.7	0.00260015	+27.48
Protease inhibitor 1	114053193	3	21.2	0.00352086	+24.11
Moricin-like peptide C1	146737994	2	15.4	0.00051967	+16.76
Carboxylic ester hydrolase	189181680	1	28.3	0.04116623	+16.47
Uncharacterized protein	189234613	3	15.5	0.0006457	+16.31
Peptidoglycan-recognition protein-LB	112702923	5	82.9	0.00492795	+15.85
Transgelin	183979237	10	41	0.0265224	+15.03
Prophenol oxidase activating enzyme 3	56718390	14	37.3	0.0003844	+11.91
Chemosensory protein 7	112983052	5	25.6	0.01430817	+7.77
Diazepam binding inhibitor-like protein	49532886	2	20.6	0.00644493	+7.61
Serpin-4B	45594226	4	50	0.0084069	+5.69
Cobatoxin-like protein	23208544	2	15.8	0.0196549	+4.75
Multi-binding protein	148298818	6	17.4	4.3737E-05	+4.73
Heat shock protein 25.4	169646838	12	37.7	0.0004958	+4.37
Serpin-like protein (SEP-LP)	112983872	9	22.3	0.02332921	+3.66
Serine protease inhibitor dipetalogastin (Dipetalin)	34921426	13	28.8	0.00040434	+3.28
Hemolin (Fragment)	55139149	14	55.3	0.01619809	+2.94
Hemolin	186703381	4	47.9	0.01791658	+2.83
Uncharacterized protein	156968291	19	36	0.00531285	+2.40

Dimeric dihydrodiol dehydrogenase	170058562	4	11.7	0.03131801	+2.11
Selenium-binding protein 1-like Protein	91092064	5	17.2	0.00846074	+2.05
Hemicentin-like protein 1	83583693	4	10.1	0.01539092	+2.01
Apolipoprotein D-like Protein	91084741	16	40.6	0.02955129	+2.00
Serpin-11	226342884	10	25	0.01016827	+1.99
Peptidyl-prolyl cis-trans isomerase (PPIase)	114052472	10	33.3	0.00982785	+1.95
Sensory appendage protein 1	6560637	14	31.5	0.02891969	+1.81
Cellular retinoic acid binding protein	49532918	18	37.1	0.0393115	+1.72
Nucleoside diphosphate kinase	153791847	10	51.2	0.02598259	+1.69
Scolexin	153791206	17	28.2	0.01604641	+1.67
Peptidoglycan recognition protein	112983994	11	51.5	0.00036311	+1.64
Peptidoglycan recognition-like protein B	23208535	14	34	0.01740053	+1.64
Uncharacterized protein	189181680	24	53.1	0.00656844	+1.54
hypothetical protein	183979392	33	63.4	0.034947	+1.47
Methionine-rich storage protein 2	159528	87	83.8	0.02980711	-1.67
3-dehydroecdysone 3beta-reductase	4753912	11	32.1	0.0482085	-1.75
Apolipophorins	2498144	14	88.5	0.00076796	-2.14
Apolipophorin 2	2498144	5	31.1	0.02021973	-3.08
Prophenoloxidase subunit 2	34556399	3	37.3	1.1621E-06	-89.07

Table A8.2. *G. mellonella* larval hemolymph proteins altered in abundance (increased [red] and decreased [green] in larvae injected with 20 µl of heat killed *Staphylococcus aureus* (OD 0.1) and incubated at 30 ºC for 24 h as compared to larvae injected with 20 µl and incubated at 30 ºC for 24 h.

Protein Name	GI Number	Peptides	Sequence coverage [%]	p value	Fold Change
Cecropin-D-like peptide	156630481	2	14.5	0.01765798	+22.23
Protease inhibitor 1	114053193	3	21.2	0.00517567	+15.41
Carboxylic ester hydrolase	189181680	1	28.3	0.02048221	+13.00
Putative defense protein Hdd11	74873244	9	60.7	0.00820801	+12.61
Prophenol oxidase activating enzyme 3	56718390	14	37.3	0.00217978	+5.96
Seroin	9087200	2	7.9	0.00424547	+3.85
Multi-binding protein	148298818	6	17.4	0.00047964	+3.50
Lysozyme-like protein 1	145286562	7	14.3	0.04001537	+2.65
Serine protease inhibitor dipetalogastin (Dipetalin)	34921426	13	28.8	6.3202E-06	+2.41
Hemolin	55139149	14	55.3	0.03956266	+2.32
Heat shock protein 25.4	169646838	12	37.7	0.00134118	+2.31
Peptidoglycan recognition protein	112983994	11	51.5	1.4485E-05	+2.13
Peptidoglycan recognition-like protein B	23208535	14	34	0.00450313	+2.06
Peptidyl-prolyl cis-trans isomerase (PPIase)	114052472	10	33.3	0.00527059	+1.66
Carboxylic ester hydrolase	162462783	5	8.5	0.04066615	+1.66
Uncharacterized protein	183979392	33	63.4	0.00118004	+1.64
Gelsolin precursor	170036627	27	39.2	0.03909879	+1.57
Uncharacterized protein	242004672	12	51.9	0.04316683	+1.51
arylphorin	384243	20	57.1	0.00176914	-1.51
Apolipophorins	2498144	5	31.1	0.01748001	-1.88

Selenium-binding protein 1-like Protein	91092064	5	17.2	0.02120065	-2.08
Hexamerin storage srotein PinSP1	14599862	72	77.6	0.01216279	-2.73
Prophenoloxidase subunit 2	34556399	3	37.3	1.8895E-06	-48.90

Table A8.3. *G. mellonella* larval hemolymph proteins altered in abundance (increased [red] and decreased [green] in larvae injected with 20 µl of PBS and incubated at 37 °C for 24 h as compared to larvae injected with 20 µl and incubated at 30 °C for 24 h.

Protein Name	GI Number	Peptides	Sequence coverage [%]	p value	Fold Change
UDP-glucose-1-phosphate uridylyltransferase 2	189239301	7	47.3	0.00198903	+8.74
Diazepam binding inhibitor-like protein	49532886	2	20.6	0.01482494	+4.95
Gustatory receptor	125629089	5	36.2	0.03787865	+2.43
Apolipoprotein D-like Protein	91084741	16	40.6	0.04148138	+2.28
Uncharacterized protein	145504735	6	21.1	0.01225063	+2.26
Uncharacterized protein	183979392	33	63.4	0.00047867	+1.73
Kazal-type proteinase inhibitor	114052484	5	21.4	0.00052863	+1.54
Selenium-binding protein 1-like Protein	91092064	5	17.2	0.00735239	-2.06
Serpin-11	226342884	10	25	0.01455724	-2.22
Thioredoxin	148298796	3	13.6	0.04390221	-3.35
Carboxylic ester hydrolase	162462783	19	62.5	0.02016574	-4.21
Carboxylic ester hydrolase	162462783	15	46.7	0.02646954	-10.43
Prophenoloxidase subunit 2	34556399	3	37.3	0.02687033	-46.57

Table A9.1. Proteins changed (increased [+] and decreased [-]) in abundance in *A. fumigatus* mycelium exposed to LL-37 (5 µg/ml) for 24 h.

Fold Change	Uniprot Identifier	Protein Name	Peptides	Sequence coverage [%]
+16.30	AFUB_004430	Eukaryotic translation initiation factor eIF-5A	3	16.7
+9.95	AFUB_028280	allergen Asp F13	5	53.3
+9.53	AFUB_032070	translation initiation factor 4B	9	22.5
+6.88	AFUB_011640	translation elongation factor EF-Tu, putative	9	19.8
+5.06	AFUB_064030	UBX domain protein, putative	5	20.6
+4.71	AFUB_061010	aspartic endopeptidase Pep1	4	15.7
+4.41	AFUB_019230	40S ribosomal protein S10a	2	22.4
+2.07	AFUB_019880	KH domain RNA-binding protein	3	8.5
+1.87	AFUA_3g00350	Ortholog of A. nidulans FGSC A4	5	38.3
+1.71	AFUB_018250	1,3-beta-glucanosyltransferase Gel1	8	20.8
+1.61	AFUB_047850	Aegerolysin family protein	7	51.8
-1.92	AFUB_037350	phosphoglucomutase PgmA	9	15.1
-1.95	AFUB_052200	CRAL/TRIO domain protein	5	14.2
-2.03	AFUB_018100	myo-inositol-phosphate synthase, putative	6	13.7
-2.12	AFUB_007840	dimeric dihydrodiol dehydrogenase, putative	7	19.9
-2.13	AFUB_051000	thiamine biosynthesis protein	13	39.8
-2.15	AFUB_023230	protein disulfide isomerase Pdi1, putative	7	14.1
-2.29	AFUB_049190	GNAT family acetyltransferase, putative	6	20.2
-2.36	AFUB_024860	thiamine biosynthetic bifunctional enzyme, putative	7	13.5
-2.41	AFUB_030310	eukaryotic translation	9	18.5

		initiation factor 3 subunit EifCd, putative		
-2.46	AFUB_028939	aminotransferase family protein, putative	6	8.2
-2.54	AFUB_072510	phosphomannomutase	3	13.1
-2.95	AFUB_073730	alanine aminotransferase, putative	6	14.2
-2.97	AFUB_040970	fumarylacetoacetate hydrolase family protein	2	12.3
-3.10	AFUB_076700	ATP citrate lyase subunit	5	9.3
-3.16	AFUB_078170	FKBP-type peptidyl-prolyl isomerase, putative	6	58.9
-3.73	AFUB_031410	poly A + RNA transport protein	10	11.7
-3.94	AFUB_037500	fructose-bisphosphate aldolase, class II	6	8.3
-4.22	AFUB_068370	saccharopine dehydrogenase	7	16.2
-5.62	AFUB_040710	inorganic diphosphatase, putative	6	18.9
-6.85	AFUB_024920	secreted dipeptidyl peptidase	16	26.4
-9.34	AFUB_061150	triosephosphate isomerase	13	33.6

Table A9.2. Proteins changed (increased [+] and decreased [-]) in abundance in *A. fumigatus* mycelium exposed to LL-37 (5 µg/ml) for 48 h.

Fold Change	**Uniprot Identifier**	**Protein Name**	**Peptides**	**Sequence coverage [%]**
+27.37	Q4WGP3	Malate dehydrogenase	14	46.8
+9.35	Q4WL81	Uncharacterized protein	3	15
+8.99	Q4WY97	Glutathione peroxidase	6	26.8
+8.90	Q4WJV5	Ribosomal protein L15	6	26.3
+8.71	Q4WPT7	Aspartate aminotransferase, putative	13	22.7
+8.70	Q4WT27	Aminomethyltransferase	8	24.3
+8.41	Q4WRB8	Translationally-controlled tumor protein	7	23.5

		homolog		
+7.87	Q4WCM2	Hsp70 chaperone	24	40.4
+7.48	Q4WJB3	High expression lethality protein Hel10, putative	4	39.6
+6.84	Q4WY15	Arginase	5	13.9
+6.83	Q4WV27	Cofilin	5	29.2
+6.48	Q4WQK3	Glutamine synthetase	7	32.1
+6.05	Q4WK14	Eukaryotic translation initiation factor eIF-5A	9	29.2
+5.96	Q4WJR3	60S acidic ribosomal protein P0	4	20.4
+5.51	Q4WIJ4	Tryptophanyl-tRNA synthetase	8	20.7
+5.25	Q4WJV9	Alcohol dehydrogenase, zinc-containing, putative	7	25.9
+5.01	Q4WMX7	Thiamine thiazole synthase	5	21.7
+4.55	Q4X1F3	Uncharacterized protein	9	30.9
+4.29	Q4WTK5	UPF0160 domain protein MYG1, putative	4	19
+4.12	Q4WAZ0	Dual-functional monooxygenase/methyltransferase psoF	14	20.6
+4.05	Q4WNI1	Methylthioribose-1-phosphate isomerase	9	29.2
+4.02	Q4WD51	Short-chain dehydrogenase/reductase family protein, putative	6	23.7
+3.77	Q4WTB4	Uncharacterized protein	3	46.9
+3.67	P67875	Ribonuclease mitogillin	8	44.3
+3.62	Q4WXC3	Threonine synthase Thr4, putative	8	18.6
+3.58	Q4WDH2	Actin Act1	7	27
+3.55	Q4WE17	Peroxiredoxin	5	29.7
+3.48	Q4WHX4	FK506-binding protein 2	6	41.8
+3.43	Q4WV35	Pyridoxamine phosphate oxidase, putative	4	9
+3.38	Q4WJT1	Proliferating cell nuclear antigen	4	26
+3.38	Q4WNW5	Ornithine carbamoyltransferase	8	30.2
+3.35	Q4WJ44	Uncharacterized protein	7	18.6
+3.31	Q4WYI3	Methyltransferase, putative	7	25.4
+3.28	Q4WI29	14-3-3 family protein ArtA, putative	20	67
+2.79	Q4X1W4	Peptidyl-prolyl cis-trans	2	13.1

		isomerase		
+2.78	Q4WP16	Phosphoribosylaminoimidazolecarboxamide formyltransferase/IMP cyclohydrolase	19	40.2
+2.73	Q4WAY7	Methionine aminopeptidase 2-1	6	23.5
+2.68	Q4WX43	ATP-dependent RNA helicase eIF4A	9	18.7
+2.65	Q4WCU7	Esterase, putative	8	27.4
+2.63	Q4WZT3	Phytanoyl-CoA dioxygenase family protein	4	25.5
+2.63	Q4WAP3	Indoleamine 2,3-dioxygenase family protein	14	36.3
+2.52	O60022	Allergen Asp f 15	4	45.4
+2.52	Q4WB00	Methyltransferase psoC	24	67.5
+2.11	Q4WAS3	Adenine phosphoribosyltransferase 1	6	29.5
+2.10	Q4W9S5	Uncharacterized protein	5	20.1
+2.03	Q4WT14	Tubulin beta chain	4	9.7
+1.91	Q4WEY2	Ser/Thr protein phosphatase family	5	9.1
+1.88	Q4WVI8	Posttranscriptional regulation nuclease	12	20.9
+1.87	Q4WPC4	Phospho-2-dehydro-3-deoxyheptonate aldolase	15	49.8
+1.73	Q7Z8P9	Nucleoside diphosphate kinase	10	66
+1.72	Q4WN17	Lactoylglutathione lyase	15	47.5
+1.69	Q4WRK8	Glutathione reductase	14	34.7
+1.68	Q4X1H5	Mitochondrial Hsp70 chaperone	27	32
+1.57	Q4WPS4	Phosphotransmitter protein Ypd1, putative	7	39.2
+1.53	Q4X1F8	ATP-dependent	7	30.7
-1.52	Q4WDW6	Transesterase	5	17.4
-1.52	Q4WHZ9	Inosine-5'-monophosphate dehydrogenase	12	24.7
-1.57	Q4WHL9	Uncharacterized protein	7	34.7
-1.61	Q00050	Asp-hemolysin	10	54
-1.62	Q4WEN2	Cdc48-dependent protein degradation adaptor protein	8	18.8

-1.68	Q4WRV1	2-isopropylmalate synthase	19	26.9
-1.69	Q4WGB5	Geranylgeranyl transferase type-2 subunit beta	3	12.2
-1.71	Q4WGD4	Proteasome subunit beta	9	34.8
-1.76	Q4WMR7	Proteasome subunit alpha type	6	25.1
-1.76	Q4WJT9	Probable NAD (P)H-dependent D-xylose reductase xyl1	10	27.3
-1.85	Q4WPU7	Mitochondrial chaperone Frataxin, putative	6	31.3
-1.86	Q4WXR1	Uncharacterized protein	8	33.9
-1.88	Q4WDE1	1,2-dihydroxy-3-keto-5-methylthiopentene dioxygenase	5	25
-1.88	Q4WZM7	Translation initiation factor 4B	8	21.1
-1.96	Q4WW00	Hsp90 binding co-chaperone	9	70.6
-1.99	Q4WI96	ATP-dependent DNA helicase II subunit 2	7	11
-2.02	Q4X267	Probable Xaa-Pro aminopeptidase pepP	13	23.3
-2.10	Q4WHM1	Proteasome component Pup1, putative	3	12.1
-2.10	Q4WLP1	Protein transport protein sec24	3	4.8
-2.28	Q4WRV9	Probable Xaa-Pro aminopeptidase AFUA_1G14920	13	20.3
-2.28	Q4W913	Uncharacterized protein	6	40.9
-2.39	Q4WPF8	Cytochrome c peroxidase, mitochondrial	10	27.6
-2.44	Q4W8Y5	Carboxypeptidase	5	9.3
-2.47	Q4WT77	Pyridoxal reductase	4	13.7
-2.47	Q4WNH5	Proteasome endopeptidase complex	9	23.7
-2.55	Q4WLQ0	Dienelactone hydrolase family protein	16	58.4
-2.57	Q4WWN8	Sulfate adenylyltransferase	18	34.8
-3.07	P0C7S9	1,3-beta-glucanosyltransferase gel1	11	25.9
-3.74	Q4WMI8	Uncharacterized protein	10	38.5

-4.04	Q4WMS1	Assimilatory sulfite reductase	11	13.6
-4.34	Q4WEP6	WW domain protein	4	16.6
-6.69	Q4WNZ8	Proteasome subunit beta	3	14.6

Table A10.1. List of proteins which are decreased in abundance in N-Chlorotaurine (6.8 mM) treated *A. fumigatus* (ATCC 26933) mycelium as compared to untreated mycelium.

Accession Number	Protein Name	Peptides	ANOVA P value	Sequence Coverage (%)	Fold Change
Q4WAP3	Indoleamine 2,3-dioxygenase family protein	26	0.01327	67.5	-32.0
Q4WW28	Glucose repressible protein Grg1, putative	4	0.00082	81.2	-18.2
Q4WII2	NACHT domain protein	17	0.01280	11.2	-9.0
Q4WYN6	Pyoverdine/dityrosine biosynthesis family protein, putative	9	0.00027	29.1	-8.9
Q4WPB8	Short chain dehydrogenase, putative	13	0.03839	61	-8.4
Q4WFC6	NRPS-like enzyme, putative	22	0.00070	30.9	-7.3
Q4WAY3	Fumagillin dodecapentaenoate synthase	16	0.02215	11	-6.5
Q4WS84	Phenol 2-monooxygenase, putative	13	0.00020	26.2	-5.4
Q4WAZ8	Alpha/beta hydrolase psoB	14	0.02140	37.3	-5.4
A0A067Z9B6	O-methyltransferase af390-400	28	0.00313	72.8	-5.2
Q4WAY4	Polyketide transferase af380	11	0.00181	63.7	-5.0
Q4WBD0	NmrA-like family protein	6	0.00246	33.4	-4.8
Q4WB00	Methyltransferase psoC	24	0.00017	71.2	-4.3
A4D9Z0	GNAT family N-acetyltransferase, putative	4	0.00028	35.7	-4.3
Q4X168	Triosephosphate isomerase	6	0.00544	35.5	-4.2
Q4WC13	Uncharacterized protein	4	0.03081	22.8	-4.2
Q4WWZ2	ABC1 domain protein	10	0.03758	22.1	-4.1
Q4WAZ9	PKS-NRPS hybrid synthetase psoA	130	0.00876	48.7	-3.9
Q4WAB4	Aldo-keto reductase	18	0.00272	60	-3.8
Q4WAZ5	Acetate-CoA ligase, putative	15	0.01918	36.6	-3.8
Q4WAZ6	Multifunctional cytochrome P450 monooxygenase af510	14	0.00168	40.7	-3.6
Q4WFJ9	Uncharacterized protein	3	0.00704	49.4	-3.4
Q4X074	Oxidoreductase, short-chain dehydrogenase/reductase family	3	0.00558	13.2	-3.3
Q4WWQ7	ThiJ/PfpI family protein	9	0.00015	26.9	-3.2
Q4WAG6	Phytase, putative	7	0.00758	19.7	-3.2
Q4WIG9	5-demethoxyubiquinone hydroxylase, mitochondrial	7	0.02061	38.9	-3.2
Q4WGX8	NADPH-dependent FMN reductase Lot6, putative	7	0.04570	62.6	-3.1
Q4WN44	Cytochrome c oxidase assembly	10	0.00394	20.9	-3.1

	protein cox15				
Q4WAZ0	Dual-functional monooxygenase/methyltransferase psoF	35	0.00036	50.1	-3.0
Q4WQ18	Carbonic anhydrase	15	0.00195	61.7	-3.0
Q4WLZ6	Nucleoside-diphosphate-sugar epimerase family protein	11	0.02876	54.1	-3.0
Q4WCN2	O-methyltransferase, putative	10	0.00320	50.6	-2.9
Q4WU44	Ribosome-releasing factor 2, mitochondrial	7	0.01445	16	-2.8
Q4WEL0	Flavin dependent monooxygenase, putative	5	0.01278	19.1	-2.8
Q4WAY9	Uncharacterized protein	11	0.03179	80.3	-2.8
Q4WAY7	Methionine aminopeptidase 2-1	11	0.01623	38.3	-2.7
Q4WZY9	DUF636 domain protein	6	0.00460	81.6	-2.5
A4D9Y3	YjgH family protein	9	0.01426	66.9	-2.4
Q92450	Superoxide dismutase [Mn], mitochondrial	22	0.00556	94.3	-2.3
A4D9U4	Uncharacterized protein	11	0.00360	57.6	-2.2
Q4WUK8	Epoxide hydrolase, putative	10	0.00493	41.4	-2.2
Q00050	Asp-hemolysin	12	0.00777	73.4	-2.1
A4D9H6	Uncharacterized protein	6	0.02463	48.7	-2.1
Q4WHK6	Alternative oxidase	21	0.00056	56.5	-2.1
Q4WY15	Arginase	15	0.01478	81.2	-2.1
Q4WDX7	Glyceraldehyde-3-phosphate dehydrogenase	35	0.00043	84.3	-2.0
Q4WDD6	Molecular chaperone	21	0.00383	41.1	-2.0
Q4WBQ3	3-hydroxy-3-methylglutaryl coenzyme A synthase	20	0.01866	57	-2.0
Q4WFL0	Porphyromonas-type peptidyl-arginine deiminase superfamily	16	0.01200	61.6	-2.0
Q4WTK7	mRNA stability protein	6	0.01490	35.3	-2.0
Q4WAT9	mRNA processing protein	14	0.01839	33.8	-2.0
Q4X1L3	Mitochondrial genome maintenance protein Mgm101, putative	10	0.00029	49.7	-2.0
Q4X174	Alcohol dehydrogenase, putative	8	0.00798	32.5	-2.0
Q4WEA5	Uncharacterized protein	8	0.00100	41.9	-1.9
Q4WQP8	Thiol methyltransferase, putative	5	0.00401	20.2	-1.9
Q4WEH6	DnaJ domain protein	10	0.01436	18.5	-1.9
Q4WG56	Oxidoreductase, 2-nitropropane dioxygenase family, putative	10	0.00765	45.4	-1.9
Q4WCA3	Oxidoreductin	14	0.01521	38.3	-1.9
Q4WHL4	Tyrosine decarboxylase, putative	17	0.00398	44.1	-1.9
Q4WXE5	CAIB/BAIF family enzyme	23	0.00313	69.2	-1.9
Q4W9Q1	Uncharacterized protein	9	0.00455	26.6	-1.9
Q4WWZ9	Cytochrome c oxidase copper	6	0.00036	59.2	-1.8

	chaperone Cox17, putative				
Q4WF68	FAD binding monooxygenase, putative	31	0.00202	70.5	-1.8
Q4WPM7	Uncharacterized protein	14	0.00291	65.5	-1.8
Q4WTB4	Uncharacterized protein	8	0.00226	85.2	-1.8
Q4WPG1	L-ornithine aminotransferase Car2, putative	26	0.01156	83.8	-1.8
Q4WY65	Transcription regulator PAB1642, putative	4	0.01981	13.2	-1.8
Q4WQJ4	Citrate lyase beta subunit, putative	2	0.03260	7.6	-1.8
Q4WT30	Prolyl-tRNA synthetase	13	0.00755	37.2	-1.7
Q4WFX1	Uncharacterized protein	12	0.00708	58.5	-1.7
Q4X0R5	Pterin-4-alpha-carbinolamine dehydratase family protein	3	0.01968	17.9	-1.7
Q4WJ50	6-phosphofructo-2-kinase 1	16	0.00389	29.4	-1.7
Q4WNB2	Uncharacterized protein	5	0.04123	11.3	-1.7
Q4W913	Uncharacterized protein	7	0.00552	66.5	-1.7
Q4WIQ2	Mitochondrial import inner membrane translocase subunit tim9	7	0.00335	75.6	-1.7
Q4WJG0	Uncharacterized protein	16	0.00574	45.2	-1.7
Q4W9P6	Uncharacterized protein	5	0.02176	12.8	-1.7
A4D9B0	Aminotransferase family protein	32	0.01020	79.7	-1.6
A4D9L8	Cell surface protein, putative	9	0.00510	48.2	-1.6
Q4WX56	Aspartyl aminopeptidase	11	0.00189	42.7	-1.6
Q4WWW4	Uncharacterized protein	7	0.00340	31.2	-1.6
Q4WD10	Uncharacterized protein	8	0.00804	35.3	-1.6
Q4WGC4	Serine/threonine protein kinase, putative	9	0.04905	24.9	-1.6
Q4WY00	Class V chitinase, putative	12	0.01592	44.9	-1.6
Q4WXC6	Regulatory protein SUAPRGA1	14	0.00335	50.3	-1.6
Q4X0L8	Phenylalanyl-tRNA synthetase alpha subunit	22	0.00505	54.8	-1.6
Q4WNT6	Asparagine synthetase Asn2, putative	20	0.00543	41	-1.6
Q4WTJ0	Uncharacterized protein	18	0.01626	42.7	-1.6
Q4WIT4	Aldehyde dehydrogenase, putative	22	0.04059	57.7	-1.6
Q4WAK1	Cystathionine gamma-synthase	5	0.01168	26.3	-1.6
Q4WIA0	HAD superfamily hydrolase, putative	14	0.00786	49.1	-1.6
Q4WGS0	Uncharacterized protein	8	0.01590	56	-1.6
Q4WQ50	Superoxide dismutase	10	0.00129	74.2	-1.6
Q4WBX7	Fructosyl amino acid oxidase, putative	10	0.00311	32.1	-1.6
Q4WQ91	Phosphatidylinositol phospholipase C	10	0.01537	29.6	-1.6
Q4WIH5	Uncharacterized protein	7	0.03262	23.7	-1.6

Q4X083	Uncharacterized protein	9	0.02678	51.8	-1.6
Q4WWL3	Rho GTPase activator	16	0.00996	33.3	-1.6
Q4WNT5	14-alpha sterol demethylase Cyp51A	21	0.01576	48.9	-1.5
Q4WNC5	Uncharacterized protein	6	0.00691	60	-1.5
Q4WJA1	Metacaspase-1A	18	0.02077	60.3	-1.5
Q4WTY5	NADH dehydrogenase [ubiquinone] 1 alpha subcomplex subunit	11	0.01447	76.8	-1.5
Q4WCP3	Dienelactone hydrolase family protein	15	0.01181	53	-1.5
Q4WKX1	Short chain dehydrogenase/reductase family protein	19	0.00375	85.4	-1.5
Q4WQ89	Anthranilate phosphoribosyltransferase, putative	12	0.00144	55	-1.5
Q4WI90	Mitochondrial inner membrane AAA protease Yta12, putative	38	0.00028	54.1	-1.5
Q4WV50	Mitochondrial ATP-dependent RNA helicase Suv3, putative	5	0.04929	9.7	-1.5
Q4WJT9	Probable NAD	14	0.03045	55.6	-1.5
Q4WWC9	Protein-L-isoaspartate O-methyltransferase	7	0.00030	50.2	-1.5
Q4WEP7	Endochitinase A1	6	0.01376	7.4	-1.5

Table A10.1. List of proteins which are increased in abundance in N-Chlorotaurine (6.8 mM) treated *A. fumigatus (*ATCC 26933) mycelium as compared to untreated mycelium.

Accession Number	Protein Name	Peptides	ANOVA P value	Sequence Coverage (%)	Fold Change
Q4WGB8	Ribosomal protein S28e	4	0.00188	50	+23.1
Q4WWK4	Cytochrome c oxidase subunit VIa, putative	8	0.00002	30.9	+12.4
Q4WVN4	Nonribosomal peptide synthetase 8	39	0.00032	6.5	+11.7
Q4WRP3	Oxidoreductase, zinc-binding dehydrogenase family, putative	13	0.00000	66.9	+11.0
Q4WG10	NAD dependent epimerase/dehydratase family protein	12	0.00080	59.6	+10.4
Q4WHD9	Agmatinase, putative	12	0.00241	47.1	+8.4
Q9Y8D9	Superoxide dismutase [Cu-Zn]	9	0.00801	77.9	+7.7
Q4WT66	Nonribosomal peptide synthetase 1	115	0.00185	29.6	+7.0
Q4WN13	Cell division control protein 2 kinase, putative	7	0.00017	21.7	+6.6

Q4WNG3	Heat shock protein Hsp30-like, putative	5	0.00099	52.8	+5.6
Q4WNN3	Ribosomal biogenesis protein Gar2	8	0.00021	18.7	+5.5
Q4WG26	Short chain dehydrogenase	9	0.00697	32.1	+5.1
Q4WGW1	NADH-dependent flavin oxidoreductase, putative	40	0.00001	92.2	+5.1
Q4WVV7	Ribosome assembly factor mrt4	9	0.00377	50.6	+5.1
Q4WP01	Small nucleolar ribonucleoprotein complex subunit, putative	13	0.00662	23.2	+4.6
Q4W8Y2	NmrA-like family protein	14	0.00073	68.2	+4.0
Q4WP70	Zinc-containing alcohol dehydrogenase, putative	19	0.00027	71.3	+3.8
Q4WGU6	Cyanamide hydratase, putative	10	0.02320	59.8	+3.6
Q4WQI6	Sorting nexin-4	8	0.00383	25.6	+3.3
Q4WIQ4	1-aminocyclopropane-1-carboxylate deaminase, putative	10	0.00307	49.4	+3.3
Q4WDF9	DNA-directed RNA polymerase I and III 14 kDa polypeptide	2	0.03877	23.6	+3.2
Q4WE16	ThiJ/PfpI family protein	12	0.00829	61.9	+3.1
Q4WP65	Pescadillo homolog	10	0.02924	21	+3.1
Q4WYI3	Methyltransferase, putative	14	0.00002	57.6	+3.1
Q4WKF7	rRNA processing protein Pwp1, putative	4	0.02056	10.9	+3.0
Q4WN79	mRNA splicing factor	6	0.03570	14.3	+2.9
Q4WCM0	Uncharacterized protein	6	0.00136	24.1	+2.9
Q4WAJ1	MFS peptide transporter Ptr2, putative	6	0.00830	17	+2.7
Q4WE18	NADH-dependent flavin oxidoreductase, putative	9	0.01096	35.7	+2.7
Q4WMF5	Uncharacterized protein	6	0.02913	61.4	+2.7
Q4WD57	mRNA-nucleus export ATPase	17	0.01779	20.1	+2.5
Q4WYW9	Heat shock protein Hsp30/Hsp42, putative	9	0.00017	62.8	+2.5
Q4WBK5	CobW domain protein	18	0.00100	39.8	+2.4
Q4WIH0	Low molecular weight phosphotyrosine protein phosphatase, putative	3	0.00662	9.7	+2.4
Q4WJP0	RNA cytidine acetyltransferase	23	0.00099	33.3	+2.3
Q4WQM4	ATP-dependent RNA helicase has1	14	0.04628	30.7	+2.2
Q4WUW5	Nitroreductase family protein, putative	16	0.00073	71.9	+2.2
Q4WGC6	Na/K ATPase alpha 1 subunit, putative	18	0.01349	20	+2.2
Q4WK52	Uncharacterized protein	9	0.00242	31.6	+2.2
Q4WJ94	40S ribosomal protein S26	5	0.00699	37.8	+2.2
Q4WMS1	Assimilatory sulfite reductase	28	0.00384	38.2	+2.1
Q4WHT7	Maleylacetoacetate isomerase	13	0.01846	52.8	+2.1

	MaiA				
Q4WWI8	Ubiquitin conjugating enzyme	4	0.03716	38.1	+2.1
Q4WG12	Extracellular phytase, putative	4	0.02294	10.9	+2.0
Q4WCI4	Uncharacterized protein	19	0.00223	21.5	+1.9
Q4WCN8	Flavin-binding monooxygenase-like protein	9	0.04915	24	+1.9
Q4WA80	Uncharacterized protein	12	0.00377	42.4	+1.9
Q4WGN6	Translation elongation factor eEF-3, putative	79	0.00064	81.2	+1.9
Q4WZV9	Sulfite reductase, putative	49	0.00200	49.7	+1.9
Q4WT60	Uncharacterized protein	12	0.04454	18.8	+1.9
E9QUP9	Citrate synthase	13	0.04592	45.6	+1.9
Q4WAV3	WD repeat protein	8	0.03660	15.4	+1.9
Q4WCK3	Carboxypeptidase	14	0.00006	37.6	+1.9
Q4WN87	Sreptomyces cyclase/dehydrase family protein	3	0.01118	25.6	+1.9
Q4WMQ0	Oxidoreductase, short-chain dehydrogenase/reductase family	5	0.02456	29.9	+1.8
Q4WFX6	Amine oxidase	24	0.01064	52.9	+1.8
Q4WGR4	Cytokinesis EF-hand protein Cdc4, putative	5	0.00079	35.3	+1.8
Q4WUY4	NRPS-like enzyme, putative	32	0.00666	36.8	+1.8
Q4WLT1	Ran-interacting protein Mog1, putative	7	0.01496	66.7	+1.8
Q4WHT9	Homogentisate 1,2-dioxygenase	28	0.00070	90	+1.8
Q4WD45	Fumipyrrole biosynthesis protein C	19	0.00590	57.1	+1.8
Q4WR90	Translation elongation factor eEF-1B gamma subunit, putative	14	0.00591	64.1	+1.8
Q4WMV5	FK506-binding protein 4	14	0.00440	36.6	+1.8
E9R0R8	Glutathione S-transferase GstA	16	0.03331	61.4	+1.7
Q4WMB7	Zinc finger protein ZPR1	18	0.03239	55.4	+1.7
Q4X040	Oxidoreductase, putative	14	0.03309	38.3	+1.7
Q4WEF7	Uncharacterized protein	16	0.02864	55.2	+1.7
H9CJR6	Cytochrome c oxidase subunit 2	6	0.04109	19.4	+1.7
Q4WX73	60S ribosomal protein L35Ae	6	0.04405	47.1	+1.7
Q4W9W9	NmrA-like family protein	4	0.00326	14.4	+1.7
Q4W9N1	Pre-mRNA-splicing factor	14	0.03261	20.4	+1.7
Q4WWN8	Sulfate adenylyltransferase	33	0.00342	72.5	+1.6
Q4WD43	Amino acid oxidase fmpA	24	0.02315	58.8	+1.6
Q4WA31	NmrA-like family protein, putative	12	0.01546	69.8	+1.6
Q4WHT8	Fumarylacetoacetate hydrolase FahA	20	0.00093	69.8	+1.6
Q4W8Y5	Carboxypeptidase	11	0.00080	27.6	+1.6
Q4WC62	Oxidoreductase, short chain dehydrogenase/reductase family	13	0.03745	74.9	+1.6

Q4WEF9	Oxidoreductase, short-chain dehydrogenase/reductase family	12	0.04013	76.3	+1.6
Q4WNS8	Protein ecm33	14	0.00526	45	+1.6
E9QRL5	Nuclear segregation protein	29	0.00871	59.2	+1.6
Q4WII3	Methionine aminopeptidase 2-2	22	0.02738	62.6	+1.6
Q4WWU0	Vacuolar carboxypeptidase Cps1, putative	10	0.01383	25.7	+1.6
Q4WK81	60S ribosomal protein L12	8	0.01687	50.6	+1.6
Q4WZR4	rRNA biogenesis protein RRP5, putative	35	0.00788	29.6	+1.6
Q4WC67	Fumarate reductase Osm1, putative	21	0.00123	44.9	+1.6
Q4WC61	Uncharacterized protein	7	0.00277	72.3	+1.6
Q4WJH1	Ribosomal protein L16a	15	0.02443	44.1	+1.6
Q4WF91	Phosphoglucomutase, putative	13	0.00183	37	+1.6
Q8J0P4	Probable glycosidase crf1	12	0.03899	50.9	+1.5
Q4WSG1	60S ribosomal protein L5, putative	22	0.02875	56.8	+1.5
Q4WE44	Cytochrome P450 phenylacetate 2-hydroxylase, putative	22	0.00227	53.2	+1.5
Q4WQD6	Conserved lysine-rich protein, putative	20	0.01173	40.7	+1.5
Q4WI64	Aldehyde reductase, putative	10	0.02947	43.7	+1.5
Q4WJR7	Protein mitochondrial targeting protein	17	0.02737	56.9	+1.5
Q4WT23	Adenylyl-sulfate kinase	13	0.00425	76.3	+1.5
Q4WJD7	60S ribosomal protein L27	16	0.02859	46.2	+1.5
Q4WPA5	Aldehyde dehydrogenase, putative	25	0.00851	63.5	+1.5
Q4WAL1	Acetamidase, putative	10	0.02527	24.2	+1.5
Q4WEE3	MFS multidrug transporter, putative	9	0.03076	23.8	+1.5
Q4WG82	Protein kinase C substrate, putative	17	0.02353	38.5	+1.5